



UNIVERSITÀ DEGLI STUDI DI PALERMO

Dottorato in Energia e Tecnologie dell'Informazione
Dipartimento di Ingegneria
Settore Scientifico Disciplinare ING-IND/11 – Fisica Tecnica Ambientale

DESALINATION AND SEA WAVE TO PRODUCE FRESHWATER AND ENERGY FROM THE SEA. THE PROPOSAL OF A LINEAR GENERATOR FOR A WAVE ENERGY CONVERTER AND EVALUATION OF CASE STUDIES IN SMALL ISLANDS

IL DOTTORE
ING. DOMENICO CURTO
Matricola 0660289

IL COORDINATORE
PROF. MAURIZIO CELLURA

IL TUTOR
PROF. VINCENZO FRANZITTA

CONTENTS

Contents.....	I
Figures	V
Tables	XIII
Equations.....	XVII
I Introduction	1
I.1 Energy statistics	2
I.2 Freshwater demand.....	7
I.3 Research topics.....	9
I.4 Publications on this topic	11
II Desalination.....	15
II.1 State of art.....	17
II.1.a Multi-Effects Distillation (MED).....	20
II.1.b Multi-Stages Flash (MSF).....	22
II.1.c Vapor Compression (VC).....	24
II.1.d Reverse Osmosis (RO)	26
II.1.e Forward Osmosis (FO)	32
II.1.f Nanofiltration (NF)	33
II.1.g Electro-Dialysis (ED)	34
II.1.h Capacitive Deionization (CDI).....	35
II.1.i Hydration (HY)	36
II.1.j Secondary Refrigerant Freezing (SRF)	37
II.1.k Membrane Distillation (MD).....	38
II.1.l Ions Exchange Resin (IXR).....	39
II.1.m Solar Still Distillation (SSD)	40
II.1.n Solar Chimney (SC)	40
II.1.o Humidification Dehumidification (HDH)	41
II.2 Statistics on desalination	42
II.3 Publications on this topic	48
III Sea wave	49
III.1 Marine energy	49

III.2 Definitions	52
III.3 State of art.....	61
III.3.a Oscillating Water Column	63
III.3.b Wave-activated bodies	68
III.3.c Overtopping device	75
III.3.d Power Take Off	77
III.4 Publications on this topic	79
IV Solutions for sea wave exploitation	81
IV.1 Introduction on linear generators	81
IV.2 The starting point: the prototype of linear generator	84
IV.2.a No load voltage simulation	86
IV.2.b No load voltage test.....	89
IV.3 Improvement of the linear generator	94
IV.3.a Regularization of the magnetic steps	94
IV.3.b Variation of the air gap	97
IV.3.c Variation of the magnetic step	99
IV.3.d Preliminary sizing	101
IV.3.e Cogging analysis	106
IV.3.f Proposed system.....	125
IV.3.g Lumped model.....	132
IV.3.h Energy performances	138
IV.4 Other system: the mechanical motion converter	141
IV.5 Publications on this topic	145
V Small islands and energy planning	149
V.1 Energy supply for public buildings in Ustica.....	155
V.1.a The case study of Ustica	155
V.1.b Mathematical approach.....	159
V.1.c Results	160
V.2 An energy mix for Balearic Islands and Fiji.....	163
V.2.a Balearic Islands	163
V.2.b Fiji.....	165
V.2.c Methodology	166
V.2.d Results	169

V.3 An energy mix for Aeolian Islands.....	183
V.3.a The case study of Aeolian Islands	183
V.3.b Mathematical approach	185
V.3.c Results	188
V.4 The proposal of a RES mix in Lampedusa and the analysis of grid stability	195
V.4.a The case study of Lampedusa.....	196
V.4.b The proposed energy mix.....	198
V.4.c Grid stability analysis.....	204
V.5 The introduction of energy flexibility in Pantelleria through the modulation of desalination plant and the production of domestic hot water	211
V.5.a The case study of Pantelleria.....	211
V.5.b Modulation of desalination plant.....	217
V.5.c Case study 1: Desalination unit flexibility.....	224
V.5.d Case study 2: Desalination unit and DHW storages flexibility + equipment installation	227
V.6 Publications on this topic	230
VI Conclusion	233
VII All publications.....	237
VIII Abbreviations.....	241
IX References.....	243

FIGURES

Figure I.1 World electricity production by regions and share of energy sources	3
Figure I.2 Annual trend of the addition of power generation capacity	3
Figure I.3 Worldwide installed power and annual energy production from RES.....	4
Figure I.4 Worldwide investment on the electrical energy sector.....	4
Figure I.5 World average trend of the capacity factor of RES technologies in 2010-2017 ...	5
Figure I.6 World average trend of the unitary cost for RES installation in 2010-2017	5
Figure I.7 World average trend of the LCOE of RES technologies in 2010-2017	6
Figure I.8 Local average value of the LCOE of RES technologies (2016-2017)	6
Figure I.9 Water distribution on the Earth's surface	7
Figure I.10 Annual rainfall distribution on the Earth's surface	8
Figure I.11 Population distribution on the Earth's surface.....	8
Figure II.1 Classification of desalination technologies by working principle.....	17
Figure II.2 Classification of desalination technologies by main energy input.....	18
Figure II.3 Possible coupling between desalination technologies and RES	20
Figure II.4 Scheme of a Multi-Effect Distillation unit.....	21
Figure II.5 Scheme of a Multi-Flash Stages desalination unit	22
Figure II.6 Scheme of a more efficient Multi-Flash Stages desalination unit.....	23
Figure II.7 Scheme of a simple Mechanical Vapor Compression desalination unit.....	24
Figure II.8 Scheme of a simple Thermal Vapor Compression desalination unit.....	25
Figure II.9 Scheme of a TVC and MED unit	25
Figure II.10 Osmosis phenomenon	26
Figure II.11 Solvent flow as function of the external pressure gradient.....	27
Figure II.12 Diagram of a simple Reverse Osmosis Desalination unit.....	28
Figure II.13 Scheme of a RO unit with a Pelton Turbine	29
Figure II.14 Scheme of a RO unit with a Turbocharger.....	29
Figure II.15 Scheme of a RO unit with a Dual Turbine System	29
Figure II.16 Scheme of a RO unit with a HEMI System	30
Figure II.17 Scheme of a RO unit with a Pressure Exchanger	30
Figure II.18 Working principle of a Rotary Pressure Exchanger [69]	31
Figure II.19 Working principle of a Piston-type Work Exchanger	31
Figure II.20 Scheme of a Forward Osmosis desalination unit.....	33
Figure II.21 Working principle and scheme of a nanofiltration unit	33
Figure II.22 Filtration technologies by required gradient pressure and porous size [63] (Elsevier license n. 4707241281962)	34
Figure II.23 Working principle of an Electro-Dialysis desalination unit.....	35
Figure II.24 Working principle of a Capacitive Deionization unit	36
Figure II.25 Scheme of Hydration desalination plant	36
Figure II.26 Scheme of a Secondary Refrigerant Freezing desalination unit	37
Figure II.27 Possible configurations of a Membrane Distillation unit	38
Figure II.28 Scheme of an Ions Exchange Resin desalination plant	39
Figure II.29 Solar Still Distillation unit	40

Figure II.30 Solar Chimney desalination unit	41
Figure II.31 HDH unit using a heat pump with a water refrigerated condenser	41
Figure II.32 HDH unit using a heat pump with an air refrigerated condenser	42
Figure II.33 Trend of installed capacity and operative desalination plants [44] (Elsevier license n. 4707250081904)	43
Figure II.34 Desalination plants around the world, by size and technology [44]	44
Figure II.35 Least work as function of recovery ratio and salinity of feedwater and freshwater [104] (CC BY-NC-SA 3.0).....	45
Figure II.36 Exergy analysis of several desalination technologies	46
Figure III.1 Wave parameters	52
Figure III.2 Particle motion in sea wave [136] (Elsevier license n. 4707201328819)	54
Figure III.3 Qualitative comparison of Pierson Moskowitz and JONSWAP spectra.....	57
Figure III.4 Examples of scatter tables, in the island of Pantelleria (Italy) [146]	60
Figure III.5 Global wave power GIS map [142] (Elsevier license n. 4707211026493)	62
Figure III.6 Classification of WEC based on wave direction	62
Figure III.7 Classification of WEC based on the distance from the coastline	63
Figure III.8 Sectional drawing (left) and view (right) of the Kværner Brug's OWC plant [153] (Elsevier license n. 4707220801868)	64
Figure III.9 Axonometric view (left) and section view (right) of the OWC device at Vizhinjam [155].....	65
Figure III.10 LIMPET OWC plant installed on the island of Islay (Scotland, UK) [158] (Elsevier license n. 4707221496823).....	65
Figure III.11 Back view of the OWC plant installed on the island of Pico (Azores, Portugal) [158] (Elsevier license n. 4707221496823)	66
Figure III.12 OWC plant installed in the bay of Mutriku (Spain) [160].....	66
Figure III.13 Working principle of REWEC3 [161].	67
Figure III.14 Back (left) and perspective views (right) of OWC plant at Yongsoo [134] (CC BY 4.0)	67
Figure III.15 Section of Backward Bent Duct Buoy [151] (Elsevier license n. 4707220104485)	68
Figure III.16 Sloped Buoy (left) [163], Spar Buoy (middle) [163] e Mighty Whale (right) [164].....	68
Figure III.17 Norwegian buoy, working principle of Danish buoy and Swedish buoy [151] (Elsevier license n. 4707220104485).....	69
Figure III.18 Rendering view (left) [151] and external view (right) [171] of Wavebob (Elsevier license n. 4707220104485 and 4707231054751)	70
Figure III.19 Principle of operation [169] and external view of PowerBuoy [172] [169] (CC BY-NC-ND 3.0).....	71
Figure III.20 Working principle of Archimedes Wave Swing [173] (CC BY-NC-SA 3.0) .	71
Figure III.21 CETO external view [175] and working principle [174]	72
Figure III.22 Salter's Nodding Duck. Section (left) [177] and rendering view (right) [176] (Elsevier license n. 4707240043865).....	72
Figure III.23 Working principle [178] (CC BY 4.0) and external view of Pelamis [179]....	73
Figure III.24 Working principle of Oyster [180].....	73

Figure III.25 Rendering view of Waveroller [182]	74
Figure III.26 Rendering view of Wavestar [183], [184].....	74
Figure III.27 Eco Wave Systems (left) [185] and Seahorse power take off system (right) [186]	75
Figure III.28 View (left) [187] and schematic plan view (left) [151] of Tapchan (Elsevier license n. 4707220104485)	76
Figure III.29 Views of the small scale Wave dragon (left) [151] and its working principle (right) [189].....	76
Figure III.30 External view (left) [134] and section view (right) [190] of Slot-Cone (CC BY 4.0).....	77
Figure III.31 Different paths for WEC systems [191] (CC BY-NC 4.0)	77
Figure IV.1 Linear machine from a rotary machine	82
Figure IV.2 Different magnetization schemes	83
Figure IV.3 Stator details	84
Figure IV.4 Coils shape	84
Figure IV.5 Terminal plate	85
Figure IV.6 Lateral and front views of the stator	85
Figure IV.7 Rendering view of the translator	85
Figure IV.8 Coils connection scheme in six lines	87
Figure IV.9 No-load voltage trends on the stator block A, at a speed of 1 m/s	87
Figure IV.10 No-load voltage trends on the stator block B, at a speed of 1 m/s.....	88
Figure IV.11 Measuring board, voltage divider and equivalent circuit	90
Figure IV.12 Control panel for the data acquisition	91
Figure IV.13 Normally open button to produce the starting signal.....	91
Figure IV.14 Drive system to test the generator.....	91
Figure IV.15 Comparison of no-load voltage trends from the experiment and the simulation.....	93
Figure IV.16 Rendering view of the generator on the FEM tool.....	94
Figure IV.17 No-load voltage trends on the block A using 40 magnets and the prototype stator.....	94
Figure IV.18 No-load voltage trends on the block B using 40 magnets and the prototype stator.....	95
Figure IV.19 Rendering view of the generator with a regular stator	96
Figure IV.20 No-load voltage trends on the block A using 40 magnets and a regularized stator.....	96
Figure IV.21 No-load voltage trends on the block B using 40 magnets and a regularized stator.....	97
Figure IV.22 Trends of the amplitudes of the first and third harmonics of no-load voltages as function of the airgap between magnets and stator.....	99
Figure IV.23 First and third harmonics in case of different width of the stator teeth	100
Figure IV.24 Location of the measuring buoys of RON.....	101
Figure IV.25 No-load voltage trends, adopting a regular stator having teeth 5.5 mm wide and an airgap of 2.5 mm.....	103

Figure IV.26 Amplified no-load voltage trends, assuming a three-phase connection scheme	104
Figure IV.27 Three-phases connection scheme	104
Figure IV.28 No-load voltage trends according to the changes from the pre-sizing.	105
Figure IV.29 Detailed shape of the stator with 72 coils (Stator 72).	106
Figure IV.30 Shape of the “Stator 72” modelled in Ansys Maxwell	106
Figure IV.31 Resultant of cogging force considering the configuration “Stator 72”	109
Figure IV.32 Cogging force produced by a magnet and the entire translator with “Stator 72”	110
Figure IV.33 Shape of the “Stator 144 A”, modelled in Ansys Maxwell	110
Figure IV.34 Resultant of cogging force considering the configuration “Stator 144 A” .	113
Figure IV.35 Shape of the “Stator 144 B” modelled on Ansys Maxwell.....	114
Figure IV.36 Resultant of cogging force considering the configuration “Stator 144 B” ..	117
Figure IV.37 Cogging force produced by a magnet and the entire translator with “Stator 144 B”	118
Figure IV.38 Shape of the “Stator 144 C” modelled on Ansys Maxwell	118
Figure IV.39 Resultant of cogging force in the configuration “Stator 144 C”	121
Figure IV.40 Cogging force produced by a magnet and the entire translator with “Stator 144 C”	121
Figure IV.41 Shape of the “Stator 144 D”, modelled on Ansys Maxwell	122
Figure IV.42 Cogging force produced by a magnet and the entire translator with “Stator 144 D”	122
Figure IV.43 Resultant of cogging force in the configuration “Stator 144 D”	125
Figure IV.44 Different views of the stator of the proposed linear generator.....	126
Figure IV.45 A 3D view of the stator.....	127
Figure IV.46 3D view of the translator	127
Figure IV.47 External view of the proposed Wave Energy Converter	129
Figure IV.48 Sectional view of the internal buoy and detail of the movable part	130
Figure IV.49 Probability density function of the Peak Period in three measuring stations in Sicily	131
Figure IV.50 Layout of a potential wave farm based on the proposed WEC	132
Figure IV.51 Internal scheme of the linear generator.....	133
Figure IV.52 Ratio of force produced by PTO as function of translator speed	136
Figure IV.53 Evaluation of the immersed volume	136
Figure IV.54 Discretized approach to evaluation of the immersed volume	137
Figure IV.55 Working principle of the mechanical motion converter	142
Figure IV.56 Internal view of WEC, equipped with the mechanical motion converter..	142
Figure IV.57 Electrical efficiency in the first scenario	143
Figure IV.58 Electrical efficiency in the second scenario.....	144
Figure IV.59 Power trend with different testing masses and a fixed load resistance (20 Ω)	144
Figure V.1 Small islands in the world [209] (CC BY-NC-ND 3.0).....	149
Figure V.2 Share of RES and installed power (data in kW) in small Italian islands.....	154
Figure V.3 Location of Ustica in the Mediterranean Sea	155

Figure V.4 Electrical consumption by uses	156
Figure V.5 Annual trend of electricity consumption by uses.....	156
Figure V.6 Protected areas in Ustica	157
Figure V.7 Freshwater production by the desalination plant in Ustica	158
Figure V.8 Data on solar and sea wave climate in Ustica	160
Figure V.9 Electricity production from the proposed renewable energy mix	161
Figure V.10 Discounted cash flow of the project.....	162
Figure V.11 Comparison of energy mix used for the electrical production in Balearic Islands and Spain during 2017.....	164
Figure V.12 Energy consumption by sources in Balearic Islands.	164
Figure V.13 Electricity production in Fiji by energy sources	165
Figure V.14 Power output of wind turbine as function of wind speed.	168
Figure V.15 Reference points in Balearic Islands for the evaluation of renewable energy potential	170
Figure V.16 Wind speed classes in the reference points in Balearic Islands	172
Figure V.17 Comparison of Weibull distribution based on two different data set in the reference point W1.	173
Figure V.18 Comparison of monthly electricity demand and potential energy production from renewable energy sources in Balearic Islands.....	174
Figure V.19 Electricity production by sources and share of RES in Balearic Islands. (A) Wind evaluation based on Weibull distribution. (B) Wind evaluation based on wind speed classes	175
Figure V.20. Discounted cash flow for the realization of the proposed RES mix in Balearic Islands. Case 1: Investment based on world average prices. Case 2: Investment based on European average prices	176
Figure V.21. Reference points in Fiji for the evaluation of renewable energy potential .	177
Figure V.22 Wind speed classes in the reference points in Vanua Levu (Fiji)	178
Figure V.23 Wind speed classes in the reference points in Viti Levu (Fiji)	179
Figure V.24 Comparison of Weibull distribution based on two different data set in the reference point W1	180
Figure V.25 Comparison of monthly electricity demand and potential energy production from renewable energy sources in Fiji using the wind speed classes approach.	181
Figure V.26 Electricity production by sources and share of RES in Fiji. (A) Wind evaluation based on Weibull distribution. (B) Wind evaluation based on wind speed classes.....	182
Figure V.27 DCF for the realization of the proposed RES mix in Fiji. Case 1: Investment based on world average prices. Case 2: Investment based on Oceanian average prices	182
Figure V.28 Aeolian Islands in the Tyrrhenian Sea (Italy).....	183
Figure V.29 PVP plants in Vulcano [208]	185
Figure V.30 Availability of wind source for each island during the year	189
Figure V.31 Wind power production as function of wind speed	190
Figure V.32 Electricity demand and potential renewable energy production.....	193
Figure V.33 Share of each source in Aeolian Islands Energy Scenario.	194
Figure V.34 Flow chart of the methodology	196
Figure V.35 Daily energy production MWh [2014]	197

Figure V.36 Layout of the MV network of Lampedusa island	198
Figure V.37 Availability of wind source by wind speed classes	199
Figure V.38 Solar radiation on horizontal and tilted surface (31°) and sea wave power flux	199
Figure V.39 Electricity demand and potential renewable energy production	204
Figure V.40 Scenario A: Typical load profile at different RES penetrations in a summer week	205
Figure V.41 Scenario A: Typical load profile at different RES penetrations in a winter week	206
Figure V.42 Scenario B: Typical load profile at different RES penetrations in a summer week	206
Figure V.43 Scenario B: Typical load profile at different RES penetrations in a winter week	206
Figure V.44 Trend inertial response in RES presence: (a) Scenario A, winter; (b) Scenario A, summer; (c) Scenario B, winter; (d) Scenario B, summer.	207
Figure V.45 Grid frequency in the case of 3-phase short-circuit in the grid: (a) Scenarios A0 and B0, (b) Scenarios A1 and B1 and (c) Scenarios A2 and B2.	209
Figure V.46 Position and satellite view of Pantelleria.	211
Figure V.47 Monthly fuel consumption and average specific fuel consumption	213
Figure V.48 Comparison of monthly electricity production in 2011, 2016 and 2018.	213
Figure V.49 Hourly electricity production in monthly typical days in 2016	214
Figure V.50 Electricity consumptions by users: (a) Yearly trend; (b) 2016 share [80].	214
Figure V.51 Freshwater production in 2015 and 2018.....	215
Figure V.52 Share of electricity consumption in residential sector by main loads, in 2011	216
Figure V.53 Annual trend of electricity consumption for DHW in residential sector	216
Figure V.54 Scheme of the energy system in Pantelleria: (a) AS-IS scenario; (b) TO-BE scenario 1; (c) TO-BE scenario 2.	217
Figure V.55 Diesel generators efficiency vs. load estimated trend and piecewise averaging	219
Figure V.56 Optimal daily schedule of diesel generators and desalination units in May (minimum load month) in case study 1.....	224
Figure V.57 Optimal daily schedule of diesel generators and desalination units in January (average load month) in case study 1.....	224
Figure V.58 Optimal daily schedule of diesel generators and desalination units in August (maximum load month) in case study 1.	225
Figure V.59 Percentage of diesel generators operating hours inside and outside maximum efficiency region, in case study 1.	225
Figure V.60 Monthly DES flexible consumption in case study 1.	226
Figure V.61 Monthly economic and emission saving in case study 1.	226
Figure V.62 STC size influence in monthly optimizations in case study 2.	227
Figure V.63 Optimal daily schedule of diesel generators and desalination units in May (minimum load month) in case study 2.....	228

Figure V.64 Optimal daily schedule of diesel generators and desalination units in January (average load month) in case study 2.	228
Figure V.65 Optimal daily schedule of diesel generators and desalination units in August (maximum load month) in case study 2.	229
Figure V.66 Percentage of diesel generators operating hours inside and outside maximum efficiency region in case study 2.	229
Figure V.67 Monthly economic and emission saving in case study 2.	230

TABLES

Table II.1 State of art of commercial desalination technologies	44
Table III.1 Potential installable capacity and energy production from marine energy sources.....	52
Table III.2 Sea States Codes based on Douglas Sea Scale.....	58
Table III.3 Average values of the energy efficiency of PTO [191].....	78
Table IV.1 Main properties of the permanent magnets	86
Table IV.2 Fourier series coefficients of no-load voltage trends in the prototype.....	89
Table IV.3 Resistance values and measurable voltage range	90
Table IV.4 Fourier series coefficients of no-load voltage trends by using a long translator and the prototype stator	95
Table IV.5 Fourier series coefficients of no-load voltage trends by using a regular long translator and a regular stator	97
Table IV.6 Fourier series coefficients of no-load voltage trends by using a regular long translator and a regular stator	98
Table IV.7 Coefficients of Fourier series in case of different width of stator teeth	100
Table IV.8 Wave speed distribution according to the data from the RON stations of Catania, Mazara del Vallo and Palermo.....	102
Table IV.9 Fourier series coefficients of no-load voltage trends by using a long translator and a regular stator having teeth 5.5 mm wide and an airgap of 2.5 mm.....	103
Table IV.10 x-axis component of cogging forces generated in the configuration “Stator 72”	107
Table IV.11 Fourier series coefficients of cogging force, considering the configuration “Stator 72”	109
Table IV.12 x-axis component of cogging forces generated in the configuration “Stator 144 A”	111
Table IV.13 Comparison of Fourier series coefficients considering “Stator 72” and “Stator 144 A”	113
Table IV.14 Sum of harmonics	114
Table IV.15 x-axis component of cogging forces generated in the configuration “Stator 144 B”	115
Table IV.16 Comparison of Fourier series coefficients considering “Stator 72” and “Stator 144 B”	117
Table IV.17 x-axis component of cogging forces generated in the configuration “Stator 144 C”	119
Table IV.18 Comparison of Fourier series coefficients in the case “Stator 72” and “Stator 144 C”	121
Table IV.19 x-axis component of cogging forces generated in the configuration “Stator 144 D”	123
Table IV.20 Comparison of Fourier series coefficients considering all different stators. .	125
Table IV.21 Significant height distribution according to the data from the RON stations of Catania, Mazara del Vallo and Palermo.....	128

Table IV.22 Simulated power output (kW) of the proposed WEC, by using the mathematical model	138
Table IV.23 Simulated power output (kW) of the proposed WEC, by using OpenWEC	138
Table IV.24 Simulated annual energy production by using the mathematical model in Catania.....	139
Table IV.25 Simulated annual energy production by using OpenWEC in Catania	139
Table IV.26 Simulated annual energy production by using the mathematical model in Mazara	140
Table IV.27 Simulated annual energy production by using OpenWEC in Mazara.....	140
Table IV.28 Simulated annual energy production by using the mathematical model in Palermo.....	140
Table IV.29 Simulated annual energy production by using OpenWEC in Palermo	141
Table V.1 Targets and data on small islands according to decree 14 February 2017 [240], [241].....	153
Table V.2 Data on desalination plants installed in small Italian islands.....	154
Table V.3 Electrical consumption in public buildings and facilities in Ustica	158
Table V.4 Details on the solar wave energy farm.....	161
Table V.5 Details on the roof-integrated photovoltaic plants.....	161
Table V.6 Economic parameters used in the discounted cash flow	162
Table V.7 Main parameters of photovoltaic panels [264]	167
Table V.8 Main parameters of the chosen wind turbines [271], [272]	168
Table V.9 Data of monthly-average daily solar radiation in Balearic Islands	170
Table V.10 Data of wind source in Balearic Islands	171
Table V.11 Estimation of the Weibull distribution coefficients and fit quality in W1 (Balearic Islands)	173
Table V.12 Data of Sea Wave Energy Flux in Balearic Islands	173
Table V.13 Details of the renewable energy mix for Balearic Islands.....	176
Table V.14 Data of Sea Wave Energy Flux in Fiji	177
Table V.15 Data of the monthly-average daily solar radiation in Fiji.....	178
Table V.16 Data of wind source in Fiji	178
Table V.17. Estimation of the Weibull distribution coefficients and fit quality in W1 (Fiji)	179
Table V.18 Details of the renewable energy mix for Fiji Islands.	181
Table V.19 Main data of Aeolian Island.....	184
Table V.20 Installed plants and targets for Aeolian Archipelago	184
Table V.21 Monthly solar radiation data [kWh/m ²] for each island [253]	189
Table V.22 Wave energy flux [kW/m] [296]	189
Table V.23 Values of main parameters used in the evaluation on Lipari island	191
Table V.24 LCOE as function of photovoltaic and wind ratio, without constrains.....	191
Table V.25 Matrix of constrains for the renewable energy mix.....	192
Table V.26 Constrained LCOE matrix for Lipari island	193
Table V.27 Proposal of energy mix for the Aeolian Islands.....	194
Table V.28 Rated power of diesel generators installed in Lampedusa	197
Table V.29 Values of main economic parameters.....	200

Table V.30 LCOE (€/MWh) as function of photovoltaic and wind ratio (%), without constrains.....	201
Table V.31 Matrix of constrains for the renewable energy mix	202
Table V.32 Constrained LCOE matrix for Lampedusa	203
Table V.33 Proposal of energy mix for Lampedusa.....	203
Table V.34 Simulated events overview.	208
Table V.35 Generation groups in Pantelleria.....	212
Table V.36 Characteristic of water reserves in Pantelleria network.....	215
Table V.37 Electricity demand in monthly standard days	222
Table V.38 DHW and freshwater demands in monthly standard days.	222
Table V.39 Economic parameters [33].....	223
Table V.40 Technical and environmental parameters [33]	223
Table V.41 Operating hours of diesel generators in case study 1.....	225
Table V.42 Operating hours of diesel generators in case study 2.....	229
Table V.43 PV and STC in twelve monthly optimizations.	229

EQUATIONS

II.1.....	26
II.2.....	28
II.3.....	45
II.4.....	46
II.5.....	46
III.1.....	52
III.2.....	53
III.3.....	53
III.4.....	53
III.5.....	54
III.6.....	54
III.7.....	54
III.8.....	54
III.9.....	55
III.10.....	55
III.11.....	55
III.12.....	55
III.13.....	56
III.14.....	56
III.15.....	56
III.16.....	56
III.17.....	56
III.18.....	56
III.19.....	57
III.20.....	58
III.21.....	59
III.22.....	59
III.23.....	59
III.24.....	59
III.25.....	59
III.26.....	59
III.27.....	60
III.28.....	60
III.29.....	60
III.30.....	60
III.31.....	61
III.32.....	61
IV.1.....	88
IV.2.....	88
IV.3.....	88
IV.4.....	89

IV.5.....	90
IV.6.....	92
IV.7.....	92
IV.8.....	92
IV.9.....	92
IV.10.....	93
IV.11.....	93
IV.12.....	99
IV.13.....	99
IV.14.....	101
IV.15.....	105
IV.16.....	105
IV.17.....	131
IV.18.....	131
IV.19.....	131
IV.20.....	133
IV.21.....	134
IV.22.....	135
IV.23.....	135
IV.24.....	135
IV.25.....	135
IV.26.....	136
IV.27.....	136
IV.28.....	137
IV.29.....	137
IV.30.....	137
IV.31.....	139
IV.32.....	142
IV.33.....	143
V.1.....	159
V.2.....	159
V.3.....	159
V.4.....	159
V.5.....	159
V.6.....	160
V.7.....	166
V.8.....	167
V.9.....	167
V.10.....	168
V.11.....	169
V.12.....	169
V.13.....	169
V.14.....	185
V.15.....	185

V.16.....	186
V.17.....	186
V.18.....	187
V.19.....	203
V.20.....	205
V.21.....	205
V.22.....	210
V.23.....	219
V.24.....	220
V.25.....	220
V.26.....	220
V.27.....	220
V.28.....	220
V.29.....	220
V.30.....	221
V.31.....	221
V.32.....	221
V.33.....	221
V.34.....	221
V.35.....	221
V.36.....	221
V.37.....	221
V.38.....	221
V.39.....	221
V.40.....	221
V.41.....	221
V.42.....	221
V.43.....	221
V.44.....	221

I INTRODUCTION

In the last decade, the term “water-energy nexus” gained popularity in the international research field [1]-[3]. Despite there is no official definition, this term underlines the relevant links existing between energy and water sectors.

Historically, in 1994 Peter Henry Gleick analyzed for the first time the connections existing between these two fields [4]. Indeed, the entire energy sector depends on the availability of water in different ways. Starting from the raw energy sources, water is required to extract fossil fuels and to irrigate the feedstock crops used as biomass. Water is also utilized as processing fluid, for example to refine and transport the fossil fuels, or in other industrial processes to transform foods and other materials.

Water is adopted as energy carrier, for example in the local heating district network. In steam power plants, water is used as working fluid and cooling energy carrier. Finally, in hydropower plants water is used as energy source, converting its potential energy into electrical energy.

At the same time, water needs several treatments requiring huge amounts of energy in order to make it usable for industrial applications or for drinking purposes. Indeed, energy is required to transport water from a region to another one or to remove bacteria, sediments, salts and other undesired substances [4]. Among these processes, desalination is undoubtedly the most energy consuming treatment required to obtain freshwater [5].

It is remarkable that energy and water sectors do not form a closed loop, however the several examples above reported highlight the strong relations existing between these two sectors. Consequently, the increasing of the energy demand corresponds to a growth in water consumption and vice versa.

The water-energy nexus is also considered in the international developing plans. As an example, in 2014 the US Department of Energy published the official report “The Water-Energy Nexus: Challenge and Opportunities”, resuming firstly the several relations existing between these two fields, then listing the potential consequences from the climate change, and finally reporting the possible solutions to limit the effects [3].

Due to the population and economy growth in many regions of the world, the water and energy demands are currently increasing, representing a relevant problem to deal with.

In order to assure a sustainable development, water and energy demand must be managed properly. In fact, both topics are considered in the 2030 Agenda for Sustainable Development, emitted by the General Assembly in September 2015 [6].

In detail, the Agenda considers 17 Sustainable Development Goals. Among these, the goal 6 is “Ensure availability and sustainable management of water and sanitation for all” and the goal 7 is “Ensure access to affordable, reliable, sustainable and modern energy for all” [6].

Focusing on the energy sector, the ratification of the Kyoto Protocol (2005) and the following Paris Agreement (2015) represented two important milestones in the hard endeavor of the global warming containment [7], [8].

The main target is the limitation of global warming to “well below 2 °C”, in comparison with the preindustrial levels [9]. In particular, the Paris Agreement imposed a maximum global warming of just 1.5°C as threshold. With the signature of the agreement, 174 Countries (plus the European Union) are now obliged to adopt specific energy policies in order to contain the CO₂ emissions [7].

This international cooperation is due by the fact that the consequences of global warming could be dramatic for the mankind: melting of glaciers, increasing of the deserts extension, increasing of the sea level, increasing of the probability of extreme weather conditions like hurricanes and storms, water scarcity and limited availability of foodstuffs [10].

I.1 Energy statistics

It is estimated that the energy sector is related to the emission of about two-thirds of all anthropogenic greenhouse-gas emissions, with a special relevance of CO₂ [11].

To limit the effects on the environment, recent studies prescribe the applications of immediate energy policies in order to achieved the zero net anthropogenic greenhouse gas emission before the second half of the 21st century [12], [13].

As well known in literature, there are two main techniques to contain the rate of greenhouse gas emission in a sustainable way [14]:

- Abandon inexorably the use of fossil fuels, promoting the installation of power plants supplied by Renewable Energy Sources (RES);
- Reduce the primary energy demand in final users, through the adoption of more efficient technologies and smart control of the systems, optimizing the energy consumption.

Both approaches are necessary to maximize the benefits from an environmental and economic point of view, since the different targets. Indeed, the adoption of the first method reduces the impacts on the environment, not modifying the total energy demand but transferring the energy production from fossil fuels to RES. On the contrary, the second approach modifies the total energy demand of final users, by the introduction of more efficient and smart technologies.

As shown in Figure I.1 (left), in the last three decades the world electricity demand has been growing from 11.88 PWh/y in 1990 to 26.59 PWh/y in 2018, with an almost linear trend [15].

The main growing contribution is related to Asia, whose annual electricity production has been expanding from 2.25 PWh/y in 1990 to 12.01 PWh/y in 2018, so almost six times in about 30 years. About the share of energy sources adopted for the electricity production, fossil fuels continue to have a dominant role, although natural gas

is nowadays preferred to oil, as shown in Figure I.1 (right) [16]. It is important to underline that each item in the graph has increased in absolute terms in the period 2000-2017.

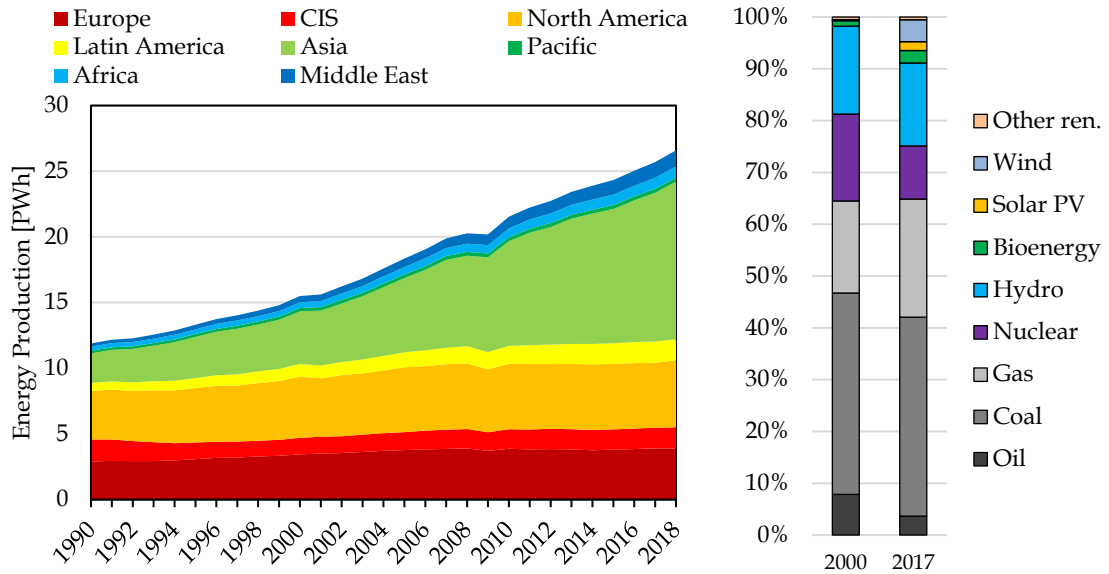


Figure I.1 World electricity production by regions and share of energy sources

Indeed, as shown in Figure I.2 in the last years new power plants supplied by fossil fuels have been installed, however from 2015 the growth of RES has been greater than the fossil fuels [16].

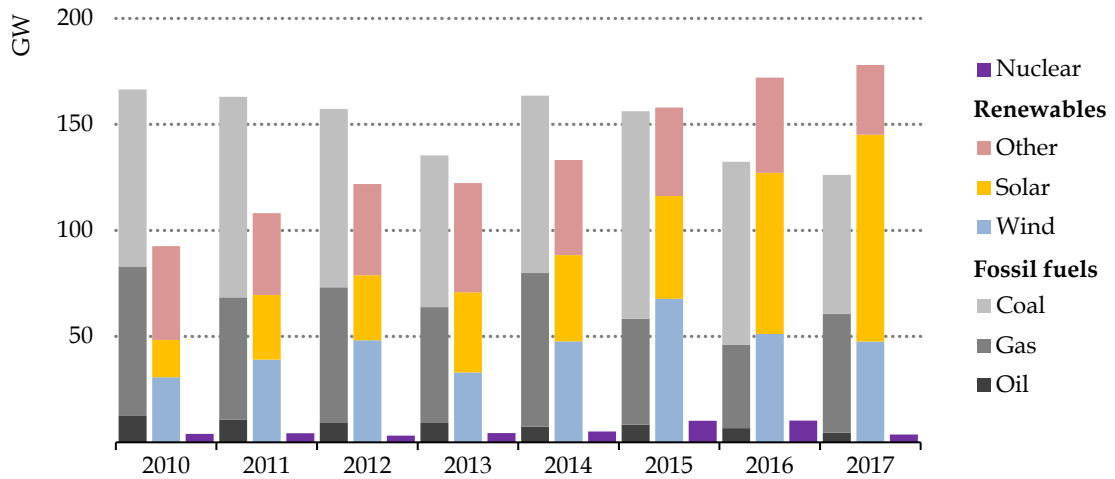


Figure I.2 Annual trend of the addition of power generation capacity

A recent IRENA report highlights the noteworthy expansion of the worldwide installed power capacity from RES: in less than 20 years, it is practically tripled, passing from 753.95 GW in 2000 to 2350.76 GW in 2018. Plant supplied by RES are currently concentrated in Asia (1023.5 GW, 43.54%), Europe (536.4 GW, 22.82%), North America (366.5 GW, 15.59%) and South America (211.27 GW, 8.99%) [17]. The worldwide trends of the installed power capacity and the annual electricity production from RES by region are reported in Figure I.3 [17].

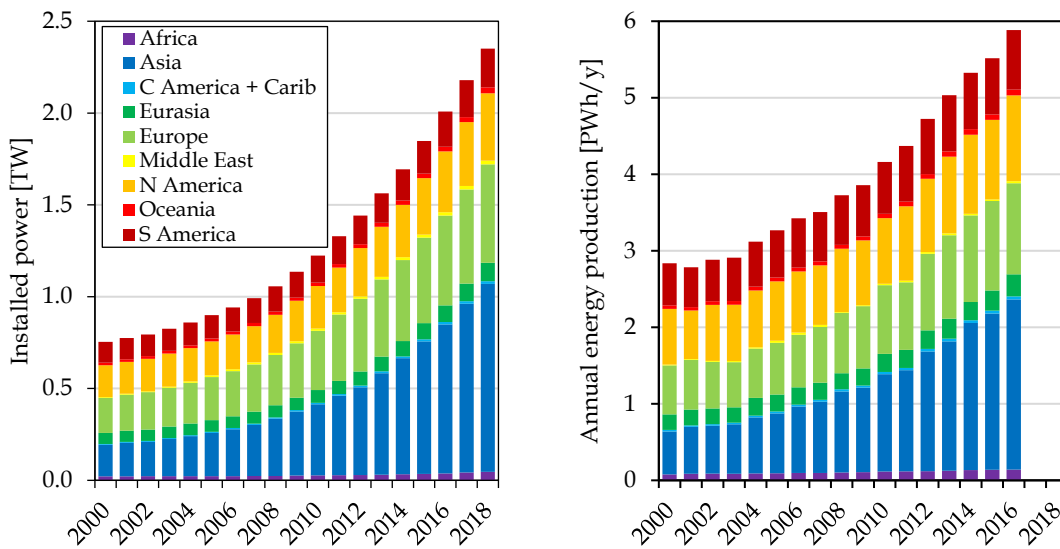


Figure I.3 Worldwide installed power and annual energy production from RES.

Considering the last year, the worldwide installed power by RES is equal to 2350.76 GW, that is composed by 1292.60 GW (54.99%) from hydropower, 563.73 GW (23.98%) from wind, 485.83 GW (20.67%) from solar panels, 115.73 GW (4.92%) from biomass and 13.33 GW (0.57%) from geothermal energy.

Huge investments are required for the energy transition from fossil fuel to RES. In detail, Figure I.4 shows the trend of the worldwide investment on the sector of the electrical power generation, by using 2018 US dollar constant currency [18]. It is possible to observe a progressive increase of the annual expenditure, from 460 billion USD in 2005 to 775 billion USD in 2018. Focusing on RES, the worldwide investment was equal to 120 billion USD in 2005 and 305 billion USD in 2018 [18].

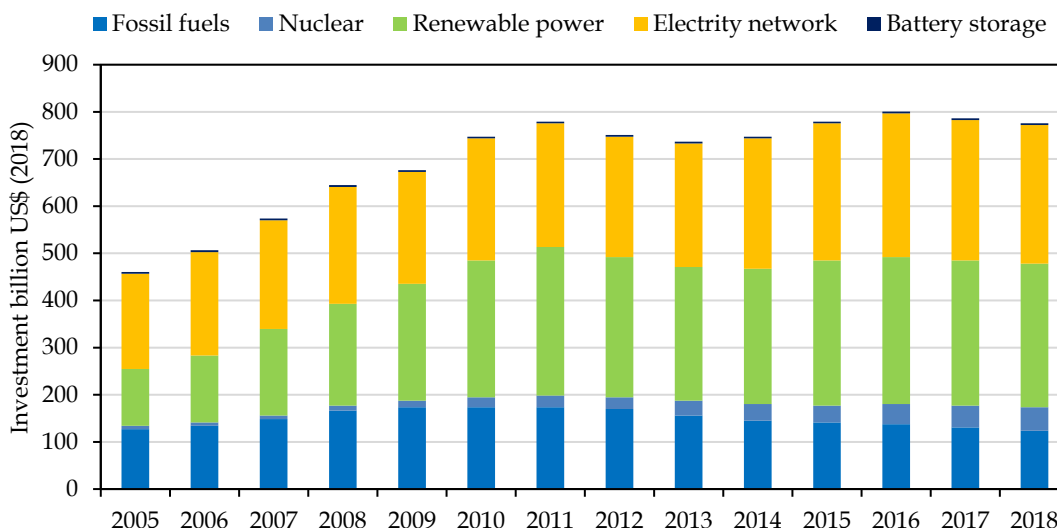


Figure I.4 Worldwide investment on the electrical energy sector.

The diffusion of RES is producing important effects on the corresponding technologies [17]:

- Improvement of the capacity factor, i.e. the ratio between the annual electricity production and the maximal production if the system works at rated power in the entire year;
- Reduction of the unitary cost for the installation of power plants;
- Reduction of the Levelized Cost of Electricity (LCOE), i.e. the minimal selling price of the lifetime energy production of a specific technology in order to overcome its lifecycle costs (the initial investment, the operative and maintenance costs, the decommissioning and the bank interest) [19].

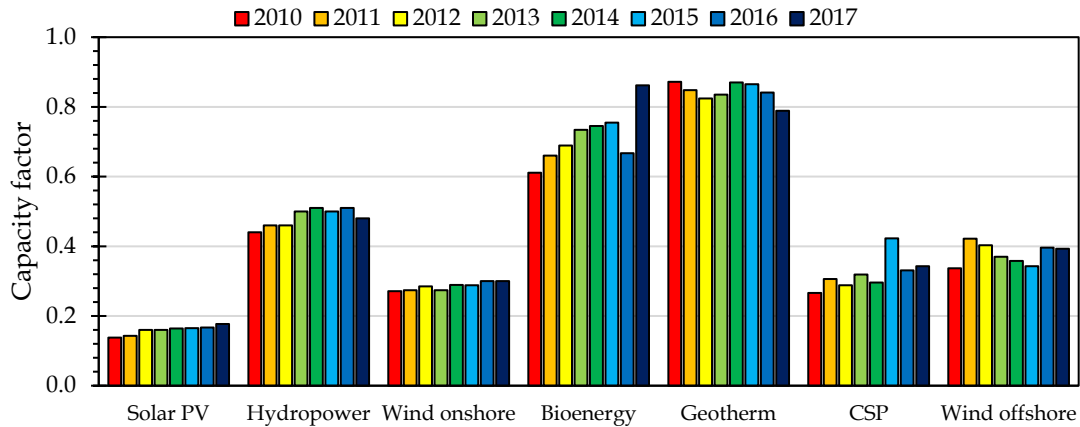


Figure I.5 World average trend of the capacity factor of RES technologies in 2010-2017

Figure I.5 reports the world weighted values of the capacity factor of each RES in the period 2010-2017 [17]. The abbreviation CSP is referred to Concentrated Solar Power. Figure I.6 shows the trends of the world average price for the installation of a unitary power of each RES technology [17].

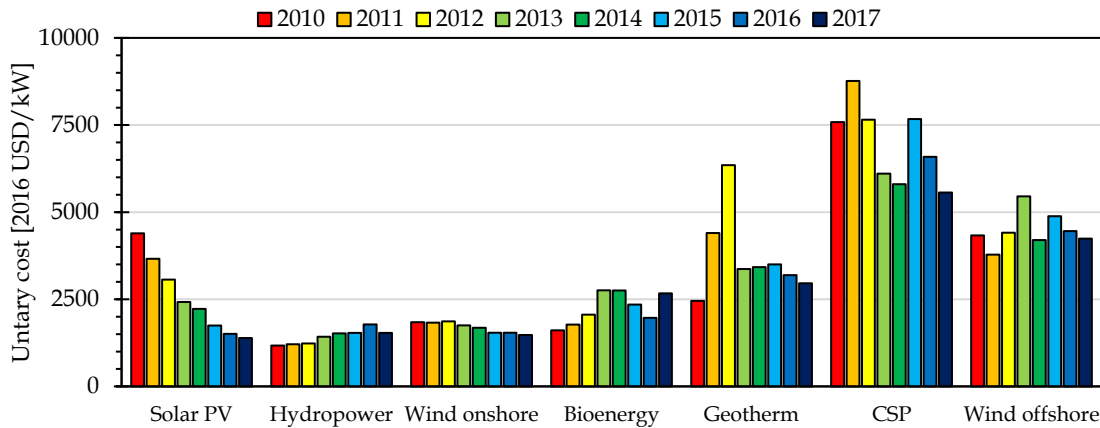


Figure I.6 World average trend of the unitary cost for RES installation in 2010-2017

Similarly, Figure I.7 reports the corresponding values of the LCOE for each RES technology [17]. Finally, Figure I.8 shows the local average values of the LCOE considering the available data in the period 2016-2017. All data are available in [17].

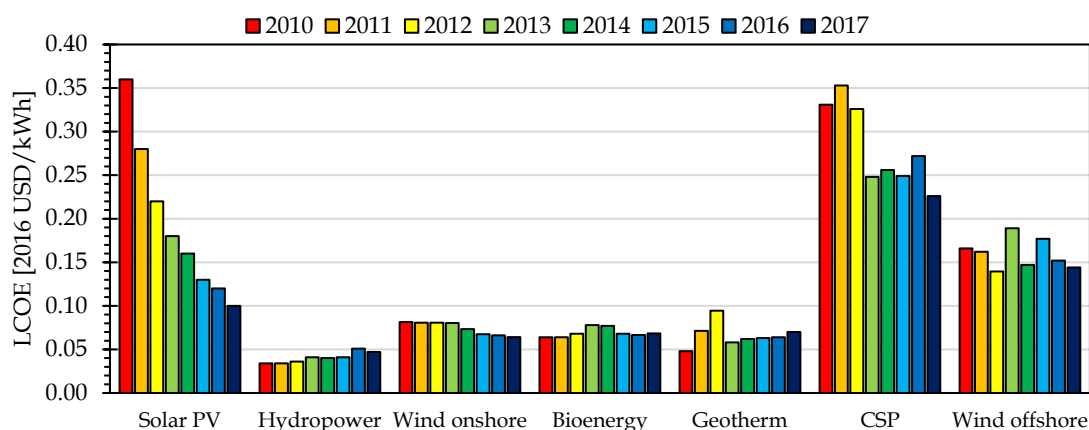


Figure 1.7 World average trend of the LCOE of RES technologies in 2010-2017

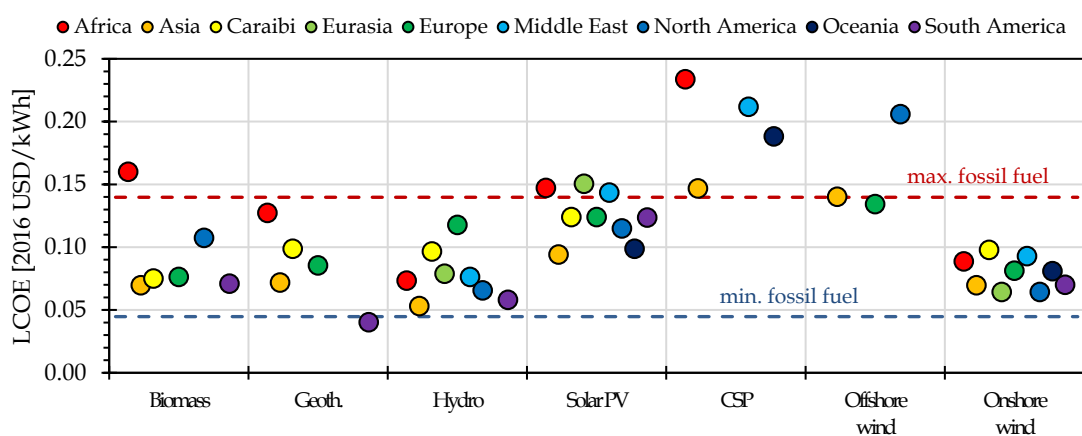


Figure 1.8 Local average value of the LCOE of RES technologies (2016-2017)

It is remarkable that nowadays a relevant part of RES technologies has a LCOE in the same range of the technologies supplied by fossil fuels [17].

While the capacity factor depends deeply on the availability of the energy sources, the unitary cost to install RES plants is highly related to the technological development. Indeed, it is interesting to observe the significant reduction of the unitary cost to install photovoltaic panels. This is essentially due to the technological progress with a consequential benefit also in term of LCOE.

Hydropower represents a very mature technology. The limited growth of the unitary cost and LCOE is essentially due to the fact that nowadays small plants are also spreading, that are affected by higher specific costs. The comparison between onshore and offshore wind turbines reveals similar results: both technologies show a limited increase of the capacity factor and the reduction of the unitary cost and LCOE. Since the wind source is stronger and more regular in case of offshore installation, the capacity factor is higher in this case than in onshore installation. Otherwise, the unitary cost for the installation is higher due to major role of infrastructure in the offshore condition.

I.2 Freshwater demand

As introduced before, the water demand is related to the energy demand in several ways. In this section, some data on the freshwater demand are reported.

Despite the 71% of Earth's surface is covered by water with an estimate volume of 1.386 billion cubic kilometers, a limited volume ratio is composed by freshwater (about 2.53%) [20]. Indeed, the most of water comprises the saltwater of seas and oceans (96.54%) and brackish¹ water (0.93%), as shown in Figure I.9.

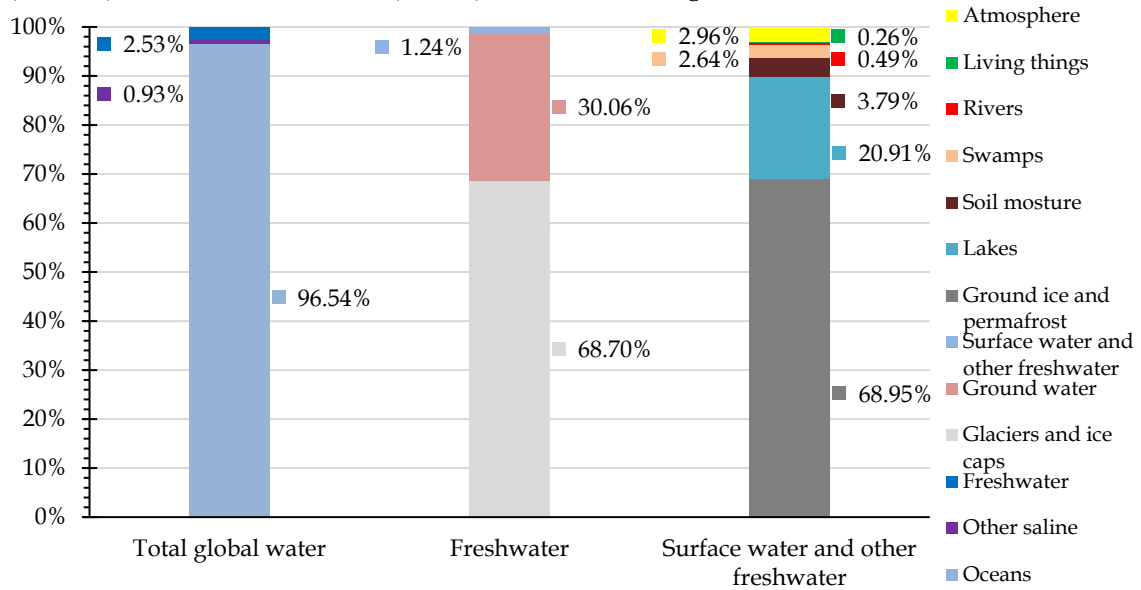


Figure I.9 Water distribution on the Earth's surface

Furthermore, a limited amount of freshwater can be reasonably used. In fact, about 68.70% of freshwater is frozen in glaciers and ice caps, about 30.06% is ground water, thus only the 1.24% of freshwater is located on the Earth's surface [20]. Considering this amount, only 20.91% is concentrated in lakes, 2.64% in swamps and 0.49% in rivers, for a total of 104590 cubic kilometers (0.0075% of the water volume on the Earth's surface) [20].

As well known, according to the hydrological cycle, water is subjected to a continuous process of evaporation and condensation, promoted by the solar radiation.

It is estimated that on the Earth's surface the total rainfalls achieve the value of 505 thousand cubic kilometers per year.

However, rainfalls are irregularly distributed around the world, as shown in Figure I.10 [21]. Several regions, as South America, Middle Africa, India, Indonesia, have high values of rainfalls, over one meter per year. In other areas, like west part of North America, Middle East, Australia, north part of Asia, rainfalls are limited, with value between 100 and 500 mm/y. Finally, other regions, like North Africa, are characterized by an extreme water scarcity (rainfalls lower than 100 mm/y).

¹ Brackish water is characterized by a limited salinity, from 0.5 to 30 grams of salts per litre.

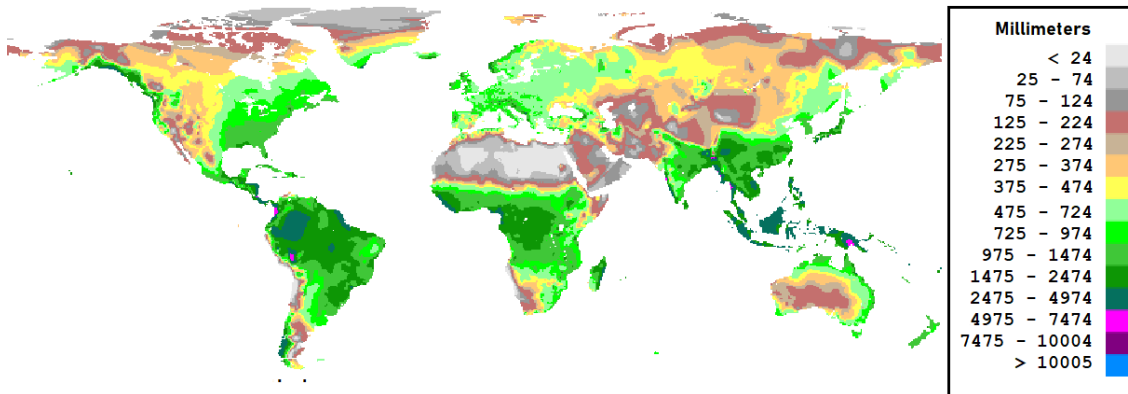


Figure I.10 Annual rainfall distribution on the Earth's surface

At the same time, it is interesting to analyze also the population distribution around the world. As shown in Figure I.11, the population is mainly concentrated in temperate areas and along the coastline. The comparison with Figure I.10 reveals that population is distributed in areas with a medium water availability (500-1500 mm/y).

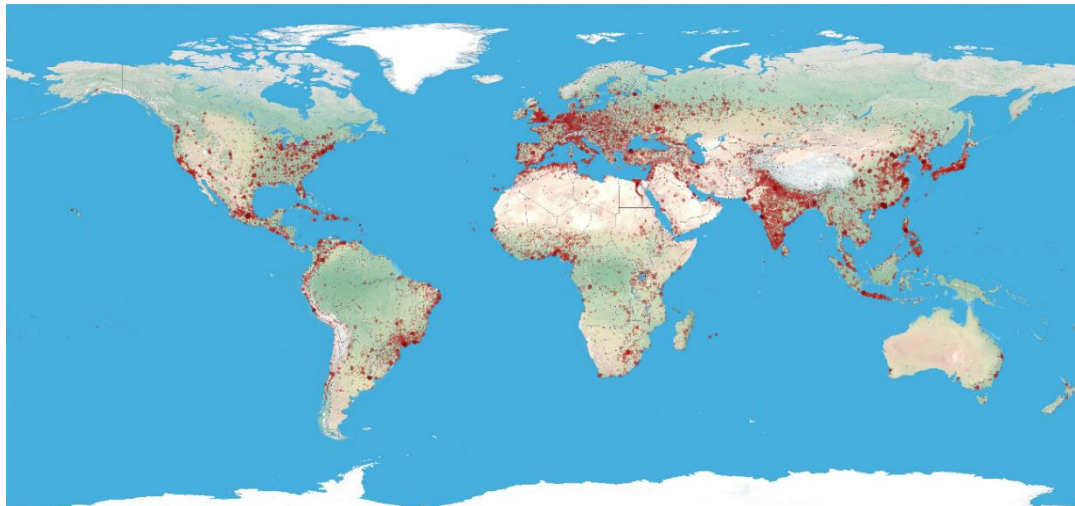


Figure I.11 Population distribution on the Earth's surface

It should be reminded that the population will increase furthermore in the next future, achieving 9.7 billion people by 2050. In developing countries, towns will gain population with a growing rate of 70 million people more each year [22].

About 2.8 billion people will stay in regions affected by water scarcity at least for one month per year; about 1.2 billion will live in areas with severe difficulties to have the access to clean water [23]. To feed the even increasing population, the water demand in agricultural production will growth of 60% [22].

Based on the water consumption trend in the past century, the manufacturing and household sectors will increase their water demand by 400% and 130%, respectively, between now and 2050 [24]. The main contribution will due to emerging economies and developing countries [25].

Furthermore, over 1.3 billion people worldwide still lack the access to the electrical energy supply; most of them are located in sub-Saharan Africa or East-Asia [26]. The

access to water reserves could produce conflicts and political instability in several countries [27].

Moreover, the water demand is increased by the cultivation of biomass, used for energy purpose. This is the case of Latin American countries, where ethanol is produced by the fermentation of sugarcane to reduce the fossil fuel consumption for the transportation sector [28]. This approach could have serious local consequences. The cultivation of biomass generates a competition with the local production of foodstuffs, reducing the territories reserved to this purpose and consequently increasing the price of foods.

From an environmental point of view, the biomass cultivation reduces the local biodiversity. Deforestation could be also a consequence of the biomass cultivation. Finally, the adoption of chemical fertilizers to improve their growth rate introduces the risk of ground water pollution, aggravating the problem of freshwater availability [29].

To overcome this problem, a solution is represented by desalination, an industrial process able to obtain freshwater from saltwater and brackish [30].

The state of art on the current technologies and new research areas is reported in the next chapter.

I.3 Research topics

Considering the water-energy nexus introduced above, this thesis investigates the possibility to produce electrical energy from sea wave in order to supply desalination plants or a generic electrical load in small islands.

While the desalination sector is full of technologies well developed and commercially mature, the exploitation of sea wave as energy source is quite back. It is relevant to underline that when the Ph.D. research project started, most of desalination plants in small Italian islands were based on thermally driven technologies [31]. In the meantime, these plants have been replaced by Reverse Osmosis units (see Table V.2 in Chapter V), that represent the current Best Available Technology (BAT) for desalination. Therefore, the application of BAT in small islands is already implemented, as shown in the case studies [32]-[34].

Thence, the introduction of RES is the remaining frontier to increase the energy sustainability in small islands. The research behind this thesis comprises several elements, among which there are:

- Review of the state of art of desalination technologies in order to find the BAT;
- Review of the state of art of sea wave energy exploitation;
- Proposal of a wave energy converter;
- Designing of an innovative power take off, i.e. the main component of the wave energy converter;

- Realization of lumped-parameters models to estimate the electrical energy production of the wave energy converters in different sea wave climate conditions;
- Evaluation of the monthly and annual electrical production of the system;
- Analysis of specific case studies, focusing on the small islands in the Mediterranean Sea;
- Proposal of mathematical model in order to size an energy mix based on sea wave and other RES, such as solar and wind.

This work represents a personal advancement of the research started with the Master Decree thesis, entitled “Improvement of the Energy Performance of an Innovative Sea Wave Electrical Energy Generator” (written in Italian with the title “Ottimizzazione delle Performances Energetiche di un Innovativo Generatore di Energia Elettrica da Moto Ondoso”).

Since the topic of this thesis is quite huge, the analysis of the state of art for desalination has been finalized to identify the BAT, as reported in Chapter II.

Chapter III addresses the topic of sea wave utilization as energy source. First, the phenomenon is described, introducing the main parameters used to evaluate this source. The state of art of the technologies for its exploitation are consequently reported.

Chapter IV reports the design process of a wave energy converter, with an attention on the power take off. Starting from the prototype investigated in the Master Decree Thesis, the chapter considers few changes required to improve the power output, the limitation of undesired phenomena (mainly the cogging force), the evaluation of the energy performance and the development of a lumped-parameters model to estimate the electrical energy production under specific sea wave conditions.

Finally, Chapter V reports some energy scenarios, considering small islands. As below reported, in several small islands equipped with desalination plants the BAT has been already implemented, in the recent installation of reverse osmosis units to contain the energy consumptions.

Thus, the case studies investigate the possibility to supply a part of the local loads, by using sea wave energy and, eventually, other energy sources (mainly wind and solar).

In this way, desalination represents a generic electrical load. Simplified mathematical models are introduced in order to evaluate the monthly and annual energy production from each energy source. The stability of the electrical grid is also evaluated, considering the case of a high penetration of Renewable Energy Sources (RES) in a small standalone electrical grid.

Finally, the possibility to manage the scheduling of desalination plant is considered in order to improve the energy efficiency in the power generation. This approach could be extended in the next future to enhance the grid stability in case of a significant contribution from RES.

I.4 Publications on this topic

- A. Viola, V. Franzitta, M. Trapanese, and D. Curto, "Nexus Water & Energy: A Case Study of Wave Energy Converters (WECs) to Desalination Applications in Sicily," *Int. J. Heat Technol.*, vol. 34, no. Special Issue 2, pp. S379–S386, Oct. 2016.
- V. Franzitta, D. Curto, D. Milone, and D. Rao, "Assessment of Renewable Sources for the Energy Consumption in Malta in the Mediterranean Sea," *Energies*, vol. 9, no. 12, p. 1034, Dec. 2016.
- V. Franzitta, D. Curto, D. Rao, and A. Viola, "Hydrogen Production from Sea Wave for Alternative Energy Vehicles for Public Transport in Trapani (Italy)," *Energies*, vol. 9, no. 10, p. 850, Oct. 2016.
- V. Franzitta, D. Curto, D. Milone, and A. Viola, "The desalination process driven by wave energy: A challenge for the future," *Energies*, vol. 9, no. 12, pp. 1–16, Dec. 2016.
- V. Franzitta, D. Curto, and D. Rao, "Energetic Sustainability Using Renewable Energies in the Mediterranean Sea," *Sustainability*, vol. 8, no. 11, p. 1164, Nov. 2016.
- A. Viola, D. Curto, V. Franzitta, and M. Trapanese, "Sea water desalination and energy consumption: A case study of wave energy converters (WEC) to desalination applications in Sicily," in *OCEANS 2016 MTS/IEEE Monterey*, 2016, pp. 1–5.
- V. Franzitta, D. Rao, D. Curto, and A. Viola, "Greening island: renewable energies mix to satisfy electrical needs of Pantelleria in Mediterranean Sea," in *OCEANS 2016 MTS/IEEE Monterey*, 2016, pp. 1–6.
- V. Franzitta, D. Curto, D. Rao, and D. Milone, "Near zero energy island with sea wave energy: The case study of Pantelleria in Mediterranean Sea," in *OCEANS 2016 - Shanghai*, 2016, pp. 1–5.
- M. Trapanese, F. Raimondi, D. Curto, and A. Viola, "Evaluation of the wave energy density on the Sicilian coast," in *OCEANS 2016 - Shanghai*, 2016, pp. 1–4.
- V. Franzitta, D. Curto, D. Rao, and A. Viola, "Renewable energy sources to fulfill the global energy needs of a country: The case study of Malta in Mediterranean Sea," in *OCEANS 2016 - Shanghai*, 2016, no. 1012, pp. 1–5.
- D. Curto and M. Trapanese, "Experimental tests on hydrogen production from sea waves energy," in *OCEANS – Anchorage*, 2017, 2017, pp. 1–5.
- A. Viola and D. Curto, "Numerical simulation of wave energy production through experimental tool," in *2017 IEEE International Conference on Environment and Electrical Engineering and 2017 IEEE Industrial and Commercial Power Systems Europe (EEEIC / I&CPS Europe)*, 2017, no. January, pp. 1–5.
- V. Franzitta and D. Curto, "Sustainability of the Renewable Energy Extraction Close to the Mediterranean Islands," *Energies*, vol. 10, no. 4, p. 283, Feb. 2017.

- V. Franzitta, P. Catrini, and D. Curto, "Wave Energy Assessment along Sicilian Coastline, Based on DEIM Point Absorber," *Energies*, vol. 10, no. 3, p. 376, Mar. 2017.
- V. Franzitta, D. Curto, D. Milone, and M. Trapanese, "Energy Saving in Public Transport Using Renewable Energy," *Sustainability*, vol. 9, no. 1, p. 106, Jan. 2017.
- V. Franzitta, D. Curto, and A. Viola, "Renewable Energy Assessment in Italy and Brazil: An Economic and Political Comparison," in *Proceedings of SWC2017/SHC2017*, 2017, pp. 1-8.
- D. Curto and M. Trapanese, "A Renewable Energy mix to Supply the Balearic Islands: Sea Wave, Wind and Solar," in *2018 IEEE International Conference on Environment and Electrical Engineering and 2018 IEEE Industrial and Commercial Power Systems Europe (EEEIC / I&CPS Europe)*, 2018, pp. 1-6.
- D. Curto and D. Milone, "Improvement of Energy Efficiency for Indoor Lighting in a Big Shopping Center," in *2018 IEEE International Conference on Environment and Electrical Engineering and 2018 IEEE Industrial and Commercial Power Systems Europe (EEEIC / I&CPS Europe)*, 2018, pp. 1-6.
- D. Curto, F. Montana, and D. Milone, "Energy Saving Optimizing the Ventilation Control in a big shopping center," in *2018 IEEE International Conference on Environment and Electrical Engineering and 2018 IEEE Industrial and Commercial Power Systems Europe (EEEIC / I&CPS Europe)*, 2018, pp. 1-6.
- F. M. Raimondi, D. Milone, and D. Curto, "An innovative mechanical motion converter for sea wave applications," in *2018 Thirteenth International Conference on Ecological Vehicles and Renewable Energies (EVER)*, 2018, pp. 1-6.
- F. M. Raimondi, D. Curto, V. Franzitta, and D. Milone, "Energy savings for indoor lighting in a shopping mall: A case of study," in *2018 Thirteenth International Conference on Ecological Vehicles and Renewable Energies (EVER)*, 2018, pp. 1-6.
- D. Curto, S. Neugebauer, A. Viola, M. Traverso, V. Franzitta, and M. Trapanese, "First Life Cycle Impact Considerations of Two Wave Energy Converters," in *2018 OCEANS - MTS/IEEE Kobe Techno-Oceans (OTO)*, 2018, pp. 1-5.
- Crainz et al., "Flexibility Services to Minimize the Electricity Production from Fossil Fuels. A Case Study in a Mediterranean Small Island," *Energies*, vol. 12, no. 18, p. 3492, Sep. 2019.
- D. Curto, V. Franzitta, S. Longo, F. Montana, and E. Riva Sanseverino, "Investigating energy saving potential in a big shopping center through ventilation control," *Sustain. Cities Soc.*, vol. 49, no. January, p. 101525, Aug. 2019.
- D. Curto, V. Franzitta, A. Viola, M. Cirrincione, A. Mohammadi, and A. Kumar, "A renewable energy mix to supply small islands. A comparative study applied to Balearic Islands and Fiji," *J. Clean. Prod.*, p. 118356, Sep. 2019.

- M. Trapanese, D. Curto, V. Franzitta, Z. Liu, L. McNabb, and X. Wang, "A Planar Generator for a Wave Energy Converter," *IEEE Trans. Magn.*, vol. 55, no. 12, pp. 1-7, Dec. 2019.

II DESALINATION

To overcome the ever increasing freshwater demand related to the growth of population and welfare, in the end 1950s first desalination plants were installed [35], [36].

First technologies were based on the thermal supply, as the low cost of fossil fuels (3 \$ for one barrel of oil).

As the progressive growth of the energy cost, two lines of research have been pursued, in order to minimize the total cost for the water treatment [35]:

- Increase the energy efficiency of commercial technologies;
- Investigation and proposal of new solutions.

For example, in the first case the number of stages in the multistage flash distillation has been progressively increased from 8-12 to 20 [37], [38]. As regards the proposal of innovative solutions, the introduction of semipermeable membranes represents a radical change in the desalination sector. In fact, nowadays the reversal osmosis is the most used technology for this purpose [39].

The term “desalination” is referred to the technological process to extract freshwater from brackish or saltwater. Sea water is often the raw water source to supply this process. Historically, the idea behind the desalination process was introduced by the Royal Navy (United Kingdom's naval warfare force) in the end of 18th century with the purpose to increase the navigation autonomy without storing more water on the ships [40].

As in that period ships were equipped with steam engines, the first desalination technology was the single flash distillation, that was improved in the following years into the more efficient Multi-Effect Flash distillation (MEF).

The first type of desalination unit was realized by the G. & J. Weir in 1885 at Glasgow (Scotland) [41]. This company, converted into Weir Westgarth, had practically the monopoly as desalination unit builder until World War II.

In the following years, desalination plants for civil purpose had been installed around the world. During 1907, a Dutch company installed the first desalination plant in the Arabian Gulf countries in the city of Jeddah [42]. By the order of King Abdulaziz Al Saud, the same plant was replaced in 1928, installing two units produced by the Weir Westgarth with an installed capacity of 135 m³/day [42].

In 1953 other desalination plants were installed in Qatar and Kuwait. In detail, 5 units were installed in Qatar, with a total capacity equal to 682 m³/day and 10 units in Kuwait, with a total capacity of 4545.5 m³/day. In 1955 other 10 units were installed in Shuwaikh (Kuwait), having the same size [42]. From this moment on, desalination plants had been expanded around the world, with the born of many companies as Krupp in Germany, Westinghouse in USA, SIR (Società Italiana Resine) in Italy [40].

The other mainstream technique is the Reversal Osmosis (RO), based on semipermeable membranes. The physical osmosis phenomenon was observed the first time in 1748 by Jean-Antoine Nollet, without any application for about two centuries [43].

In USA first studies were started by the researchers Sidney Loeb and Srinivasa Sourirajan in 1956 at the University of California and the University of Florida, respectively. The first membrane was realized in 1959 while the first pilot plant was installed in 1965, with a capacity of 19 m³/day [40].

An improvement of this technique was introduced by the asymmetric membrane that shows a different porosity moving from a face to the other one, allowing a greater water flux through the membrane [43].

The slow diffusion of reversal osmosis was initially due to the high electricity consumption to produce freshwater in comparison with other techniques and the limited life of semipermeable membranes [40]. First application was related to brackish water, due to its lower osmotic pressure in comparison with sea water.

The first desalination plant, based on reversal osmosis, for municipality was realized in 1977 in USA, with an installed capacity of 11350 m³/day. In the same area, in 1985 another big desalination plant was realized, having an installed capacity equal to 56800 m³/day [43].

The great technological progresses occurred in the reversal osmosis process, thanks to the increase of the membrane lifetime and the adding of energy recover devices to reduce the energy requirement for the process. So, nowadays the reversal osmosis is applied to sea water and is economic competitive with the other technologies. This improvement was realized during the 1990s, thanks to the introduction of an energy recovery system, based on the introduction of hydro turbines or similar systems before the returning of brackish water to the sea [40].

Currently, the Reversal Osmosis (RO) is the most spread technology, followed by the Multi-Stages Flash (MSF) desalination and Multi-Effect Distillation (MED). According to statistics, in the last year the total installed capacity was based essentially on three technologies: RO (68.7%), MSF (17.6%), MED (6.9%). The other technologies had a marginal role (6.8%) [44]. Desalination plants are installed around the world but are mainly concentrated in Middle East and North Africa (47.5% of the world capacity). The main raw water source is represented by sea water (70.5% of the world capacity) [44].

Several technologies are currently under investigation, with the goal to reduce the energy demand for the freshwater production.

After this brief history review, in the following section, the state of art of desalinating technologies is reported, describing the working principles. Finally, the chapter reports some technical statistics, among which the specific energy demand, the world installed capacity and the development status.

II.1 State of art

Today, desalination can be realized using several technologies. In general, a desalination plant includes several processes to obtain freshwater, among which the desalination unit is the most energy expensive component. A desalination plant normally includes [38]:

- Intake, composed by pumps and pipes to take water from the source (sea or brackish water);
- Pre-treatment, consisting in a filtration of raw water to remove solid components and adding of chemical substances to reduce the salts precipitation and the corrosion inside the desalination unit;
- Desalination, where freshwater is extracted from saltwater;
- Post-treatment, to correct pH by adding selected salts to meet the requirements of the final uses.

As introduced before, the desalination process represents the most energy consuming water treatment, for this reason it is analyzed in this section with some details.

Before analyzing the specific solutions, a classification is required. Alkaiasi suggested three main categories [45]: Evaporation & Condensation, Filtration and Crystallization.

The following Figure II.1 shows the classification proposed by Alkaiasi, integrating also the new technologies under investigation.

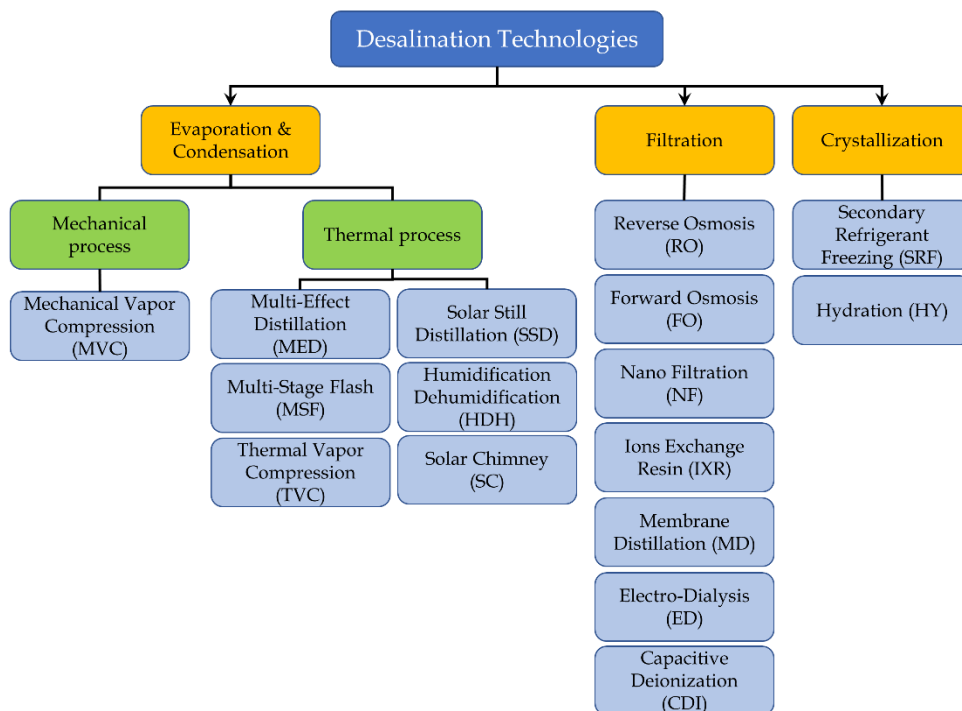


Figure II.1 Classification of desalination technologies by working principle

Evaporation & Condensation technologies are the first desalination techniques to be introduced and used for civil freshwater production. The idea is that of providing energy to seawater in order to produce a vapor and then condensate it. This energy can be given by using a thermal process, i.e. heat supply, or through a mechanical process. In the first case, the most common technologies are Multi-Effect Distillation (MED), Multi-Stage Flash (MSF) and Thermal Vapor Compression (TVC). Currently other solutions are under investigation, among these we can find few new solutions, supplied by solar radiation: Solar Still Distillation (SSD), Solar Chimney (SC) and Humidification-Dehumidification (HDH) desalination.

Regarding to the mechanical processes to produce freshwater through the evaporation and condensation of sea water, the main technique is the Mechanical Vapor Compression (MVC) [46].

In case of Filtration technologies, all solutions are essentially based on semipermeable membrane, i.e. a layer that show a different attitude to be crossed according to sizes or nature of molecules. The only exception is Ions Exchange Resins (IXR), where natural or artificial materials are used to capture the dissolved ions, in a chemical way [47].

In this context the Reversal Osmosis (RO) is the most used technology for desalination. The Electro-Dialysis (ED) and Ion Exchange Resin (IXR) are used to produce water with a very limited concentration of salts. Other techniques, as Membrane Distillation (MD), Forward Osmosis (FO), Nano Filtration (NF) and Capacitive Deionization (CDI) are in developing step [48].

Finally, the Crystallization category comprises techniques that extract freshwater producing ice as intermediate product. As example, the main techniques are Secondary Refrigerant Freezing (SRF), Hydration (HY) and Vacuum Freezing (VF) desalination. All these approaches are under investigation [49].

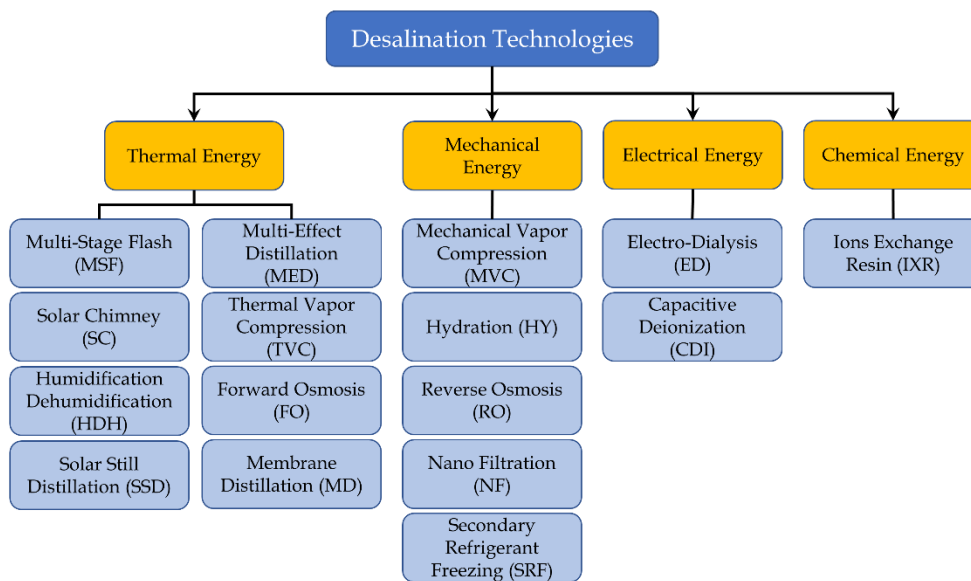


Figure II.2 Classification of desalination technologies by main energy input

Another useful classification can be realized, by considering the kind of energy mainly required to run the process, as shown in Figure II.2. This aspect is important in order to select renewable energy sources to supply the desalination process. In detail, four kinds of energy are considered:

- Thermal energy
- Mechanical energy
- Electrical energy
- Chemical energy

The first category could be supplied by solar thermal or geothermal energy sources. It comprises the following technologies: MSF, MED, TVC, FO, MD, SC, HDH and SSD. In particular, the last three approaches are designed in order to exploit directly the solar radiation.

The group of technologies requiring a Mechanical Energy input comprises MVC, RO, NF, SRF, HY. All these techniques are characterized by the presence of pumps and compressors, that requires the major part of the total energy demand for the process.

The last two categories have limited examples. The Electro-Dialysis and Capacitive Deionization desalination require the generation of an electric field, between two electrodes, separated by an anion membrane and a cation membrane (selective membranes that allow to be crossed by positive and negative ions, respectively). In this case, electricity is the only way to supply the process.

As regards the Ions Exchange Resin, the working principle is the chemical replacement of positive and negative ions.

It is important to underline that mechanical energy and electricity can be easily converted in both directions, with high efficiency. For this reason, the technologies that require a mechanical energy input, through pumps or compressors, can be easily supplied by electricity by using common electrical motors. Similarly, mechanical energy can be converted by alternators into electricity in order to supply the desalination processes that require electrical energy as input.

Thermal energy is a different case, because it can be easily obtained from electricity, through Joule Effect or Heat Pumps. The conversion from thermal energy into mechanical or electrical energy is obtained by using thermal machines or plants, affected by a low energy efficiency in comparison with the previous cases, for thermodynamic and technical reasons.

It is important to underline that thermal sources can be successfully adopted to produce electricity, in specific conditions. For example, in case of high temperature geothermal source, a power plant can be realized.

Thus, in order to supply desalination process with renewable energy sources, it is convenient to distinguish the energy sources that can be used to produce electricity (or mechanical energy) from those producing thermal energy.

With this goal, the renewable energy sources can be sorted in the following categories, according to the usual energy output that can be produced:

- **Electricity producers**, such as wind, hydro, tidal, sea wave
- **Thermal and electrical energy producers**, such as solar, geotherm, biomass. The energy output is usually selected according to the features of the local energy resource.

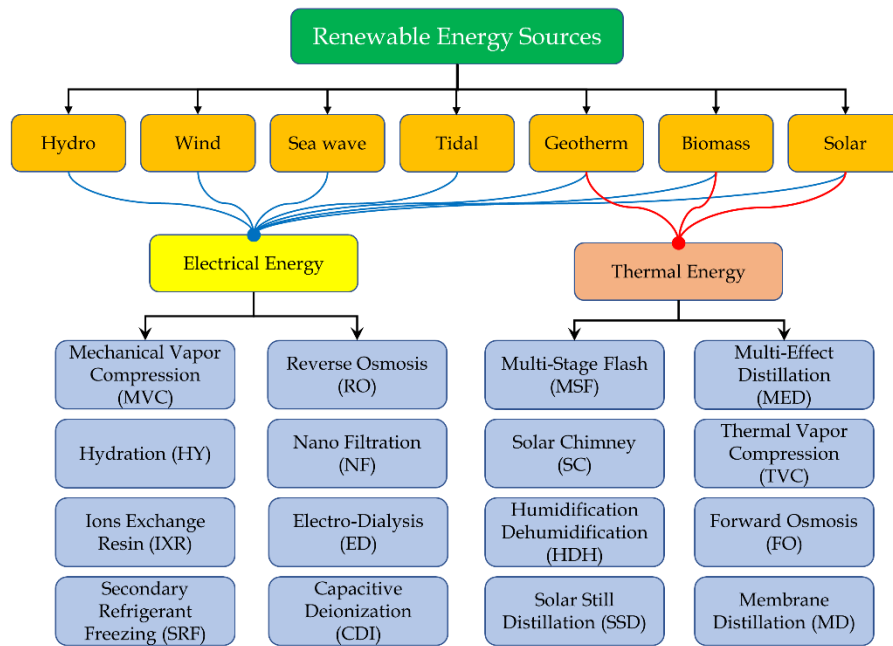


Figure II.3 Possible coupling between desalination technologies and RES

In the following paragraphs, each technology is analyzed in detail, describing the entire process and reporting the state of art.

II.1.a Multi-Effects Distillation (MED)

The first MED plant was realized in Kuwait in 1950s, using a triple effect submerged tube evaporator. Despite it was the first technology for desalination to be introduced, MED did not spread because it is particularly affected by the scaling problem on the pipes in comparison with other thermally supplied desalination technologies [50]. However, from 1980s several researches have been realized on MED, investigating lower temperatures to reduce the scaling and the corrosion of pipes [51]. MED is also currently used in food industries to extract juice from sugarcane, and to produce salts from seawater [52].

MED units can be arranged in several configurations, considering the shape of heat exchangers or the brine flow direction regarding the vapor direction. The effects can be assembled in one line or in two parallel lines, working with different pressure in order to optimize the heat recovery [50]. According to the Top Brine Temperature (TBT), MED can be classified as Low Temperature (below 90°C) or High Temperature (over 90°C).

To reduce the energy costs, steam is usually spilled from a steam turbine inside a power plant or recovered from a waste energy source in industrial processes [51]. As the primary steam is not in direct contact with saline water, the condensate inside the evaporator is normally recycled to the boiler for reuse [51].

The maximal temperature of brine is limited to 120°C by the calcium sulphate scaling while the minimal is related to the available temperature in the sea wave. Figure II.4 shows the diagram of a MED plant with horizontal tubes [51], [53], [54].

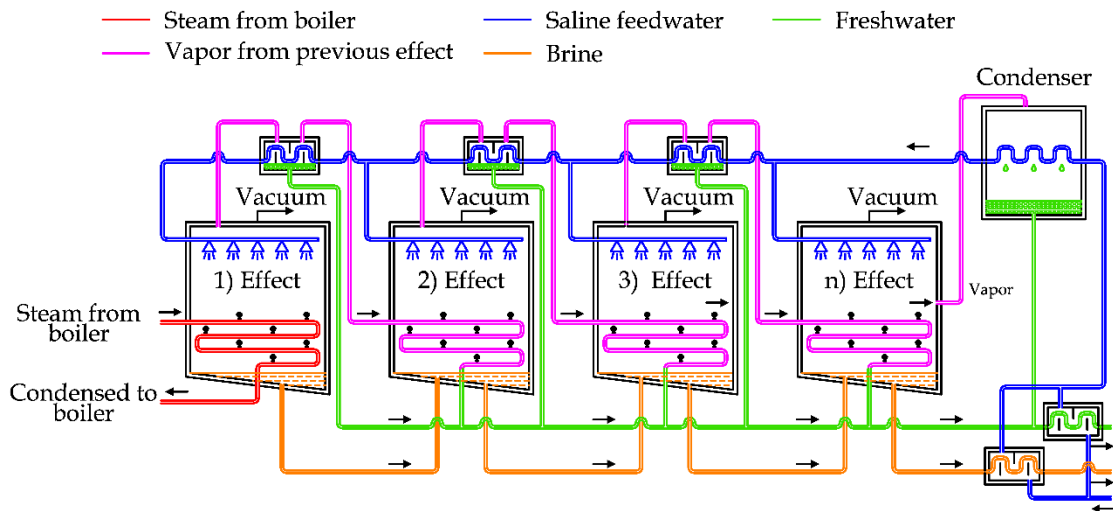


Figure II.4 Scheme of a Multi-Effect Distillation unit

In general, this plant is composed by a steam supply, several effects, heat recovery exchangers, a condenser and a venting system [50].

In detail, the saline water can be split in two lines, in order to recover the thermal energy of freshwater and brine produced by the system, as depicted in Figure II.4. After this step, saline water is used as cooling fluid for the condenser, then preheated by using heat recovery exchangers, that are supplied by the steam produced in each effect chamber [37].

The preheated water is sprayed in the first chamber on the evaporator surface, producing a thin film to promote the rapid boiling and the evaporation thanks to the low pressure inside the chamber and the external thermal energy supply [51].

The vapor produced inside this chamber is transferred by pipes in the following chamber. As the pressure inside the second chamber is lower than the first one, the boiling temperature is also lower. In this way, it is possible to condensate the vapor produced in the first chamber inside the pipes and at the same time produce other vapor inside the second chamber [55].

This process is repeated in the subsequent chambers in the same way, using the steam generated in the previous flash chamber to produce other vapor at lower pressure. In the last chamber, the vapor is finally condensed inside the condenser, cooled by the saline feedwater.

The brine produced in the previous chambers is usually transferred inside the subsequent chambers, in order to force the extraction of other feedwater, thanks to the lower pressure inside them [51].

The pressure inside chambers is kept below the atmospheric condition, using a dedicate vacuum system. The energy efficiency of MED units depends on the number of effects, normally ranging between 4 and 21 [52].

MED units are used to produce freshwater with a flowrate ranging from 2000 to 20000 m³/day. To improve the energy efficiency, MED can be coupled with a Thermal or Mechanical Vapor Compression unit [55]. The biggest desalination plants are concentrated in China and Middle East [56].

II.1.b Multi-Stages Flash (MSF)

The first MSF plant was realized in 1950s in Scotland and after few years it became the most used desalination technology [52]. MSF is commonly used also on ships to produce freshwater from seawater and along the coastline in several parts of the world, like USA, Middle East and Korea [57].

MSF process shows some similitudes with MED, previously described. In fact, an initial heat supply is also required, using steam spilled from a power plant, and the decreasing pressure is used to force the vapor production [37]. Electricity is required to run the several pumps distributed along the desalination plant [58].

Figure II.5 shows the diagram of a once-through MSF unit [51], [53], [54]. The plant can be conceptually divided in two sections: the first is the brine heater section, where the feedwater receives heat from an external supply, the latter one is the heat recovery section, where the thermal energy is recovered to preheat the feedwater [38].

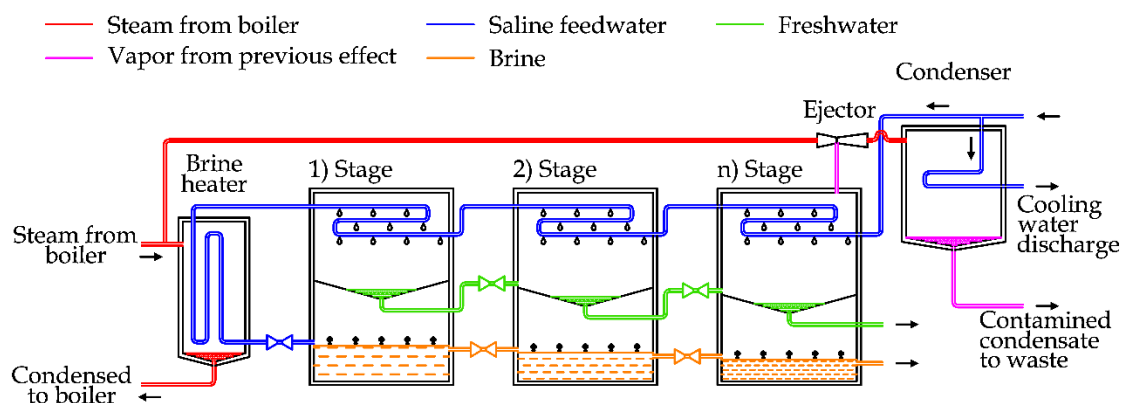


Figure II.5 Scheme of a Multi-Flash Stages desalination unit

Focusing the attention on the picture above reported, the saline feedwater is firstly used as cooling water for the condenser and then as raw source to produce freshwater.

The saline water increases progressively its temperature, flowing inside the pipes, forming the heat exchangers inside the flash stages. To start the process, the saline water is heated inside the brine heater, by using steam usually spilled from a power plant. This

steam condenses inside the brine heater (outside the tube bundle), so it can be reused in the steam power plant [52].

As the saline feedwater flows inside pipes in the brine heater and in the flash stages, the maintenance operations to remove the scaling are simpler than in MED [51]. For this reason, MSF is the most spread thermally driven desalination technology, representing the 17.6% of the total installed desalination capacity in the world [44].

After the initial heating, saline water is laminated inside the first flash stage. The vapor produced inside the chamber condenses thanks to the heat removal by the saline feedwater inside the heat exchanger. The brine collected in the lower part of the chamber is laminated in the subsequent chambers, where the internal pressure is reduced linearly from the first stage to the terminal one [57]. The vacuum is obtained by the utilization of steam ejectors, supplied by high pressure steam (as shown in Figure II.5), or using vacuum pumps [38].

Thanks to the pressure drop, the introduction of heated saline water produces the “flashing effect”, for which the saline water boils rapidly inside the chamber, producing vapor [52].

To maximize the energy efficiency of the system, MSF unit are typically composed by several flash stages, with a total number ranging from 15 to 25 stages (greater values are related to bigger MSF plants). This technology is able to satisfy a freshwater demand of about 4000 to 57000 m³/d, requiring heat at 90°-110°C [51].

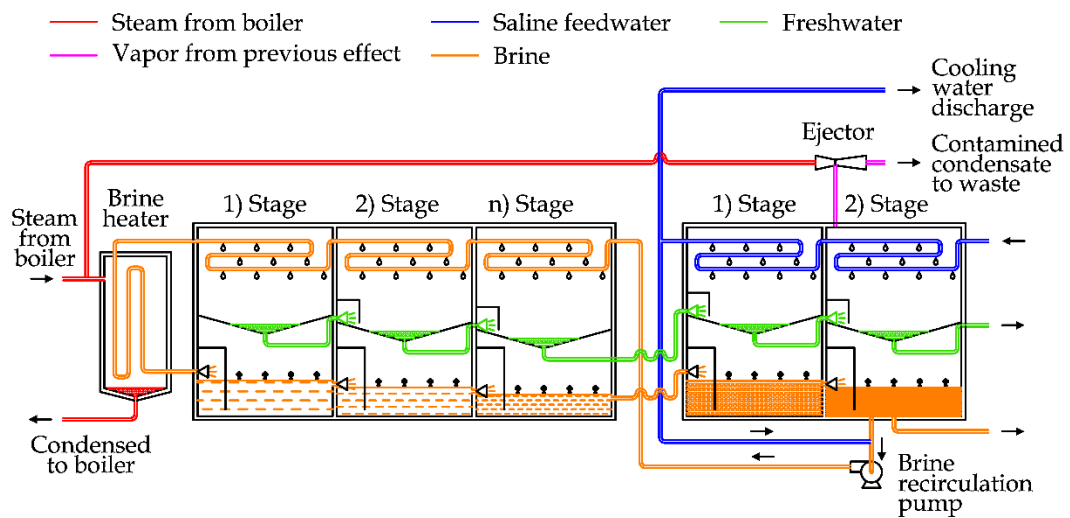


Figure II.6 Scheme of a more efficient Multi-Flash Stages desalination unit

In more recent plants, few changes are introduced. Instead of the condenser, a heat rejection section is inserted, that is composed by two or three flash stages (see Figure II.6). In detail, sea water is used as cooling fluid in this section. After this step, a part of seawater is rejected, the other part is mixed with a part of brine extracted by the last flash stage. This salt solution is used in the main section of the desalination unit, in the same way shown in the previous diagram. This technique is applied to increase the energy efficiency in big desalination plants, composed by 19-40 flash stages and 2-3 heat rejection stages [38], [58].

In the last two decades, the reliability of the system has been improved thanks to the a scaling control (adding substances to limit the phenomenon), the introduction of automation and control systems and the choice of better materials for the realization of the desalination units [51].

Similarly to MED, the MSF desalination is spread where the thermal energy cost is low, like in Saudi Arabia, United Arab Emirates and Kuwait [52].

II.1.c Vapor Compression (VC)

Vapor Compression is a common technique used in desalination sector, based on the liquid-vapor phase transition.

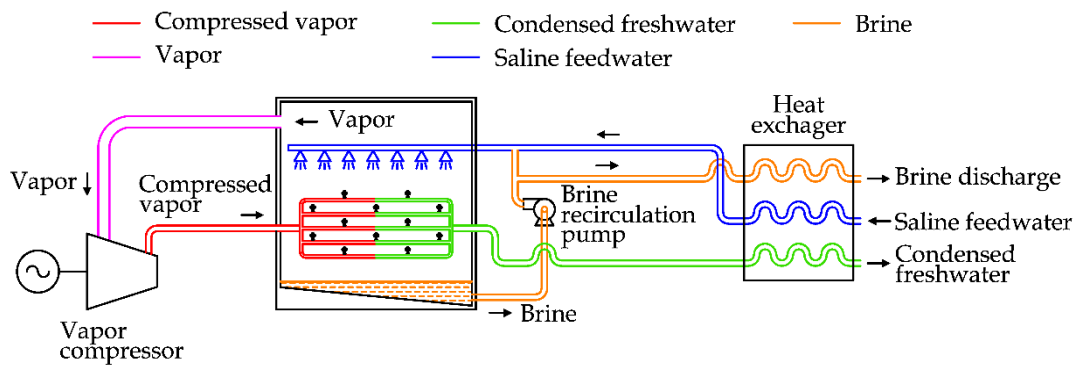


Figure II.7 Scheme of a simple Mechanical Vapor Compression desalination unit

To clarify the process, Figure II.7 is considered, reporting the case of a Mechanical Vapor Compression (MVC) unit.

A vapor compressor is used to extract vapor produced inside the chamber. Due to the compression, the vapor increases its temperature and pressure. As the rising of the temperature and by using a heat exchanger, the pressurized vapor can transfer heat to the saline water, inside the chamber and produce other vapor.

To minimize the energy consumption of the process, a heat recovery exchanger is used to transfer heat from the brine discharge and the condensed feedwater to the saline feedwater [58].

After the preheating, the saline water is mixed with a brine recirculation flow. This solution is sprayed externally on the main heat exchanger inside the desalination unit.

MCV requires essentially electricity to run the process; therefore, small stand-alone desalination unit can be realized to satisfy a freshwater demand ranging from 100 to 3000 m³/day.

The same approach is adopted in the Thermal Vapor Compression (TVC) unit, reported in Figure II.8.

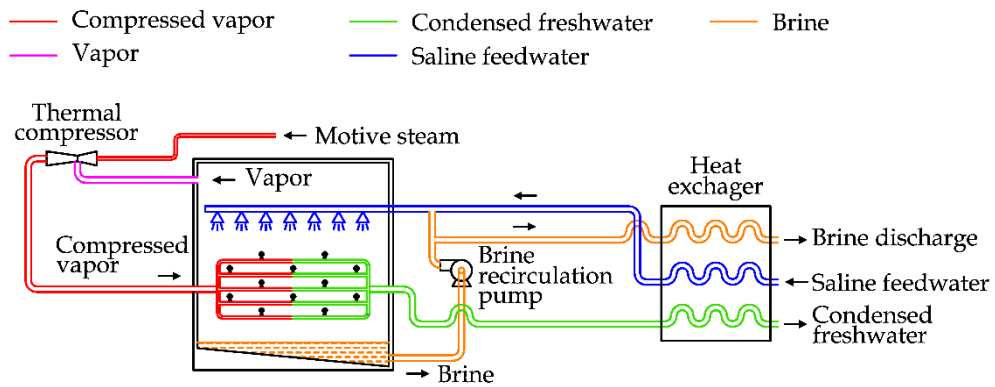


Figure II.8 Scheme of a simple Thermal Vapor Compression desalination unit

The only significant difference is related to the way used to increase the vapor pressure. In TVC a thermal compressor is adopted, that is supplied by high pressure steam, normally spilled from a power plant.

TVC requires thermal and electrical energy. The first one is used for the thermal compression, the latter one for the circulation pumps. TVC is sometimes assembled with MED unit, realizing a hybrid system defined as MED-TVC desalination plant, as shown in Figure II.9.

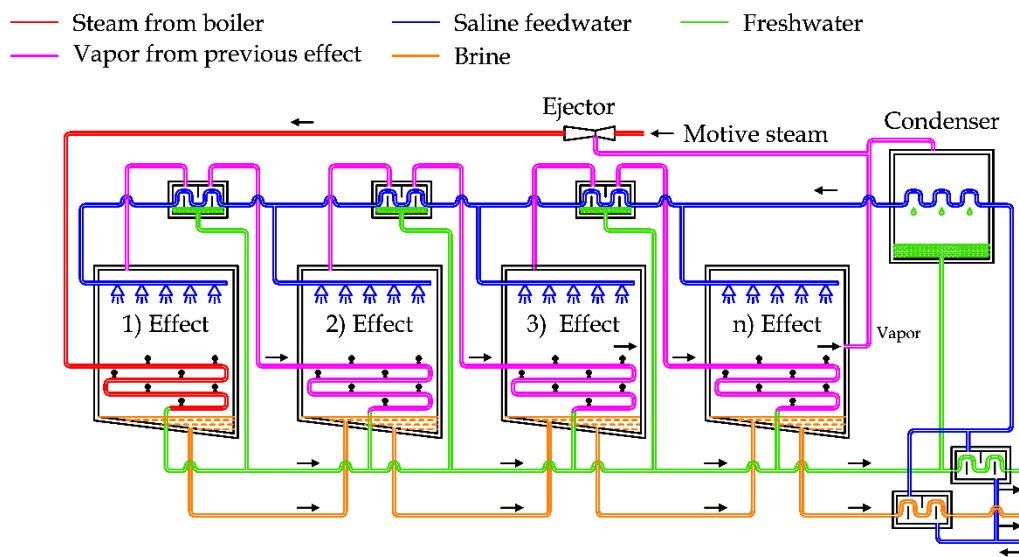


Figure II.9 Scheme of a TVC and MED unit

The comparison of the picture, reported above, and the MED diagram shows few differences. The steam supply is used to produce the vacuum inside the condenser and the last effect of MED unit. The contaminated steam is condensed inside the first effect and added to the freshwater output [59]. This configuration is used to satisfy significant freshwater demand, between 10000 and 30000 m³/day [38].

II.1.d Reverse Osmosis (RO)

RO is a desalination technology based on semipermeable membranes, that are specific layers allowing the passage only to selected molecules.

In nature, if two solutions with different concentrations of solutes are separated by a semipermeable membrane, the solvent flows spontaneously from the more diluted solution to the more concentrated one, in order to balance the energy potential of both solutions, as shown in Figure II.10 (see case a). This flow can be progressively reduced if an increasing external pressure gradient Δp is applied to the semipermeable membrane (see case b) [60].

The exact value able to stop the solvent flow is defined as Osmotic Pressure Δp_{osm} (see case c). If the external pressure gradient is greater than the osmotic pressure, the solvent flows is inverted, so the solvent can be extracted from the concentrated solution (see case d) [60].

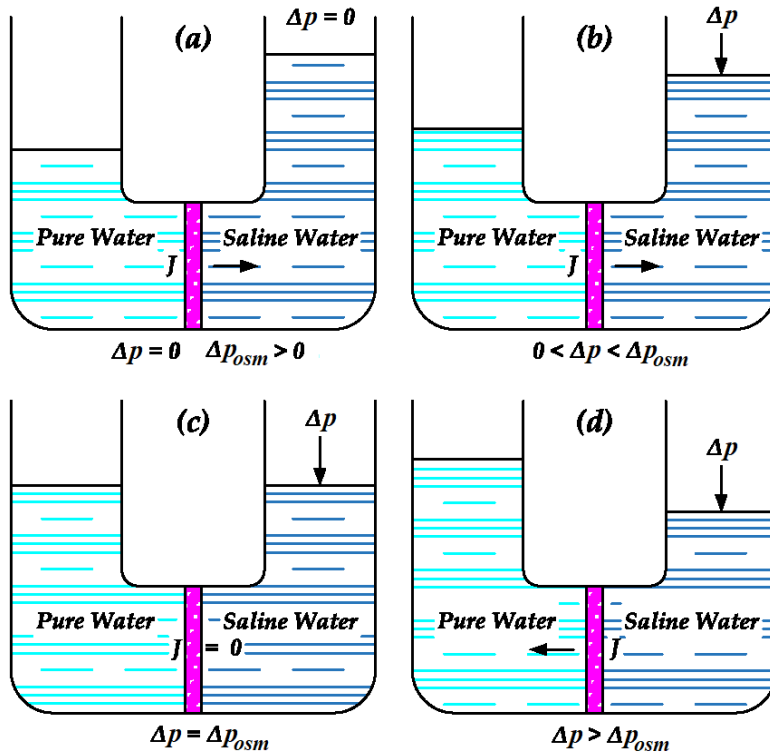


Figure II.10 Osmosis phenomenon

For each solution the absolute osmotic pressure p_{osm} can be defined according to the van't Hoff's equation [60], [61] ²:

$$p_{osm} = \iota[c]R\tau \quad II.1$$

² In chemistry, the amount $\iota[c]$ is called "normality", indicating the number of equivalents in a unitary volume. The equivalent represents the amount of a specific substance able to react with (or supply) one mole of hydrogen (H^+) in an acid-base reaction or react with (or supply) a mole of electrons in a redox reaction.

- ι is the dimensionless van't Hoff index (called also number of osmotically active particles), given by the relation $\iota = 1 + \epsilon(\nu - 1)$, where ϵ is the degree of dissociation representing the ratio of how many original solute molecules are dissociated, and ν the number of ions formed by the molecule dissociation (stoichiometric coefficient of dissociation reaction). As an example, in the case of sodium chloride (NaCl), $\epsilon \approx 1$, $\nu = 2$, consequently $\iota = 2$;
- $[c]$ is the molar concentration of solute;
- R is the ideal gas constant equal to $8.31441 \text{ J K}^{-1} \text{ mol}^{-1}$;
- τ is the absolute temperature of the solution.

As the salt concentration is negligible in the freshwater and consequently its osmotic pressure, the minimal pressure required to stop the solvent flow is equal to the osmotic pressure of saline water. For seawater, the salt concentration ranges between $0,51 \div 0,68 \text{ mol L}^{-1}$ [60]. Thus, considering an environmental temperature equal to 25°C , the osmotic pressure according to the van't Hoff's equation ranges between $25 \div 33 \text{ bar}$. Greater values can be measured, as in the extreme case of Dead Sea, where the osmotic pressure is equal to 290 bar [60].

Figure II.11 visualizes the osmosis phenomenon: until the external pressure gradient is lower than the osmotic pressure, the solvent flows from the more diluted solution to the more concentrated one. In this working region, it is also possible to extract energy from the mixing of two solutions having different concentrations. This approach can be used in the estuary of the rivers. The exploitation of the saline gradient energy source is currently under development [62].

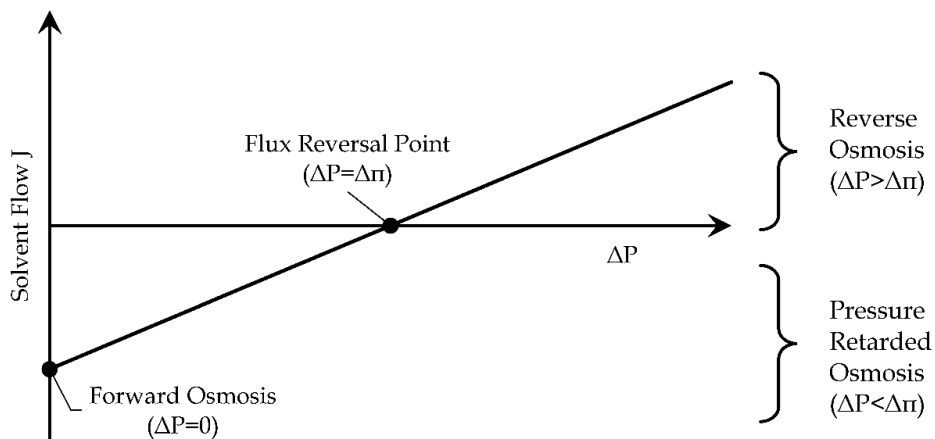


Figure II.11 Solvent flow as function of the external pressure gradient

The case without an external pressure gradient is identified as “Forward Osmosis”, which condition is used in the other osmosis desalination technique, analyzed in the following subsection.

Applying an external pressure gradient greater than the osmotic pressure, freshwater is extracted from saltwater. For desalination purpose, an external pressure

between 15 and 25 bar is normally applied for brackish, between 54 and 80 for seawater [51], [63].

Thus, according to the values reported above, the RO requires essentially electrical (or mechanical) energy to run the pumps to increase significantly the seawater pressure, before the semipermeable membrane. A simple diagram of a RO desalination unit is depicted in Figure II.12 [32].

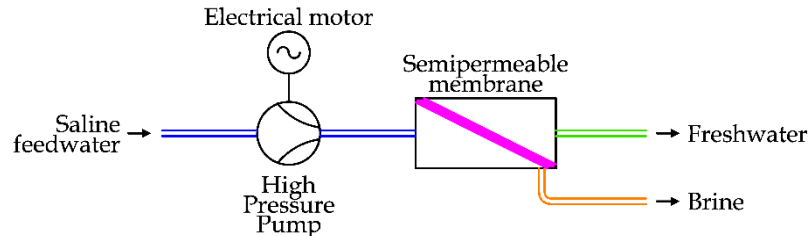


Figure II.12 Diagram of a simple Reverse Osmosis Desalination unit

Seawater, after a pre-treatment to remove solid particles, is pressurized by a High Pressure Pump (HPP) in order to supply the RO desalination unit [64].

In desalination application, the Recovery Ratio (RR) is defined as the ratio between the freshwater flow and the saline feedwater flow [44].

$$RR = \frac{Q_f}{Q_s} \quad II.2$$

Considering the working condition, RR assumes values between 35% and 50%, so practically only half (or lower than) seawater flow becomes freshwater and the remaining part is expelled as brine. To increase the freshwater extraction, the pressure before the semipermeable membrane should be increased, but there are several technical constrains, related essentially to the mechanical resistance of the membrane. As semipermeable membranes are not perfect, a limited amount of salts can be found in the freshwater output [51].

The brine flow has a high energy potential, as its pressure is practically the same of the saline input water. In fact, the pressure drop inside the brine circuit is about 2 - 3 bar [32].

To reduce the total energy consumption for desalination, since the 1970s several researches have been realized. In addition to the improvement of membrane properties, the main goal was the energy recovery from the brine flow, by the introduction of an Energy Recovering Device (ERD). The solutions can be classified as [65]:

- Centrifugal device
- Isobaric device

In the first case, two technologies have been proposed. The first, introduced in 1980s, is the installation of a hydro turbine (Pelton) in order to recover the energy of brine flow and transfer it to the main HPP. To complete the energy demand of the pump,

an electrical motor is used. The pressure increase is realized by the main HPP to the entire saline feedwater flow. This solution is depicted in Figure II.13 [32].

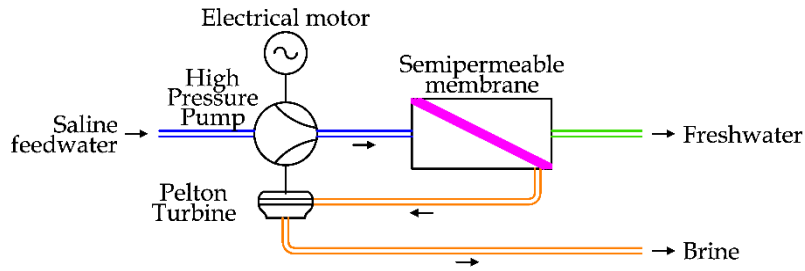


Figure II.13 Scheme of a RO unit with a Pelton Turbine

Pelton turbines are normally used in hydropower to exploit high head, between 300 m and 1000 m. Of course, only a part of the available energy of brine flow (about 70%) is transferred to the saline feedwater, as the double energy conversion (from the fluid to the mechanical shaft and then to the fluid) [66].

In the end of 1980s, another centrifugal ERD solution was introduced, represented by the turbocharger ERD. The working principle of this system is shown in Figure II.14.

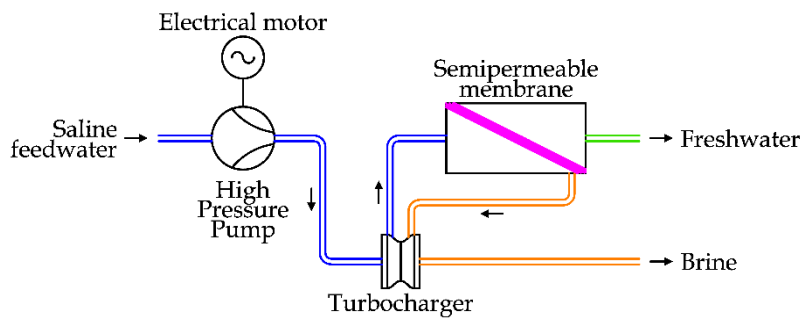


Figure II.14 Scheme of a RO unit with a Turbocharger

In detail, the saline water is pressurized in two steps: the first one is entrusted to an HPP, driven by an electrical motor, the latter one is realized by a turbocharger device, that is composed by a hydro turbine and a pump, directly coupled. This solution shows a greater energy efficiency, in comparison with the previous one, as the rotary speed of turbocharger can be modulated independently by the HPP [67].

To improve the energy efficiency also in part-load, limiting the adoption of passive regulating systems, a Dual Turbine Systems has been proposed.

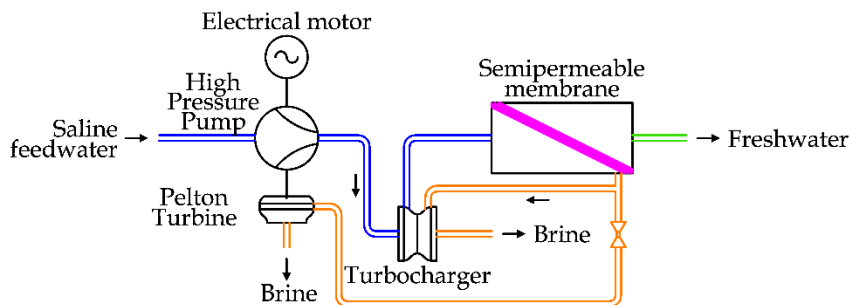


Figure II.15 Scheme of a RO unit with a Dual Turbine System

Considering the turbocharger system, shown in Figure II.14, a part of brine flow is spilled to run a Pelton turbine in order to reduce the power load of the electrical motor in the HPP. A scheme of this solution is reported in Figure II.15 [32].

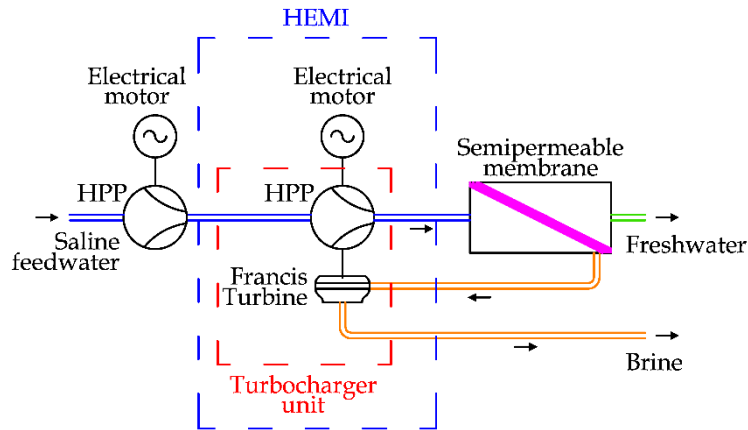


Figure II.16 Scheme of a RO unit with a HEMI System

The last centrifugal solution is represented by the HEMI (Hydraulic Energy Management Integration) proposed by FEDCO (Fluid Equipment Development Company) [68]. In detail, the HEMI solution consists in the adoption of an electrical motor in the turbocharger system, modulating the final pressure of the saline feedwater before the semipermeable membrane. In Figure II.16, the HEMI solution is depicted.

The Isobaric Devices are recent solutions to transfer energy from the brine flow to the saline feedwater flow, without intermediate energy conversions. The idea is depicted in Figure II.17.

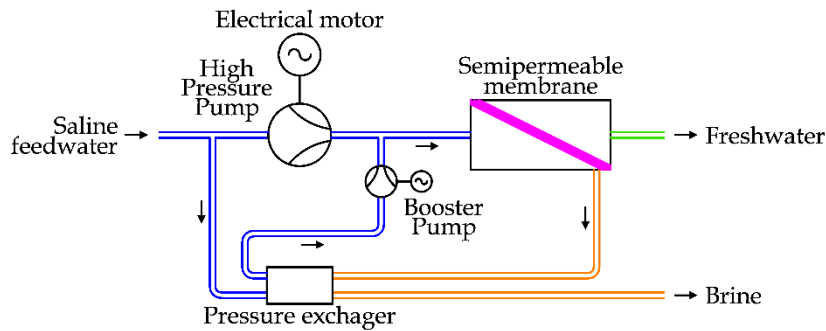


Figure II.17 Scheme of a RO unit with a Pressure Exchanger

The saline feedwater is divided in two flows: the first one is pressurized by the main HPP, driven by an electrical motor, the latter one is pressurized by the ERD.

The HPP treats a part of the total saline feedwater flow, so this component is smaller in comparison with the previous cases, considering the same freshwater flow. At the same time, this kind of ERD shows higher energy efficiency, reducing the total energy expenditure in the desalination process.

A commercial solution is the Rotary Pressure Exchanger (RPX), depicted in Figure II.18 [69].

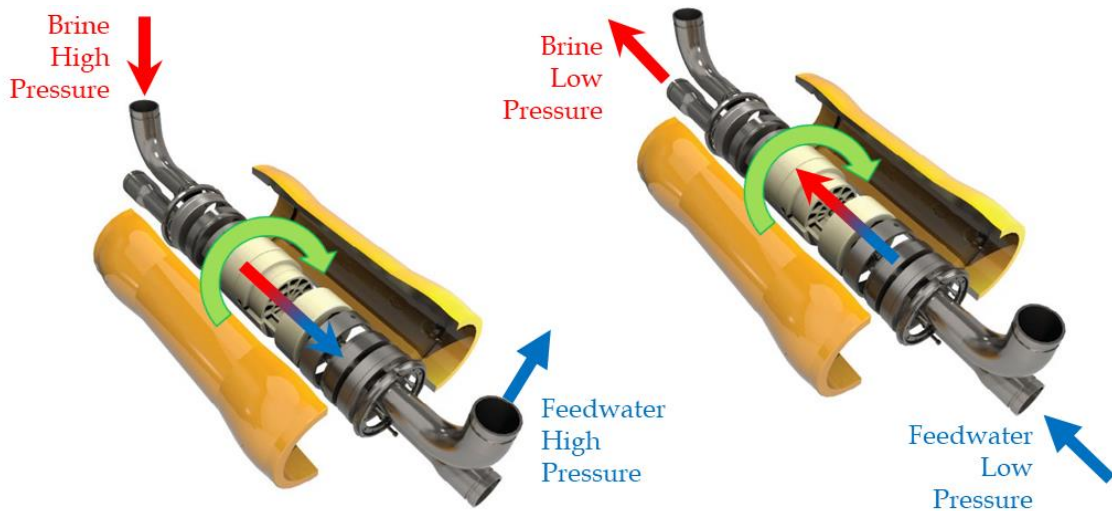


Figure II.18 Working principle of a Rotary Pressure Exchanger [69]

Inside the device, a ceramic matrix is taken in rotation by the brine flow, that enters with a tangential speed component. The channels inside the rotative matrix are alternatively connected to the Brine High-Pressure and the Freshwater High-Pressure pipes or to the Feedwater Low-Pressure and the Brine Low-Pressure pipes. In the first case, the channel, previously filled by feedwater, is now refilled by brine, pushing the feedwater inside the FHP pipe near at the same high pressure of brine water. In fact, a very limited pressure drop is measured, as the rotational motion of the channel matrix. Similarly, in the second case, the saline water is pushed by the feedwater, refilling the channel with feedwater at low pressure [32]. The process is practically continuous, because the high rotary speed of the matrix and the number of internal channels.

The same idea is applied in another way, by the Dual Work Exchanger Energy Recovery (DWEER™), proposed by Calder AG (now Flowserve Corporation) [32], [70]. The DWEER system is presented in Figure II.19. In detail, the device is composed by two cylinders, with two commanded valves (LinX® valve) to control the brine flow, and four automatic valves for the saline feedwater flow [71].

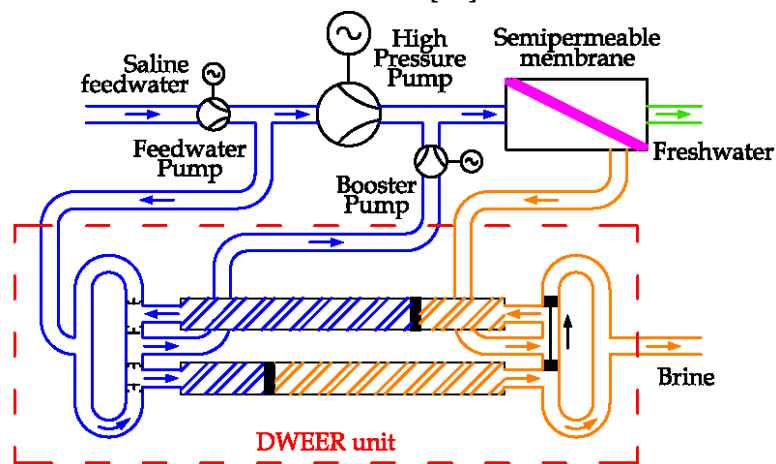


Figure II.19 Working principle of a Piston-type Work Exchanger

According to the position of the LinX valve, the brine flow from the desalination unit can be introduced in one piston or in the other one. As the high pressure of the input water, the automatic valve (on the left side of the picture) is opened, transferring the saline feedwater to the booster pump. During this step, the piston is filled with brine water. Changing the position of the LinX valve, now the brine side of the cylinder is connected to the brine discharge pipe. As the water from the feedwater pump has a greater pressure than the brine discharge, the automatic valve is open, refilling the piston with saline water. The system is composed by two cylinders, in this way alternatively one is refilled by the saline water (low pressure) and the other one with the brine water (high pressure) [32].

II.1.e Forward Osmosis (FO)

As introduced in the previous subsection, the Forward Osmosis is referred to the natural process, for which solvent flows from a more diluted solution to a concentrated one, if they are put in contact and separated by a semipermeable membrane.

It is interesting to observe that two solutions with different solutes have the same osmotic pressure if they have the same equivalent concentration and temperature, as introduced by the van't Hoff equation (see the Reverse Osmosis subsection).

Therefore, it is possible to extract freshwater by using a solution of glucose more concentrated than the saline water. This approach is applied in the "hydration bags", that is an emergency kit equipped with a semipermeable membrane and containing inside sugar. The bag is used to produce an ingestible draw solution in case of emergency, if a water source is available (rivers, seas, puddles, ponds), avoiding also the contamination from pathogens or toxins [72].

FO can be used also in a continuative process. In 2005, a research team from the Yale University proposed the utilization of ammonia carbon dioxide as thermolytic draw solute [73]. The freshwater extraction from seawater produces the dilution of the ammonia carbon dioxide. These components can be easily recovered, using a low temperature distillation. In this way, the main energy input is represented by thermal energy. Renewable energy sources could be exploited, such as solar and geothermal energy sources.

However, this technical solution is not applicable for drinking purpose, because of the presence of traces of ammonia in the freshwater [74]. In fact, according to the World Health Organization the maximal value of ammonia in freshwater for drinking purpose should be lower than 1.5 mg/L, but this condition cannot be achieved by this technology [73].

Several researchers are investigating alternative draw solutions and more performing membranes, in order to use this technique in big desalination plants [55]. In order to minimize the energy expenditure to separate the draw solution, different techniques are under investigation, as temperature or pH variation, the adoption of electro-magnetic field or light [75].

A possible solution has been proposed by Trevi Systems. The layout of the plant is reported in Figure II.20 [76].

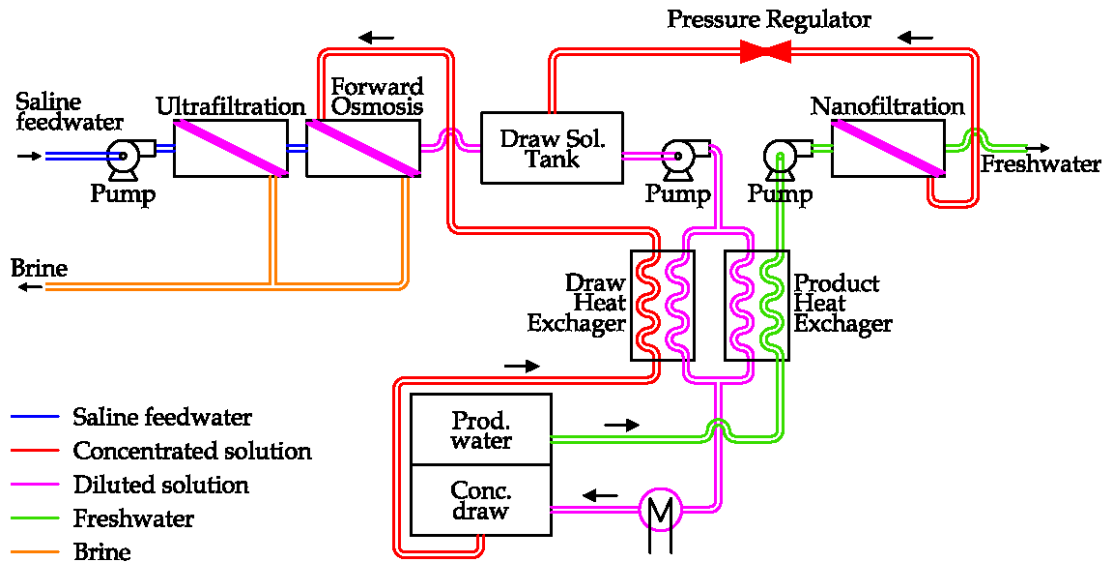


Figure II.20 Scheme of a Forward Osmosis desalination unit

In detail, saltwater after a preliminary filtration is introduced into the Forward Osmosis unit. As in the other side of semipermeable membrane the solution is more concentrated, freshwater is extracted from saline water, diluting the raw solution. Thanks to an external thermal supply, the diluted solution can be separated in two flows: the concentrated raw solution, that is sent to the FO unit, and the freshwater flow, that is furthermore filtered before the storage [76]. This technology is in development step.

II.1.f Nanofiltration (NF)

Nanofiltration is a membrane filtration process used to remove dissolved ions or organic matter to produce soft water, i.e. a water with a limited number of ions that are responsible of scaling phenomenon (Ca^{2+} , Mg^{2+} ...). This technique is conceptually similar to the reverse osmosis. The main difference is the attitude to remove ions from saltwater, as shown in Figure II.21.

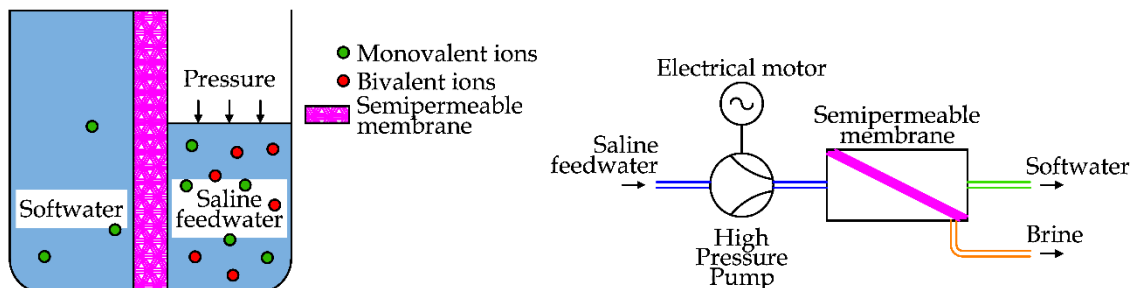


Figure II.21 Working principle and scheme of a nanofiltration unit

NF is used in several applications as water and wastewater, pharmaceutical and food processing [77]. The applications for desalination of seawater are limited, since

these semipermeable membranes are more porous, allowing the passage of some dissolved solids [51].

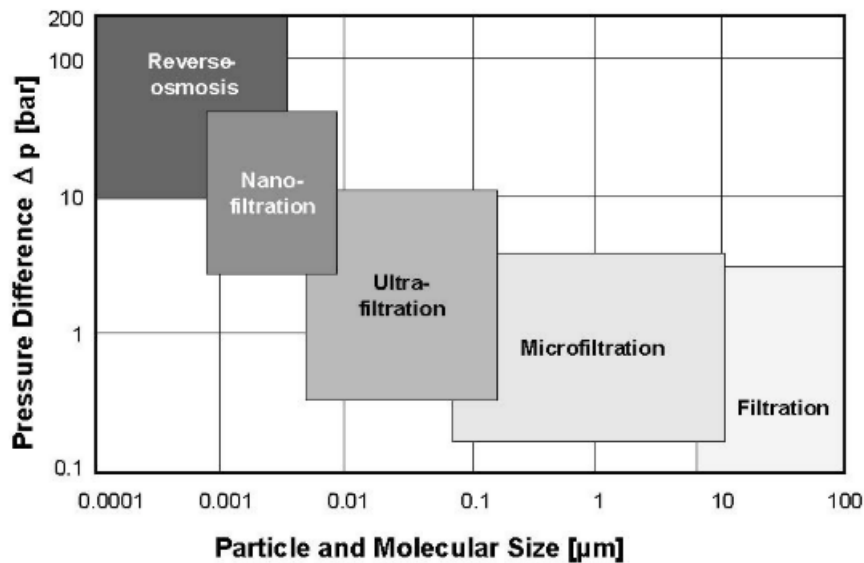


Figure II.22 Filtration technologies by required gradient pressure and porous size [63]
(Elsevier license n. 4707241281962)

As shown in Figure II.22, filtration technologies are classified according to the size of particles and molecules that are stopped by the membrane [63].

The prefix “Nano” is related to the pore sizes, ranging from 1 to 10 nanometers, so smaller than other filtration techniques (microfiltration and ultrafiltration) but larger than in the RO. As consequence, this technology removes mostly divalent ions (e.g., Ca^{+2} and Mg^{+2}), with an efficiency between 90% and 98%. The removal of monovalent ions is limited (between 60% and 85%) [36].

As the soft water produced by the NF process has a greater ions concentration than RO, a lower pressure gradient must be applied to the semipermeable membrane (between 34 to 48 bar) [36]. As NF requires a lower energy demand than RO, this solution is under investigation for seawater desalination, introducing a dual-stage unit [77].

II.1.g Electro-Dialysis (ED)

The Electro-Dialysis (ED) is an electrochemical desalination process. This technology uses the combination of semipermeable membranes and the generation of an electric field to remove the dissolved ions from the solution [78]. The working principle is shown in Figure II.23 [51], [52].

The electric field is generated by two electrodes, supplied in direct current voltage. Each ion has an electric charge (positive or negative). As a consequence of the electric field, each ion is affected by an electric force, directly proportional to the amplitude of the electric field and the value of the ion charge. The cations (positive ions, as Na^+ , Ca^{2+}) are attracted by the anode, while the anions (negative ions, as Cl^- , HCO_3^- , CO_3^{2-}) by the cathode [78].

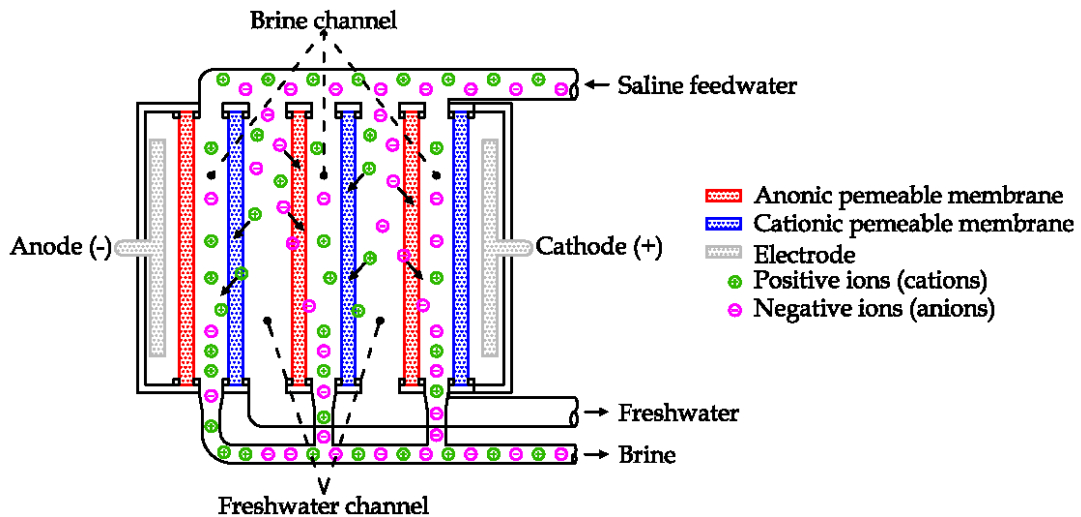


Figure II.23 Working principle of an Electro-Dialysis desalination unit

Anionic and cationic semipermeable membranes are alternatively installed in the region between the two electrodes. The first one allows the flow to the anions, the latter to cations [51]. In this way, the migration of ions generated by the electric field is selectively stopped by the semipermeable membranes. As an example, a positive ion during its motion to the anode (on the left in the picture), can cross the cationic membrane but not the anionic one. Thus, the electric field causes the motion of positive charges to the right side, while the anionic membrane stops the motion to the electrode. In the same way the negative ions migrate to the cathode but are stopped by the cationic membranes. As a result, ions are confined inside the brine channels, removing ions from the freshwater channels (see Figure II.23) [52].

First ED units were commercially introduced in the early 1970s. As a solution to avoid the deposition of salts on membranes, at regular interval the polarity of electrodes is inverted for few minutes, changing the motion of the ions inside the unit. The feedwater channels work temporarily as brine channels and vice versa [51]. This technology is currently used to produce freshwater from brackish (salinity up to 2000 ppm) [42].

II.1.h Capacitive Deionization (CDI)

Like the electro dialysis reversal, in the Capacitive Deionization (CDI) an electric field is produced between two carbon electrodes supplied with direct current voltage. As consequence of the electric field, the dissolved ions are absorbed within the carbon micropores of electrodes [79]. To regenerate them, a reverse voltage is applied, releasing ions from the electrodes to the saltwater. The co-ion adsorption phenomenon limits the efficiency of this technology, i.e. the adsorption of ions by electrodes having the same surface charge. To improve the energy efficiency, an anion exchange membrane and a cation exchange membrane could be installed on the electrodes, as shown in Figure II.24 [79]. This solution is defined as Membrane Capacitive Deionization (MCDI) [80].

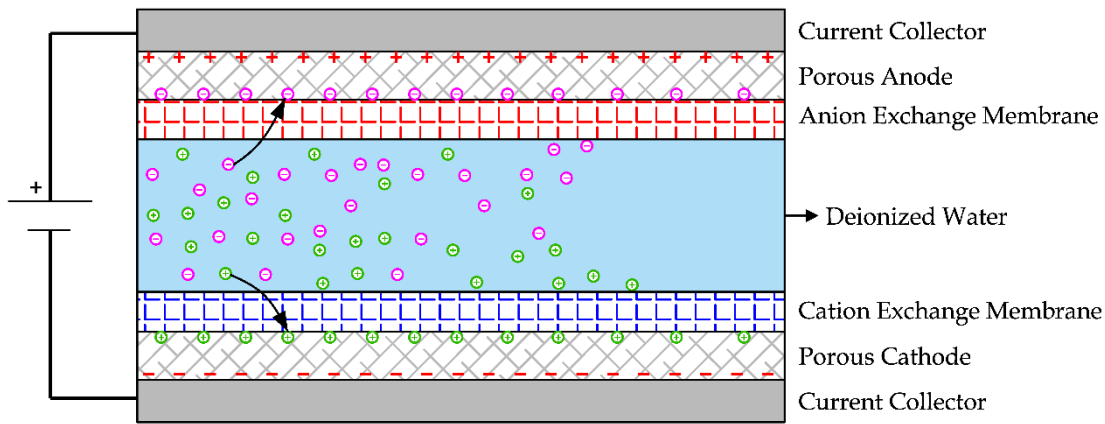


Figure II.24 Working principle of a Capacitive Deionization unit

According to literature, this technology requires a lower energy consumption for the desalination of brackish water and lower maintenance operations than the electro dialysis reversal units. Despite these advantages, CDI is a process under investigation, as the recent introduction in the context of saltwater desalination [79], [81].

II.1.i Hydration (HY)

Desalination by Hydration (HY) is based on the production of gas hydrates, that are crystalline solids composed by water (host) and gas molecules (guest) like nitrogen, carbon dioxide and methane. The dissociation of 1 m³ of hydrates can produce 0.8 m³ of water and 164 m³ of gas in standard conditions [49].

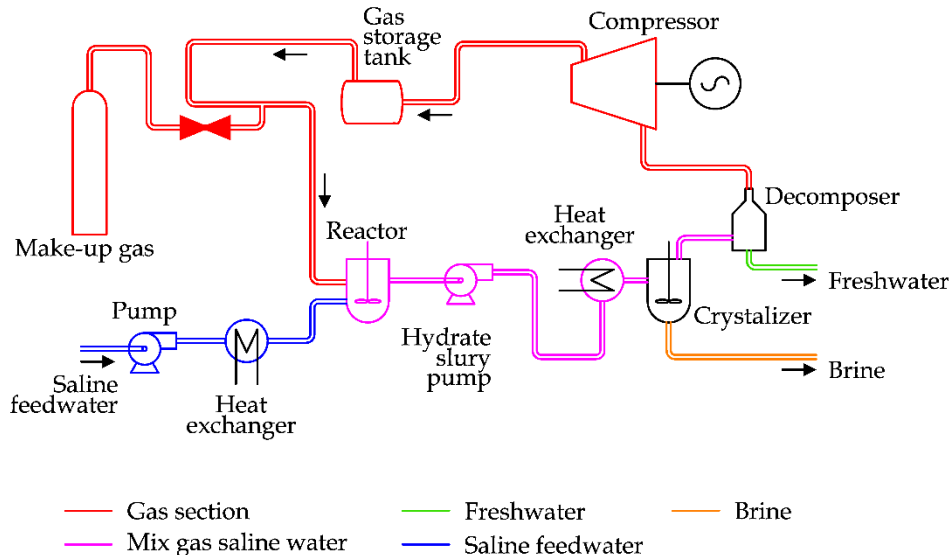


Figure II.25 Scheme of Hydration desalination plant

As the generation of hydrates requires less severe thermodynamic conditions ($T < 20\text{ }^{\circ}\text{C}$ and $P > 30\text{ bar}$) than other phase transition desalination techniques, the idea behind HY desalination is the production of hydrates and then the separation into the

components (gas and water). A scheme of Hydration plant is reported in Figure II.25 [49].

In detail, after a preliminary refrigeration seawater is mixed inside a reactor with a mixture of propane and carbon dioxide. This mixture is transferred inside the crystallizer, where hydrates are formed thanks to the low temperature and high pressure. The hydrate slurry is separated from the brine and transferred inside a decomposer. Thanks to the heat supply, hydrates are converted into freshwater and gas. The last one is recovered to be reused to produce hydrates [49].

This technology should require a lower energy expenditure in comparison with MSF and RO, however no commercial plants are available, as the high capital costs [49].

II.1.j Secondary Refrigerant Freezing (SRF)

The Secondary Refrigerant Freezing (SRF) is a desalination process based on the liquid solid phase transition. As the formed ice contains a limited amount of salts, this technique can be used to produce freshwater from seawater. A refrigerant is used to freeze the saline water. The main problem is the removal of the ice produced in the process [55].

A possible solution is depicted in Figure II.26 [55]. This system is composed by two chambers, a reversing heat pump and solenoid valves. The unit works producing alternatively ice and freshwater in the tank on the left (L) or in the other one on the right (R).

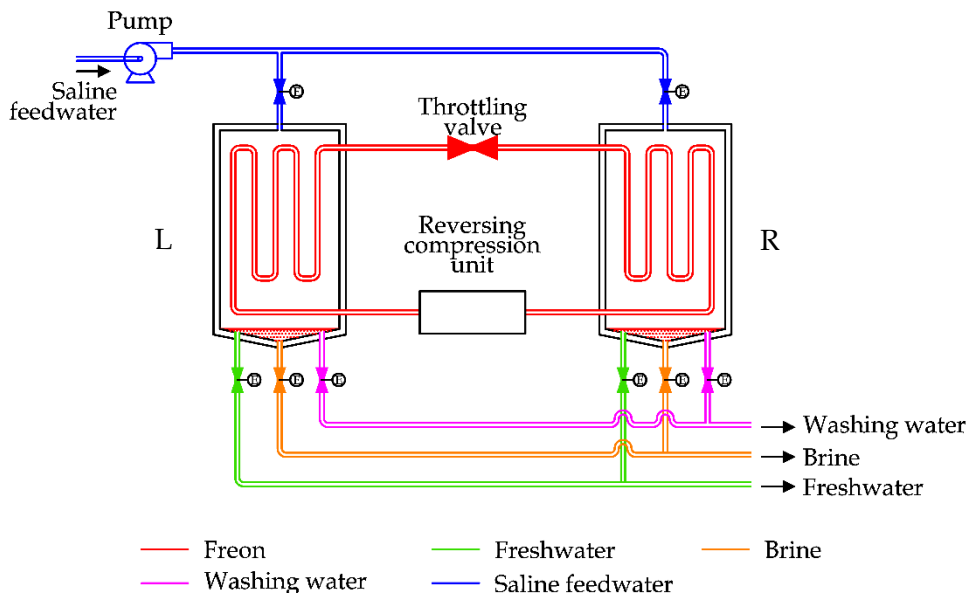


Figure II.26 Scheme of a Secondary Refrigerant Freezing desalination unit

In the first case seawater is introduced in the tank L. The heat pump is used to transfer heat from this chamber to the other one. As a consequence of the heat transfer, saline water is converted in a slurry of ice and brine inside the tank L, while in the tank R ice already formed in a previous step is melted. Stopping the process, brine is drained

out, by opening the valve in the bottom of the tank L while tank R is refilled with saline water. Reverting the heat pump, inside the tank L ice is melted thanks to the heat supply, producing freshwater. In the meantime, inside the tank R other ice is produced and the cycle is repeated. This desalination technique is currently under development [55].

II.1.k Membrane Distillation (MD)

Membrane Distillation (MD) is a desalting process, based on hydrophobic membranes. This kind of membranes can be crossed by water as vapor molecules. To promote the phase transition liquid vapor, a low temperature thermal supply is required. Solar source has been investigated to supply MD [55].

This technology works at lower temperature than other thermal-driven phase transition technologies (MSF, MED). Similarly, the required pressure is lower than other technology based on membrane (RO).

MD units can be assembled in four configurations, as shown in Figure II.27 [82]. The simplest one is the Direct Contact Membrane Distillation (DCMD), where two solutions are in direct contact with the hydrophobic membrane. As the difference of pressure between the two solutions, the vapor produced on the hot solution surface is able to cross the membrane, going inside the cold solution. This technology is common used in desalination and concentration processes of aqueous solutions in the food industry [83], [84].

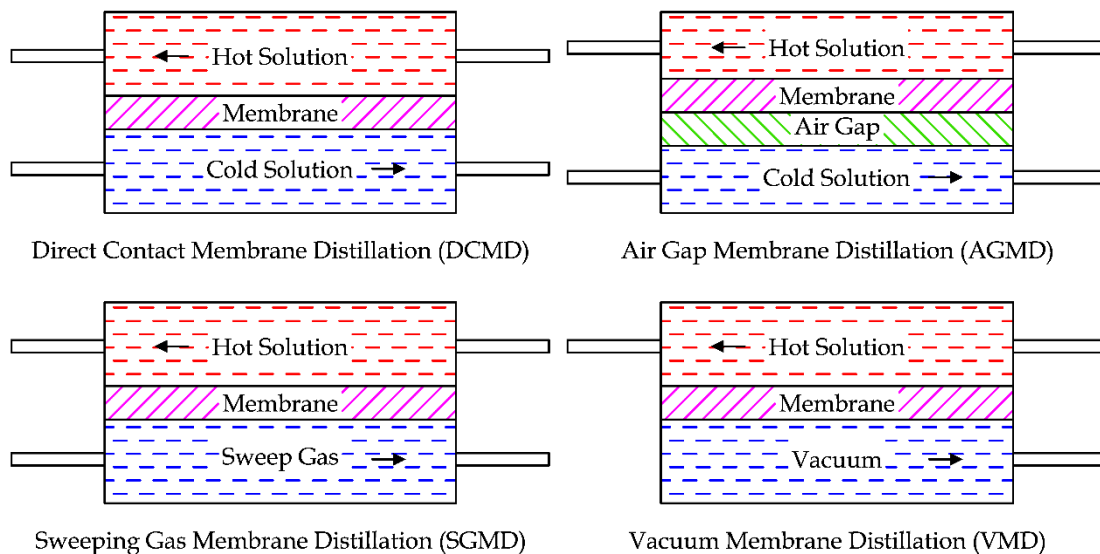


Figure II.27 Possible configurations of a Membrane Distillation unit

In the Air Gap Membrane Distillation (AGMD) a layer of stagnant air is added between the membrane and the cold solution. The reason is the reduction of the thermal energy expenditure, as the air gap increases the thermal resistance between the two fluids. However, the adding of the air gap obstacles the mass flow through the membrane. This technology can be used in desalination application or to remove volatile compounds from an aqueous solution [82], [85].

Another technology is the Sweeping Gas Membrane Distillation (SGMD), where the hydrophobic membrane separates the hot solution from a sweep gas. Like the AGMD, the thermal efficiency is higher than the DCMD. The mass transfer is promoted by the sweep gas, since it is not stationary. As disadvantage a large condenser is required. This technique can be used to remove volatile compound from aqueous solutions [86].

The last technique is the Vacuum Membrane Distillation, where the sweep gas (or the air gap) is replaced by the vacuum produced by a pump. The condensation is externally realized by the distillation unit. This solution has a high thermal efficiency and is used to separate volatile aqueous solutions [87].

II.1.1 Ions Exchange Resin (IXR)

With the term “ion-exchange resin” (IXR) is indicated a variety of organic compounds, chemically treated in order to react with the ions of a solution, capturing ions from the solution and releasing other ions from the resin to the solution. In the past zeolites were used, i.e. minerals having this characteristic.

Ions exchange resins are used in industrial and domestic applications, like the soft water production, the sugar purification, and the extraction of precious elements, such as gold, silver and uranium from mineral ores.

IXR can be classified according to the functional group [88]:

- Strongly acid, realized with sulfonic acid groups;
- Strongly basic, based on quaternary amino groups;
- Weakly acidic, realized with carboxylic acid groups;
- Weakly basic, based on primary, secondary or tertiary amino groups.

The acid resins (called also cation resins) are designed to capture positive ions (Ca^{2+} , Na^+ , Mg^{2+} , K^+ , Mn^{2+} , Fe^{3+} ...) and release H^+ ions. As a consequence, the hardness of water is reduced and the acidity is increased, since the pH is increased by the greater concentration of H^+ ions. The basic resins (called also anion resin) are utilized to capture negative ions as Cl^- , NO_3^{2-} , SO_4^{2-} , SiO_2^- , CO_3^{2-} and release OH^- ions.

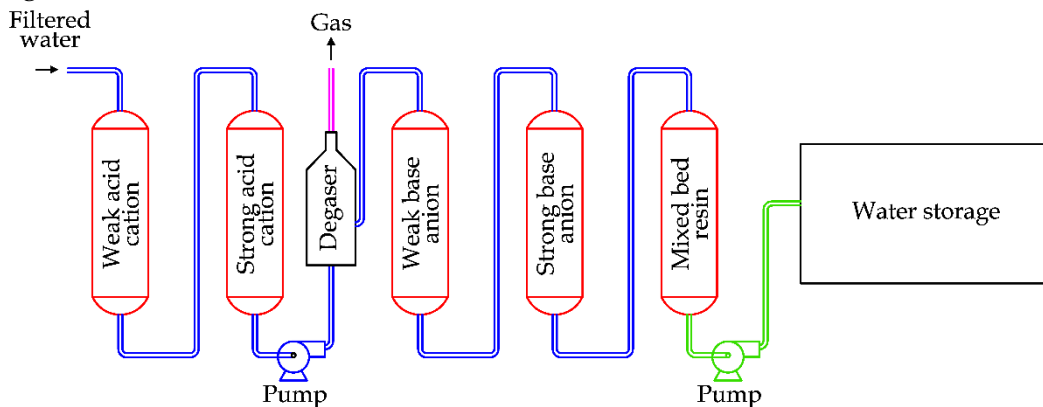


Figure II.28 Scheme of an Ions Exchange Resin desalination plant

This technology was developed in the end of 1960s [89]. A classical arrangement of a desalination plant based on IXR is reported in Figure II.28.

The saline water flows firstly through the weakly acid resin and the strongly acid resin. After this step, the water acidity is increased. A degasser is required, as bicarbonates inside the water react with H^+ ions, producing carbon dioxide.

After this step, water flows through the weakly basic resin and the strongly basic resin, reducing the water acidity. An amphoteric resin (a mix of acid and basic) is normally added to complete the removal of ions.

During the normal process, resins are progressively saturated by the ions exchange. Thence, a regeneration is periodically required to restore the resins. The regeneration uses acid solutions (H_2SO_4 and HCl) for the acid resins and basic solutions ($NaOH$ and NH_4OH) for the basic resins.

II.1.m Solar Still Distillation (SSD)

A Solar Still Distillation (SSD) can be realized by using a blackened tank, containing saline water and air [55], [90]. The device is covered with an inclined glass. In this way the solar radiation enters the system, increasing the temperature and facilitating the evaporation of freshwater. The internal humidity condenses on the glass surface, as the lower temperature of this part. The condensate is collected, obtaining freshwater. A possible solution is depicted in Figure II.29 [51], [52]. The condensate is characterized by a high quality, with a daily production about 2-3 lt./ m^2 . Consequently, this system can be used only in small applications.

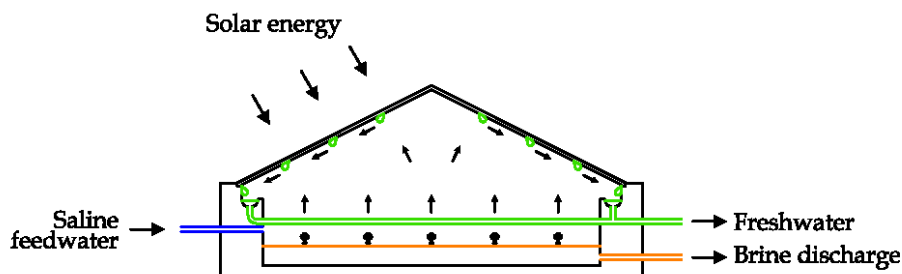


Figure II.29 Solar Still Distillation unit

II.1.n Solar Chimney (SC)

A Solar Chimney (SC) desalination unit can be assembled in the way shown in Figure II.30 [55]. A large solar collector is used to convert the solar radiation into kinetic energy of air, thanks to the shape of the chimney, that is realized in a transparent material (glass or plastic). The air flow inside the system can be used to produce electricity, if a small wind turbine is installed. The solar collector is composed by several small SSD units, in this way the solar source is also used to produce freshwater. This technology is under investigation [55].

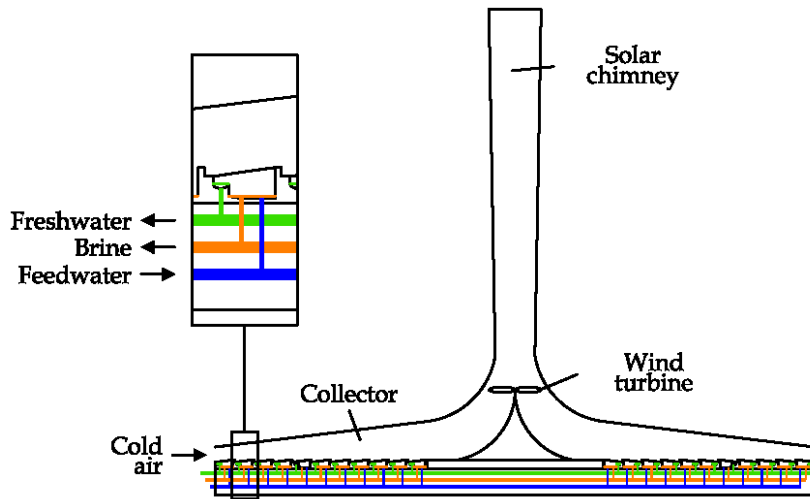


Figure II.30 Solar Chimney desalination unit

II.1.o Humidification Dehumidification (HDH)

The Humidification Dehumidification (HDH) system is a recent carrier-gas based thermal desalination technique. In detail, freshwater can be obtained by condensing the air humidity. The essential components are the humidifier and the dehumidifier. Lawal et al. proposed two possible solutions, adding a heat pump to improve the energy efficiency [91].

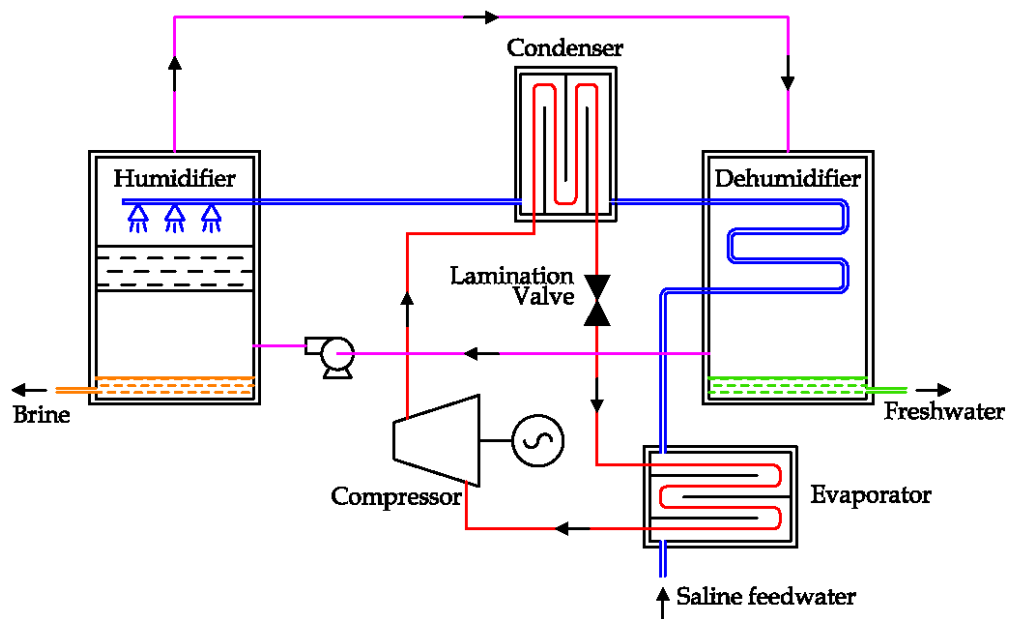


Figure II.31 HDH unit using a heat pump with a water refrigerated condenser

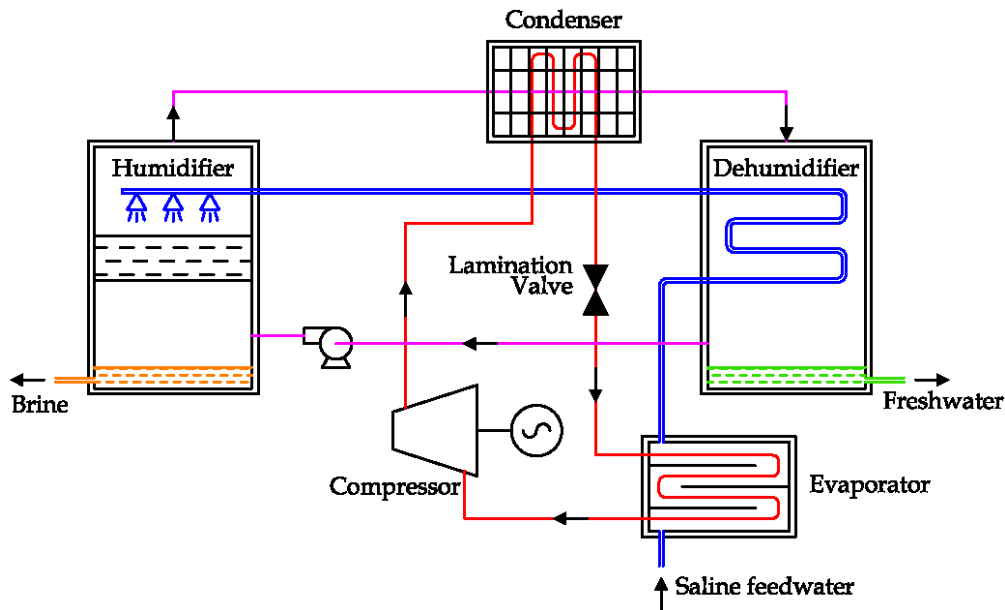


Figure II.32 HDH unit using a heat pump with an air refrigerated condenser

Both solutions are equipped with three different circuits: air, water, freon. The last one is confined inside the pipes and the main components of the heat pump (compressor, condenser, lamination valve and evaporator). Air is recirculated by a fan in a close loop, going through two chambers, where the humidification and the dehumidification occur. Only the water circuit is open, as saline water is the input, while brine and freshwater are the outputs [91].

Considering the scheme reported in Figure II.31, saline feedwater is firstly refrigerated, by the condenser of the heat pump. The cold saline water is used to promote the condensation of air humidity inside the dehumidification chamber (on the right), where freshwater is produced. During this process, the saline water temperature increases. After that, saline feedwater is nebulized inside the humidification chamber (on the left), promoting the evaporation of feedwater.

In the solution reported in Figure II.31, the thermal supply from the condenser is transferred to the saline water, after the dehumidifier unit. The alternative solution proposed by the same authors is reported in Figure II.32, where the thermal supply from the condenser is transferred to the air coming from the humidifier unit [91].

Instead of the forced air circulation, a natural air circulation system has been proposed, where the thermal supply is given by a solar panel [55], [92], [93]. In any case, HDH desalination is a technology under investigation.

II.2 Statistics on desalination

As introduced in the previous subchapters, several technologies have been proposed for desalination. The research is currently investigating new solutions to reduce the energy consumption and improve the environmental sustainability, considering renewables as energy source to supply the process.

The greatest part of technologies described above are under investigation, so limited data are available.

Considering the commercial technologies for desalination, the trends of installed capacity and number of plants are reported in Figure II.33 [44]. As introduced above, thermally driven desalination plants (MSF and MED) dominated this sector until 1990s [50], [63]. As the freshwater demand is still growing, new plants are installed. MSF continues to grow linearly, while the installed capacity by RO is increasing very quickly [94].

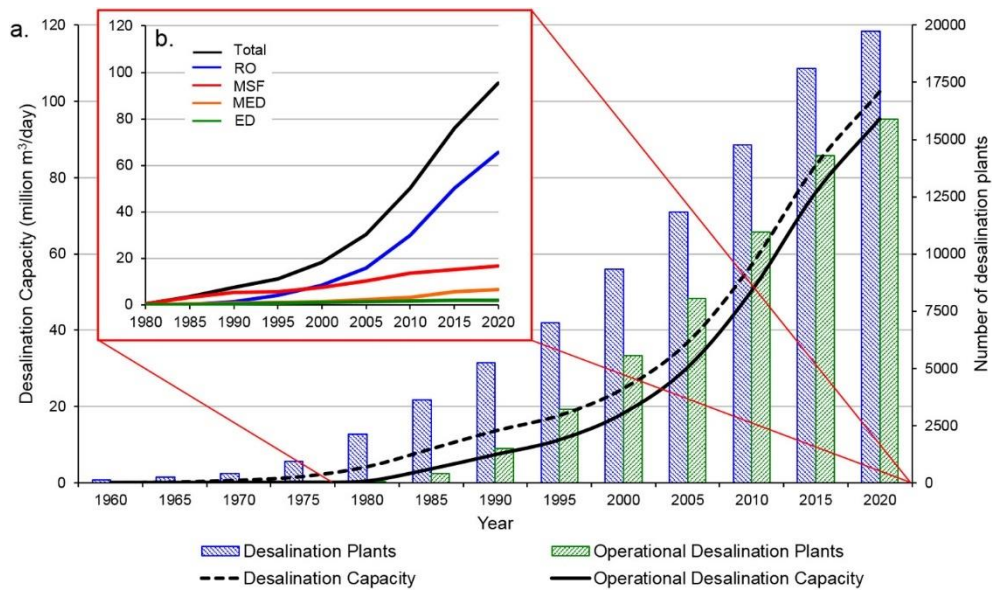


**Figure II.33 Trend of installed capacity and operative desalination plants [44]
(Elsevier license n. 4707250081904)**

A recent journal article reports statistics on the current big desalination plants installed around the world [44], using data from the Global Water Intelligence (GWI) [95]. In detail, GWI is a database containing information on the installed desalination plants, about their status, operational years, installed capacity, geographic position, technology and water sources.

Considering the desalination technology, the world installed capacity ($95.37 \cdot 10^6 \text{ m}^3/\text{day}$) is composed by RO (68.7%), MSF (17.6%) MED (6.9%) NF (3.4%) ED (2.4%), other (1.0%) [44].

Figure II.34 reports graphically the world distribution of desalination plants, considering size, technology and the water source used to produce freshwater [44].

Most of desalination plants is installed along coastline to adopt sea as water source. Indeed, 60.8% of world installed capacity uses sea as water source whereas brackish is utilized for 20.6% [44].

Middle East and North Africa region is currently equipped with 4826 plants, with an installed capacity equal to $45.32 \cdot 10^6 \text{ m}^3/\text{day}$ (47.5% of the world installed capacity). The remaining desalination plants are distributed in the following way: 3505 plants in East Asia and Pacific (18.4% of world installed capacity), 2341 in North America (11.9%), 2337 in Western Europe (9.2%), 1373 in Latin America and Caribbean (5.7%), 655 in

Southern Asia (3.1%), 566 in Eastern Europe and Central Asia (2.4), and 303 in Sub-Saharan Africa (1.9%) [44]. The main sectors are industry (7757 plants with a capacity of 28.8×10^6 m³/day) and municipality (6055 plants, 59.39×10^6 m³/day).

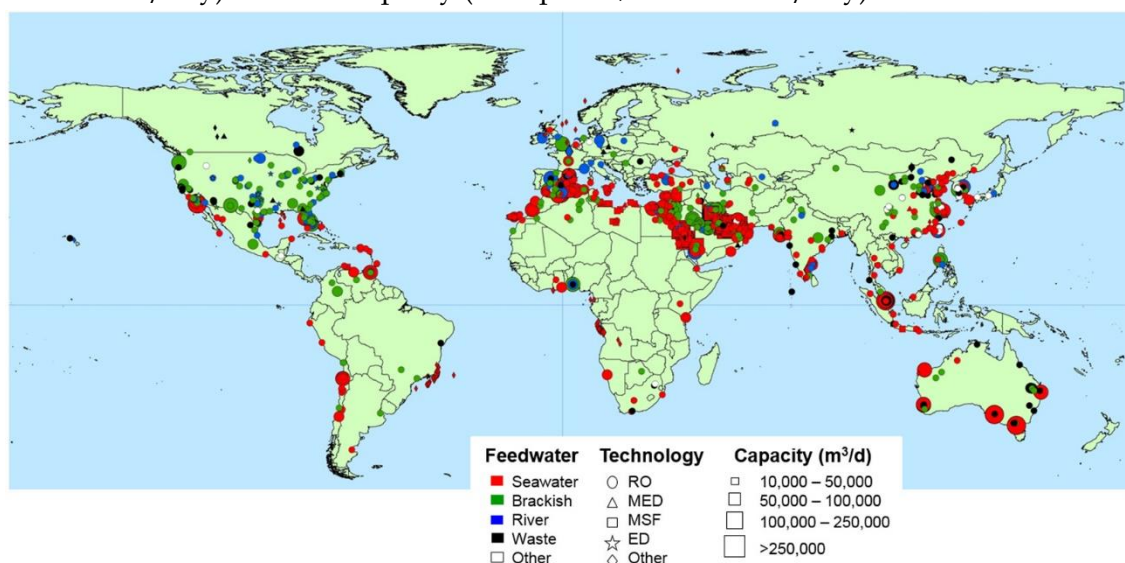


Figure II.34 Desalination plants around the world, by size and technology [44]
(Elsevier license n. 4707250081904)

Table II.1 shows statistics on the state of art of operative desalination plants [37], [44]–[46], [58], [96]. According to these data, RO is the most adaptable solution to exploit sea and brackish water, with an average capacity ranging from 1,000 (or lower) to 320,000 m³/day. About the energy supply, RO requires exclusively electricity (or mechanical energy) to run the pumps in the water circuits. This feature simplifies the potential coupling with renewable energy sources, as demonstrated by several studies [63], [96]–[98]. The water cost is lower than other desalination technologies, explaining the quick diffusion around the world.

Table II.1 State of art of commercial desalination technologies

Technology	Average capacity [10 ³ m ³ /day]	Input	Recovery Ratio	Water quality [ppm]	Energy consumption		Water cost [\$/m ³]
					Electrical [kWh/m ³]	Thermal [kJ/kg]	
MED	0.6–30	SW	0.25	10	1.5–2.5	230–390	0.52–1.5
TVC	10–35	SW	0.25	10	1.5–2.5	145–390	0.87–0.95
MSF	50–70	SW	0.22	10	4–6	190–390	0.56–1.75
MVC	0.1–3	SW		10	6–12	no	2.0–2.6
SWRO	1–320	SW	0.42	400–500	3–6	no	0.45–1.72
BWRO	Up to 98	BW	0.65	200–500	1.5–2.5	no	0.26–1.33
RED	Up to 145	BW	0.9	150–500	2.64–5.5	no	0.6–1.05

Note: SW is the abbreviation of Sea Water; BW brackish water.

To improve the energy efficiency of desalination technologies, the exergy analysis has been recently proposed in several researches [99]–[103]. Introducing the Second

Thermodynamic Law, exergy represents the maximal available energy related to a system, obtainable if reversible processes are only used to achieve the equilibrium condition with the environment (dead state). On the contrary, exergy represents also the minimal energy required by a system to achieve a desired condition, starting from the environmental state and adopting only reversible processes.

In this optic, the efficiency analysis performed according to the Second Thermodynamic Law is a successful tool to suggest solutions to improve the energy efficiency of the existing desalination technologies. A detail exergy analysis is reported in [99], where each component is firstly modelled and then analyzed.

In the case of desalination plants requiring a mechanical energy input (or electricity), the exergy efficiency is evaluated by Eq. II.3, defining W_{least}^{min} as the least work of separation required for an infinitesimal recovery ratio (RR, see Eq. II.2.)

$$\eta_{ex} = \frac{W_{least}^{min}}{W_{sep}} = \frac{W_{least}^{min}}{W_{least}^{min} + \tau_0 S_{gen}^{TDS}} = \frac{W_{least}^{min}}{W_{least}^{min} + \tau_0 S_{gen}^{RDS}} \quad II.3$$

W_{sep} is the work required by the real desalination plant, that can be expressed as sum of the least work, plus the total entropy generation S_{gen}^{TDS} (referred to the Total Dead State), multiplied by the absolute environmental temperature τ_0 .

According to the definition of W_{least}^{min} , this value is achievable if all processes are reversible and the freshwater production is infinitesimal. As a real process is designed to produce a significant amount of freshwater, the least work demand is introduced W_{least} . This term has a greater value than W_{least}^{min} , as it includes the entropy generation associated to the condition $RR > 0$. The remaining entropy generation S_{gen}^{RDS} (related to the Restricted Dead State) is associated only to the irreversibility of the adopted technologies (finite thermal differences, pressure drops, etc.).

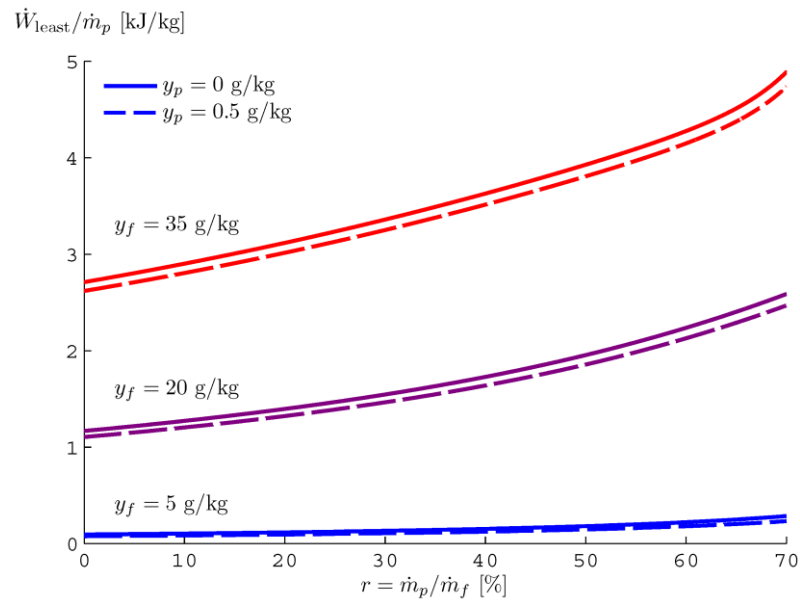


Figure II.35 Least work as function of recovery ratio and salinity of feedwater and freshwater [104]
(CC BY-NC-SA 3.0)

The trend of W_{least} is reported in Figure II.35, as function of the recovery ratio and the salinity concentration of freshwater and feed water. As introduced before, W_{least}^{min} is equal to W_{least} if the recovery ratio is equal to zero. In case of sea water (salinity 35 g/kg), zero salinity in produced freshwater and environmental temperature fixed to 25°C, W_{least}^{min} is equal to 2.71 kJ/kg (of freshwater) [99], [104].

In case of desalination plants supplied by thermal energy, Eq. II.5 can be adopted, where Q_{least}^{min} is the least thermal energy required with an infinitesimal recovery ratio. This term depends also on the temperature of the thermal source τ_H , introducing the Carnot factor $(1 - \frac{\tau_0}{\tau_H})$, that represents physically the ratio of heat that can be converted into exergy, using a reversible thermal machine.

$$Q_{least}^{min} = W_{least}^{min} \left(1 - \frac{\tau_0}{\tau_H}\right)^{-1} \quad II.4$$

So, the exergy efficiency can be evaluated by Eq. II.5, defining Q_{sep} as the thermal requirement for the real plant.

$$\eta_{ex} = \frac{Q_{least}^{min}}{Q_{sep}} = \frac{Q_{least}^{min}}{Q_{least}^{min} + \tau_0 S_{gen}^{TDS} \left(1 - \frac{\tau_0}{\tau_H}\right)^{-1}} = \frac{Q_{least}^{min}}{Q_{least} + \tau_0 S_{gen}^{RDS} \left(1 - \frac{\tau_0}{\tau_H}\right)^{-1}} \quad II.5$$

Similarly, the term Q_{least} is introduced, representing the least thermal input requirement, assuming a significant freshwater production (RR>0).

Mistry et al. analyzed the energy performances of developed desalination technologies, obtaining the results reported in Figure II.36 (based on data reported in [99]). The graph reports the exergy efficiency, according to Eq. II.3 for technologies requiring mechanical (or electrical) energy and Eq. II.5 in case of technologies thermally supplied.

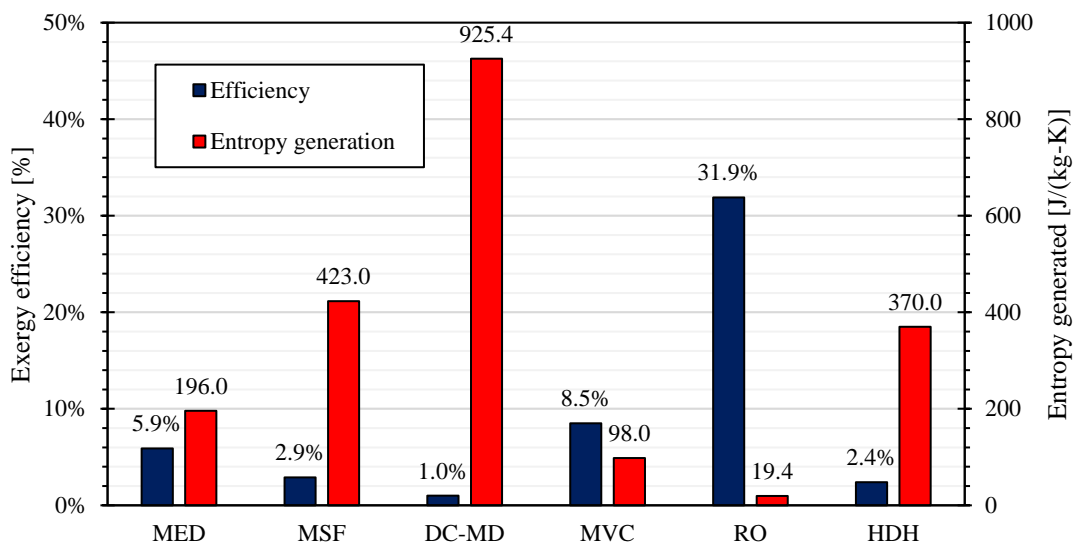


Figure II.36 Exergy analysis of several desalination technologies

The authors considered a seawater salinity equal to 4.2% in case of MED and MSF units, 3.5% (common seawater) in the other cases. The graph emphasizes the high exergy efficiency of RO and the low value of DC-MD; on the contrary if entropy generation is considered as indicator [99].

In the case of MED unit, the high entropy generation is essentially related to the finite temperature differences between fluids. In fact, considering a simple unit with 6 effects, Mistry et al. demonstrated that the entropy generation is essentially related to the effects (56.5%), the feed heaters (12.3%) and the condenser (21.8%). It is significant to underline that a significant amount of energy is irreversibly wasted as the produced brine and freshwater have a higher temperature than the environment condition. Because of the limited temperature difference between the fluids and the environments, the entropy generation is only the 6.2% [99].

MSF unit are also affected by the thermal gradient between fluids. It is evaluated that the entropy is mainly generated by feed heaters (73.9%) and brine heater (12.5%), where the temperature difference is higher. The temperature disequilibrium between produced freshwater and brine affects also MSF, causing an entropy generation equal to 10% [99].

The only solution to improve the exergy efficiency of thermally driven desalination processes is the increasing of the sizes or the number of heat exchangers in order to reduce the temperature difference between primary and secondary fluids. However, this approach is limited by the fact that increasing the sizes of the heat exchangers raises the initial investment of the plant that which may not be counterbalanced by the economic value of the energy saving [100].

The direct contact membrane distillation is a very energy consuming process. As shown in Figure II.36, the exergy efficiency is equal to 1%, with an entropy generation equal to 925.4 J/(kg-K). The entropy is essentially generated by four items: pressure drop through the module (34.5%), temperature difference in the heater (26.3%), temperature disequilibrium between feedwater, freshwater and brine (22.9%) and temperature difference inside the regenerator (16.3%).

In the case of MVC units, the entropy is essentially generated by the finite temperature difference inside the evaporator-condenser (57.2%), the irreversibility of the mechanical compressor (28.1%) and the temperature difference in the regenerator (10.9%). To improve the exergy efficiency, the main solution is the reduction of the temperature difference between the condensing steam and the evaporating brine inside the evaporator-compressor. As a consequence, the irreversibility from the heat transfer and the mechanical compressor are both reduced, thanks to the reduction of the compression work. On the other side, the cost for the desalination unit is increased [46].

According to data reported above, the RO unit represents the most efficient technology for desalination, if the energy recovery system is adopted. The exergy efficiency is equal to 31.9% in the case reported by Mistry et al. [99]. The main irreversibility is associated to the pressure drop between the two sides of the semipermeable membrane (54.8%), the irreversibility of the main high-pressure pump

(20%) and the chemical disequilibrium (15.9%). To improve further the exergy efficiency of the system, a solution is splitting the desalination process in two (or more) steps. As the osmotic pressure is function of the saline concentration of inlet and outlet fluid, in the first step a lower pressure increase is required, reducing significantly the pumping work. In the following step, a lower saline water is treated, achieving in the end the same final pressure in comparison with the case of a traditional RO unit [105].

Finally, the HDH unit is essentially affected by the finite temperature difference between fluids. In particular, entropy is generated by the dehumidifier (53.6%), the humidifier (13.2%), the heater (17.3%) and the temperature disequilibrium of produced fluids with respect to the environmental condition (15.9%) [99]. It is important to underline that this technology is currently under development, so the exergy efficiency could be increased in the next future [91].

In conclusion, RO unit represents the BAT for desalination, according to the previous statistics. Furthermore, the possibility to adopt electrical energy as input would simplify the coupling with RES, thanks to the adoption of commercial technologies like photovoltaic panels and wind turbines [2], [106]. In this way, it is possible to install small desalination units in minor islands, hopefully supplied by RES, in order to satisfy the freshwater demand in a sustainable way [107], [108].

II.3 Publications on this topic

- Viola, V. Franzitta, M. Trapanese, and D. Curto, "Nexus Water & Energy: A Case Study of Wave Energy Converters (WECs) to Desalination Applications in Sicily," *Int. J. Heat Technol.*, vol. 34, no. Special Issue 2, pp. S379–S386, Oct. 2016.
- V. Franzitta, D. Curto, D. Milone, and A. Viola, "The desalination process driven by wave energy: A challenge for the future," *Energies*, vol. 9, no. 12, pp. 1–16, Dec. 2016.
- A. Viola, D. Curto, V. Franzitta, and M. Trapanese, "Sea water desalination and energy consumption: A case study of wave energy converters (WEC) to desalination applications in Sicily," in *OCEANS 2016 MTS/IEEE Monterey*, 2016, pp. 1–5.
- V. Franzitta, D. Rao, D. Curto, and A. Viola, "Greening island: renewable energies mix to satisfy electrical needs of Pantelleria in Mediterranean Sea," in *OCEANS 2016 MTS/IEEE Monterey*, 2016, pp. 1–6.
- V. Franzitta, D. Curto, D. Rao, and D. Milone, "Near zero energy island with sea wave energy: The case study of Pantelleria in Mediterranean Sea," in *OCEANS 2016 - Shanghai*, 2016, pp. 1–5.
- Crainz et al., "Flexibility Services to Minimize the Electricity Production from Fossil Fuels. A Case Study in a Mediterranean Small Island," *Energies*, vol. 12, no. 18, p. 3492, Sep. 2019.

III SEA WAVE

III.1 Marine energy

Several researches indicate sea wave as a promising renewable energy source for the next future, especially for countries having favourable climatic conditions and a long coastline [109]-[112].

Sea wave is only one of the different kinds of energy related to the sea. In general, the term “marine energy” is usually referred to the following energy resources [60], [113], [114]:

- **Waves**, i.e. the sea motion due to the wind interaction with the sea surface;
- **Tidal range** (tidal rise and fall), i.e. the local variation of sea level caused by the gravitational attraction of sea water by the celestial bodies (Sun and Moon);
- **Tidal current**, i.e. the water flow produced by the tidal range during the process of refilling and emptying of coastal areas;
- **Ocean current**, i.e. the marine water flow generated by the wind interaction and the thermohaline circulation;
- **Ocean thermal energy conversion**, i.e. the exploitation of the temperature difference between superficial water and deep water in the oceans;
- **Saline gradient**, i.e. the recovering of the chemical energy released during the mixing of freshwater from the rivers and the saltwater of the oceans.

As introduced before, this thesis is focused on the exploitation of sea wave energy source. Thus, in the following paragraph, some information is reported about the other kinds of energy sources associated to the marine environment.

Tidal range and currents are two phenomena related to the Earth's oceanic tides. Because of the Moon's orbit around the Earth, the orbit of this one around the Sun and the Earth's rotation, a huge amount of sea water flows around the world surface, modifying locally the sea level. The effects are locally different due to the irregular distribution of lands around the world. In any case, the tides are a regular phenomenon, whose effects can be accurately predicted. Thus, tides represent an interesting renewable energy source, that can be exploited as tidal stream or tidal range.

In the first case, a hydro turbine could be installed on seabed to exploit the marine current. Several projects have been proposed. For example, SeaGen was the first full scale tidal stream generator, developed by the “Marine Current Turbine”. A device was installed in Strangford Narrows (Northern Ireland) and connected to the electrical grid in 2008. This system had a rated power of 1.2 MW, producing electricity for 18 - 20 hours per day. It was essentially composed by two hydro turbines, each one having a two-blades rotor and connected to a submersible section, in order to extract this part

from water in case of maintenance operations [115]. This system was removed in 2017. Several solutions have been proposed: some of them are under investigation (RITE Project [116], Kobold [117]), other ones were stopped after failures or project closure for funding reasons (Delta Stream Turbine [118], Oceanflow Energy's 35kW Evopod unit [119], Open Hydro [120]). No commercial technologies are currently available [121], [122].

About the exploitation of tidal range, there are locations where the sea level changes significantly as an effect of tides. A well-known example is the power plant installed on the estuary of La Rance river (France) in 1966 and still working. The plant is composed by a barrage, 750 m long, where 24 hydro turbines are installed. The rated power is 240 MW, producing annually about 500 GWh. In 2011 the Sihwa Lake Tidal Power Station (South Korea) was completed, having a rated power of 254 MW and producing 552 GWh/y [123].

Other smaller plants are: Annapolis Royal Generating Station (Canada, 20 MW, opened in 1984, producing 50 GWh/y), Jiangxia (China, 3.2 MW, 1985, 6.5 GWh/y), Udolmolk (South Korea, 1.5 MW, 2013, 2.4 GWh/y), Kislaja Guba (Russia, 1.7 MW, opened in 1968 and upgraded in 2004, 0.54 GWh/y) [122].

The term ocean current is used to underline the different origin of this kind of marine currents in relation to the tidal currents, previously described. Ocean currents are seawater circulations promoted by solar radiation. In fact, the heat irradiated by sun increases the water temperature and consequently reduces the water density. At the same time, the freshwater reversed by rivers into the seas causes a local density variation due to the different salinity.

Since the solar radiation varies with the latitude and considering the irregular distribution of the lands on the Earth's surface and the orography of seabed, the variation of water density produces water flows that are extended for thousands of kilometres. Superficial currents are also created by the wind interactions with the sea surface. Summing all these contributions, the thermohaline circulation is generated. The Gulf Stream is a famous ocean current (about 100 km wide and 800 m to 1200 m deep) that is originated from the Gulf of Mexico and flows up the North Pole with a speed of about 2.5 m/s [124]. Other famous currents are the Kuroshio Current (on the west side of Pacific Oceans) [125] and the Agulhas Current (on the south-eastern part of Indian Ocean, along the coastline of South Africa) [126].

Ocean currents are characterized by a high regularity, having a prevailing direction (temporary variations are also possible) [124]. In any case, in this step no commercial devices are available, despite recent investigations underline the huge energy potential [127], [128].

About the Ocean Thermal Energy Conversion (OTEC), the idea is the installation of a thermal machine able to use the superficial sea water as thermal source and the deep water as thermal sink [129]. The energy potential is very high, between 30 and 90 PWh, considering that about the 15% of the total solar energy is irradiated on the oceans and converted into thermal energy [113].

Like other energy sources, favourable places can be found around the world, especially in tropical regions where the difference of temperature can exceed 20°C between the superficial water (25°C) and deep water (5°C, 1 km in depth) [114]. The main problem is the low energy efficiency of this system, also in the best cases. Considering the installation of an ideal Carnot heat engine to exploit the available thermal sources, the energy efficiency is no more than 7%. Consequently, introducing the irreversibility of a real system, the power plant requires huge dimensions (especially the heat exchangers) to obtain a significant power output; thence the required investments are high. Two layouts for a possible OTEC power plant have been proposed: open cycle and closed cycle [113].

In the first case the warm water from the sea surface is flashed to produce steam, and then condensed by using the cold deep water. The main disadvantages are related to the operative conditions. Indeed, in order to use steam, the entire plant works under vacuum, so infiltrations are possible. At the same time, the specific mass of steam is quite high (30 - 100 m³/kg), hence the system requires large pipe for a small power output. The main advantage is the production of freshwater from the condenser [129].

The latter solution is the closed cycle. The warm superficial water is used to evaporate a working fluid, normally used in the chilling sector such as ammonia, propane or chlorofluorocarbon [130]. This vapor is used to run a turbine, then is condensed using the deep water as refrigerant [131]. The advantage is that the system works under pressure, so the air infiltration is avoided. As a disadvantage, huge heat exchangers are required. The first small pilot plant was tested in 1930 in Cuba but failed to achieve the desired net power output due to the limited availability of the thermal source in the testing site. In 1935 another plant (2.2 MW) was proposed, using a floating system to produce ice for Rio de Janeiro, but this project failed in numerous attempts to install the vertical long pipe to collect the deep water. After several years, a 210 kW plant was installed in Hawaii and operated from 1993 to 1998, demonstrating the feasibility of this system [131]. However, the high investment discouraged the installation of full-scale plants. A small plant (50 kW) is currently operating in the small island of Kumejima (Japan) since 2013 [132].

About the saline gradient energy source (called also Osmotic Power), the idea is the exploitation of chemical energy released when the freshwater from rivers is mixed with saltwater in the sea.

As introduced in the subsection II.1.d about the RO desalination, two solutions having different ions concentrations are characterized by different values of osmotic pressure. A solution, proposed in 1937, is the Pressure Retarded Osmosis, where the saltwater is pressurized before a semipermeable membrane. As reported in Figure II.11 (see subsection II.1.d), if the external pressure gradient is lower than the osmotic pressure, water flows from the diluted solution to the concentrated one. A brackish water is consequently produced, having the same pressure of saline water but with a greater flow. Using a hydro turbine is possible to collect more energy than the pumping expenditure, producing an electrical output [60]. In 2009 a pilot plant was installed in

Norway, having a rated power of 4 kW. Commercial systems are no currently available, in any case research is investigating new possible solutions [133].

To conclude this brief introduction on marine energy sources, some statistics are reported in Table III.1 [134]. According to the following data, sea wave represents one of the most abundant energy sources related to the marine environment.

Table III.1 Potential installable capacity and energy production from marine energy sources

	Capacity (GW)	Potential generation (TWh/y)
Marine currents	5000	50000
Osmotic salinity	20	2000
OTEC	1000	10000
Tide	90	800
Sea wave	1000-9000	8000-80000

III.2 Definitions

As introduced in the previous section, sea wave is a form of marine energy due to the several forces acting to the water surface, such as the friction generated by wind, the Coriolis force (related to the Earth rotation), the celestial bodies attraction (tidal) or other unpredictable phenomena as earthquake and volcanic eruptions (tsunami) [135]. In any case, to describe this energy source, some definitions are required.

A regular wave is classically modelled by a sine (or cosine) function of time and position, introducing the amplitude *A*, the wavelength λ and the period *T*, reported in Eq. III.1.

$$z_w(x, t) = A \sin\left(\frac{2\pi}{T}t - \frac{2\pi}{\lambda}x\right) \tag{III.1}$$

In detail, fixing the observing time *t*₀, the wavelength λ represents the minimal distance over which the wave shape is repeated, as shown in Figure III.1.

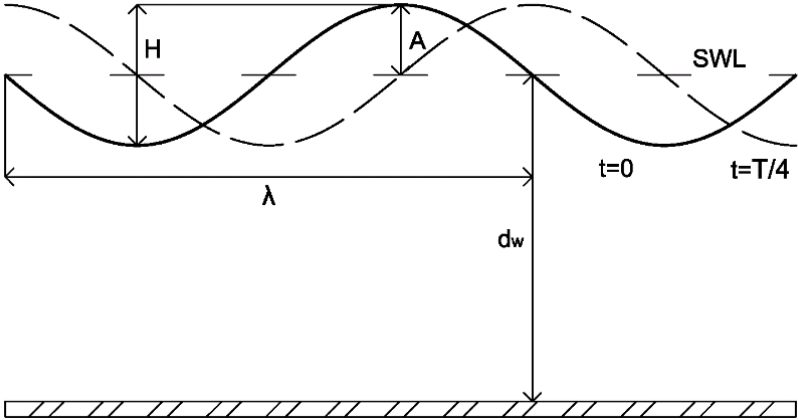


Figure III.1 Wave parameters

Similarly, selecting the observing point x_0 , the period T represents the minimal time required to complete a single oscillation. Both conditions are expressed by the relations reported in Eq. III.2, considering n as a generic natural number.

$$\begin{aligned} z_w(x + n\lambda, t_0) &= z_w(x, t_0) \\ z_w(x_0, t + nT) &= z_w(x_0, t) \end{aligned} \quad III.2$$

The rate of propagation (called also phase velocity) v_p represents the speed at which the wave profile travels and is given by the ratio λ/T .

The amplitude A represents the measure of the entire oscillating phenomenon in a single period. Two definitions are commonly used:

- Peak amplitude, i.e. the difference between the peak and the Surface Water Level (SWL). This definition is commonly used in electronic sector;
- Peak to peak, i.e. the difference between the crest (the highest value during the oscillation) to the trough (the lowest one).

To avoid misunderstanding, in sea wave sector the term “height” (symbol H) is normally used to indicate the peak to peak amplitude (see Figure III.1).

Eq. III.1 can be used also to introduce other two parameters. The amount $2\pi/T$ is called angular frequency and indicated with the Greek letter ω . Similarly, the amount $2\pi/\lambda$ is the wavenumber and indicated with k . Finally, the steepness is a nondimensional number given by the ratio H/λ .

The parameters above introduced are commonly used to analyze periodic signal, also irregular, by introducing the Fourier series. Considering only a time dependent function to simplify, a generic period signal can be approximated by Eq. III.3, where A_0 is the average value of the signal, $A_{s,i}$ and $A_{c,i}$ the amplitude of the harmonics used to approximate the input signal.

$$z_w(t) = A_0 + \sum_{i=1}^n A_{s,i} \sin\left(\frac{2\pi i}{T} t\right) + \sum_{i=1}^n A_{c,i} \cos\left(\frac{2\pi i}{T} t\right) \quad III.3$$

The motion of a single particle of fluid during sea motion was described by the Airy wave equations (published by Sir George Biddell Airy in 1845), representing a linear solution to the hydrodynamic equations.

$$\begin{aligned} \Delta x &= -\frac{H \cosh k(z_0 + d_w)}{2 \sinh kd_w} \cos(kx_0 - \omega t - \phi) \\ \Delta z &= \frac{H \sinh k(z_0 + d_w)}{2 \sinh kd_w} \sin(kx_0 - \omega t - \phi) \end{aligned} \quad III.4$$

The particle describes an elliptical motion around the mean position (x_0, z_0) according to Eq. III.4, tending to be circular in the surface ($z_0 = 0$) and practically horizontal near to seabed ($z_0 = -d_w$), as depicted Figure III.2 [136].

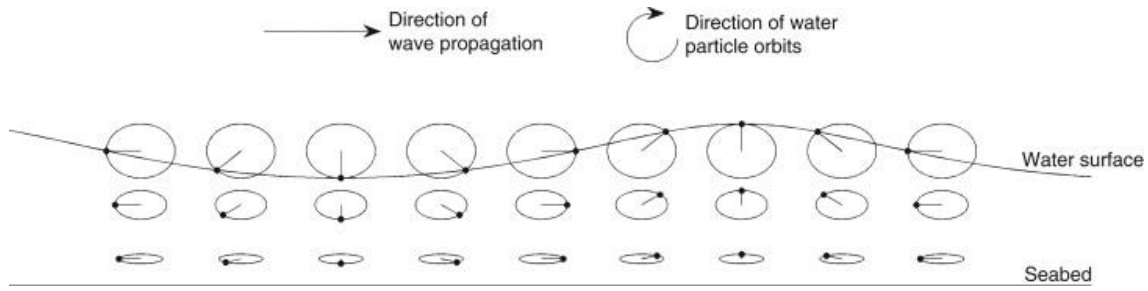


Figure III.2 Particle motion in sea wave [136] (Elsevier license n. 4707201328819)

Indeed, if the quote z_0 tends to $-d_w$ (seabed), the factor $\cosh k(z_0 + d_w)$ is equal to 1 while $\sinh k(z_0 + d_w)$ is equal to 0.

If the water depth d_w tends to ∞ , the Eq. III.4 can be simplified in Eq. III.5, corresponding to the case of a circular motion.

$$\begin{aligned}\Delta x &= -\frac{H}{2} e^{kz_0} \cos(kx_0 - \omega t - \phi) \\ \Delta z &= \frac{H}{2} e^{kz_0} \sin(kx_0 - \omega t - \phi)\end{aligned}\tag{III.5}$$

However, sea wave phenomenon is an example of random wave, thence a statistical approach is normally used. The following definitions are commonly adopted during a measuring campaign in the open sea. The classical approach considers the sea wave phenomenon as sum of a large number of sine wave components, each one having different amplitude A_i , period T_i , wavelength λ_i and direction ϑ_i [136]. The term ϕ_i represents the wave phase, considered randomly distributed in the interval $[0, 2\pi]$.

$$z_w(x, y, t) = \sum_{i=1}^n A_i \sin \left[\frac{2\pi}{\lambda_i} (x \cos \vartheta_i + y \sin \vartheta_i) - \frac{2\pi}{T_i} t + \phi_i \right]\tag{III.6}$$

Using a statistical approach, it is possible to introduce a directional variance spectrum $s(f, \vartheta)$ indicating how the energy in the wave field is distributed with respect to frequency and direction [136].

The directional variance spectrum $s(f, \vartheta)$ can be decomposed in two functions (see III.7): $s(f)$ represents the total energy at each frequency independently of wave direction, while $D(f, \vartheta)$ expresses how the energy at a specific frequency is distributed according to the wave direction.

$$s(f, \vartheta) = s(f)D(f, \vartheta)\tag{III.7}$$

By the integration over the entire space, the omnidirectional spectrum or frequency spectrum is obtained in Eq. III.8:

$$S(f) = \int_0^{2\pi} s(f)D(f, \vartheta) d\vartheta\tag{III.8}$$

where the directional distribution function $D(f, \vartheta)$ satisfies the conditions III.9:

$$\int_0^{2\pi} D(f, \vartheta) d\theta = 1 \quad \text{III.9}$$

$$D(f, \vartheta) \geq 0 \quad \forall \theta \in [0, 2\pi]$$

The definition of frequency spectrum $S(f)$ is fundamental, since several statistical parameters used in sea wave analysis are defined on this basis. The n -th order momentum of frequency spectrum m_n is defined by III.10:

$$m_n = \int_0^{\infty} f^n S(f) df \quad \text{III.10}$$

The Significant Height H_s is equal to four times the standard deviation of the surface elevation or equivalently as four times the square root of the zeroth-order moment of the wave spectrum [137], so:

$$H_s = 4\sqrt{m_0} = 4 \sqrt{\int_0^{\infty} S(f) df} \quad \text{III.11}$$

In the past, the significant height was traditionally defined as the mean wave height of the highest third of the waves [138], according to III.12.

$$H_s \cong H_{1/3} = \frac{1}{n/3} \sum_{j=1}^{n/3} H_j \quad \text{III.12}$$

It is important to underline that the two definitions are practically equivalent as a more accurate correlation shows that $H_{1/3} = 4.01\sqrt{m_0}$, so the difference is negligible [137].

In literature sometimes other parameters are used to describe the wave height:

- $H_m = H_{1/1}$ Mean wave, that represents the average value of all measured waves in the measuring period;
- $H_{1/10}$ Wave one-tenth that is the mean wave height of the highest tenth of the waves;
- H_{max} Maximum wave height, that is the maximum value measured in the site. It is relevant to design structures that are exposed to sea wave.

In literature, the average period T_m represents the average value of all waves, measured in a fixed interval (as example 30 minutes or 1 hour). A more rigorous definition is given by Eq. III.13 [136]:

$$T_m = \frac{m_0}{m_1} = \frac{\int S(f)df}{\int fS(f)df} \quad III.13$$

Another common period is the mean wave period T_z defined as the square root of the zero-order momentum and the second order momentum of frequency spectrum (see Eq. III.14):

$$T_m = \sqrt{\frac{m_0}{m_2}} = \sqrt{\frac{\int S(f)df}{\int f^2 S(f)df}} \quad III.14$$

It is also possible to define a Peak Period T_p corresponding to the peak of the variance density spectrum $S(f)$.

Finally, the wave energy period T_e is defined as the variance-weighted mean period of the one-dimensional period variance density spectrum $S(f)$ [139]. Analytically, the energy period is defined by III.15:

$$T_e = \frac{m_{-1}}{m_0} = \frac{\int f^{-1}S(f)df}{\int S(f)df} \quad III.15$$

This parameter is commonly used to evaluate the potential energy production. As Eq. III.15 is quite complex to perform, simplified correlations are available in literature.

As an example, the Atlas of UK Marine Renewable Energy Resources suggests the correlation between the energy period and the average period, expressed by Eq. III.16 [139]:

$$T_e = 1.14 T_p \quad III.16$$

The energy period can be also evaluated from the peak period T_p , according to Eq. III.17. The value 0.86 is obtained in the case of Pierson Moskowitz spectrum [110]. This value is commonly used in surrounded sea with a limited surface, like the Mediterranean Sea [140].

$$T_e = 0.86 T_m \quad III.17$$

The Pierson Moskowitz spectrum, above cited, is modelled by Eq. III.18, where α_{PM} e β_{PM} are two parameters related to the sea state, defined by the significant height H_s and the peak period T_p (or equivalently the peak frequency $f_p = 1/T_p$) [141], [142]:

$$S_{PM}(f) = \frac{\alpha_{PM}}{f^5} e^{-\beta_{PM}/f^4} \quad III.18$$

$$\alpha_{PM} = \frac{5}{16} H_s^2 f_p^4 \beta_{PM} = \frac{5}{4} f_p^4$$

In the original work, the Pierson Moskowitz spectrum was related to the wind speed measured at 19.5 m above the average sea level, using a similar formulation [135].

Another common spectrum is the JONSWAP (acronym of Joint North Sea Wave Observation Project) spectrum, obtained from Pierson Moskowitz spectrum multiplied by an extra peak enhancement factor $\gamma^{\delta(f)}$:

$$S_{JONSWAP}(f) = S_{PM}(f)\gamma^{\delta(f)}$$

$$\delta(f) = \exp\left[-\frac{1}{2}\left(\frac{f - f_p}{\sigma f_p}\right)^2\right]$$

$$\sigma = \begin{cases} 0.07 & \text{for } f < f_p \\ 0.09 & \text{for } f \geq f_p \end{cases}$$
III.19

In the JONSWAP distribution, all parameters are obtained from the observed sea [136]. A qualitative comparison of Pierson spectrum and JONSWAP spectrum is reported in Figure III.3, where the x-axis is normalized by the peak frequency and the y-axis by the maximum value of the Pierson Moskowitz spectrum. The graph underlines the effect produced by extra peak enhancement factor introduced in the JONSWAP spectrum, as in the real application all parameters are calculated in order to approximate the measuring data [135].

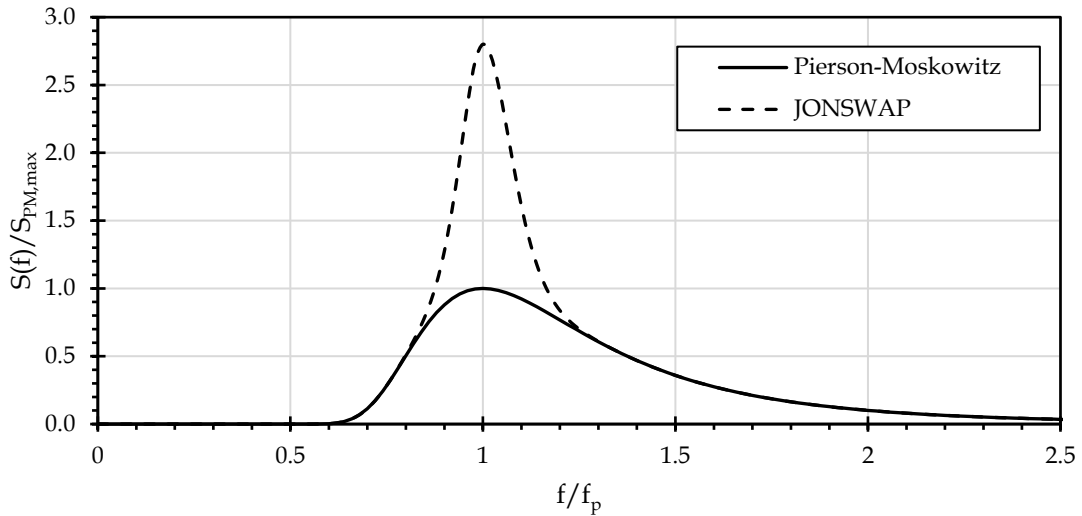


Figure III.3 Qualitative comparison of Pierson Moskowitz and JONSWAP spectra

Sea waves can be classified in different ways, considering the parameters above defined:

- Introducing the ratio d_w/λ (water depth divided by wavelength) [141]
 - Shallow water or long wave $\frac{d_w}{\lambda} < \frac{1}{20}$;
 - Intermediate water $\frac{1}{20} < \frac{d_w}{\lambda} < \frac{1}{2}$;
 - Deep water or short wave $\frac{d_w}{\lambda} > \frac{1}{2}$;

- Wave period T [135], [143]
 - Capillary waves ($T < 0.1 s$), generated by wind and restored by surface tension;
 - Ultra-gravity waves ($0.1 s < T < 1 s$) generated by wind and restored by surface tension and gravity;
 - Gravity waves ($1 s < T < 30 s$) generated by wind and restored by gravity;
 - Infra-gravity waves ($30 s < T < 5 min$), caused by wind and atmospheric pressure gradients and restored by gravity;
 - Long-period waves (seiches, storm surges, tsunamis, with a period $5 min < T < 12 h$), caused by atmospheric pressure gradients and earthquake and restored by gravity;
 - Ordinary tidal waves ($12 h < T < 24 h$), due to the gravitational attraction of celestial bodies (moon and sun) and restored by gravity and Coriolis force;
 - Trans-tidal waves ($T > 24 h$), due to storms and gravitational attraction and restored by gravity and Coriolis force.

In oceanography, the term “sea state” is used to indicate the temporary (about half hour) and local condition of the sea surface (with respect to wind waves and swell) as consequence of wind interaction. The World Meteorological Organization (WMO) defines the sea states according to the Douglas Sea Scale, reported in Table III.2:

Table III.2 Sea States Codes based on Douglas Sea Scale

Code	H_s	Characteristics
0	0	Calm (glassy)
1	<0.1	Calm (rippled)
2	0.1-0.5	Smooth (wavelets)
3	0.5-1.25	Slight
4	1.5-2.5	Moderate
5	2.5-4	Rough
6	4-6	Very rough
7	6-9	High
8	9-14	Very high
9	>14	Phenomenal

Analysing the phenomenon of sea wave propagation, the group velocity v_g is introduced, representing the velocity at which wave energy travels and defined by Eq. III.20:

$$v_g = \frac{d\omega}{dk} \quad III.20$$

In general, the phenomenon is influenced by the water depth. In fact, considering a finite water depth d_w , the wavenumber $k = 2\pi/\lambda$ and the angular frequency $\omega = 2\pi/T$ are related by the dispersion relation, expressed by Eq. III.21.

$$\omega^2 = gk \tanh(kd_w) \quad III.21$$

It is interesting to observe that in case of deep water ($d_w/\lambda > 1/2$), the term $\tanh(kd_w)$ is close to 1; in the case of shallow water ($d_w/\lambda < 1/20$) the same term is equivalent to kd_w [141]. Thus, in these cases, Eq. III.21 is replaced by Eq. III.22:

$$\omega^2 = \begin{cases} gk & \text{for } \frac{d_w}{\lambda} > \frac{1}{2} \\ gk^2 d_w & \text{for } \frac{d_w}{\lambda} < \frac{1}{20} \end{cases} \quad III.22$$

Combining the equations above reported, the velocity group is given by Eq. III.23 [139]:

$$v_g = \frac{1}{2} v_p \left(1 + \frac{2kd_w}{\sinh 2kd_w} \right) \quad III.23$$

that can be simplified in two forms, according to the case of shallow water and deep water, respectively (see Eq. III.24).

$$v_g = \begin{cases} v_p & \text{for } \frac{d_w}{\lambda} < \frac{1}{20} \\ \frac{1}{2} v_p & \text{for } \frac{d_w}{\lambda} > \frac{1}{2} \end{cases} \quad III.24$$

With the target to exploit sea wave as a renewable energy source, it is important to evaluate the amount of energy associate to the phenomenon.

It is possible to define the total energy related to sea wave for a unitary surface E_t (sum of kinetic and potential energy) according to Eq. III.25:

$$E_t = \frac{\rho g}{8} H^2 \quad III.25$$

The value 8 (instead of 2) at the denominator is due to the fact that wave height is double the wave amplitude.

The wave energy flux is defined as the power of a unitary wave front, that is given by Eq. III.26:

$$\varphi = \frac{\rho g}{8} H^2 v_g \quad III.26$$

Eq.s III.25 and III.26 can be applied only for a monochromatic wave spectrum. Since the real sea states are represented by a sum of several monochromatic waves, an approximation is given by Eq.s III.27 and III.28, using the definition of significant height.

$$E_t \approx \frac{\rho g}{16} H_s^2 \quad \text{III.27}$$

$$\varphi \approx \frac{\rho g}{16} H_s^2 v_g \quad \text{III.28}$$

The phase velocity for gravity wave is given by Eq. III.29:

$$v_p = \frac{\lambda}{T} = \sqrt{\frac{g}{k}} = \sqrt{\frac{g\lambda}{2\pi}} = \frac{gT}{2\pi} \quad \text{III.29}$$

consequently, in the case of deep water (where $v_g = v_p/2$), the wave energy flux is finally obtained, according to Eq. III.30:

$$\varphi = \frac{\rho g^2}{64\pi} H_s^2 T_e \quad \text{III.30}$$

In literature, this equation is universally adopted to estimate the wave energy potential in a specific site, knowing the energy period T_e and the significant height H_s [112], [139], [144], [145].

As introduced before, the sea state, identified by the significant height and the energy period, represents one of the several possible conditions that can be observed in the site.

A simple way to report data on the measured sea states is the scatter table (see Figure III.4), reporting the equivalent hours in which a specific condition (T_e, H_s) is measured (picture on the left) or the corresponding annual energy availability (picture on the right).

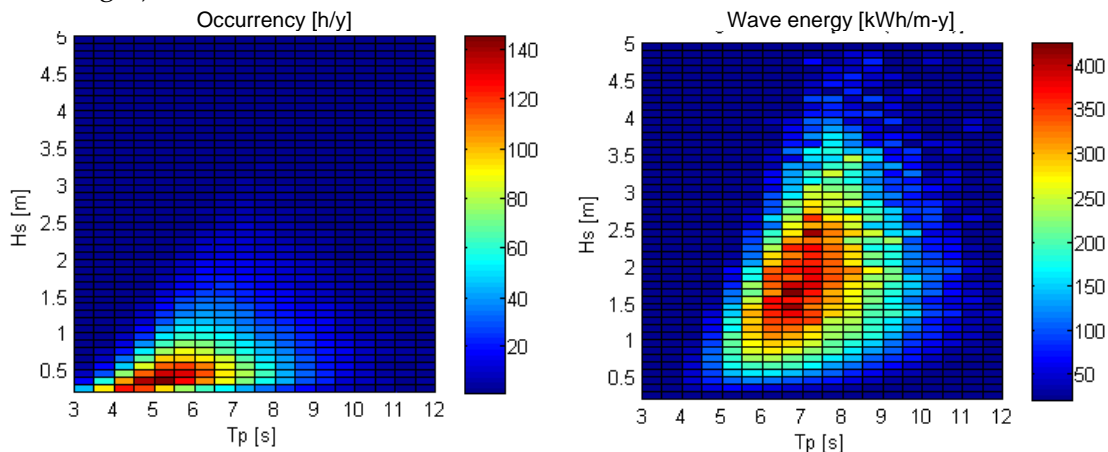


Figure III.4 Examples of scatter tables, in the island of Pantelleria (Italy) [146]

A generic device to exploit the sea wave energy source is affected by an energy efficiency, due to the transferring of energy from sea wave to the device (hydraulic efficiency η_{hy}) and the internal transformation to electricity (electrical efficiency η_e). According to the definition of sea wave flux (power per unitary length of wave front), the electricity production from sea wave can be estimated by Eq. III.31:

$$E_{sw} = d_c \sum_{i=1}^n \sum_{j=1}^m \frac{\rho g^2}{64\pi} H_{s,i}^2 T_{e,j} \eta_{hy}(H_{s,i}, T_{e,j}) \eta_e(H_{s,i}, T_{e,j}) t_{i,j} \quad III.31$$

where d_c is the equivalent diameter of the system that recovers the energy from sea wave, $H_{s,i}$ is the i -th class of significant height, $T_{e,j}$ is the j -th class of energy period and $t_{i,j}$ the number of hours in which the condition $(H_{s,i}, T_{e,j})$ is measured.

A simplified equation is also adopted in this thesis, if a monthly average wave energy flux $\varphi_{m,i}$ is available:

$$E_{sw} = d_c \eta_{hy} \eta_e \sum_{i=1}^n \varphi_{m,i} t_i \quad III.32$$

assuming an average hydraulic efficiency η_{hy} , an average electrical efficiency η_e of the system $\eta_{e,w}$, and indicating with h_i the number of hours per month [109].

III.3 State of art

Wave energy represents a “new entry” in the renewable energy sector, however a common opinion suggests that in near future sea wave might have a key role for the electrical energy production, due to its huge energy potential [121], [142]. It is also evident how this source will be able to exploit areas which are not used nowadays, creating important supply chains and local job opportunities [147].

Recent international reports underline that the total theoretical wave energy potential is about 30 PWh/year, not evenly distributed throughout the world [121], [148]. The red areas in Figure III.5 are defined as hot spots, i.e. regions with high values of wave energy potential. Thus, the Southern part of Australia, Africa and America are exposed to the highest values of wave energy potential. Other more moderate areas can be found in the regions between USA, Canada and Japan in the Pacific Ocean and between European Union, Greenland, USA and Canada in the Atlantic Ocean. Unfortunately, all these areas are affected by extreme bad weather conditions, due to the high level of energy potential, complicating the utilization of this renewable energy source [149], [150].

In this context, the device able to extract energy from sea wave and produce electrical energy or other useful energy output is commonly defined as Wave Energy Converters (WEC) [151].

Historically, the first patent was registered in France in 1799 by Monsieur Girard and his son [151]. After that, many types of WEC have been proposed over time.

These systems are classified using different criteria like the position with respect to the coastline, the typical size, the orientation with respect to the direction of wave propagation or the working principle.

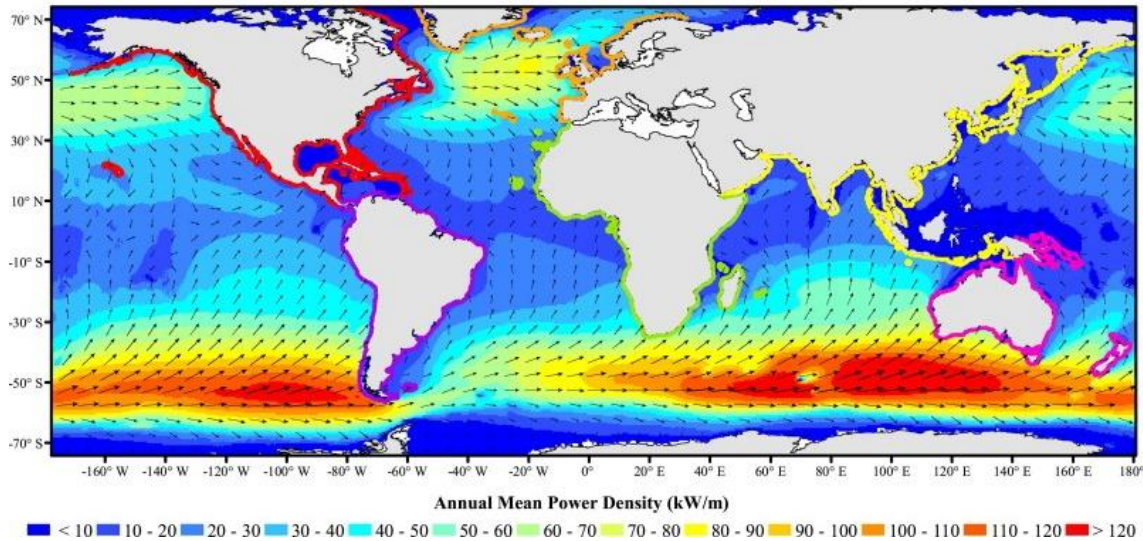


Figure III.5 Global wave power GIS map [142] (Elsevier license n. 4707211026493)

As shown in Figure III.6, considering the orientation of the system with respect to the direction of wave propagation, it is possible to define [152]:

- **Attenuators**, these systems are oriented parallel to the wave direction. Since the device has a length of the same order of the wavelength, it adapts its shape to the wave profile, extracting energy from sea wave;
- **Point absorbers**, these systems work independently of wave direction due to their small sizes in comparison with the wavelength;
- **Terminators**, these systems are oriented perpendicular to the direction of wave propagation. Sea wave ends on the device, transferring its energy.

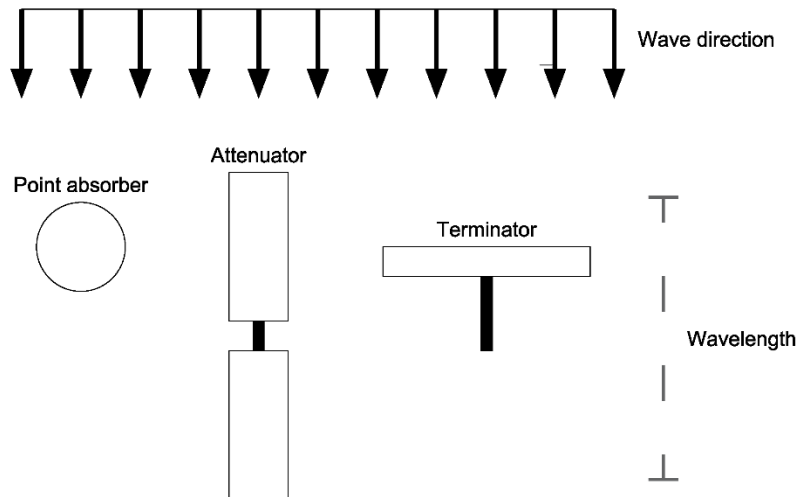


Figure III.6 Classification of WEC based on wave direction

Considering the working principle, the following categories are identified [151]:

- **Oscillating water column**, in this system sea wave enters inside a chamber open to the atmosphere. Inside the chamber, sea wave produces a vertical water oscillation. The air inside the chamber is pressurized and depressurized by the water oscillation, producing a bidirectional air flow

usable to run special wind turbines. The system can be installed on the coastline or integrated in a floating device.

- **Wave-activated bodies**, in this case sea wave produces relative motions on the systems, running the energy converters. This kind of system can be assembled in several configurations in order to produce a rotation or a translation. About the installation, there are floating systems and submerged ones.
- **Overtopping devices**, in this case, sea water is conveyed in a reservoir, using a ramp to convert the kinetic energy of sea wave into potential energy. The water is consequently spilled from the reservoir and used to produce electricity, by using a low head hydro turbine.

About the distance from the coastline, it is common to define the following regions (see Figure III.7):

- **Onshore**, in this case the system is directly fixed on the mainland, simplifying the maintenance and the installation of the device.
- **Nearshore**, it represents the transition region between the shoreline and the effective offshore area. In this zone, sea wave energy starts to be dissipated by seabed. In simple term, nearshore region starts where the water depth is about half of the wavelength and ends where the depth is one twentieth of wavelength (the same conditions reported in Eq. III.22 in the previous subsection).
- **Offshore**, the region where the sea wave phenomenon is practically not influenced by seabed. In this area, waves are strong and regular.

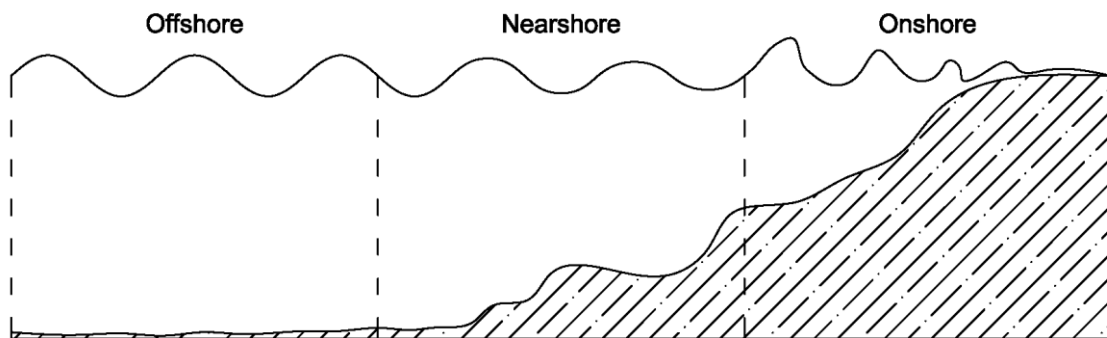


Figure III.7 Classification of WEC based on the distance from the coastline

In the following subsections, some examples of Wave Energy Converters are reported, according to the classification based on the working principle [151]. Finally, a focus on the Power Take Off is reported.

III.3.a Oscillating Water Column

Several Oscillating Water Column (OWC) devices have been proposed in the past. According to the position of the system from the coastline, OWC devices can be classified as fixed or floating [148].

In the first case, the OWC plant is installed via a fixed structure on the shoreline or close to it, or in natural or artificial structures, such as breakwaters and rock cliffs [148].

The installation of WEC directly on the shoreline has several benefits. The maintenance operations are simplified, reducing the relative costs. At the same time, the costs for the mooring system is minimized. Furthermore, the entire electrical equipment for the energy conversion is installed out of the water [151].

As mentioned before, the OWC devices are designed to produce a vertical oscillation of water inside a chamber in order to produce the alternative compression and expansion of the air inside the same chamber. Since the air flow changes continually its direction, the traditional horizontal-axis air turbines cannot be adopted. A solution is represented by Wells turbine, developed in the mid-1970s by Alan Arthur Wells (in that period professor at Queen's University of Belfast) [151].

The Wells turbine is a low-pressure air turbine, characterized by the ability to rotate in one direction independently of the air flow direction. The blades are characterized by a symmetrical air foil where the plane of the symmetry is the same of the plane of rotation and perpendicular to the air flow direction. As reported in [151], the Wells turbine is affected by a low (or negative) torque in case of small air flow rate; significant aerodynamic losses and noise in comparison with other wind turbines. Thus, this turbine requires a greater section to achieve the same power output of other turbines. Nevertheless, Wells turbine has been applied in several OWC plants.

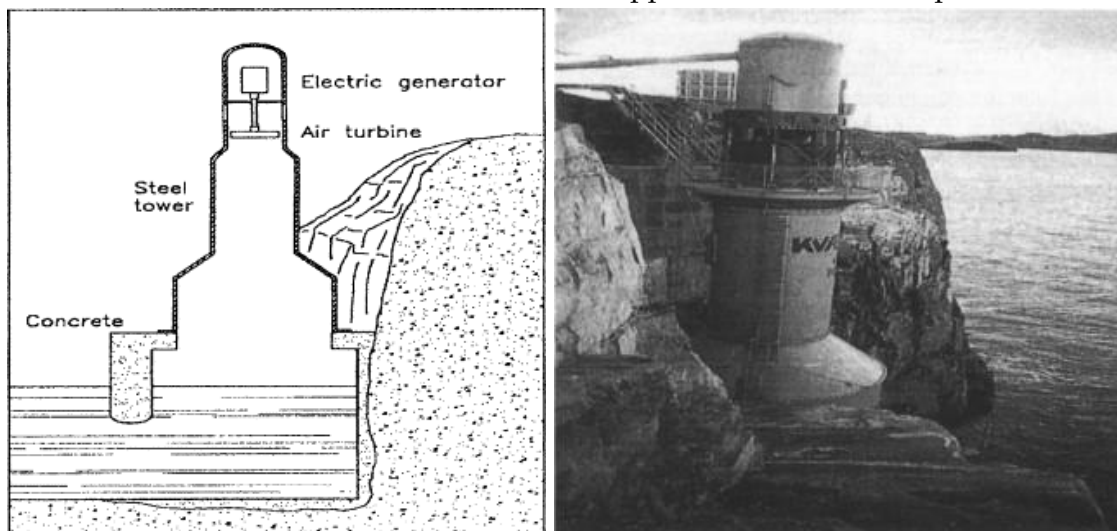


**Figure III.8 Sectional drawing (left) and view (right) of the Kværner Brug's OWC plant [153]
(Elsevier license n. 4707220801868)**

As an example of full-scale OWC system, the Kværner Brug's OWC plant was realized at Toftesfjallen (Norway) in 1985, with an electrical rated power of 500 kW [154].

The lower part was realized in concrete, with a height of 3.5 m above sea level. As reported in Figure III.8 [153], this part of the system formed a chamber, communicating to the sea under the water level. The upper part (steel tower), achieving the height of 21 m, was equipped with a self-rectifying air turbine, with a rated power of 500 kW. Unluckily, this plant was destroyed by a severe storm in the end of 1988 [155]. Despite

the proposal to replace the damaged part, the system was decommissioned, keeping only the concrete part on the testing site. In its short operative life, the Kværner Brug's OWC plant delivered 29 MWh to the electrical grid [156].

In 1991 an OWC system was installed at Vizhinjam (Kerala, India), composed by a concrete caisson and installed near to the original breakeven structure. The project considered the installation of a Wells turbine coupled with an induction generator (150 kW) in order to be directly coupled with the electrical grid [155].

In reality the results were under the expectation: the output power was highly variable in the range 0-60 kW in few seconds and the induction motor frequently was an electrical load instead a generator, consuming more energy than it produced [157]. The plant was inactive for a long period. In 2004 the plant was investigated to supply a RO desalination plant. This OWC device was finally decommissioned in 2011 [115].

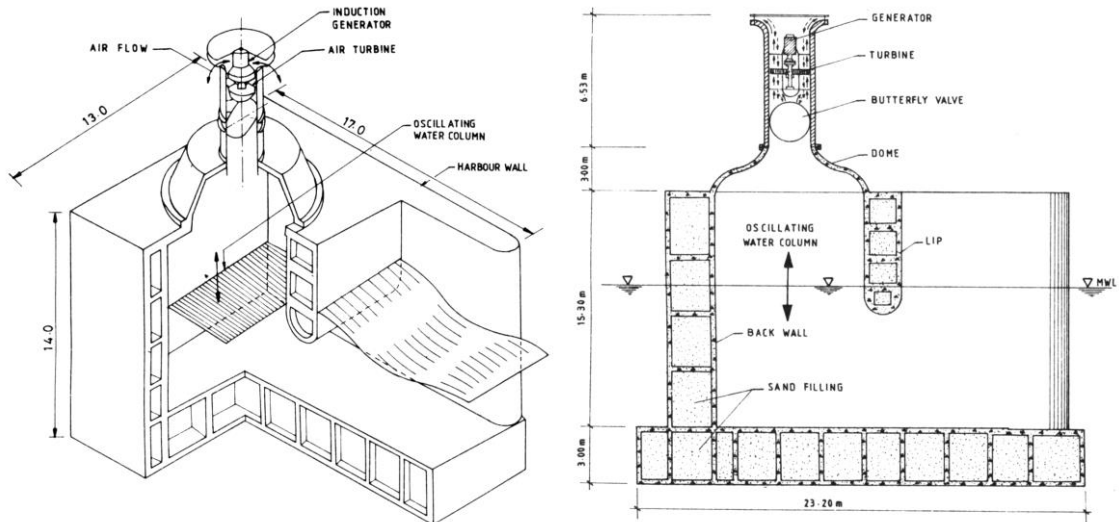


Figure III.9 Axonometric view (left) and section view (right) of the OWC device at Vizhinjam [155].

Based on the same principle, in 2000 the Islay LIMPET (Land Installed Marine Power Energy Transmitter) was installed on the Scottish island of Islay. This plant was realized and operated by Wavegen in cooperation with Queen's University of Belfast. Islay LIMPET was the full-scale version of a previous prototype (75 kW) realized in 1991.



Figure III.10 LIMPET OWC plant installed on the island of Islay (Scotland, UK) [158] (Elsevier license n. 4707221496823)

The envelope of LIMPET was entirely realized in concrete on the shoreline. It was equipped with two Wells turbines, each one with a rated power of 250 kW [134], [158].

The plant was decommissioned in 2012 and today only the concrete building remains on the shoreline.

A similar technology was also developed in Portugal, under the supervision of Instituto Superior Técnico of Lisbon. In 1999 a full scale (400 kW) OWC plant was realized in Pico Island (Azores, Portugal) [158]. Some problems were due to malfunctions of Wells turbine and its support. The project was concluded on January 2018, demonstrating the feasibility of this technology [159].



Figure III.11 Back view of the OWC plant installed on the island of Pico (Azores, Portugal) [158] (Elsevier license n. 4707221496823)



Figure III.12 OWC plant installed in the bay of Mutriku (Spain) [160]

In 2011, an OWC plant was inaugurated in the bay of Mutriku (Spain) (see Figure III.12) [160]. The power plant is 100 m long and has an installed power of 296 kW. It is composed by 16 OWC chambers, each one equipped with a Wells turbine. The producer indicated a total electricity production equal to 1.6 GWh (updated to the end of June 2018) [160].

An OWC system, called REWEC3 (REsonant Wave Energy Converter), has been developed in Italy, by the University of Reggio Calabria. This system is designed to be incorporated into a traditional vertical breaker in the harbour. In comparison with other OWC devices, the main difference is the U-shape connection between the internal chamber and the sea (see Figure III.13 [161]), that is chosen in order to adapt the

resonance frequency of the system to sea wave. Thus, it is possible to maximize the energy extraction [161]. In the port of Civitavecchia, a full scale plant has been installed, composed by 136 chambers and a rated power of 2.5 MW [134]. In 2016 the system, with a length of 100 m, produced 500 MWh/y. After the optimization, the designers want to achieve an annual production of 800 MWh/y.

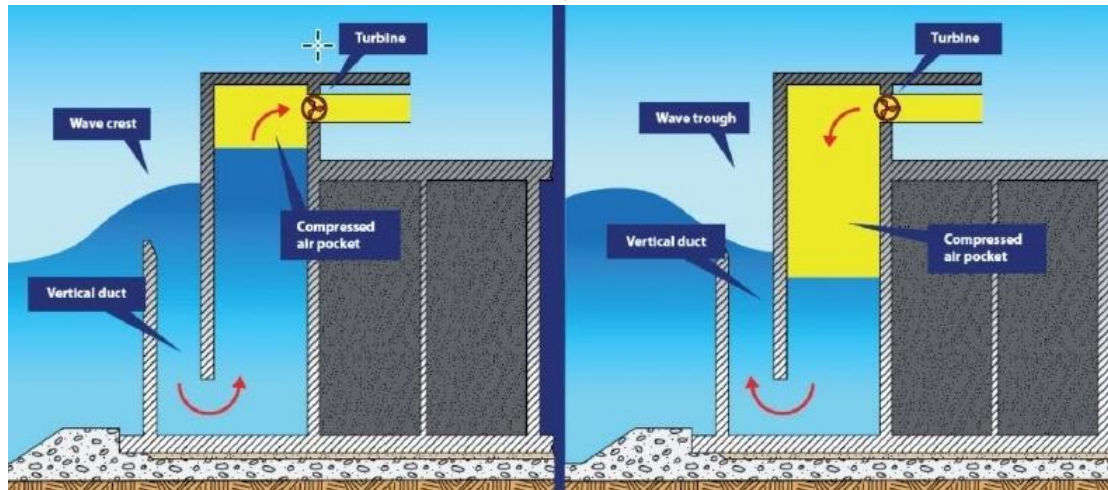


Figure III.13 Working principle of REWEC3 [161].

The Yongsoo plant (see Figure III.14) [134] is another fixed OWC system, that was recently completed near to Jeju Island (Republic of Korea). The system is installed on seabed, at 1 km from the coastline. It is equipped with two horizontal axis impulse turbines, connected to different kinds of generators (a synchronous generator and an induction generator), both with a rated power of 250 kW [134]. The plant has a length of 37 m and a width of 31 m.

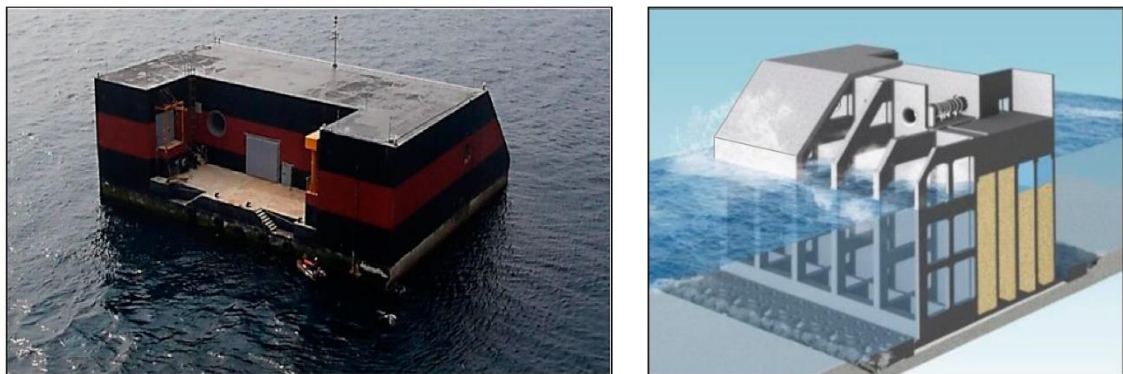


Figure III.14 Back (left) and perspective views (right) of OWC plant at Yongsoo [134] (CC BY 4.0)

The other family of OWC devices is composed by the floating systems. The working principle is the same. The main difference is related to the structure, where the OWC device is installed. Indeed, the most popular solution is represented by the adoption of floating buoys, equipped with chambers used to produce the water oscillation.

One of the first floating OWC was developed in Japan between 1960s and 1970s by the team of Yoshio Masuda. The system, called Backward Bent Duct Buoy (BBDB), is composed by a floating buoy, anchored to seabed and equipped with a L-profiled

chamber [162]. This one is open in the back to the sea, under the water level while in the upper part to the atmosphere, through a Wells turbine, as shown in Figure III.15 [151].

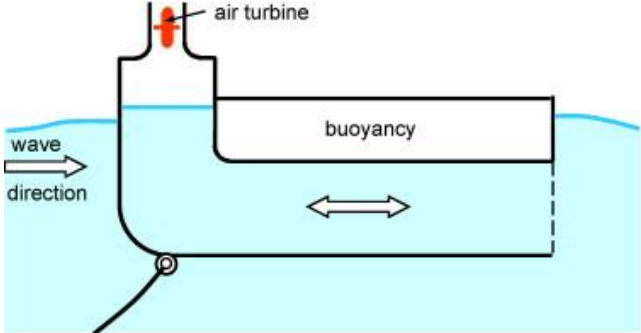


Figure III.15 Section of Backward Bent Duct Buoy [151] (Elsevier license n. 4707220104485)

Some years later, other similar systems were developed. Among these, the best known are Sloped Buoy, Spar Buoy and Mighty Whale, reported in Figure III.16 [163]. In detail the Sloped buoy is composed by three parallel pipes installed on a floating buoy with a tilt angle of 45°. The lower part is open to the sea while the upper part to the atmosphere.

The Spar Buoy is a vertical pipe installed in a floating buoy, that has a cylindrical shape. This aspect improves the energy extraction from sea wave, because the system works independently of wave direction. For this reason, it is classified as Point Absorber.



Figure III.16 Sloped Buoy (left) [163], Spar Buoy (middle) [163] e Mighty Whale (right) [164]

It is interesting to report the case of Mighty Whale, composed by a buoy having a shape like a whale (50 m long and 30 m wide), as shown in Figure III.16 [164], [165]. It was based on OWC and equipped with three Wells turbines, with a total installed power equal to 120 kW [166].

III.3.b Wave-activated bodies

The category of Wave-Activated Bodies (WAB) comprises several kinds of solutions for the sea wave exploitation. These systems are generally composed by two or more parts, arranged in order to produce a relative motion and run the energy converter [167].

These systems are generally designed for a nearshore or offshore installation, in order to exploit the more regular waves of the open sea, in comparison with the systems installed on the coastline. However, the installation far away from the coastline increases the number of problems. Indeed, long underwater cables or pipes are required to transfer the energy collected by the WEC to the mainland. These devices need also a mooring system, strong enough to resist to the extreme weather conditions [168].

Since there is a number of WAB, a classification is introduced by considering the working principle of the device as criterium [151]:

- Single body heaving buoys;
- Two-body heaving systems;
- Fully submerged heaving systems;
- Pitching devices;
- Bottom-hinged systems;
- Many-body systems.

Single Body Heaving Buoys

The first group includes systems composed essentially by a single floating buoy. In case of sea wave, the buoy produces an oscillation that is used by an energy converter to produce electricity.

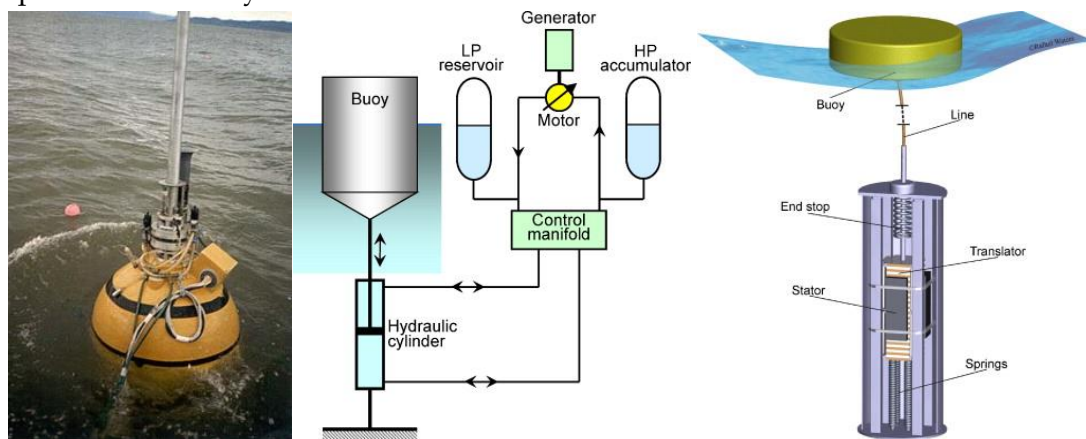


Figure III.17 Norwegian buoy, working principle of Danish buoy and Swedish buoy [151] (Elsevier license n. 4707220104485)

An example was the Norwegian Buoy, shown in Figure III.17 [151], [169], composed essentially by a spherical buoy able to move along a metallic strut anchored to seabed by a universal joint. The idea was the exploitation of this vertical motion to pressurize an air reserve and consequently run an air turbine in a regular way [170]. A prototype, having a buoy one meter diameter, was tested in 1983 in the Trondheim Fjord (Norway), replacing the air turbine with an orifice [151]. In 1990s, a similar device was developed in Denmark. This system was composed by a buoy fixed to a structure on seabed by using a long cable. The relative motion was used to run a piston pump to pressurize water and run a hydro turbine (see Figure III.17). An alternative solution

(Lysekil Project) was developed at Uppsala University (Sweden), installing a linear generator inside a structure fixed to seabed [151], [169].

Two-Body Heaving Buoys

The category “two body heaving systems” was introduced to solve the problem of the distance between the floating buoy and the fixed structure on seabed, where the energy production occurs. In this case, the WEC is composed by two floating buoys in order to produce a relative motion usable to extract energy. The shapes of two floaters are normally different in order to maximize the relative motion.

As shown in Figure III.18 [151], [171], Wavebob is an example of two body heaving system. To improve the relative motion between the two parts of the WEC, the central buoy is equipped with a big mass, increasing the inertia and limiting the vertical motion. The inferior buoy is designed to be submerged at depth enough to minimize the interference with sea wave. The vertical motion produced by the upper buoy (body 1) is used to run an oil pumping system. A small-scale (1:4) prototype was tested in the Galway Bay (Ireland) [151], [171].

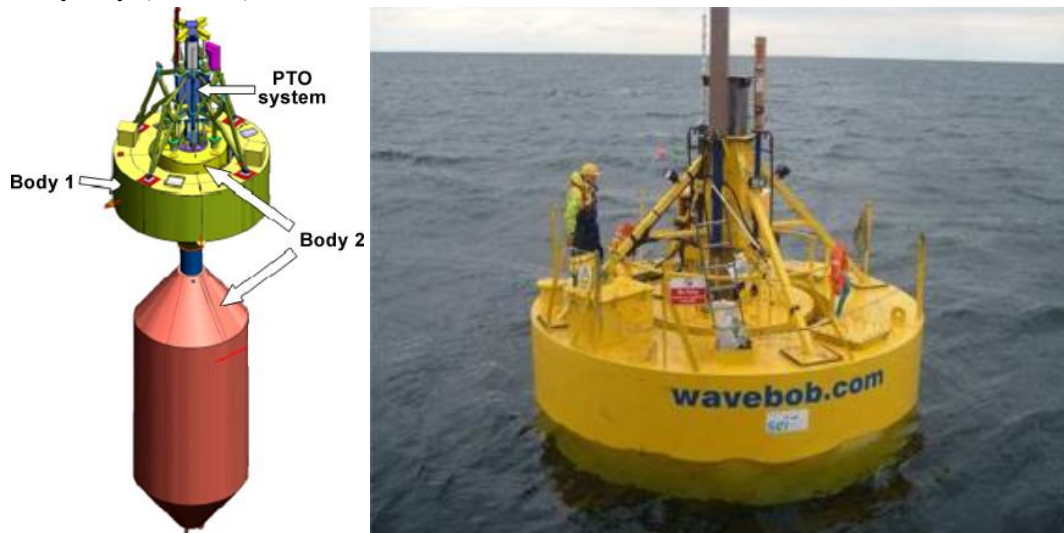


Figure III.18 Rendering view (left) [151] and external view (right) [171] of Wavebob (Elsevier license n. 4707220104485 and 4707231054751)

PowerBuoy is another example of two body heaving system, developed by the American company Ocean Power Technologies. As shown in Figure III.19 [169], [172], this WEC is composed by a floater, that is free to move up and down according to sea wave, and a submerged body, having a disk shape adopted to improve the inertia and hydrodynamic resistance of this part and maximize the relative motion between the two main parts of the device. The idea is the realization of a wave energy farm, installing several devices, each one producing electricity. To minimize the cost of the electrical connection with the mainland, an offshore substation could be realized, as shown in Figure III.19. In 2005 a pilot plant (40 kW) was tested in an offshore site, close to Atlantic City (New Jersey, USA) [169]. In 2008, another plant of the same size was installed off the coast of Santoña (Spain) [151].

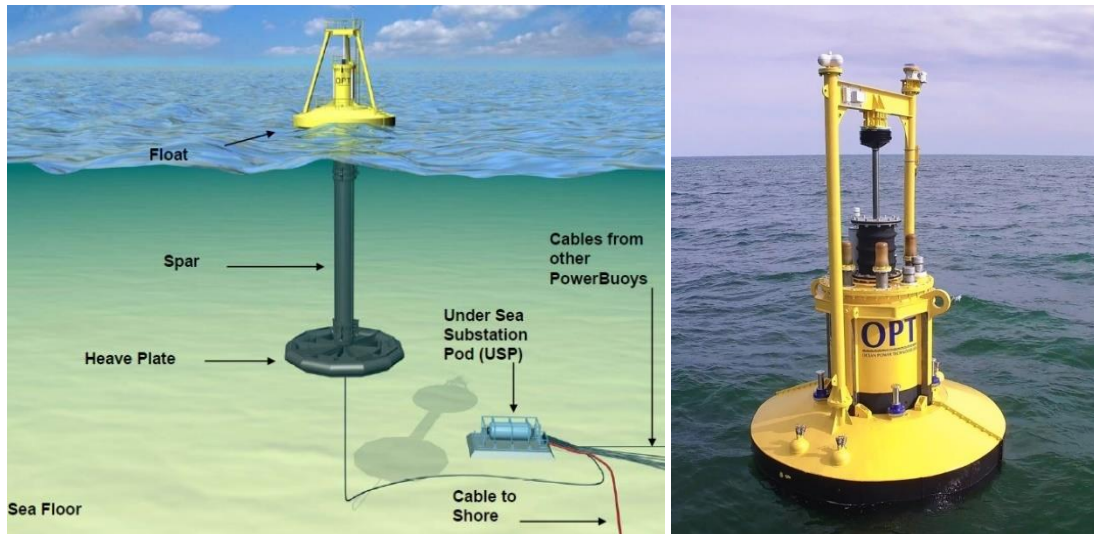


Figure III.19 Principle of operation [169] and external view of PowerBuoy [172] [169] (CC BY-NC-ND 3.0)

Fully Submerged Heaving Systems

About the fully submerged heaving systems, an example is the Archimedes Wave Swing, developed in Holland.

As shown in Figure III.20 [173], the system is composed by two parts: a basement, that is anchored to seabed, and a floater. The device works by using the variation of the hydrostatic pressure applied to the floater, that pushes up and down a linear generator installed inside. In 2004, a pilot plant was tested in Portugal [151].

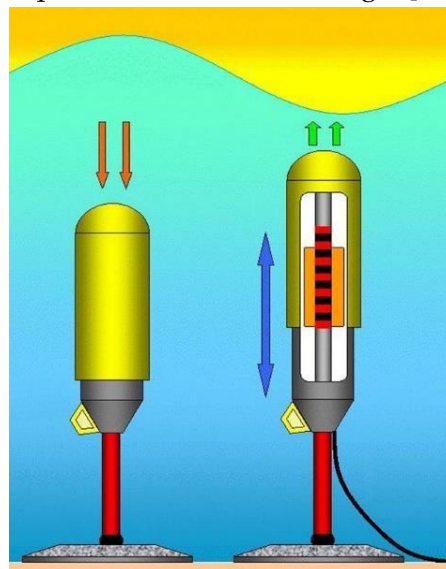


Figure III.20 Working principle of Archimedes Wave Swing [173] (CC BY-NC-SA 3.0)

CETO (name inspired by a Greek ocean goddess) is another full submerged device, proposed by Carnegie Clean Energy. This system is designed to be installed in the nearshore, a few meters below the sea level. The previous version (CETO 5) was designed to pump water for a station located on the coast where electricity and

freshwater are produced, by using a RO unit [174], [175]. The company is currently working on a new device (CETO 6) to produce electricity directly on the WEC.

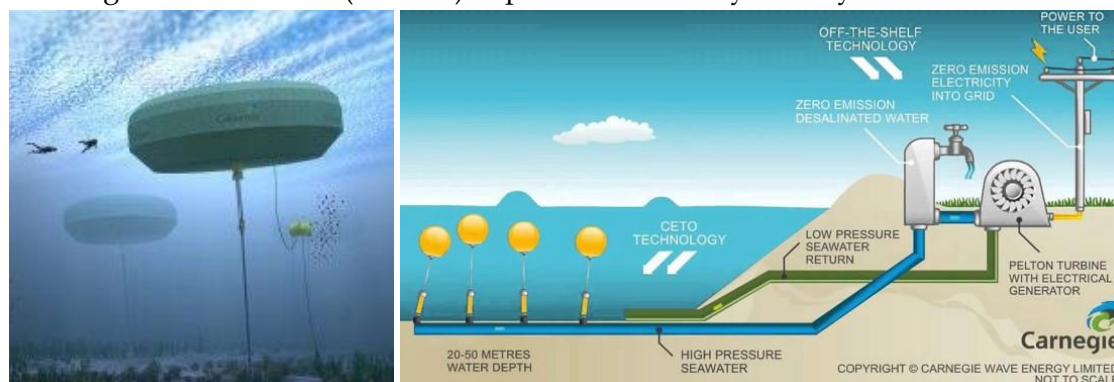


Figure III.21 CETO external view [175] and working principle [174]

Pitching Devices

In the pitching devices, the main motion is a relative rotation (usually pitch) among the parts. A first example was the Salter's Duck (called also the nodding Duck), developed by the team of Prof. Stephen Salter at the University of Edinburg (UK), between 1970s and 1980s. In detail, this device is composed by a floater, having a cam shape (see Figure III.22) [176], [177]. As first solution, a hydraulic pumping system was proposed to convert the rotary motion into electricity. As alternative solution, a gyroscope system was proposed some years later [177].

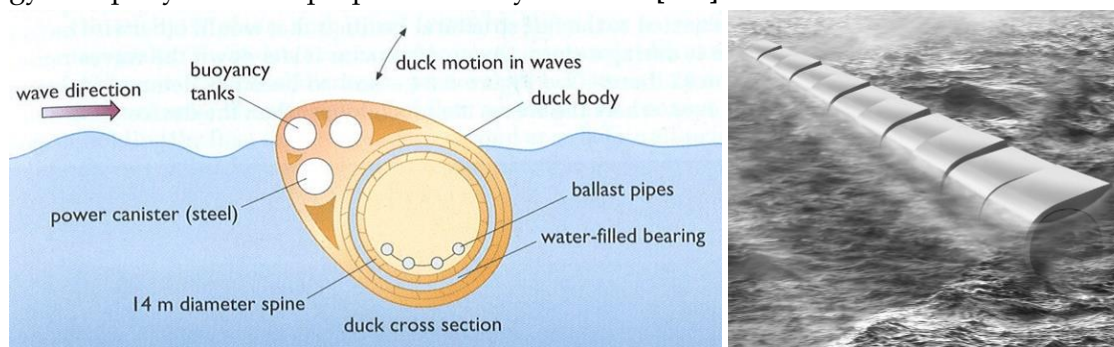


Figure III.22 Salter's Nodding Duck. Section (left) [177] and rendering view (right) [176] (Elsevier license n. 4707240043865)

Pelamis was another famous example of pitching device [151]. It was developed in UK by Scottish company "Pelamis Wave Power Ltd". A first prototype, connected to the electrical grid, was tested in Orkney (Scotland) between 2004 and 2007. In 2008 a wave farm with three devices was installed at Aguçadoura (Portugal). Unluckily, the wave farm worked only for two months due to technical failures, causing financial problems to the company. The intellectual property was transferred to the Scottish government in November 2014. This WEC was composed by four cylindrical buoys, connected by three Power Conversion Modules (PCM), as depicted in Figure III.23 [178], [179].

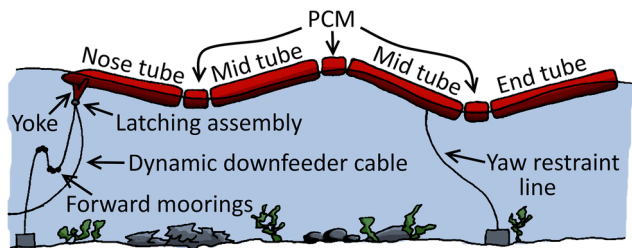


Figure III.23 Working principle [178] (CC BY 4.0) and external view of Pelamis [179]

In detail, the system had a shape like a snake, oriented according to the wave direction, achieving a length of 120 m and a rated power of 750 kW. The working principle of Pelamis was based on the generation of a relative rotation on the PCM, equipped with hinged joints, in order to pump oil at high-pressure into accumulators and then run hydraulic motors coupled with induction generators.

Bottom Hinged Systems

The Bottom Hinged Systems are designed to exploit sea wave in shallow water (10 - 15m), where the sea motion is mainly horizontal. An example is Oyster, that is illustrated in Figure III.24 [180].

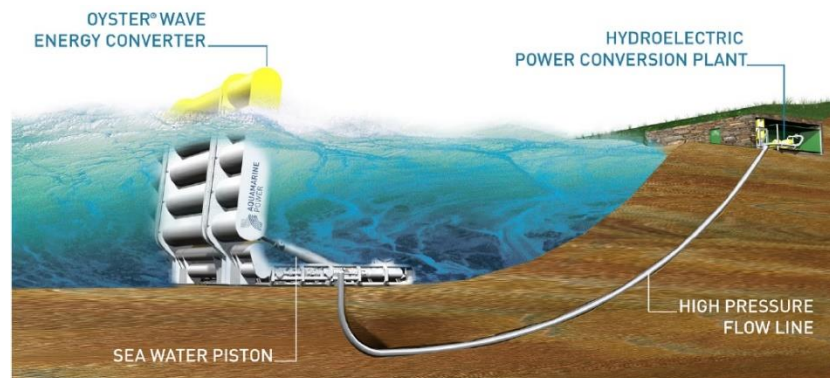


Figure III.24 Working principle of Oyster [180]

This device consists essentially in a barrier, made by five cylinders horizontally stacked. Since the barrier is fixed by a horizontal hinge, the braking wave produces a rotation, activating a high-pressure pump. The pressurized water is conveyed along pipes to the coastline, where hydro turbines and alternators are installed to produce electricity. This kind of WEC was proposed by the team of Professor Trevor Whittaker, from the Queen's University of Belfast. The company Aquamarine Power developed and tested two full-scale plants at the European Marine Energy Centre's Billia Croo test site: Oyster 1 (315 kW) and Oyster 2 (800 kW). The second version was connected to grid in 2012 until 2015, when the company ceased trading [181].

AW Energy (a Finnish company) proposed a similar system called Waveroller (see Figure III.26) [182]. In 2007, a small scale (1:4) prototype was tested in Portugal.

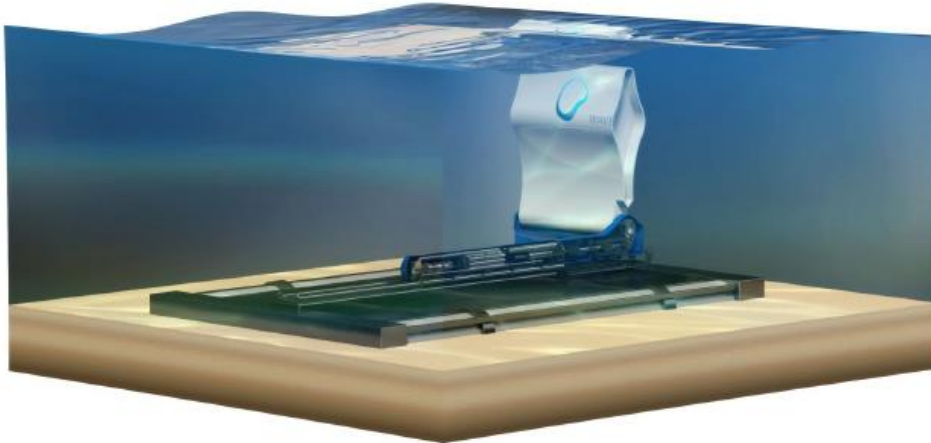


Figure III.25 Rendering view of Waveroller [182]

A full-scale prototype was installed in Järvenpää (Finland) in 2015, in order to optimize the technology. The device is designed to be installed at 0.3 – 2 km from the shoreline, where the sea depth is between 8 and 20 meters. The device has a rated power of 350 kW, equipped with a flap 18 m long and 10 m high. The company is currently working for new projects in Portugal, Mexico and Southeast Asia [182].

Many-body systems

Wavestar is an example of many-body systems [151]. The first study on this device was started in 2000 by Niels and Keld Hansen in Denmark. A small-scale prototype (1:40) was tested in 2004 at the laboratory of Aalborg University. In 2005, a grid connected small scale (1:10) pilot plant was installed at Nissum Bredning. Finally, in 2009 a 1:2 scale prototype was connected to grid in Hanstholm. The plant was taken down in 2013 [183]. Like other systems described above, Wavestar uses the relative rotation of the buoys to pump oil at high-pressure and runs hydraulic motors [151].

The researchers are currently working on the full scale of the device. As shown in Figure III.26 [183], [184], Wavestar is composed by 20 buoys (10 m diameter), arranged in two lines, and able to extract until 6 MW according to the climatic conditions of the North Sea. The system could be also assembled with a star shape, using 60 buoys and achieving a total rated power of 18 MW [183], [184].



Figure III.26 Rendering view of Wavestar [183], [184]

The same working principle can be applied along the coastline and the breakers of the harbours. An example is the EcoWave System, composed by several floaters, which rise and fall according to the hydrodynamic interaction with sea wave.

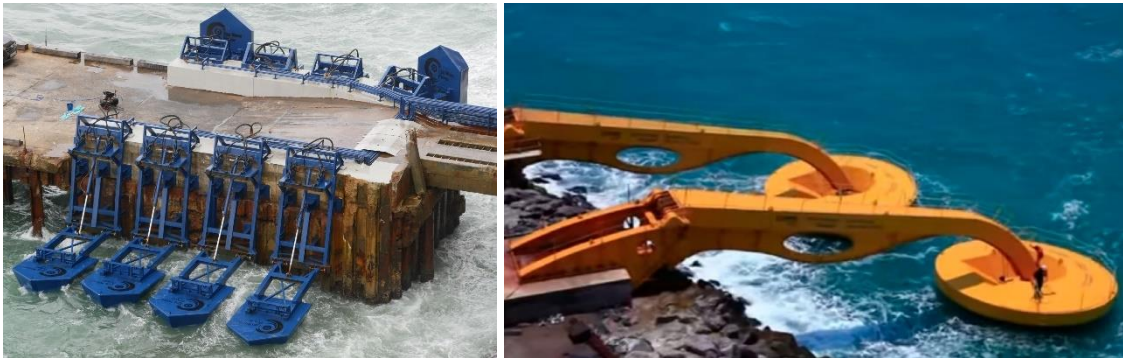


Figure III.27 Eco Wave Systems (left) [185] and Seahorse power take off system (right) [186]

Using robust arms, the system pressurizes a fluid to run a generator installed on the coastline (see Figure III.27 on the left) [185]. In 2016 a wave farm was opened at Gibraltar, located at the southern tip of the Iberian Peninsula. The plant has currently a rated power of 100 kW but it is planned to achieve 5 MW of installed power [134].

Based on the same approach, the Seahorse system (50 kW) was installed in 2012 at the Port of Pecem (Brazil) [134], [186]. The device was developed by the Federal University of Rio de Janeiro and is composed by two arms, each one equipped with a circular buoy (see Figure III.27 on the right) [134], [186].

III.3.c Overtopping device

In the Overtopping Devices (OD), the exploitation of sea wave is based on the conversion of the kinetic energy of water into potential energy, usable by a low head hydro turbine.

An artificial water reserve should be created at a level superior than the sea level. To refill the system, a ramp is required to convey sea wave inside the water reserve. Historically, the first OD pilot plant was the Tapchan (Tapered Channel Wave Power Device), realized at Toftestallen (Norway) in 1985 (see Figure III.28) [151], [187]. The collector was carved into a rocky cliff, realizing an entrance about 60 m wide and lifting water up into a reservoir 3 m above sea level and with a surface of 8500 m². To convert the potential energy into electricity, a low-head Kaplan-type hydro turbine was adopted, having a rated power of 350 kW. This plant was damaged by the storm in 1988. The plant was decommissioned in 1991.

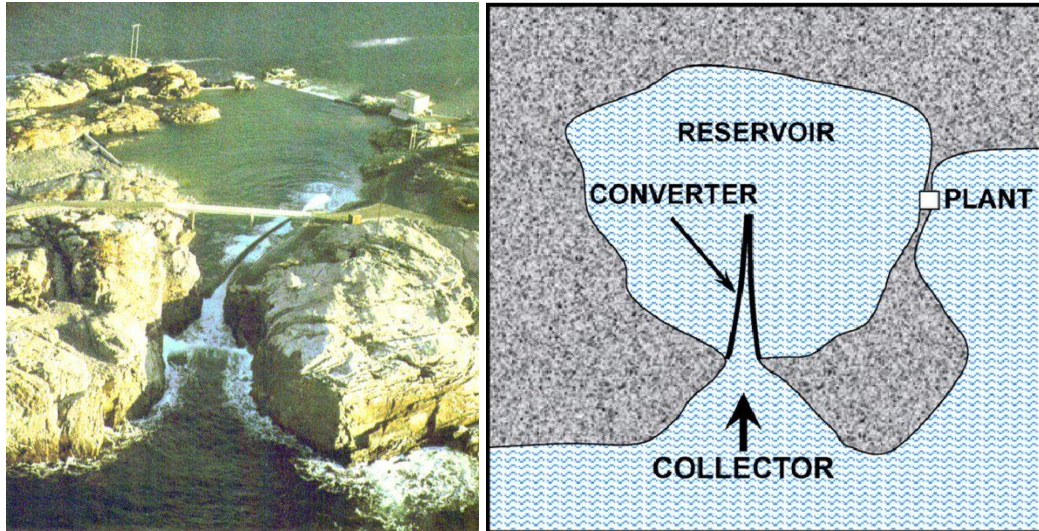


Figure III.28 View (left) [187] and schematic plan view (left) [151] of Tapchan (Elsevier license n. 4707220104485)

It is also possible to realize an OD for an offshore application. As an example, the Wave Dragon was a floating slack moored WEC, developed by the Danish company “Wave Dragon Aps”. In March 2003 a 20 kW prototype (scale 1:4.5) was installed and tested in the Nissum Bredning fjord until January 2005 [188]. Another pilot plant (4 MW) was installed in 2006 and scrapped in 2011.

In detail, Wave Dragon is composed by a floating water reserve, refilled with sea wave by using two reflectors (see Figure III.29) [151], [189] and a ramp to convert the kinetic energy into potential energy through the increasing of water level [189]. This kind of energy can be used by Kaplan turbines to run permanent magnets rotary generators. To work properly, the system should be fixed to seabed by moorings and faced to the wave direction [169].



Figure III.29 Views of the small scale Wave dragon (left) [151] and its working principle (right) [189] (Elsevier license n. 4707220104485 and 4707240446626)

The last OD project is called Seawave Slot-Cone Generator, depicted in Figure III.30 [134], [190]. This system is designed for an onshore installation.



Figure III.30 External view (left) [134] and section view (right) [190] of Slot-Cone (CC BY 4.0).

In detail the system is composed by three chambers, located at different heights. Each chamber has an opening, located at the superior point. The system has externally a ramp shape, in order to increase the water height and fill the internal chambers. A multistage low-head hydro turbine is adopted to transform the potential energy of water inside each chamber into electricity.

Two pilot plants have been planned for the realization along the west Norwegian coasts [190].

III.3.d Power Take Off

As reported in the previous paragraphs, there are several technologies under investigation for the exploitation of the wave energy potential.

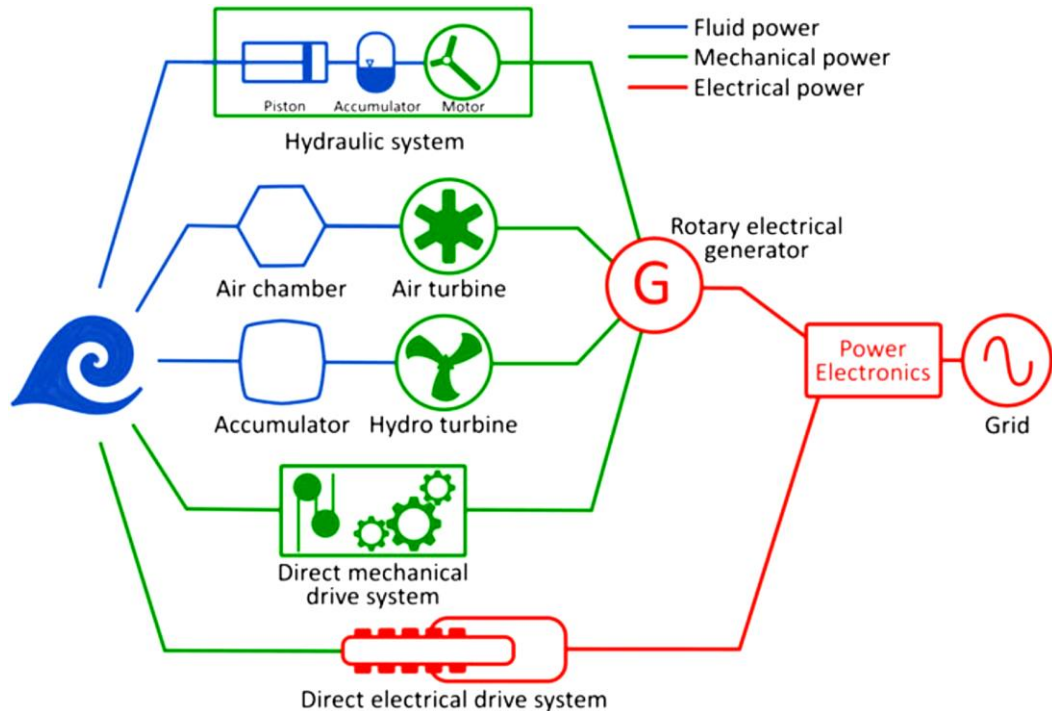


Figure III.31 Different paths for WEC systems [191] (CC BY-NC 4.0)

The main component of a sea wave energy converter is defined as Power Take Off (PTO), that is the mechanism used to transfer the mechanical energy of wave to the electrical energy generator [191].

As suggested by Figure III.31, the energy transmission from buoys to the energy generators can be performed in different ways, in particular:

- **High pressure oil hydraulic systems.** In this case, WEC is designed to produce a relative motion among the main components in order to run a piston pump to pressurize a fluid (normally oil). From the high-pressure tank the fluid is spilled to run a hydraulic motor, coupled with alternators in order to produce the electrical energy. This approach is normally adopted in the wave-activated buoys WEC.
- **Air turbine systems.** As described in paragraph III.3.a on OWC systems, in this case sea wave enters and leaves a chamber open to sea under the water level. The alternative motion of the wave produces the pressurization and the depressurization of the chamber, forcing the air flow through an air turbine. The main problem is related to the fact that the air flow is bidirectional, so the air turbine must be designed in order to rotate in the same direction independently of the air flow. The Wells turbine is the most popular solution, coupled with alternator to produces electrical energy.
- **Low head water turbine systems.** As explained in the paragraph III.3.c on the overtopping devices, a possible solution to exploit the sea wave energy is the recovery of the kinetic energy of the wave, transforming it into potential energy. The water of sea wave is conveyed inside a reservoir, installed at a quote higher than the sea level, thanks to the adoption of ramps. The potential energy of the water stored in the reserve can be used by a low-head water turbine, coupled with alternators, in order to produce electrical energy.
- **Mechanical motion converting systems.** In this case the relative motion (linear or rotary) is transformed into a unidirectional rotary motion, in order to run alternators to produce electrical energy.
- **Direct electrical producing systems.** In this technique, the WEC devices are designed to produce a bidirectional motion directly usable by linear generators in order to obtain electrical energy.

Table III.3 Average values of the energy efficiency of PTO [191].

PTO system	Efficiency (%)
Hydraulic	65
Air	55
Water	85
Mechanical	90
Direct drive	95

As introduced in the first chapter, in this thesis an innovative linear generator is designed and proposed as PTO for a WEC. Indeed, as shown in Table III.3, the adoption of direct drive systems could allow the achievement of high energy efficiency [191].

For this reason, in the next chapter a prototype already analyzed in a previous research is presented. Geometrical changes are introduced in order to improve the

power output and limit disturbing phenomena, like the cogging force. The proposal of a WEC is also presented.

A lumped-parameters model is introduced, in order to realize a preliminary energy assessment of the energy production in different sea wave conditions.

III.4 Publications on this topic

- V. Franzitta, D. Curto, D. Milone, and D. Rao, "Assessment of Renewable Sources for the Energy Consumption in Malta in the Mediterranean Sea," *Energies*, vol. 9, no. 12, p. 1034, Dec. 2016.
- V. Franzitta, D. Curto, D. Rao, and A. Viola, "Hydrogen Production from Sea Wave for Alternative Energy Vehicles for Public Transport in Trapani (Italy)," *Energies*, vol. 9, no. 10, p. 850, Oct. 2016.
- V. Franzitta, D. Curto, D. Milone, and A. Viola, "The desalination process driven by wave energy: A challenge for the future," *Energies*, vol. 9, no. 12, pp. 1–16, Dec. 2016.
- V. Franzitta and D. Curto, "Sustainability of the Renewable Energy Extraction Close to the Mediterranean Islands," *Energies*, vol. 10, no. 4, p. 283, Feb. 2017.
- A. Viola, V. Franzitta, M. Trapanese, and D. Curto, "Nexus Water & Energy: A Case Study of Wave Energy Converters (WECs) to Desalination Applications in Sicily," *Int. J. Heat Technol.*, vol. 34, no. Special Issue 2, pp. S379–S386, Oct. 2016.
- V. Franzitta, D. Rao, D. Curto, and A. Viola, "Greening island: renewable energies mix to satisfy electrical needs of Pantelleria in Mediterranean Sea," in *OCEANS 2016 MTS/IEEE Monterey*, 2016, pp. 1–6.
- A. Viola, D. Curto, V. Franzitta, and M. Trapanese, "Sea water desalination and energy consumption: A case study of wave energy converters (WEC) to desalination applications in Sicily," in *OCEANS 2016 MTS/IEEE Monterey*, 2016, pp. 1–5.
- M. Trapanese, F. Raimondi, D. Curto, and A. Viola, "Evaluation of the wave energy density on the Sicilian coast," in *OCEANS 2016 - Shanghai*, 2016, pp. 1–4.
- V. Franzitta, D. Curto, D. Rao, and D. Milone, "Near zero energy island with sea wave energy: The case study of Pantelleria in Mediterranean Sea," in *OCEANS 2016 - Shanghai*, 2016, pp. 1–5.
- V. Franzitta, D. Curto, D. Rao, and A. Viola, "Renewable energy sources to fulfill the global energy needs of a country: The case study of Malta in Mediterranean Sea," in *OCEANS 2016 - Shanghai*, 2016, no. 2012, pp. 1–5.
- V. Franzitta, D. Curto, and D. Rao, "Energetic Sustainability Using Renewable Energies in the Mediterranean Sea," *Sustainability*, vol. 8, no. 11, p. 1164, Nov. 2016.

- V. Franzitta, A. Colucci, D. Curto, V. Di Dio, and M. Trapanese, "A linear generator for a waveroller power device," in *OCEANS 2017 - Aberdeen*, 2017, pp. 1-5.
- V. Franzitta, D. Curto, A. Viola, V. Di Dio, V. Boscaino, and M. Trapanese, "Guidelines proposal for a good and durable WEC design," in *OCEANS 2017 - Aberdeen*, 2017, pp. 1-7.
- D. Curto and M. Trapanese, "Experimental tests on hydrogen production from sea waves energy," in *OCEANS - Anchorage*, 2017, 2017, pp. 1-5.
- V. Franzitta, P. Catrini, and D. Curto, "Wave Energy Assessment along Sicilian Coastline, Based on DEIM Point Absorber," *Energies*, vol. 10, no. 3, p. 376, Mar. 2017.
- V. Franzitta, D. Curto, D. Milone, and M. Trapanese, "Energy Saving in Public Transport Using Renewable Energy," *Sustainability*, vol. 9, no. 1, p. 106, Jan. 2017.
- D. Curto and M. Trapanese, "A Renewable Energy mix to Supply the Balearic Islands: Sea Wave, Wind and Solar," in *2018 IEEE International Conference on Environment and Electrical Engineering and 2018 IEEE Industrial and Commercial Power Systems Europe (EEEIC/I&CPS Europe)*, 2018, pp. 1-6.
- F. M. Raimondi, D. Milone, and D. Curto, "An innovative mechanical motion converter for sea wave applications," in *2018 Thirteenth International Conference on Ecological Vehicles and Renewable Energies (EVER)*, 2018, pp. 1-6.
- D. Curto, S. Neugebauer, A. Viola, M. Traverso, V. Franzitta, and M. Trapanese, "First Life Cycle Impact Considerations of Two Wave Energy Converters," in *2018 OCEANS - MTS/IEEE Kobe Techno-Oceans (OTO)*, 2018, pp. 1-5.
- D. Curto, V. Franzitta, A. Viola, M. Cirrincione, A. Mohammadi, and A. Kumar, "A renewable energy mix to supply small islands. A comparative study applied to Balearic Islands and Fiji," *J. Clean. Prod.*, p. 118356, Sep. 2019.
- M. Trapanese, V. Boscaino, G. Cipriani, D. Curto, V. Di Dio, and V. Franzitta, "A Permanent Magnet Linear Generator for the Enhancement of the Reliability of a Wave Energy Conversion System," *IEEE Trans. Ind. Electron.*, vol. 0046, no. c, pp. 1-1, 2018.

IV SOLUTIONS FOR SEA WAVE EXPLOITATION

In the previous chapters, the current technologies for the utilization of sea as energy and water sources have been presented.

As reported in the introduction, this work was focused on the exploitation of sea wave as renewable energy source. Desalination represents a possible electrical load that can be supplied by sea wave, solving two problems at the same time: the production of freshwater in area affected by water scarcity, such as small islands, and the balance of the electrical grid. Indeed, desalination plants could be managed in a flexible way and supplied by aleatory renewable energy sources, helping the stability control of the local electrical grid.

This chapter shows the proposal of innovative energy converters that could be used as Power Take Off in sea wave application in order to produce electricity.

In detail, the main solution is based on the adoption of linear generators, a machine able to produce electricity by using the mechanical energy introduced in the form of a bidirectional linear motion.

As reported in literature, the adoption of linear generation reduces the numbers of energy conversion steps to the minimum, increasing the energy efficiency of the entire energy conversion chain. At the same time, the limited numbers of components could increase also the reliability of the wave energy converter [191]. For this reason, the development of linear generators is considered. In the end of the chapter, an alternative solution is also presented, suggesting the realization of a mechanical motion converter. This system transforms a directional linear motion into a unidirectional rotary motion, in order to run a commercial multipolar alternator and produce electrical energy.

The following introduction on linear generators was published in the paper “**A New Solution for Sea Wave Energy Harvesting, the Proposal of an Ironless Linear Generator**” in *Journal of Marine Science and Engineering* [192].

IV.1 Introduction on linear generators

In electrotechnics the term “generator” is associated to a machine able to convert mechanical energy into electrical energy. Classifications are introduced, considering different aspects, like the type of motion (rotary or linear), type of current (alternative current or direct current), way to produce the magnetic field (permanent magnets or field coils), number of magnetic poles, presence or absence of synchronization between the electrical frequency and the angular speed of the generator (synchronous or asynchronous machine) [193].

While rotary machines have been well developed from a long time, linear generators still need a significant improvement, because the limited application of these systems [194].

It is interesting to observe that the rotary machines are designed to work in steady state regime at a fixed angular speed (for example 1500 rpm in case of a two pairs pole alternator supplying a 50 Hz electrical grid), while linear generators have to work in a non-steady condition because of the nature of the input motion. The first kind of motion is very popular in the energy sector, since most of the energy sources are exploited by primary motors that produce a rotary motion, such as wind and hydro turbines, internal combustion engines, steam and gas turbines.

The adoption of rotary machine is also under investigation in sea wave application, as shown in the previous chapter. An alternative solution is represented by the adoption of linear generators, having the benefits to limit the number of components required for the energy conversion chain. Focusing on the electrical machine, rotary generators and motors are composed by a stator (the fixed part) and a rotor (the movable part, that turns around the axis). In the same way, linear machines are composed by two parts: the stator (fixed) and the translator (the component subjected to a bidirectional linear motion).

From a conceptual point of view, it is possible to obtain a linear machine, making a cut along the axis of the rotary machine and then unrolling the system in order to obtain a planar configuration, as shown in Figure IV.1. According to the type of cut, it is possible to obtain different geometries [193].

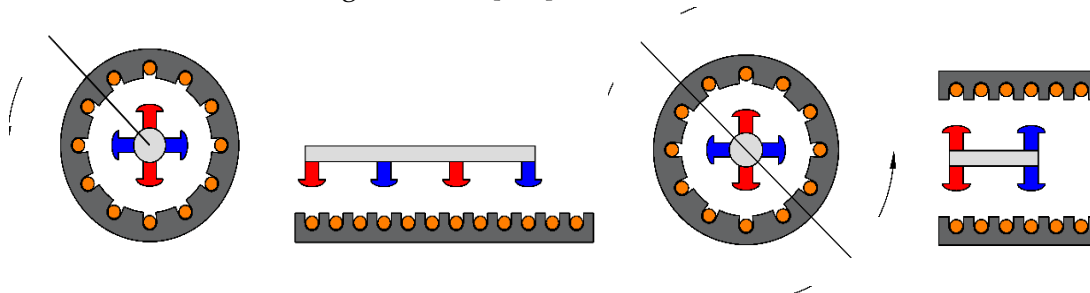


Figure IV.1 Linear machine from a rotary machine

A detailed classification of linear generators is reported in [195]. About linear generators equipped with permanent magnets, the following topologies can be adopted:

- Considering the shape of the generator
 - Structure of generator
 - *Flat structure* (generator having a shape like the example in Figure IV.1) vs. *tubular structure* (stator and translator are designed in order to have an axial symmetry, like two coaxial cylinders).
 - Length of translator in comparison with the stator
 - *Long translator* (if the translator is longer than the stator) vs. *short translator* (in the other case).
 - Position of translator in comparison with the stator
 - *External translator* (if the translator moves in a region outside the stator) vs. *internal translator* (if the translator is installed inside the stator region).

- Place where the permanent magnets are installed
 - *Stator PM* (if magnets are installed on the stator) vs. *translator PM* (if magnets are located on the translator).
- Flux Path
 - Installation of permanent magnets
 - *Radial, axial, Halbach and quasi-Halbach*. Considering a tubular generator, in the radial scheme, PM are magnetized along the radius. Poles are alternated as reported in Figure IV.2. In the axial configuration, PM are magnetized along the same axis of the translator. In the Halbach scheme, PM are magnetized along the axis, but are oriented in order to oppose the same poles. To assemble the stator, a ferromagnetic material is installed between the magnets. As effect, the resulting magnetic field is oriented in the radial direction. Finally, in the quasi-Halbach configuration, axial and radial magnets are alternated, in order to minimize the magnetic field inside the translator and maximize outside.
 - Position of winding with respect to the translator motion
 - *Transverse Flux* (if the flux path through coils is perpendicular in comparison with the translator motion) vs. *Longitudinal Flux* (if the flux path is parallel).
- Core Type
 - *Iron-cored* (the stator is realized with a ferromagnetic material) vs. *Air-cored* (the stator is with a non-magnetic material, equivalent to air)

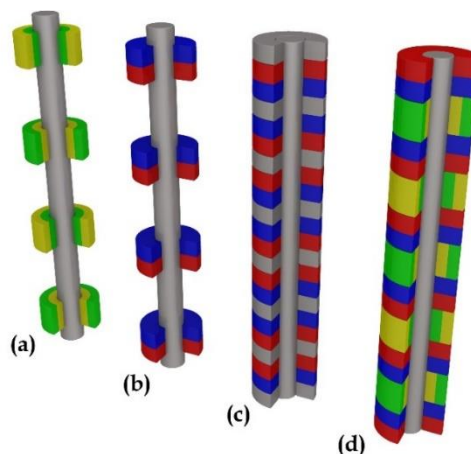


Figure IV.2 Different magnetization schemes
(a) Radial, (b) Axial, (c) Halbach, (d) Quasi-Halbach

Finally, in literature another kind of generator is investigated: *linear switched reluctance generator*. In this case, the magnetization is realized by coils, that require a control system, function of the translator position [193].

IV.2 The starting point: the prototype of linear generator

As introduced before, in this thesis the development of a linear permanent magnet generator is presented. A small-scale prototype was realized at the University of Palermo and partially investigated for my Master Decree Thesis. Thus, in this section it is useful to present the features of this machine, in order to better understand the aspects investigated during the Ph.D. researches.

In Figure IV.3 the geometric details of the stator are reported. This part is split in two symmetrical blocks, obtained by overlapping 126 AISI 1008 sheets, achieving a total height of 65 mm. Each sheet has a size of 972 mm (length) and 60 mm (width) and is cut by laser in order to realize the several holes required to assemble the stator with bolts and threaded bars and install the coils. In detail, each block has 8 holes, used to assemble the stator, and 39 slots for the installation of 36 coils.

This machine was originally designed according to the short translator configuration. For this reason, it was possible to reduce the width of the first three and the last three slots, where only a single coil takes place. Indeed, as reported in Figure IV.3, these slots have a width of 8 mm while the other 30 internal slots are 12 mm wide. All teeth have a width of 13.5 mm.

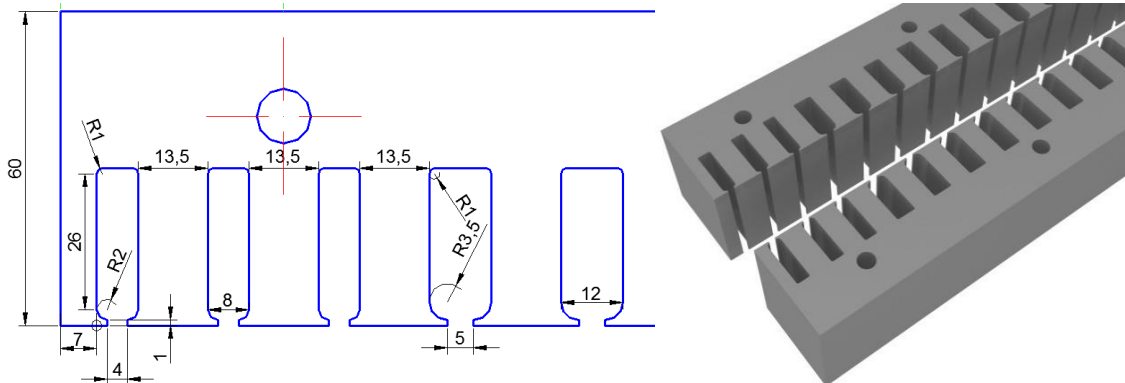


Figure IV.3 Stator details

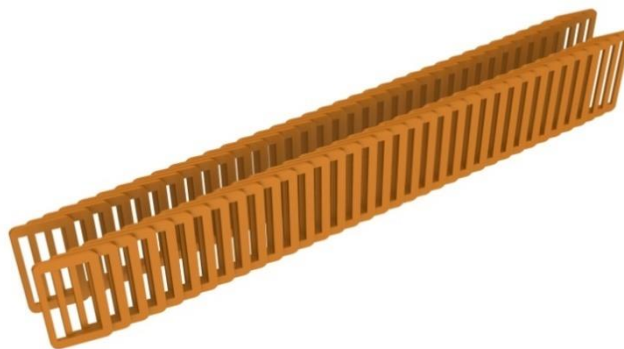


Figure IV.4 Coils shape

Coils are realized in enameled copper, 0.5 mm diameter. Each coil is composed by 375 turns having a rectangular shape (averagely 85x135 mm), for a total mass of 278 g.

All coils end on the terminal plate, installed in the upper part of the device, through which is possible to adopt different schemes of connection.

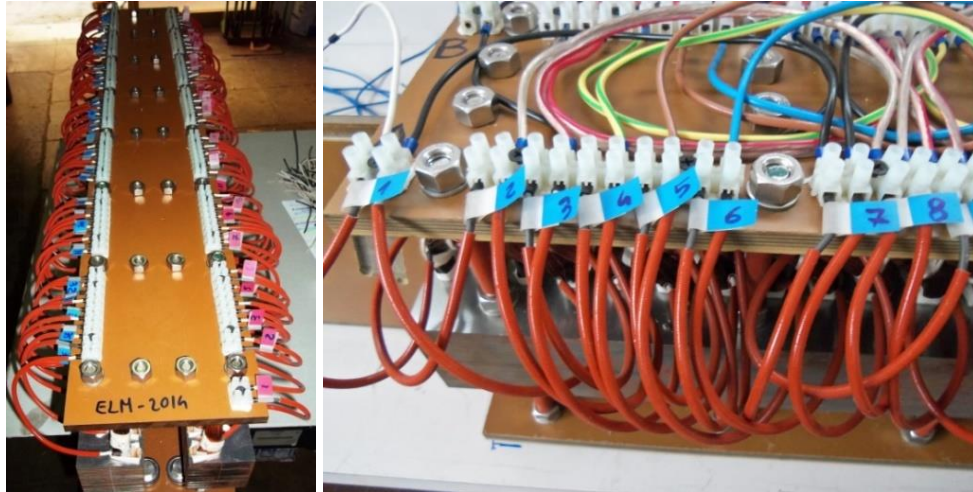


Figure IV.5 Terminal plate

The linear generator is assembled by using also two bakelite sheets, on which four lines of bearing are installed, allowing the relative motion between the translator and the stator (see Figure IV.6). Overall, the stator has a mass of 74.5 kg, with a parallelepipedal shape having the sizes of 972 mm long, 260 mm high and 160 mm wide.

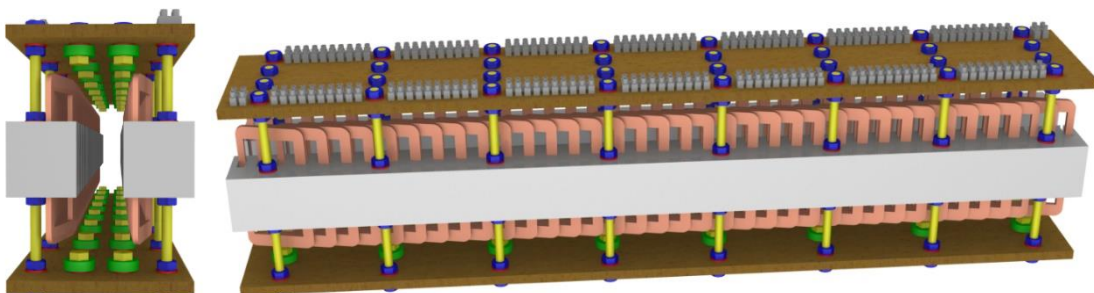


Figure IV.6 Lateral and front views of the stator

The other main component is the translator, that consists of a bakelite sheet where 12 permanent magnets are installed, as shown in Figure IV.7 (left). Indeed, the sheet was shaped in order to allow the installation of 40 magnets (see Figure IV.7 right). The translator has a mass of 7.25 kg in the first case, 13 kg in the latter one. The sheet has the following sizes: 1.6 m long, 11 mm wide and 20.5 cm high.

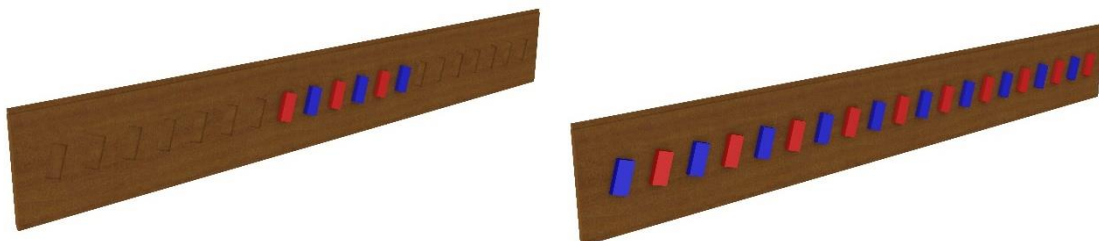
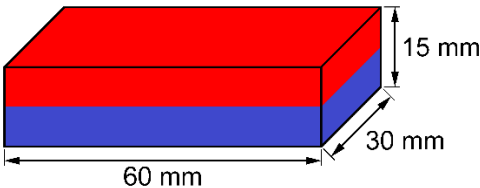


Figure IV.7 Rendering view of the translator

The translator presents a groove along the long edge, in order to slide through the bearings mounted on the stator. About the magnets, the main properties are reported in Table IV.1 [196].

Table IV.1 Main properties of the permanent magnets

Parameter	Value
Sigle	Q-60-30-15-N
Sizes	60 x 30 x 15 mm
Pole faces	60 x 30 mm
Size tolerance	±0.1 mm
Material	Nd-Fe-B
Coating	Nickel plated (Ni-Cu-Ni)
Direction of magnetization	Along the shortest size
Magnetization	N40
Strength	549 N
Weight	205.2 g
Maximal working temperature	80°C
Curie temperature	310°C
Residual magnetization Br	1.26 ÷ 1.29 T
Coercive field strength bHc	860 ÷ 955 kA/m
Coercive field strength iHc	≥ 955 kA/m
Energy product (BxH) max	303 ÷ 318 kJ/m ³



Finally, it is important to underline that the PM are installed with a tilt angle of 17° clockwise. This value was obtained in the previous study on the minimization of the cogging force due to the interaction between teeth, slots and magnets.

IV.2.a No load voltage simulation

The geometry of the device was initially implemented during the previous research for my Master Decree Thesis. In this section it is useful to report just the results from that simulations and the following experimental test used to validate the model.

The prototype was preliminary simulated on Ansys Maxwell, a specific Finite Element Method (FEM) tool for electromagnetic investigations.

The generator was initially connected according to the scheme reported in Figure IV.8, obtaining six phases for each block of the stator. Each line is equipped with six coils series connected.

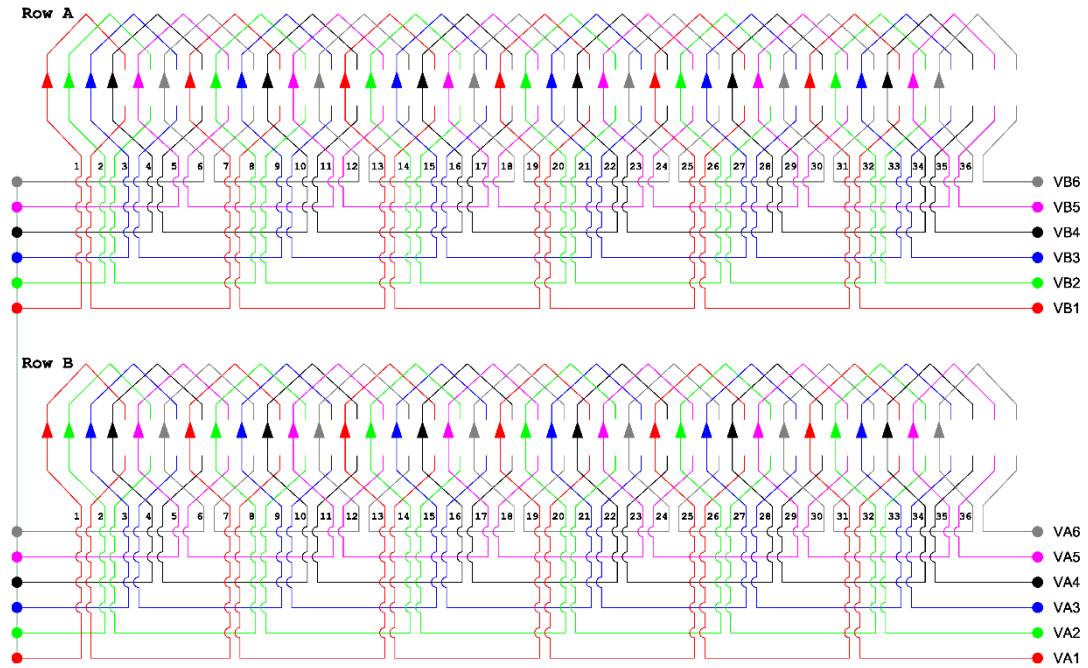


Figure IV.8 Coils connection scheme in six lines

In the FEM tool, the no-load voltage trend was simulated in the case of a linear motion applied to the translator, assuming a constant speed of 1 m/s and a total movement of 54.4 cm. This motion corresponds to the maximal distance covered by a 12 PM translator, keeping all magnets inside the stator region. The simulation was performed, collecting data with a timestep of 0.08 s and saving separately the induced voltage produced by each coil. In this way, the results from the simulation can be arranged in order to obtain the total equivalent voltage trends, available at the terminals of the generator, as sum of the single induced voltages, according to the preferred connecting scheme (as example see Figure IV.8).

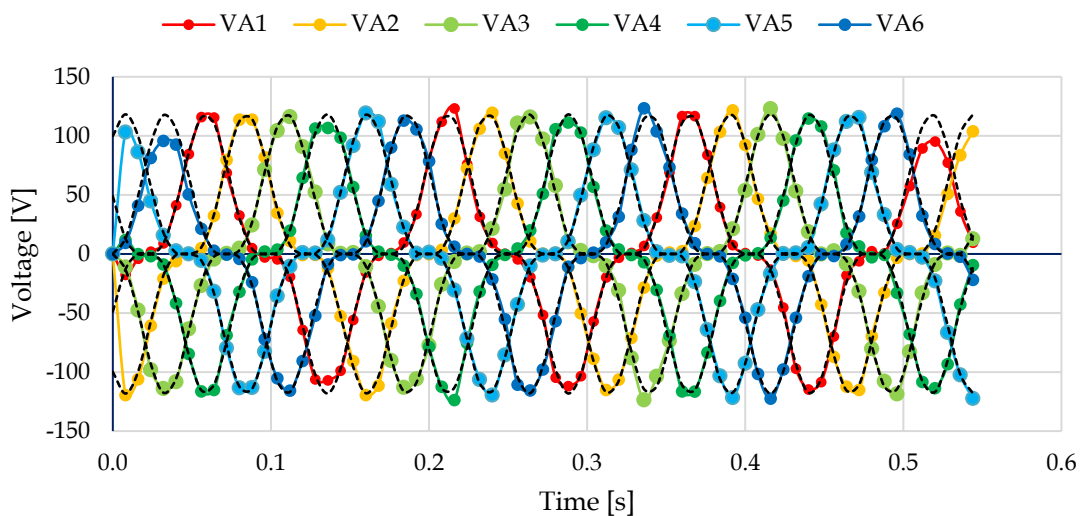


Figure IV.9 No-load voltage trends on the stator block A, at a speed of 1 m/s

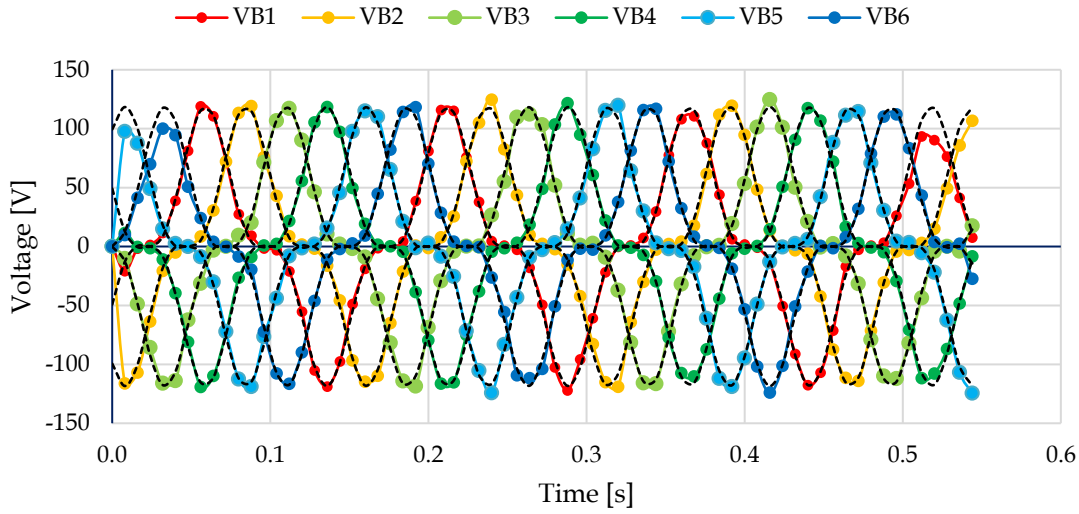


Figure IV.10 No-load voltage trends on the stator block B, at a speed of 1 m/s

The no-load voltages trends of both stator blocks are reported in Figure IV.9 and Figure IV.10. The comparison of the graphs reveals similar values of the corresponding lines (example VA1 and VB1). Since in the step between two magnets with the same pole there are exactly six coils, for each trend is possible to find another one that is in the opposite phase (example VA1 and VA4).

Since the simulation is realized at a fixed speed, the signals above reported are characterized by a frequency given by the following relation, where v is the speed of the translator and λ_m the step between two magnets having the same pole.

$$f = \frac{v}{\lambda_m} \quad IV.1$$

In the stator of the prototype $\lambda_m = 0.153m$, thus in the simulation above reported the frequency of the voltages is equal to 6.536 Hz.

The Fourier series was performed in both stator blocks, evaluation the coefficients by considering the following relation among the six voltage trends reported in Figure IV.9 and Figure IV.10:

$$V_i(t) = A_0 + \sum_{j=1}^n A_j \sin \left[j\omega t + \theta_j + (i-1) \frac{j\pi}{3} \right] \quad IV.2$$

Where A and θ are the amplitude and the phase of the j -th harmonic. The angular frequency is given by the relation:

$$\omega = 2\pi f \quad IV.3$$

The results of the Fourier series are reported in Table IV.2. The calculation was performed considering only the data in the interval 0.040 s to 0.054 s in order to remove the signal distortions due to:

- Initial condition imposed to the voltage trend
- Different width of the first three and last three coils in the stator.

Both aspects are visible in Figure IV.9 and Figure IV.10.

Table IV.2 Fourier series coefficients of no-load voltage trends in the prototype

Harmonic	Block A		Block B		Average signal	
	Amplitude	Phase	Amplitude	Phase	Amplitude	Phase
0	-0.151		-0.174		-0.163	
1	87.543	-0.850	87.440	-0.853	87.491	-0.852
2	0.096	-0.704	0.126	-0.505	0.110	-0.591
3	30.629	0.590	30.917	0.571	30.771	0.581
4	0.118	-1.347	0.117	-1.415	0.118	-1.381
5	0.747	2.263	1.572	1.906	1.144	2.020
6	0.121	0.662	0.148	0.365	0.133	0.499
7	0.516	0.447	0.116	-1.131	0.264	0.225
8	0.040	1.848	0.137	2.305	0.087	2.202
9	0.446	2.138	0.848	2.799	0.616	2.575
10	0.051	4.147	0.085	4.263	0.068	4.220

As shown in the Table, the most significant terms are the first and the third harmonics, despite there are also other odd harmonics. Thus, the Fourier series can be expressed by Eq. IV.4.

$$V_i(t) = A_1 \sin \left[\omega t + \theta_1 + (i - 1) \frac{\pi}{3} \right] + A_3 \sin [3\omega t + \theta_3 + (i - 1)\pi] \quad IV.4$$

IV.2.b No load voltage test

In order to validate the model developed in the FEM tool, an experimental campaign was realized on the prototype. With this purpose, a measuring bench was realized, putting together:

- a measurement and data acquisition system;
- a drive system.

The first part is composed by a data acquisition board (NI USB 6008 National Instrument). This card can measure until four differential analogic inputs in the range ± 10 V, adopting 12 bits of resolution. The power supply is entrusted to the USB connection, through which it is possible to manage the card on Labview. In order to increase the measurable voltage range, a voltage divider is also realized (see Figure IV.11).

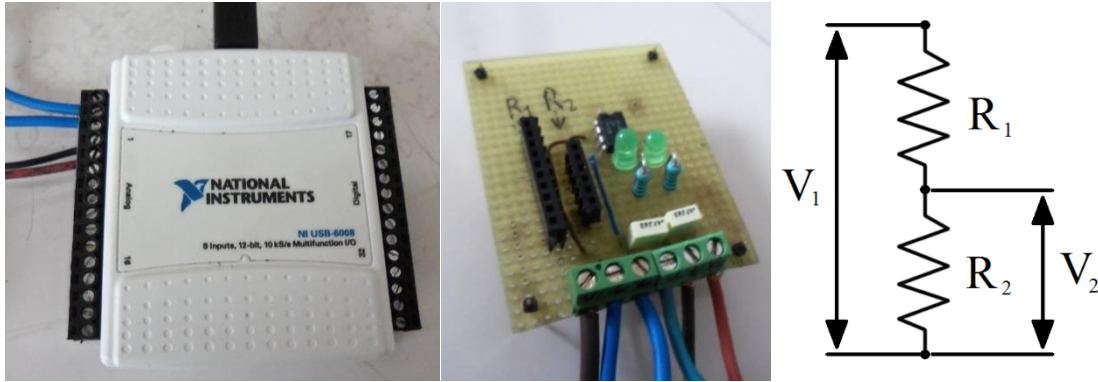


Figure IV.11 Measuring board, voltage divider and equivalent circuit

If the voltage divider is composed by two resistances R_1 and R_2 series connected according to scheme in Figure IV.11, the input voltage V_1 applied to the resistance series generates an output voltage V_2 at the terminals of the resistance R_2 given by the relation:

$$V_2 = V_1 \frac{R_2}{R_1 + R_2} \quad IV.5$$

In order to limit the current on the measuring board, R_1 was fixed to $1.2 \text{ M}\Omega$ while R_2 was varied according to the desired range, choosing the values reported in Table IV.3.

Table IV.3 Resistance values and measurable voltage range

Resistance R_2	Maximum measurable voltage V_1
22 kΩ	555.45 V
100 kΩ	130.00 V
220 kΩ	64.55 V
470 kΩ	35.53 V
1.2 kΩ	20.00 V
3.3 kΩ	13.64 V

The data acquisition is managed by the control panel implemented in Labview (see Figure IV.12). In detail, the measurement starts with the click of the button, having the shape of an arrow. In order to correlate the voltage trend with the motion of the stator, two voltages trends are measured in two separated channels. In the first one, the voltages produced by the generator and scaled by the voltage divider is measured, in the latter a digital signal (ON-OFF) produced by a button that is commanded by the translator (see Figure IV.13). In detail, this normally open button is kept in the closed position by the translator. When the translator starts to move, the button is released, generating a binary signal.

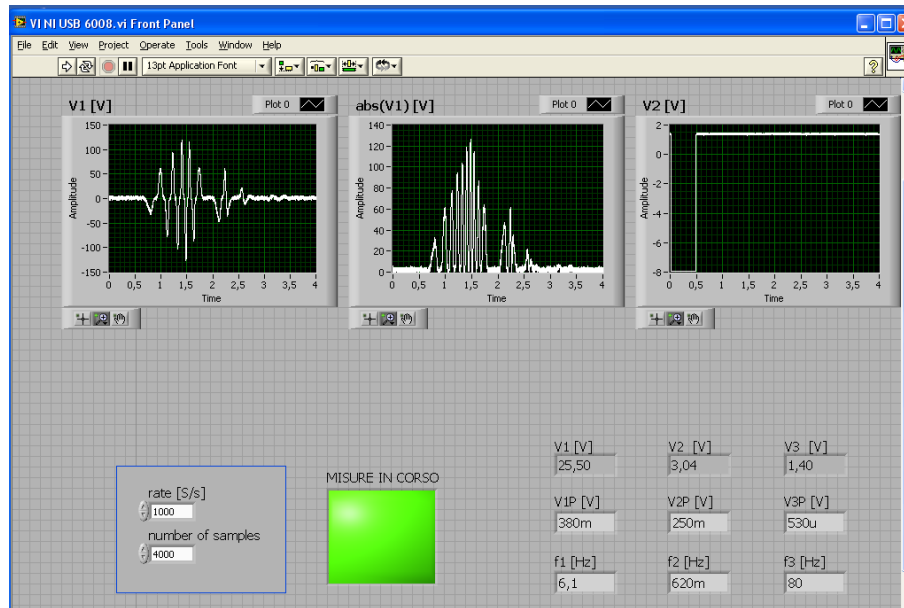


Figure IV.12 Control panel for the data acquisition

This approach was introduced since the measuring system can monitor only one voltage trend at a time. Thus, in order to measure all the no-load voltage trends produced by the generator, the test must be repeated at least six times.



Figure IV.13 Normally open button to produce the starting signal

Focusing on the drive system, the translator is forced to move by the utilization of a weight and a pulley, as depicted in Figure IV.14.



Figure IV.14 Drive system to test the generator

In general, the motion of the translator is given by Eq. IV.6, assuming that F_g is the weight force produced by the test weight having a mass m_w , F_f is the sum of all friction forces, F_c is the cogging force, F_e is the braking force due to the production of electrical power in the stator, m_t is the mass of the translator, a is the linear acceleration of weight and translator, α is the angular acceleration of the pulley, having a radius r_p and an inertia I_p .

$$F_g - F_f - F_c - F_e = (m_w + m_t)a + \frac{I_p}{r_p}\alpha \quad IV.6$$

Since the experiment investigated the no-load voltage trends, the term F_e is practically equal to zero (there is a negligible power loss due to the generation of eddy currents in the stator).

Since the pulley is composed by a cylinder with a mass m_p and a radius r_p , the inertia is equal to $I_p = m_p r_p^2$. The angular acceleration of the pulley is related to the linear acceleration $\alpha = a/r_p$. Finally, $F_g = m_w g$, where g is the gravity acceleration. Thus, Eq. IV.6 can be converted into Eq. IV.7:

$$m_w g - F_f - F_c = (m_w + m_t + m_p)a \quad IV.7$$

Introducing the average values in Eq. IV.7, it is possible to evaluate the average value of the friction force \bar{F}_f , by considering that the average value of cogging force is equal to zero (see Eq. IV.8).

$$\bar{F}_f = m_w g - (m_w + m_t + m_p)\bar{a} \quad IV.8$$

In the test reported below, the test weight has a mass of 1.89 kg, the translator 7.25 kg, the pulley 3.15 kg. Since the average value of linear acceleration is equal to 1.235 m/s², according Eq. IV.8 the average friction force is estimated equal to 3.35 N.

The experiment was realized in the condition of uniformly accelerated motion, while the simulation was performed in the case of constant motion. For this reason, the simulation should be manipulated in order to obtain the equivalent trend in the same condition of the experiment.

In this case, it is important to remind the Lenz's law, reported in Eq. IV.9:

$$\varepsilon(t) = -N \frac{d\Phi_B(t)}{dt} = -N \frac{d\Phi_B(t)}{dx} \frac{dx(t)}{dt} = -Nv(t) \frac{d\Phi_B(x(t))}{dx} \quad IV.9$$

In other words, it is possible to evaluate the induced voltage $\varepsilon(t)$ of N coils from the spatial variation of the magnetic flux Φ_B , considering for each time step the position $x(t)$ and the speed of the translator $v(t)$.

As reported in the previous section, the output voltage trends can be expressed with a Fourier series, composed only by the first and the third harmonics. Thus, combining Eq. IV.2 with Eq. IV.9, the following relation is obtained:

$$V_i(t) = \frac{v(t)}{v_0} \left\{ A_1 \sin \left[\frac{\omega_0}{v_0} x(t) + \theta_1 + (i-1) \frac{\pi}{3} \right] + A_3 \sin \left[3 \frac{\omega_0}{v_0} x(t) + \theta_3 + (i-1) \pi \right] \right\} \quad IV.10$$

where v_0 is the reference speed in the case of constant motion (1 m/s) and ω_0 is the amount $2\pi/\lambda_m$. This equation is usable in case of variable motion, if position and speed trends are known.

Since the experiment was realized in the condition of uniformly accelerated motion, Eq. IV.11 is obtained, assuming initial position and speed both equal to zero.

$$V_i(t) = at \left\{ A_1 \sin \left[\frac{at^2 \omega_0}{2 v_0} + \theta_1 + (i-1) \frac{\pi}{3} \right] + A_3 \sin \left[3 \frac{at^2 \omega_0}{2 v_0} + \theta_3 + (i-1) \pi \right] \right\} \quad IV.11$$

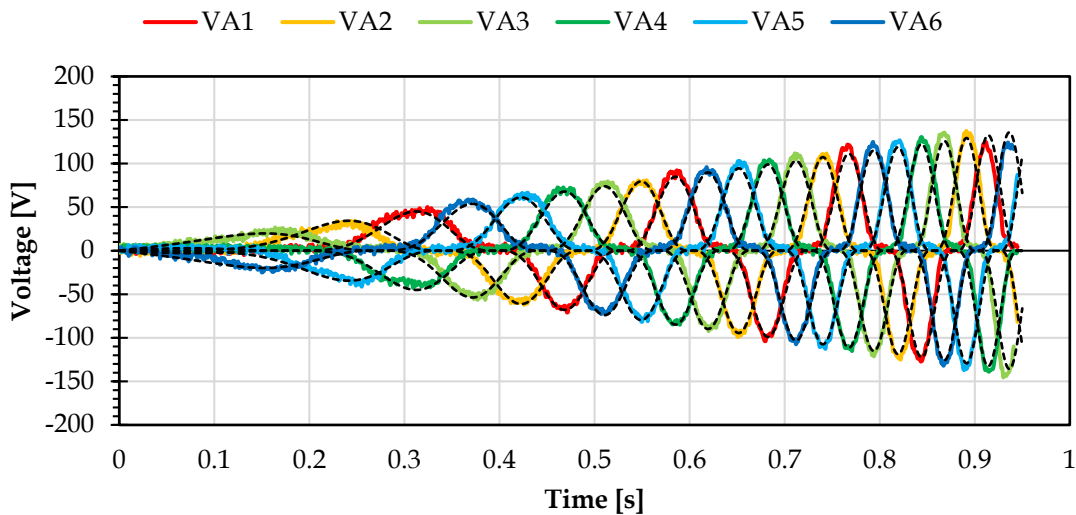


Figure IV.15 Comparison of no-load voltage trends from the experiment and the simulation

The equation reported above represents the theoretical preview of the output voltages, based on the results obtained from the simulation at constant speed and transformed in order to adopt the same motion conditions used in the experiment.

The comparison of the experimental results and the theoretical trends is reported in Figure IV.15, revealing a good correspondence between the adapted simulation results (dashed black lines) and the measurements on the prototype.

In the next section, the optimization process of the electrical generator is reported, simulating different shapes of the stator on the FEM tool.

IV.3 Improvement of the linear generator

In order to improve the electrical output of the generator, some changes of the stator shape are considered. The target is the realization of a linear generator able to produce up to 10 kW, exploiting sea wave energy in the Mediterranean Sea.

IV.3.a Regularization of the magnetic steps

The linear generator analyzed above is characterized by a short stator, in fact only a part of the translator is equipped with magnets in order to oscillate inside the stator region. Since the linear generator should be designed to exploit sea wave characterized by a wave height of few meters, the translator must be modified by the adoption of a long translator configuration (see Figure IV.16).

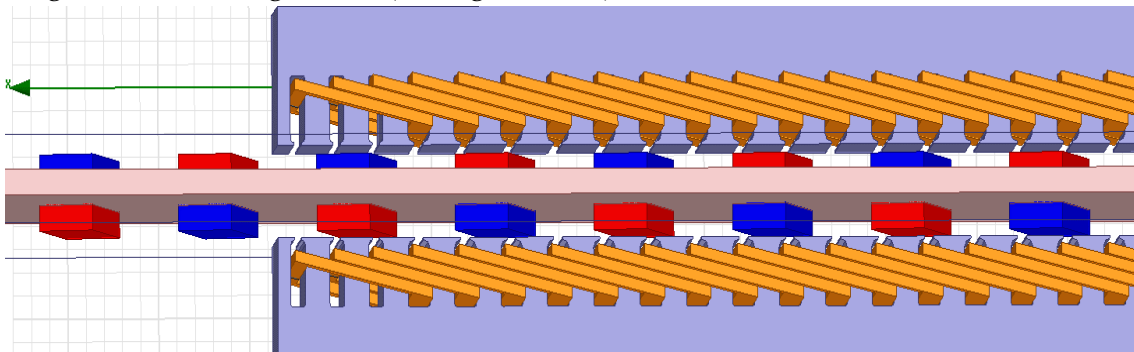


Figure IV.16 Rendering view of the generator on the FEM tool

As first solution, the same geometry of the prototype described above was simulated, considering the adoption of the translator equipped with 40 magnets instead of 12. In this way, the entire stator is simultaneously excited by magnets, increasing the potential power output of the generator.

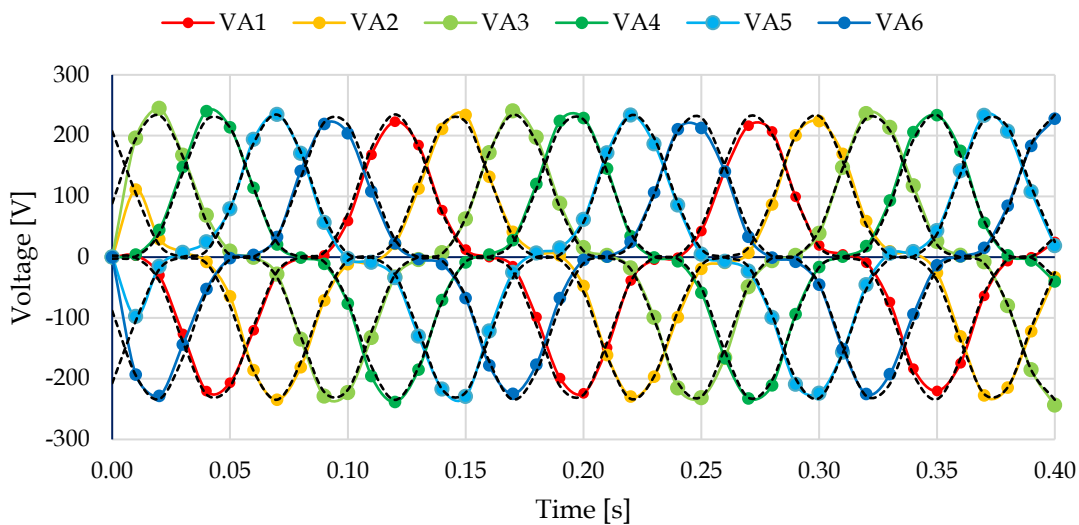


Figure IV.17 No-load voltage trends on the block A using 40 magnets and the prototype stator

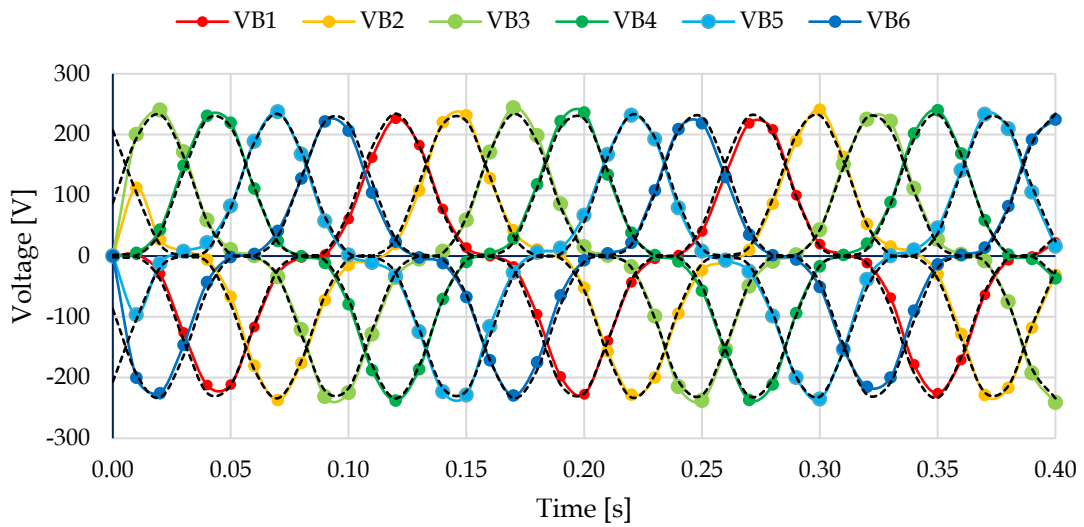


Figure IV.18 No-load voltage trends on the block B using 40 magnets and the prototype stator

The simulation was performed considering a constant speed of 1 m/s and assuming a total movement of 40 cm, since the signal is periodical after few time steps, when the initial conditions are relevant. Indeed, the evaluation of the Fourier series considered the interval from 0.04 s to 0.40 s.

The no-load voltage trends obtained in this condition are reported in Figure IV.17 and Figure IV.18.

The coefficients of Fourier series are reported in the following Table IV.5. Like in the previous simulation, each block of the stator was analyzed separately, in order to compare the results from the simulation.

While the first and third harmonics are characterized by similar coefficient in both blocks, the no-load voltage trend in the block A reveals the presence of a seventh harmonic, while block B has a fifth harmonic.

Table IV.4 Fourier series coefficients of no-load voltage trends by using a long translator and the prototype stator

Harmonic	Block A		Block B		Average signal	
	Amplitude	Phase	Amplitude	Phase	Amplitude	Phase
0	0.044		0.066		0.056	
1	175.745	2.904	174.793	2.904	175.240	2.941
2	0.469	-0.122	0.476	-0.505	0.468	-0.238
3	59.137	-0.716	59.529	-0.718	59.244	-0.607
4	0.112	2.913	0.205	2.114	0.137	2.566
5	0.623	4.151	2.530	1.653	1.049	1.985
6	0.376	3.800	0.173	3.663	0.262	3.541
7	2.225	1.066	1.016	1.987	1.470	1.624
8	0.175	0.738	0.201	-1.007	0.120	0.021
9	0.425	3.724	0.797	4.328	0.809	4.667
10	0.246	3.957	0.034	-1.055	0.140	4.533

These high order harmonics are due to two geometric aspects, as shown in Figure IV.16:

- The coils are installed without the adoption of a planar symmetry;
- The first and last three teeth have a different width in comparison with the other internal teeth.

For these reasons, the first improvement is represented by a regularization of the shape of the stator, imposing a planar symmetry of coils and the same shape to all teeth of the stator.

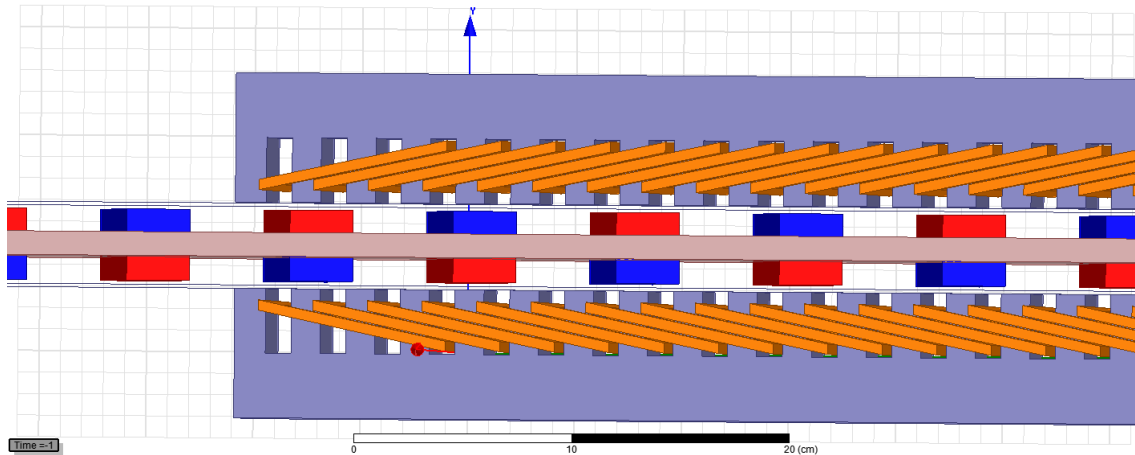


Figure IV.19 Rendering view of the generator with a regular stator

The simulation was repeated obtaining the trends reported in Figure IV.20 and Figure IV.21.

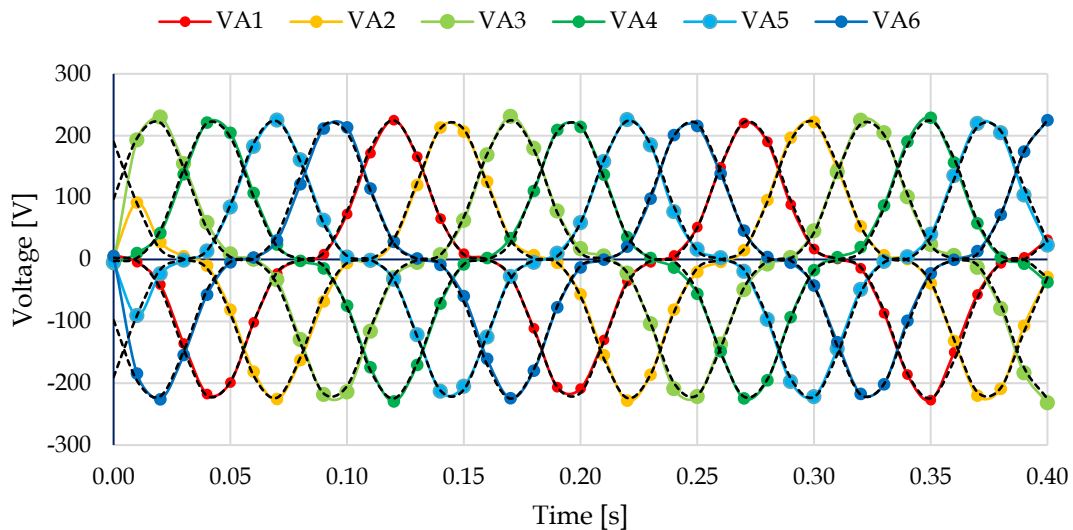


Figure IV.20 No-load voltage trends on the block A using 40 magnets and a regularized stator

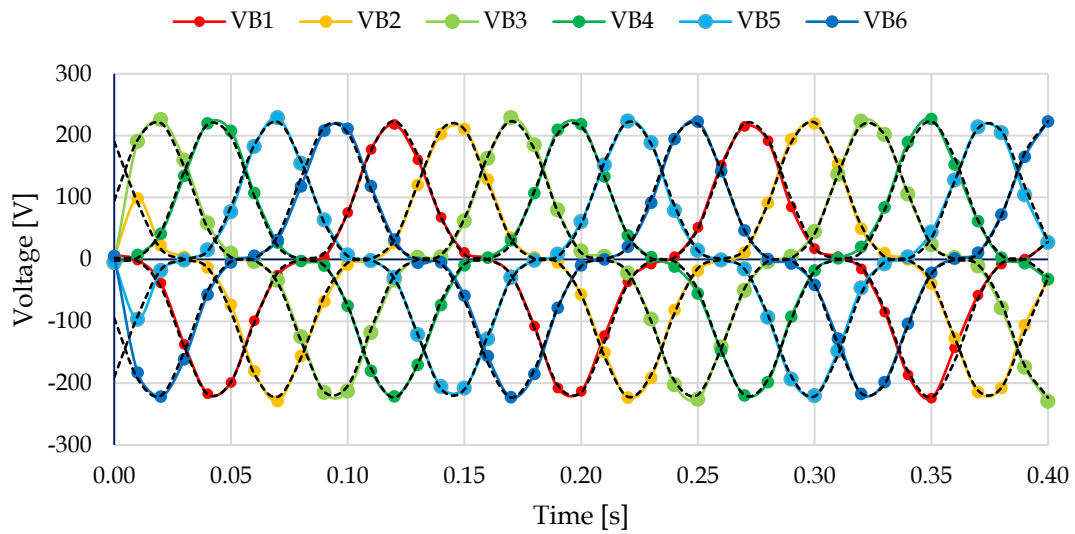


Figure IV.21 No-load voltage trends on the block B using 40 magnets and a regularized stator

The Fourier series was also performed, obtaining the coefficients reported in Table IV.5. In this case, the voltage trends are practically the same in both stator blocks, with the presence of a small fifth harmonic while the other high-order harmonics are practically negligible.

Table IV.5 Fourier series coefficients of no-load voltage trends by using a regular long translator and a regular stator

Harmonic	Block A		Block B		Average signal	
	Amplitude	Phase	Amplitude	Phase	Amplitude	Phase
0	-0.100		-0.072		-0.086	
1	169.460	2.949	168.193	2.942	168.826	2.946
2	0.132	2.110	0.189	2.923	0.148	2.593
3	55.503	-0.567	55.244	-0.596	55.367	-0.582
4	0.029	-0.423	0.163	-1.537	0.089	-1.389
5	2.017	2.248	2.097	2.213	2.057	2.230
6	0.232	0.496	0.265	0.917	0.243	0.721
7	0.400	-0.355	0.579	4.192	0.323	-1.436
8	0.141	2.825	0.104	2.301	0.118	2.603
9	0.218	-0.130	0.514	-1.453	0.303	-1.097
10	0.080	-0.951	0.079	1.057	0.043	0.042

IV.3.b Variation of the air gap

In this section the effects produced by the variation of the airgap between the stator and the magnetics installed on the translator is investigated.

The idea is to modify this parameter in order to evaluate the variation of the no-load voltage trends. From a theoretical point of view, the reduction of the airgap should increase the voltage trends in the system. Despite this, practical aspects should be also considered, like the tolerance adopted to assemble the machine and the local forces produced by the interaction between magnets and stator. As a consequence, there are

some limitations on the minimal air gap and the requirement to increase the rigidity of the translator, for example by the addition of other bearing in the stator.

About the no-load voltage trend, the simulation was realized starting from the previous configuration and removing or adding space in the airgap. Considering that the prototype is assembled with an airgap of 3.5 mm between magnets and stator, the airgap was varied adding a space ds_{gap} ranging between - 1 mm to 3 mm, with a step of 1 mm.

The Fourier series was performed in each case, obtaining the coefficients reported in Table IV.6 , considering the average trend produced by blocks A and B of the stator. Like in the previous case, this evaluation considers only the results in the interval 0.04 s to 0.40 s in order to remove the influence of the initial conditions.

After this analysis, the trends of the amplitude of the first and the third harmonics were evaluated and reported in Figure IV.22. In this range, both amplitudes are affected by a linear trend: an increment of the airgap equal to 1 mm produces the reduction of 9.7 V in the first harmonics and 7.7 V in the third one.

Since the main goal is the increasing of the power output of the generator, these simulations suggest the reduction of the airgap to the value of 2.5 mm, that is 1 mm thinner than the airgap adopted in the prototype.

Table IV.6 Fourier series coefficients of no-load voltage trends by using a regular long translator and a regular stator

Coefficient	Additive air gap [mm]				
	-1.0	0.0	+1.0	+2.0	+3.0
K	-0.08	-0.12	-0.04	-0.08	-0.06
A_1	180.56	168.34	158.77	150.57	141.02
A_2	0.09	0.03	0.11	0.05	0.01
A_3	67.59	56.37	46.35	42.91	36.03
A_4	0.21	0.06	0.09	0.10	0.07
A_5	2.35	2.04	0.69	0.48	0.40
A_6	0.20	0.23	0.18	0.07	0.04
A_7	2.04	0.52	0.81	0.45	0.41
A_8	0.20	0.14	0.08	0.03	0.04
A_9	1.30	0.27	0.48	0.06	0.38
A_{10}	0.23	0.08	0.08	0.02	0.06
ϑ_1	3.057	3.056	3.059	3.056	3.058
ϑ_2	-0.362	0.890	1.068	-0.646	1.764
ϑ_3	-0.251	-0.269	-0.236	-0.261	-0.232
ϑ_4	3.508	4.060	3.979	-1.164	-1.320
ϑ_5	2.797	2.652	2.419	3.222	2.881
ϑ_6	-0.196	-1.103	0.675	2.479	2.808
ϑ_7	2.278	2.616	3.270	4.352	2.637
ϑ_8	1.630	1.164	0.235	0.440	2.688
ϑ_9	-0.911	-1.070	-1.310	0.516	-0.765
ϑ_{10}	-1.077	-0.357	2.667	3.878	1.671

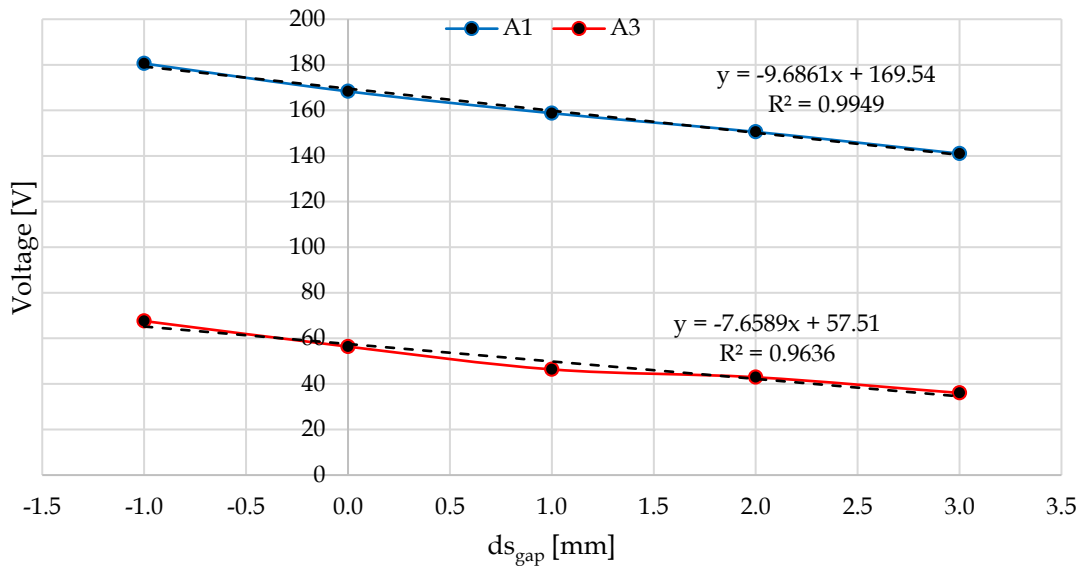


Figure IV.22 Trends of the amplitudes of the first and third harmonics of no-load voltages as function of the airgap between magnets and stator

IV.3.c Variation of the magnetic step

In order to improve the power output of the generator, a possible technique is the reduction of the step between the magnets installed on the translator.

Several simulations were performed, assuming a constant speed of the translator equal to 1 m/s and fixing that the distance λ_m between two magnets having the same pole is equal to six times the sum of tooth width w_t and slot width w_s .

$$\lambda_m = 6(w_t + w_s) \quad IV.12$$

The same airgap of the prototype was considered in this step. The proposed stator is characterized by a regular alternance of teeth and slots. Since the width of the slot is related to the number of turns of each coil, the simulations were realized by modifying only the width of the tooth considering the addition of iron. This amount is expressed by the parameter dw_t that ranges between -12 mm to +2 mm with a step of 2 mm. The extreme case of the complete removal of teeth is also considered (-13.5 mm).

$$w_t = w_{t,0} + dw_t \quad IV.13$$

Each simulation was analyzed, evaluating the coefficients of the equivalent Fourier series. Data reported in Table IV.7 are referred to the average signals produced by blocks A and B of the stator. The trends of the first and the third harmonics are shown in Figure IV.23.

Table IV.7 Coefficients of Fourier series in case of different width of stator teeth

Coefficient	Additive iron in the teeth of stator [mm]								
	-13.5	-12.0	-10.0	-8.0	-6.0	-4.0	-2.0	0.0	+2.0
K	-0.06	-0.25	-0.13	-0.22	-0.23	0.01	-0.09	-0.25	-0.34
A_1	39.10	218.51	213.21	208.35	203.00	192.09	177.76	169.89	160.44
A_2	0.10	0.18	0.14	0.01	0.06	0.08	0.07	0.07	0.04
A_3	0.05	1.79	4.02	12.15	20.24	34.35	46.31	54.81	62.22
A_4	0.07	0.08	0.10	0.07	0.11	0.06	0.03	0.03	0.10
A_5	0.14	0.59	0.39	0.32	1.59	0.78	0.78	1.45	3.97
A_6	0.16	0.22	0.03	0.48	0.15	0.30	0.31	0.22	0.07
A_7	0.04	0.49	0.18	0.08	0.26	0.61	0.73	0.69	1.35
A_8	0.06	0.01	0.10	0.17	0.12	0.03	0.07	0.18	0.03
A_9	0.05	0.54	0.10	0.76	0.36	0.53	0.86	0.05	0.86
A_{10}	0.09	0.06	0.03	0.11	0.04	0.19	0.11	0.11	0.13
ϑ_1	-1.50	0.00	0.00	0.00	0.00	0.00	0.00	0.00	0.00
ϑ_2	4.31	2.15	-0.28	2.68	-1.25	0.67	2.26	3.60	-1.53
ϑ_3	-0.35	3.73	4.63	-0.68	-0.12	2.45	-1.04	2.92	1.00
ϑ_4	3.51	0.34	2.44	-1.45	-0.57	-1.11	3.65	1.38	-1.46
ϑ_5	2.39	4.11	0.50	1.47	4.62	-0.31	2.03	-0.15	2.64
ϑ_6	2.47	1.55	0.14	2.50	2.36	0.19	1.37	-0.57	-1.43
ϑ_7	1.35	1.00	-1.51	-0.31	1.67	4.35	4.61	1.97	1.03
ϑ_8	0.73	0.02	-1.05	2.33	4.54	1.02	4.62	3.92	1.16
ϑ_9	2.84	-1.46	-0.49	3.03	1.40	-0.61	2.51	0.71	3.99
ϑ_{10}	2.92	3.78	2.70	4.17	4.68	0.98	0.06	3.18	0.95

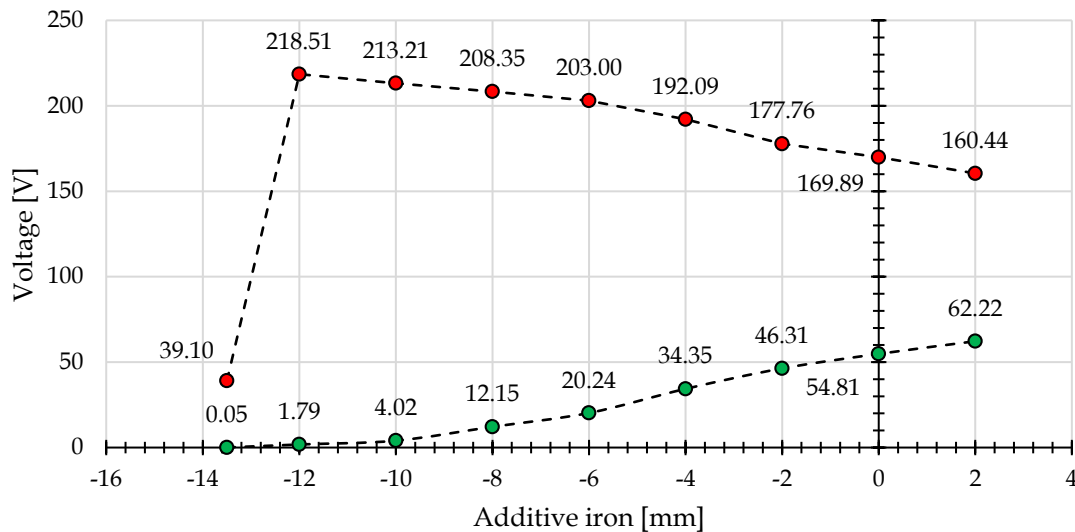


Figure IV.23 First and third harmonics in case of different width of the stator teeth

It is interesting to observe how the reduction of the width of the stator teeth increases the value of the first harmonic and reduces the value of the third one. This aspect is important to increase and level the power output, since in a three-phases system the first term is responsible of a constant power output, while the third one produces a pulsating component.

Although the best condition from an electrical point of view is $dDe = -12$ mm, in the next analysis the condition $dDe = -8$ mm is assumed in order to ensure a width of the

stator teeth (5.5 mm) enough to resist to the mechanical solicitations produced by coils during the electrical power generation.

IV.3.d Preliminary sizing

As introduced before, the goal is the sizing of a linear generator able to exploit the energy potential of sea wave in the Mediterranean Sea.

Considering the simplified case of a regular wave in Eq. III.1 and assuming that in the best case the Wave Energy Converter moves up and down following the crest of sea wave, the speed of the device can be evaluated by Eq. IV.14

$$\dot{z}(t) = \frac{d}{dt} \left[\frac{H_s}{2} \sin \left(\frac{2\pi}{T} t - \frac{2\pi}{\lambda} x \right) \right] = \frac{\pi H_s}{T} \cos \left(\frac{2\pi}{T} t - \frac{2\pi}{\lambda} x \right) \quad IV.14$$

from which it is possible to estimate the maximal speed archivable by the device by the term $\pi H_s/T_e$.



Figure IV.24 Location of the measuring buoys of RON

In order to create a data bank about the wave energy potential along the Italian coastline, the project RON (in Italian “Rete Ondometrica Nazionale”, i.e. the national

network for the wave energy measurement) was started in 1989 by ISPRA (in Italian “Istituto Superiore per la Protezione e Ricerca Ambientale”, i.e. the “Superior Institute for the Environmental Protection and Research”). After the last upgrade in the period 2009-2014, RON is currently composed by 15 measuring buoys, type WatchKeeper™, built by the Canadian society AXYS Ltd. In detail, RON is used to measure the Significant Height, the average period of waves, the peak period, the average direction of waves. The location of the measuring buoy of RON is depicted in Figure IV.24.

The data bank from three different buoys around Sicily were analyzed in order to find the maximal value of the vertical speed, according to the previous Eq. IV.14.

The discretized distribution of wave speed $f_v(v)$ is reported in Table IV.8, representing each value the frequency with which the speed v is observed. The wave speed is discretized in bins having the width of 0.1 m/s.

Table IV.8 Wave speed distribution according to the data from the RON stations of Catania, Mazara del Vallo and Palermo.

v [m/s]	f(v)			v [m/s]	f(v)		
	Catania	Mazara	Palermo		Catania	Mazara	Palermo
0.1	0.0657	0.0330	0.0550	1.6	0.0005	0.0073	0.0034
0.2	0.1651	0.0843	0.1444	1.7	0.0003	0.0046	0.0019
0.3	0.1990	0.1068	0.1572	1.8	0.0003	0.0031	0.0012
0.4	0.1816	0.1177	0.1382	1.9	0.0001	0.0018	0.0008
0.5	0.1368	0.1190	0.1150	2.0	0.0000	0.0011	0.0004
0.6	0.0903	0.1040	0.0958	2.1	0.0000	0.0004	0.0002
0.7	0.0593	0.0935	0.0785	2.2	0.0000	0.0002	0.0001
0.8	0.0405	0.0803	0.0582	2.3	0.0000	0.0001	0.0001
0.9	0.0252	0.0700	0.0453	2.4	0.0000	0.0000	0.0000
1.0	0.0156	0.0555	0.0350	2.5	0.0000	0.0000	0.0000
1.1	0.0090	0.0405	0.0252	2.6	0.0000	0.0000	0.0000
1.2	0.0049	0.0316	0.0176	2.7	0.0000	0.0000	0.0000
1.3	0.0029	0.0212	0.0132	2.8	0.0000	0.0000	0.0000
1.4	0.0017	0.0146	0.0077	2.9	0.0000	0.0000	0.0000
1.5	0.0012	0.0094	0.0054	3.0	0.0000	0.0000	0.0000

According to the data reported above, the maximal value of the observed wave speed is equal to 2.3 m/s (this value is observed with an annual frequency of 10^{-4} in the measuring stations of Palermo and Mazara del Vallo).

As introduced in the previous sections, in order to improve the power output of the linear generator, two approaches were introduced:

- Reduce the air gap between the stator blocks and the magnets installed on the translator;
- Reduce the width of the teeth of the stator and consequently the distance between the magnets.

In order to perform a more accurate analysis, the prototype was modified, adopting stator teeth 5.5 mm wide (-8.0 mm in comparison with the prototype) and an airgap of 2.5 mm (-1.0 mm in comparison with the prototype).

Table IV.9 Fourier series coefficients of no-load voltage trends by using a long translator and a regular stator having teeth 5.5 mm wide and an airgap of 2.5 mm

Harmonic	Block A		Block B		Average signal	
	Amplitude	Phase	Amplitude	Phase	Amplitude	Phase
0	-0.247	0.000	-0.216	0.000	-0.231	0.000
1	222.129	2.679	224.726	2.680	223.427	2.679
2	0.033	3.287	0.006	-0.851	0.015	3.453
3	18.324	-1.418	17.588	-1.320	17.935	-1.370
4	0.160	0.334	0.307	1.460	0.201	1.093
5	4.395	4.203	2.160	3.881	3.240	4.097
6	0.438	2.232	0.235	3.164	0.304	2.548
7	1.646	4.504	0.421	-0.072	0.821	-1.522
8	0.375	1.988	0.180	1.913	0.277	1.964
9	1.467	-0.069	0.490	2.468	0.550	0.187
10	0.096	-0.619	0.045	-1.220	0.068	-0.806

The no-load voltage trends were simulated and analyzed in order to obtain the coefficients of the Fourier series (see Table IV.9). The comparison between results and the Fourier series approximation (first and third harmonics) is reported in Figure IV.25.

It is interesting to compare the results in Table IV.9 with the reference case reported in Table IV.5. Considering the average signal, the first harmonic increased from 169.889 V to 223.427 V (+31.5 %) while the third harmonic was reduced from 54.809 V to 17.935 V (-67.3%). These values are slightly better than the previsions based on the results of the previous simulations.

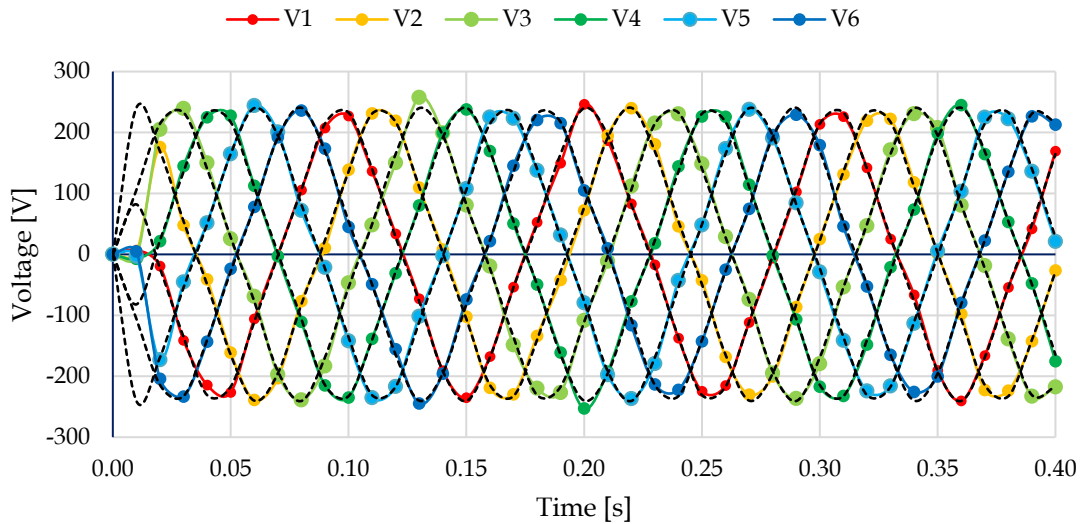


Figure IV.25 No-load voltage trends, adopting a regular stator having teeth 5.5 mm wide and an airgap of 2.5 mm

At this point, a simplified evaluation of the maximal power output is realized according to the following procedure:

- The no-load voltage trends should be amplified according to the maximal wave speed, according to the data of the Mediterranean Sea (2.3 m/s);

- The maximal allowable current should be chosen according to the state of art of similar machines. In the case of motor is commonly chosen a current density between 5 and 6 A/mm². Since the prototype is realized by using enameled copper coils, having a diameter of 0.5 mm (corresponding to 0.1964 mm²), the maximal current \bar{I} could be fixed to 1.05 A.
- In order to increase the power output, the number of turns per coil and the total number of coils could be increased.

Thus, assuming a constant speed equal to 2.3 m/s, the no-load voltage trends were amplified, obtaining the values in Figure IV.26, by considering a three-phases scheme connection reported in Figure IV.27.

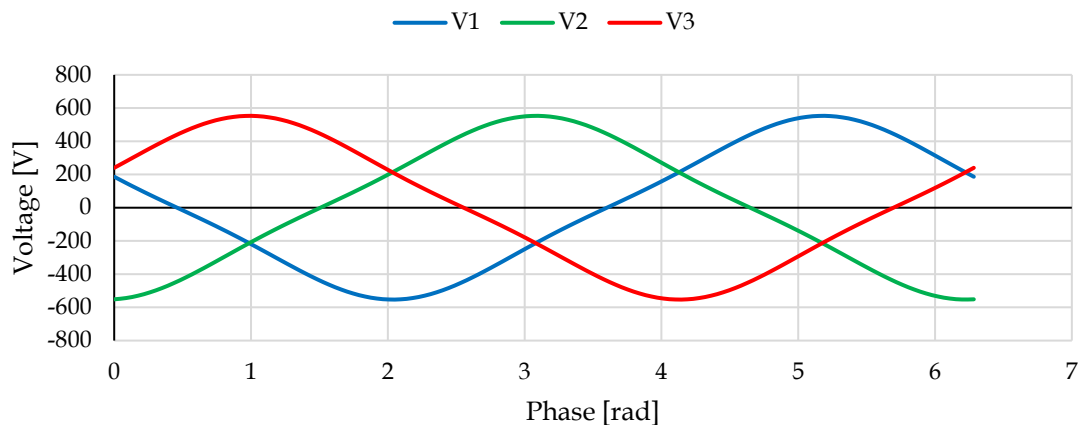


Figure IV.26 Amplified no-load voltage trends, assuming a three-phases connection scheme

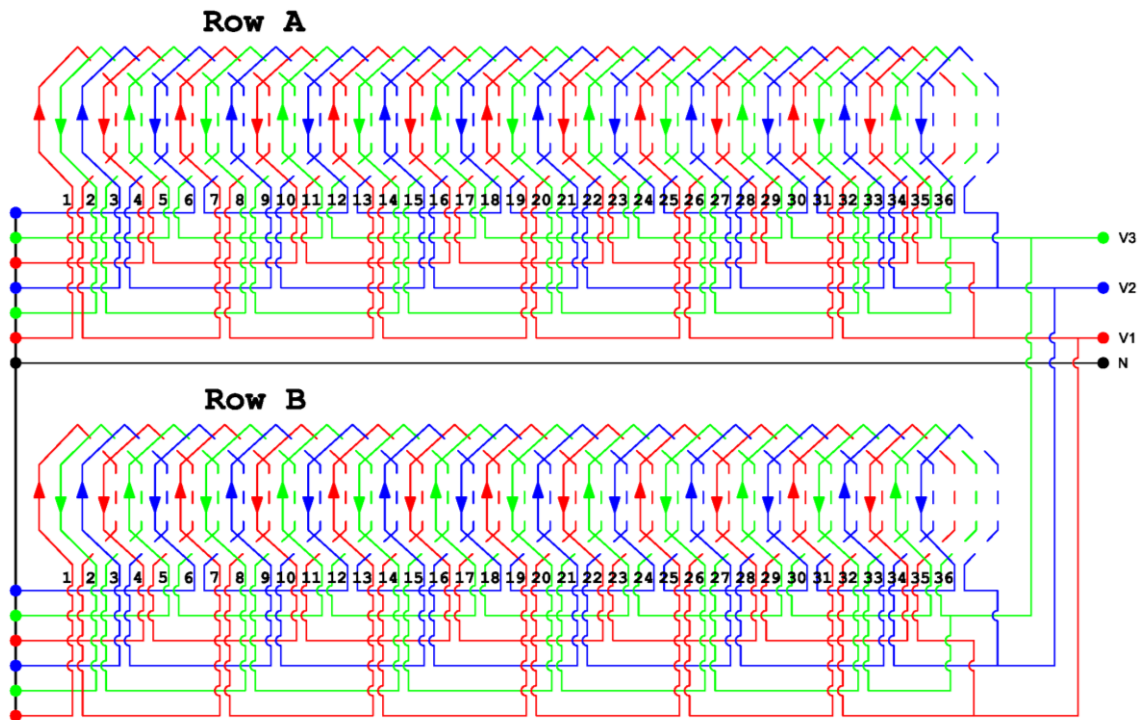


Figure IV.27 Three-phases connection scheme

Pondering a single period, the peak value of no-load voltage is equal to 552.61 V, while the effective value \bar{V} is equal to 362.49 V. Thus, the power output of the systems is equal to:

$$P_o = 3n_{l,o}\bar{V}\bar{I} \cos \varphi_{VI} \quad IV.15$$

assuming that $n_{l,o}$ is the number of lines in parallel per each phase (4 according to the scheme), and $\cos \varphi_{VI}$ is the power factor, fixed to 0.8.

In this condition, the power output of the system P_o is equal to 3654 W. Thus, the ratio between the desired rated power (10 kW) and the modified prototype is equal to 2.6378. To increase the power output, there are two techniques:

- Increase the number of turns (corresponding to an increase of the voltage)
- Increase the number of coils (corresponding to an increase of the total current available for the load).

Thus, the solution of the problem is to double up the number of coils ($n_{l,n} = 2n_{l,o}$) and increase the number of turns per coil of the amount:

$$n_{turns,n} = n_{turns,0} \frac{P_n n_{l,0}}{P_o n_{l,n}} = 513.1 \quad IV.16$$

Rounding the previous value, the proposed system will be equipped with 144 coils, each one having 515 turns per coil. The size of the slot is modified by increasing the depth from 3.0 cm to 3.9 cm.

A simulation was realized to confirm the data above reported, considering a linear generator with 72 coils, 515 turns per coil, airgap 2.5 mm, stator teeth width of 5.5 mm and the adoption of chamfered slots (the same shape used in the prototype). The no-load voltage trends are reported in Figure IV.28.

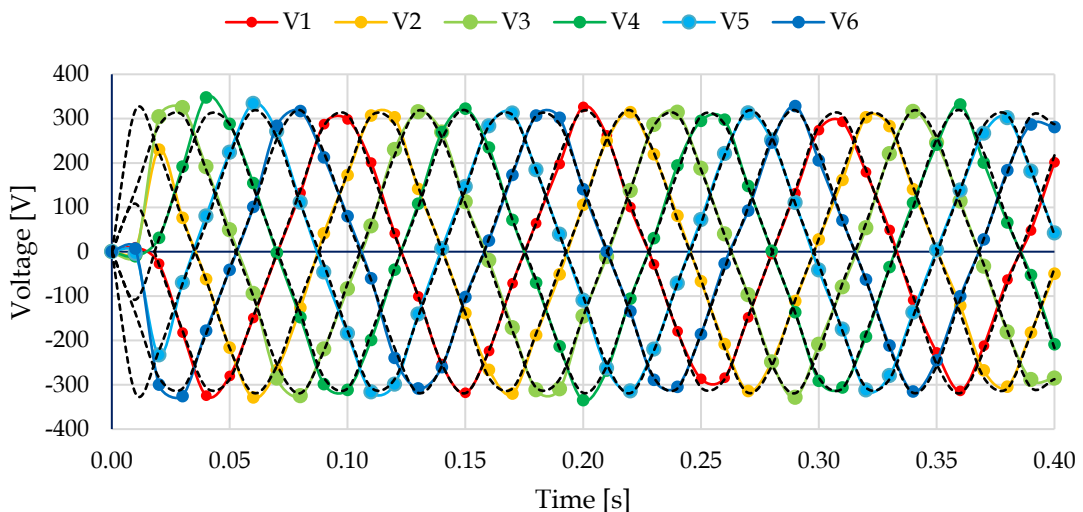


Figure IV.28 No-load voltage trends according to the changes from the pre-sizing.

In this case, the effective voltage is equal to 482.1 V while the increasing of coils suggested the achievement of an effective voltage equal to 497.8 V. Since the difference is limited (3.26%), in order to achieve the rated power of 10 kW, a solution is the increasing of the effective current from 1.05 A to 1.09 A, corresponding to a current density equal to 5.55 A/mm².

IV.3.e Cogging analysis

In the previous section, the preliminary sizing of the linear generator was performed. The results above indicate the need to double the number of coils, in order to achieve the desired rated power of the linear generator. The starting point is represented by the stator obtained from the previous analyses, having the sizes shown in Figure IV.29. This stator, split in two parts, presents 78 slots in order to install 72 coils. This configuration is identified in the following as “Stator 72”.

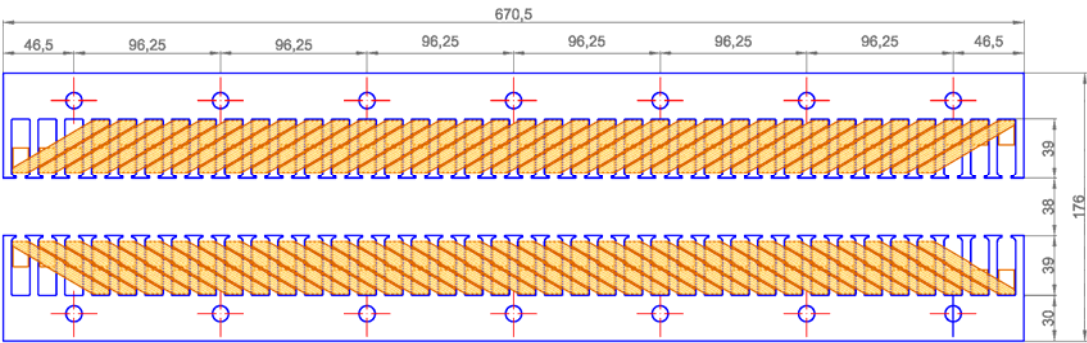


Figure IV.29 Detailed shape of the stator with 72 coils (Stator 72).

As first step, the configuration reported above was considered in order to evaluate the cogging force generated by the magnetic interaction between the iron of the stator and the permanent magnets installed on the translator. In absence of currents in stator coils, this force pulls the translator into the condition of minimal energy potential, i.e. where the magnetic flux is maximized or equivalently the reluctance of the magnetic circuit is minimized. Cogging force is a disturbing phenomenon, because it is responsible of the creation of vibration, noise and an irregular power production [197].

A simulation on Ansys Maxwell was performed, numerating the magnets from the left with the numbers 1 - 39. The goal is the investigation of the cogging force that affects each magnet and the entire translator with the stator.

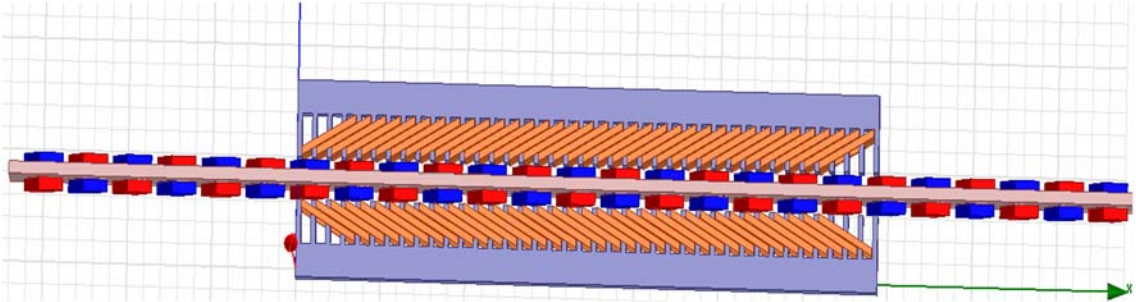


Figure IV.30 Shape of the “Stator 72” modelled in Ansys Maxwell

In the following analysis, the initial position represents the condition for which the middle point of the first magnet is located at -30 cm to the origin of the x-axis. Indeed, the geometry of the stator start from the origin of the coordinate system, as shown in Figure IV.30. The simulation considers a total displacement of the translator equal to 10.5 cm, that is the distance between two magnets having the same pole.

In Table IV.10 the trends of the cogging forces produced by each magnet are reported, considering only the component along the x-axis, since the components along the y-axis and z-axis are equal to zero for the planal symmetry of the device.

Table IV.10 x-axis component of cogging forces generated in the configuration “Stator 72”

dX [cm]	0.0	0.5	1.0	1.5	2.0	2.5	3.0	3.5	4.0	4.5	5.0
<i>Tot</i>	-320.3	-204.2	-11.0	-5.6	77.4	296.8	283.0	62.6	6.6	-39.7	-252.7
<i>M1</i>	72.5	72.8	72.3	72.7	72.9	72.6	72.1	72.6	72.4	72.7	73.4
<i>M2</i>	-5.4	-5.3	-5.9	-5.5	-5.7	-5.9	-5.8	-5.3	-5.0	-5.5	-5.4
<i>M3</i>	0.6	1.3	1.0	0.6	1.1	1.3	0.7	0.3	0.4	0.5	0.6
<i>M4</i>	-0.9	-0.8	-0.4	-0.2	0.3	0.9	1.3	1.2	2.1	2.0	2.3
<i>M5</i>	3.3	1.4	0.1	-2.0	-5.3	-10.2	-16.3	-24.0	-31.7	-39.1	-42.8
<i>M6</i>	-42.2	-33.0	-8.8	45.6	127.4	183.9	181.8	137.5	81.9	20.5	-23.3
<i>M7</i>	-27.7	-11.6	1.6	-5.0	-7.1	4.4	3.8	-5.7	-0.4	6.9	-1.4
<i>M8</i>	-6.6	-0.3	6.8	-2.8	-5.7	6.2	4.4	-5.6	0.5	7.5	-1.9
<i>M9</i>	-5.7	-0.6	8.7	-2.4	-5.5	5.9	4.3	-5.6	-1.2	7.0	-3.1
<i>M10</i>	-6.1	-0.3	7.6	-2.3	-5.1	5.4	4.0	-5.7	0.1	7.8	-2.0
<i>M11</i>	-6.0	-0.6	7.2	-2.0	-5.2	5.7	4.0	-6.2	-0.5	7.7	-1.9
<i>M12</i>	-6.5	-0.7	6.6	-2.5	-5.7	5.2	4.6	-5.8	-0.4	7.6	-2.4
<i>M13</i>	-6.1	0.5	6.6	-1.8	-5.4	5.3	3.7	-6.3	-0.2	7.8	-2.1
<i>M14</i>	-5.9	0.7	6.6	-2.5	-5.5	5.2	4.1	-6.1	-0.5	7.0	-2.0
<i>M15</i>	-6.4	-1.0	7.1	-1.9	-5.5	4.2	4.4	-6.4	-0.7	6.5	-2.1
<i>M16</i>	-6.4	0.0	8.0	-2.0	-4.7	5.0	4.1	-5.9	0.7	7.1	-1.8
<i>M17</i>	-6.7	-0.4	6.8	-2.0	-5.2	6.7	3.7	-6.9	-0.4	6.8	-2.8
<i>M18</i>	-6.3	0.4	6.7	-2.2	-5.4	5.2	4.5	-6.7	1.3	7.0	-1.2
<i>M19</i>	-5.8	1.3	8.6	0.0	1.0	21.3	25.4	-16.3	-74.4	-132.1	-180.3
<i>M20</i>	-191.4	-167.8	-94.4	-19.1	20.7	38.4	43.0	40.0	32.6	25.1	17.4
<i>M21</i>	13.8	7.6	3.7	1.3	-1.0	-2.3	-2.1	-2.7	-2.5	-1.6	-1.7
<i>M22</i>	-0.7	-0.7	-0.5	-0.4	-0.3	0.1	0.2	0.6	0.2	-0.1	-0.1
<i>M23</i>	0.3	0.6	-0.1	-0.3	-0.4	-0.3	0.0	0.1	-0.3	-0.5	-0.2
<i>M24</i>	-0.1	-0.2	0.2	-0.1	0.0	-0.3	0.0	0.6	0.0	0.3	0.0
<i>M25</i>	0.1	0.1	-0.1	0.1	-0.1	-0.2	0.1	-0.1	-0.4	0.3	0.2
<i>M26</i>	0.4	0.1	-0.2	-0.1	-0.1	0.3	0.7	0.3	0.1	-0.1	0.3
<i>M27</i>	0.0	-0.4	0.0	0.0	0.0	-0.4	0.0	-0.1	-0.3	0.3	-0.1
<i>M28</i>	-0.6	-0.6	0.3	0.3	0.3	0.2	-0.1	-0.2	0.1	0.0	0.1
<i>M29</i>	0.1	-0.2	0.0	0.2	0.3	0.5	-0.2	0.2	0.6	0.2	-0.1
<i>M30</i>	-0.1	0.1	-0.4	0.4	0.2	0.0	-0.1	-0.1	-0.4	0.0	0.0
<i>M31</i>	0.5	-0.1	-0.2	0.4	-0.4	0.0	-0.1	0.2	-0.3	-0.4	0.0
<i>M32</i>	0.3	-0.2	-0.7	0.1	0.0	0.4	0.1	0.5	-0.2	-0.2	0.7
<i>M33</i>	-0.5	0.1	0.0	-0.2	-0.3	-0.6	-0.1	-0.3	0.1	0.2	0.7
<i>M34</i>	0.3	-0.2	0.3	0.1	0.3	0.2	0.4	0.2	0.0	-0.1	0.4
<i>M35</i>	-0.4	-0.1	0.0	-0.6	0.5	-0.2	-0.5	-0.4	0.2	-0.2	0.0
<i>M36</i>	-0.1	0.2	0.4	0.2	-0.1	0.6	0.7	0.0	0.2	-0.2	0.1
<i>M37</i>	-0.5	-1.3	-0.8	-0.7	-0.8	-0.8	-0.9	-0.8	-1.0	-0.7	-1.5
<i>M38</i>	5.4	5.9	5.7	5.6	5.1	5.7	5.4	5.3	5.8	5.2	5.4
<i>M39</i>	-71.9	-71.5	-72.2	-72.1	-72.3	-72.5	-72.1	-72.0	-71.5	-71.7	-72.1

dX [cm]	5.5	6.0	6.5	7.0	7.5	8.0	8.5	9.0	9.5	10.0	10.5
<i>Tot</i>	-301.8	-96.6	13.5	7.8	194.0	328.5	165.9	8.2	1.5	-132.5	-317.4
<i>M1</i>	72.4	72.9	72.6	72.3	72.8	72.8	73.1	72.7	72.3	72.9	73.0
<i>M2</i>	-5.8	-6.0	-5.6	-5.9	-5.8	-5.8	-5.6	-6.1	-6.2	-6.0	-5.5
<i>M3</i>	0.8	0.9	1.2	1.4	2.3	2.7	3.3	3.4	4.1	4.2	4.2
<i>M4</i>	2.2	0.9	-1.4	-3.9	-7.9	-13.4	-20.8	-28.4	-36.4	-41.9	-42.6
<i>M5</i>	-38.7	-22.8	14.1	87.1	162.2	190.9	162.1	110.5	51.2	-4.4	-27.7
<i>M6</i>	-22.1	-2.9	0.1	-9.1	-1.5	6.9	-2.2	-5.1	4.2	4.4	-6.3
<i>M7</i>	-5.1	4.9	4.4	-6.0	-0.2	7.1	-2.2	-5.5	5.2	4.2	-5.9
<i>M8</i>	-4.8	4.9	4.1	-6.1	-0.1	7.1	-2.1	-5.2	5.2	3.6	-5.1
<i>M9</i>	-4.5	5.3	3.6	-6.2	0.4	6.8	-2.7	-3.9	5.4	4.5	-6.1
<i>M10</i>	-5.6	4.6	3.6	-5.6	-0.2	7.2	-2.8	-5.3	5.0	3.7	-6.3
<i>M11</i>	-6.1	5.3	3.6	-6.9	-0.1	7.0	-3.1	-5.6	5.1	3.5	-5.9
<i>M12</i>	-4.5	5.3	3.6	-6.0	0.5	6.8	-3.2	-5.8	4.8	4.5	-6.0
<i>M13</i>	-5.5	4.9	4.3	-6.5	0.5	5.4	-2.6	-4.8	4.9	4.1	-5.2
<i>M14</i>	-6.1	5.1	5.3	-7.2	1.2	7.5	-2.6	-5.8	5.3	4.4	-6.0
<i>M15</i>	-5.4	4.8	4.3	-6.7	-0.5	7.7	-2.9	-5.6	6.2	4.0	-6.4
<i>M16</i>	-5.6	5.1	4.4	-6.6	-0.6	6.9	-1.8	-5.5	4.9	4.9	-6.6
<i>M17</i>	-5.1	4.7	4.2	-7.0	0.4	7.6	-0.5	-5.5	4.7	4.0	-4.9
<i>M18</i>	-5.4	6.2	6.3	-1.8	10.3	26.7	10.4	-44.6	-103.7	-157.4	-190.9
<i>M19</i>	-188.0	-135.4	-53.3	4.7	31.0	41.4	42.0	36.6	28.9	21.2	13.9
<i>M20</i>	10.8	5.1	2.2	0.2	-1.8	-3.0	-2.5	-3.1	-2.4	-2.2	-1.7
<i>M21</i>	-1.4	-0.2	-0.7	0.0	0.3	0.3	0.4	0.4	0.7	0.2	0.8
<i>M22</i>	0.0	0.2	0.3	0.1	-0.3	-0.6	-0.1	-0.8	-0.4	-0.3	-0.4
<i>M23</i>	0.2	-0.3	0.1	0.3	0.0	0.0	0.5	0.5	0.3	-0.1	0.0
<i>M24</i>	0.1	-0.2	0.1	-0.2	0.1	0.6	0.2	-0.6	-0.2	0.0	0.3
<i>M25</i>	-0.2	-0.7	-0.2	0.0	0.1	0.4	-0.3	-0.4	-0.3	-0.6	0.1
<i>M26</i>	-0.1	-0.2	0.4	0.5	0.3	0.1	-0.3	0.2	0.3	0.0	0.0
<i>M27</i>	0.0	0.2	-0.1	0.2	-0.2	-0.3	0.1	-0.2	-0.4	-0.5	-0.3
<i>M28</i>	0.5	0.2	0.7	-0.2	0.0	0.1	0.0	0.5	0.1	-0.4	0.1
<i>M29</i>	-0.4	-0.1	0.1	-0.1	-0.1	-0.1	0.0	0.0	0.5	-0.2	-0.4
<i>M30</i>	-0.2	-0.3	0.1	0.3	-0.3	-0.3	-0.4	0.0	0.0	0.2	0.2
<i>M31</i>	-0.1	0.1	-0.7	-0.2	-0.4	0.2	0.2	0.2	-0.2	-0.3	0.0
<i>M32</i>	0.8	0.0	-0.1	0.2	0.3	0.2	-0.1	-0.1	-0.2	0.1	0.1
<i>M33</i>	0.4	-0.5	-0.3	0.4	-0.2	0.1	0.0	-0.1	0.0	0.1	0.3
<i>M34</i>	0.0	-0.1	0.2	0.0	-0.3	-0.1	-0.1	-0.2	-0.2	0.3	-0.4
<i>M35</i>	-0.2	-0.1	-0.4	-0.2	-0.1	-0.2	0.1	-0.5	0.1	0.5	-0.6
<i>M36</i>	-0.1	0.2	0.1	-0.5	0.2	0.3	0.1	0.1	0.1	-0.3	0.1
<i>M37</i>	-1.2	-0.5	-0.6	-0.6	-1.2	-1.2	-0.8	-0.9	-0.5	-0.8	-0.7
<i>M38</i>	5.5	4.9	5.4	5.4	5.7	5.6	5.0	5.3	5.6	5.3	5.2
<i>M39</i>	-72.4	-72.4	-71.5	-72.2	-71.9	-72.3	-72.3	-71.9	-72.2	-72.2	-71.8

The values in red are related to the generation of the end effect, i.e. the contribution to the cogging force due to the entrance and exit of magnets through the region between the stator. The resultant cogging force of each magnet is due to the interaction with the other closer magnets and the iron of the stator. In the case of the magnets from 2 to 38, the attraction component between magnets is balanced, since for each magnet there are two magnets symmetrical places, that produce a null component. In the case of the last and the first magnets, this condition is not verified, consequently it is possible to observe a constant value (about ± 73 N), related to the attractive force of these magnets to the closest ones.

Summing all the contribution from each magnet, the translator is subjected to a resultant force, which trend is reported in the Figure IV.31.

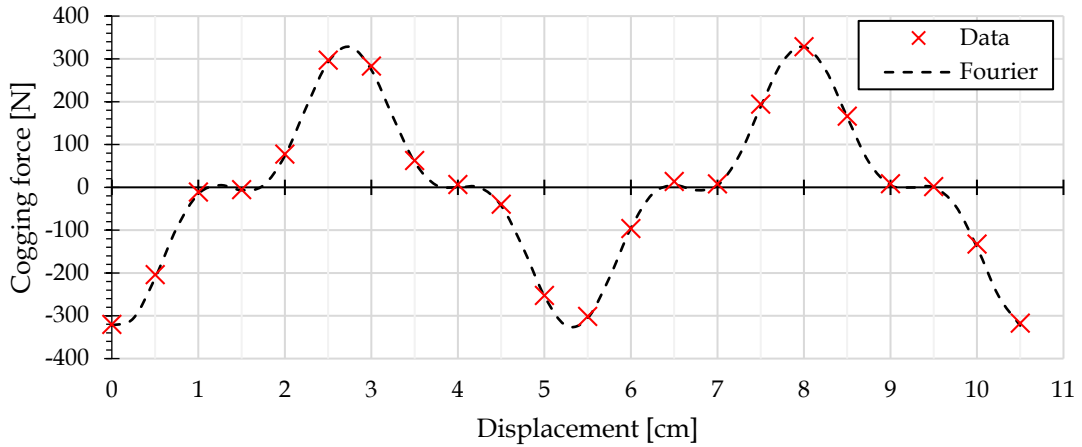


Figure IV.31 Resultant of cogging force considering the configuration “Stator 72”

The points obtained from the simulation were analyzed, evaluating the Fourier series, considering a wavenumber equal to 59.84 rad/m. This value is given by the ratio $2\pi/\lambda_m$, where λ_m is the distance between two magnets having the same pole (10.5 cm). The value of the amplitude and phase of each harmonics of Fourier series are reported in Table IV.11. It is interesting to observe that the main terms are the second and the sixth harmonics. These results carry out that:

- The end effect is not influenced by the verse of magnetization of the magnets, since the phenomenon is related to the second harmonic instead of the first one;
- The alternance of teeth and slots during the motion produce an important component (sixth harmonic), since the distance of two magnets of the same pole is exactly six time the sum of the widths of slots and teeth of the stator. Thus, each magnet inside the stator give a contribution.

Table IV.11 Fourier series coefficients of cogging force, considering the configuration “Stator 72”

Order	Amplitude [N]	Phase [rad]
0	3.95	-
1	0.89	0.4197
2	237.20	4.6044
3	2.20	1.7066
4	6.06	-0.1106
5	0.92	-0.1159
6	90.92	4.4002
7	0.62	3.9536
8	0.29	1.5004
9	2.65	4.2856
10	0.68	0.5510

The data above reported in Table IV.10 can be rearranged, in order to analyze the contribution of a single magnet, crossing the entire region inside the stator. This can be obtained, excluding the contribution of first and the last magnets, if the translator is long enough to permit this movement to the observed magnet. In detail, the trend below reported in Figure IV.32 shows the contribution to the cogging force produced by the second magnet installed on the translator and the comparison with the total force generated by the translator. The vertical green lines indicate the starting and ending points of the stator geometry. It is possible to observe the end effect produced by the magnet, close to the border of the stator and the effect of the alternance of slots and teeth. It should be reminded that the end effect is due only to the magnets closest to the borders of the stator, so the peak of the cogging force of a single magnet has the same order of the peak of the total force produced by the translator. Differently, the alternance of teeth and slots is linked to about eleven magnets, so the small oscillation of the cogging force produced by a single magnet inside the stator region is amplified by one order.

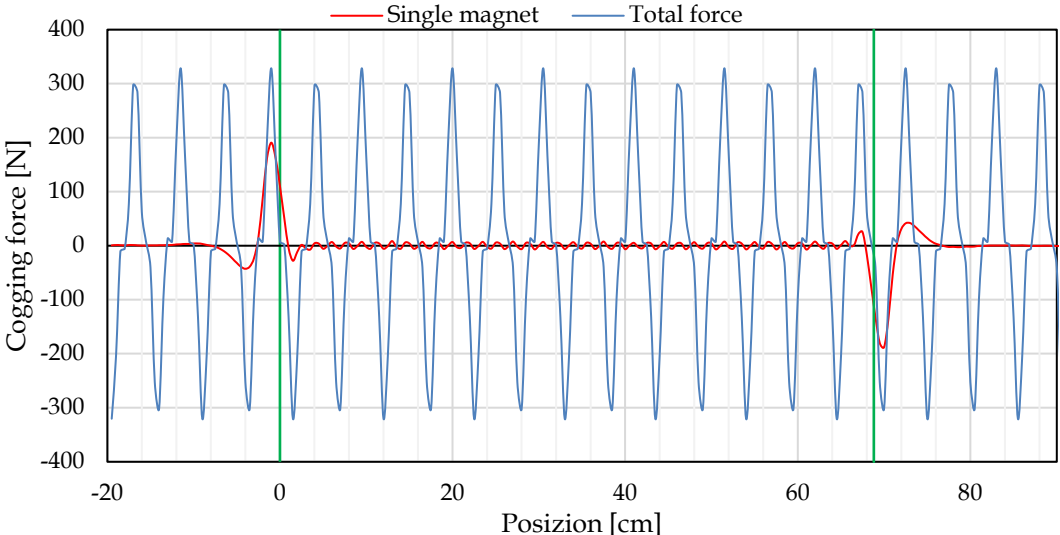


Figure IV.32 Cogging force produced by a magnet and the entire translator with “Stator 72”

As introduced before, the main goal is the achievement of the desired power output, thus according to the results in the previous section, the number of coils in the stator should be doubled.

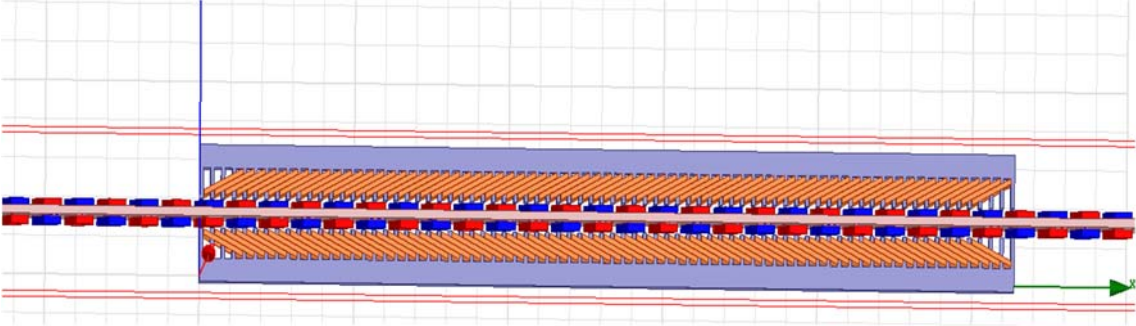


Figure IV.33 Shape of the “Stator 144 A”, modelled in Ansys Maxwell

A simple way is to maintain the shape of teeth and slots and increase their numbers in order to allow the installation of 144 coils, as reported in Figure IV.33. This configuration is identified as “Stator 144 A”. The cogging force was evaluated in this case, obtaining the results reported in Table IV.12. The end effect now is due to the magnets 4-7 and 30-33 since the increasing of the length of the stator. At the same time, the number of magnets that are related to the generation of the sixth harmonic is increased.

Table IV.12 x-axis component of cogging forces generated in the configuration “Stator 144 A”

dX [cm]	0.0	0.5	1.0	1.5	2.0	2.5	3.0	3.5	4.0	4.5	5.0
<i>Tot</i>	-403.9	-218.6	71.0	-41.5	8.3	341.8	324.1	-20.4	-5.2	38.7	-284.0
<i>M1</i>	72.7	72.5	72.8	72.7	73.0	72.6	72.7	72.5	72.6	72.5	72.7
<i>M2</i>	-5.8	-6.0	-5.9	-6.0	-6.0	-5.6	-6.0	-5.7	-5.9	-6.1	-6.0
<i>M3</i>	1.4	1.3	1.4	1.6	1.2	0.9	1.1	1.0	0.8	0.7	0.9
<i>M4</i>	-1.4	-1.3	-0.6	-0.7	0.0	0.6	0.9	1.9	2.2	2.6	2.6
<i>M5</i>	2.8	1.7	0.8	-1.3	-4.5	-9.6	-15.9	-23.1	-31.0	-39.2	-42.5
<i>M6</i>	-42.5	-33.4	-9.9	43.2	124.7	181.3	180.2	135.1	79.9	20.1	-23.7
<i>M7</i>	-27.9	-12.3	0.8	-6.3	-7.2	4.6	3.8	-6.7	-0.5	6.8	-2.8
<i>M8</i>	-7.4	-1.3	7.1	-2.7	-5.3	5.3	4.0	-6.9	-1.3	7.7	-2.3
<i>M9</i>	-6.9	-0.6	7.5	-2.0	-5.9	5.0	3.3	-6.4	-1.1	6.9	-3.1
<i>M10</i>	-6.8	-0.7	6.9	-2.7	-5.8	4.7	3.3	-6.7	-0.7	7.0	-2.5
<i>M11</i>	-6.7	-0.7	7.4	-3.3	-5.4	4.6	4.3	-6.3	-1.3	7.2	-2.6
<i>M12</i>	-6.5	-0.6	6.7	-2.7	-6.1	4.5	3.8	-5.9	-0.5	6.3	-2.2
<i>M13</i>	-6.8	-0.7	7.1	-2.9	-5.8	4.9	4.1	-6.8	-1.0	6.6	-2.0
<i>M14</i>	-7.8	-0.9	7.5	-3.1	-5.8	4.5	3.8	-6.9	-0.3	6.8	-2.3
<i>M15</i>	-6.4	-1.1	6.7	-2.4	-5.1	3.7	3.9	-6.4	-0.9	7.2	-2.1
<i>M16</i>	-6.3	-0.6	6.2	-2.7	-5.9	4.5	3.8	-6.9	0.5	6.7	-2.0
<i>M17</i>	-6.8	-0.4	7.0	-2.8	-4.9	5.1	3.4	-7.3	-0.6	6.6	-2.9
<i>M18</i>	-5.8	-0.7	6.2	-2.4	-5.0	5.2	3.8	-5.7	-0.7	6.9	-3.3
<i>M19</i>	-6.1	-1.1	6.6	-2.4	-5.4	5.2	4.4	-6.4	-0.3	6.1	-1.8
<i>M20</i>	-6.6	-0.8	6.6	-2.4	-5.4	5.2	4.4	-6.3	-1.0	6.9	-3.0
<i>M21</i>	-6.1	-0.3	6.4	-2.7	-5.3	4.5	2.9	-6.3	-0.5	7.0	-2.7
<i>M22</i>	-6.5	-0.4	6.3	-2.3	-5.7	4.2	4.0	-6.6	0.0	6.6	-2.0
<i>M23</i>	-6.3	-1.4	6.8	-2.6	-5.3	3.5	4.1	-6.6	0.0	6.8	-3.3
<i>M24</i>	-6.6	-0.6	7.5	-2.9	-5.9	4.3	4.0	-6.5	0.1	7.5	-3.0
<i>M25</i>	-6.6	-0.4	6.8	-2.5	-5.6	4.8	3.4	-6.9	-0.8	6.3	-2.7
<i>M26</i>	-6.6	-0.4	6.8	-2.8	-5.9	5.1	4.4	-6.4	-0.3	6.4	-2.3
<i>M27</i>	-6.6	-1.4	7.2	-2.5	-5.4	4.8	4.4	-6.5	-0.3	6.0	-2.0
<i>M28</i>	-6.1	-0.3	6.9	-2.6	-5.0	5.0	4.1	-6.8	0.3	7.3	-2.2
<i>M29</i>	-6.9	-0.8	6.9	-2.0	-5.8	4.0	3.2	-6.6	-0.7	5.9	-2.0
<i>M30</i>	-7.0	-0.2	7.6	-2.4	-5.4	5.3	4.7	-7.1	-0.1	7.3	-1.8
<i>M31</i>	-7.2	0.8	9.3	0.8	1.6	20.8	25.0	-14.7	-74.5	-130.8	-176.8
<i>M32</i>	-187.6	-164.9	-92.1	-17.5	21.5	38.7	42.9	39.9	33.0	24.9	16.8
<i>M33</i>	13.1	7.3	3.6	0.7	-1.6	-2.5	-2.9	-3.2	-2.6	-2.4	-1.5
<i>M34</i>	-1.6	-1.1	-0.3	0.0	-0.1	0.4	0.3	1.0	0.2	1.0	0.2
<i>M35</i>	-0.2	0.1	0.1	-0.3	0.3	-0.5	0.0	0.0	-0.4	-0.3	-0.6
<i>M36</i>	0.5	0.3	0.1	0.2	0.8	0.7	0.5	0.7	0.7	0.7	0.7
<i>M37</i>	-1.3	-1.2	-1.3	-1.5	-1.9	-1.7	-1.3	-1.7	-1.4	-1.4	-1.5
<i>M38</i>	5.8	6.4	6.1	5.5	5.9	5.9	6.2	6.1	5.8	6.3	6.0
<i>M39</i>	-72.6	-72.5	-72.6	-72.8	-72.3	-72.6	-72.9	-72.4	-72.5	-72.7	-72.4

(Table follows in the next page).

dX [cm]	5.5	6.0	6.5	7.0	7.5	8.0	8.5	9.0	9.5	10.0	10.5
<i>Tot</i>	-363.2	-38.6	54.7	-75.5	177.4	405.0	125.4	-62.7	55.4	-89.2	-401.0
<i>M1</i>	72.7	72.8	72.6	72.9	73.0	72.6	72.6	72.6	72.9	72.6	72.6
<i>M2</i>	-5.8	-5.6	-6.0	-5.8	-6.3	-6.6	-6.5	-6.5	-6.8	-6.4	-6.9
<i>M3</i>	1.0	1.6	1.7	2.0	2.2	3.0	3.4	3.8	4.3	4.3	4.6
<i>M4</i>	1.7	0.5	-0.7	-3.6	-8.4	-13.0	-20.8	-28.4	-36.3	-42.4	-43.0
<i>M5</i>	-38.8	-23.8	11.9	83.7	159.6	188.2	160.6	108.3	50.5	-4.7	-27.7
<i>M6</i>	-23.1	-3.3	-0.1	-8.9	-1.4	6.9	-3.2	-5.4	4.4	4.1	-6.9
<i>M7</i>	-5.4	4.7	3.2	-7.2	-0.5	6.6	-2.2	-5.9	5.2	3.9	-6.6
<i>M8</i>	-5.4	5.0	3.1	-6.5	-1.0	5.9	-2.2	-6.1	4.2	3.8	-7.1
<i>M9</i>	-5.6	4.2	3.7	-7.1	-0.5	6.8	-2.4	-5.5	4.7	3.5	-6.7
<i>M10</i>	-4.6	4.9	4.4	-6.7	-1.0	6.8	-3.3	-5.7	5.0	3.5	-6.8
<i>M11</i>	-5.0	4.9	4.0	-6.8	-0.1	7.0	-3.1	-5.7	4.7	3.8	-6.4
<i>M12</i>	-5.5	4.8	3.7	-5.8	-0.6	6.7	-3.3	-6.0	4.3	4.1	-6.8
<i>M13</i>	-5.6	5.3	3.9	-6.9	-0.5	6.2	-2.3	-5.5	5.1	3.8	-6.7
<i>M14</i>	-5.5	4.5	3.5	-6.7	0.0	6.7	-2.1	-5.5	4.4	4.0	-6.1
<i>M15</i>	-5.6	5.2	3.9	-6.0	-1.6	7.0	-2.0	-5.4	5.3	3.4	-6.6
<i>M16</i>	-5.1	4.8	4.3	-6.2	-0.7	6.7	-2.6	-5.8	4.7	3.4	-7.2
<i>M17</i>	-5.1	4.3	3.4	-6.7	-0.6	6.9	-2.8	-5.2	4.7	3.5	-6.8
<i>M18</i>	-4.7	5.2	3.7	-6.8	-0.7	7.7	-3.0	-5.8	5.0	3.0	-6.8
<i>M19</i>	-5.1	5.0	3.6	-6.6	-1.0	7.2	-3.2	-5.2	4.7	4.4	-6.4
<i>M20</i>	-5.5	4.4	3.5	-6.4	-0.4	6.5	-3.0	-6.5	5.4	4.0	-6.0
<i>M21</i>	-5.7	4.7	3.3	-6.7	-0.6	7.1	-2.1	-5.4	4.9	3.6	-6.4
<i>M22</i>	-6.2	5.0	4.2	-7.0	-1.2	6.9	-3.4	-5.2	5.5	4.2	-6.1
<i>M23</i>	-6.0	5.6	3.3	-6.6	-0.1	6.6	-3.1	-5.5	5.2	3.0	-7.2
<i>M24</i>	-5.3	4.8	2.9	-6.8	-1.2	6.3	-2.7	-6.4	4.5	3.9	-6.6
<i>M25</i>	-4.8	4.4	3.6	-7.3	-1.2	6.8	-2.7	-5.9	5.2	3.7	-6.0
<i>M26</i>	-5.5	4.6	3.6	-6.6	-1.0	6.6	-2.8	-5.4	4.2	3.6	-6.3
<i>M27</i>	-5.8	4.0	4.5	-7.2	-0.9	6.2	-2.3	-5.6	4.4	4.7	-7.0
<i>M28</i>	-5.6	4.7	3.8	-7.0	-0.4	7.1	-2.5	-5.3	4.9	3.4	-6.6
<i>M29</i>	-4.8	4.8	3.6	-5.9	0.0	7.0	-2.4	-5.1	4.3	4.3	-5.7
<i>M30</i>	-5.6	6.2	6.8	-1.2	10.6	27.2	9.6	-43.8	-102.7	-155.5	-187.6
<i>M31</i>	-183.9	-132.7	-50.7	6.5	32.3	42.1	42.0	36.7	28.9	20.7	13.5
<i>M32</i>	10.3	5.1	2.1	-0.1	-1.7	-2.7	-2.8	-3.2	-2.5	-2.0	-1.5
<i>M33</i>	-1.2	-0.8	-0.6	0.0	-0.1	0.7	0.4	0.3	0.1	0.5	0.2
<i>M34</i>	0.3	0.6	0.0	0.4	0.1	0.0	-0.1	-0.1	-0.3	-0.2	0.4
<i>M35</i>	-0.4	-0.5	-0.1	-0.5	-0.3	-0.2	-0.3	-0.5	0.0	0.1	-0.1
<i>M36</i>	0.6	0.4	0.5	0.4	0.7	0.2	0.3	0.5	0.2	0.2	0.3
<i>M37</i>	-1.5	-1.7	-1.0	-1.1	-1.0	-1.3	-1.4	-1.4	-1.5	-1.1	-1.9
<i>M38</i>	5.9	5.6	6.1	6.0	6.4	5.7	5.5	5.7	6.0	6.1	6.4
<i>M39</i>	-72.1	-72.8	-72.5	-72.7	-72.5	-72.8	-72.3	-71.8	-72.4	-72.4	-72.5

The Fourier series was evaluated in order to realize a comparison with the results of the previous simulation. The comparison of the Fourier series coefficients is reported in Table IV.13. The trend of the cogging force obtained in the configuration “Stator 144 A” is reported in Figure IV.34.

The comparison confirms the correlation between harmonics and number of magnets:

- The second harmonic assumes more or less the same value in both conditions, since the number of magnets that interact with the borders of the stator is the same;

- The sixth harmonic is linearly amplified with the number of active magnets able to interact with the teeth of the stator or equivalently with the total number of teeth realized on the translator. Indeed, in the previous configuration there are 40 teeth, while in this one 76, thus the ratio is 1.9:1. The same value is obtained dividing the corresponding amplitudes of the sixth harmonic.

Table IV.13 Comparison of Fourier series coefficients considering “Stator 72” and “Stator 144 A”

Order	Stator 72		Stator 144 A	
	Amplitude [N]	Phase [rad]	Amplitude [N]	Phase [rad]
0	3.95	-	0.02	-
1	0.89	0.4197	1.56	-0.8706
2	237.20	4.6044	233.95	4.6055
3	2.20	1.7066	2.13	2.3769
4	6.06	-0.1106	6.57	-0.1917
5	0.92	-0.1159	1.62	4.2413
6	90.92	4.4002	172.83	4.3956
7	0.62	3.9536	0.84	4.2314
8	0.29	1.5004	0.34	-0.1109
9	2.65	4.2856	6.30	3.7086
10	0.68	0.5510	1.13	2.1534

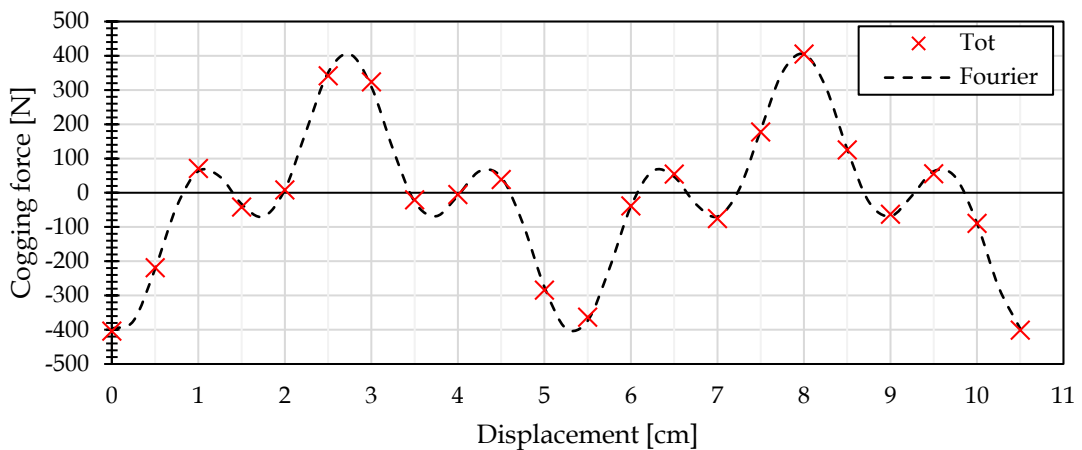


Figure IV.34 Resultant of cogging force considering the configuration “Stator 144 A”

As shown in Figure IV.34, the peak of cogging force is about 400 N. This value is not acceptable, so a solution is required. Instead of creating a unique uniform stator, it is possible to realize two separate stators, located at a distance able to minimize the total cogging force generated by the translator.

As reported in Table IV.13, the main contributions to the cogging force are the second and the sixth harmonics, so a distance able to nullify these terms can be found. As demonstrated in Table IV.14, this condition is verified if the second term is out of phase by the amount $\pi/4$. However, there are also collateral effects: all odd harmonics are amplified by $\sqrt{2}$ while the fourth and the eighth harmonics are doubled.

Table IV.14 Sum of harmonics

Order	Terms	Equivalent to	Result
1	$\sin(x) + \sin\left(x + \frac{\pi}{2}\right)$	$\sin(x) + \cos(x)$	$\sqrt{2} \sin\left(x + \frac{\pi}{4}\right)$
2	$\sin(2x) + \sin\left(2x + 2\frac{\pi}{2}\right)$	$\sin(2x) - \sin(2x)$	0
3	$\sin(3x) + \sin\left(3x + 3\frac{\pi}{2}\right)$	$\sin(3x) - \cos(3x)$	$\sqrt{2} \sin\left(2x - \frac{\pi}{4}\right)$
4	$\sin(4x) + \sin\left(4x + 4\frac{\pi}{2}\right)$	$\sin(4x) + \sin(4x)$	$2 \sin(4x)$
5	$\sin(5x) + \sin\left(5x + 5\frac{\pi}{2}\right)$	$\sin(5x) + \cos(5x)$	$\sqrt{2} \sin\left(5x + \frac{\pi}{4}\right)$
6	$\sin(6x) + \sin\left(6x + 6\frac{\pi}{2}\right)$	$\sin(6x) - \sin(6x)$	0
7	$\sin(7x) + \sin\left(7x + 7\frac{\pi}{2}\right)$	$\sin(7x) - \cos(7x)$	$\sqrt{2} \sin\left(7x - \frac{\pi}{4}\right)$
8	$\sin(8x) + \sin\left(8x + 8\frac{\pi}{2}\right)$	$\sin(8x) + \sin(8x)$	$2 \sin(8x)$
9	$\sin(9x) + \sin\left(9x + 9\frac{\pi}{2}\right)$	$\sin(9x) + \cos(9x)$	$\sqrt{2} \sin\left(9x + \frac{\pi}{4}\right)$
10	$\sin(10x) + \sin\left(10x + 10\frac{\pi}{2}\right)$	$\sin(10x) - \sin(10x)$	0

Thus, an alternative solution is the realization of two stators, separated by a distance able to create a phase shift equal to $\pi/4$. As first solution, the geometry reported in Figure IV.35 was considered. The space between the two stators is equal to 2.075 cm. In detail this amount was obtained by considering the initial point of the second machine located at 7 times the distance λ_m reduced by one quarter of λ_m . This new configuration is denominated "Stator 144 B".

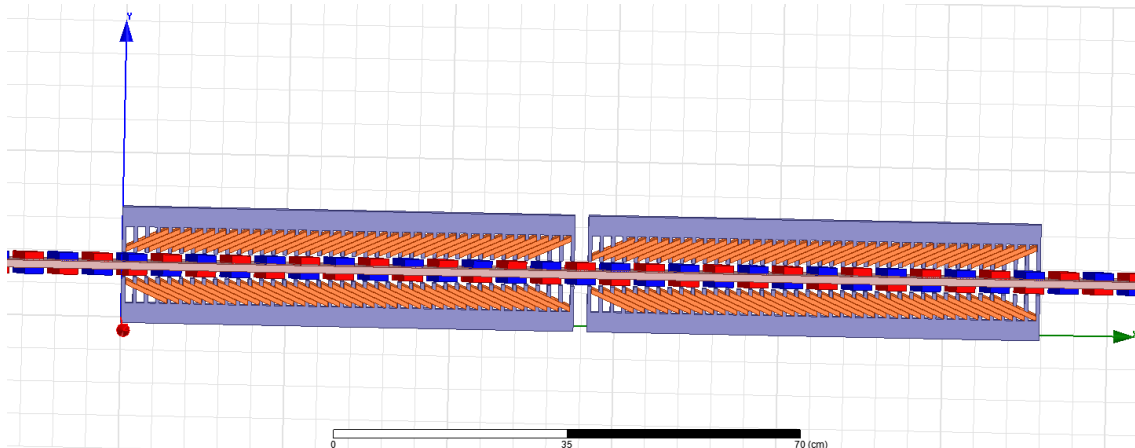


Figure IV.35 Shape of the "Stator 144 B" modelled on Ansys Maxwell

Similar to the previous case studies, Table IV.15 reports the results of the simulation about the cogging force, showing the contribution of each magnet and the total resultant force applied to the translator. The red lines are related to the end effects. In comparison with the previous case, it is possible to observe the contribution of the central magnets 18-20 to the end effect.

Table IV.15 x-axis component of cogging forces generated in the configuration "Stator 144 B"

dX [cm]	0.0	0.5	1.0	1.5	2.0	2.5	3.0	3.5	4.0	4.5	5.0
<i>Tot</i>	-17.0	47.6	74.1	54.3	40.3	0.0	-6.4	-33.4	-63.2	-67.6	-46.8
<i>M1</i>	72.4	72.8	72.5	72.3	72.6	72.2	72.7	73.3	72.6	72.8	72.6
<i>M2</i>	-5.5	-5.7	-5.7	-5.6	-5.1	-5.9	-5.7	-5.3	-5.7	-5.3	-5.3
<i>M3</i>	0.9	1.4	1.1	0.7	0.8	1.1	0.5	0.7	0.1	0.8	0.8
<i>M4</i>	-0.7	-0.7	-0.3	-0.1	0.0	0.7	1.7	1.7	2.6	2.4	2.1
<i>M5</i>	2.5	1.5	0.2	-2.1	-5.3	-10.5	-16.6	-23.8	-32.1	-39.4	-42.4
<i>M6</i>	-41.9	-32.0	-7.2	46.8	130.7	186.9	184.4	138.3	81.2	20.7	-23.9
<i>M7</i>	-28.9	-12.1	1.3	-6.3	-7.0	3.6	3.0	-6.7	-0.5	7.8	-3.1
<i>M8</i>	-6.7	-1.1	6.5	-2.4	-5.5	5.0	3.1	-7.1	-0.2	7.6	-2.9
<i>M9</i>	-6.9	-0.6	7.2	-2.1	-6.2	4.7	4.1	-6.6	-0.5	6.1	-2.2
<i>M10</i>	-7.2	-1.0	7.4	-3.7	-5.2	4.7	3.5	-6.4	0.3	6.3	-1.3
<i>M11</i>	-5.7	-0.5	7.1	-2.8	-5.3	4.7	3.2	-6.2	-0.9	6.6	-3.7
<i>M12</i>	-6.6	-0.4	6.6	-2.6	-5.1	5.7	4.3	-6.7	0.0	7.0	-2.6
<i>M13</i>	-6.6	0.0	6.9	-3.1	-6.0	5.6	3.7	-6.9	-1.0	7.0	-3.0
<i>M14</i>	-6.2	0.3	7.3	-1.9	-4.8	5.7	3.6	-6.5	-0.6	7.7	-2.1
<i>M15</i>	-7.2	-1.1	6.6	-2.2	-6.2	3.7	3.7	-6.3	-0.5	5.6	-2.9
<i>M16</i>	-6.7	-0.3	6.0	-2.4	-5.3	4.4	4.9	-4.9	-0.4	6.7	-3.1
<i>M17</i>	-7.2	-0.9	6.9	-2.8	-5.3	4.4	3.1	-6.0	-0.8	6.1	-3.2
<i>M18</i>	-6.6	-0.6	7.1	-3.0	-5.1	4.5	3.8	-5.9	-1.1	6.8	-2.5
<i>M19</i>	-6.7	0.6	7.9	0.3	-4.7	6.5	-1.1	-45.2	-82.2	-63.8	-24.9
<i>M20</i>	-8.4	30.9	69.3	79.5	38.3	-1.5	-5.8	4.8	0.3	-7.9	2.1
<i>M21</i>	6.4	0.3	-6.7	2.1	6.3	-5.0	-3.8	7.0	-0.5	-6.8	2.0
<i>M22</i>	6.3	1.1	-7.2	3.5	7.2	-4.5	-3.3	6.9	0.9	-7.0	2.2
<i>M23</i>	6.1	0.8	-6.9	1.7	6.2	-6.4	-4.1	6.4	0.9	-5.6	0.8
<i>M24</i>	5.9	1.3	-6.4	2.7	6.1	-4.9	-2.6	6.9	0.6	-6.5	1.8
<i>M25</i>	5.8	0.8	-6.6	1.9	6.1	-5.8	-2.9	5.9	-0.4	-6.7	3.7
<i>M26</i>	6.5	0.9	-6.4	3.1	6.1	-6.0	-3.2	6.5	0.6	-6.6	2.8
<i>M27</i>	7.1	0.4	-7.1	1.8	5.0	-5.8	-4.5	5.6	0.1	-7.0	1.9
<i>M28</i>	6.6	0.6	-6.2	1.8	6.1	-5.7	-3.6	6.0	1.3	-7.0	1.4
<i>M29</i>	5.7	-0.2	-6.5	2.0	5.9	-5.4	-3.0	6.7	-0.1	-4.9	1.9
<i>M30</i>	6.1	0.6	-7.1	2.5	6.2	-5.1	-3.2	6.9	0.8	-6.0	1.7
<i>M31</i>	6.8	0.5	-7.1	0.9	6.0	-5.4	-3.1	6.8	1.3	-7.0	3.1
<i>M32</i>	7.8	0.9	-6.4	3.2	7.0	-5.0	-2.5	7.4	4.1	-1.3	16.3
<i>M33</i>	25.3	19.3	-29.1	-90.8	-145.9	-188.8	-181.5	-117.8	-36.3	12.1	33.9
<i>M34</i>	39.7	42.5	38.5	30.8	22.9	16.0	9.5	5.2	1.8	-0.2	-1.6
<i>M35</i>	-2.4	-3.0	-2.6	-2.8	-2.2	-1.8	-1.4	-0.9	-0.6	-0.1	0.3
<i>M36</i>	0.3	0.6	0.3	0.7	0.2	0.4	0.7	0.3	0.1	-0.2	0.0
<i>M37</i>	-0.9	-1.3	-0.8	-0.8	-1.2	-1.1	-0.8	-0.6	-0.2	-1.3	-0.6
<i>M38</i>	6.0	5.4	5.4	5.8	5.7	6.1	5.8	5.6	5.1	5.6	5.4
<i>M39</i>	-72.1	-72.5	-72.0	-72.3	-72.1	-72.5	-72.3	-71.8	-71.8	-72.3	-72.3

(Table follows in the next page).

dX [cm]	5.5	6.0	6.5	7.0	7.5	8.0	8.5	9.0	9.5	10.0	10.5
<i>Tot</i>	32.8	59.3	78.1	42.4	18.5	4.6	-25.8	-45.4	-79.0	-53.9	-18.6
<i>M1</i>	72.4	72.3	72.1	72.6	72.9	73.2	72.5	73.2	73.0	72.7	72.6
<i>M2</i>	-5.4	-5.5	-5.4	-6.0	-6.0	-5.9	-6.5	-5.9	-6.3	-5.8	-5.7
<i>M3</i>	0.8	0.8	1.5	1.6	1.9	2.6	2.9	3.5	4.0	4.0	3.3
<i>M4</i>	1.5	0.4	-0.8	-4.1	-8.3	-14.0	-20.8	-28.7	-36.5	-41.8	-42.3
<i>M5</i>	-37.9	-21.7	15.1	88.2	163.7	193.6	164.5	110.0	50.9	-5.7	-28.4
<i>M6</i>	-22.7	-2.6	-1.1	-9.7	-0.8	6.7	-2.7	-5.2	3.8	3.2	-7.0
<i>M7</i>	-5.1	4.0	4.2	-5.2	0.4	6.6	-2.0	-6.1	4.2	4.0	-6.3
<i>M8</i>	-4.9	4.3	4.6	-6.0	0.5	6.9	-3.9	-5.0	4.1	4.1	-7.5
<i>M9</i>	-5.8	5.1	3.3	-6.2	0.0	7.4	-2.4	-6.2	5.1	4.3	-6.6
<i>M10</i>	-5.9	4.2	4.1	-6.3	-1.8	6.7	-2.5	-5.3	5.4	4.0	-6.3
<i>M11</i>	-5.1	4.8	3.3	-6.7	0.6	6.5	-2.1	-5.0	4.9	4.2	-7.2
<i>M12</i>	-5.0	5.3	4.0	-6.6	-0.7	7.0	-2.3	-6.3	4.1	4.4	-6.8
<i>M13</i>	-6.0	4.2	5.4	-6.9	-1.1	7.3	-2.0	-4.5	4.9	2.9	-5.9
<i>M14</i>	-5.3	5.6	4.6	-7.8	-0.1	6.8	-2.2	-5.8	4.1	3.4	-6.6
<i>M15</i>	-4.8	4.7	3.9	-6.3	-0.7	7.1	-2.0	-5.0	4.2	3.9	-6.6
<i>M16</i>	-5.2	5.4	3.3	-7.2	-1.2	6.4	-2.4	-5.2	4.2	4.8	-7.5
<i>M17</i>	-5.9	5.5	4.4	-6.3	-0.7	6.9	-2.3	-5.7	6.2	4.0	-7.6
<i>M18</i>	-6.6	5.7	5.1	-5.0	0.9	7.2	-20.8	-68.7	-79.2	-45.7	-7.7
<i>M19</i>	13.5	51.0	81.6	62.6	14.2	-7.5	0.4	3.7	-5.5	-4.2	6.9
<i>M20</i>	6.9	-5.6	-3.9	6.7	0.0	-6.7	2.3	5.5	-6.0	-3.0	6.5
<i>M21</i>	6.3	-5.7	-3.3	7.0	1.5	-6.8	2.8	6.2	-5.0	-3.4	6.3
<i>M22</i>	5.9	-5.3	-2.6	5.6	0.3	-6.7	2.0	5.9	-6.8	-2.5	6.8
<i>M23</i>	6.2	-5.7	-2.4	6.0	0.9	-6.5	2.1	6.3	-4.7	-3.3	6.4
<i>M24</i>	5.9	-5.7	-3.9	6.0	0.5	-7.2	1.6	5.9	-5.6	-2.8	5.9
<i>M25</i>	5.9	-4.8	-3.2	6.5	-0.2	-5.9	2.2	6.0	-4.5	-3.8	5.5
<i>M26</i>	5.7	-5.5	-3.2	5.3	0.6	-6.3	2.9	5.9	-4.8	-3.6	5.7
<i>M27</i>	7.0	-4.7	-3.8	6.5	1.2	-6.3	1.7	6.5	-5.3	-3.7	6.6
<i>M28</i>	6.1	-5.3	-2.4	6.6	0.3	-6.0	2.1	5.8	-5.5	-3.0	6.5
<i>M29</i>	6.2	-5.2	-2.8	6.9	0.0	-6.3	3.8	5.4	-4.9	-3.3	5.6
<i>M30</i>	6.4	-5.8	-3.5	5.5	1.3	-5.9	2.0	6.6	-5.5	-3.3	7.0
<i>M31</i>	5.9	-5.1	-4.1	7.2	1.5	-6.5	3.5	8.7	-1.0	5.1	25.6
<i>M32</i>	29.1	-1.2	-59.8	-120.0	-172.1	-193.2	-156.1	-75.8	-7.3	25.7	39.6
<i>M33</i>	41.8	41.3	35.2	27.0	18.9	12.6	7.3	3.2	0.5	-0.9	-2.7
<i>M34</i>	-2.3	-2.9	-2.7	-2.2	-1.6	-1.2	-1.0	-0.4	0.3	0.7	0.2
<i>M35</i>	0.3	0.1	0.4	1.0	0.5	-0.1	0.7	0.4	-0.2	0.0	-0.5
<i>M36</i>	-0.3	-0.3	-0.1	-0.2	-0.4	0.1	-0.1	-0.1	0.0	0.3	0.0
<i>M37</i>	-0.5	-1.1	-0.8	-0.9	-1.1	-1.1	-0.7	-1.1	-0.8	-0.9	-1.1
<i>M38</i>	5.5	5.1	5.2	5.3	5.4	5.4	5.5	5.4	5.4	5.3	5.1
<i>M39</i>	-71.6	-72.1	-72.5	-72.1	-72.7	-71.9	-71.9	-71.6	-72.1	-72.0	-71.8

In this case, a significant reduction of the resultant cogging force is observed, as reported in Figure IV.36. In this configuration the peak is about 80 N in comparison with the case “Stator 144 A” (400 N) and “Stator 72” (320 N).

The Fourier series coefficients were evaluated. As expected, all the odd harmonics are increased, the only exception is the third one. As reported in Table IV.16, the new configuration shows a remarkable reduction (-75%) of the second harmonic and the complete removal of the sixth one. Thus, in this new configuration the Fourier series practically comprises second, fourth and ninth harmonics.

Table IV.16 Comparison of Fourier series coefficients considering “Stator 72” and “Stator 144 B”

Order	Stator 72		Stator 144 B	
	Amplitude [N]	Phase [rad]	Amplitude [N]	Phase [rad]
0	3.95	-	0.60	-
1	0.89	0.4197	1.30	4.5724
2	237.20	4.6044	65.27	-0.1094
3	2.20	1.7066	0.28	4.1394
4	6.06	-0.1106	19.00	-0.2043
5	0.92	-0.1159	1.52	3.0082
6	90.92	4.4002	0.77	0.0251
7	0.62	3.9536	1.40	-1.2708
8	0.29	1.5004	1.03	-1.0038
9	2.65	4.2856	7.91	3.5752
10	0.68	0.5510	1.46	-0.4297

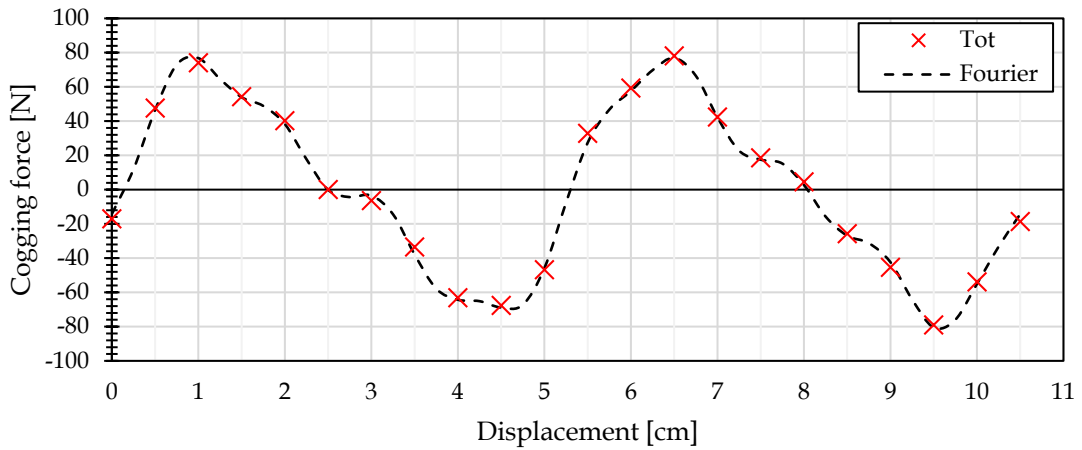


Figure IV.36 Resultant of cogging force considering the configuration “Stator 144 B”

However, according to Table IV.14, it was expected the complete removal of the second harmonic.

This different result is related by the fact that the two stators are too close, thus the magnets at the border are not able to produce a strong component able to balance the forces produced by the other terminal magnets. This is evident in Figure IV.37, comparing the cogging force produced by the magnet when it is located close to 0 cm and 140 cm and when the magnet is in the middle position corresponding to the transition from one stator to the other. Anyway, it is relevant that the resultant cogging force generated by the translator has a peak lower than the peak of the cogging force produced by a single magnet.

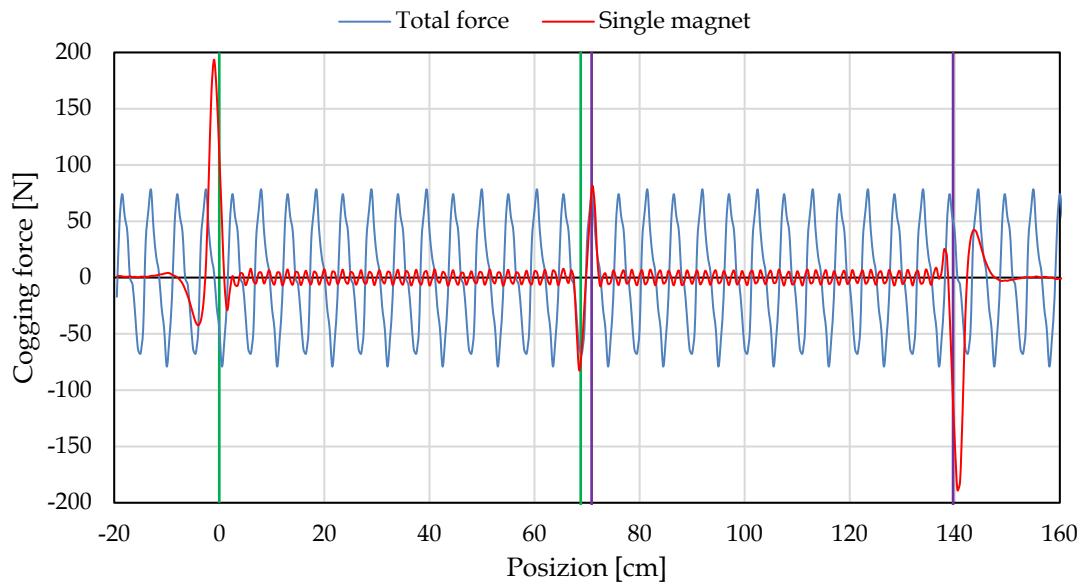


Figure IV.37 Cogging force produced by a magnet and the entire translator with “Stator 144 B”

In order to reduce furthermore the resultant cogging force, another configuration was considered, increasing the space between the two stators to the value 7.325 cm (equal to the distance λ_m reduced by one quarter). This solution is called “Stator 144 C”.

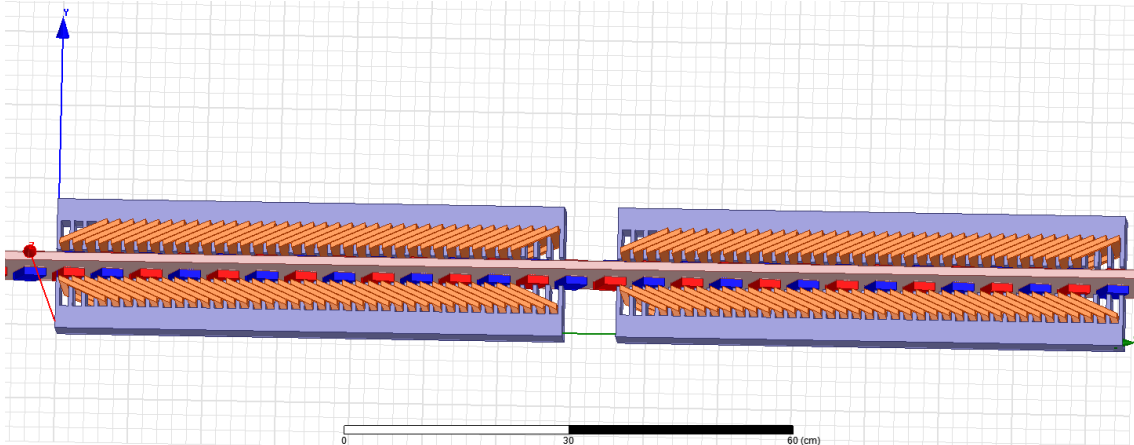


Figure IV.38 Shape of the “Stator 144 C” modelled on Ansys Maxwell

Like in the other cases, the new configuration was simulated on Ansys Maxwell in order to evaluate the contribution of each magnet to the generation of the cogging force. As reported in Table IV.17, in this configuration there is one more row of magnets in the middle position that generate a contribution to the end effect of cogging force.

Table IV.17 x-axis component of cogging forces generated in the configuration "Stator 144 C"

dX [cm]	0.0	0.5	1.0	1.5	2.0	2.5	3.0	3.5	4.0	4.5	5.0
<i>Tot</i>	-11.1	7.1	4.1	-11.4	-11.5	-13.6	13.6	18.9	6.9	-6.5	-15.2
<i>M1</i>	72.8	72.5	72.6	72.5	72.5	72.5	72.5	72.3	72.7	72.3	72.8
<i>M2</i>	-5.4	-5.7	-6.0	-5.8	-5.8	-6.1	-5.2	-5.6	-5.1	-5.1	-5.4
<i>M3</i>	1.3	1.1	0.7	1.2	0.9	1.1	0.3	1.0	-0.1	1.0	0.6
<i>M4</i>	-0.9	-0.5	-0.3	0.0	0.4	0.7	1.3	1.7	2.0	2.3	2.2
<i>M5</i>	2.5	2.1	0.8	-1.8	-5.1	-10.1	-16.2	-23.4	-32.2	-39.1	-42.5
<i>M6</i>	-42.7	-33.7	-8.8	44.7	127.6	183.9	182.7	137.6	80.9	20.2	-23.3
<i>M7</i>	-29.1	-13.2	0.8	-5.9	-7.7	4.2	3.8	-6.9	0.1	7.0	-2.6
<i>M8</i>	-6.8	-2.0	5.9	-2.7	-6.7	4.3	3.6	-6.7	-0.3	7.3	-2.7
<i>M9</i>	-6.0	-0.2	6.4	-2.4	-5.0	5.6	3.8	-6.8	-0.7	6.3	-2.9
<i>M10</i>	-7.0	-0.5	7.1	-2.6	-5.4	5.6	3.4	-7.2	-0.2	7.3	-2.7
<i>M11</i>	-6.4	-0.9	6.9	-3.1	-5.2	4.7	3.4	-6.7	-0.3	6.5	-1.8
<i>M12</i>	-6.8	-0.5	6.5	-1.3	-5.1	5.7	4.4	-6.0	-0.8	7.8	-2.2
<i>M13</i>	-5.6	-1.0	6.2	-1.8	-6.0	4.9	4.5	-6.0	-0.7	5.9	-2.3
<i>M14</i>	-6.1	-1.6	6.3	-2.9	-5.2	5.8	3.6	-7.1	-0.8	6.7	-2.7
<i>M15</i>	-5.9	-1.2	6.5	-3.0	-5.5	4.5	3.5	-6.1	-1.0	6.9	-2.7
<i>M16</i>	-6.6	-1.5	7.8	-3.1	-5.3	5.8	3.3	-5.2	-0.4	6.0	-2.6
<i>M17</i>	-6.5	1.1	7.6	-2.2	-5.2	5.3	4.5	-6.7	-1.2	5.7	-2.0
<i>M18</i>	-7.3	0.2	7.9	-1.2	-5.8	5.1	3.9	-5.4	-0.6	6.9	-2.0
<i>M19</i>	-6.7	0.7	8.4	2.4	1.3	21.7	26.0	-15.0	-75.9	-138.1	-190.6
<i>M20</i>	-204.9	-189.1	-124.4	-55.8	-22.0	-5.9	6.9	25.5	63.8	135.4	195.2
<i>M21</i>	206.5	183.3	128.1	66.6	6.2	-28.2	-18.5	0.2	-2.9	-8.0	1.8
<i>M22</i>	5.8	-0.5	-7.6	2.0	6.0	-5.1	-3.9	6.4	0.3	-6.7	2.6
<i>M23</i>	6.4	1.1	-6.5	2.2	6.3	-5.2	-3.3	7.0	0.5	-7.3	2.1
<i>M24</i>	6.7	0.1	-7.0	2.4	6.0	-5.4	-3.4	5.9	0.1	-7.2	2.5
<i>M25</i>	6.8	1.6	-7.4	2.6	6.5	-5.4	-4.0	6.6	1.7	-7.9	2.0
<i>M26</i>	6.0	0.6	-7.5	1.9	6.7	-6.0	-3.9	6.6	1.3	-7.1	1.2
<i>M27</i>	6.7	0.7	-6.6	3.1	5.7	-4.4	-3.5	6.9	0.0	-7.1	1.7
<i>M28</i>	5.3	0.2	-7.0	2.0	5.8	-6.4	-3.9	5.9	0.3	-6.3	1.8
<i>M29</i>	5.9	1.0	-5.7	2.7	5.2	-5.3	-3.7	6.3	0.0	-6.3	2.6
<i>M30</i>	6.5	0.1	-7.2	2.0	5.9	-5.7	-3.1	7.5	0.5	-6.3	2.6
<i>M31</i>	6.3	0.7	-6.0	2.0	6.3	-5.4	-3.3	6.9	0.9	-6.1	2.2
<i>M32</i>	6.8	0.8	-6.1	1.7	6.1	-5.0	-3.5	6.5	0.2	-5.7	2.8
<i>M33</i>	6.0	1.1	-6.5	1.9	5.8	-4.3	-3.8	9.1	4.4	-1.1	15.0
<i>M34</i>	25.2	18.6	-30.9	-90.3	-144.1	-187.1	-179.8	-114.6	-33.8	14.1	35.1
<i>M35</i>	40.2	43.0	38.1	30.8	22.7	14.8	9.0	4.3	1.4	-0.6	-2.0
<i>M36</i>	-2.2	-2.9	-2.5	-2.6	-2.0	-1.6	-0.5	-0.5	-0.3	0.1	0.2
<i>M37</i>	-0.7	-0.1	-0.2	-0.6	-0.7	-0.5	-0.4	-0.6	-0.9	-1.0	-1.1
<i>M38</i>	5.5	5.2	5.4	5.7	5.1	5.6	6.0	5.6	5.2	5.4	5.6
<i>M39</i>	-72.1	-72.1	-72.2	-72.3	-72.0	-72.2	-72.6	-71.9	-72.2	-72.1	-71.9

(Table follows in the next page).

dX [cm]	5.5	6.0	6.5	7.0	7.5	8.0	8.5	9.0	9.5	10.0	10.5
<i>Tot</i>	9.8	4.0	4.4	-16.2	-9.5	2.9	11.5	16.6	-5.9	-7.7	-11.1
<i>M1</i>	72.5	72.4	72.7	73.1	72.2	72.4	72.9	72.3	73.2	73.2	72.5
<i>M2</i>	-5.4	-5.4	-5.5	-5.6	-5.4	-5.8	-5.6	-6.0	-6.1	-6.1	-5.9
<i>M3</i>	0.5	0.9	1.4	1.4	2.1	2.3	3.2	3.4	4.0	3.8	3.0
<i>M4</i>	1.7	0.7	-0.7	-3.5	-7.8	-13.2	-20.5	-28.7	-36.8	-42.5	-42.8
<i>M5</i>	-38.9	-23.8	13.5	85.8	162.7	191.0	162.7	109.7	51.8	-5.7	-28.3
<i>M6</i>	-22.3	-3.5	0.2	-8.9	-0.9	6.7	-3.2	-6.3	4.6	3.3	-6.8
<i>M7</i>	-6.0	4.4	4.2	-7.0	-0.2	7.5	-2.7	-5.1	3.6	3.4	-6.8
<i>M8</i>	-5.6	5.2	4.1	-6.5	-0.3	7.1	-3.0	-6.1	4.1	3.8	-6.5
<i>M9</i>	-6.1	5.0	3.5	-6.7	-0.3	6.7	-2.8	-4.7	5.3	3.3	-6.6
<i>M10</i>	-5.2	5.2	4.6	-6.3	0.5	6.6	-2.7	-5.6	4.4	4.0	-7.2
<i>M11</i>	-5.0	3.8	3.7	-6.5	-0.7	7.4	-1.6	-5.5	4.5	4.3	-7.3
<i>M12</i>	-5.3	5.1	4.1	-7.6	0.0	6.2	-2.2	-5.2	3.5	3.5	-7.1
<i>M13</i>	-6.2	4.1	3.1	-6.8	-1.5	6.8	-2.4	-5.3	4.8	4.7	-6.5
<i>M14</i>	-6.1	4.2	5.0	-6.0	-0.7	6.3	-2.5	-5.5	5.0	3.8	-6.4
<i>M15</i>	-5.3	3.6	4.3	-5.0	0.5	7.1	-2.8	-4.9	5.7	4.2	-6.3
<i>M16</i>	-4.8	4.9	3.9	-5.7	-0.1	7.3	-2.9	-6.1	4.6	3.0	-5.8
<i>M17</i>	-5.6	5.4	3.9	-6.7	1.0	6.9	-2.3	-5.9	5.4	3.9	-7.9
<i>M18</i>	-5.8	6.6	6.4	-2.7	11.1	29.4	10.6	-45.8	-107.3	-166.4	-205.5
<i>M19</i>	-205.1	-160.4	-86.8	-35.1	-12.2	1.0	15.2	40.5	97.8	170.6	206.5
<i>M20</i>	201.8	158.0	98.8	35.4	-16.9	-26.9	-8.0	1.6	-7.6	-4.6	6.7
<i>M21</i>	6.0	-4.7	-4.3	5.8	1.1	-7.5	1.6	6.4	-5.6	-3.5	5.8
<i>M22</i>	5.4	-4.1	-3.0	7.3	0.7	-7.1	2.1	5.4	-5.2	-2.8	5.5
<i>M23</i>	6.2	-5.6	-3.8	6.9	0.3	-7.0	1.1	5.7	-4.8	-3.3	5.7
<i>M24</i>	6.5	-5.7	-3.5	6.3	0.6	-6.1	2.3	6.8	-4.5	-3.2	5.9
<i>M25</i>	6.4	-5.4	-3.1	6.3	0.0	-7.6	3.0	6.2	-5.8	-4.2	6.2
<i>M26</i>	6.1	-4.8	-3.3	6.9	1.7	-6.8	2.9	5.1	-5.1	-3.9	6.8
<i>M27</i>	5.3	-4.4	-3.6	6.3	-0.4	-6.8	2.4	5.7	-5.4	-3.1	6.9
<i>M28</i>	6.5	-4.8	-3.5	7.2	1.7	-7.5	2.1	5.6	-5.5	-3.4	5.8
<i>M29</i>	6.3	-5.6	-3.5	6.9	0.3	-5.8	2.2	6.4	-5.2	-2.8	6.9
<i>M30</i>	5.7	-5.3	-3.6	6.2	0.0	-7.1	2.1	6.3	-5.2	-4.4	5.4
<i>M31</i>	6.1	-6.5	-4.7	5.7	1.1	-6.2	2.5	6.4	-5.3	-3.5	5.9
<i>M32</i>	7.0	-6.3	-3.6	6.7	1.5	-5.7	4.4	7.8	-0.3	5.4	25.4
<i>M33</i>	27.8	-1.2	-61.3	-120.2	-169.5	-191.6	-153.2	-73.7	-5.6	26.9	40.1
<i>M34</i>	43.0	41.9	35.3	26.6	19.4	11.8	6.8	3.0	0.7	-1.6	-2.5
<i>M35</i>	-2.7	-2.6	-3.3	-2.6	-1.9	-1.6	-1.1	-0.8	0.0	-0.1	0.2
<i>M36</i>	0.6	0.5	0.4	0.7	0.8	0.3	0.0	0.6	0.4	0.5	0.1
<i>M37</i>	-1.3	-1.0	-1.1	-1.1	-1.0	-0.6	-1.0	-0.8	-0.8	-0.7	-0.7
<i>M38</i>	5.2	5.7	5.9	5.5	5.4	5.6	5.8	5.9	5.7	4.8	5.3
<i>M39</i>	-71.8	-71.9	-71.9	-72.6	-72.2	-72.4	-72.3	-72.3	-72.1	-72.1	-71.9

The Fourier series was evaluated, considering the resultant cogging force generated by the translator. As reported in Table IV.18, it is possible to observe that the configuration “Stator 144 C” is able to reduce almost completely the second harmonic (from 232.7 to 5.4 N), while the sixth is negligible. As expected from Table IV.14, the fourth harmonic is almost double. It is interesting to observe the presence of a ninth harmonic, but this term could be related to the precision adopted in the simulation.

Table IV.18 Comparison of Fourier series coefficients in the case "Stator 72" and "Stator 144 C"

Order	Stator 72		Stator 144 C	
	Amplitude [N]	Phase [rad]	Amplitude [N]	Phase [rad]
0	3.95	-	-0.42	
1	0.89	0.4197	1.34	4.4671
2	237.20	4.6044	5.41	3.3862
3	2.20	1.7066	0.45	1.9930
4	6.06	-0.1106	13.19	-0.2839
5	0.92	-0.1159	1.36	3.7133
6	90.92	4.4002	1.05	0.1550
7	0.62	3.9536	0.52	-0.3815
8	0.29	1.5004	0.76	-1.2519
9	2.65	4.2856	5.15	3.7531
10	0.68	0.5510	1.33	-0.2584

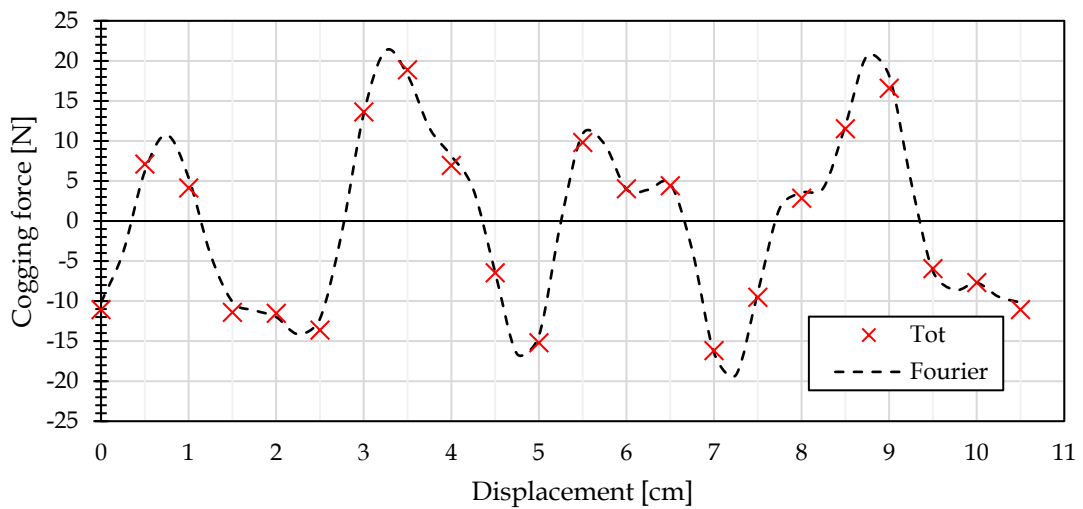


Figure IV.39 Resultant of cogging force in the configuration "Stator 144 C"

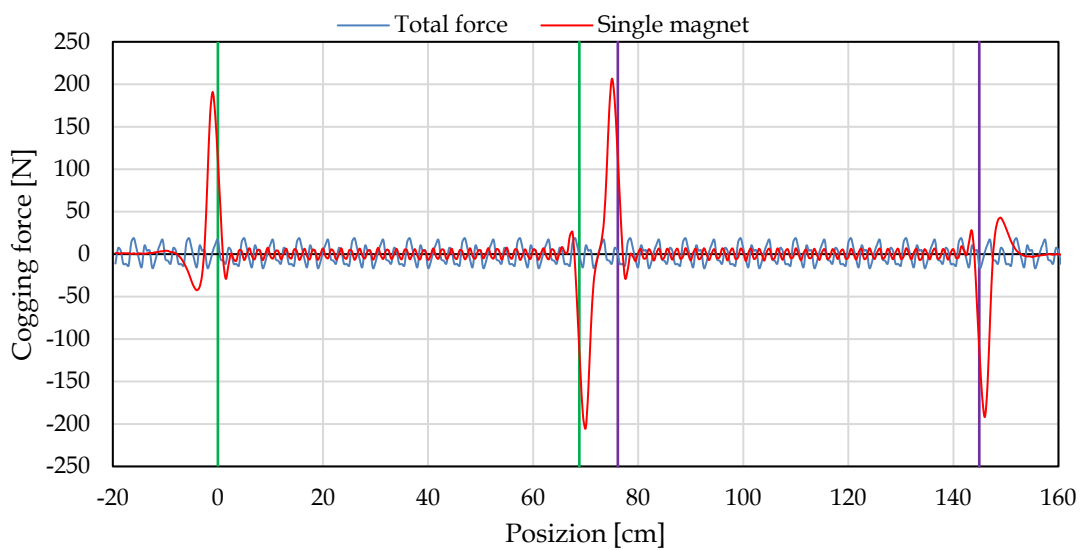


Figure IV.40 Cogging force produced by a magnet and the entire translator with "Stator 144 C"

The trend of cogging force reported in Figure IV.39 is acceptable, since the peak is about 20 N, in comparison with the configuration “Stator 144 A” that is affected by a peak of 400 N. Anyway, Figure IV.40 emphasized the local stress that are also applied to the stator: the entrance and exit of magnets produces a peak of cogging force equal to 200 N. Since the last hypothesis considers the realization of two stators, these parts should be fixed on a rigid structure in order to maintain exactly their relative position. It should also be reminded that the stators are normally realized by stacking iron sheets in order to minimize the eddy currents. For this reason, supposing to fix the two stators at the correct distance, the local component of cogging force could create a misalignment of the sheets after a while.

Thus, the last solution (“Stator 144 D”) was introduced, considering the union of the two stators in a unique one. In this way, all the stresses produced by magnets are applied to a single stator, limiting the potential misalignment of the iron sheets.

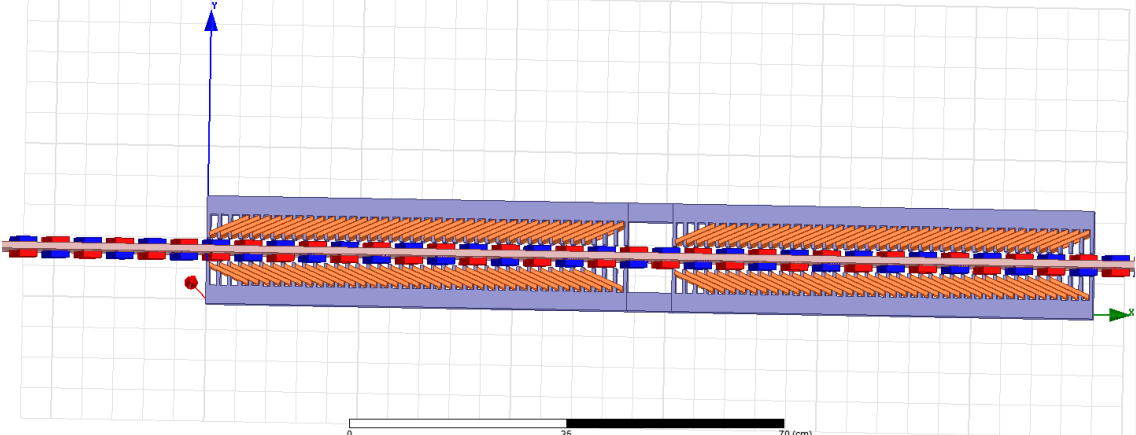


Figure IV.41 Shape of the “Stator 144 D”, modelled on Ansys Maxwell

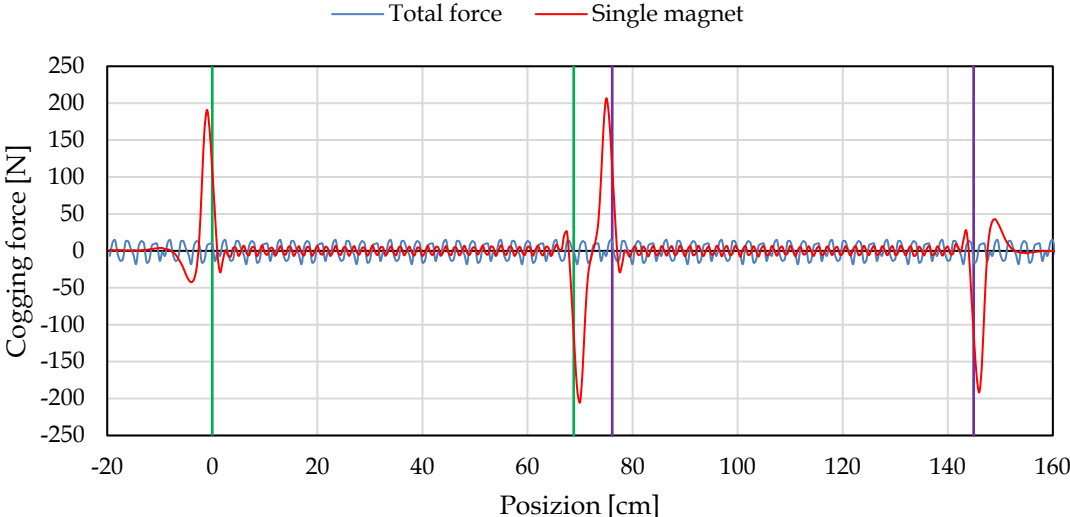


Figure IV.42 Cogging force produced by a magnet and the entire translator with “Stator 144 D”

Table IV.19 x-axis component of cogging forces generated in the configuration "Stator 144 D"

dX [cm]	0.0	0.5	1.0	1.5	2.0	2.5	3.0	3.5	4.0	4.5	5.0
<i>Tot</i>	-6.7	11.0	14.5	-4.3	-13.5	-10.8	12.6	12.9	2.7	-5.3	-17.9
<i>M1</i>	72.8	72.5	73.0	73.0	72.4	72.8	72.4	72.5	72.3	72.9	72.4
<i>M2</i>	-5.5	-6.2	-6.1	-5.0	-5.2	-5.6	-5.8	-5.3	-4.9	-5.1	-5.7
<i>M3</i>	1.2	1.0	1.0	1.2	0.8	0.8	0.1	1.0	0.2	0.6	0.5
<i>M4</i>	-1.0	-0.7	-0.2	-0.2	0.5	0.8	1.2	1.6	2.5	2.9	2.3
<i>M5</i>	3.0	2.0	0.6	-1.1	-5.2	-10.1	-16.0	-23.6	-32.2	-39.9	-43.5
<i>M6</i>	-43.4	-34.1	-9.8	43.6	125.9	184.2	182.1	138.5	83.2	21.9	-24.0
<i>M7</i>	-28.0	-11.6	0.9	-5.9	-6.9	3.6	3.2	-6.6	-1.0	7.0	-2.6
<i>M8</i>	-7.0	-0.6	6.6	-3.0	-5.4	5.8	4.4	-6.5	-0.5	6.9	-2.2
<i>M9</i>	-6.3	0.0	7.0	-2.3	-6.2	4.4	3.5	-6.3	0.6	6.9	-2.3
<i>M10</i>	-5.8	0.2	7.2	-2.8	-6.1	5.2	4.0	-6.8	-0.9	6.7	-2.8
<i>M11</i>	-6.6	0.0	6.0	-2.6	-6.1	5.2	2.8	-5.9	-0.3	6.8	-3.3
<i>M12</i>	-7.2	-2.4	6.4	-2.5	-5.8	5.5	4.0	-6.3	-0.1	6.4	-2.5
<i>M13</i>	-6.4	-0.7	7.1	-3.2	-5.3	5.5	3.5	-7.1	-0.1	7.5	-2.8
<i>M14</i>	-7.0	-0.4	6.8	-2.5	-5.4	5.2	3.3	-5.8	-0.7	7.9	-2.1
<i>M15</i>	-6.5	-1.2	7.4	-2.2	-6.4	4.7	4.0	-6.7	-1.5	6.7	-2.7
<i>M16</i>	-7.7	-0.6	7.2	-1.9	-5.7	4.3	3.9	-6.3	-0.5	7.8	-2.7
<i>M17</i>	-6.7	0.0	6.3	-2.2	-5.5	4.2	3.3	-6.8	-1.1	7.2	-2.6
<i>M18</i>	-6.8	-1.3	6.3	-2.1	-5.7	5.5	4.3	-6.4	-0.7	6.6	-2.2
<i>M19</i>	-6.1	-0.2	9.2	2.0	1.5	21.0	24.1	-16.1	-77.5	-137.6	-187.7
<i>M20</i>	-200.2	-185.9	-117.5	-49.8	-17.9	-4.0	5.6	21.5	57.5	128.8	189.4
<i>M21</i>	202.1	180.5	128.7	68.2	8.3	-25.7	-18.2	0.1	-3.2	-8.5	2.4
<i>M22</i>	5.3	0.2	-6.2	1.9	5.7	-5.8	-4.1	7.0	0.8	-6.8	2.2
<i>M23</i>	5.3	0.6	-6.9	2.2	5.2	-4.9	-4.2	6.0	1.5	-6.7	2.3
<i>M24</i>	5.4	0.7	-7.4	2.1	6.6	-5.2	-3.8	5.9	0.5	-5.6	2.4
<i>M25</i>	6.4	1.6	-6.9	4.0	5.5	-4.5	-3.6	6.7	1.3	-7.0	2.2
<i>M26</i>	5.9	1.0	-6.4	1.9	6.0	-4.7	-3.8	6.8	0.6	-6.2	2.0
<i>M27</i>	6.5	1.2	-6.1	1.9	6.2	-4.9	-3.3	6.4	0.8	-7.4	2.6
<i>M28</i>	6.1	0.5	-7.1	2.5	7.2	-5.9	-3.3	6.8	0.4	-5.7	3.1
<i>M29</i>	6.1	1.1	-6.4	1.9	6.6	-5.8	-3.6	5.7	-0.9	-6.8	1.7
<i>M30</i>	7.2	0.1	-6.7	1.5	5.9	-5.2	-2.8	5.8	0.8	-6.7	1.9
<i>M31</i>	7.5	1.5	-6.2	2.9	6.3	-5.8	-3.8	7.1	0.4	-7.0	2.5
<i>M32</i>	6.3	-0.6	-6.4	2.4	6.0	-5.7	-2.7	6.7	0.1	-6.5	2.1
<i>M33</i>	8.0	0.5	-6.6	3.1	5.3	-5.3	-2.4	8.0	4.3	-0.2	15.6
<i>M34</i>	25.0	19.0	-30.5	-90.8	-147.6	-186.4	-178.2	-113.9	-32.4	15.7	37.0
<i>M35</i>	41.2	43.3	39.0	30.6	23.0	15.2	9.2	4.3	0.9	-1.1	-1.8
<i>M36</i>	-1.9	-2.9	-2.8	-2.3	-2.3	-2.3	-1.0	-0.4	-0.3	0.5	0.3
<i>M37</i>	-0.5	-0.4	-0.4	-1.0	-0.5	-0.6	-0.7	-0.7	-0.9	-0.7	-0.8
<i>M38</i>	5.6	5.4	5.4	5.6	5.5	5.5	4.9	5.3	5.5	5.4	5.5
<i>M39</i>	-72.2	-72.1	-72.0	-72.3	-72.5	-72.0	-72.0	-71.9	-72.2	-72.2	-72.5

(Table follows in the next page).

dX [cm]	5.5	6.0	6.5	7.0	7.5	8.0	8.5	9.0	9.5	10.0	10.5
<i>Tot</i>	6.5	13.3	9.8	-15.6	-12.9	7.0	9.5	9.5	-13.6	-1.3	-7.7
<i>M1</i>	72.6	72.8	72.7	73.0	72.9	72.9	72.9	73.1	72.6	72.8	72.8
<i>M2</i>	-5.4	-5.5	-5.8	-6.0	-5.8	-6.1	-5.6	-6.3	-6.0	-6.0	-5.9
<i>M3</i>	1.1	1.0	1.1	1.5	1.9	2.4	2.9	3.4	4.2	4.5	4.1
<i>M4</i>	1.3	1.0	-1.1	-3.9	-8.0	-13.6	-20.7	-28.3	-37.2	-43.1	-43.1
<i>M5</i>	-39.2	-25.0	11.9	84.7	160.9	191.3	164.2	111.4	52.7	-4.1	-27.4
<i>M6</i>	-21.7	-2.2	-0.8	-10.0	-2.0	6.8	-3.1	-6.5	5.3	3.0	-7.3
<i>M7</i>	-5.6	5.0	4.0	-6.8	0.1	6.1	-2.4	-5.6	4.7	4.5	-6.8
<i>M8</i>	-5.1	5.3	4.0	-6.5	-0.8	6.6	-2.6	-5.8	4.0	3.6	-6.9
<i>M9</i>	-5.1	4.6	2.7	-5.8	-0.7	6.9	-3.7	-5.3	5.0	4.9	-6.6
<i>M10</i>	-5.9	4.9	4.2	-6.3	-0.4	6.8	-3.3	-6.5	4.1	4.6	-8.6
<i>M11</i>	-5.6	4.5	4.2	-6.7	-0.2	6.8	-2.9	-5.4	4.8	4.5	-6.4
<i>M12</i>	-5.6	5.9	4.6	-6.1	-0.3	6.7	-2.7	-5.3	4.8	4.8	-6.2
<i>M13</i>	-5.4	4.4	3.7	-6.5	0.7	7.0	-3.1	-4.7	5.5	4.4	-6.2
<i>M14</i>	-6.5	6.0	4.2	-6.8	-0.5	6.6	-3.2	-5.4	3.6	3.3	-7.2
<i>M15</i>	-6.3	4.8	4.9	-7.9	-0.4	7.0	-2.1	-5.8	4.5	3.8	-6.7
<i>M16</i>	-5.8	4.4	3.8	-7.1	-0.6	8.3	-2.2	-5.3	4.0	3.1	-6.5
<i>M17</i>	-6.1	5.9	4.3	-6.9	-0.3	6.3	-2.0	-5.5	5.9	5.0	-6.3
<i>M18</i>	-5.2	6.5	6.6	-2.3	10.1	27.1	9.9	-47.2	-108.6	-164.3	-201.1
<i>M19</i>	-201.1	-154.3	-80.0	-30.6	-10.2	0.9	12.5	35.5	90.5	164.5	200.7
<i>M20</i>	199.1	156.6	99.1	37.5	-14.5	-26.1	-6.8	1.2	-8.3	-4.7	6.0
<i>M21</i>	5.6	-4.9	-3.6	5.6	0.7	-6.7	2.6	6.8	-5.4	-3.1	7.9
<i>M22</i>	5.7	-5.1	-3.6	6.7	0.6	-6.0	2.2	6.3	-5.6	-2.7	6.9
<i>M23</i>	5.9	-5.2	-3.7	6.9	1.2	-6.3	2.6	5.4	-5.2	-2.5	6.3
<i>M24</i>	5.6	-5.9	-3.5	6.8	0.5	-5.5	3.0	5.0	-5.9	-2.8	6.4
<i>M25</i>	5.9	-5.3	-4.5	6.3	0.9	-7.3	3.2	5.5	-5.3	-1.7	6.4
<i>M26</i>	5.7	-5.5	-2.9	6.6	-0.3	-6.1	2.1	6.5	-4.9	-3.5	6.8
<i>M27</i>	6.6	-4.9	-3.6	6.3	-0.1	-6.2	1.9	5.7	-4.2	-3.3	7.2
<i>M28</i>	5.5	-5.6	-3.3	6.3	0.6	-6.3	2.8	5.9	-5.4	-3.1	5.8
<i>M29</i>	5.6	-5.4	-3.2	5.8	0.6	-6.9	1.8	6.1	-4.6	-3.8	7.2
<i>M30</i>	5.5	-5.0	-2.6	5.5	0.5	-5.8	2.1	5.3	-5.8	-3.8	5.8
<i>M31</i>	5.2	-6.1	-3.6	6.5	0.2	-7.2	2.3	6.2	-6.0	-2.6	5.9
<i>M32</i>	6.4	-4.4	-3.6	6.6	0.6	-6.2	3.7	6.8	-0.9	5.0	24.4
<i>M33</i>	25.3	-2.3	-60.9	-120.0	-170.9	-190.2	-152.8	-72.0	-4.1	27.5	41.3
<i>M34</i>	43.5	42.2	35.5	27.4	19.7	12.1	6.3	3.1	0.4	-1.5	-2.3
<i>M35</i>	-3.0	-3.4	-3.5	-2.5	-2.3	-1.6	-0.7	-0.5	-0.1	-0.1	0.2
<i>M36</i>	0.2	0.6	0.3	0.3	0.7	0.7	0.1	0.0	0.4	0.1	-0.3
<i>M37</i>	-0.9	-1.2	-1.2	-1.6	-1.1	-1.3	-1.0	-1.1	-1.0	-1.2	-1.2
<i>M38</i>	5.6	5.5	5.9	5.8	5.7	5.5	5.3	5.4	5.6	5.7	5.5
<i>M39</i>	-71.9	-72.2	-72.4	-72.4	-72.6	-72.0	-72.3	-72.8	-72.0	-71.5	-72.3

According to Figure IV.43 the resultant cogging force in the case “Stator 144 D” has a peak about 20 N, that is the same of the case “Stator 144 C”, previously considered.

In conclusion a comparison of the Fourier series coefficients is reported in Table IV.20. It is possible to observe that in the configuration “Stator D” the second and the sixth harmonics are negligible, the fourth is almost double than the same in the configuration “Stator 72”. This term is the main component of the cogging force in the configuration “Stator 144 D”. Like in the case “Stator 144 C”, it is observable the presence

of a ninth harmonic, but this term, as introduced before, could be related to the tolerance adopted in the simulation.

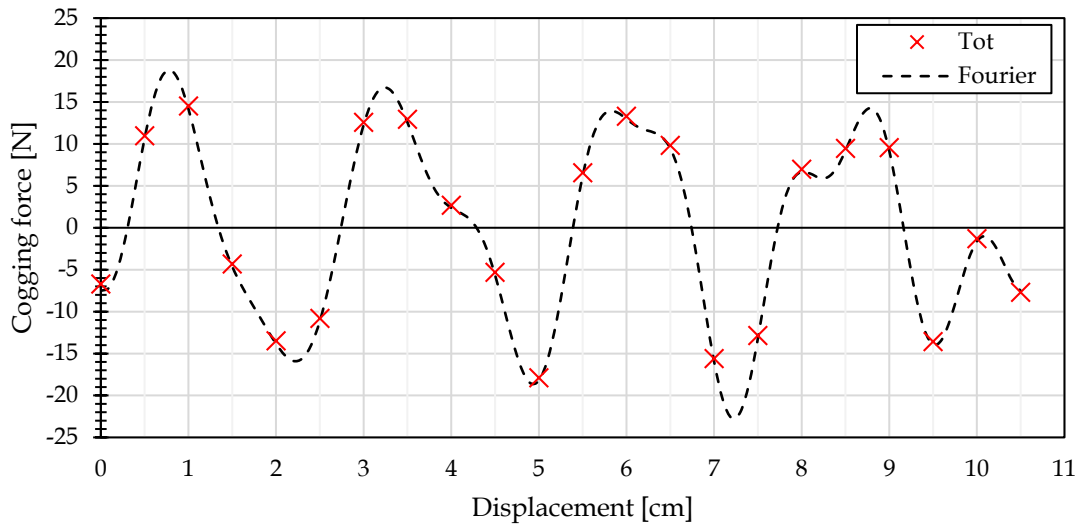


Figure IV.43 Resultant of cogging force in the configuration “Stator 144 D”

Table IV.20 Comparison of Fourier series coefficients considering all different stators

Order	Stator 72		Stator 144 A		Stator 144 B		Stator 144 C		Stator 144 D	
	Amp. [N]	Phase [rad]	Amp. [N]	Phase [rad]	Amp. [N]	Phase [rad]	Amp. [N]	Phase [rad]	Amp. [N]	Phase [rad]
0	3.95	-	0.02	-	0.60	-	-0.42	-	0.33	-
1	0.89	0.4197	1.56	-0.8706	1.30	4.5724	1.34	4.4671	0.25	0.2450
2	237.20	4.6044	233.95	4.6055	65.27	-0.1094	5.41	3.3862	0.62	2.6055
3	2.20	1.7066	2.13	2.3769	0.28	4.1394	0.45	1.9930	1.19	1.2329
4	6.06	-0.1106	6.57	-0.1917	19.00	-0.2043	13.19	-0.2839	13.96	-0.2434
5	0.92	-0.1159	1.62	4.2413	1.52	3.0082	1.36	3.7133	2.25	2.6310
6	90.92	4.4002	172.83	4.3956	0.77	0.0251	1.05	0.1550	3.09	4.0576
7	0.62	3.9536	0.84	4.2314	1.40	-1.2708	0.52	-0.3815	0.94	2.6005
8	0.29	1.5004	0.34	-0.1109	1.03	-1.0038	0.76	-1.2519	0.88	4.2331
9	2.65	4.2856	6.30	3.7086	7.91	3.5752	5.15	3.7531	4.86	3.6350
10	0.68	0.5510	1.13	2.1534	1.46	-0.4297	1.33	-0.2584	1.81	-1.2515

In conclusion, the configuration “Stator D” can achieve the desired rated power. The cogging force is minimized, and the stator has a structure that is more solid than the other solutions previously analyzed. In the next section, a description of the proposed device is given.

IV.3.f Proposed system

In this section, a description of the proposed Wave Energy Converter (WEC) is reported.

Starting from the linear generator, Figure IV.44 shows the shape and two sections of the stator.

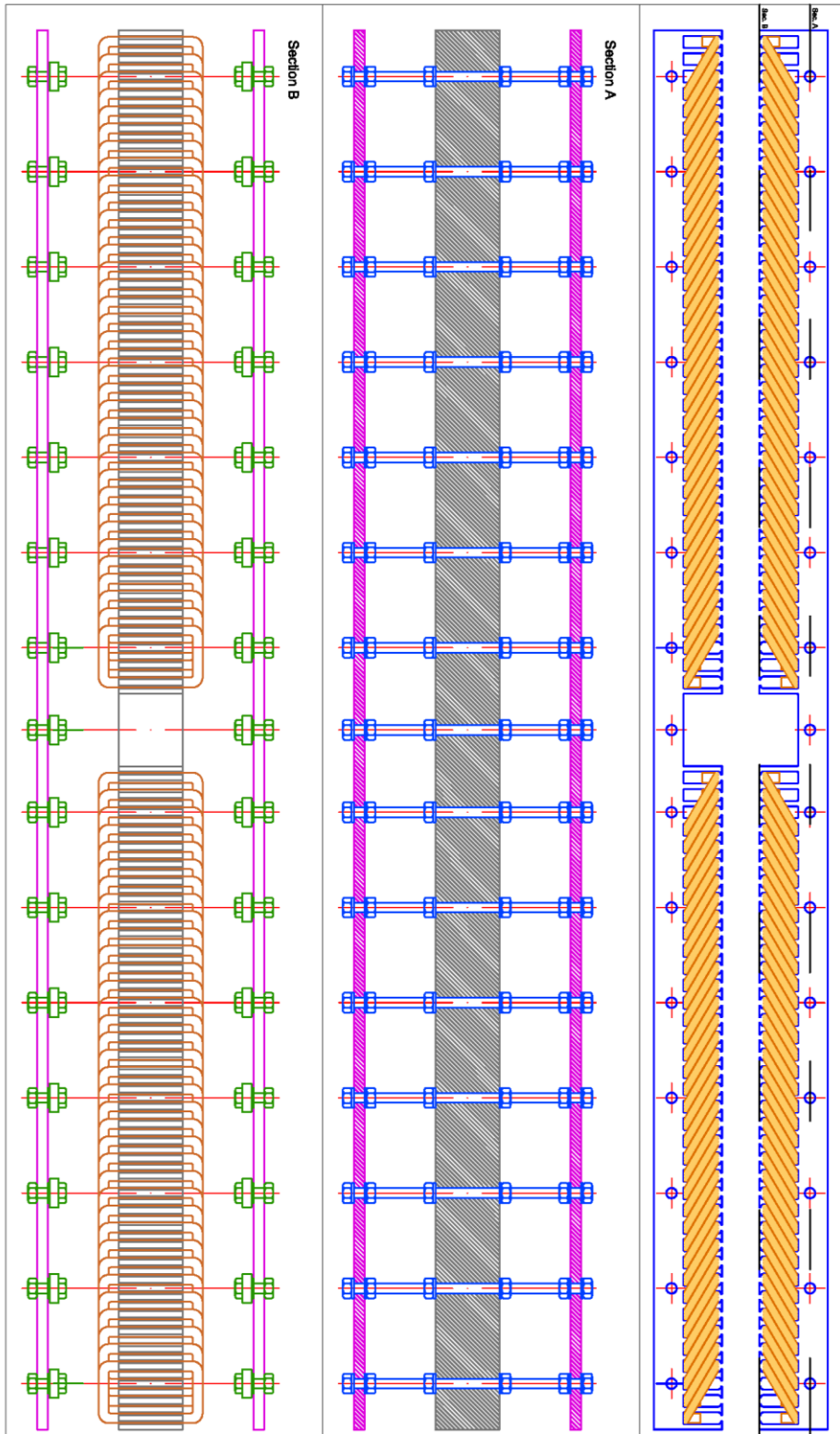


Figure IV.44 Different views of the stator of the proposed linear generator.

Each block of the stator has a length of 1449 mm, a height of 65 mm and a width 69 mm. It is equipped with 80 teeth and 78 slots, in order to install 72 coils in each block.

Considering the shape and the density of iron (7850 k/m^3), it is estimated a mass of 20.24 kg for each block of the stator (excluding threaded bars and coils).

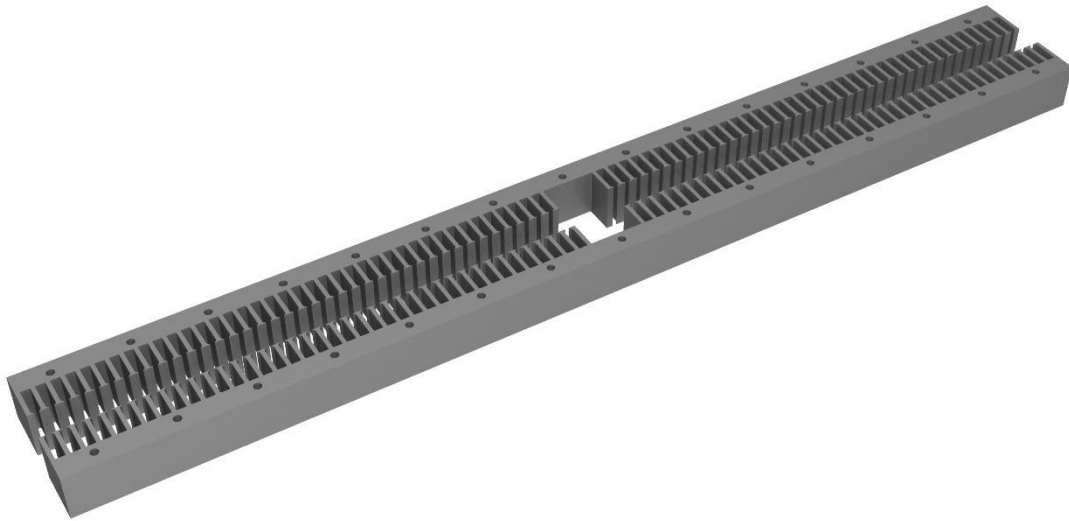


Figure IV.45 A 3D view of the stator

About coils, each one has a rectangular shape, about 62.5 mm wide and 95 mm high, thus considering commercial value of resistance and weight (enameled copper 0.5 mm diameter) a mass of 283.34 g and a resistance of 14.25Ω were estimated.

Thus, the stator should have a total mass equal to 82.5 kg, including the iron blocks, the coils and the threaded bars.

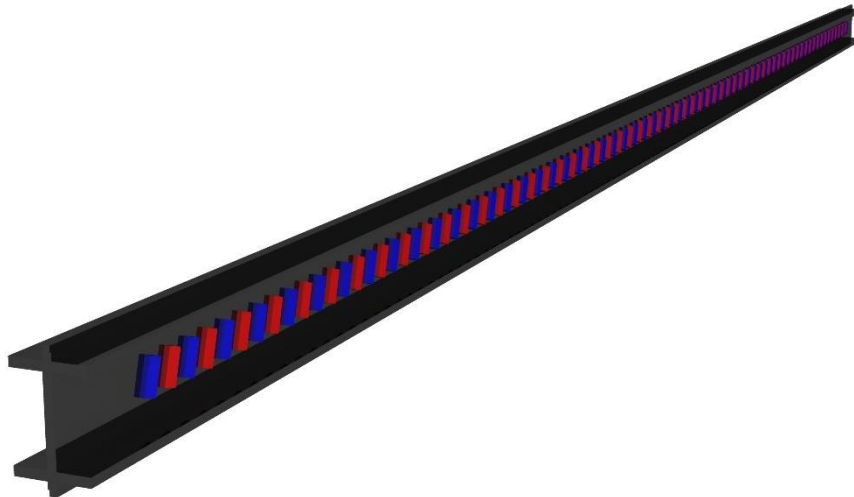


Figure IV.46 3D view of the translator

As regards the translator (see Figure IV.46), the length was chosen according to the maximal value of significant height measured around the Sicilian coastline. As reported in Table IV.21, a significant height of 5 m represents a remote condition measurable during the year. In order to exploit also this sea state, the length of translator was fixed equal to 6949 mm.

Table IV.21 Significant height distribution according to the data from the RON stations of Catania, Mazara del Vallo and Palermo

Hs [m/s]	f(Hs)			v [m/s]	f(Hs)		
	Catania	Mazara	Palermo		Catania	Mazara	Palermo
0.2	0.2067	0.1118	0.2277	3.2	0.0011	0.0052	0.0030
0.4	0.3427	0.1573	0.2041	3.4	0.0010	0.0042	0.0022
0.6	0.1725	0.1495	0.1450	3.6	0.0005	0.0029	0.0016
0.8	0.0956	0.1241	0.1060	3.8	0.0003	0.0023	0.0012
1.0	0.0597	0.0995	0.0804	4.0	0.0002	0.0019	0.0010
1.2	0.0409	0.0774	0.0611	4.2	0.0002	0.0013	0.0007
1.4	0.0265	0.0636	0.0431	4.4	0.0002	0.0012	0.0005
1.6	0.0183	0.0535	0.0329	4.6	0.0001	0.0007	0.0002
1.8	0.0106	0.0422	0.0260	4.8	0.0000	0.0007	0.0003
2.0	0.0077	0.0313	0.0193	5.0	0.0000	0.0003	0.0003
2.2	0.0053	0.0226	0.0143	5.2	0.0000	0.0002	0.0001
2.4	0.0035	0.0155	0.0109	5.4	0.0000	0.0003	0.0001
2.6	0.0026	0.0120	0.0074	5.6	0.0000	0.0002	0.0000
2.8	0.0021	0.0095	0.0057	5.8	0.0000	0.0001	0.0000
3.0	0.0018	0.0073	0.0045	6.0	0.0000	0.0001	0.0000

The shape remembers a double T profile, with an extension in both sides and was chosen in order to constrain the translator to the guide, composed by bearing installed on the stator. Considering the distance between the magnets and the length of the translator, the solution depicted in Figure IV.46 requires the installation of 250 magnets (125 in each side). Assuming the realization of the translator in carbon fiber, this component should have a mass of 130.9 kg, of which 79.6 kg due to the mechanical support and 51.3 kg for the magnets.

In order to exploit the sea wave energy potential, a linear generator can be used in the following system designed to be installed in offshore areas.

This solution is essentially composed by two floating buoys, as depicted in Figure IV.47. Each buoy has a specific purpose: the central one is anchored to seabed and contains the energy converters, while the external buoy is adopted to extract energy from sea wave. The idea is the generation of a relative motion between the buoys. This is possible by the fact that the external buoy can move up and down, following the crest of sea wave while the internal buoy is almost motionless. The mobility of the central buoy is limited by the fact that this part has a greater weight, due to the components located inside, and to the addition of a stabilizing weight, represented by the cylinder installed in the lower part. This component increases also the hydrodynamic resistance of the buoy, so the vertical mobility of the central buoy is further limited.

Thanks to its geometrical symmetry, this system works independently of wave direction propagation, thus it can be defined as "Point Absorber" according to the classification introduced in the previous chapter.

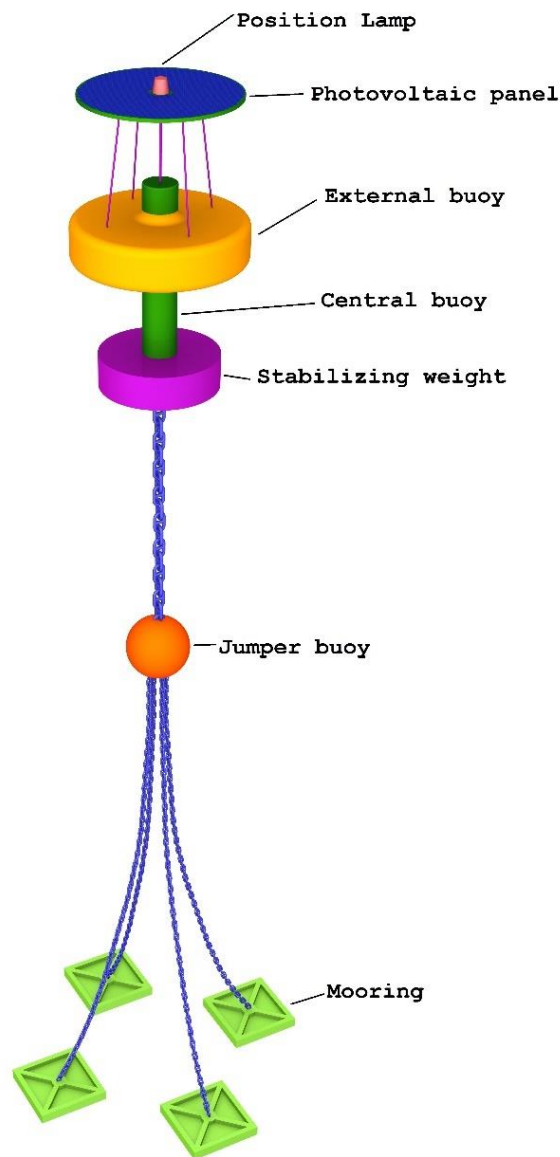


Figure IV.47 External view of the proposed Wave Energy Converter

The central buoy is anchored to seabed through a long chain and four moorings. A jumper buoy is used to avoid potential damages of seabed. Indeed, the four chains, connecting the moorings and jumper, are constantly maintained in traction, avoiding the scraping of seabed. This solution is chosen in order to install the point absorber in an offshore configuration.

The electricity production is entrusted to eight linear generators, above described, that are installed inside the central buoy. As shown in Figure IV.48, the relative motion between the external and internal buoys is transferred to the central buoy through a long bar, connected to eight linear generators.

This modular solution is used to simplify the achievement of greater rated power, without other changes of the generator design, since the proposed electrical machine has

a maximal power of 10 kW. Furthermore, it is possible to maximize the power extraction, optimizing the WEC response to sea wave by changing the number of active generators. Optionally, a photovoltaic plant could be integrated on the top, increasing the annual electrical energy production. The height of the internal buoy is chosen in order to allow the entire stroke to the translators of the linear generators.

The stators of the generators are fixed on the framework that is anchored to the internal buoy. Two end stroke springs are installed in order to avoid damages in case of extreme sea states, when the wave oscillation could exceed the maximal stroke of the device.

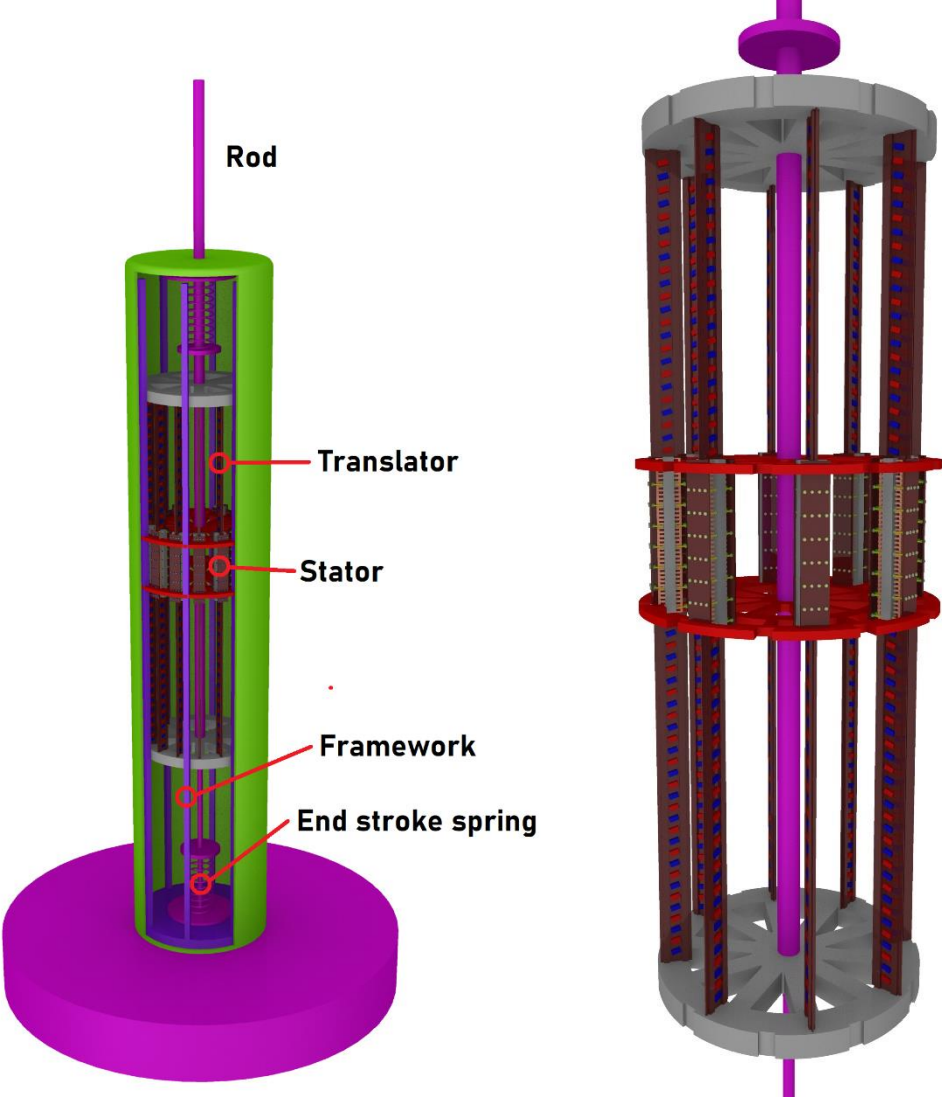


Figure IV.48 Sectional view of the internal buoy and detail of the movable part

An important aspect is the sizing of the external buoy. As reported in [198], the diameter of the heave buoy must be chosen in order to maximize the extraction of power. This condition is realized by Eq. IV.17, where λ is the wavelength.

$$d_{max,power} = \frac{\lambda}{2\pi} \quad IV.17$$

Since in case of deep water, the wavelength is related to the energy period by Eq. IV.18, it is possible to evaluate the diameter of the external buoy in order to maximize the extraction of power output, as a function of the energy period according to Eq. IV.19.

$$\lambda = \frac{g}{2\pi} T_e^2 \quad IV.18$$

$$d_{max,power} = \frac{g}{4\pi^2} T_e^2 \quad IV.19$$

Considering the probability density function of the peak period (see Figure IV.49), based on data collected by RON measuring stations in Sicily, the WEC external diameter should be equal to 6.28 m (Catania), 6.82 m (Palermo) and 7.43 m (Mazara).

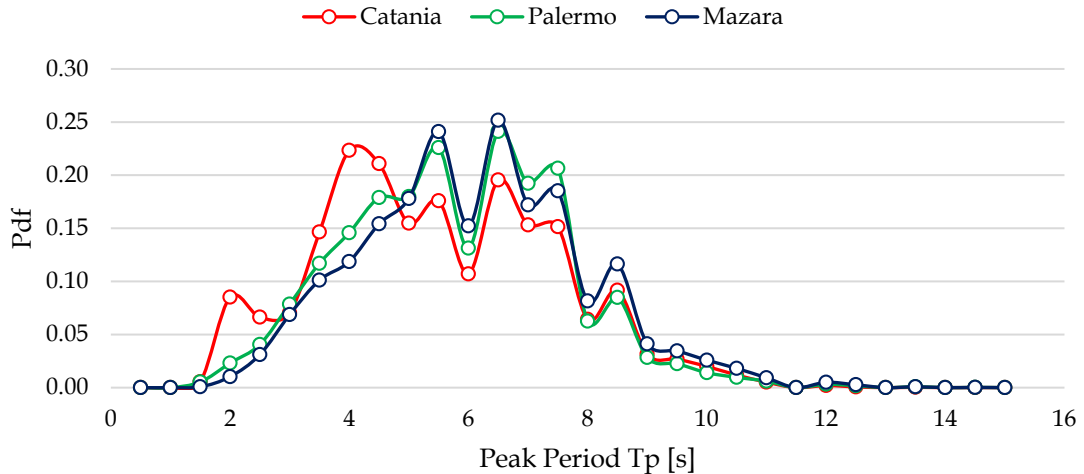


Figure IV.49 Probability density function of the Peak Period in three measuring stations in Sicily

Thus, from the mean of the previous values, an external diameter of 6.84 m is suggested.

Like wind farm, this WEC could be installed in order to form a wave farm, composed by several buoys. The distance between each buoy should be chosen in order to minimize the mutual interference phenomena [199]. A distance 5.1 times the diameter of the external buoy is adopted in Figure IV.50, according to the results reported in a previous work [109].

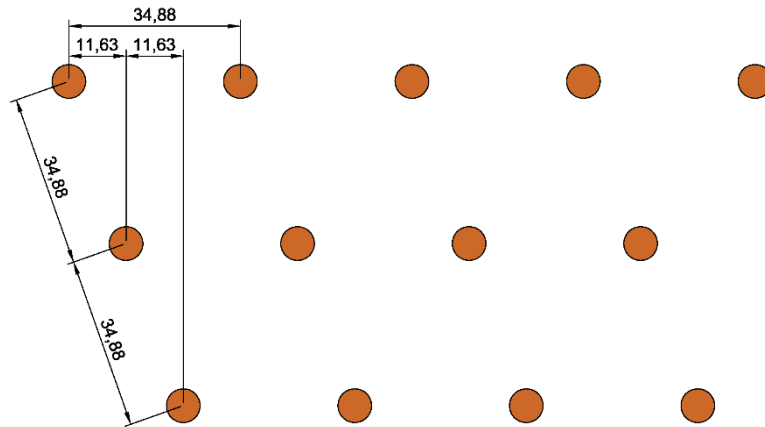


Figure IV.50 Layout of a potential wave farm based on the proposed WEC

In another work [200], the benefits of this solution were underlined, evaluating also the potential environmental impacts:

- Limited visibility of the device from the coastline, especially in case of offshore installation;
- Absence of pressurized fluid that could be dispersed in case of failure;
- Limited number of components and absence of complex mechanical motion converters, composed by belts, freewheels, racks, etc.
- Simplest energy conversion chains, increasing the energy efficiency.

Thus, the proposed WEC shows limited environmental impacts, like marker buoys used in reserved areas, with the benefits of the electrical energy production. In this case, an intermittent red light can be installed on top of the buoy, making visible the WEC up to several nautical miles away.

As described in the next chapter, this technology could be a valid solution to supply the electrical grid (or big loads like desalination plants) in small islands, where the environmental constraints do not allow the installation of devices supplied by other renewable energy sources.

IV.3.g Lumped model

As described above, the point absorber is composed by two coaxial cylindrical buoys. The central buoy is fixed to the seabed, while the external one can move vertically. Thus, ignoring the fixed buoy, the sea wave energy converter can be modelled as a single body having one degree of freedom along the vertical axis z [201].

As reported in Eq. IV.20, several forces are responsible of the movement of the buoy, in particular:

- F_g represents the gravity force applied to the total mass m_{tot} of the components subjected to the vertical oscillation, indicating with g the gravity acceleration;

- $F_b(t)$ is the buoyancy force, called also Archimedes force, that is related to the immersed volume of the buoy under the sea level. Assuming a buoy with a constant horizontal section at different heights, if the sizes of the buoy are small in comparison with the wavelength, the immersed volume is linearly dependent to the vertical position of the buoy z and the local level of the sea z_w .
- $F_e(t)$ represents the force produced by the PTO in order to produce electrical power, considering the speed of the device equal to $\dot{z}(t)$.
- $F_l(t)$ is the viscous damping force due to the relative motion between sea wave and the buoy. It is essentially related to the square of the relative speed, given by the difference $\dot{z}(t) - \dot{z}_w(t)$. The drag coefficient C_D is assumed equal to 0.5, according to the average conditions during sea wave [202].

$$F_g + F_b(t) + F_e(t) + F_l(t) = m_{tot}\ddot{z}(t)$$

$$F_g = -m_{tot}g$$

$$F_b(t) = \rho gV(t)$$

IV.20

$$F_e(t) = -\frac{P_e(t)}{\dot{z}(t)}$$

$$F_l(t) = -\frac{1}{2}C_D\rho S_b[\dot{z}(t) - \dot{z}_w(t)] * |\dot{z}(t) - \dot{z}_w(t)|$$

In order to define the reaction from PTO, the power generation should be expressed as function of the vertical speed of the converter.

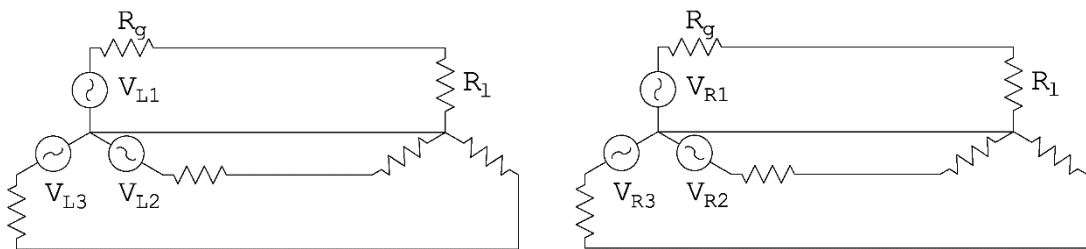


Figure IV.51 Internal scheme of the linear generator

Considering each linear generator, connected to two three-phases resistive loads (see Figure IV.27 and Figure IV.51) and neglecting the internal inductance of the generator, the total electrical power production is given by Eq. IV.21, indicating with $V_{Li,0}$ the no load voltages produced by the left part of the generator and with $V_{Ri,0}$ the right ones at the reference speed (1 m/s).

$$P_e(t) = \dot{z}^2 \frac{n_g}{v_0^2 R_t} \sum_{i=1}^3 V_{Li,0}^2(t) + V_{Ri,0}^2(t)$$

$$V_{Li,0}(t) = A_1 \sin\left(kz(t) + \theta_1 + (i-1)\frac{2\pi}{3}\right) + A_3 \sin(3kz(t) + \theta_3) \quad IV.21$$

$$V_{Di,0}(t) = A_1 \sin\left(kz(t) + \varphi\theta_1 + \frac{\pi}{2} + (i-1)\frac{2\pi}{3}\right) + A_3 \sin\left(3kz(t) - \frac{\pi}{2} + \theta_3\right)$$

The constant $n_g = 8$ represents the number of generators installed inside the proposed WEC. Since the no-load voltage trends are linearly dependent to the vertical speed of buoy, in the evaluation of the electrical power production the square of the vertical speed \dot{z}^2 is introduced. Comparing the definition of the no-load voltages, the phase shifting can be recognized by the addition of the amount $\pm \frac{\pi}{2}$ in the definition of $V_{Di,0}(t)$.

Replacing the terms in Eq. IV.21, the following relations are obtained:

$$\begin{aligned} \sum_{i=1}^3 V_{Li,0}^2(t) &= A_1^2 \sum_{i=1}^3 \sin^2\left(kz(t) + \theta_1 + (i-1)\frac{2\pi}{3}\right) + A_3^2 \sum_{i=1}^3 \sin^2(3kz(t) + \theta_3) \\ &\quad + 2A_1A_3 \sum_{i=1}^3 \sin\left(kz(t) + \theta_1 + (i-1)\frac{2\pi}{3}\right) \sin(3kz(t) + \theta_3) \end{aligned}$$

$$\begin{aligned} \sum_{i=1}^3 V_{Ri,0}^2(t) &= A_1^2 \sum_{i=1}^3 \sin^2\left(kz(t) + \theta_1 + \frac{\pi}{2} + (i-1)\frac{2\pi}{3}\right) + A_3^2 \sum_{i=1}^3 \sin^2\left(3kz(t) - \frac{\pi}{2} + \theta_3\right) \\ &\quad + 2A_1A_3 \sum_{i=1}^3 \sin\left(kz(t) + \theta_1 + \frac{\pi}{2} + (i-1)\frac{2\pi}{3}\right) \sin\left(3kz(t) - \frac{\pi}{2} + \theta_3\right) \end{aligned}$$

Considering the trigonometric properties

$$\sin^2(x) + \sin^2\left(x + \frac{2\pi}{3}\right) + \sin^2\left(x - \frac{2\pi}{3}\right) = \frac{3}{2}$$

$$\sin(x) + \sin\left(x + \frac{2\pi}{3}\right) + \sin\left(x - \frac{2\pi}{3}\right) = 0$$

$$\sin\left(x - \frac{\pi}{2}\right) = -\cos(x)$$

$$\sin^2(x) + \cos^2(x) = 1$$

the previous relation can be simplified in:

$$\sum_{i=1}^3 V_{Li,0}^2(t) = \frac{3}{2}A_1^2 + 3A_3^2 \sin^2(3kz(t) + \theta_3)$$

$$\sum_{i=1}^3 V_{Ri,0}^2(t) = \frac{3}{2}A_1^2 + 3A_3^2 \cos^2(3kz(t) + \theta_3)$$

Thus, the electrical power production and the corresponding force are finally given by Eq. IV.22 and IV.23.

$$P_e(t) = 3n_g \dot{z}^2 \frac{A_1^2 + A_3^2}{v_0^2 R_t} \quad IV.22$$

$$F_e(t) = 3n_g \dot{z} \frac{A_1^2 + A_3^2}{v_0^2 R_t} \quad IV.23$$

It is possible also to demonstrate the more general case, where the inductance of the generator L_g is not negligible. In this case, Eq. IV.24 and IV.25 should be used, considering that λ_m is the distance between two magnets having the same pole (10.5 cm).

$$P_e(t) = 3n_g \dot{z}^2 \left[\frac{A_1^2 R_t}{v_0^2 \left(R_t + \frac{2\pi \dot{z}}{\lambda_m} L_g \right)^2} + \frac{A_3^2 R_t}{v_0^2 \left(R_t + \frac{6\pi \dot{z}}{\lambda_m} L_g \right)^2} \right] \quad IV.24$$

$$F_e(t) = 3n_g \dot{z} \left[\frac{A_1^2 R_t}{v_0^2 \left(R_t + \frac{2\pi \dot{z}}{\lambda_m} L_g \right)^2} + \frac{A_3^2 R_t}{v_0^2 \left(R_t + \frac{6\pi \dot{z}}{\lambda_m} L_g \right)^2} \right] \quad IV.25$$

These equations are obtained assuming steady state conditions and a constant speed \dot{z} . In case of sea wave exploitation, the speed of translator changes continuously, thus the response of the PTO could differ from the Eq. IV.24 and IV.25. It is interesting to observe that in the case of $L_g = 0$, these equations assume the expression of the previous Eq. IV.22 and IV.23.

Considering different values of the internal inductance of the device, the ratio between the force evaluated by Eq. IV.25 and the force from Eq. IV.23 is graphically reported in Figure IV.52. Thus, the presence of an internal inductance reduces the value of force produced by PTO and this effect is more evident by increasing the value of the internal inductance and the speed of the translator. For example, an internal inductance of 0.2 H (per each phase of a single part of the generator) reduces the electrical reaction of PTO to 54% at the speed of 3 m/s.

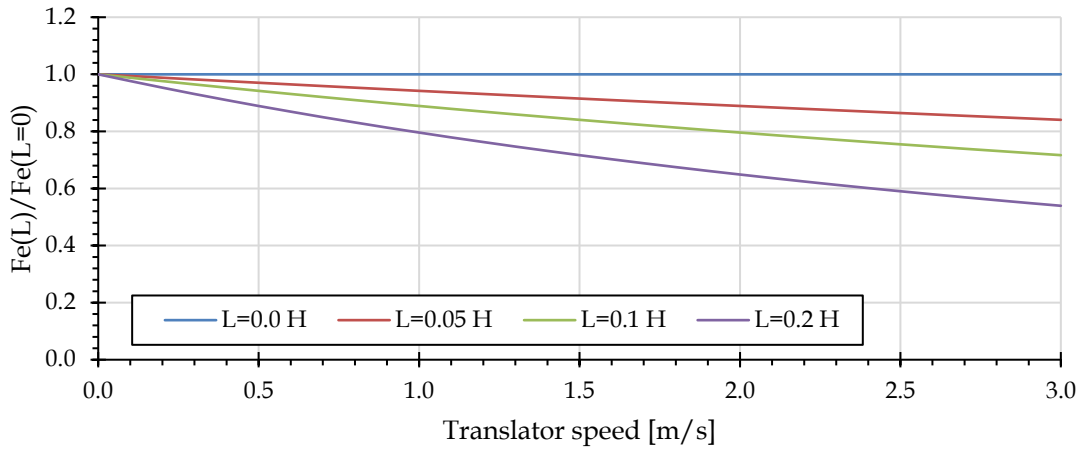


Figure IV.52 Ratio of force produced by PTO as function of translator speed

Finally, it should be reminded that in the linear theory of PTO, the reaction force is evaluated according to Eq. IV.26

$$F_{PTO}(t) = -b_{PTO}\dot{z}(t) - c_{PTO}z(t) \quad IV.26$$

assuming a term proportional to the speed of the translator (related to the power extraction of PTO) and a term proportional to the position of PTO in order to model the introduction of spring to restore the equilibrium condition and create a resonant oscillating device [203].

Before to realize a dynamic simulation of PTO, an approach to evaluate the immersed volume is required.

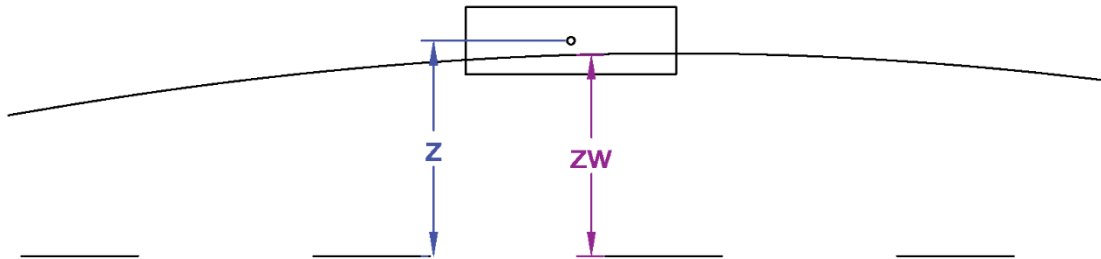


Figure IV.53 Evaluation of the immersed volume

As shown in Figure IV.53, if the diameter of the buoy is negligible in comparison with the wavelength, the immersed volume is given by Eq. IV.27:

$$F_b(t) = f(x) = \rho g S \begin{cases} z_w - z \leq -h_{inf} & 0 \\ -h_{inf} \leq z_w - z \leq h_{sup} & h_{inf} + z_w - z \\ z_w - z > h_{sup} & h_{inf} + h_{sup} \end{cases} \quad IV.27$$

Indicating with S the base area of the buoy, h_{inf} and h_{sup} are the distances between the steady state buoyancy level and respectively the bottom and the top of the buoy.

Since the system is designed in order to maximize the energy extraction from sea wave, the diameter was chosen according to Eq. IV.19, thus the hypothesis behind Eq. IV.27 is not verified.

An alternative approach is the discretization of buoy in a finite number of elements and for each of them verify the relative position in comparison with the sea level, as reported in Figure IV.54.

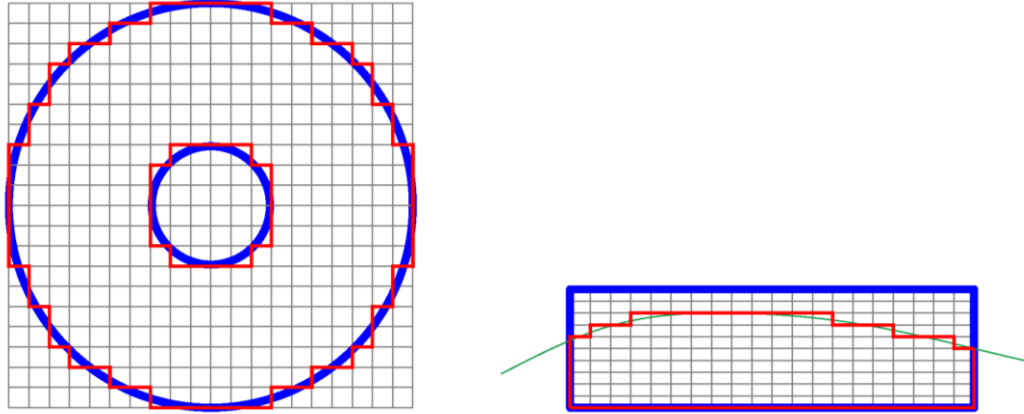


Figure IV.54 Discretized approach to evaluation of the immersed volume

Each rectangle is identified by the center coordinate (x_i, y_j, z_k) . The parallelepiped is considered submerged if:

$$\begin{cases} z_k \leq z_w \\ r_i^2 \leq x_i^2 + y_j^2 \leq r_e^2 \end{cases} \quad IV.28$$

To close the problem, the distribution of the local level of water is assumed given by a regular wave, according to Eq. IV.29

$$z_w(x, t) = \frac{H_s}{2} \sin \left[\frac{2\pi}{T_e} \left(t - \frac{2\pi x}{gT_e} \right) \right] \quad IV.29$$

The condition reported in Eq. IV.29 represents a strong simplification of the mathematical model, because it assumes a wave distribution equivalent to the case of absence of any obstacle. The presence of a buoy influences the wave distribution creating an additive force, called radiation force that is composed by [198]:

- a term proportional to vertical acceleration $\ddot{z}(t)$ of the buoy, multiplied by the added mass m_a , representing the mass of water moved by the buoy;
- a term proportional to the vertical speed of the buoy $\dot{z}(t)$, multiplied by the hydrodynamic damping coefficient R_D .

$$F_R(t) = -m_a \ddot{z}(t) - R_D \dot{z}(t) \quad IV.30$$

Since this evaluation requires the evaluation of complex functions, in order to simplify the mathematical model, this term is neglected. As a consequence, the

numerical complexity of the problem is reduced. The results obtained could be an overestimation of the energy production but allows the realization of quick evaluations of the annual energy production of WEC in a specific context.

In the next section, the model is adopted to estimate the annual energy production in the three measuring points around the Sicilian coastline.

IV.3.h Energy performances

The mathematical model was applied by considering the three different measuring stations located around the Sicilian coastline (Catania, Mazara del Vallo, Palermo).

As first step, the power output of the proposed WEC was simulated considering a finite number of sea states, represented by the values H_s and T_e . It was assumed that the external buoy has an external diameter of 6.84 m, according to Eq. IV.17, an internal diameter of 2 m and an immersed volume equal to 0.5 m. Since in the equilibrium condition the gravity force of the entire system applied to the external buoy is equal to the mass of the water displaced by the immersed volume, the total mass considered in this simulation is estimated equal to 16.8 tons.

Table IV.22 Simulated power output (kW) of the proposed WEC, by using the mathematical model

		Energy period T_e [s]										
		2	3	4	5	6	7	8	9	10	11	12
Significant Height H_s [m]	0.5	0.0	3.8	2.8	1.9	1.3	1.0	0.7	0.6	0.4	0.4	0.3
	1.0	0.1	15.4	11.1	7.4	5.1	3.8	2.8	2.2	1.8	1.5	1.3
	1.5	1.1	38.3	25.2	16.6	11.4	8.5	6.4	5.0	4.0	3.3	2.8
	2.0	2.6	73.7	46.1	29.5	20.3	15.0	11.3	8.9	7.1	5.9	5.0
	2.5	4.8	117.8	73.7	46.5	31.7	23.5	17.7	13.9	11.1	9.2	7.8
	3.0	8.5	161.6	108.3	67.7	45.8	33.9	25.5	20.1	16.0	13.3	11.2
	3.5	13.8	191.9	149.5	93.2	62.6	46.1	34.6	27.3	21.8	18.1	15.3
	4.0	21.1	202.4	197.0	122.8	82.3	60.3	45.3	35.7	28.4	23.6	20.0
	4.5	30.8	200.8	249.6	156.3	104.8	76.5	57.3	45.2	36.0	29.9	25.3
	5.0	43.4	198.9	303.8	193.7	130.2	94.6	70.8	55.7	44.5	36.9	31.2

Table IV.23 Simulated power output (kW) of the proposed WEC, by using OpenWEC

		Energy period T_e [s]										
		2	3	4	5	6	7	8	9	10	11	12
Significant Height H_s [m]	0.5	0.4	1.5	1.7	1.4	1.0	0.8	0.6	0.5	0.4	0.3	0.3
	1.0	1.6	5.8	6.7	5.5	4.2	3.2	2.5	2.0	1.6	1.4	1.2
	1.5	3.5	13.1	15.1	12.4	9.4	7.2	5.6	4.5	3.7	3.0	2.6
	2.0	6.2	23.3	26.9	22.0	16.6	12.8	10.0	8.0	6.6	5.4	4.6
	2.5	9.8	36.4	42.0	34.4	26.0	20.0	15.7	12.4	10.3	8.5	7.3
	3.0	14.1	52.5	60.5	49.5	37.5	28.8	22.6	17.9	14.8	12.2	10.4
	3.5	19.1	71.4	82.3	67.4	51.0	39.2	30.7	24.4	20.1	16.6	14.2
	4.0	25.0	93.3	107.5	88.0	66.6	51.2	40.1	31.8	26.3	21.7	18.6
	4.5	31.6	118.1	136.1	111.4	84.3	64.8	50.8	40.3	33.2	27.4	23.5
	5.0	39.0	145.7	168.0	137.5	104.1	80.0	62.7	49.7	41.0	33.9	29.0

In order to evaluate the quality of the previous simulations, a comparison was realized by using OpenWEC, an open source tool that can be used to model the response of simplified system, like cylinders. The reaction of PTO is modelled by Eq. IV.26, introduced above.

It should be reminded that the external buoy is composed by a cylinder with a cylinder cavity, required by the coupling with the internal buoy. In order to make a comparison, at least the same immersed volume is required, thus the external buoy was modelled with a cylinder having the diameter that satisfies Eq. IV.31:

$$\frac{\pi}{4}d_c^2 h_{imm} = \pi(r_e^2 - r_i^2)h_{imm} \quad IV.31$$

The comparison between the two tables reveals greater values in the MatLab simulation, in comparison with OpenWEC. It is interesting to observe that OpenWEC reports a quadratic trend of the power output for each fixed value of the energy period, while the MatLab simulations show the existence of points where the power output is maximized.

Table IV.24 Simulated annual energy production by using the mathematical model in Catania

		Energy period Te [s]										
		2	3	4	5	6	7	8	9	10	11	12
Significant Height [m]	0.5	10.8	2209	5082	1596	1024	892	236	69.2	35.3	12.2	1.39
	1.0	0	295	1809	3944	1191	1707	738	149	38.6	2.52	0.3
	1.5	0	0	91.6	1182	1158	1257	1154	415	130	11.3	0.34
	2.0	0	0	0	71.5	381	675	579	369	316	62.3	0
	2.5	0	0	0	5.63	38.4	333	330	209	276	87.2	6.62
	3.0	0	0	0	0	5.55	94.3	160	146	232	167	12.2
	3.5	0	0	0	0	7.59	16.8	54.5	49.6	100	142	18.5
	4.0	0	0	0	0	0	0	21.9	34.6	62	62.9	19.3
	4.5	0	0	0	0	0	0	0	0	30.5	57.9	9.18
	5.0	0	0	0	0	0	0	0	6.75	21.5	0	0

Table IV.25 Simulated annual energy production by using OpenWEC in Catania

		Energy period Te [s]										
		2	3	4	5	6	7	8	9	10	11	12
Significant Height [m]	0.5	176	851	3060	1179	827	745	206	60.8	32.4	11.2	1.3
	1.0	0	112	1092	2944	975	1447	651	132	35.4	2.3	0.28
	1.5	0	0	54.9	883	950	1070	1023	370	119	10.3	0.32
	2.0	0	0	0	53.3	313	575	514	330	292	57.1	0
	2.5	0	0	0	4.16	31.5	283	292	187	255	79.9	6.15
	3.0	0	0	0	0	4.54	80.2	142	130	215	154	11.4
	3.5	0	0	0	0	6.18	14.2	48.4	44.3	92.5	131	17.2
	4.0	0	0	0	0	0	0	19.4	30.8	57.2	57.7	18
	4.5	0	0	0	0	0	0	0	0	28.2	53.1	8.54
	5.0	0	0	0	0	0	0	0	6.02	19.9	0	0

To evaluate the annual producibility, the previous tables were multiplied for the occurrence matrix, obtained from the analysis of raw data from three stations of RON (the Italian measuring network).

Both evaluations are reported in the following tables. Each cell contains the corresponding annual energy production (kW/y) related to a specific sea state.

The estimated annual energy production in Catania for a single WEC is equal to 23.68 MWh/y (OpenWEC) and 31.71 MWh/y (model).

Table IV.26 Simulated annual energy production by using the mathematical model in Mazara

		Energy period T_e [s]										
		2	3	4	5	6	7	8	9	10	11	12
Significant Height [m]	0.5	1.29	1970	1942	1642	759	438	157	27	9.69	2.31	0.06
	1.0	0	379	3615	3836	3075	1965	593	199	119	45.6	4.4
	1.5	0	0	306	2959	3691	4345	1426	364	212	102	15.7
	2.0	0	0	4.74	565	2455	4535	2425	536	191	77.2	14.4
	2.5	0	0	0	28.7	470	2217	2306	861	297	85.4	23.3
	3.0	0	0	0	0	23.6	818	1634	1015	480	80.6	17.3
	3.5	0	0	0	0	19.3	104	713	708	560	184	17.3
	4.0	0	0	0	0	0	12.4	182	349	515	248	45.2
	4.5	0	0	0	0	0	0	17.7	186	318	194	44.2
	5.0	0	0	0	0	0	0	14.6	86	142	110	12.8

Table IV.27 Simulated annual energy production by using OpenWEC in Mazara

		Energy period T_e [s]										
		2	3	4	5	6	7	8	9	10	11	12
Significant Height [m]	0.5	20.9	759	1169	1213	613	366	137	23.7	8.91	2.12	0.06
	1.0	0	143	2183	2863	2519	1665	524	177	109	41.5	4.06
	1.5	0	0	184	2211	3031	3700	1264	325	195	93.1	14.5
	2.0	0	0	2.77	421	2014	3860	2153	479	176	70.8	13.4
	2.5	0	0	0	21.2	385	1886	2046	769	274	78.3	21.6
	3.0	0	0	0	0	19.3	696	1449	906	444	74	16.1
	3.5	0	0	0	0	15.7	88.7	632	632	517	169	16.1
	4.0	0	0	0	0	0	10.5	161	311	475	227	42
	4.5	0	0	0	0	0	0	15.7	166	294	178	41.1
	5.0	0	0	0	0	0	0	12.9	76.7	131	101	11.9

The estimated annual energy production in Mazara del Vallo for a single WEC is equal to 48.16 MWh/y (OpenWEC) and 60.15 MWh/y (model).

Table IV.28 Simulated annual energy production by using the mathematical model in Palermo

		Energy period T_e [s]										
		2	3	4	5	6	7	8	9	10	11	12
Significant Height [m]	0.5	1.75	2039	3017	2255	804	707	159	33.1	12	1.94	0.21
	1.0	0	206	2291	2978	3286	2310	486	180	84.5	26.7	5.46
	1.5	0	0	132	1244	2087	4171	1150	229	126	60.5	10.3
	2.0	0	0	0	152	721	3273	1850	411	169	66.1	10.3
	2.5	0	0	0	5.31	120	1301	1809	607	157	64.3	3.56
	3.0	0	0	0	0	5.23	298	1014	703	330	80.4	20.5
	3.5	0	0	0	0	0	47.4	261	436	338	97	12.2
	4.0	0	0	0	0	0	6.89	56.8	163	347	135	18.2
	4.5	0	0	0	0	0	0	0	67	169	106	11.5
	5.0	0	0	0	0	0	0	0	25.5	60.9	122	10.7

Table IV.29 Simulated annual energy production by using OpenWEC in Palermo

		Energy period T_e [s]										
		2	3	4	5	6	7	8	9	10	11	12
Significant Height [m]	0.5	28.4	786	1816	1666	650	590	138	29.1	11	1.78	0.2
	1.0	0	77.9	1384	2222	2691	1957	428	160	77.4	24.3	5.04
	1.5	0	0	79.4	930	1714	3552	1020	204	116	55.3	9.54
	2.0	0	0	0	113	591	2786	1643	367	156	60.6	9.54
	2.5	0	0	0	3.92	98	1107	1606	542	145	58.9	3.31
	3.0	0	0	0	0	4.28	253	900	628	305	73.7	19.1
	3.5	0	0	0	0	0	40.3	232	390	312	89	11.4
	4.0	0	0	0	0	0	5.84	50.4	145	321	124	17
	4.5	0	0	0	0	0	0	0	59.8	156	97	10.7
5.0	0	0	0	0	0	0	0	22.7	56.2	112	9.94	

The estimated annual energy production in Palermo for a single WEC is equal to 36.16 MWh/y (OpenWEC) and 45.76 MWh/y (model).

IV.4 Other system: the mechanical motion converter

As alternative solution, a mechanical motion converter was also considered for the exploitation of sea wave energy.

The idea is the adoption of the same point absorber, described above, by replacing the linear generator with a commercial alternator. To achieve this purpose, a motion converter should be implemented in order to transform a bidirectional and variable linear motion into a unidirectional rotary motion.

From a technical point of view, the adoption of commercial generators simplifies the designing process of the wave energy converter. In this case, the research is focused on the designing of mechanical components.

The idea is based on the use of freewheels and a bifacial rack. To better understand the working principle, Figure IV.55 shows the device composed by two freewheels (picture on the left), split in two subsystems (pictures in the middle and on the right). Imagining that the bifacial rack is pulled down by the weight of external buoy, the freewheel B starts to convert the linear motion into rotative one, transferring this motion to the wheel C, connected in the same axis of the freewheel. A belt is used to transfer the motion from the wheel C to the output axis E. Thanks to the adoption of wheels having different radiuses, it is possible to increase the angular speed of the output axis, in order to reduce the geometrical sizes of electrical machine.

This simple approach exploits only one of the two alternative strokes of the racks, producing a pulsating rotative motion in the output axis. Indeed, if the linear motion is inverted, the freewheel disconnects the torque transferred from the rack to the output axis, giving the ability to continue the rotation of this part thanks to the exploitation of its residual kinetic energy, accumulated during the previous step.

If a second freewheel F is installed in the other face of the rack, it is also possible to use the linear motion from the bottom to the top in order to run the same output axis E.

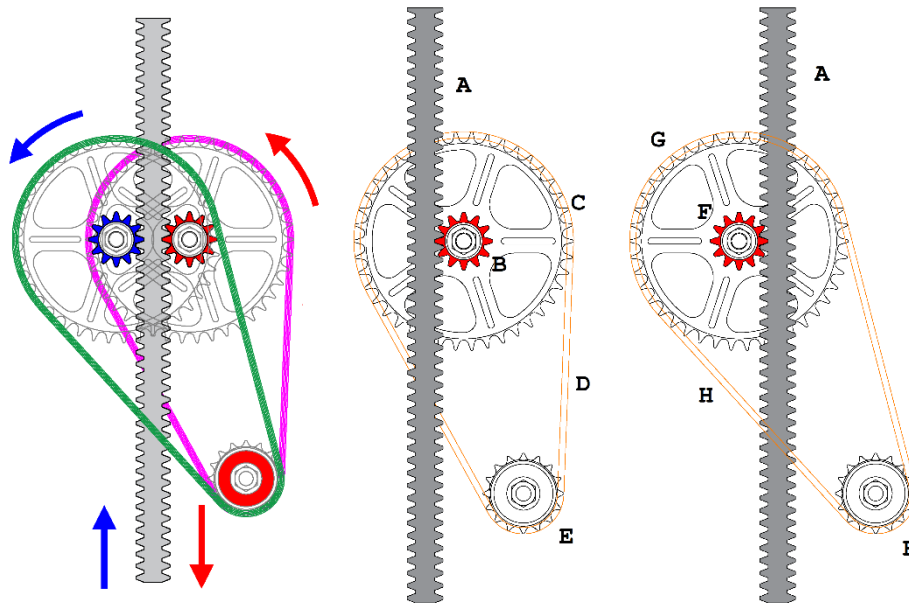


Figure IV.55 Working principle of the mechanical motion converter

As introduced before, the mechanical motion converter can be installed inside the same point absorber, described in the previous section. A rendering view is reported in Figure IV.56

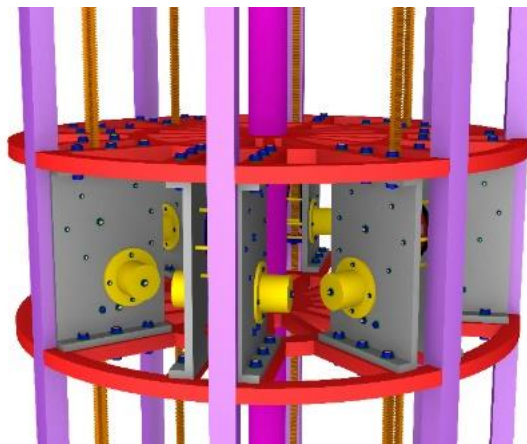


Figure IV.56 Internal view of WEC, equipped with the mechanical motion converter

Focusing the attention on the mechanical motion converter, the following mathematical approach can be used to analyze the working process.

The Eq. IV.32 evaluates the angular speed of output wheel, considering the linear speed of rack $\dot{z}(t)$, the number of teeth per length ζ , the number of teeth in the first freewheel n_1 (B), the radius of second wheel r_2 (C) and the radius of output wheel r_3 (E).

$$\omega_3(t) = \frac{2\pi\zeta r_2}{n_1 r_3} |\dot{z}(t)| = \gamma |\dot{z}(t)| \quad IV.32$$

The absolute value of linear speed velocity is introduced, considering the use of two opposite freewheels that convert the bidirectional motion into unidirectional.

The angular speed of alternators, thanks to the installation of a freewheel in the output axis, can be evaluated by these conditions:

$$\begin{cases} \text{if } \omega_3 < \omega_{alt} \rightarrow I_{alt} \frac{d\omega_{alt}}{dt} = -\tau_e - \tau_f \\ \text{else} \rightarrow \omega_{alt}(t) = \omega_3(t) = \gamma|v(t)| \end{cases} \quad IV.33$$

Indeed, if the angular speed ω_3 produced by the linear motion of the rack is lower than the instantaneous angular speed of alternators ω_{alt} , the output wheel does not receive drive torque from the mechanical converter; therefore, the alternators transform their kinetic energy into electricity (producing the corresponding torque τ_e) and a marginal energy loss by friction (corresponding to τ_f). In the second case, thanks to the adoption of freewheels, the output wheel is forced to rotate at the angular speed, set by the mechanical converter.

As preliminary evaluation of the energy performance, the mechanical motion converter was numerically simulated by considering the gravity force of a testing mass as input for the linear motion. Several tests have been realized, changing the value of electrical load resistance (ranging from 0 Ω to 100 Ω) and the value of testing mass (10 kg, 25 kg, 50 kg, 75 kg, 100 kg, 150 kg and 200 kg). In this simulation the parameter γ is fixed to 143.4 m^{-1} , while the friction torque is assumed equal to 0.3 Nm.

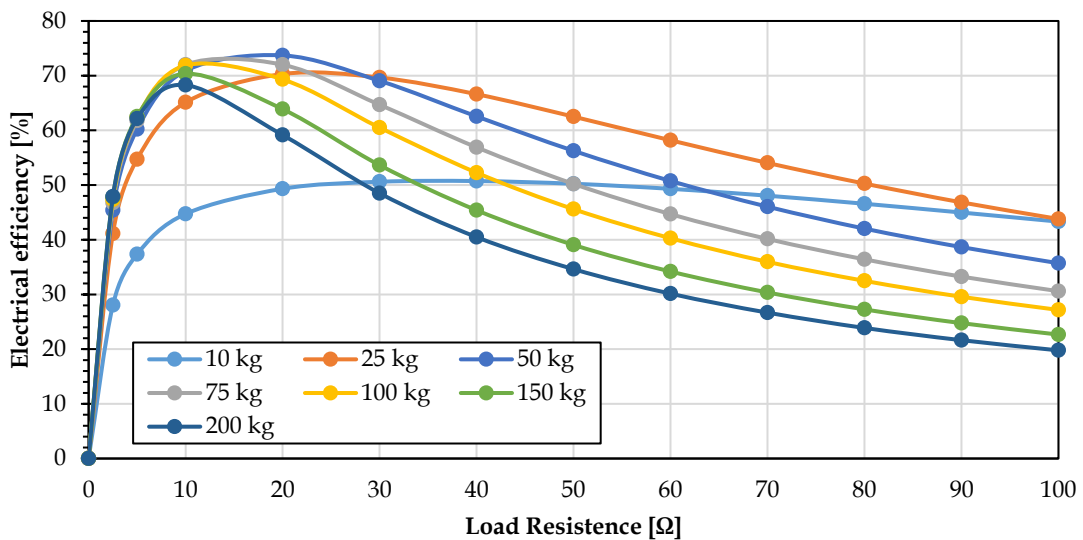


Figure IV.57 Electrical efficiency in the first scenario

Using the same set of values for the load resistance and the testing mass, two different approaches are considered: in the first test, the measuring interval is stopped at the end of the stroke. In this scenario, the alternators and secondarily the testing mass present a significant kinetic energy at the end of the stroke. Thanks to the installation of a freewheel in the output axis, the alternators can convert the residual kinetic energy into

electrical. Thence, in the second scenario, the measuring time is stopped when the alternators have finished their motion.

Figure IV.57 shows the electrical efficiency of the system in the first scenario, changing the testing mass and the electrical load resistance; similarly, Figure IV.58 reports the electrical efficiency in the second scenario.

Both figures show that the increasing of testing mass improves the electrical efficiency, since the internal braking torque by friction was assumed independent of the testing mass.

In the first scenario, the increasing of load resistance produces a significant reduction of the electrical efficiency, caused by the increasing of the fraction of kinetic energy of alternators and testing mass at the end of the stroke (see Figure IV.57).

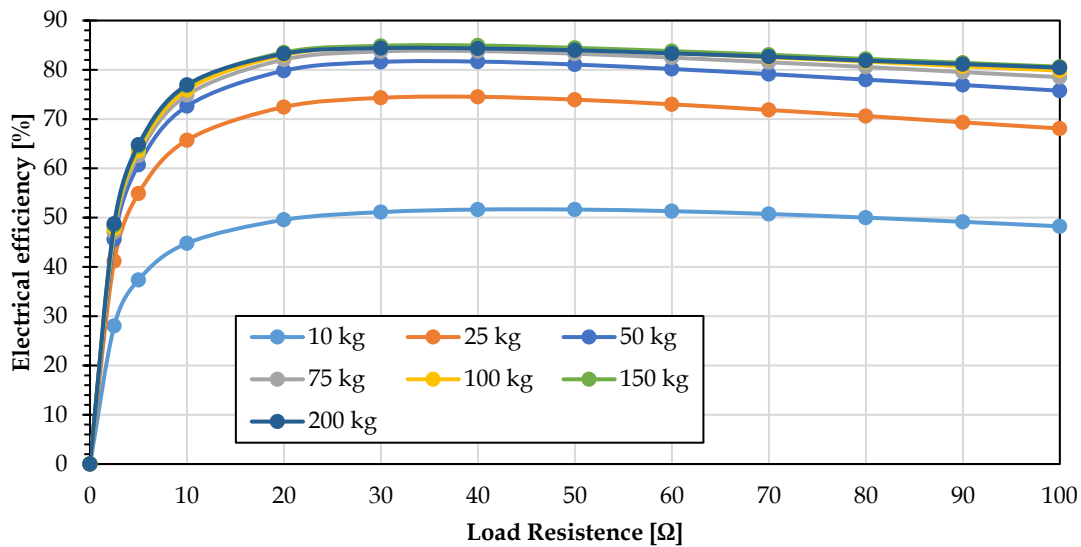


Figure IV.58 Electrical efficiency in the second scenario

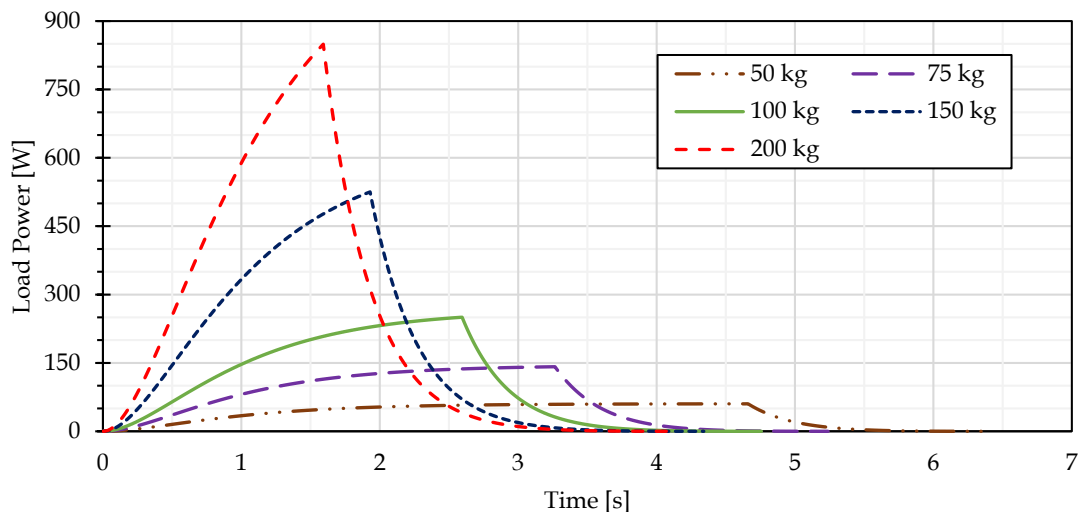


Figure IV.59 Power trend with different testing masses and a fixed load resistance (20 Ω)

In the second scenario (see Figure IV.58), the major part of kinetic energy of alternators is converted into electricity, hence the increasing of the electrical load

resistance produces a limited reduction of electrical efficiency (it is not possible recovers the kinetic energy of testing mass).

As regards the electrical output, increasing of testing mass improves the speed of rack and consequently increases the angular speed of alternators and the output voltages; the transient time of the phenomenon is reduced, as shown in Figure IV.59, where the load resistance is fixed to 20 Ω .

To conclude this chapter on the PTO, it should be noted that Eq. IV.26 can be also used to model the equivalent reaction of this system, thus the same approach reported in the previous section can be applied to estimate the power extraction from sea wave.

IV.5 Publications on this topic

- A. Viola, V. Franzitta, M. Trapanese, and D. Curto, “Nexus Water & Energy: A Case Study of Wave Energy Converters (WECs) to Desalination Applications in Sicily,” *Int. J. Heat Technol.*, vol. 34, no. Special Issue 2, pp. S379–S386, Oct. 2016.
- V. Franzitta, D. Curto, D. Milone, and D. Rao, “Assessment of Renewable Sources for the Energy Consumption in Malta in the Mediterranean Sea,” *Energies*, vol. 9, no. 12, p. 1034, Dec. 2016.
- V. Franzitta, D. Curto, D. Rao, and A. Viola, “Hydrogen Production from Sea Wave for Alternative Energy Vehicles for Public Transport in Trapani (Italy),” *Energies*, vol. 9, no. 10, p. 850, Oct. 2016.
- V. Franzitta, D. Curto, D. Milone, and A. Viola, “The desalination process driven by wave energy: A challenge for the future,” *Energies*, vol. 9, no. 12, pp. 1–16, Dec. 2016.
- M. Trapanese, F. Raimondi, D. Curto, and A. Viola, “Evaluation of the wave energy density on the Sicilian coast,” in *OCEANS 2016 - Shanghai*, 2016, pp. 1–4.
- V. Franzitta, D. Curto, D. Rao, and D. Milone, “Near zero energy island with sea wave energy: The case study of Pantelleria in Mediterranean Sea,” in *OCEANS 2016 - Shanghai*, 2016, pp. 1–5.
- V. Franzitta, D. Curto, D. Rao, and A. Viola, “Renewable energy sources to fulfill the global energy needs of a country: The case study of Malta in Mediterranean Sea,” in *OCEANS 2016 - Shanghai*, 2016, no. 2012, pp. 1–5.
- V. Franzitta, D. Curto, and D. Rao, “Energetic Sustainability Using Renewable Energies in the Mediterranean Sea,” *Sustainability*, vol. 8, no. 11, p. 1164, Nov. 2016.
- V. Franzitta, D. Rao, D. Curto, and A. Viola, “Greening island: renewable energies mix to satisfy electrical needs of Pantelleria in Mediterranean Sea,” in *OCEANS 2016 MTS/IEEE Monterey*, 2016, pp. 1–6.

- A. Viola, D. Curto, V. Franzitta, and M. Trapanese, “Sea water desalination and energy consumption: A case study of wave energy converters (WEC) to desalination applications in Sicily,” in *OCEANS 2016 MTS/IEEE Monterey*, 2016, pp. 1–5.
- V. Franzitta and D. Curto, “Sustainability of the Renewable Energy Extraction Close to the Mediterranean Islands,” *Energies*, vol. 10, no. 4, p. 283, Feb. 2017.
- V. Franzitta, P. Catrini, and D. Curto, “Wave Energy Assessment along Sicilian Coastline, Based on DEIM Point Absorber,” *Energies*, vol. 10, no. 3, p. 376, Mar. 2017.
- A. Viola and D. Curto, “Numerical simulation of wave energy production through experimental tool,” in *2017 IEEE International Conference on Environment and Electrical Engineering and 2017 IEEE Industrial and Commercial Power Systems Europe (EEEIC / I&CPS Europe)*, 2017, no. January, pp. 1–5.
- V. Boscaino et al., “Experimental validation of a distribution theory-based analysis of the effect of manufacturing tolerances on permanent magnet synchronous machines,” *AIP Adv.*, vol. 7, no. 5, p. 056650, May 2017.
- V. Franzitta, A. Colucci, D. Curto, V. Di Dio, and M. Trapanese, “A linear generator for a waveroller power device,” in *OCEANS 2017 - Aberdeen*, 2017, pp. 1–5.
- V. Franzitta, D. Curto, A. Viola, V. Di Dio, V. Boscaino, and M. Trapanese, “Guidelines proposal for a good and durable WEC design,” in *OCEANS 2017 - Aberdeen*, 2017, pp. 1–7.
- D. Curto and M. Trapanese, “Experimental Tests on Hydrogen Production from Seawaves Energy,” in *OCEANS – Anchorage*, 2017, 2017, pp. 1–5.
- V. Franzitta, D. Curto, D. Milone, and M. Trapanese, “Energy Saving in Public Transport Using Renewable Energy,” *Sustainability*, vol. 9, no. 1, p. 106, Jan. 2017.
- D. Curto, S. Neugebauer, A. Viola, M. Traverso, V. Franzitta, and M. Trapanese, “First Life Cycle Impact Considerations of Two Wave Energy Converters,” in *2018 OCEANS - MTS/IEEE Kobe Techno-Oceans (OTO)*, 2018, pp. 1–5.
- F. M. Raimondi, D. Milone, and D. Curto, “An innovative mechanical motion converter for sea wave applications,” in *2018 Thirteenth International Conference on Ecological Vehicles and Renewable Energies (EVER)*, 2018, pp. 1–6.
- D. Curto and M. Trapanese, “A Renewable Energy mix to Supply the Balearic Islands: Sea Wave, Wind and Solar,” in *2018 IEEE International Conference on Environment and Electrical Engineering and 2018 IEEE Industrial and Commercial Power Systems Europe (EEEIC / I&CPS Europe)*, 2018, pp. 1–6.
- M. Trapanese, V. Boscaino, G. Cipriani, D. Curto, V. Di Dio, and V. Franzitta, “A Permanent Magnet Linear Generator for the Enhancement of the Reliability of

a Wave Energy Conversion System,” *IEEE Trans. Ind. Electron.*, vol. 0046, no. c, pp. 1–1, 2018.

- D. Curto, V. Franzitta, A. Viola, M. Cirrincione, A. Mohammadi, and A. Kumar, “A renewable energy mix to supply small islands. A comparative study applied to Balearic Islands and Fiji,” *J. Clean. Prod.*, p. 118356, Sep. 2019.
- M. Trapanese, D. Curto, V. Franzitta, Z. Liu, L. McNabb, and X. Wang, “A Planar Generator for a Wave Energy Converter,” *IEEE Trans. Magn.*, vol. 55, no. 12, pp. 1–7, Dec. 2019.
- D. Curto, A. Viola, V. Franzitta, M. Trapanese, and F. Cardona, “A New Solution for Sea Wave Energy Harvesting, the Proposal of an Ironless Linear Generator,” *J. Mar. Sci. Eng.*, vol. 8, no. 2, p. 93, Feb. 2020.

V SMALL ISLANDS AND ENERGY PLANNING

As reported in the introduction, power plants supplied by RES are spreading around the world, increasing the sustainability of the energy sector.

Despite the availability of commercial technologies, in several remote areas and small islands the electricity production is nowadays realized through obsolete plants, supplied by fossil fuels [204]. This approach causes negative effects for the environment, like the pollution of air [205], water and soil, as well as the generation of noise [206].

Moreover, small islands normally do not have local fossil sources, for this reason fuels are shipped from the mainland. Bad weather conditions sometimes represent a real risk for the energy security of these territories. Long underwater cables rarely connect the small islands to the mainland, since these projects require huge investments in comparison with the local energy consumption [207]. For these reasons, the electrical power generation presents higher costs than in mainland [208].

These aspects are more relevant in the Small Islands Developing States (SIDS). This term, introduced in 1994 by UN (United Nations), is currently used to identify a group of islands with common peculiarities from a geographical or economic point of view.

There are more than 50,000 islands in the world but only a limited part of them is classified as SIDS. Indeed, Figure V.1 shows the numerous island communities around the world, both SIDS and small islands belonging to big countries [209]. In detail, Blechinger et al. indicates that over 21 million of people live in about 2050 small islands (each one with a population between 1,000 and 100,000 inhabitants). The electricity demand to supply all these communities is estimated equal to 52690 GWh/y, using mainly fossil fuel [209].

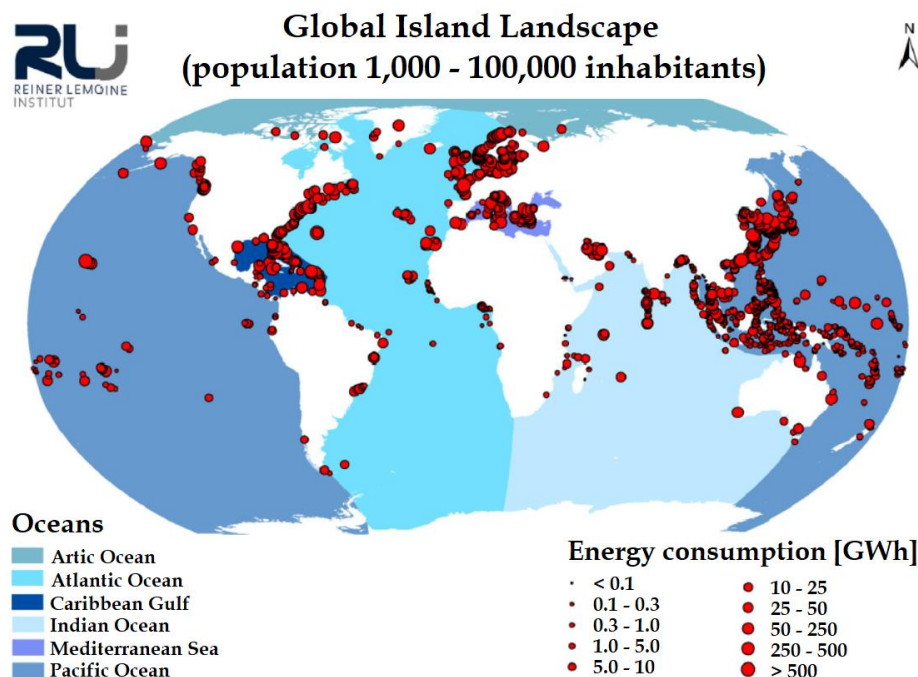


Figure V.1 Small islands in the world [209] (CC BY-NC-ND 3.0)

According to the United Nations Department of Economic and Social Affairs the SIDS list includes 58 countries, divided in Caribbean (29 countries), Pacific (20 countries) and AIMS (acronym of Africa, Indian Ocean, Mediterranean and South China Sea, including 9 countries) [210].

The introduction of RES represents a valid solution to limit the energy dependence on fossil fuel. This aspect is common in small islands around the world, with a relevance in the case of SIDS (Small Islands Developing Countries) [211]. There are limited exceptions, like Fiji and Dominica, where hydropower is used to cover a significant share of the local energy demand [212].

In any case, the fuel consumption in SIDS implies the importation of energy resources from other countries. Trinidad and Tobago and Papua New Guinea are the only exception because these countries have local reserves [210].

Small island communities and in particular SIDS have in common the following peculiarities [213]-[215]:

- high seasonal variation in inhabitants, especially in touristic destinations;
- annual growth of the energy demand, especially in developing countries;
- limited utilization of RES, despite their availability;
- high fuel cost due to the need to import it from the mainland or far foreign countries;
- limited freshwater reserves, thence desalination plants sometimes are required;
- the installation of RES could be limited for the preservation of the landscape.

Unlike the small islands belonging to developed countries, SIDS are directly exposed to the international markets of oil, making the local economy fragile. Furthermore, in SIDS population and welfare show an increasing trend, implying a rapid growing of the energy demand. Finally, SIDS are generally located in the tropical zone [216], that is quite exposed to extreme weather conditions, causing disasters [217].

Pelling et al. studied and established the degree and past scale of vulnerability of SIDS offering a structure of the types of global pressure in islands [218]. However, Szabo et al. realized a cost effective analysis of electricity generation for islands [219]. They suggested new political subsidies to increase the development of RES.

Weisser discussed the benefits in SIDS's economy by using renewable energies or other technologies that cut the cost for the electricity generation [220].

Several researches indicate the most promising RES for this application [2], [221], [222]. The current focus is on wind, solar, biomass and sea wave [223]. Due to the small available surface in SIDS, specific solutions must be implemented, avoiding the installation of land consuming technologies in order to preserve their fragile ecosystems [224].

Consequently, energy management for small islands must engage problems that can no longer be solved by using traditional technologies, thence renewable energy systems represent a possible solution. Indeed, most of them can become autonomous from the energy point of view by using RES, thus avoiding the considerably higher (3-4 times) costs of the conventional sources and preserving the territory at the same time.

In any case, the economic benefits from the adoption of RES in SIDS has been recently demonstrated through the evaluation of the Levelized Cost Of Electricity (LCOE) index [225].

In this context, sea wave is considered an interesting solution to supply coastal areas around the world, due to its peculiarities, such as the great regularity and huge availability, especially in case of small islands where the energy demand is limited [112], [145], [226], [227]. Several solutions have been proposed but no technologies are commercially available [228], [229].

Different RES mix have been suggested to supply several small islands around the world, as reported in the following case studies: Samsø (Denmark) [221], Azores (Portugal) [230], Skyros (Greek) [222], Maldives [2], Canary Islands (Spain) [231], Faroe Islands [232], Dongfushan Island [233] and Reunion Island (France) [234].

For example, Samsø is a small Danish island, having a surface about 114 km². It is electrically linked to the mainland [221]. Thanks to the installation of offshore wind turbines and biomass plants, since 1997 the community satisfies the electricity demand by using exclusively renewable energy sources [235].

Stenzel et al. performed a Life Cycle Assessment, considering Graciosa Island as case study. This island belongs to Azores, an autonomous archipelago in the middle of the Atlantic Ocean. Since the local electricity production is based on fossil fuels, the realization of a RES mix is proposed, considering the installation of 4.5 MW of wind turbines, 1 MW of photovoltaic panels (1 MW) and the existing diesel engines to balance the electrical grid and in case of energy backup [230].

Petrakopoulou [222] presented a hybrid power plant in order to cover the electrical demand of Skyros, a small Greek island, in the middle of Aegean Sea. The solution is composed by solar thermal and photovoltaic plants, hydro and wind turbines.

Considering the Maldives Islands, Liu recommended the installation of a RES mix, composed by solar, wind and biomass sources [2]. To stabilize the electricity flow on the local grid, the modulation of the local desalination plant and diesel power plants is proposed.

About the Canary Islands, Rusu reported a preliminary energy assessment suggesting the exploitation of sea wave energy and considering different technologies, currently in development step [231]. In the same context, Gils and Simon reported several scenarios, considering a variegated energy mix composed by solar, wind, geothermal, biomass and hydro power as energy sources and the development of the electrical grid [236].

Another case study is Faroe Islands, an autonomous country formed by 18 islands that are in the middle of the North Atlantic Ocean between Norway, Iceland and

Scotland. The archipelago is home to 50,000 inhabitants, that require an electricity demand equal to 335 GWh/y [232]. To this purpose, the current energy mix is entrusted to fossil fuels (49%), hydropower (33%) and wind source (18%) [232]. With the goal of improving the sustainability of the energy sector, Katsaprakakis et al. investigated the installation of a wind farm, photovoltaic panels and a pumping hydro plant [232].

Zhao et al. proposed a RES mix to supply Dongfushan Island, located in the eastern part of China [233]. The system is composed by solar panels, wind turbines, diesel generators and a battery storage system. A genetic algorithm is used to minimize the life cycle costs and maximize the production of electrical energy by renewable energy sources [233].

Finally, Selosse et al. [234] considered the Reunion Island, a French oversea island in the Indian Ocean, analyzing different energy scenarios based on biomass, hydropower, wind, solar, geothermal, sea wave and Ocean Thermal Energy Conversion (OTEC, i.e. the energy related to the thermal gradient between the surface water and the deep water of the sea) [114].

Considering now only the European territories, there are 362 small islands, having more than 50 permanent residents and other 286 islands with a lower population [237].

To reduce the CO₂ emissions, in 2008 the European Commission started the project called “Covenant of Mayors”, involving all European communities. After the signature of this agreement, a detailed energy assessment is required, analyzing the local energy demand, subdivided by sectors and energy carriers. The local peculiarities are also considered, like population trend, main activities and special needs. Collecting all this information, each municipality draws up the Sustainable Energy Action Plan, where the intervention plans are reported to reach the objectives for the energy saving and the promotion of RES [238].

Focusing on Italy, there are about 50 islands with a population greater than 50 habitants. In order to promote, the energy sustainability in these small islands, two decrees have been recently emitted in Italy, proposing the installation of power plants supplied by RES and the improvement of energy efficiency in the final users. The central idea is the transformation of small Italian islands into open air laboratories where sustainable and innovative energy solutions can be tested, considering the environmental and landscape restrictions [239].

In particular, the decree 14 February 2017 issued by the Italian Ministry of Economic Development considers 20 small islands (not connected to the mainland) and indicates for each one the current energy demand, the targets of electricity and thermal energy production from RES by December 31, 2020 and the financial incentives [240].

As an example, according to data reported in Table V.1, for the island of Lampedusa (south of Sicily) the Annex I of the decree 14 February 2017 indicates a current energy demand of 37.66 GWh/y and sets the requirement to achieve a total RES power of 2.14 MW. About the thermal energy production, the decree prescribes the installation of 2370 m² of solar thermal panels.

It is remarkable that the Article 6 introduces the possibility to realize “integrated innovative projects”, including offshore plants supplied by oceanic energies. Thus, sea wave energy represents a potential solution to supply small islands in a sustainable way. Indeed, it is important to underline that the greatest part of Italian small islands shows environmental constraints to preserve the natural landscape from anthropic changes, therefore the realization of extensive RES plants is currently forbidden [34].

Table V.1 Targets and data on small islands according to decree 14 February 2017 [240], [241]

Island	Surface [km ²]	Inhabitants [-]	Electrical target [kW]	Solar thermal panel target [m ²]	Electrical demand [MWh/y]	Owner of the local power plant
Alicudi	5.10	105	20	20	400	ENEL Produzione
Capraia	19.33	398	180	250	2760	ENEL Produzione
Capri	10.5	14164	1000	4850	66600	SIPPIC SpA
Favignana	19.8	3337	900	1070	15470	SEA Soc Elettrica Favignana
Filicudi	9.49	235	80	90	1400	ENEL Produzione
Giglio	24.01	1423	700	780	10300	SIE Società Impianti Elettrici
Lampedusa	20.2	5871	2140	2370	37660	SELIS Lampedusa
Levanzo	5.6	208	40	40	600	ICEL
Linosa	5.43	433	170	210	2800	SELIS Linosa
Lipari	37.29	8686	2110	2520	34800	SEL SNC Lipari
Marettimo	12.3	684	120	150	2040	SELIS Marettimo
Panarea	3.34	280	130	200	3140	ENEL Produzione
Pantelleria	84.53	7759	2720	3130	44170	SMEDE Pantelleria
Ponza	10.16	3360	720	870	11500	SEP Soc Elettrica Ponzese
Salina	26.38	2598	580	570	9160	ENEL Produzione
Stromboli	12.19	572	220	250	3870	ENEL Produzione
Tremiti	3.18 (*)	472	240	290	3920	Germano Industrie Elettriche
Ustica	8.24	1319	280	370	4870	Imp Elettrica D'Anna Bonaccorsi
Ventotene	1.75	768	170	200	2700	ENEL Produzione
Vulcano	20.87	715	300	470	7280	ENEL Produzione

(*) Entire archipelago

The decree has been in force for more than a year, but only at the beginning of 2018 the Authority published guidelines regarding methods and scheduling. However, since the objectives are also retroactive (the already operative plants contribute to the target achievement), it is interesting to check the current conditions in comparison with the target at 2020. In detail, the comparison of the current installed power and the goals fixed by the decree is reported in Figure V.2.

The island of Vulcano is the only one that reached half of the target concerning RES installed capacity (thanks to photovoltaic panels), while all the others are well below 50%. For example, the islands of Salina, Panarea, Filicudi and Alicudi have no RES supplied power plants.

Very recently, the European Union created the Clean Energy for EU Islands Secretariat in order to facilitate the energy transition from fossil fuels to RES. In this project, 26 European islands have been selected, of which three are Italian (Favignana, Salina and Pantelleria) [242].

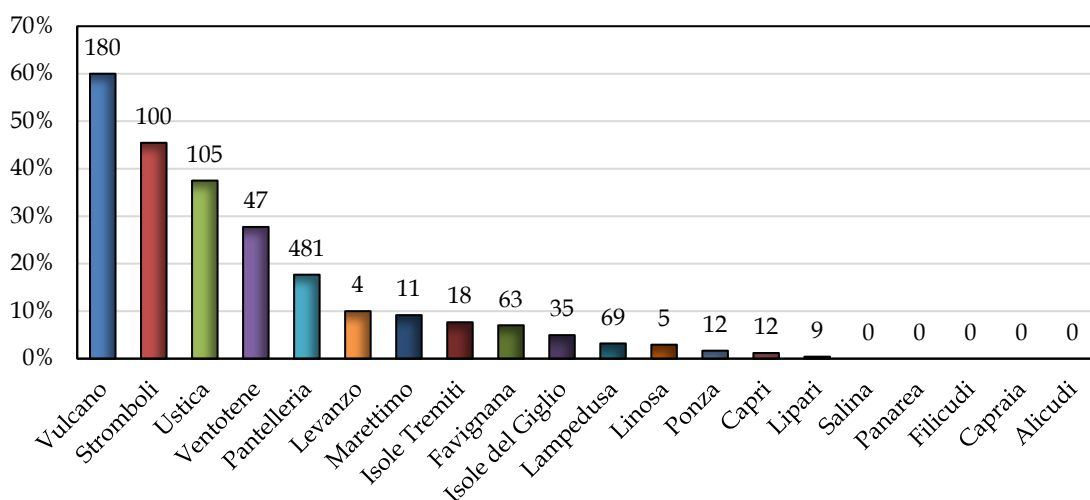


Figure V.2 Share of RES and installed power (data in kW) in small Italian islands

To reduce the energy consumption for the freshwater production, in the last years all small Italian islands replaced their desalination plants, installing new RO units. The main data are reported in Table V.2 (based on [32], [243], [244] and information provided by SO.FI.P. S.p.A., S.ME.D.E. Pantelleria S.p.A. and S.EL.I.S. Lampedusa S.p.A.).

Table V.2 Data on desalination plants installed in small Italian islands

Island	n. unit	Model	Capacity [m ³ /day]	Operating date	Annual production [m ³]
Lampedusa	2	DOW FILMTEC	1500	Dec. 2014	870897 [2019]
	1	SW30HRLE440	600		
Linosa	2	DOW FILMTEC	250	Mar. 2015	214340 [2019]
		SW30HRLE440			
Pantelleria (Sataria)	4	DOW FILMTEC	1250	Dec. 2014	742548 [2019]
		SW30HRLE440			
Pantelleria (Maggiuluvedi)	1	DOW FILMTEC SW30HRLE440	900	Jun. 2016	122880 [2019]
Ustica	2	-	864	Sep. 2015	331540 [Sep. 2015 to Aug. 2016]
Lipari	3	EuroMEC	3600	Jan. 2013	-
Vulcano	2	Veolia Water Technologies	1469	Oct. 2019	-
Capraia	1		500	2005	104531 [2016]

In conclusion, according to the great attention for small islands in the last years, in this chapter some case studies are reported, investigating the exploitation of sea wave to supply local loads, like desalination plants, public buildings and facilities or a significant part of the total electrical energy demand. About desalination plants, since the BAT is already adopted, the equivalent energy demand is considered as target to size a RES mix. The management of desalination plants is also considered in the last case study, with the purpose to improve the energy efficiency for the electricity production.

V.1 Energy supply for public buildings in Ustica

As first case study, in this section a preliminary energy assessment is reported, considering the electrical energy demand of public buildings and facilities in Ustica.

Since this energy demand represents a limited ratio of the total electricity production, the hourly balancing problem is not considered.

The proposed energy mix suggests the installation of few WEC and small photovoltaic plants, some of them integrated on the rooftop of the existing buildings and the other on the same WECs. Thus, the energy mix comprises solar and sea wave.

A limited amount of climatic data is required, in order to perform the evaluation of the annual energy production. These data are available in literature or can be obtained by using specific GIS (Geographic Information System) tools. An economic analysis is also performed.

The case study below reported is published in the paper “**A Preliminary Energy Assessment to Improve the Energy Sustainability in the Small Islands of the Mediterranean Sea**” in *Journal of Sustainable Development of Energy, Water and Environment* [245].

V.1.a The case study of Ustica

Ustica is a small Italian island, located north of Sicily in the Tyrrhenian Sea, about 67 kilometres north-west from Palermo (see Figure V.3). The island has an extension of 8.65 km², with a coastline 12 km long.

The island has a own municipality, where about 1,300 people live regularly. Ustica is equipped with a small electrical grid, not linked to the mainland. As introduced above, this condition is quite common in the small islands of the Mediterranean Sea. The only way to reach the island is the ferry service from Palermo, Trapani or Naples.



Figure V.3 Location of Ustica in the Mediterranean Sea

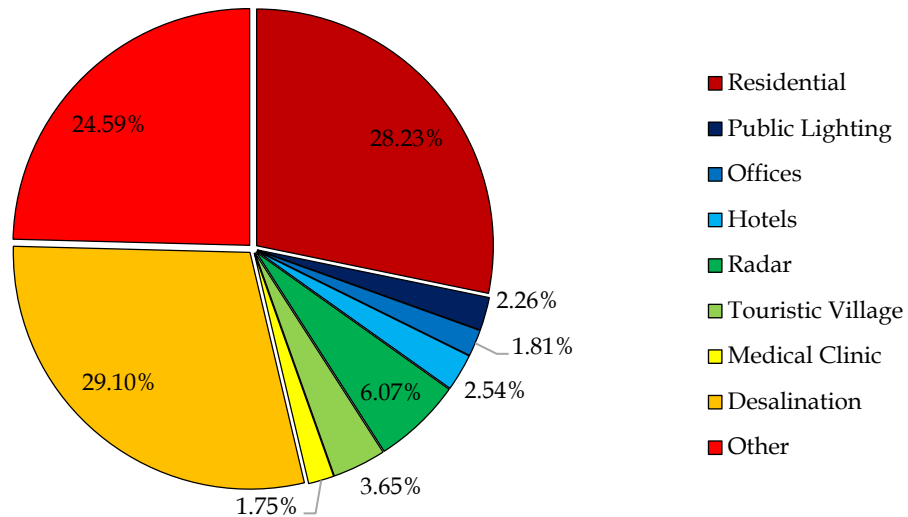


Figure V.4 Electrical consumption by uses

The electrical production is still today based on old diesel engines, producing annually about 6.5 MWh (data 2015-2016). Figure V.4 shows the main loads [32]. In detail, almost the 82% of the total energy demand is due to three kinds of uses: Residential (28.23%), Desalination (29.10%) and Other (24.59%, representing rural buildings and activities). The remaining electricity demand is related to specific activities, such as Public Lighting, Offices, Hotels, Touristic Village, Medical Clinic and Radar (for the national air traffic control).

As shown in Figure V.5, the annual trend of electrical energy consumption reveals a significant variation during the four seasons: the maximal value is achieved in August (1028 MWh), while the minimum one in February (377 MWh). This variation is essentially due to the touristic sector, that represents a relevant income for the island. The tourist arrivals are concentrated in summer (from June to September), therefore electricity and freshwater demand increases.

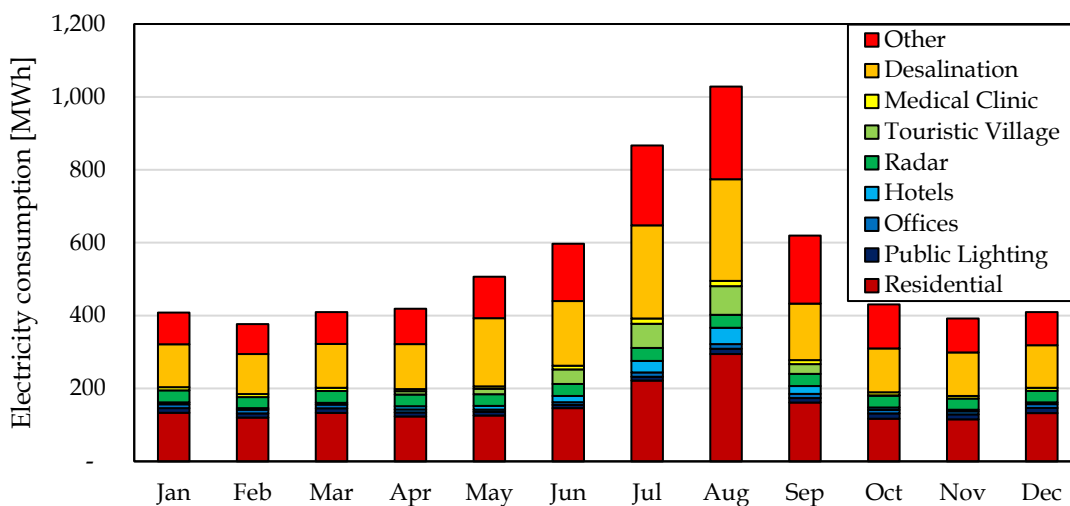


Figure V.5 Annual trend of electricity consumption by uses

The renewable energy sources are practically unused, since the environmental constraints avoid the installation of land consuming technologies, like photovoltaic panels (PVP), except the case of rooftop integrated PVP in not heritage building, or device visible at distance, like wind turbines [34].

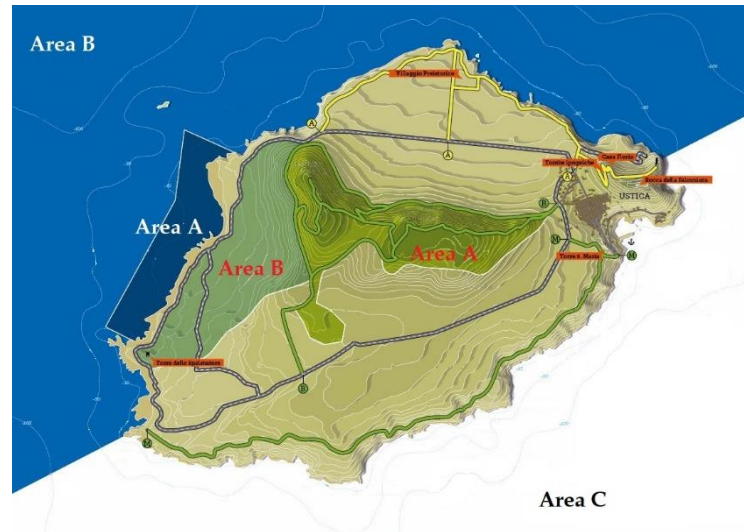


Figure V.6 Protected areas in Ustica

Indeed, the island of Ustica is included in two reserved areas (see Figure V.6). The “Protected Marine Area” was established in 1986 and is referred to about 16,000 hectares of sea around the island. It is divided in three zones, with different levels of restrictions: inside Area A any type of boats is not allowed, fishing is forbidden, bathing and snorkeling are permitted; inside Area B, it is forbidden to take any form of plant or animal life, boats and underwater activities are allowed, except fishing; finally inside the Area C, navigation and docking are allowed, professional fishing is permitted only after a specific authorization [246].

The “Terrestrial Natural Reserve” was established in 1997, including about 500 species of terrestrial flora. Inside these areas all human activities are forbidden to preserve the local flora and fauna [247].

Ustica is affected by water scarcity, since the annual rainfall achieves the 500 mm, mainly concentrated in 60 days. The water reserves are limited, since lakes and rivers are absent. The only available natural source has a capacity of 350 m³/day, not enough to cover the freshwater demand of the island [248]. Thus, the greatest part of freshwater is produced by the local desalination plant. In case of prolonged failure, freshwater had been also transported by boat from the mainland.

In 2015 the desalination plant was updated, replacing the two old MVC units, with two modern RO units. The new desalination plant has a nominal freshwater production equal to 72 m³/h (1728 m³day) [32].

This upgrade modified the load flows in the local grid, because electricity production was previously realized by dedicated diesel engines, installed in the desalination plant, while today the entire energy demand is transferred to the local power plant. The annual

freshwater trend is reported in Figure V.7 [32]. Considering also the electricity consumption for the water withdrawal from the sea, pre-treatments and post-treatments, the desalination plant produces freshwater with a unitary energy consumption equal to 5.91 kWh/m³. Like the annual electricity production, the freshwater demand increases significantly during summer (about 47 000 m³ in August in comparison with 20 000 m³ during winter).

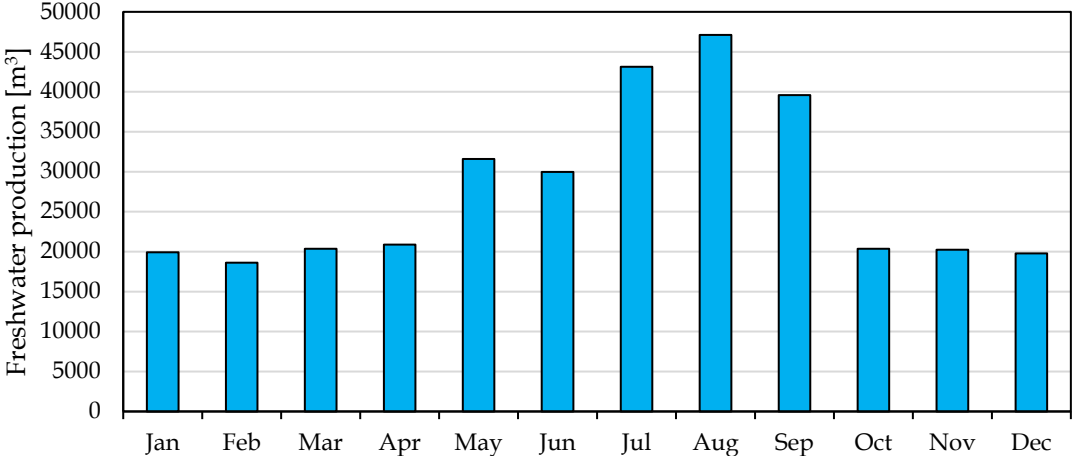


Figure V.7 Freshwater production by the desalination plant in Ustica

In this context, Ustica has some public services and offices, therefore the related costs for the electricity consumption represents expenditure money for the municipality. For example, there are public schools, municipal offices, public lighting and water purification plants.

The following Table V.3 reports the electrical consumptions measured in 2016 about the public buildings and facilities, subdivided in five categories: schools, public lighting, offices, water purification plant and other services.

Table V.3 Electrical consumption in public buildings and facilities in Ustica

	Annual electrical consumption [kWh/y]	Annual costs [€/y]
Schools	24,959	7,454
Public lighting	143,583	24,926
Offices	64,505	19,513
Water purification plant	67,126	15,014
Other services	16,667	9,730

Thus, according to the previous data, the annual electrical demand from public services in Ustica is equal to 316,840 kWh/y, with a cost of 76,637 €. It is important to underline that this energy demand represents only the 4.9 % of the annual global electrical demand in Ustica.

V.1.b Mathematical approach

In order to evaluate the electricity production from solar and sea wave energy sources, a simplified mathematical approach is reported below.

Eq. V.1 is used to calculate the monthly electrical production from solar panels $E_{PVB,i}$ installed on the roofs of public buildings:

$$E_{PVB,i} = H_{m,tilt,i} S_{PV,B} \eta_{PV,e} n_B \quad V.1$$

indicating with $H_{m,tilt,i}$ the monthly solar radiation collected by an inclined surface to the south with a tilt angle equal to the latitude; $S_{PV,B}$ represents the net area of photovoltaic panels installed above the public buildings; $\eta_{PV,e}$ is the average electrical efficiency of photovoltaic panels and, finally, n_B represents the number of photovoltaic plants [249].

As described above, the WEC proposed in the section IV.3.f can be adopted also to produce electricity from solar radiation, thanks to the possibility to install a PVP plant on the top of the device. Thus, Eq. V.2 is introduced to evaluate this energy contribution [249].

$$E_{PVF,i} = H_{m,ho,i} S_{PV,F} \eta_{PV,e} n_C \quad V.2$$

considering the monthly solar radiation $H_{m,ho,i}$ to a horizontal surface, the net area of photovoltaic panels installed on each WEC $S_{PV,F}$, the electrical efficiency of photovoltaic panels $\eta_{PV,e}$ and the number of devices installed in the solar wave energy farm n_C .

According to Eq. V.3, the monthly electrical energy production from sea wave $E_{W,i}$ is evaluated considering the monthly average sea wave power flux $\varphi_{m,i}$, the equivalent hydraulic diameter d_C of the external buoy of point absorber, the average energy efficiency η_W of the device, the number of hours in the i -th month $t_{m,i}$ and the number of wave energy converters n_C [250].

$$E_{WF,i} = \varphi_{m,i} d_C \eta_W t_{m,i} n_C \quad V.3$$

To evaluate the environmental benefits, firstly the avoided electricity production from fossil fuels is obtained as sum of the monthly electrical energy production from sea wave and solar panels (see Eq. V.4). Multiplying this value with the specific emission factor γ_{CO_2} , the annual avoided CO_2 is obtained (see Eq. V.5) [251].

$$E_{ann} = \left[\sum_{i=1}^{12} (E_{PVF,i} + E_{PVB,i} + E_{WF,i}) \right] \quad V.4$$

$$\Gamma_{CO_2} = \gamma_{CO_2} E_{ann} \quad V.5$$

Finally, in order to evaluate the economic convenience of the project, Eq. V.6 introduces the discounted cash flow [252].

$$DCF_n = -I_0 - \sum_{i=1}^n \frac{C_i}{(1 + \tau)^i} + E_{ann} c_e \sum_{i=1}^n \frac{(1 + \varepsilon)^i}{(1 + \tau)^i} \quad V.6$$

The equation considers the initial investment I_0 , the annual operative and maintenance costs C_i , the annual income from the selling of electrical energy $E_{ann} c_e$, the rate of interest for money τ and, finally, the rate of interest for energy ε .

V.1.c Results

In order to cover the energy demand of public buildings and facilities in the island of Ustica, the following energy mix is considered:

- The installation of a small solar wave energy farm, composed by two point absorbers, able to exploit solar and sea wave sources, due to the integration of photovoltaic panels in the upper part of wave energy converters;
- The installation of six photovoltaic plants on the roofs of public buildings, each one having a rated power of 3.3 kW.

Figure V.8 shows the annual trend of sea wave power flux and the monthly solar radiation to a horizontal plane and an inclined plane to the south with a tilt angle equal to 39° . Data on sea wave are obtained from the "Rete Ondametrica Nazionale", described in the previous chapter [112]. About the solar radiation, an open source GIS tool is adopted [253].

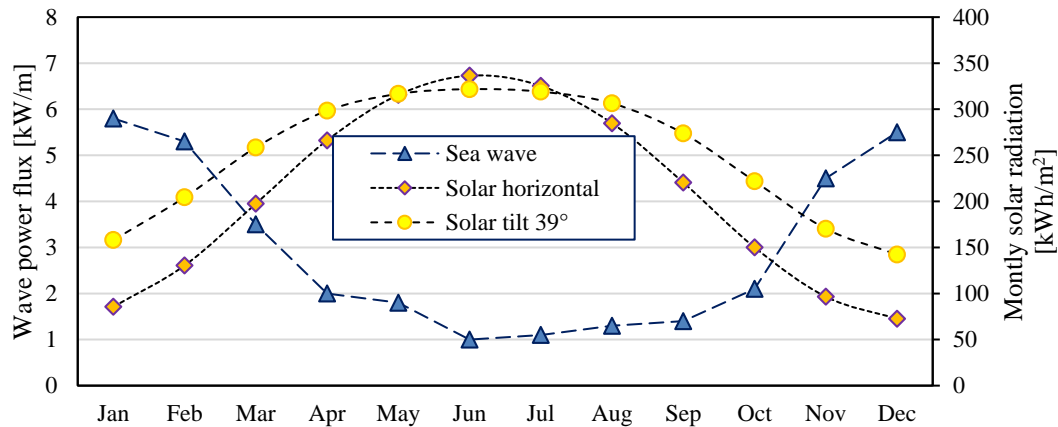


Figure V.8 Data on solar and sea wave climate in Ustica

The energy mix is sized in order to cover the annual electrical demand of public services. Applying the set of equations above reported, Figure V.9 shows the annual trend of the electrical energy production from the proposed RES mix.

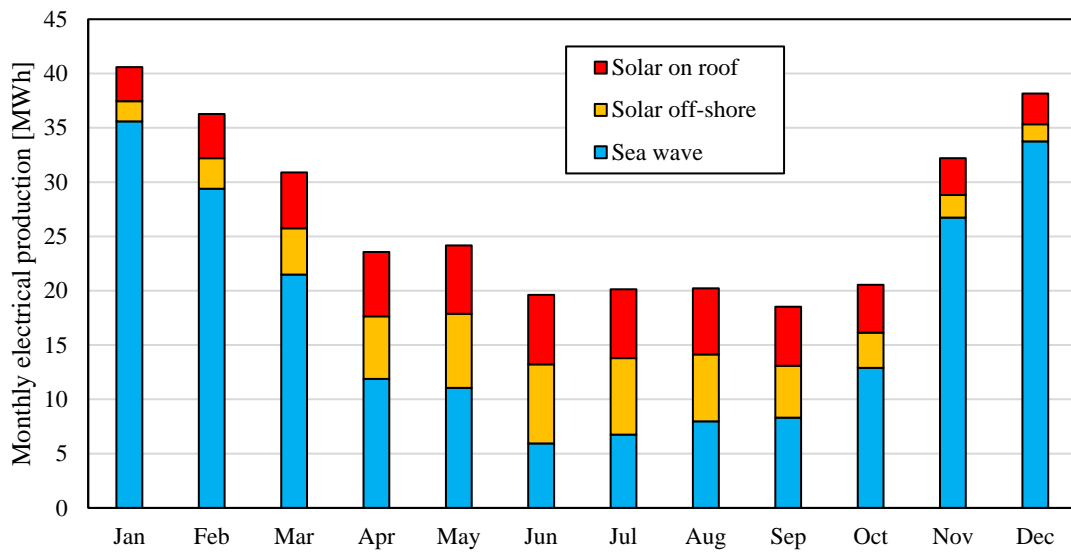


Figure V.9 Electricity production from the proposed renewable energy mix

According to the simulation, the solar wave energy farm could produce 265.43 MWh/y, of which 211.76 MWh/y from sea wave and 53.67 MWh/y from solar. The installed power is equal to 160 kW from sea wave and 21.6 kW from photovoltaic panels.

In order to regularize the annual electrical production, additional photovoltaic plants must be installed on the roofs of public buildings. In particular, it is suggested the installation of 6 photovoltaic plants, each one having a rated power of 3.3 kW, with a global installed power of 19.9 kW and a potential electricity production equal to 59.45 MWh/y.

Summing up all energy productions, the proposed RES mix could produce 324.88 MWh/y, enough to cover the annual electrical demand of public services, with a surplus of 8 MWh/y, that can be sold to the local electrical grid, reducing furthermore the electricity production from fossil fuels. Table V.4 summarizes the features of the solar sea wave energy farm while Table V.5 reports the characteristics of the PVP plants that should be installed on the roofs of public buildings.

Table V.4 Details on the solar wave energy farm

Parameters	Values
Number of buoys	2
Installed power by wave	160 kW
Installed photovoltaic power	21.6 kW
Annual electrical production by wave	211.76 MWh/y
Annual electrical production by solar	53.67 MWh/y

Table V.5 Details on the roof-integrated photovoltaic plants

Parameters	Values
Number of photovoltaic plants	6
Rated power of single photovoltaic plants	3.3 kW
Installed power by photovoltaic plants	19.9 kW
Annual electrical production	59.45 MWh/y

About the environmental benefits, the annual avoided CO₂ emission was evaluated according to Eq. V.5. It was assumed an emission factor γ_{CO_2} equal to 0.682 t CO₂/MWh, considering data from literature about similar technologies [251]. Thus, the proposed RES mix can avoid the emission of 221.6 tons of CO₂ per year.

Finally, the economic analysis was performed, evaluating the discounted cash flow according to Eq. V.6. All economic parameters are reported in Table V.6. About the cost for the installation and maintenance of photovoltaic panels, data are available in literature [17].

Table V.6 Economic parameters used in the discounted cash flow

Parameters	Values
Money discount rate	0.25%
Energy discount rate	2.0%
Initial investment	340,628 €
Annual maintenance costs	37,469 €
Selling energy price	25.0 c€/kWh
Annual energy selling	81,221 €

It is interesting to underline that to cover the additional cost for the electricity generation in small islands, the Italian authority (ARERA) admits an incentivized price. Each small island shows a different value, equal to 41.39 c€/kWh in the case study, that should be summed to the average National Unique Price (NUP, 5.32 c€/kWh) [254]. Since the renewable energy mix should be installed by the local municipality, a lower total price was assumed, practically equal to sum of the NUP and half of the incentivized price, in order to reduce the breakeven time and create a profit for the local and the national institutions. This value is close to the average price currently paid by the local municipality to purchase electricity.

The money discount rate is chosen according to the European Central Bank [255], while the energy discount rate is obtained analyzing the trend of the NUP in the last five years [256]. Thence, considering the data above reported, the discounted cash flow was performed. As reported in Figure V.10, the breakeven time is equal to 7-8 years.

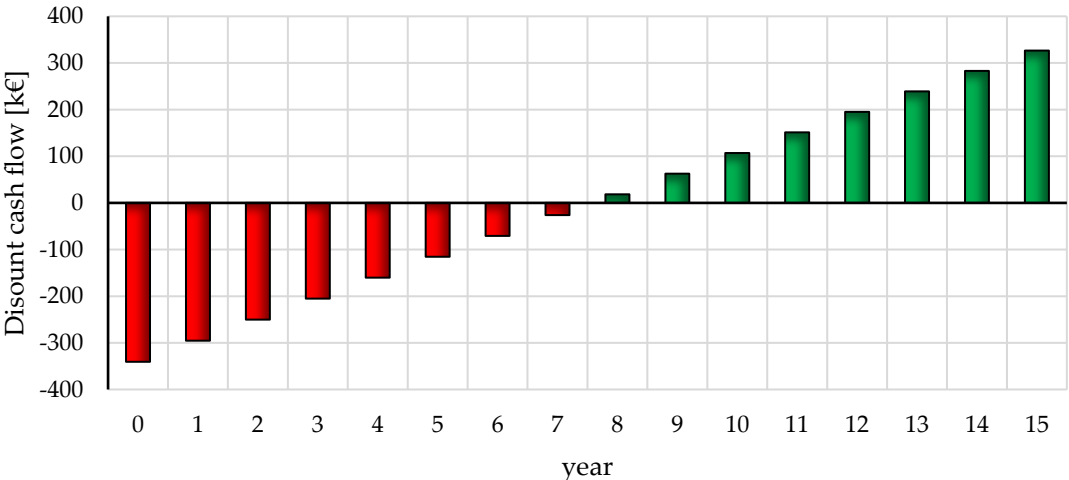


Figure V.10 Discounted cash flow of the project

V.2 An energy mix for Balearic Islands and Fiji

In this section, the proposal of an energy mix, based on solar, wind and sea wave, is reported, realizing a comparison of two archipelagos located in different areas of the world: Balearic Islands (Mediterranean Sea) and Fiji (Pacific Ocean).

Each case study is analyzed in detail, reporting the status of the electrical grid, the availability of local resources and the expected energy demand by 2025 in both contexts.

A simplified model is introduced in order to realize a preliminary energy assessment by the evaluation of the potential energy production by three different RES, the related costs for the installation and maintenance.

The model allows the estimation of the initial investment to realize the RES mix and the environmental effects, represented by the avoided CO₂ emission and electricity production from fossil fuels.

This model requires a limited amount of climatic data (a monthly resolution is enough) and the technical specifics of the selected devices for the exploitation of RES. Climatic data can be obtained from literature or using a specific software. Technical specifics are normally reported in the datasheets of the selected devices.

About wind energy, two alternative expressions are adopted, since GIS tools provide data in terms of equivalent Weibull distribution or reporting the observed number of hours per each month for fixed number of wind speed classes.

The potential electrical production from RES and the environmental benefits are calculated. From an economic point of view, the breakeven time and the discounted cash flow are evaluated.

The case studies below reported are published in the papers “**A renewable energy mix to supply small islands. A comparative study applied to Balearic Islands and Fiji**” in *Journal of Cleaner Production* [257] and “**A Renewable Energy mix to Supply the Balearic Islands: Sea Wave, Wind and Solar**” in *Conference Proceedings 2018 IEEE International Conference on Environment and Electrical Engineering and 2018 IEEE Industrial and Commercial Power Systems Europe (EEEIC / I&CPS Europe)* [249].

V.2.a Balearic Islands

Balearic Islands is a Spanish archipelago, located about two hundred kilometers from the Spanish east coast (lat. 38.55°N - 40.27°N; long. 1.05°E - 4.33°E). Altogether, the four major islands (Majorca, Menorca, Ibiza and Formentera) cover a surface of 4992 km², given hospitality to a population of 1,150,840 (data 2016). As many other islands in the Mediterranean Sea, the energy demand shows a peak during summer due to the relevance of the tourist arrivals. This region has a flourish economy with a Gross Domestic Product (GDP) per capita equal to 24,131 € (equivalent to 29,471 \$). Balearic Islands experience the Mediterranean climate, characterized by a temperature that ranges from 8.3°C (minimal in January) to 29.8°C (maximal in August), with higher rain levels in autumn and lower ones in summer [258].

About the energy sector, it is interesting to analyze the energy sources adopted to satisfy the energy demand in Spain (mainland) and in the Balearic Islands in 2017. Data are reported in Figure V.11 [259].

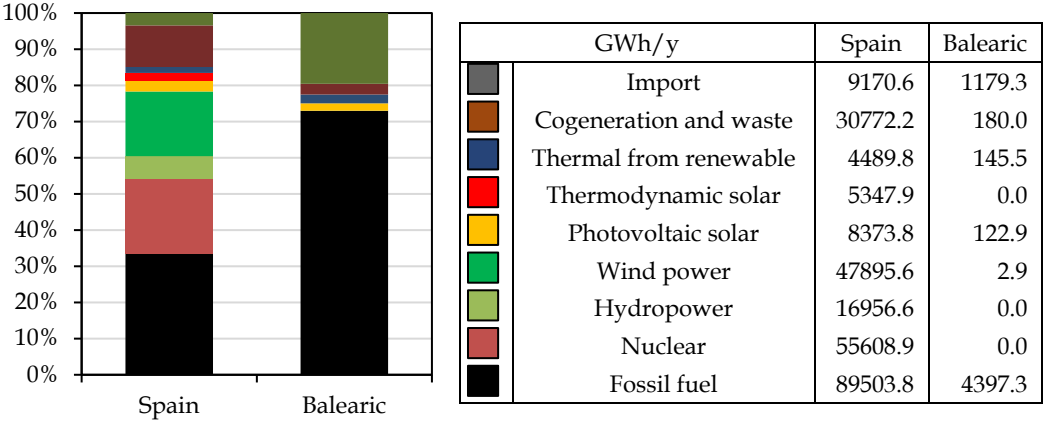


Figure V.11 Comparison of energy mix used for the electrical production in Balearic Islands and Spain during 2017.

In Spain, RES cover about 31% of the electrical energy demand whereas in Balearic Islands RES represent only 4.5%. Conversely, fossil fuels are used to cover 33.4% of the electrical demand in Spain and even 72.9% in Balearic Islands. In Spain, nuclear power is also used, meeting 20.8% of the electrical demand while this contribution is absent in the archipelago. Finally, it is interesting to underline the existence of the energy exchanges with other countries or regions. Indeed, Spain imported about 9170.6 GWh (3.42% of the electrical consumption) from other countries while the Balearic Islands about 1179.3 GWh (19.56% of the electrical consumption) from Spain.

Considering the energy demand in Balearic Islands, Figure V.12 reveals an almost stationary trend (about 6 TWh/y). Fossil fuel has a dominant role, as expected from the previous data about the energy shares, however the graph emphasizes a decreasing trend from 5682.5 GWh (97.5%) in 2006 to 4397.3 GWh (72.9%) in 2017.

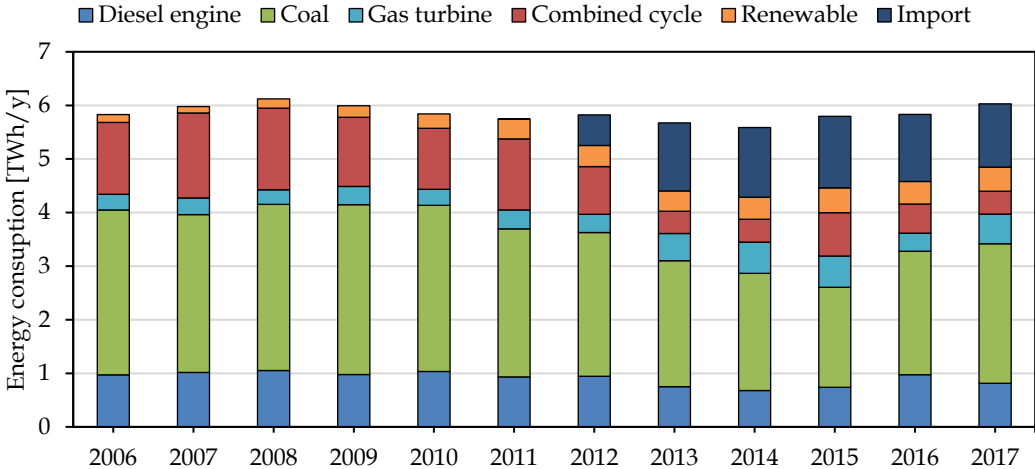


Figure V.12 Energy consumption by sources in Balearic Islands.

This is due to two reasons: first, the electrical link of Balearic Islands to Spain, second, the progressive installation of plants supplied by RES.

In detail, the connection between the archipelago and the mainland was realized in 2012, linking up Sagunto station (Valencia, Spain) to Santa Ponsa station (Majorca). This link operates in direct current (250 kV), covering a length of 237 km. Secondary links connect each other the Balearic Islands: a three-phases alternative current (132 kV) link joints Ciutadella station (Menorca) with Es Bessons station (Majorca); a double link (132 kV) connects Santa Rosa station (Majorca) to Torrent station (Ibiza); finally, a line (30 kV) links San Jorge station (Ibiza) to Formentera [259].

V.2.b Fiji

Fiji is a big archipelago, comprising over 330 islands and 500 islets, located between 15°S – 24°S and 174°W – 179°E, in the middle of the Pacific Ocean. The major islands are Vanua Levu and Viti Levu, representing 88% of the total land surface (about 18,900 km²). This archipelago has a volcanic origin, proved by geothermal activities in Vanua Levu and Taveuni.

A population of about 920,938 inhabitants lives in Fiji. This country is an example of SIDS, for geographical and economic reasons. Indeed, the GDP per capita is equal to 11,925.40 FJD (equivalent to 5,761.06 \$). About the climatic conditions, Fiji is affected by a tropical climate, thus the temperature range is limited between 21°C in July-August (winter) to 31°C in February (summer) [260]. Rainfalls are abundant, exceeding 2000 mm per year and mainly concentrated during summer. Despite this territory is not so windy, cyclones sometimes occur, especially in the period between January and February [260].

About the energy sector, Figure V.13 indicates a dominant role of hydropower and diesel supplied plants. Energy Fiji Limited (EFL) is the only national electricity producer. The energy demand is characterized by a growing trend, from 524 GWh in 2000 to 924 GWh in 2016, thus with a growth of +76.3% in 16 years.

As expected by the plenty rains, hydropower is the dominant energy source, satisfying the 53.65% of the total electrical demand in 2016.

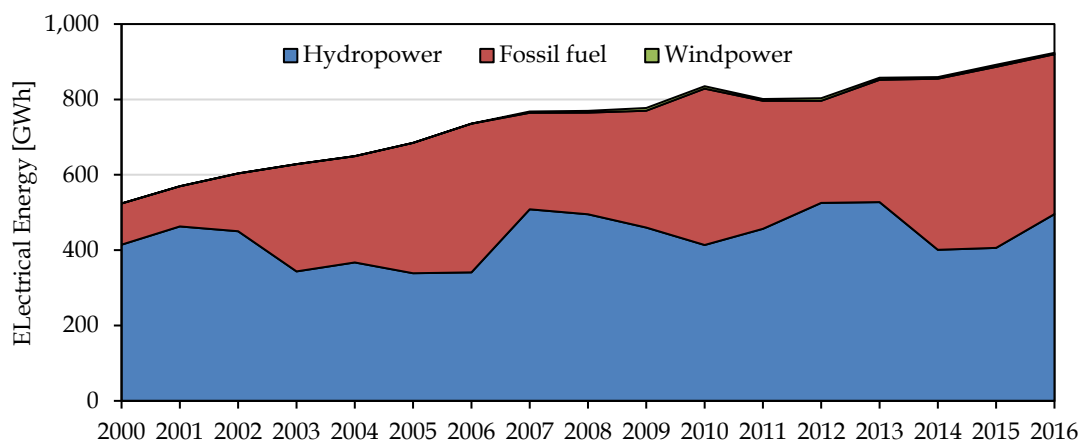


Figure V.13 Electricity production in Fiji by energy sources

In order to overcome the even increasing energy demand, fossil fuels power plants have been installed in the last years, thus the share of electricity production from hydropower is decreasing. Reporting some data, in 2002 the energy mix was composed by hydropower (74.6%) and diesel (25.4%) [261]. The total generation in 2016 was equal to 923.6 GWh, of which 424.5 GWh by diesel (46.0%) and 495.5 GWh by hydropower (53.7%). These statistics underline the rapid increase of the electricity demand and the slow growth of renewable installed capacity.

V.2.c Methodology

The sizing of the renewable energy mix in Balearic Islands and Fiji considers several aspects, as the potential increase of the local electrical demand, the presence of other renewable sources (hydropower in Fiji) and the existing electrical interconnections with other regions, like in Balearic Islands.

In this section, a mathematical model is introduced for the evaluation of the energy production from each renewable energy source (wind, solar and sea wave).

As regards wind and solar sources, commercial technologies are available, hence some technical details of the selected devices are reported. For the exploitation of sea wave, the point absorber proposed in the previous chapter is considered.

The sizing of the energy mix is based on the maximization of the Discounted Cash Flow (DCF), considering a fixed share of electricity production from RES as a goal. Some constraints are introduced, since each source is sized to produce at least the 5% of the entire electricity production from RES.

Before to define the DCF, the equations for the estimation of the electricity production from sea wave, solar and wind sources are presented.

The forecast of the annual electricity production from the sea wave energy source E_{sw} is equal to the sum of the monthly electricity production $E_{sw,i}$, according to the Eq. V.7, where the main difference with Eq. V.3 is related to the adoption of the average hydrodynamic η_{hy} and electrical $\eta_{e,w}$ efficiencies instead of an average energy efficiency of the device [251].

$$E_{sw} = \sum_{i=1}^n E_{sw,i} = \sum_{i=1}^n \varphi_{m,i} d_c n_c \eta_{hy} \eta_{e,w} t_i \quad V.7$$

In the case of deep water, the sea wave energy flux can be evaluated according Eq. III.30, introduced in the chapter about sea wave energy. The condition of deep water is verified if $d_w/L_w > 0.5$, where d_w is the water depth and L_w is the sea wavelength. These parameters are related by the "dispersion equation", that is well known in literature to describe the propagation of gravity wave [137], [262]. According to this relation, the water deep condition is practically verified, if the depth is greater of 40 m ($T_e = 7$ s), 80 m ($T_e = 10$ s) and 160 m ($T_e = 14$ s).

The following Eq. V.8 is used to evaluate the annual electricity production from solar source E_{pv} . In comparison with the previous Eq. V.2, the main difference is the adoption of the monthly-average daily solar radiation $H_{d,i}$, thus the number of days in the i -th month t_i is added [263]:

$$E_{pv} = \sum_{i=1}^n E_{pv,i} = \sum_{i=1}^n H_{d,i} S_{pv} \eta_{e,pv} t_i \quad V.8$$

The exploitation of solar source can be realized by using commercial silicon photovoltaic panels. In Table V.7, the main characteristics of the photovoltaic panel are reported.

Table V.7 Main parameters of photovoltaic panels [264]

Parameter	Value
Model	PV-MLU255HC
Number of cells per panel	120
Maximum power rating	255 W _p
Open circuit voltage	37.8 V
Short circuit current	8.89 A
Module efficiency	15.4%
Dimensions	1625x1019x46 mm
Weight	20 kg

The utilization of well-developed photovoltaic panels has been considered to minimize the cost for the realization of the renewable energy mix. The installation of several small plants on the roofs of existing buildings can solve the problem of land consumption [265].

The annual electricity production from wind power E_w is determined by Eq. IV.9. The Weibull distribution is defined by two parameters: α_j (shape parameter) and β_j (scale parameter) [266]. Eq. V.9 assumes the adoption of different Weibull distributions according to the wind direction. For this reason, the occurrence o_j is introduced representing the time ratio when wind flows from a specific direction. The estimation requires the knowledge of the turbine power output $\psi(v)$, function of wind speed v [267].

$$E_w = 8760 \sum_{j=1}^m o_j \int \frac{\alpha_j}{\beta_j} \left(\frac{v}{\beta_j}\right)^{\alpha_j-1} \exp\left[-\left(\frac{v}{\beta_j}\right)^{\alpha_j}\right] \psi(v) dv \quad V.9$$

It is also common the adoption of a single Weibull distribution to model the availability of the wind source [268].

An alternative solution is the adoption of wind classes, indicating the number of hours $h_{i,j}$ when a specific wind class v_j is measured [269], [270]. In this case, Eq. V.10 can be applied to evaluate the annual electricity production:

$$E_w = \sum_{i=1}^n E_{w,i} = \sum_{i=1}^n \sum_{j=1}^m h_{i,j} \psi(v_j) \quad V.10$$

For the exploitation of wind source, the installation of commercial horizontal axis wind turbines is considered. Table V.8 shows the main features of the selected wind turbines.

Table V.8 Main parameters of the chosen wind turbines [271], [272]

Model	MM100	6.3M152
Nominal power	2,050 kW	6,330 kW
Cut-in wind speed	3.0 m/s	3.5 m/s
Nominal wind speed	11.0 m/s	11.5 m/s
Cut-out wind speed	22 m/s	30 m/s
Hub height	80 m	80 m
Rotor diameter	100 m	152 m
Rotor area	7,854 m ²	18,146 m ²

Several aspects should be considered to select the wind turbines, such as the local energy demand, the average wind speed and the extreme weather conditions. A wind turbine, with a rated power of 2 MW, has been chosen for Fiji. However, in Balearic Islands the local energy demand is high and the extreme weather conditions are limited, therefore a bigger wind turbine (6.3 MW) is chosen to reduce the total number of devices. The power output function of both wind turbines is reported in Figure V.14.

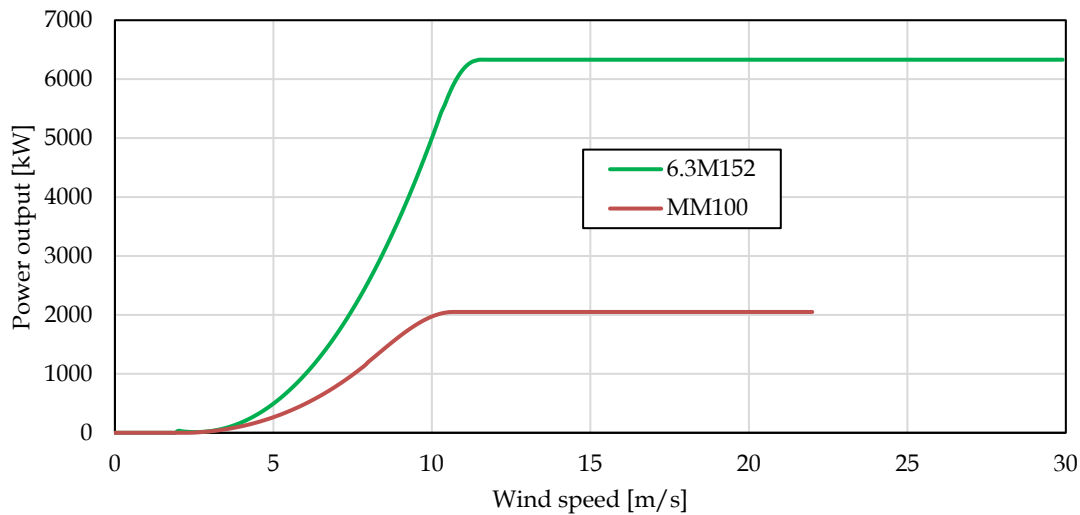


Figure V.14 Power output of wind turbine as function of wind speed.

The equations above introduced are used to evaluate the size of RES power plants to meet the local energy demand. The sizing process considers the maximization of the Discounted Cash Flow (DCF) after 20 years, as target. In general, the DCF at n-th year is given by Eq. V.11:

$$DCF(n) = -I_0 - [A_{O\&M} - (E_{sw} + E_{pv} + E_w)c_e] \sum_{i=1}^n \frac{1}{(1 + \tau)^i}$$

V.11

$$I_0 = P_{sw}c_{0,sw} + P_{pv}c_{0,pv} + P_w c_{0,w}$$

$$A_{O\&M} = P_{sw}c_{O\&M,sw} + P_{pv}c_{O\&M,pv} + P_w c_{O\&M,w}$$

Unitary costs to install one kilowatt of sea wave energy converters ($c_{0,sw}$), photovoltaic panels ($c_{0,pv}$) and wind turbines ($c_{0,w}$) are introduced. Thence, the initial investment I_0 is determined by multiplying the unitary costs for each total nominal power (P_{sw}, P_{pv}, P_w). The same approach is adopted to evaluate the annual operative and maintenance costs $A_{O\&M}$, by the introduction of the corresponding costs for each RES ($c_{O\&M,sw}, c_{O\&M,pv}, c_{O\&M,w}$). The annual income is represented by the avoided fossil fuel consumption, which is replaced by the RES production ($E_{sw} + E_{pv} + E_w$). A unitary cost c_e for the electricity production from fossil fuels is considered. The annual operative and maintenance costs of the renewable energy mix and the avoided expenditure for the electricity production from fossil fuel are normalized by the annual discount rate τ .

To evaluate the economic benefits of this project, the discounted payback time t_b (representing the time to obtain a DCF equal to zero) is also calculated by solving the Eq. V.12:

$$DCF(t_b) = 0$$

V.12

After the sizing of the renewable energy mix, the environmental benefits are finally evaluated. As the potential electricity production from RES is equal to the avoided electricity production from fossil fuels, the annual avoided CO₂ emission Γ_{CO_2} is determined by Eq. V.13.

$$\Gamma_{CO_2} = \gamma_{CO_2}(E_{sw} + E_{pv} + E_w)$$

V.13

The equation introduces the specific CO₂ emission factor γ_{CO_2} , representing the amount of CO₂ emitted to produce one kilowatt-hour of electricity, by using the current energy mix. The specific emission factor is normally available in literature for different technologies. Big energy producers indicate the average value of this parameter in official reports on energy statistics [259].

V.2.d Results

The mathematical model was applied to the two case studies. In the following sections the results are reported. Each section shows firstly the available RES, reporting the climatic data on the solar radiation, the wind speed (modelled by Weibull coefficients and wind speed classes) and the sea wave power flux. Since wind data are available in

two different ways, a comparison of the estimated electricity production from wind is reported.

Balearic Islands

The evaluation of the potential electricity production from RES requires the climatic data as input, that can be collected by using specific GIS tools [269], [270], [273], [274]. In detail, Figure V.15 shows the location of the reference points which are used in this analysis. The points are divided in three categories, representing respectively solar (red), sea wave (green) and wind (yellow) sources. The geographical positions and the main parameters, modelling the energy potential of RES, are below reported.

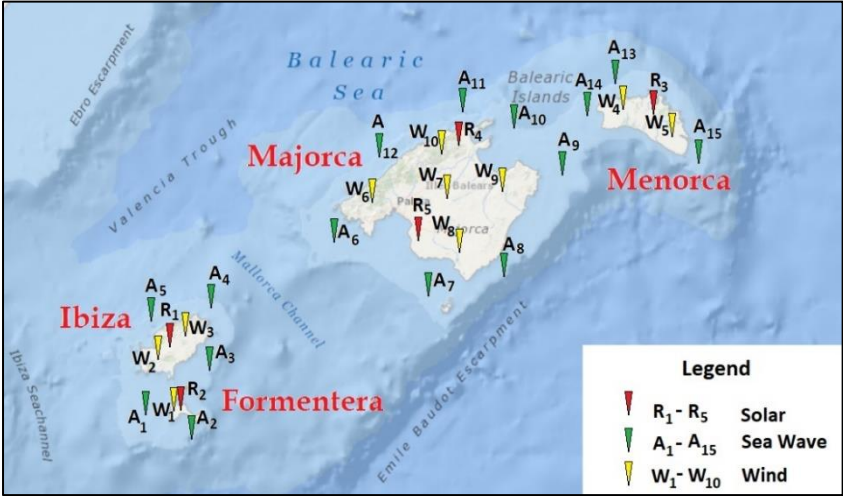


Figure V.15 Reference points in Balearic Islands for the evaluation of renewable energy potential

Table V.9 reports the values of the monthly-average daily solar radiation for each reference point. Each island is evaluated introducing one reference point, except Majorca that has two reference points, as its greater extension.

Table V.9 Data of monthly-average daily solar radiation in Balearic Islands

	Monthly-average daily solar radiation H_d [kWh/d]											
Signle	Jan	Feb	Mar	Apr	May	Jun	Jul	Aug	Sep	Oct	Nov	Dec
R1	2.6	3.7	4.6	6.1	7.6	7.8	7.9	6.6	5.2	3.7	2.8	2.2
R2	2.6	3.8	4.8	6.2	7.6	8.0	7.9	6.8	5.3	3.9	2.9	2.4
R3	2.3	3.2	4.7	5.4	7.6	7.5	7.8	6.6	5.1	3.4	2.6	2.1
R4	2.3	3.3	4.3	5.7	7.5	7.4	7.8	6.5	4.9	3.3	2.6	2.0
R5	2.5	3.5	4.6	6.0	7.5	7.5	7.9	6.7	5.1	3.6	2.7	2.2

Based on the mathematical model, the evaluation of wind potential can be realized by using the Weibull distribution. Table V.10 reports the values of the parameters (α and β) of Weibull distribution by considering 12 different directions from where wind flows. The occurrence (o) is also reported. This parameter represents the time ratio when wind flows from a specific direction. A simple evaluation can be also performed by using the equivalent Weibull distribution, neglecting the dependence from the wind direction. This information is reported in the last row in Table V.10.

Table V.10 Data of wind source in Balearic Islands

<i>Dir.</i>	W1			W2			W3			W4			W5		
	<i>o</i>	β	α	<i>o</i>	β	α	<i>o</i>	β	α	<i>o</i>	β	α	<i>o</i>	β	α
0°	0.06	7.25	2.02	0.07	7.65	2.06	0.07	7.47	2.10	0.14	10.6	1.88	0.17	10.1	1.94
30°	0.09	6.32	1.98	0.08	6.66	1.99	0.09	6.21	1.75	0.15	8.10	1.98	0.13	7.37	2.02
60°	0.17	6.42	2.37	0.14	6.21	2.23	0.14	5.85	2.08	0.08	6.40	2.15	0.08	5.92	1.99
90°	0.15	6.05	1.98	0.14	6.03	1.91	0.13	5.85	1.85	0.07	7.00	1.62	0.08	6.79	1.68
120°	0.08	4.56	1.90	0.09	4.86	2.21	0.08	4.41	1.82	0.07	7.00	1.80	0.07	6.40	1.83
150°	0.06	4.09	1.70	0.07	4.41	2.02	0.07	4.50	2.06	0.07	6.30	1.87	0.06	5.63	1.76
180°	0.05	4.19	1.65	0.06	4.77	1.97	0.06	4.95	2.11	0.07	5.90	1.90	0.05	5.34	1.76
210°	0.08	5.77	1.84	0.09	5.76	1.70	0.09	6.48	2.08	0.08	7.00	1.68	0.08	6.98	1.80
240°	0.10	7.35	1.87	0.09	7.02	1.72	0.09	7.83	1.94	0.07	6.60	1.62	0.09	7.47	2.11
270°	0.06	6.98	1.87	0.06	7.20	1.87	0.07	7.74	2.04	0.06	6.70	1.76	0.06	6.89	1.86
300°	0.06	6.98	2.07	0.06	7.02	2.21	0.05	7.02	2.12	0.07	6.60	1.66	0.06	6.89	1.88
330°	0.04	6.79	1.71	0.05	6.93	1.66	0.05	7.65	1.71	0.06	5.80	1.23	0.07	7.18	1.43
Equ.		6.14	1.84		6.12	1.81		6.21	1.79		7.30	1.63		7.28	1.70

<i>Dir.</i>	W6			W7			W8			W9			W10		
	<i>o</i>	β	α	<i>o</i>	β	α	<i>o</i>	β	α	<i>o</i>	β	α	<i>o</i>	β	α
0°	0.06	6.30	1.71	0.04	7.13	1.60	0.04	6.14	1.54	0.09	8.10	1.62	0.06	7.35	1.54
30°	0.08	7.38	2.00	0.14	7.70	1.94	0.11	7.44	1.87	0.13	8.40	2.03	0.10	8.33	1.99
60°	0.10	6.66	2.04	0.14	7.32	2.21	0.17	7.07	2.27	0.10	6.50	2.30	0.11	6.76	2.22
90°	0.11	6.30	2.00	0.12	5.32	1.48	0.15	6.32	1.73	0.10	6.20	1.54	0.10	6.08	1.62
120°	0.14	6.03	1.62	0.05	5.23	1.90	0.07	4.65	1.67	0.08	5.90	1.67	0.07	5.98	1.65
150°	0.08	4.68	1.95	0.06	3.99	1.48	0.06	4.65	2.25	0.07	5.50	1.94	0.05	5.29	1.46
180°	0.07	4.77	1.90	0.07	4.56	1.86	0.05	4.37	1.86	0.06	5.50	1.93	0.07	6.08	1.67
210°	0.07	5.58	1.63	0.08	5.70	1.72	0.07	5.49	1.76	0.05	6.60	1.99	0.09	7.35	1.51
240°	0.08	6.30	1.64	0.13	6.84	1.78	0.10	7.25	2.00	0.10	8.50	2.14	0.09	9.51	1.95
270°	0.06	5.58	1.67	0.06	6.08	2.15	0.08	6.32	2.07	0.08	6.80	2.04	0.10	8.04	2.14
300°	0.07	6.39	1.59	0.07	6.56	1.68	0.06	6.88	2.14	0.08	6.80	1.56	0.10	8.04	1.72
330°	0.08	6.93	1.63	0.04	5.70	1.36	0.06	6.51	1.74	0.06	5.70	1.40	0.05	5.59	1.30
Equ.		6.12	1.70		6.18	1.69		6.32	1.82		6.90	1.73		7.15	1.67

The wind potential evaluation can be alternatively performed by considering the wind speed classes, reported graphically in Figure V.16. This GIS tool shows a lower geographical resolution, thence the ten reference points used in Table 4 are replaced by only three different trends, reported in Figure V.16.

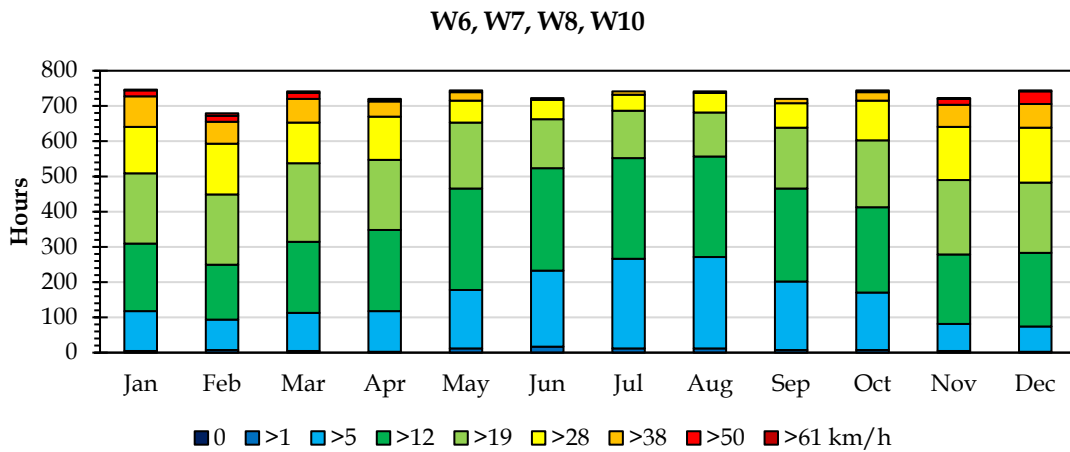
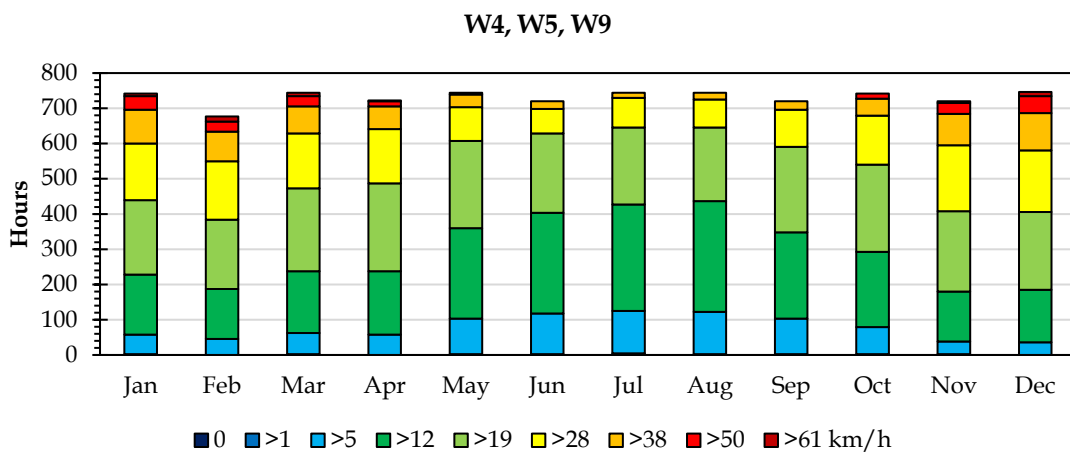
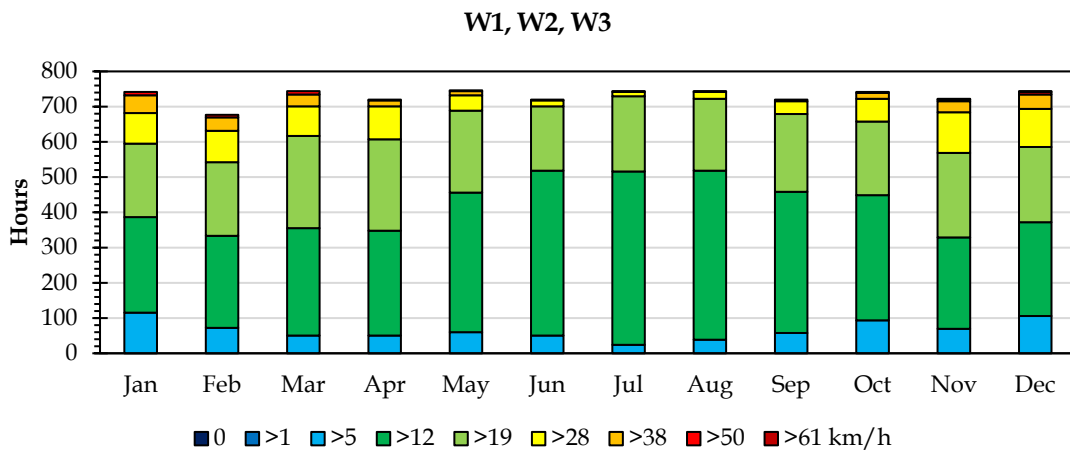


Figure V.16 Wind speed classes in the reference points in Balearic Islands

A preliminary analysis was performed to verify the consistency between the two datasets used to evaluate the wind energy source. In detail, the hourly data behind the second dataset were analyzed, evaluating the Probability Distribution Function (PDF) and the corresponding Weibull approximation.

The determination of Weibull coefficients was performed considering different approaches: the median and quartiles method, moments method, energy method, maximum likelihood method and least square fit method [275], [276].

Table V.11 Estimation of the Weibull distribution coefficients and fit quality in W1 (Balearic Islands)

Method	β	α	COD	RMSE	MAE
Median and quartiles	6.673	1.976	0.9807	0.4290	0.3752
Moments	6.244	1.875	0.9969	0.1720	0.1465
Energy	6.241	1.848	0.9974	0.1575	0.1398
Maximum likelihood	6.256	1.884	0.9969	0.1723	0.1461
Least square fit	6.402	1.957	0.9939	0.2413	0.2023

The quality of fitting was investigated, introducing the Coefficient of Determination (COD), the Root Mean Square Error (RMSE), the Mean Absolute Error (MAE) [277]–[279]. Considering the reference point W1 of Balearic Islands, the results of Weibull distribution coefficients are reported in Table V.11. In case a good fitting, COD should be close to 1 while RMSE and MAE to 0.

Figure V.17a shows the comparison of the PDF obtained from the hourly data [270], the best Weibull approximation and the corresponding Weibull distribution proposed by the other GIS tool [280]. Figure V.17b reports the evaluation of the corresponding Cumulative Distribution Function (CDF).

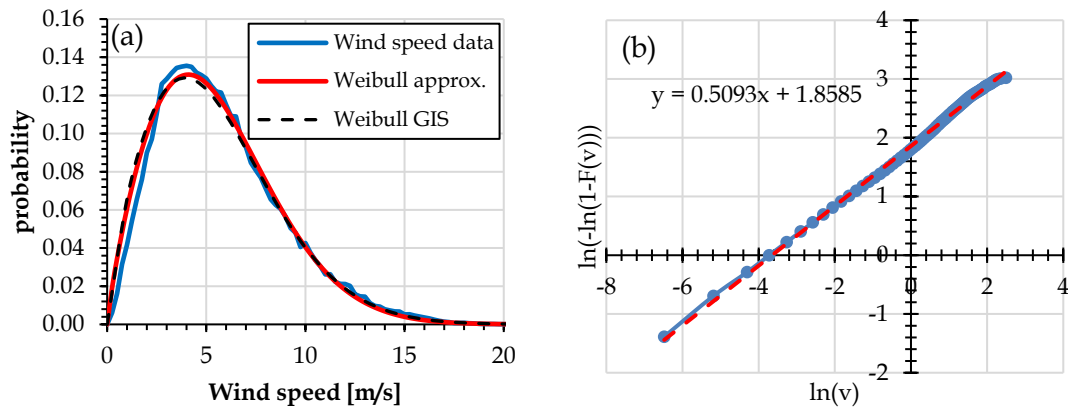


Figure V.17 Comparison of Weibull distribution based on two different data set in the reference point W1.

Table V.12 reports the annual average values of the wave energy flux and the average values measured in each quarter.

Table V.12 Data of Sea Wave Energy Flux in Balearic Islands

Stgle	A1	A2	A3	A4	A5	A6	A7	A8	A9	A10	A11	A12	A13	A14	A15
Average	2.48	2.95	2.22	1.97	3.82	2.17	2.72	2.68	5.44	6.86	6.43	5.00	9.01	6.63	9.07
Jan-Mar	3.77	4.02	2.72	2.38	5.58	3.51	4.22	3.87	7.65	9.64	9.29	7.31	13.1	9.57	13.1
Apr-Jun	1.76	2.43	1.75	1.59	2.19	1.36	1.92	2.10	3.50	3.85	3.20	2.44	4.88	3.74	5.56
Jul-Sep	0.81	1.29	1.16	1.06	1.22	0.61	0.79	0.92	2.27	2.88	2.38	1.79	3.75	2.78	3.71
Oct-Dec	3.59	4.09	3.25	2.84	6.29	3.23	3.97	3.85	8.35	11.1	10.9	8.48	14.3	10.5	13.9

From the analysis of the electrical energy sector in the last five years (2013-2017), it was estimated an annual electricity demand of 6738.7 GWh/y for 2025. This request is distributed in each month by considering the annual trends of the last five years.

By using the climatic data reported above, the energy production from the renewable energy mix was simulated. About the importation of electricity from mainland, an average trend of the last five years was considered.

Power plants are sized to cover about 46% of the estimated energy demand for 2025. Figure III.18 shows the estimated energy production from RES, and the monthly electricity demand for each of the major Balearic Islands. The wind energy production is evaluated, by using both methods (Weibull distribution and wind speed classes).

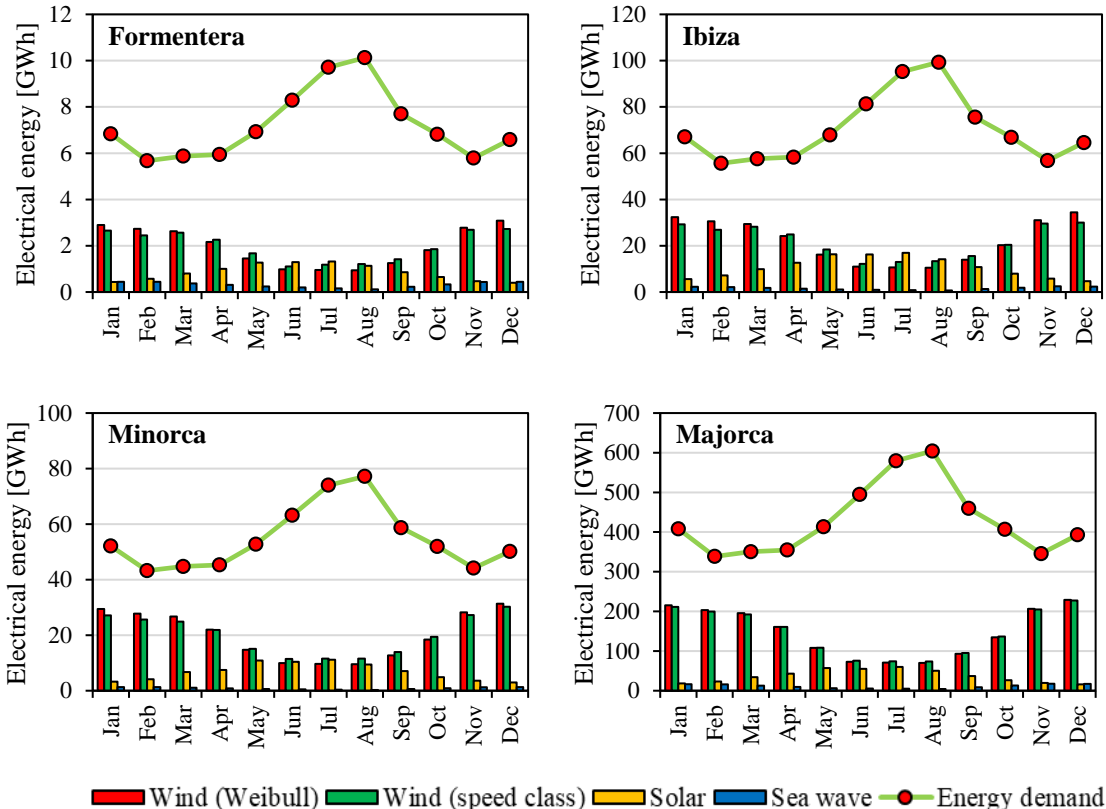


Figure V.18 Comparison of monthly electricity demand and potential energy production from renewable energy sources in Balearic Islands.

As shown in the trends above reported, the energy demand reveals a peak during summer, due to tourism. Wind and sea wave sources are characterized by a greater energy production during winter. Therefore, the installable power capacity from these sources is limited. Solar energy source produces more electricity in summer; however, this source is also limited because photovoltaic panels should be installed only on residential roofs, in order to minimize the visual impacts and not occupy other soil.

The comparison between the wind estimation based on the Weibull distribution and on wind speed classes reveals comparable results (2289 GWh/y using Weibull distribution and 2287 GWh/y using the wind speed classes). It is important to underline

that the tool based on wind speed classes has a lower resolution, therefore local variations can be found.

The share of renewable sources is selected by considering the balancing problem of electricity demand and production. This aspect could be managed by the existing local power plants and the electrical connection from mainland. Indeed, as shown in Figure V.19, fossil fuels and importation from mainland are used to balance the electrical grid. Two different shares of renewable are reported: the first represents the ratio between the electricity production by RES and the total electricity production in situ; the latter share is defined as the ratio of RES production and the total local consumption. In this way, the effect of importation from mainland is emphasized.

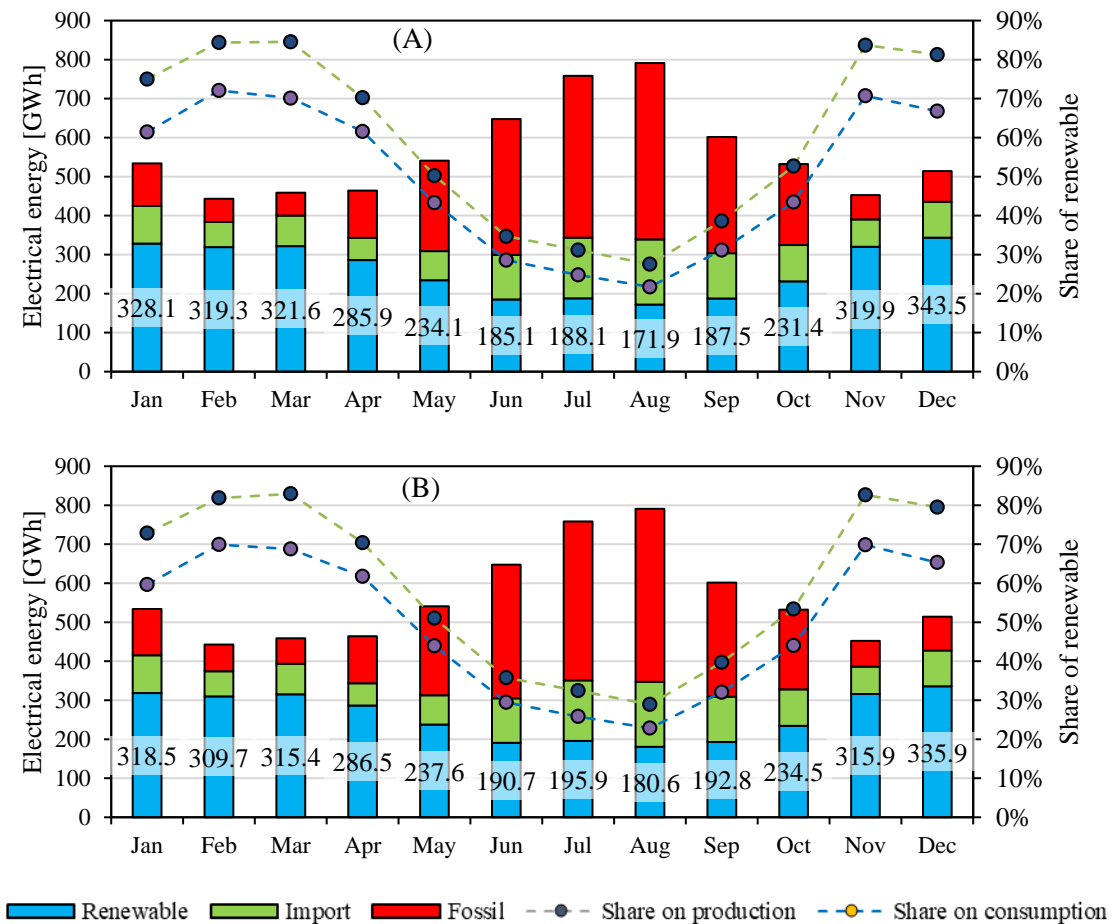


Figure V.19 Electricity production by sources and share of RES in Balearic Islands.
(A) Wind evaluation based on Weibull distribution. (B) Wind evaluation based on wind speed classes

The proposed RES mix is able to replace until the 70% of electricity production from fossil fuels in February and November; the minimum share is achievable in August (22%). As shown in Figure V.19, results are practically the same if the Weibull distribution or the wind speed classes methods are adopted. The details of the renewable energy mix are reported in Table V.13.

About wind source, the number of wind farms, the number of wind turbines per each farm, the required power and the annual potential electricity production are

reported. The same parameters are stated for sea wave. About solar source, the total required PVP surface, the total installed power and the estimated annual electricity production are provided.

Table V.13 Details of the renewable energy mix for Balearic Islands.

	Parameters	Units	Formen.	Ibiza	Minorca	Majorca
<i>Wind</i>	N. wind farm	[-]	1	2	2	5
	Devices per farm	[-]	2	11	7	25
	Total installed power	[MW]	12.6	138.6	88.2	787.5
	Energy production (Weibull)	[GWh/y]	23.66	264.61	240.55	1760.51
	Energy production (wind classes)	[GWh/y]	23.79	261.67	240.07	1761.23
<i>Sea Wave</i>	N. sea wave farm	[-]	2	3	3	7
	Devices per farm	[-]	10	35	20	40
	Total installed power	[MW]	1.6	8.4	4.8	22.4
	Energy production	[GWh/y]	3.7	19.2	10.4	132.6
<i>Solar</i>	Total area covered by PVP	[10 ³ m ²]	35	450	300	1600
	Total installed power	[MW]	5.39	69.3	46.2	246.4
	Energy production	[GWh/y]	10.2	128.3	82.1	440.7

From an environmental point of view, the renewable energy mix here proposed is able to avoid the annual emission of 2.26 million tons of CO₂, considering the emission factor equal to 0.726 t CO₂/MWh [259].

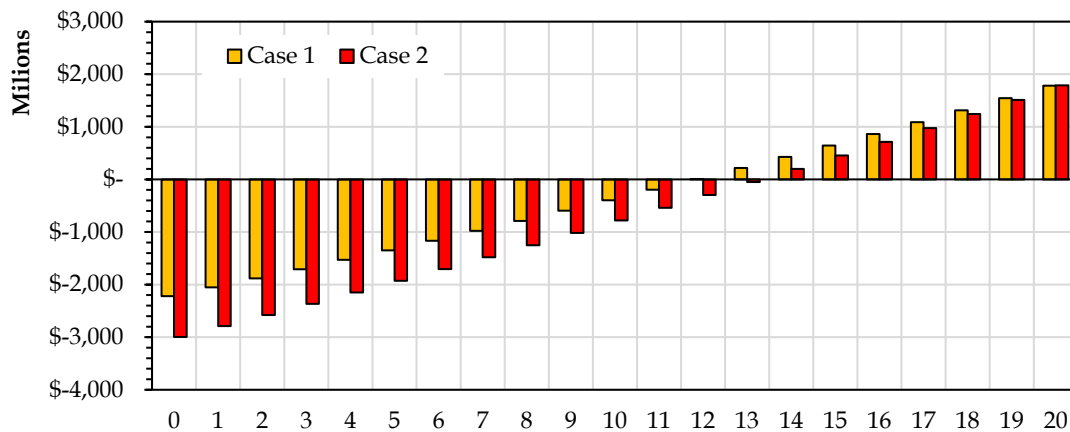


Figure V.20. Discounted cash flow for the realization of the proposed RES mix in Balearic Islands. Case 1: Investment based on world average prices. Case 2: Investment based on European average prices

As regards the economic aspect, the discounted cash flow and the breakeven time are evaluated. Two scenarios are shown in Figure V.20. The first one considers international average unitary prices for the installation of renewable energy technologies, the latter applies more specific prices for the area under investigation [17].

According to results, the initial investment ranges between 2220 to 2995 million of US dollars, with a DCF after 20 years fluctuating between 1781 to 1789 million of US dollars. The breakeven time is between 11.96 and 13.31 years.

Fiji

The same approach was applied to Fiji, evaluating the renewable energy potential from sea wave, wind and solar. All reference points are shown in Figure V.21.

The red markers represent the reference points that are used to evaluate the solar radiation, the green ones for the sea wave energy sources, the yellow ones for the wind source.

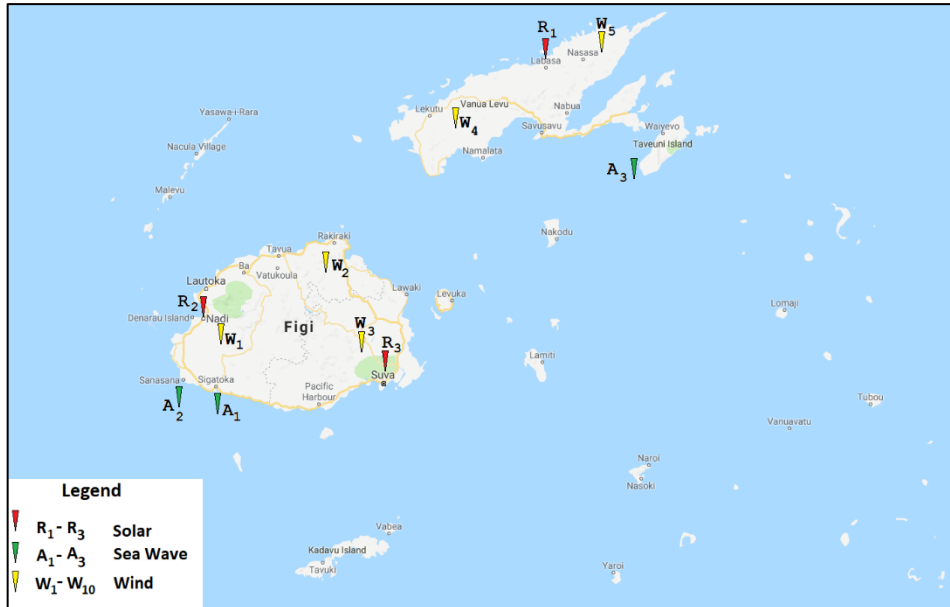


Figure V.21. Reference points in Fiji for the evaluation of renewable energy potential

Thanks to WACOP Project, financed by European Union, several reports have been published, describing the sea wave climate around the islands and analyzing also the incidence of extreme weather conditions [281]. Data about wave energy potential are reported in Table V.14.

Table V.14 Data of Sea Wave Energy Flux in Fiji

Single		Jan	Feb	Mar	Apr	May	Jun	Jul	Aug	Sep	Oct	Nov	Dec
A1	H_s	1.09	1.15	1.31	1.40	1.54	1.55	1.63	1.58	1.48	1.43	1.29	1.16
	T_e	12.94	13.39	13.84	14.20	14.17	13.94	13.67	14.02	14.26	14.14	13.46	12.90
	φ	7.55	8.62	11.69	13.56	16.45	16.48	17.73	17.17	15.29	14.23	10.90	8.45
A2	H_s	1.20	1.28	1.45	1.51	1.63	1.65	1.71	1.65	1.55	1.49	1.34	1.23
	T_e	12.75	13.18	13.76	14.12	14.12	13.95	13.67	14.13	14.29	14.16	13.43	12.86
	φ	9.00	10.63	14.25	15.75	18.36	18.55	19.63	18.90	16.84	15.42	11.88	9.51
A3	H_s	1.05	1.06	1.15	1.29	1.41	1.49	1.55	1.49	1.41	1.32	1.17	1.12
	T_e	11.13	11.96	12.59	12.64	12.63	12.43	11.87	12.05	12.03	12.16	11.76	10.95
	φ	6.05	6.61	8.15	10.28	12.35	13.54	13.99	13.12	11.76	10.46	7.87	6.76

Table V.15 shows the monthly-average daily solar radiation in three reference points in Fiji [282].

Table V.15 Data of the monthly-average daily solar radiation in Fiji

Stgle	Jan	Feb	Mar	Apr	May	Jun	Jul	Aug	Sep	Oct	Nov	Dec
R1	5.70	5.44	5.32	4.95	4.79	4.62	4.78	4.97	5.24	5.67	5.88	6.00
R2	6.56	6.05	5.80	5.45	5.15	5.00	5.25	5.54	5.86	6.30	6.54	6.83
R3	6.27	5.88	5.55	4.99	4.61	4.38	4.51	4.88	5.21	5.83	6.10	6.41

Table V.16 shows the occurrence (o) of wind direction and Weibull parameters (α and β), modelling the availability of this renewable source [280].

Table V.16 Data of wind source in Fiji

Name	W1			W2			W3			W4			W5		
	Dir.	o	β	α	o	β	α	o	β	α	o	β	α	o	β
0°	0.07	7.04	2.69	0.08	6.95	2.88	0.07	6.16	2.79	0.10	7.00	2.77	0.11	6.76	2.80
30°	0.04	5.52	2.71	0.04	5.53	2.90	0.04	4.90	2.82	0.04	5.25	2.68	0.05	5.24	2.71
60°	0.03	4.96	2.38	0.04	4.90	2.57	0.04	4.34	2.48	0.04	4.41	6.30	0.04	4.69	2.58
90°	0.03	5.20	2.46	0.03	5.06	2.59	0.03	4.55	2.54	0.04	4.41	2.35	0.04	4.42	2.39
120°	0.04	5.52	2.77	0.04	5.53	2.99	0.04	4.83	2.87	0.04	4.55	2.91	0.03	4.28	2.73
150°	0.09	6.88	2.57	0.09	6.72	2.75	0.09	6.02	2.67	0.07	5.60	2.46	0.07	5.59	2.54
180°	0.08	5.04	2.50	0.08	5.06	2.70	0.08	4.41	2.60	0.10	5.11	2.39	0.10	5.31	2.51
210°	0.05	3.76	2.59	0.05	3.71	2.77	0.05	3.29	2.69	0.06	3.43	2.47	0.06	3.45	2.60
240°	0.03	3.68	2.40	0.04	3.63	2.62	0.04	3.22	2.49	0.03	3.01	2.29	0.04	3.11	2.42
270°	0.07	6.08	2.54	0.07	6.16	2.77	0.07	5.32	2.64	0.05	4.55	2.52	0.05	4.55	2.60
300°	0.22	8.64	2.49	0.22	8.45	2.66	0.22	7.56	2.58	0.18	6.37	2.30	0.15	6.62	2.41
330°	0.23	9.44	2.69	0.23	9.40	2.89	0.23	8.33	2.79	0.26	8.54	2.64	0.26	8.35	2.71
Equ.	-	7.12	2.32	-	7.03	2.51	-	6.23	2.42	-	6.16	2.27	-	6.07	2.31

Like the case study of Balearic Islands, the wind speed classes are also considered in order to make a comparison between the two different approaches for the evaluation of the wind energy potential. The GIS tool provides a single set of values (shown in Figure V.22) to describe the wind availability in Vanua Levu, instead of the two separate reference points introduced in Table V.16. About Viti Levu, the same number of reference points are considered in both approaches (see Figure V.23).

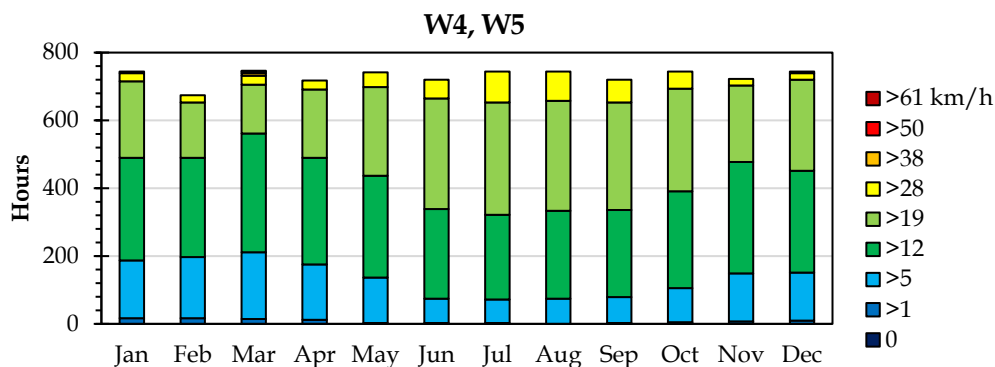


Figure V.22 Wind speed classes in the reference points in Vanua Levu (Fiji)

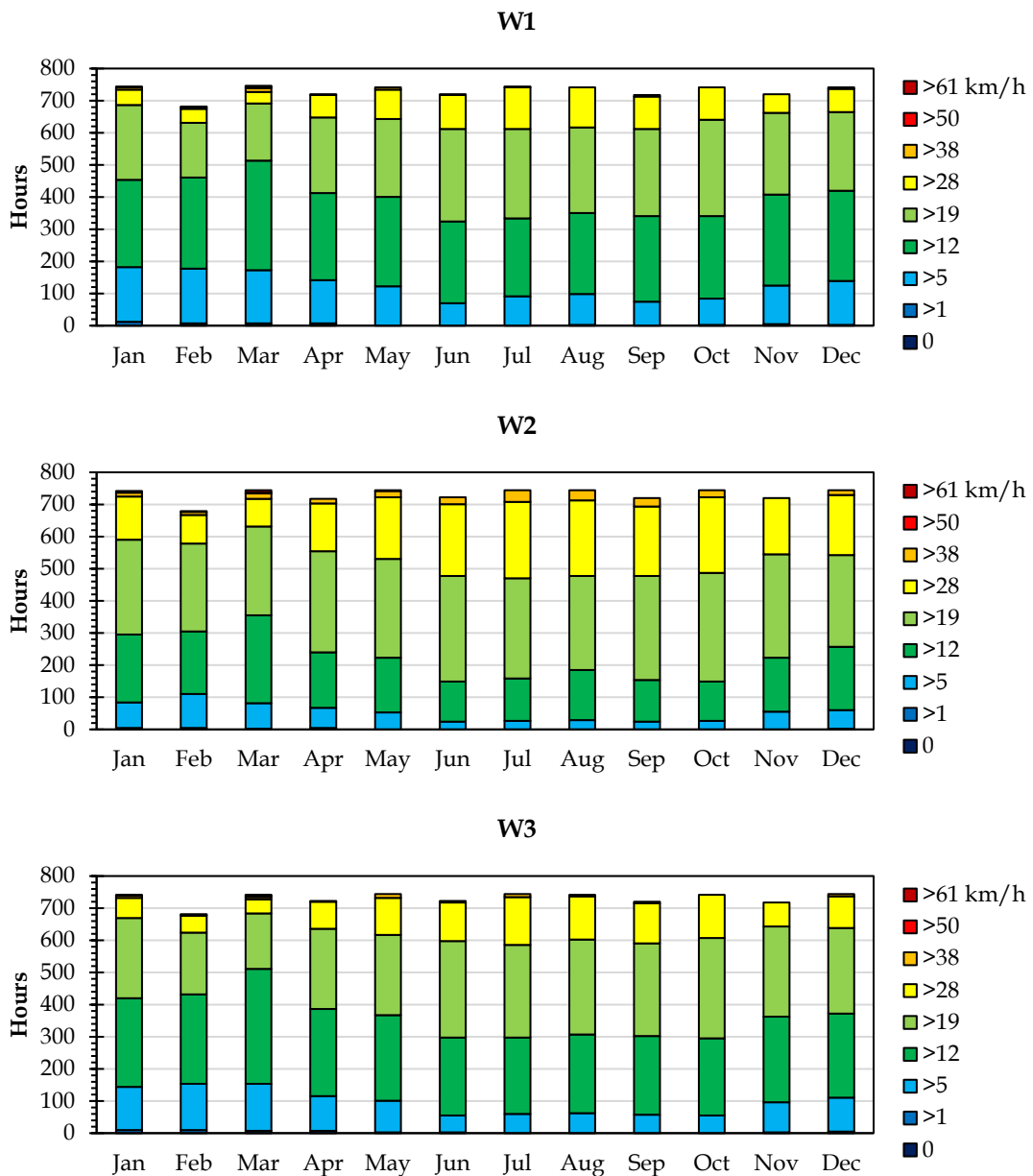


Figure V.23 Wind speed classes in the reference points in Viti Levu (Fiji)

The two datasets for the wind energy potential are preliminarily compared, using the same approach introduced in the case study of Balearic Islands.

Table V.17 shows the estimation of the Weibull distribution coefficients, by using five different approaches in the reference point W1 in Fiji [275], [276].

Table V.17. Estimation of the Weibull distribution coefficients and fit quality in W1 (Fiji)

Method	β	α	COD	RMSE	MAE
Median and quartiles	7.084	2.672	0.9785	0.4036	0.2502
Moments	6.967	2.397	0.9888	0.2914	0.1520
Energy	6.970	2.335	0.9892	0.2864	0.1826
Maximum likelihood	6.961	2.359	0.9893	0.2843	0.1716
Least square fit	7.805	2.012	0.8211	1.1636	0.8571

Figure V.24a shows the comparison of the PDF obtained from the hourly data [269], the best Weibull approximation and the corresponding Weibull distribution proposed by the other GIS tool [280]. Figure V.24b reports the evaluation of the corresponding Cumulative Distribution Function (CDF).

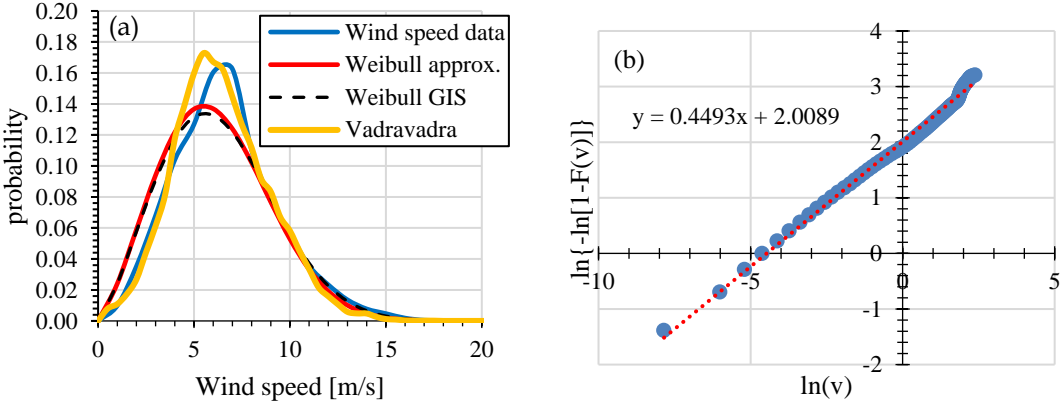


Figure V.24 Comparison of Weibull distribution based on two different data set in the reference point W1

In addition, Figure V.24a reports also the wind speed distribution, obtained from a measuring campaign, realized in the Vadravadra village, located in an intermediate position between the reference points W1 and W2.

The coefficients of the best Weibull approximation are close the others given by the other GIS tool. Despite this, the comparison of the PDF obtained from the raw wind speed data with the corresponding Weibull approximation reveals that the Weibull distribution does not model properly the wind speed availability, especially in case of low speed values [283]. Similar results were obtained in the other references points. It is important to underline that errors in the low speed region do not affect the evaluation of the energy potential, since in this area the energy production from wind turbines is very limited.

Since the goal of this case study is the suggestion of a simplified approach to evaluate the potential energy production from three different RES, both datasets were used in order to perform a comparison.

It was estimated an annual electricity demand for 2025, equal to 1170.8 GWh/y (+26.75% respect the energy consumption in 2016) by considering the growing trend in the last five years (2012-2016). The existing hydropower and fossil fuel plants could be successfully used to balance the dynamic trends of energy demand and RES production.

The same technologies are considered for the exploitation of solar and sea wave energy sources. A wind turbine having a rated power of 2 MW is adopted in this case study.

Power plants are sized to cover about 89% of the estimated energy demand for 2025. Figure V.25 shows the estimated energy production from RES, and the monthly electricity demand for Viti Levu and Vanua Levu. The wind energy production is evaluated, using both methods (Weibull distribution and wind speed classes).

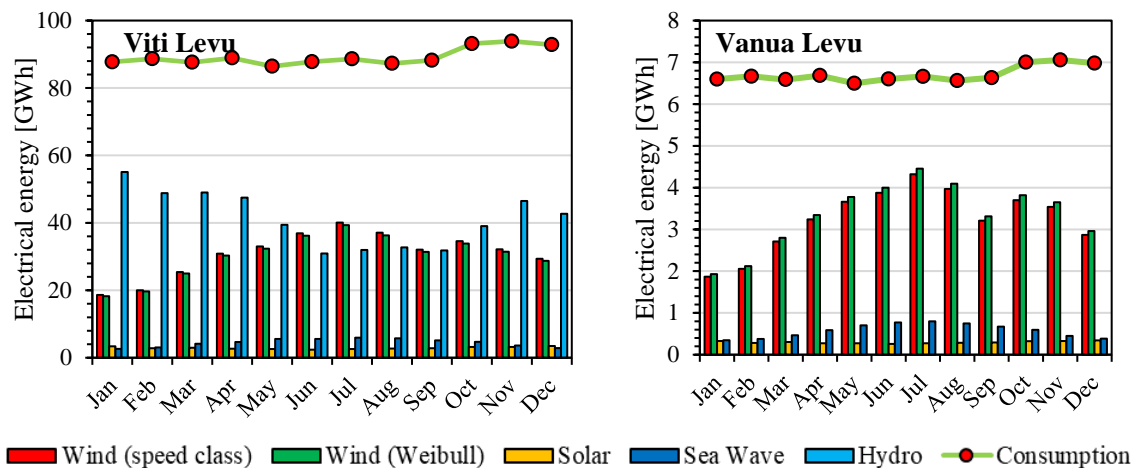


Figure V.25 Comparison of monthly electricity demand and potential energy production from renewable energy sources in Fiji using the wind speed classes approach.

As shown in the reported trends, the energy demand is practically stable during the year, while the energy production from wind and sea wave presents a peak in the period between May and October (winter). The energy demand is mainly concentrated in Viti Levu, because most of population lives in this island. In this energy scenario, hydropower is adopted only in Viti Levu, considering the utilization of the existing power plants.

Table V.18 Details of the renewable energy mix for Fiji Islands.

	Parameters	Units	Viti Levu	Vanua Levu
<i>Wind</i>	N. wind farm	[-]	3	2
	Devices per farm	[-]	20	4
	Total installed power	[MW]	139.4	16.4
	Energy production (Weibull)	[GWh/y]	362.9	39.0
	Energy production (wind classes)	[GWh/y]	370.1	40.2
<i>Sea Wave</i>	N. sea wave farm	[-]	2	1
	Devices per farm	[-]	28	10
	Total installed power	[MW]	4.5	0.8
	Energy production	[GWh/y]	53.8	6.9
<i>Solar</i>	Total area covered by PVP	[10 ³ m ²]	110	12
	Total installed power	[MW]	16.94	1.85
	Energy production	[GWh/y]	34.7	3.6

The details of the numbers of devices, the required power and the electricity production are reported for each source in Table V.18. The annual trend of electricity production is reported in Figure V.26, considering the two different ways to express the wind potential.

The two different approaches reveal similar results. In detail, focusing on the annual electricity production from wind, the method based on the Weibull distribution indicates an annual electricity production equal to 401.9 GWh/y while the wind speed classes approach suggests an annual production equal to 410.4 GWh/y.

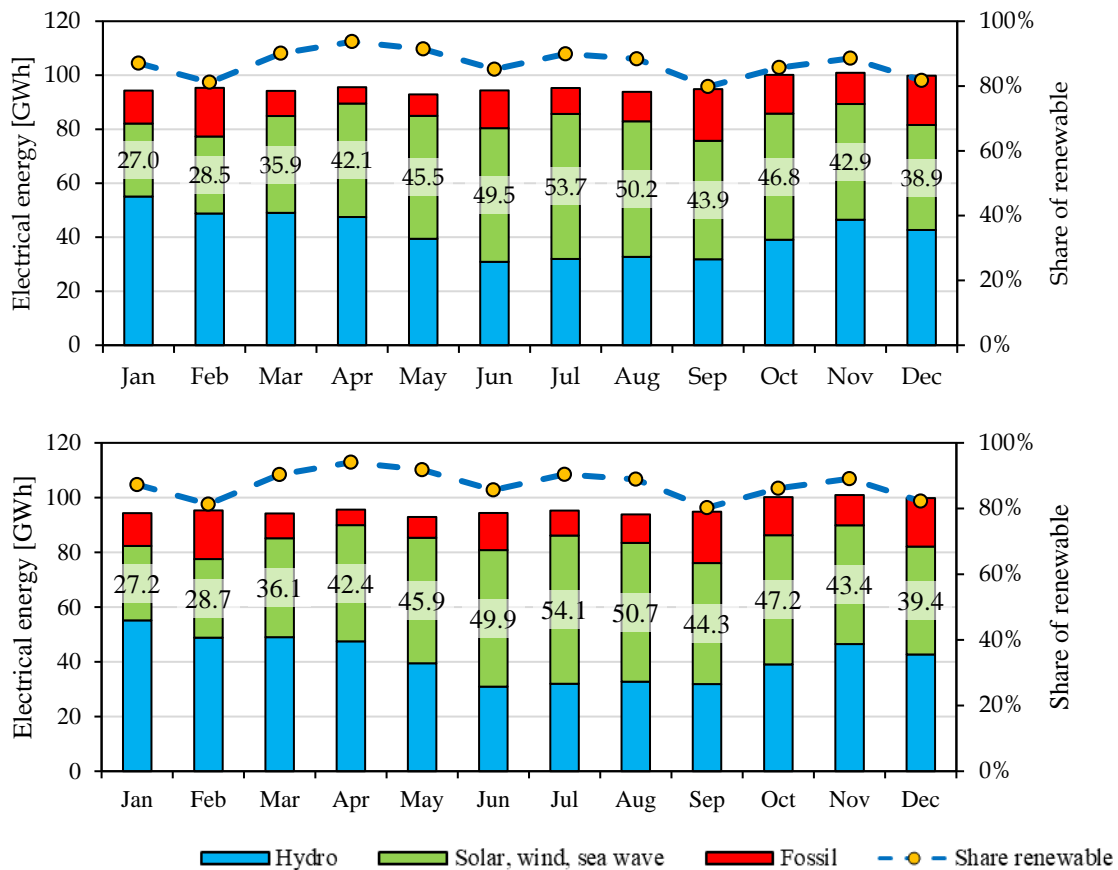


Figure V.26 Electricity production by sources and share of RES in Fiji. (A) Wind evaluation based on Weibull distribution. (B) Wind evaluation based on wind speed classes

From an environmental point of view, the renewable energy mix can avoid the emission of 260,286 tons of CO₂ per year (the value is obtained by considering an emission factor equal to 0.511 t CO₂/MWh). The economic evaluation is performed, evaluating the discounted cash flow and the breakeven time (see Figure V.27). The initial investment ranges between 258 to 339 million of US dollar, with an expected DCF after 20 years. In addition, the DCF ranges between 292 and 417 million of US dollar. The breakeven time is between 6.19 and 9.12 years.

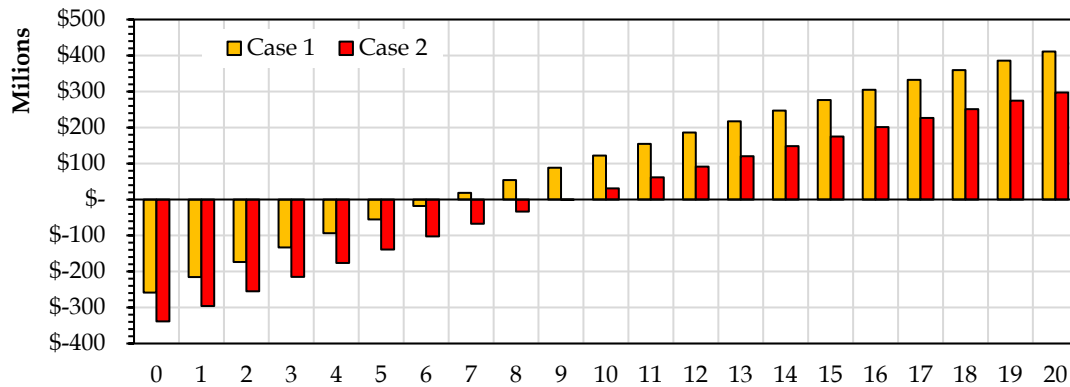


Figure V.27 DCF for the realization of the proposed RES mix in Fiji. Case 1: Investment based on world average prices. Case 2: Investment based on Oceanian average prices

V.3 An energy mix for Aeolian Islands

As introduced before, most small islands in the Mediterranean Sea are equipped with standalone electrical grid, supplied by fossil fuels. In this context, the introduction of RES represents a valid solution to increase the energy sustainability.

With this goal, in this section the Aeolian Islands are investigated in order to find the best RES mix able to satisfy a significant energy demand. Considering the utilization of wind, solar and sea wave, the sizing is based on an economic criterium.

The case studies below reported are published in the conference paper “**Supplying small islands with solar, wind and sea wave. An economic approach to find the best energy share**” in the conference proceeding *Oceans - 2019 Seattle*. [284]

V.3.a The case study of Aeolian Islands

The Aeolian Islands are an Italian archipelago, located in the Tyrrhenian Sea at north of Sicily, close to Messina. The main islands are Alicudi, Filicudi, Lipari, Panarea, Salina, Stromboli and Vulcano (see Figure V.28). The name of the archipelago has a Greek origin, indeed, according to the mythology Aeolus (demigod of the winds) lived there. The Aeolian islands are affected by volcanic activities. Actually, Vulcano and Stromboli are two famous active volcanos, characterized by sulfurous fumaroles, hot springs and volcanic muds. Eruptions occasionally occur.



Figure V.28 Aeolian Islands in the Tyrrhenian Sea (Italy).

From an economic point of view, the Aeolian Islands live on tourism, especially in summer, attracting up to 200,000 visitors per year. A ferry service connects the Aeolian Islands to Sicily (Messina, Milazzo and Palermo) and other cities in the southern part of Italy (Naples and Reggio Calabria). The archipelago is characterized by a Mediterranean climate, having mild winter, dry summer and temperate middle seasons. As regards the administration, all islands belong to the Lipari’s municipality, except the island of Salina,

that is split in three municipalities (Leni, Malfa and Santa Marina Salina). Some data about Aeolian islands are reported in Table V.19 [285].

All islands are affected by water scarcity, for this reason some of them are equipped with desalination plants. Freshwater is also transported by boat from Sicily.

Table V.19 Main data of Aeolian Island

Island	Water supply / Wastewater treatment	Inhabitants	Area [km ²]	Electrical consumption [MWh/y]	Electrical Society
Alicudi	Boat / No	105	5.1	400	Enel Produzione
Filicudi	Boat / No	235	9.5	1,400	Enel Produzione
Lipari	Desalination / Yes	11386	37.6	34,800	SEL SNC Lipari
Panarea	Boat / No	241	3.4	3,140	Enel Produzione
Salina	Boat / No	2300	26.4	9,160	Enel Produzione
Stromboli	Boat / No	400	12.6	3,870	Enel Produzione
Vulcano	Desalination / Yes	733	21	7,280	Enel Produzione

Like many other small islands in the Mediterranean Sea, the electricity production is based on fossil fuels. In Lipari, the power plant is owned by the private company “Società Elettrica Liparese S.r.l.”, producing about 34.8 GWh/y. In the other islands, the power plants are owned by the Italian big company “Enel Produzione S.p.A.”, producing about 25.3 GWh/y.

As introduced before, small Italian islands are obligated to promote the introduction of RES in order to achieve the targets fixed by the decree 14 February 2017. Table V.20 shows the targets imposed to the Aeolian Islands and the current installed plants [34].

Table V.20 Installed plants and targets for Aeolian Archipelago

Island	Installed PVP [kW]	Target electricity by RES [kW]	Installed thermal panels [m ²]	Target thermal panels [m ²]
Alicudi	-	20	-	20
Filicudi	-	80	-	8
Lipari	8.9	2110	79.9	2520
Panarea	-	130	-	200
Salina	-	580	24	570
Stromboli	100	220	-	250
Vulcano	180	300	-	470

The data reported in Table V.20 reveal a very limited penetration of RES in the local electrical grid. Indeed, in 1984 a silica monocrystalline photovoltaic park was installed in Vulcano, characterized by a rated power 180 kW and an energy efficiency of 9% (see Figure V.29) [208]. On the other volcanic island (Stromboli), a hybrid power system was installed in 2004 [208]. The system comprises a 100 kW PVP plant and a diesel generator (160 kW), supplying 140 homes in Ginostra. The overproduction is used to supply the local desalination plant.



Figure V.29 PVP plants in Vulcano [208]

V.3.b Mathematical approach

In this section, a simplified approach is reported in order to size a renewable energy mix, based on solar, wind and sea wave. To detect the optimal energy mix, a Levelized Cost of Electricity (LCOE) is defined [286], [287]. This economic parameter represents the minimal selling price of electricity, covering the initial investments and the annual operative and maintenance costs for the new installed capacity supplied by RES and the annual operative and maintenance costs of existing power plants supplied by fossil fuels [288], [289].

Eq. V.14 suggests the general definition of LCOE, introducing the Total Life Cycle Cost (TLCC) that represents the sum of the initial investment and the annual operative and maintenance costs of the system [290]. The term E_i represents the annual energy output corresponding to the realization of power plant.

$$LCOE * \sum_{i=1}^n \frac{E_i}{(1 + \tau)^i} = TLCC \quad V.14$$

This concept is normally applied to a single technology in literature [17], [19], [287], [288], [291], [292]. The idea is to extend this definition to the entire energy mix in order to find the best profitable solution. Thus, the parameter LCOE is obtained from the following economic balance, where the discounted cash flow is introduced. Eq. V.15 has been adapted to the specific case study, where three renewable energy sources are considered.

$$c_e E_d \sum_{z=1}^{20} \left(\frac{1 + \varepsilon}{1 + \tau} \right)^z \geq E_{fuel} c_{fuel} \sum_{z=1}^{20} \left(\frac{1 + \varepsilon}{1 + \tau} \right)^z + I_0 + (C_{m,ren} + C_{m,fuel}) \sum_{z=1}^{20} \frac{1}{(1 + \tau)^z}$$

where:

V.15

$$\begin{cases} E_{fuel} = E_d - (E_{WF} + E_w + E_{PV}) \\ I_0 = I_{0,WF} + I_{0,w} + I_{0,PV} \\ C_{m,ren} = C_{m,WF} + C_{m,w} + C_{m,PV} \end{cases}$$

In detail E_d represents the annual energy demand, c_e is the selling price for electricity, ε and τ are the inflation rate for energy sector and the monetary interest rate, respectively. E_{fuel} is the annual electricity production from existing power plant in the renewable energy mix scenario. This term can be expressed as difference of the annual energy demand and the annual energy production from sea wave E_{WF} , wind E_w and solar E_{PV} sources. With regard to the initial investment I_0 , this term is expressed as sum of the initial investment for sea wave $I_{0,WF}$, wind $I_{0,w}$ and photovoltaic panels $I_{0,PV}$. The same approach is applied to the annual operative and maintenance costs for the RES mix $C_{m,ren}$. Finally, the term $C_{m,fuel}$ represents the annual operative and maintenance cost for the existing diesel engines (except the fuel expenditure). To simplify Eq. V.15, the following assumptions are introduced:

- The economic profit for the local producer is neglected, so the inequality is converted into equation;
- The initial investment is assumed directly proportional to the installed capacity, introducing a unitary cost for each technology;
- The annual operative and maintenance costs can be expressed as fraction of the initial investment, introducing the parameters μ_{WF} , μ_w , μ_{PV} .

In these hypotheses, the Levelized Cost of Electricity can be evaluated through Eq. V.16:

$$LCOE = \frac{E_{fuel}c_{fuel} \sum_{z=1}^{10} \left(\frac{1+\varepsilon}{1+\tau}\right)^z + I_0 + (C_{m,ren} + C_{m,fuel}) \sum_{z=1}^{10} \frac{1}{(1+\tau)^z}}{E_d \sum_{z=1}^{10} \left(\frac{1+\varepsilon}{1+\tau}\right)^z} \quad V.16$$

where:

$$\begin{cases} E_{fuel} = E_d - (E_{WF} + E_w + E_{PV}) \\ I_0 = P_{WF}c_{WF} + P_w c_w + P_{PV}c_{PV} \\ C_{m,ren} = \mu_{WF}P_{WF}c_{WF} + \mu_w P_w c_w + \mu_{PV}C_{m,PV} \end{cases}$$

The equivalent working hours for each technology are introduced in V.17, dividing the energy output by the respective rated power.

$$t_{eq,PV} = \frac{E_{PV}}{P_{PV}} = \frac{\sum_{i=1}^{12} H_{m,tilt,i} S_{PV} n_{PV} \eta_{PV}}{I_{PV} S_{PV} n_{PV} \eta_{PV}} = \frac{\sum_{i=1}^{12} H_{m,tilt,i}}{I_{PV}}$$

$$t_{eq,w} = \frac{E_w}{P_w} = \frac{1}{P_w} \sum_{i=1}^{12} \sum_{j=1}^m t_{j,i} \psi(v_j) \quad V.17$$

$$t_{eq,WF} = \frac{E_{WF}}{P_{SW}} = \frac{1}{P_{SW}} \sum_{i=1}^{12} \varphi_{m,i} D_C \eta_{W,e} t_{m,i} n_C$$

About the evaluation of the electricity production from solar and sea wave, the definition reported in Eq. V.17 are based on the previous Eq. V.1, Eq. V.3 and Eq. V.10, respectively.

The parameters $t_{eq,PV}$, $t_{eq,w}$, $t_{eq,WF}$ depend on climatic data and the chosen technologies for the exploitation of RES. In detail, $t_{eq,PV}$ is function of the monthly solar radiation $H_{m,tilt,i}$ evaluated on the tilted surface S_{PV} . The term I_{PV} represents the reference radiation (1000 W/m²) used to calculate the rated peak power of PVP. Fixing a rated power, the extension of a PVP plant is related to the number of panels n_{PV} and their electrical efficiency η_{PV} .

Like the other technologies, the evaluation of the equivalent working hours for a wind turbine requires the evaluation of the annual electricity production divided by the rated power P_w of the system. According to Eq. V.10, above introduced, the annual electricity production of a single wind turbine can be calculated by using a discrete number of wind speed classes v_j and evaluating for each of them the number of hours per month $t_{i,j}$ when the speed class is measured. The equation requires the knowledge of the power output function of wind speed $\psi(v_j)$.

Finally, about the evaluation of the equivalent working hours for sea wave energy converters $t_{eq,WF}$, the equation above reported is obtained from Eq. V.3 (see subsection V.1.b), divided by the rated power of the device P_{SW} .

In order to identify the best energy mix from an economic point of view, a solution is to fix the amount of electricity production from RES and modify the distribution of the energy production from each source. For this reason, the following parameters are introduced:

- r is the ratio between the annual energy production from RES and the annual energy demand;
- a_{PV} is the ratio between the annual electricity production from PVP and the annual electricity production from RES;
- a_w is the ratio between the annual electricity production from wind and the annual electricity production from RES.

$$LCOE = (1 - r)c_{fuel} + \frac{r}{k_1} \left[\frac{a_{PV}}{t_{eq,PV}} C_{PV}(1 + k_2\mu_{PV}) + \frac{a_w}{t_{eq,w}} C_w(1 + k_2\mu_w) + \frac{1 - a_{PV} - a_w}{t_{eq,WF}} C_{WF}(1 + k_2\mu_{WF}) \right] + \frac{C_{m,fuel} k_2}{E_d k_1}$$

where:

$$\begin{cases} k_1 = \sum_{z=1}^{20} \left(\frac{1 + \varepsilon}{1 + \tau} \right)^z \\ k_2 = \sum_{z=1}^{20} \frac{1}{(1 + \tau)^z} \end{cases}$$

V.18

Thus, Eq. V.18 is finally obtained, where the variables are r , a_{pV} and a_w . In order to obtain the optimal condition for the Levelized Cost of Electricity, two constraints on the renewable energy mix are imposed:

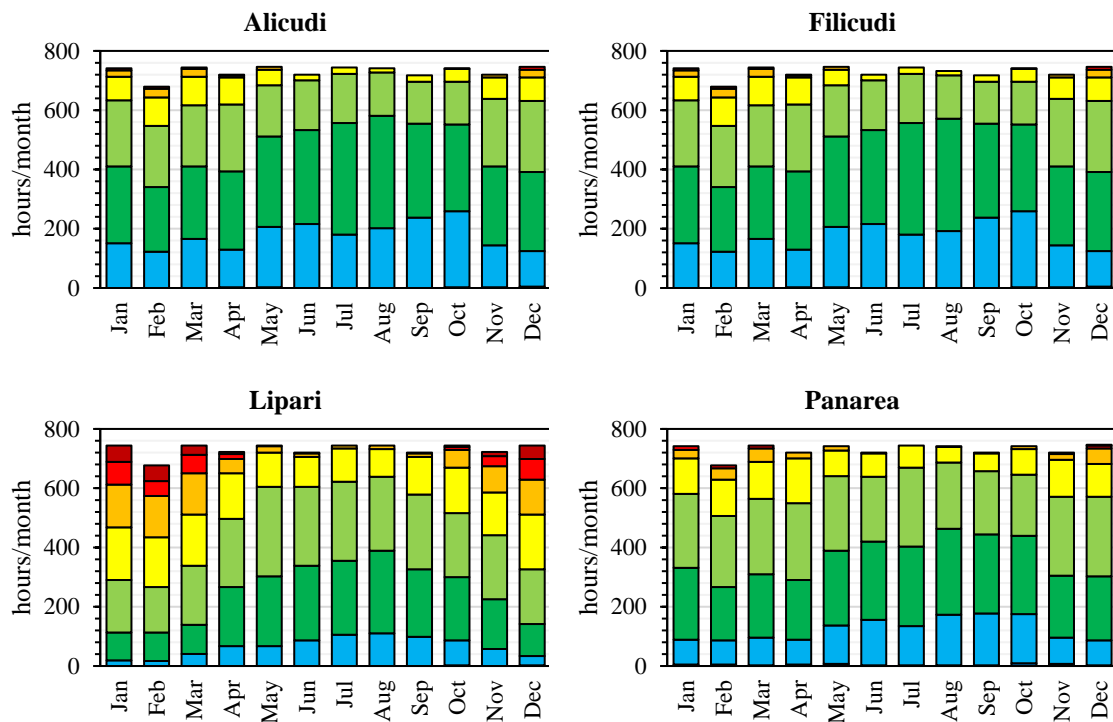
- Each source must produce almost the 10% of the total renewable energy production in each month;
- The total renewable energy production must not exceed the 90% of the monthly electricity demand, to guarantee a minimal electricity production from fossil fuels, compensating the maintenance cost of the existing power plant.

In conclusion the proposed approach is a case of constrained multivariable single objective optimization problem [293].

V.3.c Results

The mathematical model mentioned above was applied to the Aeolian islands taking into account the electrical production from renewable energy sources like solar photovoltaic, wind and sea wave [294]. The selection of the best mix is based on the evaluation of LCOE as function of the total renewable share r and the ratio of energy production from wind and solar sources, a_w and a_{pV} respectively. In order to evaluate renewable energy scenario, climate data have been collected from GIS tools [295].

Figure V.30 shows the annual availability of wind source for the Aeolian Islands. According to the previous data, wind speed assumes greater values during winter compared to summer.



(It follows in the next page)

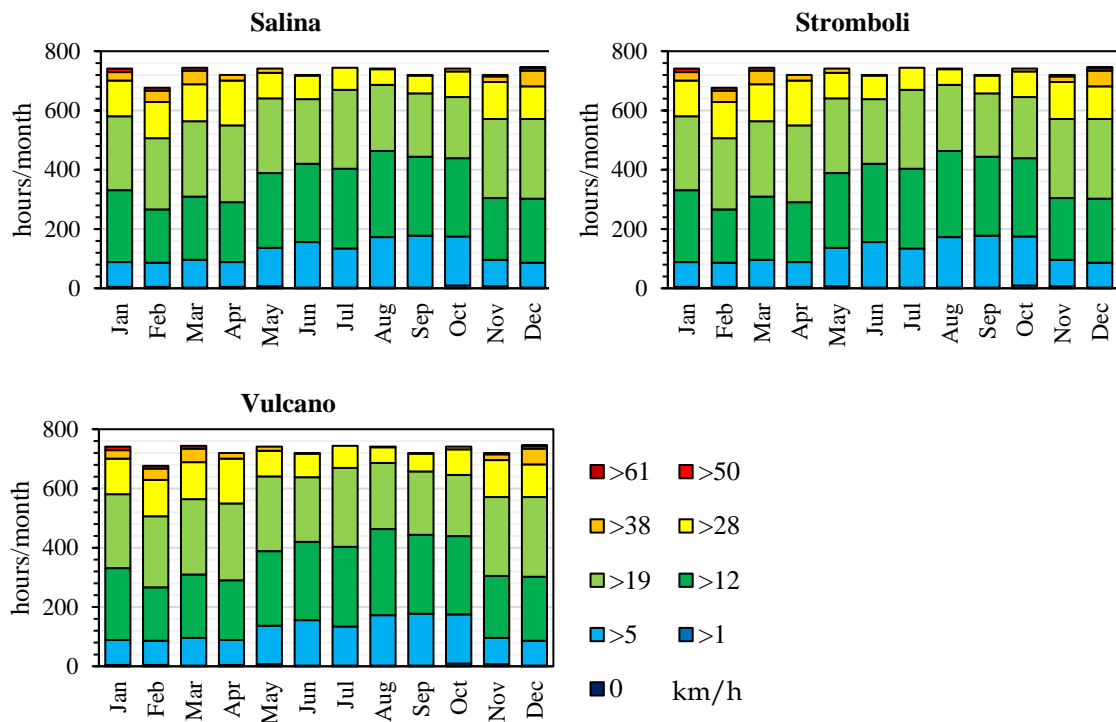


Figure V.30 Availability of wind source for each island during the year

Table V.21 Monthly solar radiation data [kWh/m²] for each island [253]

	Jan	Feb	Mar	Apr	May	Jun	Jul	Aug	Sep	Oct	Nov	Dec
Alicudi	103.9	113.1	178.3	186.6	213.0	217.2	232.8	223.5	177.6	148.5	115.8	96.1
Filicudi	115.6	133.0	196.5	196.5	218.6	218.4	235.0	229.7	192.9	170.5	127.8	105.7
Lipari	107.3	119.8	184.8	189.9	214.5	218.4	237.2	230.3	187.2	161.2	117.3	98.6
Panarea	104.2	117.9	182.0	190.2	213.9	217.5	235.0	228.5	185.4	158.7	111.9	95.8
Salina	89.0	109.2	171.1	186.9	213.3	217.5	236.2	229.7	178.8	148.5	99.9	78.4
Stromboli	83.7	103.6	169.9	192.3	215.1	220.5	238.7	231.3	183.0	147.3	94.2	76.3
Vulcano	113.5	126.0	190.0	192.3	215.5	218.4	234.1	230.7	189.6	167.7	124.2	105.1

Table V.21 shows the monthly solar radiation data [253]. Finally, Table V.22 reports the average values of wave energy flux and the location [296].

Table V.22 Wave energy flux [kW/m] [296]

	Point: Lat. / Long.	Jan-Mar	Apr-Jun	Jul-Sep	Oct-Dec
Alicudi	38.56°N / 14.32°E	7.13	2.17	1.37	5.39
Filicudi	38.57°N / 14.51°E	6.83	2.08	1.32	5.12
Lipari	38.45°N / 18.88°E	4.42	1.42	0.79	3.33
Panarea	38.66°N / 15.07°E	5.85	1.80	1.15	4.35
Salina	38.60°N / 14.78°E	5.85	1.78	1.16	4.38
Stromboli	38.83°N / 15.17°E	6.37	1.99	1.21	4.74
Vulcano	38.36°N / 14.87°E	4.60	1.47	0.85	3.48

In order to exploit solar and wind sources [297], commercial devices were considered, with power curve and efficiency noted. In particular, the trends of power production of

chosen wind turbines are reported in Figure V.31. In the case of sea wave, the point absorber, described in the previous chapter, is considered [298], [299].

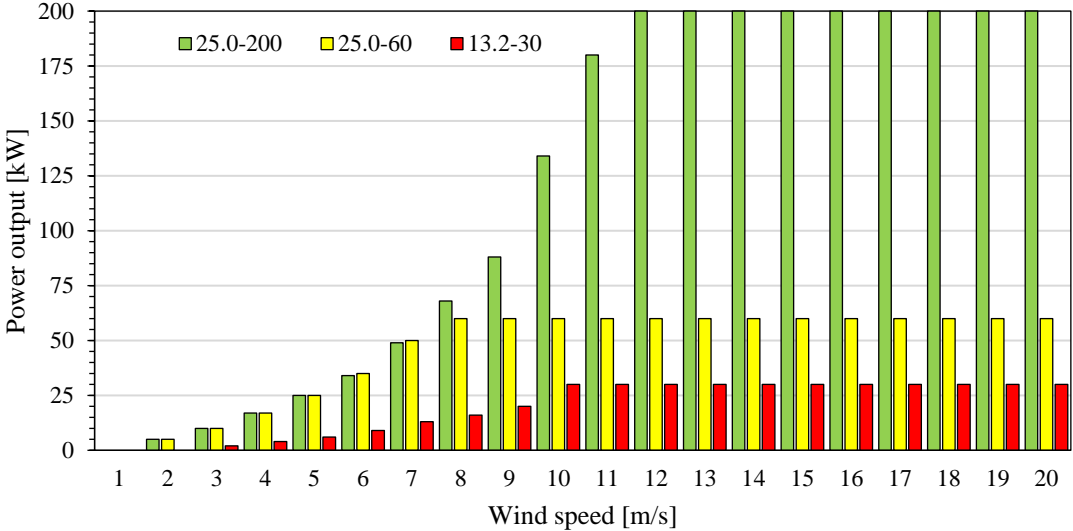


Figure V.31 Wind power production as function of wind speed

The mathematical model was applied to evaluate the Levelized Cost of Electricity (LCOE), as function of three degrees of freedom: the total share of energy production from the renewable energy mix r and the ratio of energy production from photovoltaic panels a_{PV} and wind source a_w .

In the following, the method is applied step by step to Lipari island. For the other Aeolian Islands results are directly reported.

Table V.23 shows the values of the main parameters required by the mathematical model, in the case of Lipari island. Recent statistics indicate an annual electrical energy consumption equal to 34.8 GWh [240]. With regard to the cost for electricity production through diesel engines, it was assumed equal to the sum of NUP (National Unique Price, in Italian “Prezzo Unico Nazionale”) [300] and the incentive established by the Italian Authority for Energy [301].

As the mathematical model considers the cost for energy production and operative and maintenance cost, the first term is assumed equal to the 90% of the total annual expenditure, so in conclusion the electricity cost by diesel engines is reduced by the same amount respect the sum of NUP and the incentive. The maintenance cost for diesel engines is assumed be independent from the annual energy production by fossil fuel and equal to 10% of the current annual expenditure for the electricity production by diesel engines.

Finally, the unitary cost for the installation of photovoltaic panels and wind turbines and the related annual operative and maintenance cost are extrapolated by recent reports of IRENA [17]. For the sea wave energy source, the economic parameters have been analyzed in specific works [302].

Table V.23 Values of main parameters used in the evaluation on Lipari island

Parameters	Symbols	Values
Annual energy demand	E_d	34.8 GWh/y
Electricity cost by diesel engines	c_{fuel}	0.311 €/kWh
Inflation rate for energy	ε	2.99%
Monetary interest rate	τ	1.75%
Unitary cost to install 1 kW of PVP	c_{PV}	1231 €/kW
Unitary cost to install 1 kW of wind turbines	c_w	1310 €/kW
Unitary cost to install 1 kW of sea wave	c_{WF}	5000 €/kW
Ratio of annual O&M cost on investment for PVP	μ_{PV}	0.013
Ratio of annual O&M cost on investment for wind	μ_w	0.034
Ratio of annual O&M cost on investment for wave	μ_{WF}	0.010
Annual O&M cost of diesel engines	$C_{m,fuel}$	1,824,912 €
Annual specific energy production from PVP	$t_{eq,PV}$	2066.4 kWh/kW
Annual specific energy production from wind	$t_{eq,w}$	2740.9 kWh/kW
Annual specific energy production from sea wave	$t_{eq,SW}$	1475.5 kWh/kW

Table V.24 LCOE as function of photovoltaic and wind ratio, without constrains

	a_{PV}																				
a_w	0.00	0.05	0.10	0.15	0.20	0.25	0.30	0.35	0.40	0.45	0.50	0.55	0.60	0.65	0.70	0.75	0.80	0.85	0.90	0.95	1.00
0.00	0.281	0.277	0.274	0.270	0.267	0.263	0.260	0.256	0.253	0.249	0.246	0.242	0.238	0.235	0.231	0.228	0.224	0.221	0.217	0.214	0.210
0.05	0.278	0.274	0.270	0.267	0.263	0.260	0.256	0.253	0.249	0.246	0.242	0.238	0.235	0.231	0.228	0.224	0.221	0.217	0.214	0.210	
0.10	0.274	0.270	0.267	0.263	0.260	0.256	0.253	0.249	0.246	0.242	0.239	0.235	0.231	0.228	0.224	0.221	0.217	0.214	0.210		
0.15	0.270	0.267	0.263	0.260	0.256	0.253	0.249	0.246	0.242	0.239	0.235	0.231	0.228	0.224	0.221	0.217	0.214	0.210			
0.20	0.267	0.263	0.260	0.256	0.253	0.249	0.246	0.242	0.239	0.235	0.231	0.228	0.224	0.221	0.217	0.214	0.210				
0.25	0.263	0.260	0.256	0.253	0.249	0.246	0.242	0.239	0.235	0.231	0.228	0.224	0.221	0.217	0.214	0.210					
0.30	0.260	0.256	0.253	0.249	0.246	0.242	0.239	0.235	0.232	0.228	0.224	0.221	0.217	0.214	0.210						
0.35	0.256	0.253	0.249	0.246	0.242	0.239	0.235	0.232	0.228	0.224	0.221	0.217	0.214	0.210							
0.40	0.253	0.249	0.246	0.242	0.239	0.235	0.232	0.228	0.224	0.221	0.217	0.214	0.210								
0.45	0.249	0.246	0.242	0.239	0.235	0.232	0.228	0.225	0.221	0.217	0.214	0.210									
0.50	0.246	0.242	0.239	0.235	0.232	0.228	0.225	0.221	0.217	0.214	0.210										
0.55	0.242	0.239	0.235	0.232	0.228	0.225	0.221	0.217	0.214	0.210											
0.60	0.239	0.235	0.232	0.228	0.225	0.221	0.217	0.214	0.210												
0.65	0.235	0.232	0.228	0.225	0.221	0.218	0.214	0.210													
0.70	0.232	0.228	0.225	0.221	0.218	0.214	0.210														
0.75	0.228	0.225	0.221	0.218	0.214	0.210															
0.80	0.225	0.221	0.218	0.214	0.210																
0.85	0.221	0.218	0.214	0.211																	
0.90	0.218	0.214	0.211																		
0.95	0.214	0.211																			
1.00	0.211																				

Fixing the annual renewable energy ratio r equal to 50% (in order to achieve the target of the Italian decree 14/02/2017), the previous Table V.24 shows the evaluation of LCOE as function of the remain degrees of freedom, i.e. the ratio of the annual energy production from wind turbines (a_w) and photovoltaic panels (a_{PV}). The specific annual energy production from each renewable source has been evaluated according to Eq. V.18 and climatic data above reported, considering Lipari island. Analyzing the results reported in Table V.24, it is interesting to observe the following aspects:

- As the linear model for the evaluation of the initial investment, operative cost and energy production, the LCOE assumes lower values in the case of energy mixes composed by high equivalent working hours and a low Capex and Opex.
- As sea wave is a prototypical technology, the initial investment is higher in comparison with the other two technologies, for this reason the LCOE analysis suggests a limitation of the installation of sea wave energy converters.
- The greatest part of energy mixes reported in Table IV.23 shows a LCOE lower than the current electricity cost by diesel engines.
- The choice of the energy mix is not influenced by the costs for the electricity production by diesel engines and their maintenance (of course, the values of LCOE change, but not the composition of the best energy mix).

Table V.25 Matrix of constrains for the renewable energy mix

a_w	a_{pv}																				
	0.00	0.05	0.10	0.15	0.20	0.25	0.30	0.35	0.40	0.45	0.50	0.55	0.60	0.65	0.70	0.75	0.80	0.85	0.90	0.95	1.00
0.00	0	0	0	0	0	0	0	0	0	0	0	0	0	0	0	0	0	0	0	0	0
0.05	0	0	0	0	0	0	0	0	0	0	0	0	0	0	0	0	0	0	0	0	0
0.10	0	0	0	0	0	1	1	1	1	1	1	1	1	1	1	1	1	0	0	0	0
0.15	0	0	0	0	1	1	1	1	1	1	1	1	1	1	1	1	0	0	0	0	0
0.20	0	0	0	0	1	1	1	1	1	1	1	1	1	1	1	0	0	0	0	0	0
0.25	0	0	0	0	1	1	1	1	1	1	1	1	1	1	0	0	0	0	0	0	0
0.30	0	0	0	1	1	1	1	1	1	1	1	1	1	0	0	0	0	0	0	0	0
0.35	0	0	0	1	1	1	1	1	1	1	1	1	0	0	0	0	0	0	0	0	0
0.40	0	0	0	1	1	1	1	1	1	1	1	0	0	0	0	0	0	0	0	0	0
0.45	0	0	0	1	1	1	1	1	1	1	0	0	0	0	0	0	0	0	0	0	0
0.50	0	0	1	1	1	1	1	1	1	0	0	0	0	0	0	0	0	0	0	0	0
0.55	0	0	1	1	1	1	1	1	0	0	0	0	0	0	0	0	0	0	0	0	0
0.60	0	0	1	1	1	1	1	0	0	0	0	0	0	0	0	0	0	0	0	0	0
0.65	0	0	1	1	1	1	0	0	0	0	0	0	0	0	0	0	0	0	0	0	0
0.70	0	0	1	1	1	0	0	0	0	0	0	0	0	0	0	0	0	0	0	0	0
0.75	0	0	1	1	0	0	0	0	0	0	0	0	0	0	0	0	0	0	0	0	0
0.80	0	0	1	0	0	0	0	0	0	0	0	0	0	0	0	0	0	0	0	0	0
0.85	0	0	0	0	0	0	0	0	0	0	0	0	0	0	0	0	0	0	0	0	0
0.90	0	0	0	0	0	0	0	0	0	0	0	0	0	0	0	0	0	0	0	0	0
0.95	0	0	0	0	0	0	0	0	0	0	0	0	0	0	0	0	0	0	0	0	0
1.00	0	0	0	0	0	0	0	0	0	0	0	0	0	0	0	0	0	0	0	0	0

As introduced in the mathematical model, several constrains have been introduced. In detail, it was assumed that:

- Each source must annually produce at least the 10% of the total electricity production from RES.
- The monthly energy production from RES must not exceed the 90% of the monthly electricity demand, allowing a minimal energy production from fossil fuels, necessary to balance the local electrical grid.

The results of the constrains are reported in Table V.25. The value 1 suggests that the energy mix satisfies the constrain conditions above described. Thus, multiplying the values reported in Table V.24 and Table V.25, the constrained LCOE matrix is finally obtained. Indeed, Table V.26 suggests the best energy mix from the economic point of

view. In detail, satisfying the 50% of the annual electricity demand, the best RES mix must be sized in order to produce 80% from wind, 10% from solar and 10% from sea wave. As the high energy demand and wind speed, a bigger wind turbine (200 kW) was considered in the case of Lipari, while 30 kW and 60 kW are chosen in the other cases.

Table V.26 Constrained LCOE matrix for Lipari island

α_w	α_{pv}																					
	0.00	0.05	0.10	0.15	0.20	0.25	0.30	0.35	0.40	0.45	0.50	0.55	0.60	0.65	0.70	0.75	0.80	0.85	0.90	0.95	1.00	
0.00																						
0.05																						
0.10						0.256	0.253	0.249	0.246	0.242	0.239	0.235	0.231	0.228	0.224	0.221	0.217					
0.15					0.256	0.253	0.249	0.246	0.242	0.239	0.235	0.231	0.228	0.224	0.221	0.217						
0.20					0.253	0.249	0.246	0.242	0.239	0.235	0.231	0.228	0.224	0.221	0.217							
0.25					0.249	0.246	0.242	0.239	0.235	0.231	0.228	0.224	0.221	0.217								
0.30					0.249	0.246	0.242	0.239	0.235	0.232	0.228	0.224	0.221	0.217								
0.35					0.246	0.242	0.239	0.235	0.232	0.228	0.224	0.221	0.217									
0.40					0.242	0.239	0.235	0.232	0.228	0.224	0.221	0.217										
0.45					0.239	0.235	0.232	0.228	0.225	0.221	0.217											
0.50					0.239	0.235	0.232	0.228	0.225	0.221	0.217											
0.55					0.235	0.232	0.228	0.225	0.221	0.217												
0.60					0.232	0.228	0.225	0.221	0.217													
0.65					0.228	0.225	0.221	0.218														
0.70					0.225	0.221	0.218															
0.75					0.221	0.218																
0.80					0.218																	
0.85																						
0.90																						
0.95																						
1.00																						

Figure V.32 shows the potential energy production from the proposed energy mix in comparison with the energy demand, whose trend has been modelled in similitude by using the annual trend of other Aeolian Islands [285]. The graph demonstrates that the matching of energy demand and electricity production from RES is a very difficult task.

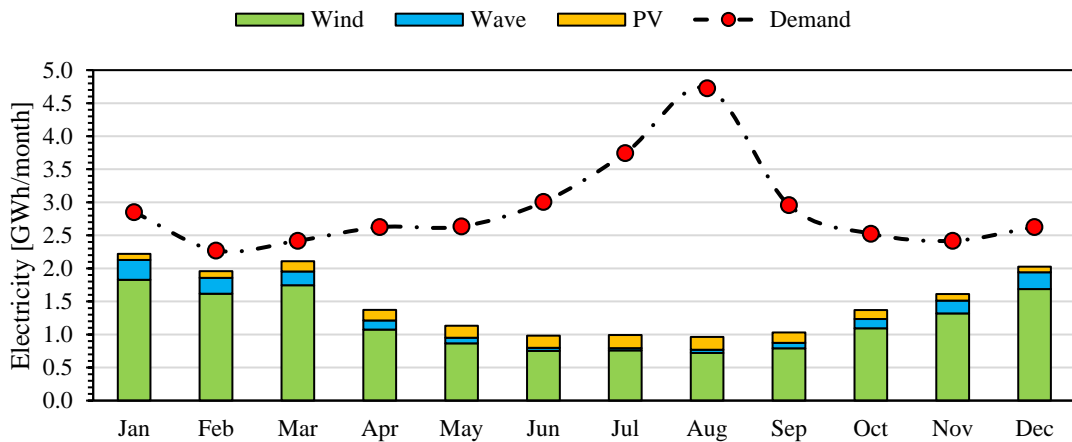


Figure V.32 Electricity demand and potential renewable energy production

Not considering the installation of energy storage system, the renewable energy mix capacity is limited by the energy demand during winter, according to the conditions above imposed. Since the electricity demand increases during summer, three solutions could be adopted if a higher RES share is introduced in the local grid:

- Increase the installed power and introduce an energy storage system, saving the energy surplus during winter and exploiting it during summer (for example hydrogen storage);
- Increase the installed power from RES, accepting to stop a part during winter;
- Interconnect all small islands to Sicily, in order to exploit the mainland electrical grid to balance the energy demand and production on Aeolian Islands.

The LCOE approach was applied to the other Aeolian Islands. The proposed energy mix (see Table V.27) considers the realization of building integrated PVP plants (each one with a rated power of 3 kW_p), the utilization of 200 kW wind turbines in Lipari (30 kW in Alicudi and 60 kW in the other islands), and the installation of several WECs. As regards the economic parameters, in the Aeolian Islands have been used the same unitary costs of Lipari, as more accurate data are not available.

Table V.27 Proposal of energy mix for the Aeolian Islands

		Alicudi	Filicudi	Lipari	Panarea	Salina	Stromb.	Vulcano
n. PVP plants	[-]	2	5	281	26	78	33	58
Total PVP power	[kW]	6	15	843	78	234	99	174
PVP production	[MWh/y]	12.0	32.1	1742.0	159.2	458.3	193.6	366.6
n. wind turbines	[-]	3	3	25	4	13	6	10
Total wind power	[kW]	90	180	5000	240	780	360	600
Wind production	[MWh/y]	187.2	693.8	13704.5	1121.4	3644.5	1682.1	2803.5
n. wave converters	[-]	0	0	15	2	4	1	4
Total wave power	[kW]	0	0	1200	160	320	80	320
Total wave production	[MWh/y]	0	0	1770.6	311.7	624.3	169.6	493.0
Total RES production	[MWh/y]	199.2	725.9	17217.1	1592.3	4727.2	2045.3	3943.5
LCOE	[€/kWh]	0.2161	0.2007	0.2192	0.2135	0.2075	0.2007	0.2022

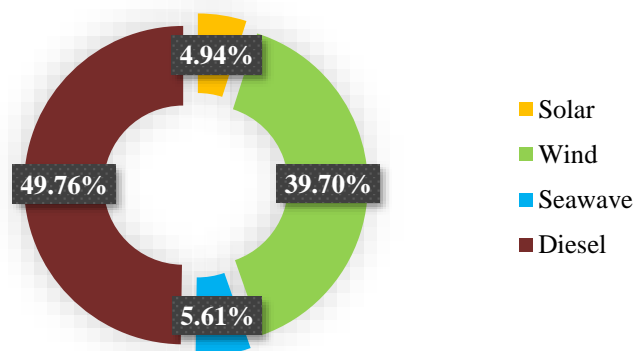


Figure V.33 Share of each source in Aeolian Islands Energy Scenario.

According to Figure V.33, the proposed RES mix can cover about the 50% of the annual energy demand. The annual economic saving is estimated equal to 9.39 million of euros. At the same time, the emission of 20386 tons of CO₂ per year is avoided.

V.4 The proposal of a RES mix in Lampedusa and the analysis of grid stability

In the previous section, a mathematical model was introduced in order to identify the best energy mix from an economic point of view. In this section, the same mathematical model is applied to Lampedusa, a small Italian island located south of Sicily. The main change is the introduction of an additional check on the energy production from RES, considering hourly trend in reference days. In this way the maximal share of monthly energy production is modified in order to remove some incompatible energy mixes. The best energy mix is furthermore investigated, evaluating the hourly trends in reference days and analyzing the frequency stability problem of the local grid.

Indeed, the installation of RES supplied power plants is realized through the utilization of electronic power converters, in order to maximize the electricity production. As a consequence, the electrical energy production from conventional power plants is reduced. This aspect represents a relevant benefit for the environment, thanks to the reduction of CO₂ emission and fossil fuel consumption. However, focusing on the electrical grid, the growth of RES production and consequently the reduction of energy production from fossil fuel supplied power plants represent a serious risk for the grid stability. Indeed, in case of load variations, traditional power plants can use the kinetic energy of rotary machines (turbines, alternators, etc.) and limit the frequency variations. This property is absent in power electronics-based RES generators, except in case of advanced controlled systems. Therefore, the growth of RES installed power reduces the systems inertia and, consequently, increases the Rate of Change of Frequency (RoCoF), an indicator used to quantify potential grid instability [303], [304].

Thence, in the case study reported below the system inertia is evaluated by considering the typical week profiles of the energy demand delivered by the local company. Two different trends of RES production are considered, in order to evaluate the energy production entrusted to the local fossil fuel supplied power plant:

- **Worst grid scenario** is referred to the worst condition for the electrical grid, assuming that the RES production is as much as possible and consequently the conventional production is at a minimum level. This load condition is obtained, if the solar production is evaluated according to the hourly solar radiation, while the production from wind and sea wave is assumed equal to the corresponding rated power.
- **Probabilistic grid scenario** is obtained by considering the hourly trends of RES in two different years and assuming for each source the condition that correspond to the maximal energy production. Consequently, the energy balance of the grid is entrusted to the traditional power plant.

Finally, 24 failure conditions are simulated by using Neplan software, analyzing the dynamic transient stability to verify the robustness of the local grid in the presence

of RES. The flow chart in Figure V.34 briefly synthesizes the step of the proposed analysis methodology.

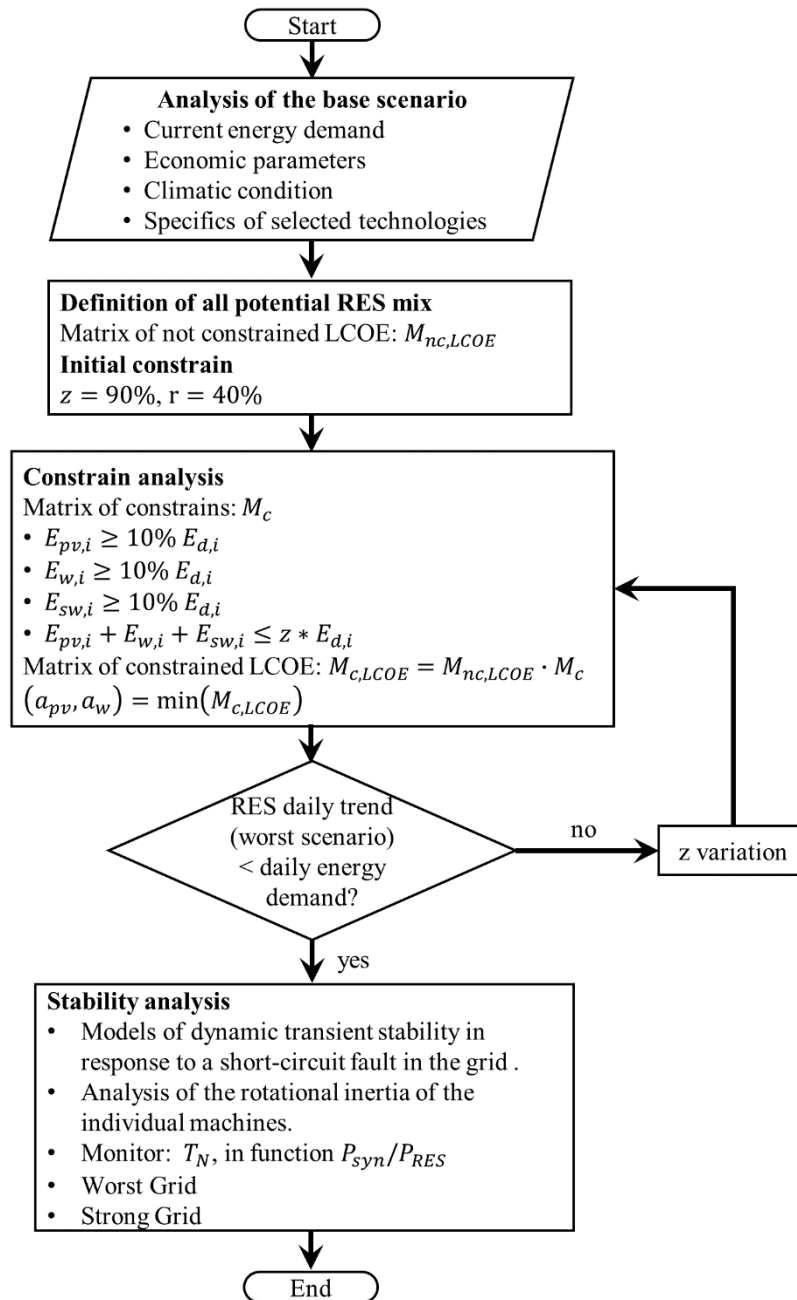


Figure V.34 Flow chart of the methodology

V.4.a The case study of Lampedusa

Lampedusa is a small Italian island, located between Sicily and North Africa, about 113 km from Tunisia and 205 km from Sicily. It covers a surface of about 20.2 km² and a coastline of about 26 km. Lampedusa belongs to Pelagie Islands, with the other small islands of Linosa and Lampione.

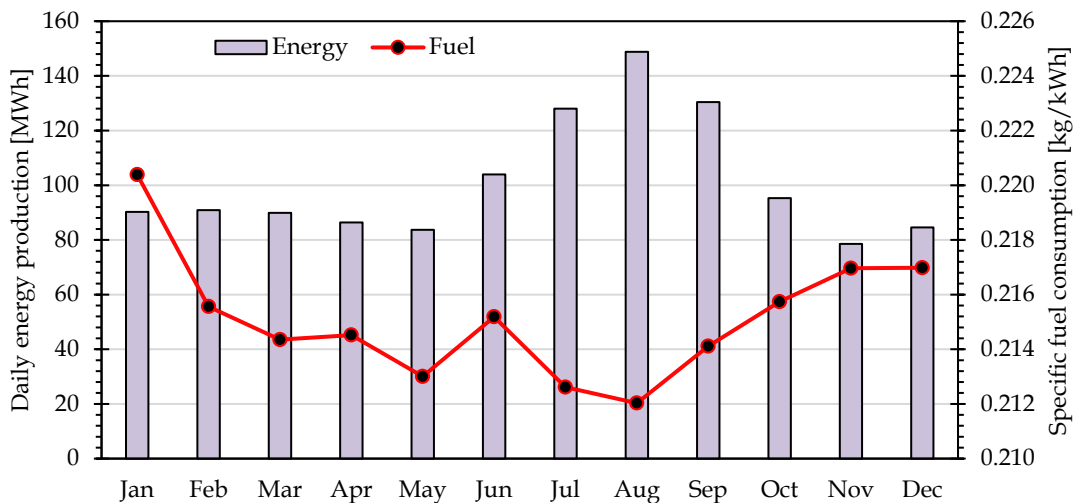


Figure V.35 Daily energy production MWh [2014]

The power system is isolated from the main national grid, because the relevant distance from the mainland. The local medium voltage network comprises 69 nodes, 39 kiosks and 13 pole-mounted 10 kV/400 V substations. The annual electricity production is about 36.2 GWh. The trend of the daily energy production is reported in Figure V.35 [305].

The entire electrical energy production is realized by the local power plant, equipped with eight diesel generators, achieving a total installed power equal to 22.5 MVA. The sizes of all generators are reported in Table V.28. The generators work with different schedules according to the prevision of the hourly electrical demand.

Table V.28 Rated power of diesel generators installed in Lampedusa

Identification	Rated power [kW]	Inertia constant [s]
G1	4100	2.85
G2	1328	1.51
G3	1470	1.53
G4	2800	2.41
G5	1893	2.01
G6	2998	2.52
G7	2935	2.47
G8	5040	2.91

A boat service refills the fuel reservoirs of the local power plant. This solution is not sustainable from an environmental point of view, because of the emission of CO₂ and pollutants, due to the diesel combustion in the local power plant and the fuel transport. Figure V.36 represents the structure of the local medium voltage network [306].

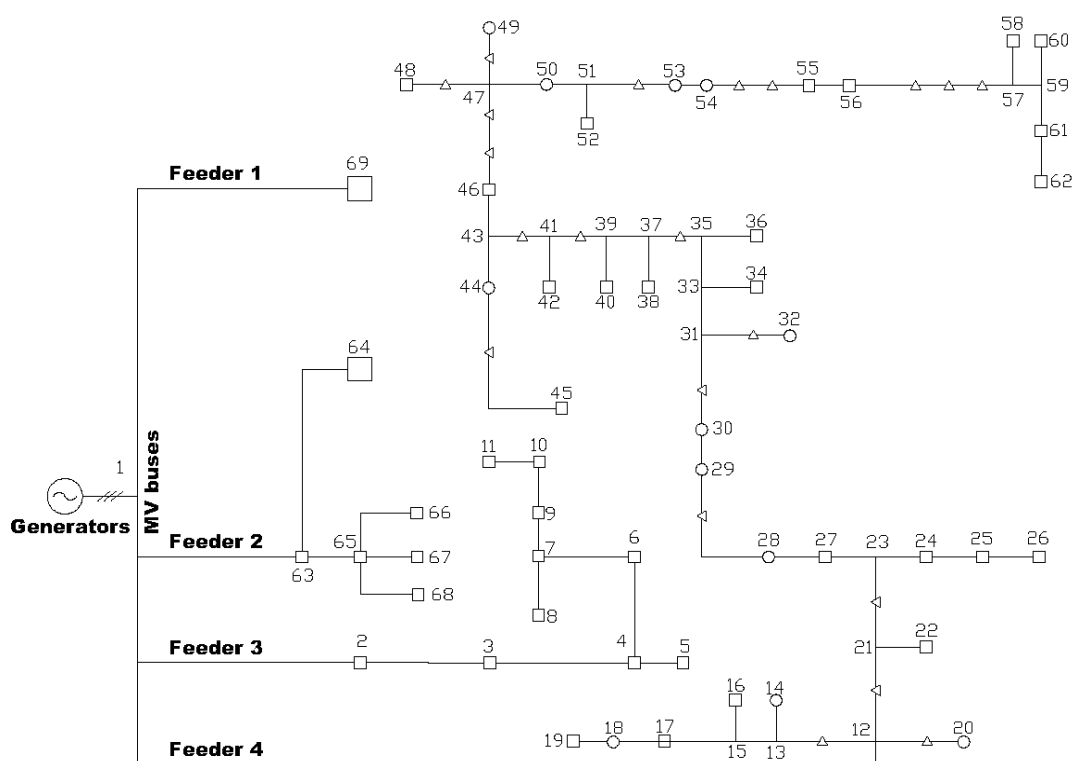


Figure V.36 Layout of the MV network of Lampedusa island

About the economic point of view, the electricity generation in Lampedusa shows greater costs in comparison with the mainland. Like the other small islands, an incentive in Italian electrical bills is used to cover this additional cost. In the case of Lampedusa, this incentive corresponds to 13 M€/y [34].

V.4.b The proposed energy mix

The same mathematical model, reported in the previous case study, was applied in the context of Lampedusa. In the evaluation of the constrained LCOE matrix, the following conditions were adopted:

- Each renewable energy source must annually produce at least the 10% of the total electricity production from RES.
- The monthly share of electricity production from RES must not exceed the parameter z , in order to guarantee a minimal electricity production from the existing power plant and balance the electrical grid. At the same time, z is calibrated in order to avoid the condition in which the hourly electricity production exceeds the energy demand, otherwise the installation of an energy storage is required. This condition is checked, by considering the hourly trend of the energy demand during a summer week and a winter one.

As shown in the flow chart reported in Figure V.34, the parameter z is evaluated with an iterative approach. It assumes firstly the value of 90% in order to evaluate preliminarily the matrix of constrains. Overlapping the matrix of constraints to the not

constrained LCOE matrix, it is possible to identify the best condition, i.e. the RES mix corresponding to the lowest LCOE. This condition is consequently verified, considering the hourly trends of energy demand and production from RES. If the proposed energy mix exceeds the energy demand in some hours of the day, the parameter z is reduced and consequently the matrix of constraints is calculated again and overlapped on the not constrained LCOE matrix to find the new best energy mix. After a few iterations, the best energy is finally obtained, verifying the hourly compatibility with the local energy demand.

The RES mix is selected according to the economic parameter LCOE seen in Eq. V.18. Solar, wind and sea wave are the considered energy sources. Climatic data have been collected, using specific GIS tools. In detail, Figure V.37 shows the annual trend of the wind source, by considering nine wind speed classes and reporting the corresponding hours when each speed class is measured. These data are based on a specific weather model having a resolution of 30 km [307].

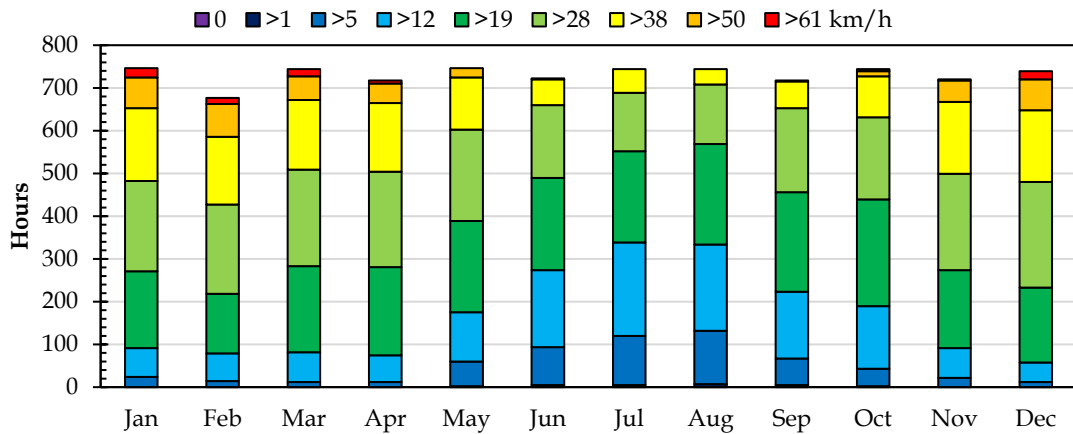


Figure V.37 Availability of wind source by wind speed classes

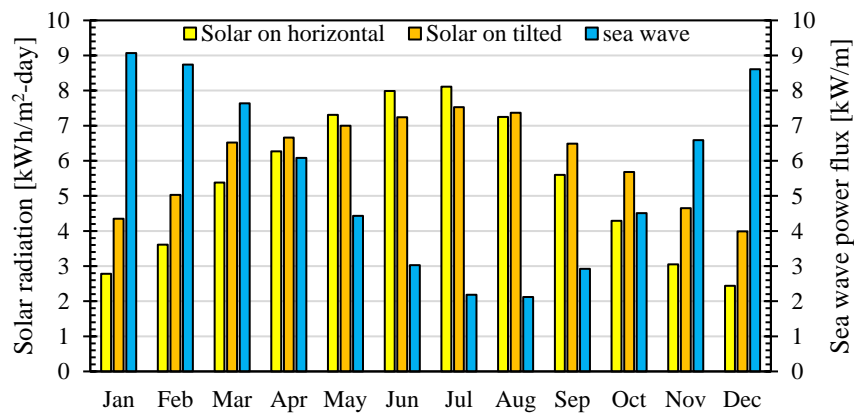


Figure V.38 Solar radiation on horizontal and tilted surface (31°) and sea wave power flux

As regards the sea wave energy source, the monthly average power flux trend is reported in Figure V.38 [296]. In the same graph, the solar source is represented by the monthly average daily solar radiation on a horizontal surface and a tilted surface (31°) [253].

About the existing power plant, the mathematical model splits the annual costs in two items: a term related to the fuel consumption to produce energy and the latter to fixed expenditure (maintenance, worker salaries, etc.). Assuming that the trend reported in Figure V.35 was the same also in 2015, the evaluation of the average price for fuel consumption has been evaluated as weighted average of the monthly average price of oil with a low concentration of sulfur (less than 1%) published by the Italian Ministry of Economic Development [308].

The total income of the local producer is given by product of the annual electricity production and the total selling price of energy. Thus, the fixed costs are evaluated as the difference of the total income and the estimated expenditure for the fuel consumption. About the cost for electricity production using traditional generators, it assumed equal to the sum of NUP [300] and the incentive established by the Italian Authority for Energy [309].

About RES, the unitary cost for the purchase and installation and for the operative and maintenance operations of each RES technology can be obtained from literature [17]. About sea wave, the economic parameters have been considered in previous researches [252].

The discount rate for energy sector has been evaluated by the authors, considering the entire data bank (from January 1996 to November 2019) on the monthly average price of oil with a low concentration of sulfur [308]. About the discount rate for money, data are available in literature [310].

Recent statistics indicate an annual electrical energy consumption equal to 36.8 GWh in Lampedusa [240]. All data are reported in Table V.29.

Table V.29 Values of main economic parameters

Parameters	Symbols	Values
Annual energy demand	E_d	36863 MWh/y
Electricity cost by diesel engines	c_f	0.205 €/kWh
Inflation rate for energy	ε	2.99%
Monetary interest rate	τ	1.14%
Unitary cost to install 1 kW of PVP	$c_{pv,0}$	1231 €/kW
Unitary cost to install 1 kW of wind turbines	$c_{w,0}$	1310 €/kW
Unitary cost to install 1 kW of sea wave	$c_{sw,0}$	5020 €/kW
Unitary O&M cost for 1 kW of PVP	$c_{pv,A}$	18 €/kW-y
Unitary O&M cost for 1 kW of wind turbines	$c_{w,A}$	50 €/kW-y
Unitary O&M cost for 1 kW of WEC	$c_{sw,A}$	75 €/kW-y
Annual O&M cost of diesel engines	$C_{f,A}$	2,830,659 €
Equivalent working hour of PVP	$t_{eq,pv}$	1953.2 kWh/kW
Equivalent working hour of wind turbine	$t_{eq,w}$	4982.6 kWh/kW
Equivalent working hour of sea wave converter	$t_{eq,sw}$	2419.5 kWh/kW

Considering the climatic data above reported, the mathematical model is applied considering a RES share set to 40%. The remaining two degrees of freedom are varied in a discretized way from 0 to 100%, as shown in Table V.30, obtaining the LCOE as function of the share of solar and wind production.

Table V.30 LCOE (€/MWh) as function of photovoltaic and wind ratio (%), without constrains

α_w	α_{pv}																				
	0.00	0.05	0.10	0.15	0.20	0.25	0.30	0.35	0.40	0.45	0.50	0.55	0.60	0.65	0.70	0.75	0.80	0.85	0.90	0.95	1.00
0.00	222	221	219	218	216	215	213	212	210	209	207	206	204	203	201	200	198	197	195	193	192
0.05	221	219	218	216	214	213	211	210	208	207	205	204	202	201	199	198	196	195	193	192	
0.10	219	217	216	214	213	211	210	208	207	205	204	202	200	199	197	196	194	193	191		
0.15	217	215	214	212	211	209	208	206	205	203	202	200	199	197	196	194	193	191			
0.20	215	214	212	211	209	208	206	204	203	201	200	198	197	195	194	192	191				
0.25	213	212	210	209	207	206	204	203	201	200	198	197	195	194	192	190					
0.30	211	210	208	207	205	204	202	201	199	198	196	195	193	192	190						
0.35	210	208	207	205	204	202	201	199	198	196	194	193	191	190							
0.40	208	206	205	203	202	200	199	197	196	194	193	191	190								
0.45	206	205	203	201	200	198	197	195	194	192	191	189									
0.50	204	203	201	200	198	197	195	194	192	191	189										
0.55	202	201	199	198	196	195	193	192	190	189											
0.60	201	199	198	196	195	193	191	190	188												
0.65	199	197	196	194	193	191	190	188													
0.70	197	195	194	192	191	189	188														
0.75	195	194	192	191	189	188															
0.80	193	192	190	189	187																
0.85	192	190	189	187																	
0.90	190	188	187																		
0.95	188	186																			
1.00	186																				

The share of electricity production from sea wave represents the complementary part to 100% of the sum of the share of electricity production from PVP and wind turbines.

The evaluation of all economic parameters considers a linear relation with the installed power of each RES. As a consequence, Table V.30 reveals the following features:

- In the case of not constrained matrix, LCOE assumes lowest value using only the renewable energy source with high annual specific energy production and low Capex and Opex (see $a_w = 100\%$).
- About sea wave, this technology is at a development step, so the initial investment is higher in comparison with the other two sources. Consequently, in the case $a_w = 0\%$ and $a_{pv} = 0\%$ LCOE assumes the highest value.
- The greatest part of the values reported in Table V.30 is lower than the equivalent cost for the electricity production from fossil fuel (see c_f in Table V.29). This aspect means that the adoption of each possible RES mix can reduce the sum of all costs to produce electricity in small islands in comparison with the as-is scenario.
- The choice of the optimal energy mix is not influenced by the change of operative and maintenance cost to produce electricity from fossil fuels.

Table V.31 Matrix of constrains for the renewable energy mix

α_w	α_{pv}																				
	0.00	0.05	0.10	0.15	0.20	0.25	0.30	0.35	0.40	0.45	0.50	0.55	0.60	0.65	0.70	0.75	0.80	0.85	0.90	0.95	1.00
0.00	0	0	0	0	0	0	0	0	0	0	0	0	0	0	0	0	0	0	0	0	0
0.05	0	0	0	0	0	0	0	0	0	0	0	0	0	0	0	0	0	0	0	0	0
0.10	0	0	0	0	0	0	0	0	0	0	1	0	0	0	0	0	0	0	0	0	0
0.15	0	0	0	0	0	0	0	0	0	1	1	0	0	0	0	0	0	0	0	0	0
0.20	0	0	0	0	0	0	0	0	0	1	1	0	0	0	0	0	0	0	0	0	0
0.25	0	0	0	0	0	0	0	0	1	1	1	0	0	0	0	0	0	0	0	0	0
0.30	0	0	0	0	0	0	0	1	1	1	1	0	0	0	0	0	0	0	0	0	0
0.35	0	0	0	0	0	0	0	1	1	1	1	0	0	0	0	0	0	0	0	0	0
0.40	0	0	0	0	0	0	1	1	1	1	1	0	0	0	0	0	0	0	0	0	0
0.45	0	0	0	0	0	1	1	1	1	1	1	0	0	0	0	0	0	0	0	0	0
0.50	0	0	0	0	0	1	1	1	1	1	1	0	0	0	0	0	0	0	0	0	0
0.55	0	0	0	0	0	1	1	1	1	1	1	0	0	0	0	0	0	0	0	0	0
0.60	0	0	0	0	1	1	1	1	1	1	1	0	0	0	0	0	0	0	0	0	0
0.65	0	0	0	0	1	1	1	1	1	1	1	0	0	0	0	0	0	0	0	0	0
0.70	0	0	0	0	1	1	1	1	1	1	1	0	0	0	0	0	0	0	0	0	0
0.75	0	0	0	0	0	0	0	0	0	0	0	0	0	0	0	0	0	0	0	0	0
0.80	0	0	0	0	0	0	0	0	0	0	0	0	0	0	0	0	0	0	0	0	0
0.85	0	0	0	0	0	0	0	0	0	0	0	0	0	0	0	0	0	0	0	0	0
0.90	0	0	0	0	0	0	0	0	0	0	0	0	0	0	0	0	0	0	0	0	0
0.95	0	0	0	0	0	0	0	0	0	0	0	0	0	0	0	0	0	0	0	0	0
1.00	0	0	0	0	0	0	0	0	0	0	0	0	0	0	0	0	0	0	0	0	0

To simplify the evaluation of all constrains, the worst scenario is considered, in which the renewable energy mix produces the maximal potential energy output: PVP plants according to the hourly solar radiation, wind turbines and WECs at rated power. Indeed, each RES should contribute at least for the 10% of the monthly energy demand and the total monthly share should not exceed the parameter z , in order to avoid the requirement of an energy storage system. According to the algorithm shown in Figure V.34, the parameter z is calibrated with an iterative approach, in order to verify the maximal RES share only for a limited number of potential RES mixes, since this investigation is based on hourly trends.

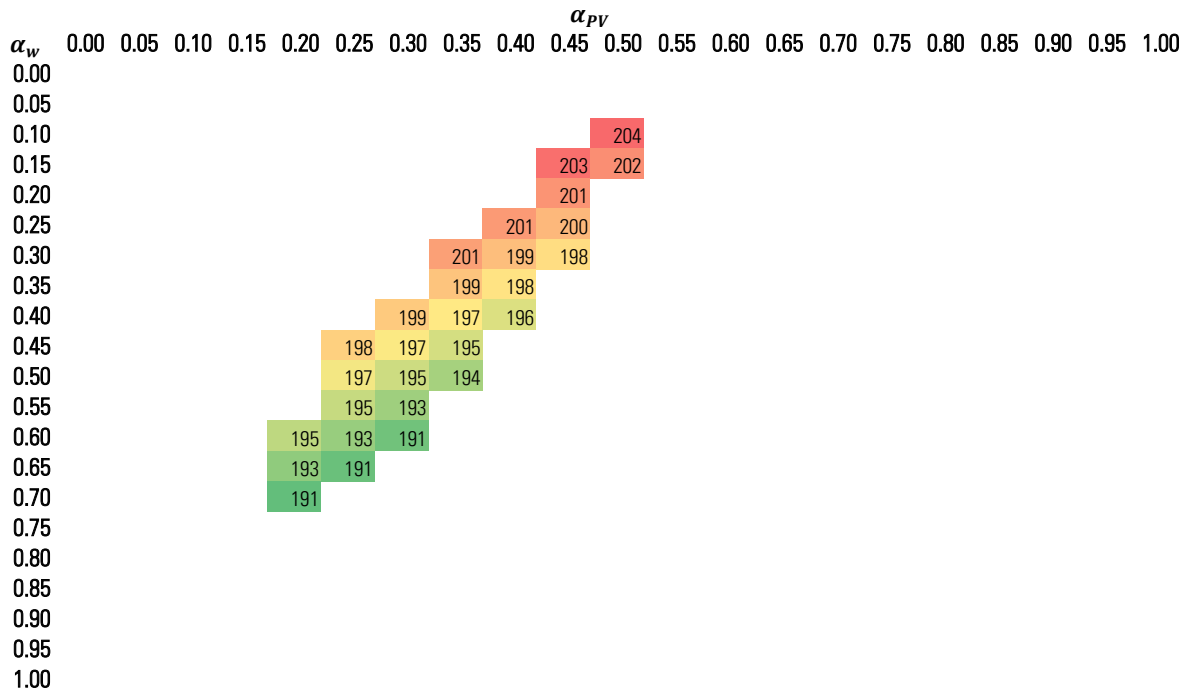
According to this analysis, z is evaluated equal to 0.53.

Table V.31 shows the RES mixes that satisfy all the conditions above reported, by using a Boolean representation. The value 1 is referred to the energy mixes that are compatible with all constrains above reported. Thus, multiplying the values reported in Table V.30 and

Table V.31, the constrained LCOE matrix is finally obtained (see Table V.32).

As shown in Table V.32, the best energy mix to cover the 40% of the annual electricity demand is composed by 70% wind, 20% solar and 10% sea wave.

Table V.32 Constrained LCOE matrix for Lampedusa



Consequently, the following Eq. V.19 are used to obtain the power to install for each source, considering the parameters already described above.

$$P_w = rE_d \frac{a_w}{t_{eq,w}} \quad P_{pv} = rE_d \frac{a_{pv}}{t_{eq,pv}} \quad P_{sw} = rE_d \frac{1 - a_w - a_{pv}}{t_{eq,sw}} \quad V.19$$

Considering that each RES supplied technology has a commercial rated power, the final values of installed power are obtained by rounding the number of required devices to achieve the desired energy production. The details of the proposed RES mix are reported in Table V.33.

Table V.33 Proposal of energy mix for Lampedusa

		Solar	Wind	Sea wave
Power to be installed	[kW]	1509	2100	640
Rated power of device	[kW]	3	60	80
n. device	[-]	503	35	8
Annual energy production	[MWh/y]	2947.4	10463.4	1548.5

In Figure V.39 the energy demand and production show different trends: the first one has a peak in summer, while the latter in winter. For this reason, the share of electricity production by RES oscillates from 23.1% in August to 53.3% in April and 53.0% in November.

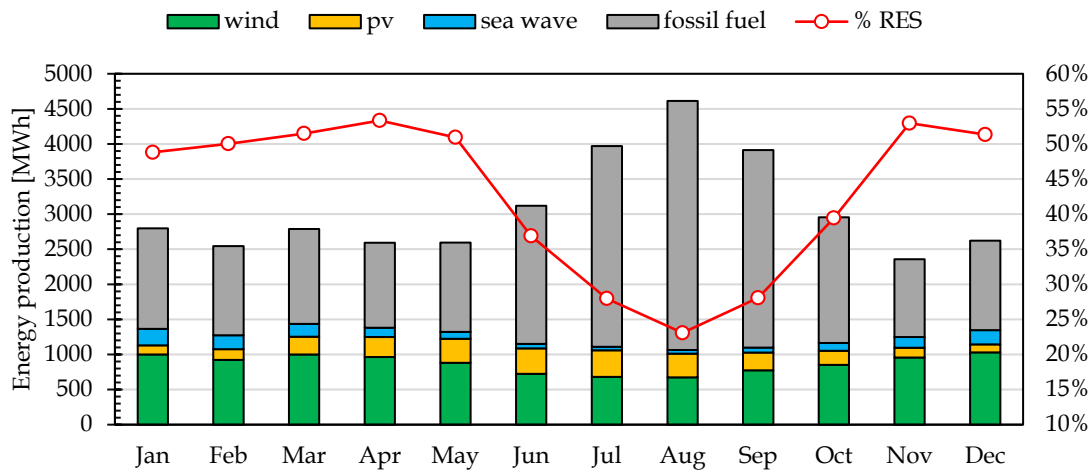


Figure V.39 Electricity demand and potential renewable energy production

In conclusion, to replace the 40% of the current electricity demand, the best energy mix from an economic point of view requires the installation of 1509 kW of PVP (subdivided into 503 small roof-integrated plants), 2100 kW of wind turbines (35 wind plants) and 640 kW of wave energy converters (8 devices). In this way, the estimated annual electricity production is equal to 2947.4 MWh/year for solar panels, 10463.4 MWh/year for wind turbines and 1548.5 MWh/y for sea wave energy converters.

The energy mix can reduce the energy price to 0.190 €/kWh from the current value equal to 0.282 €/kWh (data of 2015).

An avoided annual expenditure in the Italian bill equal to 3.384 million euros (a reduction of 32.58 % of the current expenditure) is estimated thanks to the reduction of electricity production from fossil fuels.

From an environmental point of view, the fuel consumption is reduced by 3170 tons of oil, corresponding to an avoided emission of 9963 tons of CO₂ per year.

V.4.c Grid stability analysis

Power systems security is based on frequency stability in relation to the inertia and kinetic energy variation of the synchronous generators connected to the grid. As introduced previously, two scenarios are analyzed:

- **Scenario A or Worst grid scenario.** In this case study, the hourly active power from RES P_{res} is considered equal to the sum of the rated power of wind turbines and WECs, and the maximal producibility from PVP, assuming the hourly trend of the solar radiation.
- **Scenario B or Probabilistic grid scenario.** In this case, a more realistic condition is modelled, according to data collected in two different years about sea wave, wind and solar radiation, and assuming for each source the condition that correspond to the maximal energy production.

In both scenarios, three operative conditions are considered:

- Case 0: P_{res} is 100% in service for every hour;
- Case 1: P_{res} is limited in order to allow the running of at least one synchronous generator;
- Case 2: P_{res} is in order to allow the running of at least two synchronous generators.

The trends of energy production from RES are modelled, considering the hourly energy demand in a typical summer week and in winter one. The transient stability is analyzed considering an imbalance due to the sudden load lack following a short circuit occurring at bus 65 located at two kilometers from the power plant. The fault occurs at the simulation time “1 second” [303].

The inertia constant of the running synchronous machines is determined according to Eq. V.20:

$$T_N = \frac{\sum_1^n T_i \cdot A_{n,SG,i}}{\sum_1^n A_{n,SG,i}} \quad V.20$$

where $A_{n,SG,i}$, $P_{nom,sg,n}$ and T_i are, respectively, the nominal apparent power and the inertia constant of the i -th running Synchronous Generator (SG) at the considered hour. To evaluate the number of active generators, the real daily operating plan of the diesel engines provided by the utility is considered.

Based on Eq. V.20 the hours corresponding to the maximum and minimum inertia constants of the power system are evaluated for the winter and summer weeks. For those hours, the Non-Synchronous Penetration Level (NSPL) is calculated [69], defined as the measure of the non-synchronous generation for the instantaneous simulated scenarios time, expressed in percentage according to Eq. V.21:

$$NSPL = \frac{P_w + P_{pv} + P_{sw}}{P_w + P_{pv} + P_{sw} + P_{syn}} \quad V.21$$

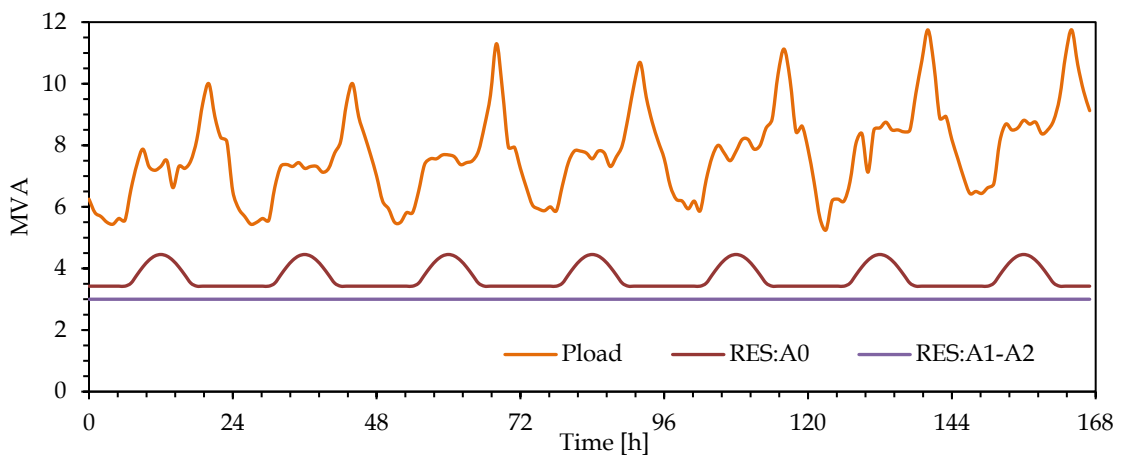


Figure V.40 Scenario A: Typical load profile at different RES penetrations in a summer week

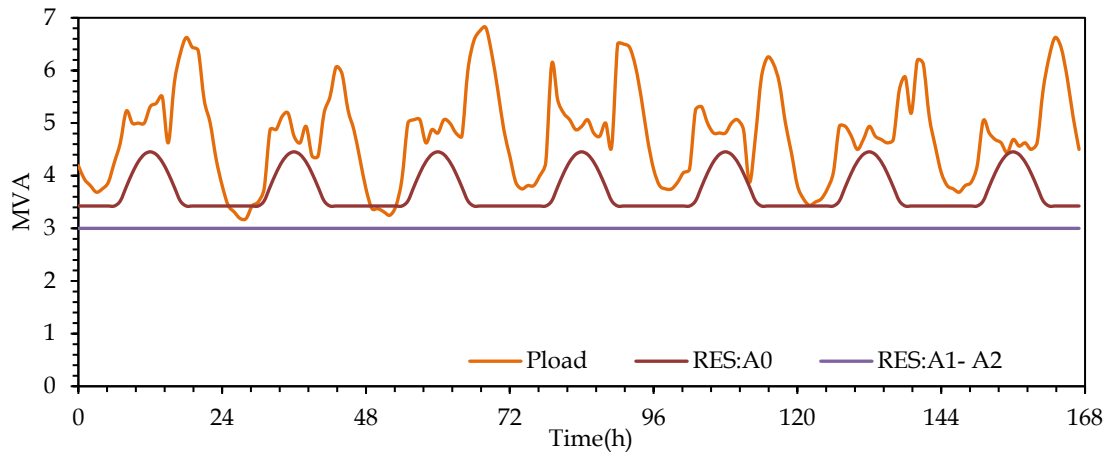


Figure V.41 Scenario A: Typical load profile at different RES penetrations in a winter week

According to the scenario A, Figure V.40 and Figure V.41 show the trends of RES production in the three different level of RES penetration, during a summer week and a winter one, respectively.

Similarly, according to the scenario B, Figure V.42 and Figure V.43 show the trends of RES production in the three different level of RES penetration, during a summer week and a winter one, respectively.

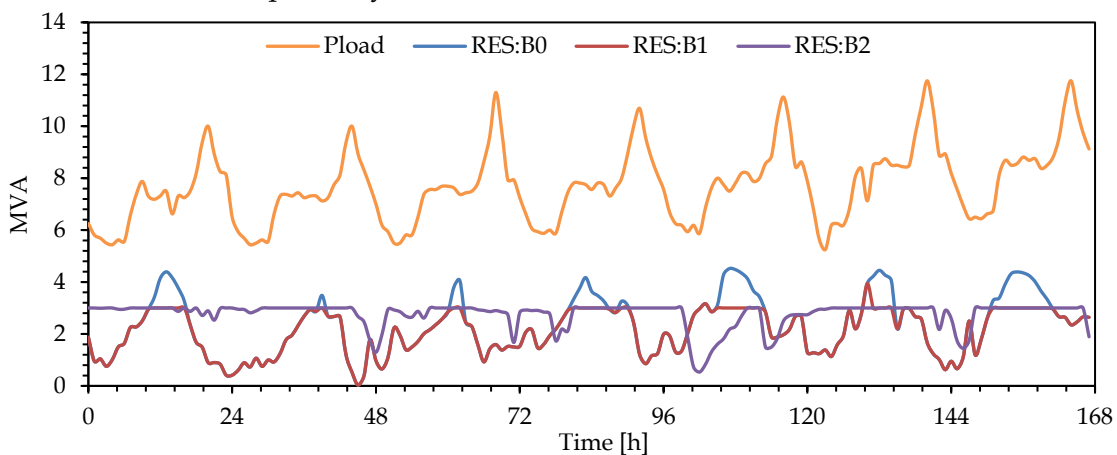


Figure V.42 Scenario B: Typical load profile at different RES penetrations in a summer week

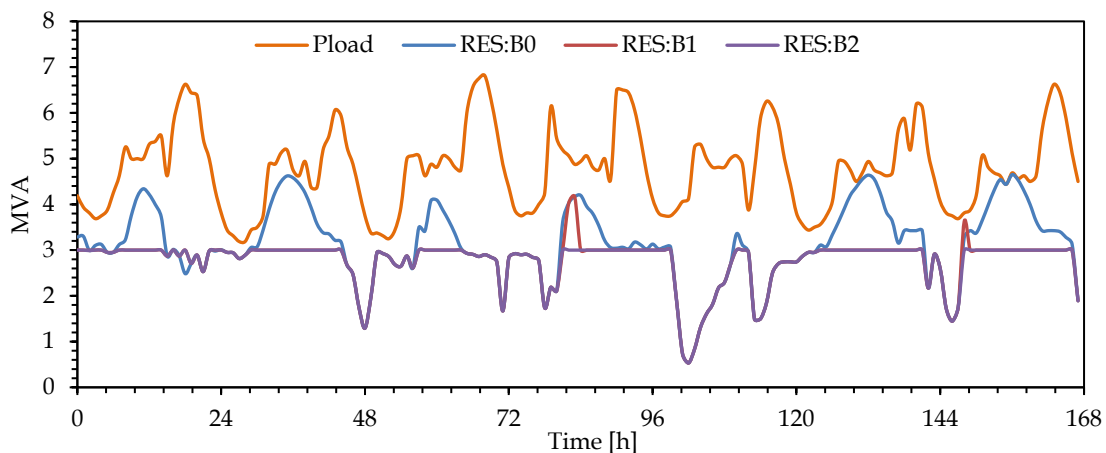


Figure V.43 Scenario B: Typical load profile at different RES penetrations in a winter week

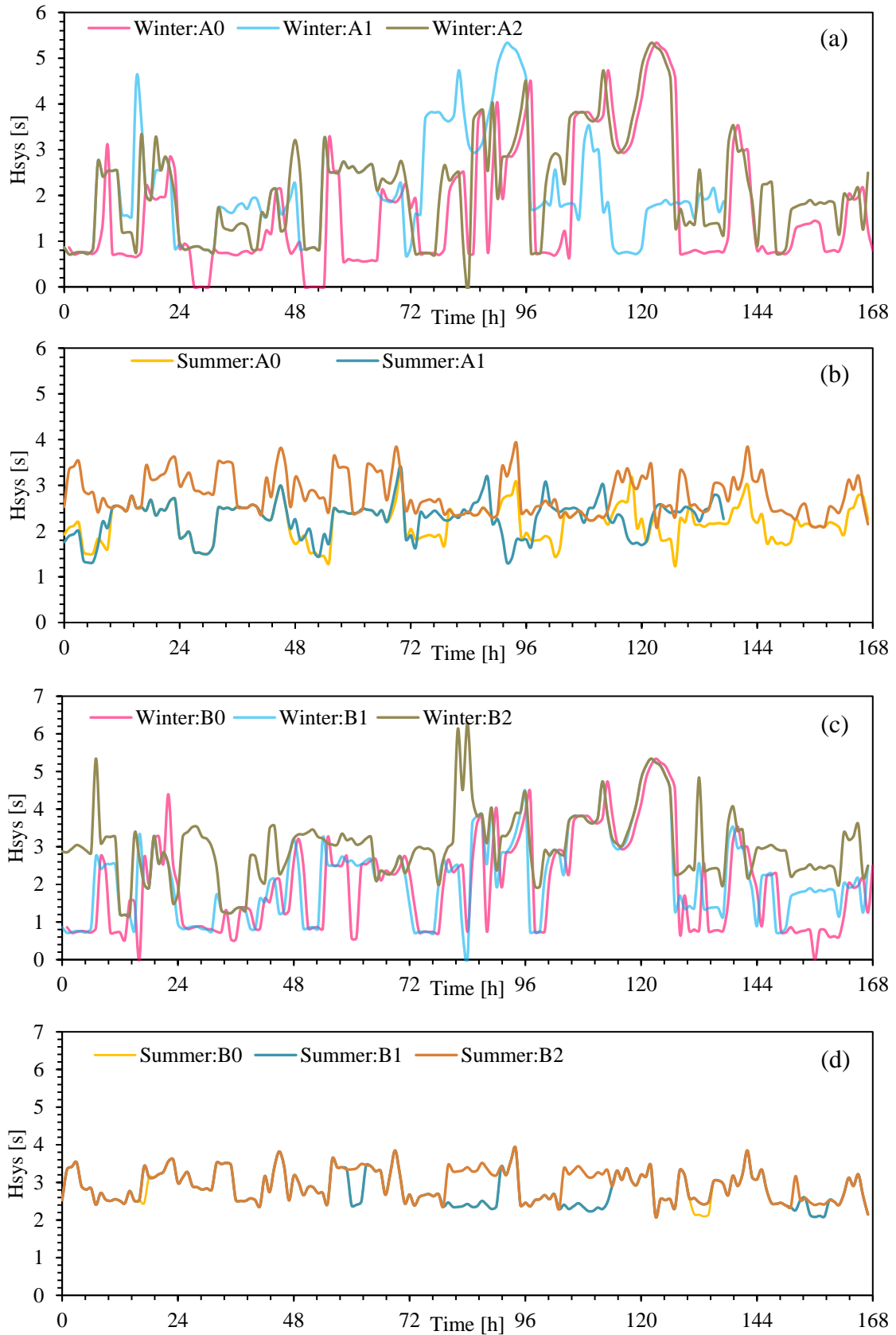


Figure V.44 Trend inertial response in RES presence: (a) Scenario A, winter; (b) Scenario A, summer; (c) Scenario B, winter; (d) Scenario B, summer.

Considering the energy production from RES and the load profiles in the previous figures, the inertia of the system is evaluated hour by hour for the two typical weeks, by using Eq. V.21. All results are reported in Figure V.44.

Table V.34 reports 24 different power system states corresponding to the minimum and maximum inertia of the system, evaluated according to Eq. V.20. Each state is identified by a code, whose structure is the following

$$\#code = x_1x_2.x_3.x_4$$

where:

x_1 indicated the scenario (A or B).

x_2 indicates the running condition (0, 1, 2)

x_3 indicates the level of the inertia constant of the system (1 for minimum; 2 for maximum).

x_4 indicates the season (1 for summer and 2 for winter).

In Table V.34, P_{CPP} is the percentage of the load provided by synchronous generators in comparison with the rated power of the active generators and CPP indicates the active synchronous generators.

Table V.34 Simulated events overview.

Sim. #	P_{CPP}	CPP	NSPL	T_N [s]	Sim. #	P_{CPP}	CPP	NSPL	T_N [s]
A0.1.1	82%	G4	58%	0.54	B0.1.1	64%	G5-G7	26%	0.91
A0.1.2	0%	-	100%	0.00	B0.1.2	0%	-	100%	0.00
A0.2.1	46%	G4-G8	43%	1.48	B0.2.1	56%	G4-G7-G8	13%	1.71
A0.2.2	0%	-	100%	0.00	B0.2.2	8%	G8	86%	2.34
A1.1.1	70%	G7	54%	0.57	B1.1.1	64%	G5-G7	26%	0.91
A1.1.2	58%	G3	74%	0.30	B1.1.2	11%	G3	75%	0.31
A1.2.1	50%	G4-G8	38%	1.48	B1.2.1	56%	G4-G7-G8	13%	1.71
A1.2.2	7%	G8	87%	2.34	B1.2.2	37%	G8	34%	1.29
A2.1.1	66%	G3-G7	45%	0.67	B2.1.1	64%	G5-G7	26%	0.92
A2.1.2	59%	G1	20%	0.92	B2.1.2	59%	G3-G5	55%	0.51
A2.2.1	73%	G7-G8	45%	1.70	B2.2.1	56%	G4-G7-G8	13%	1.71
A2.2.2	18%	G1-G8	59%	2.75	B2.2.2	17%	G1-G8	61%	2.75

For the 24 cases in Table V.34, a dynamic stability analysis is performed by using Neplan. The disturbance occurs at $t = 1$ s and the observation window is set equal to 10 seconds. The grid frequency oscillation is represented for the 24 cases in Figure V.45.

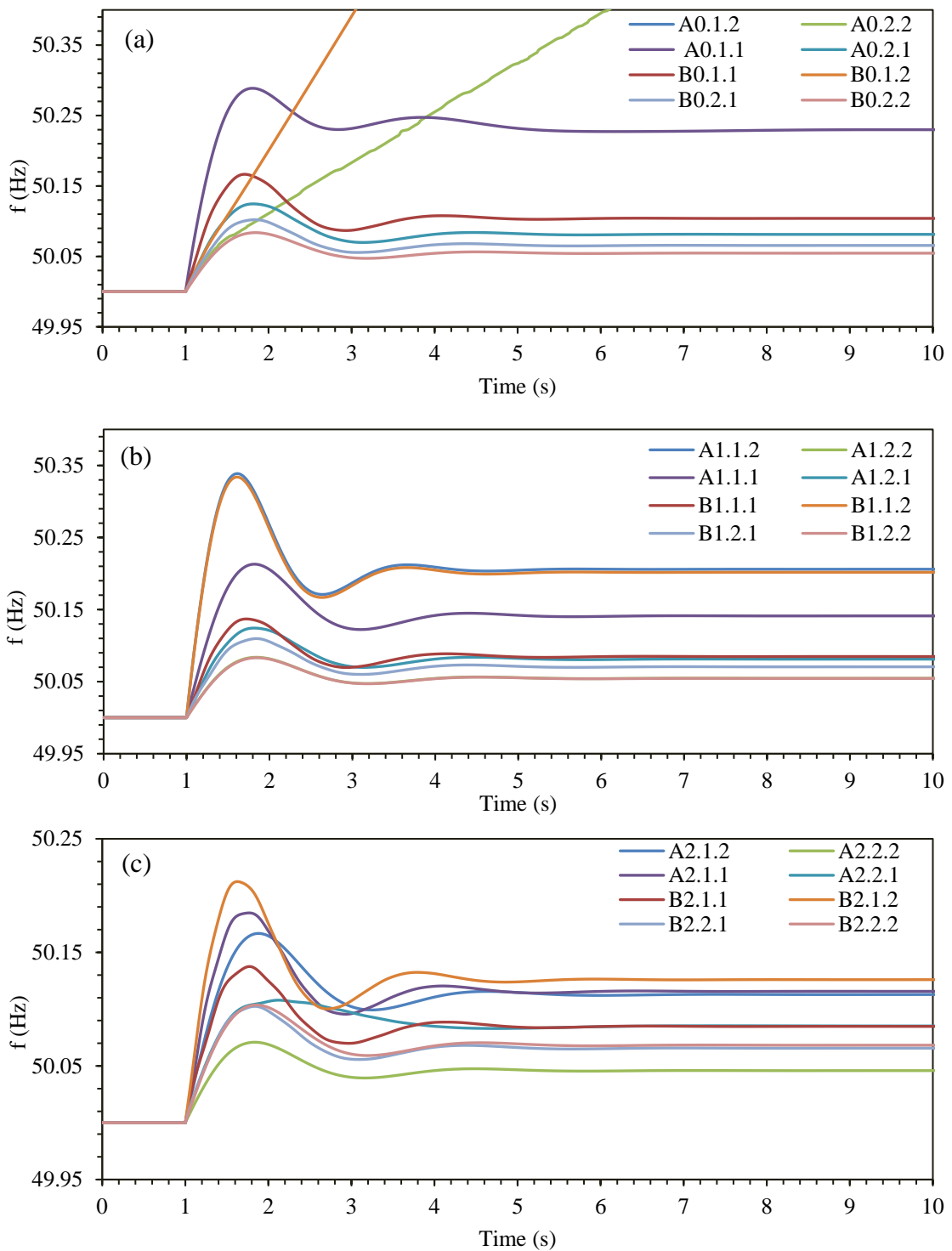


Figure V.45 Grid frequency in the case of 3-phase short-circuit in the grid: (a) Scenarios A0 and B0, (b) Scenarios A1 and B1 and (c) Scenarios A2 and B2.

The trends in Figure V.45 show that:

- in all cases the grid frequency shows a typical trend occurring in the case of load loss. In 21 out of 24 cases the frequency initially increases reaching a peak in less than one second due to the unbalance between generation

and load. Then, it decreases again reaching a new steady-state value due to the action of the speed regulators of the diesel generators;

- the frequency has greater oscillations when RES contribution is greater than 28% of the synchronous generation and when only one active synchronous generator is working. This is mainly due to lower values of both the system inertia and the primary regulation reserve of the generating systems depending only on the synchronous generators;
- in 21 out 24 cases, the system reaches a new stable condition in less than 10 seconds, therefore in a time interval totally compatible with the grid code. The new conditions area far from the upper frequency limit allowed for the isolated grid (51.5 Hz);
- the system is stable in 21 cases, with limited deviation from the rated frequency, while the upper limit frequency relays (set to 51.5 Hz) detach the synchronous generators in three cases: A0.1.2, A0.2.2, B0.1.2.

For a further analysis of the dynamic stability issue, the rate of change of frequency (RoCoF) is introduced, according to Eq. V.22:

$$RoCoF = \left. \frac{df}{dt} \right|_{t=0+} = \frac{f_o P_k}{2 \sum_{i=1}^n T_i A_{n,SG,i}} \quad V.22$$

where f_o is the rated frequency and P_k is the power disturbance in the grid (in the examined case the detachment of load due to the 3-phase short-circuit). Although in Lampedusa RoCoF protections are not present, the analysis is presented for its theoretical value. The analysis gave the following results:

- 5 cases have a RoCoF below 2%;
- 6 cases have a RoCoF between 2% and 3%;
- 13 cases have a RoCoF above 3%.

Therefore, 21 of the examined cases are acceptable from the point of view of grid stability. In presence of RoCoF protections, 13 of the examined cases should be further analyzed in order to ensure that, in every possible disturbance event, the system could maintain its stability considering the energy production from RES in the scenarios above investigated without the intervention of the RoCoF relays.

V.5 The introduction of energy flexibility in Pantelleria through the modulation of desalination plant and the production of domestic hot water

In this case study, the benefit of the modulation of the desalination plant and Domestic Hot Water (DHW) production is investigated in order to increase the energy efficiency of power generation. As case study, the energy system of Pantelleria island was accurately examined before the modelling phase, in order to identify the key points to be addressed. The study was divided in two main groups of simulations:

- the first group considers only the desalination unit flexibility service to be integrated with the local diesel generator units;
- the second group accounts also for the installation of new equipment and the flexibility of DHW storages.

The reason behind this separation was to investigate the potential benefit deriving from only new management logics (flexibility of the desalination unit activation) and from the use of new components.

The case of study below reported was published in the paper “**Flexibility Services to Minimize the Electricity Production from Fossil Fuels. A Case Study in a Mediterranean Small Island**” in the journal *Energies* [33].

V.5.a The case study of Pantelleria

Pantelleria is a small Italian island, located in the Mediterranean Sea at 100 km southwest of Sicily and 65 km east of the Tunisia, as shown in Figure V.46 [311].

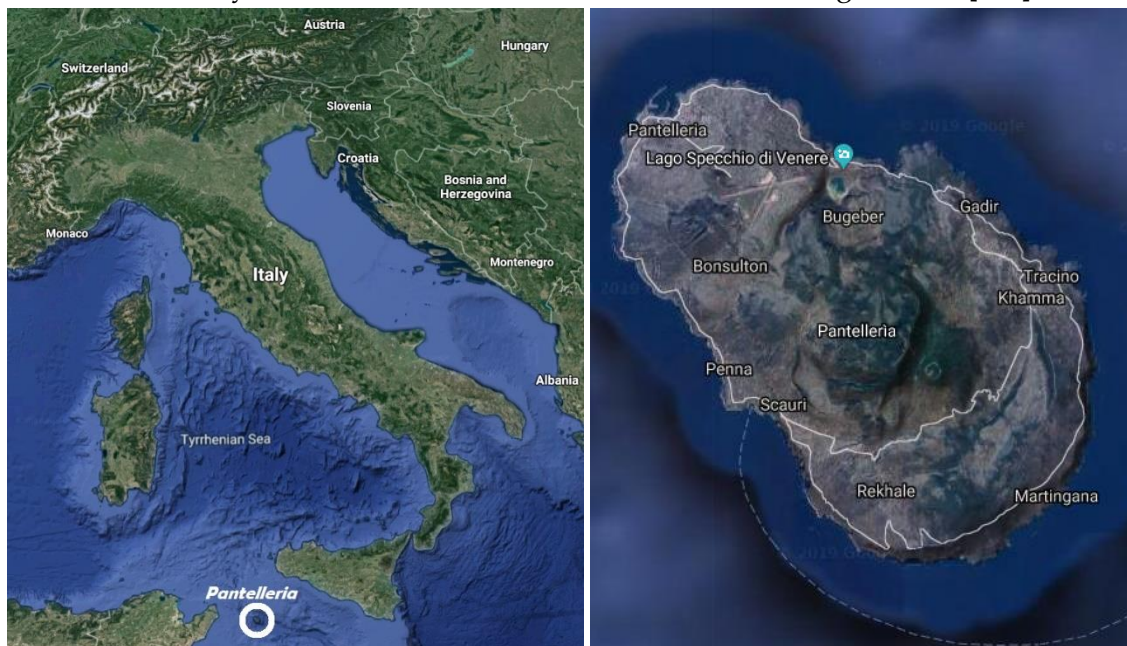


Figure V.46 Position and satellite view of Pantelleria.

It covers a surface of 84.5 km², giving hospitality to a population of 7759 inhabitants. However, this value varies during the year, since this island shows a relevant tourism, that increases the population during summer up to 10,483.

This island, characterized by mountainous territory, has a volcanic origin, confirmed by the presence of hot springs and fumaroles [312].

From 1999 most of the island is classified as reserved area, thanks to the establishment of the natural oriented reserve of Pantelleria [313]. Thus, there are specific restrictions in the local building regulation plan to avoid anthropic changes to the landscape. Indeed, the installation of PVP and wind plants requires the realization of an environmental impact assessment, however the installation of Solar Thermal Collector (STC) and PVP is forbidden on traditional local buildings, known with the term “Dammusi” [314].

As a consequence, the electricity production is based on diesel engines, installed inside the local power plant of the private company S.MED.E. Pantelleria S.p.A.. Nevertheless, as introduced before, Pantelleria is inserted in the list of small islands obliged to achieve environmental targets, according to the Ministry Decree 14 February 2017 [240]. In detail, it is required the installation of 2,720 kW of electrical RES plants and 3,130 m² of STC.

The installed RES mix is currently far to achieve these targets, because there are only two small wind turbines (total power 32 kW) and many PVP (449 kW). Thus, the RES contribution in the power generation is lower than 1%. About the production of DHW from RES, there are 20.8 m² of STC [34].

Like the other Italian small islands, the local power plant is largely oversized, if compared to the average demand, because the annual trend of the energy demand is affected by a relevant peak during summer (about 8 MW) and a minimum in middle seasons (about 2 MW). Consequently, the capacity factor of the power plant is low (equal to 0.167). The annual energy production is about 36.5 GWh (2018), with a minimum in middle seasons (2.5 GWh/month) and a maximum in August (4.6 GWh/month).

Table V.35 Generation groups in Pantelleria

Generation units	Rated power [kW]
Diesel generator 1	1,250
Diesel generator 2	5,040
Diesel generator 3	3,070
Diesel generator 4	2,920
Diesel generator 5	3,089
Diesel generator 6	2,648
Diesel generator 7	1,760
Diesel generator 8	5,220
<i>TOT Diesel generators</i>	<i>24,997</i>
PV plants	449
Wind turbines	32
<i>TOT Diesel + RES generators</i>	<i>25,478</i>

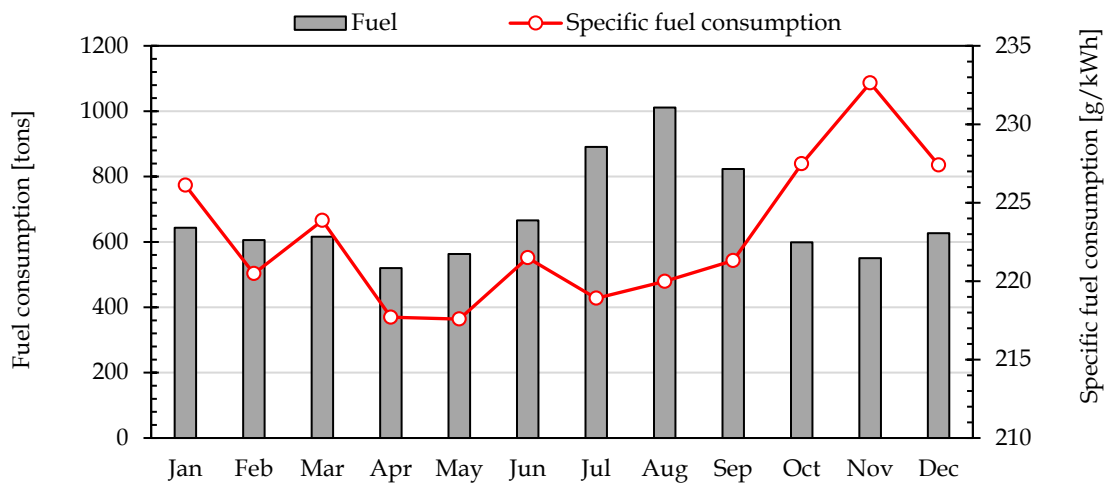


Figure V.47 Monthly fuel consumption and average specific fuel consumption

The total installed power in Pantelleria is described in Table V.35, where it is possible to confirm the limited installed power from RES. Figure V.47 reports the monthly fuel consumption and the average specific fuel consumption measured by the local producer in Pantelleria [33].

In the same way of the previous case studies, the Italian government recognizes an incentive to cover the additional costs for the electricity generation in Pantelleria in comparison with the National Unique Price. This incentive was equal to 0.2979 €/kWh in 2015, accounting for more than 9,030,840 € [315].

Pantelleria is supplied through a 10.5 kV electrical grid [316]. Due to the low voltage level, distribution losses are quite high, and outages are frequent. In 2017, the cumulated outages were 36.63 minutes per low voltage users [317].

About the annual electricity demand, Figure V.48 reports three reference years [33]. It is possible to observe the significant reduction of the energy production in the last years, due to the recent revamping of the desalination plants (in the end of 2014).

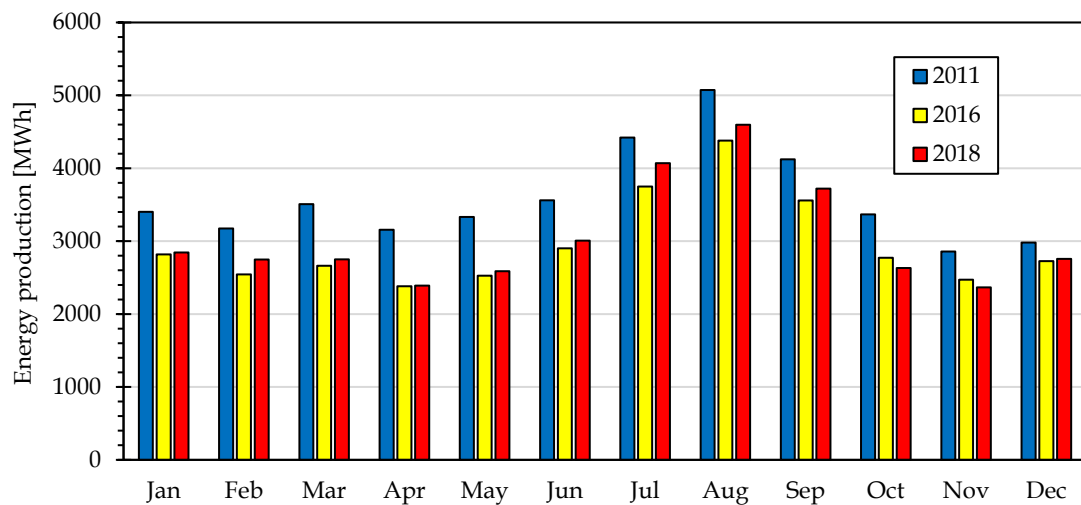


Figure V.48 Comparison of monthly electricity production in 2011, 2016 and 2018.

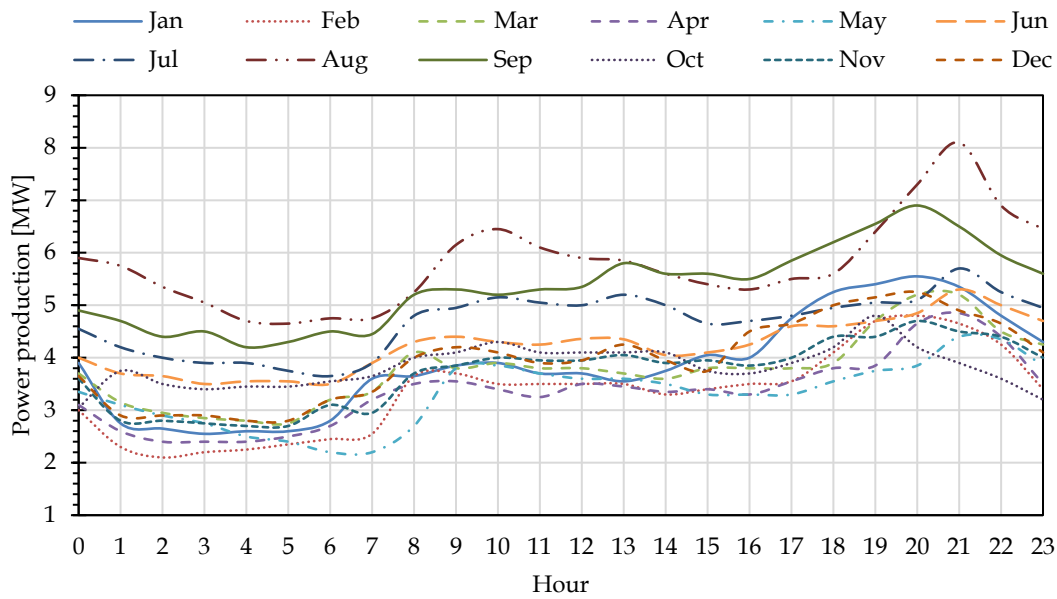


Figure V.49 Hourly electricity production in monthly typical days in 2016

In Figure V.49, the hourly trends of the electricity production from the local power plant are reported, considering one reference day per each month. Since the installed power from RES is limited, the same trend is assumed equivalent to the local energy demand, if the grid losses are neglected.

The trend of the annual energy demand by users is reported in Figure V.50a, while the 2016 share is reported in Figure V.50b. A relevant item is the residential sector, in fact, the sum of main and secondary residences corresponds to 37.20% of the local electricity demand in 2016. “Other Low Voltage users” is referred to services, offices, hotels and non-residential buildings (32.5% of the energy demand). The item “Medium Voltages users” (27.06%) is composed by desalination plants and the airport. Finally, the graph reveals the marginal share of the energy consumption for public lighting (3.23%).

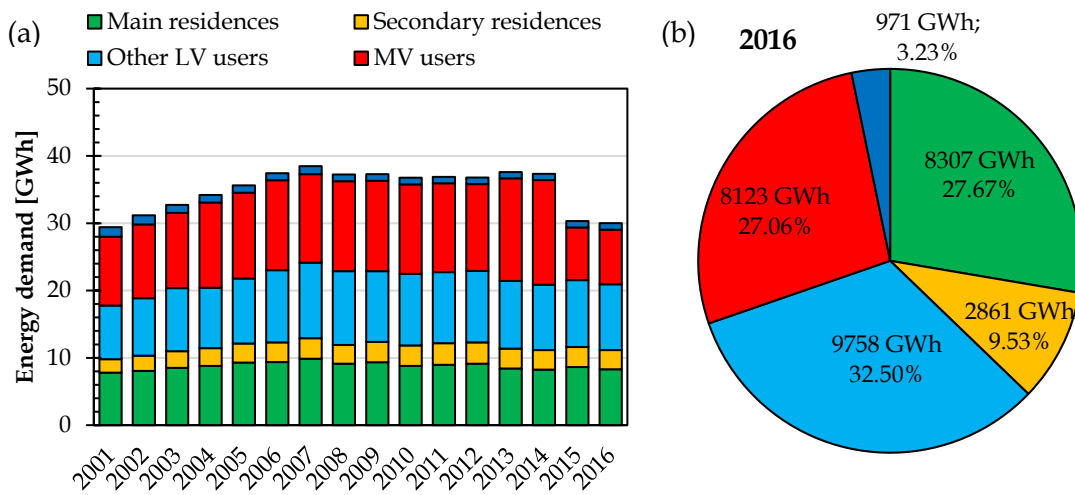


Figure V.50 Electricity consumptions by users: (a) Yearly trend; (b) 2016 share [80].

Desalination plants are big energy consumers. In detail, in 2018 their energy demand was equal to 3,300 MWh (about 10% of the whole island demand), used to produce about 870,000 m³ of freshwater.

Pantelleria is equipped with two desalination plants, named “Sataria” and “Maggiuluvedi” (by the name of areas where the plants are installed). After the recent replacement of desalination units, both plants are equipped with RO units.

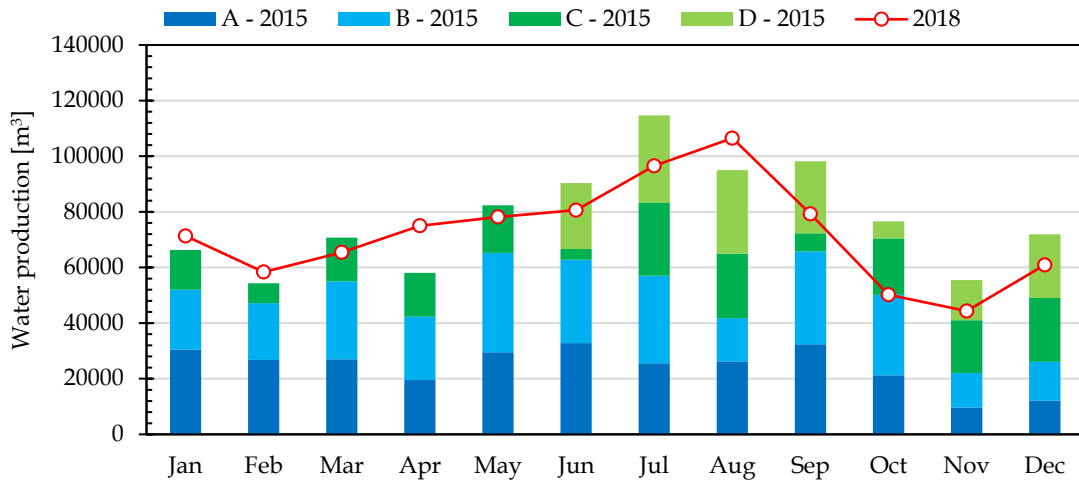


Figure V.51 Freshwater production in 2015 and 2018

Sataria plant has 4 RO units, each one having a rated capacity of 1200 m³/day of freshwater, using sea water as source, and requiring until 200 kW. The desalination plant is managed in order to run a different number of units according to the seasonal freshwater demand, ranging from 2 active units in winter until all 4 units in summer, as shown in Figure V.51.

From the desalination plant, freshwater is pumped into Kaffefi and Gelfiser reserves, each one having a capacity of 7000 m³ and located respectively at 262 and 371 m above sea level. In this way, thanks to the gravity force, freshwater is distributed into several other reserves until the final users [318].

Table V.36 Characteristic of water reserves in Pantelleria network

Locality	Altitude [m a.s.l.]	Capacity [m ³]
Kaffefi	262.0	7000
Gelfiser	371.5	7000
Zinedi	230.1	300
Sant'Elmo	117.8	850
Kuddia Bruciata	109.3	300
Lago	249.2	300
Russo	294.6	850
Runcuni di Pigna	267.2	300
Ex Vedetta	290.7	850
Arenella Vecchio	20.0	200
Arenella Nuovo	10.0	3500
Scauri	20.0	3500

The other desalination plant is installed in Maggiuluvedi. It is composed by a single RO unit, supplied with brackish water from the Valenza well. Freshwater is directly distributed to the local water network and the Arenella reserve. In Table V.36 the detail of the island water capacities is reported [318].

According to the owner of desalination plants in Pantelleria, *SOFIP S.p.A.*, the following case studies consider the possibility to modulate the freshwater production only in Sataria plant, in order to find the best schedule for the desalination plant to increase the average efficiency of the diesel engines and produce economic and environmental benefits, thanks to the reduction of fossil fuel consumption. Furthermore, during an interview, *SOFIP S.p.A.* stated that Sataria plant is equipped with a 5,000 m³ capacity storage, thus this value was adopted in the simulations.

A focus on the residential energy consumption, representing about 37% of the total electricity demand, is given in Figure V.52. Among the main loads in the residential sector, the production of DHW has the main role (31.1% in 2011), corresponding to 3.8 GWh/y, since the production of DHW in Pantelleria is commonly covered by electrical resistance boilers [319]. The annual trend of the primary energy demand for DHW production is reported in Figure V.53.

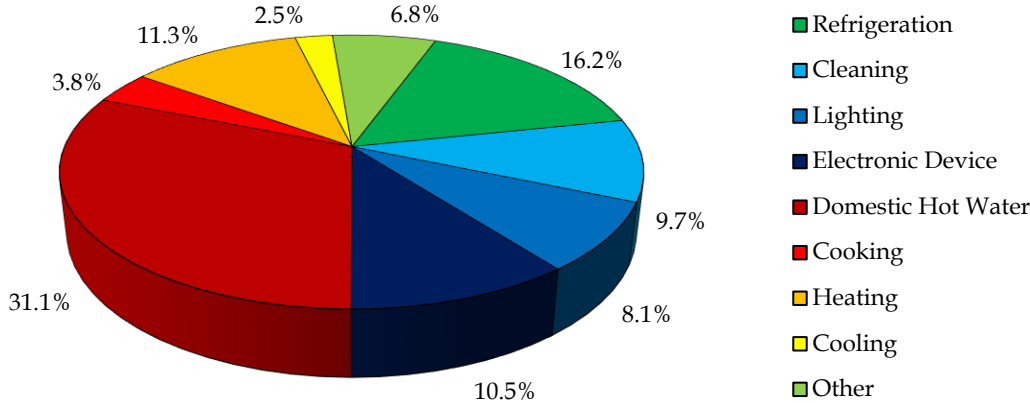


Figure V.52 Share of electricity consumption in residential sector by main loads, in 2011

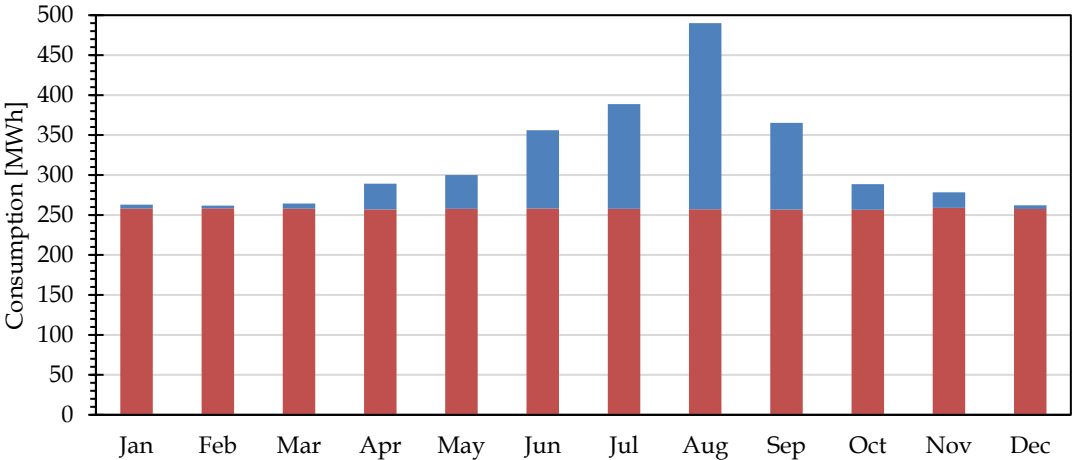


Figure V.53 Annual trend of electricity consumption for DHW in residential sector

V.5.b Modulation of desalination plant

The main goal of this study is to identify the optimal combination of components (synthesis stage), their optimal sizes (design stage) and their optimal operating schedule (operation stage) in order to minimize the annual operative costs, satisfying the energy demand in Pantelleria. The AS IS scenario is evaluated, by considering the existing layout of the energy systems (AS-IS scenario), based on diesel generators (DG), a desalination plant (DES), a freshwater storage (WSS), several heat pumps (HP) for the indoor climatization and distributed storages (HWSS) for DHW production (see Figure V.54a). As first step, the flexibility of desalination units was investigated in the TO-BE scenario 1 (Figure V.54b), assuming the same components of the AS-IS scenario. Finally, the installation of PVP, STC and electrical storage (ESS) was analyzed in the TO-BE scenario 2 (Figure V.54c).

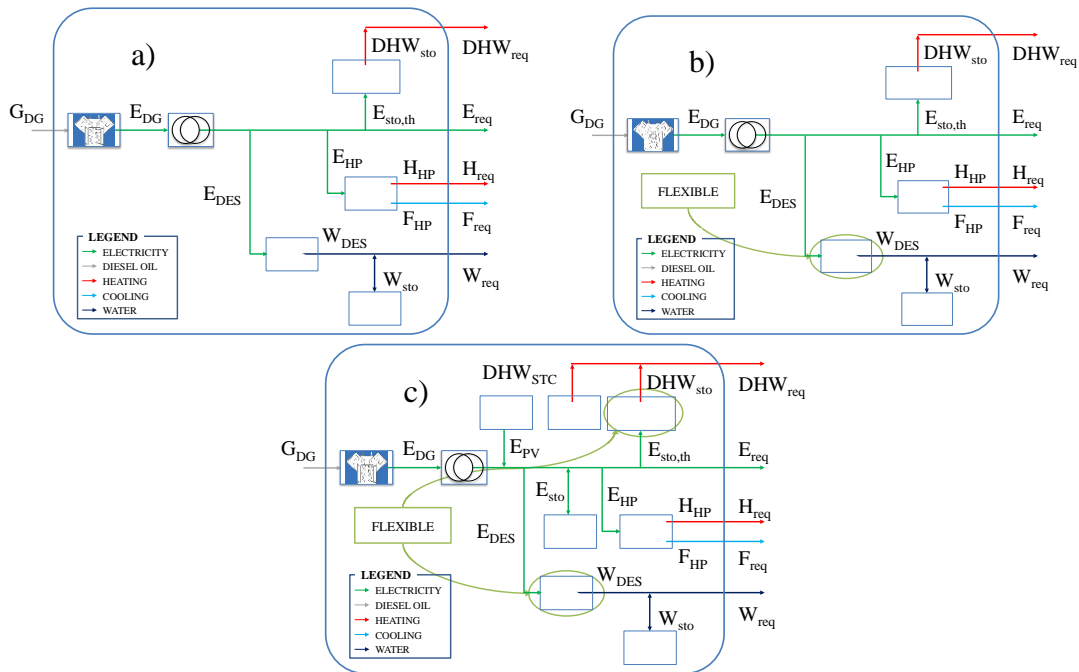


Figure V.54 Scheme of the energy system in Pantelleria: (a) AS-IS scenario; (b) TO-BE scenario 1; (c) TO-BE scenario 2.

An energy hub optimization model was implemented in *MATLAB*, in order to find the best combination of existing and new components from an economic point of view, minimizing the annualized installation and the operating costs.

The model considers various aspects related to the Pantelleria's energy system, which was deeply analyzed before the modelling phase. Indeed, a preliminary analysis of the island allowed neglecting some aspects of the system, as electricity is not imported from mainland, and natural gas distribution or district heating and cooling systems do not exist. Furthermore, as space heating and cooling demands are mainly met through electricity, the estimation of the corresponding loads appeared to be superfluous, as they are already accounted for into the power demand supplied by diesel generators (data reported in Figure V.49). Being these components already installed, their sizing was also

neglected. Although also freshwater is provided through electricity, a different approach was adopted in order to evaluate the economic feasibility of flexibility service. This approach is based on storage systems (municipality water storage), thus flexibility can be provided without the installation of new components. For these reasons, the total electrical demand of the island was divided into electricity, freshwater and DHW production [33]. The demand estimation was based on data provided by the owner of desalination plant (*SOFIP S.p.A.*) and the owner of the local power plant (*S.MED.E. Pantelleria S.p.A.*).

The mathematical model of the optimization problem is composed by energy balance equations, for each energy carrier and storage system and by relations describing each component's behavior [320], [321]. These equations were employed as equality and inequality constraints in the optimization model. The following assumptions were considered in the development of the mathematical model:

- objective function and constraints are represented by linear equations;
- energy balances are evaluated in steady state condition;
- system losses are evaluated only for components, while networks losses are neglected.

The variables of this problem can be categorized as synthesis, design and operation variables for components and energy flows from grids. Synthesis variables indicate whether a new component is selected or not, and there is one Boolean variable for electricity storage (δ_{ESS}). Four additional design variables were selected to indicate the number of PVP and STC units (N_{PV} and N_{STC}), and the size of electricity and water storages (S_{ESS} and S_{WSS}), since the possibility of rising the storage capacity was also investigated. It should be noted that PVP and STC design variables represent synthesis variables. Operation variables indicate, for each component and each timestep t , the amount of energy produced for by renewable technologies, the amount of energy absorbed or released for electricity and DHW storages, the amount of energy or water accumulated in the storages and Boolean variables indicating the state of electricity storage (since it cannot charge and discharge at the same time), and the number of desalination units. Operation variables for diesel generators are related to the load percentage of each of the 8 generators. Variables can be identified in the following equations as they are written in bold style.

Although most of components efficiencies were assumed to be constants to keep the linearity of the problem, the efficiency variation of diesel generators at partial load was considered, since it is higher than in other components. To reach this aim, the efficiency trend was simplified assuming four average values in four regions, as shown in Figure V.55.

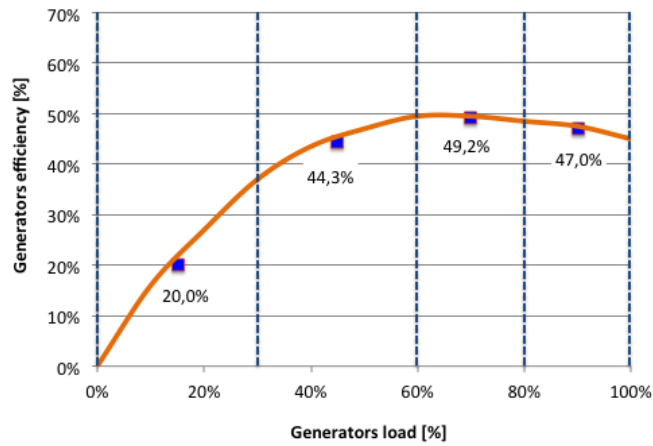


Figure V.55 Diesel generators efficiency vs. load estimated trend and piecewise averaging

Since the whole operating year was simulated assuming 12 monthly standard days, with an hourly detail, the total number of operating hours is equal to 288, with a total number of 12,674 continuous variables and 867 discrete variables. Considering lower and upper bounds of discrete variables, the search space of this problem is composed by $1.3 \cdot 10^{382}$ alternative combinations. Since this search space would lead to an unfeasible computational time, the problem was simplified through the following approach:

- first, twelve monthly optimizations were performed, both for TO-BE scenarios 1 and 2, based on standard day data with hourly detail, obtaining optimal solutions for synthesis, design and operation of each variable in each month. In this way, variables number was reduced to 1,058 continuous variables and 75 discrete variables, with $4.5 \cdot 10^{38}$ combinations for each optimization. The results are then extended to the month duration;
- for TO-BE scenario 2, since the simulations involve the design of new equipment, the optimal size of each component assumed different values depending on the monthly demand. For this reason, the obtained results were combined by selecting the highest size of each equipment, obtaining a sub-optimal solution to the problem. Nevertheless, this result is very close to the optimal solution since the diesel generators operating costs are one order of magnitude higher than investment costs for new components.

The objective function can be expressed as the annualized cost related to the island energy production, given by the sum of operating cost for diesel generators and the investment costs for components (Eq. V.23). Investment costs were annualized through the Capital Recovery Factor (CRF) of the investment, whose formula is shown in Eq. V.24.

$$\min \left\{ C_{op,DG} \cdot \sum_{t=1}^{24} \sum_{j=1}^8 \left[\frac{E_{DG,j}(t)}{\eta_{DG,j}(t)} \right] + C_{PV} \cdot N_{PV} \cdot CRF_{PV} + C_{STC} \cdot N_{STC} \cdot CRF_{STC} + \right. \\ \left. + (C_{ESS} \cdot S_{ESS} + C_{ESS,0} \cdot \delta_{ESS}) \cdot CRF_{ESS} + C_{WSS} \cdot (S_{WSS} - S_{WSS,0}) \cdot CRF_{WSS} \right\} \quad V.23$$

$$CRF = \frac{i \cdot (1+i)^{UL}}{(1+i)^{UL} - 1} \quad V.24$$

where $C_{op,DG}$ indicates operating diesel oil supply costs, $E_{DG,j}$ is the rated power of the j -th diesel generator, $\eta_{DG,j}$ is the efficiency of the j -th diesel generator, C_{PV} , C_{STC} , C_{ESS} , $C_{ESS,0}$ and C_{WSS} are the installation costs for PVP, STC, ESS and freshwater storage, respectively, $S_{WSS,0}$ is the initial water storage capacity, i is the interest rate and UL is the useful life of each component.

Although these costs may be faced by different actors of the energy system (energy production company, DES owner, final customer), they were coupled in a unique objective function, since all the costs in the energy sector are always paid by the final users through their bills.

The average electricity storage price was modelled as a linear function, with the constant term being multiplied by the synthesis variable in order to neglect this term when ESS is not selected in the optimization. Maintenance costs were neglected in this study, as were the financial subsidies to energy efficiency and renewable energies.

To describe the system, balance equations for each energy flow and each timestep have been considered as constraints. Energy balance equations were imposed as equality constraints, referring to the scheme reported in Figure V.54, for electrical energy flows, DHW flows, electricity storage, DHW storage and freshwater storage, where symbols were already defined in the nomenclature:

$$E_{DG}(t) \cdot \eta_{TR} + E_{PV}(t) - E_{sto,ch}(t) + E_{sto,disch}(t) - E_{sto,th}(t) + \delta_{DES}(t) \cdot E_{unit} = E_{req}(t) + H_{req}(t) / COP_{HP} + F_{req}(t) / EER_{HP} \quad V.25$$

$$DHW_{STC}(t) + DHW_{sto,disch}(t) - DHW_{req,flex}(t) = 0 \quad V.26$$

$$E_{sto}(t+1) = E_{sto}(t) + \eta_{ESS,ch} \cdot E_{sto,ch}(t+1) - E_{sto,disch}(t+1) / \eta_{ESS,disch} \quad V.27$$

$$DHW_{sto}(t+1) = DHW_{sto}(t) \cdot (1 - \eta_{HWSS,loss}) + \eta_{HWSS,ch} \cdot E_{sto,th}(t+1) - \frac{DHW_{sto,disch}(t+1)}{\eta_{HWSS,disch}} \quad V.28$$

$$W_{sto}(t+1) = W_{sto}(t) + K_{DES} \cdot \delta_{DES}(t+1) \cdot E_{unit} - W_{req,flex}(t+1) \quad V.29$$

In detail, Eq. V.25 is the electricity flows balance, Eq. V.26 the DWH flows balance, Eq. V.27 the energy balance on the ESS, Eq. V.28 the energy balance on the HWSS and Eq. V.29 the mass balance on the WSS. COP_{HP} and EER_{HP} are the conversion coefficients from electricity to heating and from electricity to cooling, commonly known as Coefficient Of Performance (COP) and Energy Efficiency Ratio (EER), respectively. These parameters are indicated only to show the approach to the study, since the local Distribution System Operator provided the whole island electricity demand, including also consumptions related to air conditioning.

Further equality and inequality constraints, describing the behavior of each component, were imposed. Eqs. V.30 and V.31 limits the electricity production of PVP and the DHW production of STC up to the energy provided by the solar radiation, reduced by their efficiencies. Eqs. V.32, V.33 and V.34 impose the repeatability of daily or yearly storage systems cycles. Eqs. V.35 and V.36 are the constraints describing the flexibility service for DHW storages and desalination unit, respectively, since they set the sum of these variables flows equal to the daily requirement. Eqs. V.37 - V.43 are further constraints for the ESS, avoiding that the component is charged and discharged at the same time, imposing that a minimum amount of energy, known as depth of discharge (*DoD*), is constantly stored in the system, to guarantee a longer useful life, and linking synthesis and design variables. Eq. V.44 limits the amount of freshwater in the WSS to be up to the storage capacity.

$$E_{PV} \leq \eta_{PV} \cdot I_{sun} \cdot N_{PV} \cdot A_{PV} \quad V.30$$

$$DHW_{STC} \leq \eta_{STC} \cdot I_{sun} \cdot N_{STC} \cdot A_{STC} \quad V.31$$

$$E_{sto}(1) = E_{sto}(end) \quad V.32$$

$$DHW_{sto}(1) = DHW_{sto}(end) \quad V.33$$

$$W_{sto}(1) = W_{sto}(end) \quad V.34$$

$$\sum_{t=1}^{24} DHW_{req,flex,j}(t) = DHW_{req,j,day} \quad V.35$$

$$\sum_{t=1}^{24} W_{req,flex,j}(t) = W_{req,j,day} \quad V.36$$

$$E_{sto,ch}(t) \leq \delta_{ESS,ch}(t) \cdot Q_{ESS} \quad V.37$$

$$E_{sto,disch}(t) \leq \delta_{ESS,disch}(t) \cdot Q_{ESS} \quad V.38$$

$$\delta_{ESS,ch}(t) + \delta_{ESS,disch}(t) \leq 1 \quad V.39$$

$$DoD \cdot S_{ESS} \leq E_{sto}(t) \leq S_{ESS} \quad V.40$$

$$E_{sto,ch}(t) \leq S_{ESS} \cdot (1 - DoD) \quad V.41$$

$$E_{sto,disch}(t) \leq S_{ESS} \cdot (1 - DoD) \quad V.42$$

$$S_{ESS} \leq \delta_{ESS} \cdot Q_{ESS} \quad V.43$$

$$W_{sto}(t) \leq S_{WSS} \quad V.44$$

The mathematical model depends on real and integer variables, where real variables mainly indicate energy flows and integer variables were employed for the electricity storage, for the DES units and for the solar technologies design variables. All the equations in the model, both objective function and constraints, are linear functions. For this reason, a MILP (Mixed Integer Linear Programming) algorithm was adopted for

the solution of the optimization problem. In this way, an absolute optimum solution can be derived.

It is worth to mention that, in this study, the costs optimization is also oriented to the reduction of greenhouse gases emissions during the running phase of the system, since every action aims at reducing the diesel gas consumption. Indeed, the flexibility of DES and DHW storages, as well as the installation of an ESS, fill the valleys in the load diagram ensuring a smoother and more efficient operation of generators, while the introduction of renewable systems reduces the energy demand that the diesel generators have to fulfil.

Table V.37 Electricity demand in monthly standard days

Hour	Electricity demand [kWh]											
	Jan	Feb	Mar	Apr	May	Jun	Jul	Aug	Sep	Oct	Nov	Dec
00:00	3,532	2,598	2,783	2,094	2,573	2,954	3,274	4,509	4,038	2,647	2,853	2,710
01:00	2,382	1,895	2,213	1,597	2,321	2,641	2,961	4,344	3,834	3,347	2,069	1,960
02:00	2,281	1,696	2,014	1,299	2,131	2,601	2,879	3,944	3,533	3,098	2,055	1,952
03:00	2,182	1,796	1,920	1,264	1,972	2,449	2,784	3,662	3,640	2,997	2,001	1,970
04:00	2,232	1,846	1,871	1,279	1,722	2,499	2,716	3,293	3,328	3,047	1,965	1,854
05:00	2,231	1,946	1,819	1,352	1,631	2,489	2,476	3,248	3,433	3,047	1,973	1,862
06:00	2,432	2,046	2,264	1,561	1,418	2,453	2,375	3,399	3,632	3,147	2,349	2,264
07:00	2,840	2,146	2,426	2,150	1,322	2,854	2,625	3,502	3,470	2,953	2,196	2,406
08:00	2,532	3,248	3,175	2,496	1,746	3,255	3,536	3,969	4,023	3,218	2,795	3,015
09:00	2,718	3,296	2,861	2,545	2,819	3,386	3,690	4,751	4,185	3,495	2,896	3,256
10:00	2,790	2,986	2,963	2,966	2,864	3,269	3,901	5,064	4,010	3,697	2,951	3,150
11:00	2,575	3,038	2,871	2,604	2,653	3,176	3,910	4,693	4,234	3,498	2,854	2,935
12:00	2,561	3,098	2,870	2,555	2,438	3,314	3,819	4,496	4,285	3,496	2,854	2,999
13:00	2,415	3,096	2,784	2,519	2,439	3,285	3,926	4,462	4,735	3,593	2,951	3,305
14:00	2,615	2,791	2,658	2,394	2,338	2,986	3,740	4,207	4,685	3,693	2,801	3,009
15:00	2,925	2,769	2,605	2,416	2,153	3,050	3,390	3,993	4,733	3,343	2,849	2,804
16:00	2,865	2,920	2,639	2,292	2,141	3,191	3,451	3,894	4,634	3,292	2,776	3,552
17:00	3,635	3,096	2,681	2,545	2,147	3,543	3,546	4,111	4,974	3,493	3,158	3,709
18:00	4,120	3,696	2,783	2,651	2,414	3,558	3,673	4,193	5,337	3,793	3,813	4,059
19:00	4,438	4,298	3,639	2,696	2,742	3,716	3,775	4,997	5,533	4,393	3,835	4,239
20:00	4,723	4,398	4,440	3,517	2,838	3,988	3,828	5,927	5,837	3,793	4,135	4,511
21:00	4,421	4,248	4,469	3,696	3,249	4,441	4,428	6,854	5,438	3,493	3,928	4,145
22:00	3,871	3,846	3,769	3,254	3,204	4,141	3,981	5,622	4,888	3,193	3,834	3,906
23:00	3,375	2,998	3,529	2,480	2,689	3,841	3,696	5,051	4,533	2,793	3,431	3,349

Table V.38 DHW and freshwater demands in monthly standard days.

Month	DHW demand [kWh]	Freshwater demand [m ³]
January	8,470	2,300
February	9,325	2,100
March	8,515	2,100
April	9,661	2,500
May	9,677	2,500
June	11,849	2,700
July	12,537	3,100
August	15,827	3,450
September	12,203	2,650
October	9,342	1,600
November	9,239	1,500
December	8,463	1,950

Table V.39 Economic parameters [33]

Parameter	Value
Operating cost of diesel generators (diesel oil supply cost)	650 €/m ³
Investment cost of PVP system	527 €
Investment cost of STC	650 €
Investment cost of electrical storage	165 €/kWh
Investment cost of electrical storage	2974 €
Investment cost of water storage	450 €/m ³
Interest rate in energy sector	5%
Useful life of PVP system	25 years
Useful life of STC	15 years
Useful life of electrical storage	7 years
Useful life of water storage	25 years
Capital recovery factor of PVP system	0.071
Capital recovery factor of STC	0.096
Capital recovery factor of electrical storage	0.173
Capital recovery factor of water storage	0.071

Table V.40 Technical and environmental parameters [33]

Parameter	Value
Diesel generators efficiency at part load between 0% and 30%	20.0%
Diesel generators efficiency at part load between 30% and 60%	44.3%
Diesel generators efficiency at part load between 60% and 80%	49.2%
Diesel generators efficiency at part load between 80% and 100%	47.0%
Freshwater storage initial available capacity	5,000 m ³
Lower heating value of diesel oil	41.025 MJ/kg
Transformer efficiency	99%
Specific electricity consumption for freshwater production	4 kWh/ m ³
Electricity consumption per each desalination unit	200 kW
PVP system efficiency	16.25%
PVP occupied area per unit	1.6368 m ²
PVP maximum available area	16,000 m ²
Solar collector zero-loss efficiency	79.7%
Solar collector first order heat loss coefficient	3.18 W/(m ² K)
Solar collector second order heat loss coefficient	0.008 W/(m ² K ²)
Solar collector average efficiency	69.4%
Solar collector occupied area per unit	2.5235 m ²
Solar collector maximum available area	3,500 m ²
Electricity storage charging efficiency	97%
Electricity storage discharging efficiency	97%
Electricity storage depth of discharge	20%
Electricity storage upper bound size	100,000 kWh
DHW storage charging efficiency	95%
DHW storage discharging efficiency	100%
DHW storage self-discharge rate (thermal losses)	1%/h
Annual average solar radiation	5.02 kWh/m ²

The parameters employed for this study are technical parameters (efficiencies, capacity of existing equipment, average surface occupied by the PVP and STC units), economic parameters (installation or operating costs) and environmental parameters (solar radiation and greenhouse gases emissions). These parameters are reported from Table V.37 to Table V.40. The rated powers of the diesel generators were reported in Table V.35.

V.5.c Case study 1: Desalination unit flexibility

In this section, only the improvements deriving from the flexibility provided by the DES was assessed. Thus, it is assumed that the DES produces the same amount of freshwater that it would have produced, but the hourly operation schedule is changed, according to the MILP algorithm results. More specifically, since the eight diesel generators have higher efficiencies when the power output is between 60% and 80% of their rated powers, the optimization identifies, hour-by-hour, the optimal number of desalination units whose load, added to non-flexible load of the island, allows the maximum possible generator's efficiency. This is the most interesting case for the existing situation, since it doesn't involve the installation of new components. In order to evaluate this case, the variables related to PVP, STC, ESS and HWSS were set equal to zero in the model. The standard day trends of electricity consumption in May (minimum load, Figure V.56), January (average load, Figure V.57), and August (maximum load, Figure V.58) are provided, where only the optimization variables are reported, neglecting the fixed electrical load. Indeed, notwithstanding some tourists are already visiting Pantelleria in May, the additional electricity demand required for their consumption is much lower than the demand of the residential population during the heating season.

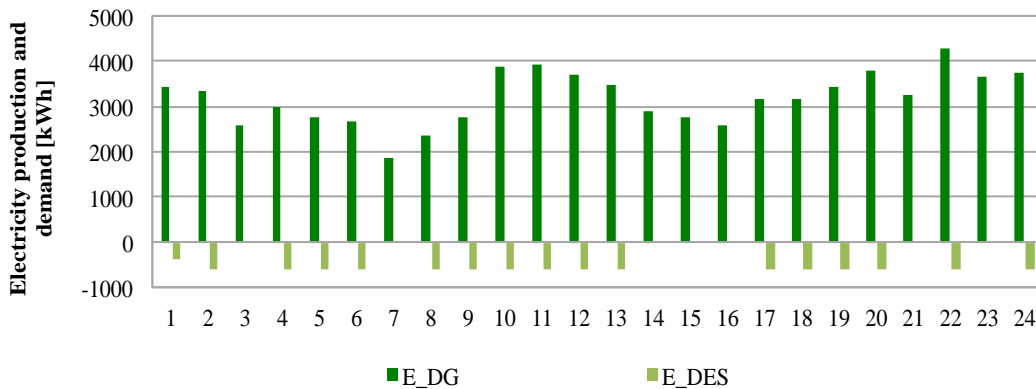


Figure V.56 Optimal daily schedule of diesel generators and desalination units in May (minimum load month) in case study 1.

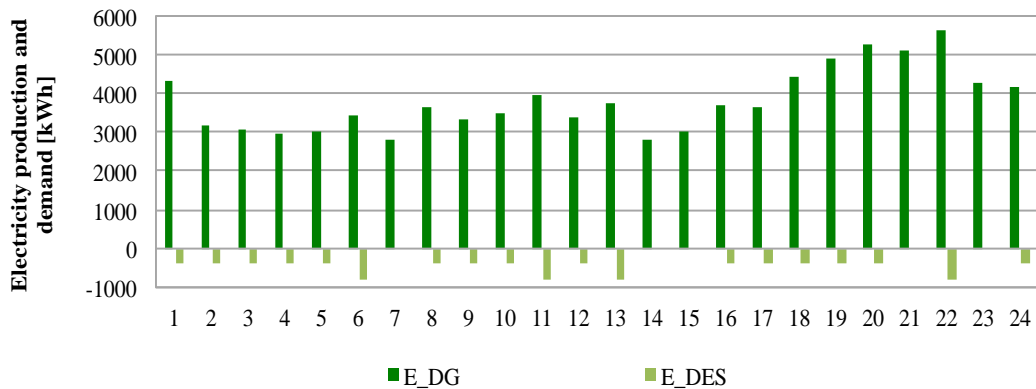


Figure V.57 Optimal daily schedule of diesel generators and desalination units in January (average load month) in case study 1

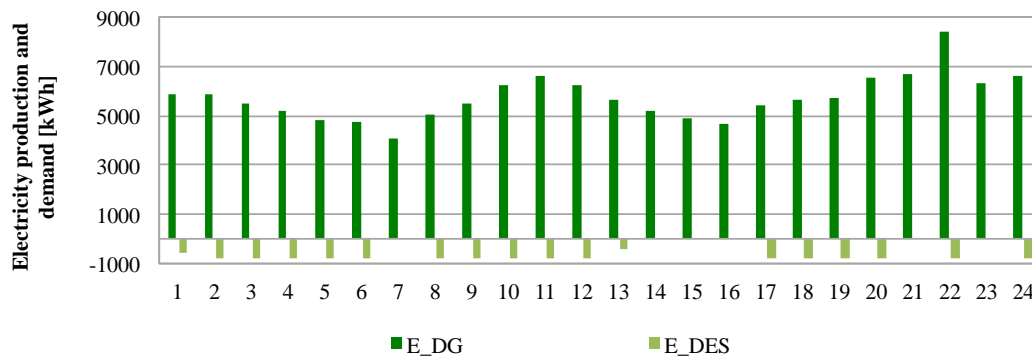


Figure V.58 Optimal daily schedule of diesel generators and desalination units in August (maximum load month) in case study 1.

From the previous graphs it is possible to see that the optimization identifies, as optimal solution, a variable production rather than a smooth operation for the generators, since in this way the generators operate with the maximum efficiency. The operation of desalination units is quite smooth, although in some hours of the day the plant has to be turned off.

Although it wasn't possible to compare the generators daily operation and the efficiency with the AS-IS scenario, the optimization allowed identifying a highly efficient schedule, with 97% of annual operating hours working with maximum efficiency. Figure V.59 shows the percentage of monthly detail.

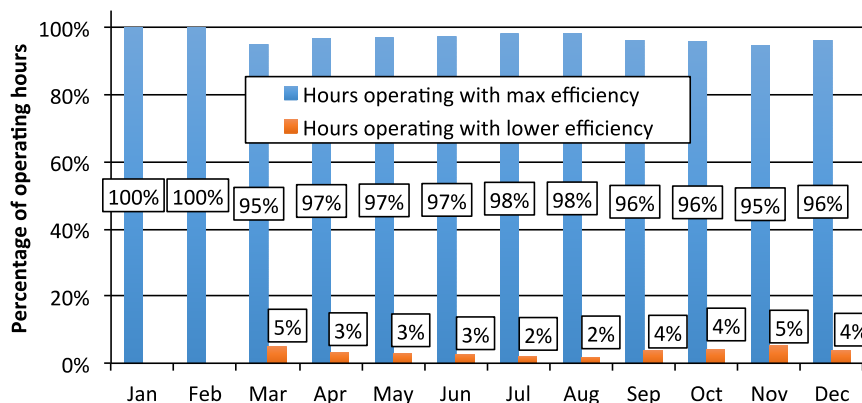


Figure V.59 Percentage of diesel generators operating hours inside and outside maximum efficiency region, in case study 1.

Since there are many possible generators combinations, a post-processing phase was performed, aimed at leveling the operating hours of the generators, since this is one of the operating criteria adopted by the company, preferring the use of the newest ones. The number of operating hours per each generator is reported in Table V.41.

Table V.41 Operating hours of diesel generators in case study 1.

	DG ₁	DG ₂	DG ₃	DG ₄	DG ₅	DG ₆	DG ₇	DG ₈
Rated power [kW]	1,250	5,040	3,070	2,920	3,089	2,648	1,760	5,220
Installation year	1976	2002	1990	1998	1981	1985	2009	2007
Operating hours [#]	1,324	1,832	1,565	1,825	1,643	1,758	2,716	2,974

Regarding the desalination units flexibility, the most important parameter to show is the amount of electricity that was deferred through the exploitation of the freshwater storage, that is reported in Figure V.60. This is the amount of electricity consumption related to the desalination of the water that was stored instead of being sent to the local distribution network. At annual level, about 274 MWh of electricity consumption was deferred, corresponding to 68,500 m³ of freshwater stored.

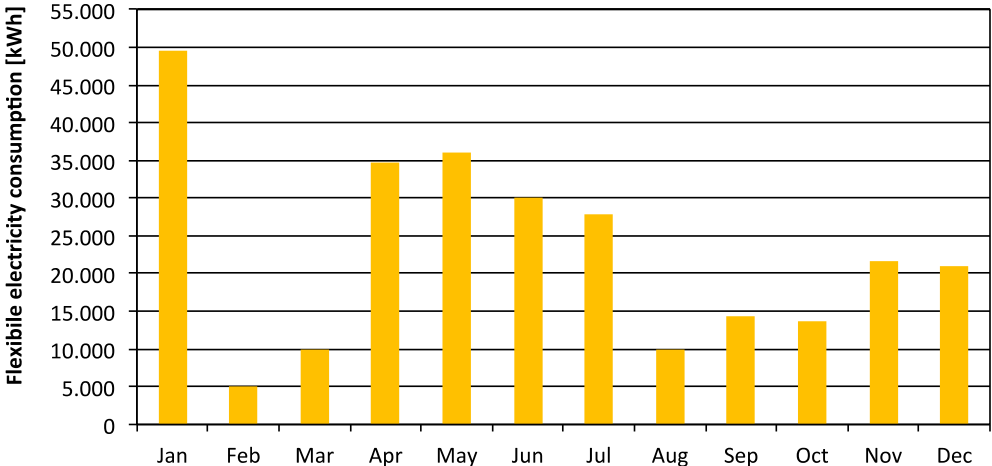


Figure V.60 Monthly DES flexible consumption in case study 1.

In this first case study, the cooperated scheduling of electricity generators and desalination units allowed to reach an annual economic saving equal to 1,360 k€ related to the diesel oil supply reduction, deriving from a very efficient operation of the generators. This value corresponds to more than the 20% of the yearly operating costs of the electrical plant related to the fuel supply. Although part of this saving would be given to the owner of the DES as a reward for the flexibility service, this value represents a high saving. In this way, the diesel oil consumption can be reduced from about 8,100 tons/year to about 6,300 tons/year. Considering an average emission of 0.267 CO₂ tons/MWh [87], the consequent saving emissions is equal to 5,385 ktons. Monthly economic and emissions reductions are provided in Figure V.61.

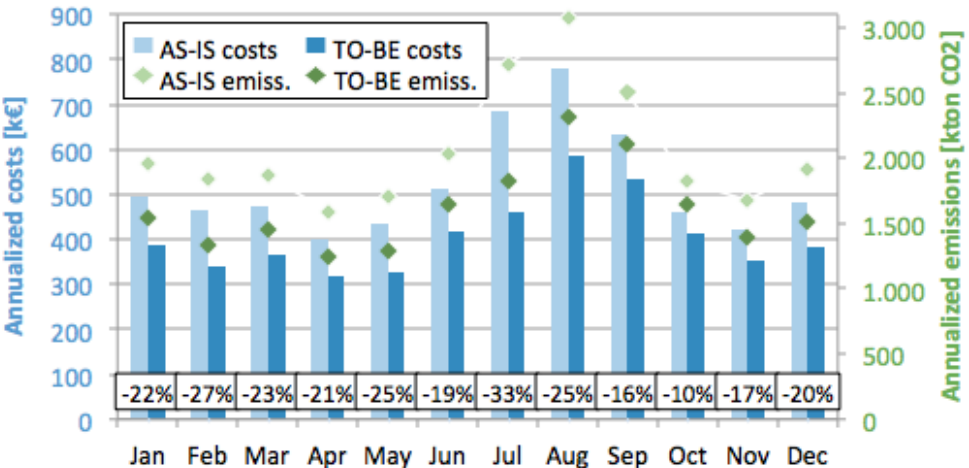


Figure V.61 Monthly economic and emission saving in case study 1.

V.5.d Case study 2: Desalination unit and DHW storages flexibility + equipment installation

In this section, the economic feasibility of the DES flexibility was assessed in a scenario where also renewable solar technologies and ESS were installed, pushed by the Ministry Decree 14 February 2017 [53]. Furthermore, since the existing literature showed that the GIWH (Grid Integrated Water Heating) technology can provide very profitable results with a limited investment, the flexibility of water heaters was also evaluated in this case study. The optimization results showed that the PVP plant is almost always profitable, since its size corresponds to the upper limit (16,000 m², corresponding to 9,775 kW) in every monthly optimization except for January, when no PVP plant is considered in the optimum, due to the combination of low solar radiation and medium electricity load. On the opposite, STC installation is optimal in every month and considered more convenient than the GIWH, that are rarely employed and only in November, December and January (92 hours during the year with a total energy produced of about 4,000 kWh). It is important to remark that the GIWH intervention is required in these months only because the STC size has reached its upper limit. The STC size is highly influenced by two factors: the average monthly solar radiation and the DHW requirement, as qualitatively shown in Figure V.62.

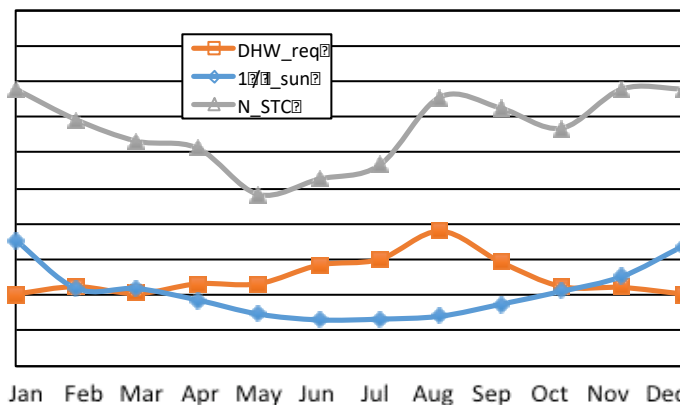


Figure V.62 STC size influence in monthly optimizations in case study 2.

Indeed, the surface needed to produce a unit amount of energy (proportional to the inverse of the solar radiation, blue trend), is lower in summer and higher in winter, while the DHW demand follows the touristic trend, with higher values in summer (orange trend). The combination of these two factors determines a variation in the optimal STC size, with the minimum value occurring in May (2,170 m²) and the maximum in November, December and January (3,500 m², equal to the upper bound), while in August the optimal size is 3,400 m² due to the high DHW demand. These results corroborate the economic convenience of the installation of RES supplied technologies in small islands, since they help to reduce the price of energy bills as well as “greening” the power system. The results also suggest that higher sizes would be profitable, but the landscape constraints in the island may conflict with this aspect. Given that the energy

production of the PVP system is low, if compared with the diesel generators contribution, the ESS is never selected, also because of the high installation cost.

The standard day trends of electricity consumption in May (minimum load, Figure V.63), January (average load, Figure V.64), and August (maximum load, Figure V.65) are provided. Comparing these trends with those related to case study 1, it is possible to see that, in general terms, the electricity load is slightly lower, thanks to the DHW that is almost totally supplied by the STC and the PVP plant that contribute, when available, to the reduction of the load covered by diesel generators. Furthermore, the DES operation is more discontinuous but with a higher number of units turned on at the same time. Furthermore, comparing the same day between case study 1 and 2:

- in May, a high fraction of the low energy demand is covered by the PVP during the central hours of the day, while the two trends are similar in the rest of the day;
- in January, the electricity production from diesel generators is very similar, since it is the unique month when the optimization doesn't select the PVP installation;
- the yearly peak, occurring at 10 pm in August, that is also the true yearly peak, as shown in Figure V.49, was reduced from 8,398 kW to 7,732 kW, also allowing minor power flow on the power grid, although this was not the aim of the optimization.

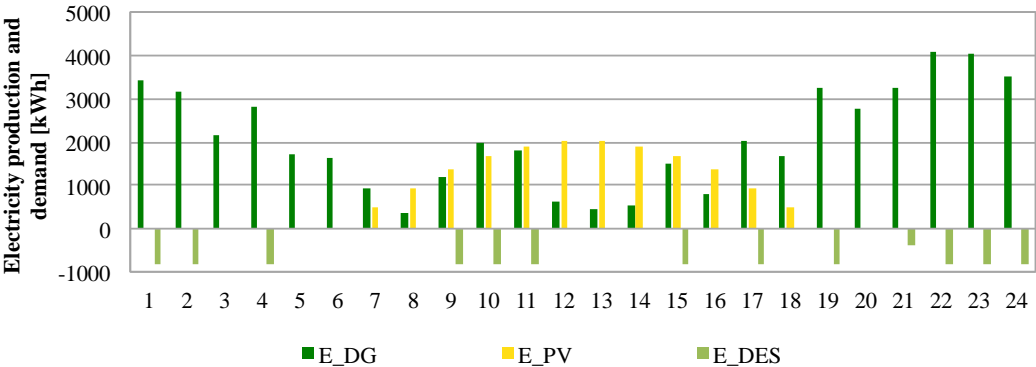


Figure V.63 Optimal daily schedule of diesel generators and desalination units in May (minimum load month) in case study 2.

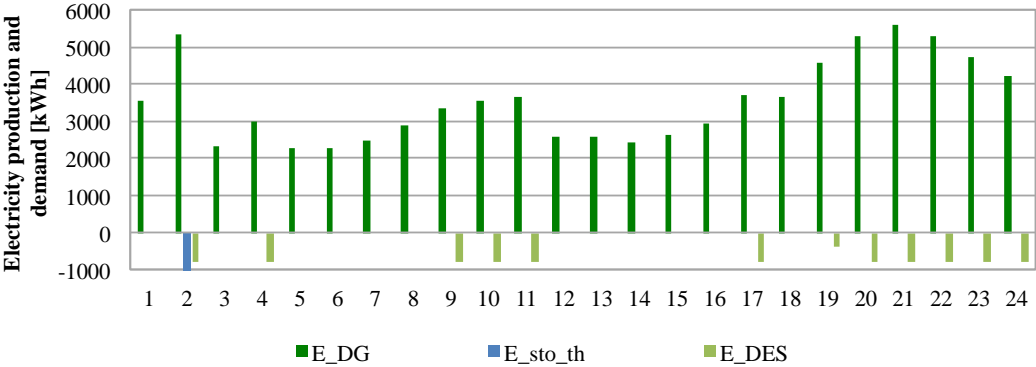


Figure V.64 Optimal daily schedule of diesel generators and desalination units in January (average load month) in case study 2.

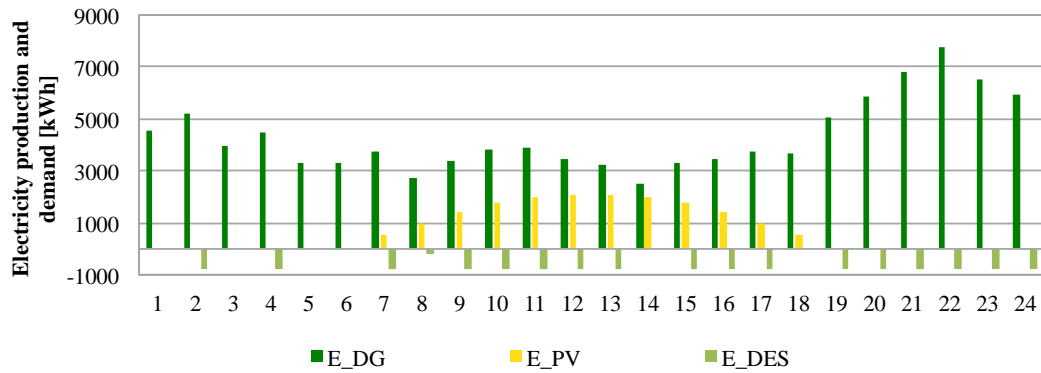


Figure V.65 Optimal daily schedule of diesel generators and desalination units in August (maximum load month) in case study 2.

The generators daily schedule results are also very efficient, although less than in the previous scenario, with 95,8% of annual operating hours working with maximum efficiency. The monthly detail is reported in Figure V.66, while Table V.42 shows the operation hours of the diesel generators during the year.

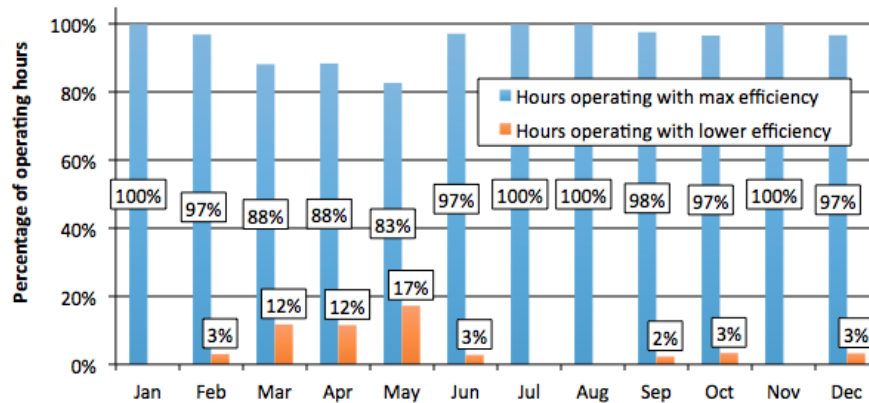


Figure V.66 Percentage of diesel generators operating hours inside and outside maximum efficiency region in case study 2.

Table V.42 Operating hours of diesel generators in case study 2.

	DG1	DG2	DG3	DG4	DG5	DG6	DG7	DG8
Rated power [kW]	1,250	5,040	3,070	2,920	3,089	2,648	1,760	5,220
Installation year	1976	2002	1990	1998	1981	1985	2009	2007
Operating hours [#]	1,645	1,497	1,004	1,075	1,020	1,393	2,160	2,618

Regarding the RES plants, since twelve monthly optimizations were performed, sizes change every month, as reported in Table V.43.

Table V.43 PV and STC in twelve monthly optimizations.

Month	A _{PV} [m ²]	A _{STC} [m ²]	Month	A _{PV} [m ²]	A _{STC} [m ²]
Jan	0	3500	Jul	16000	2539
Feb	16000	3111	Aug	16000	3399
Mar	16000	2841	Sep	16000	3258
Apr	16000	2753	Oct	16000	3005
May	16000	2170	Nov	16000	3500
Jun	16000	2362	Dec	16000	3500

Referring to the twelve optimizations on a monthly scale, the combined effect of the installation of RES plants and DES flexibility allows to reduce of about 25% the annual electricity load covered by the diesel generators and of about 40% the annual diesel oil consumption. Since these values are related to the optimization results, where different RES sizes were selected in every month, the energy and environmental saving would be higher by installing the maximum possible size of PVP and STC. Monthly detail of costs and environmental savings is provided in Figure V.67.

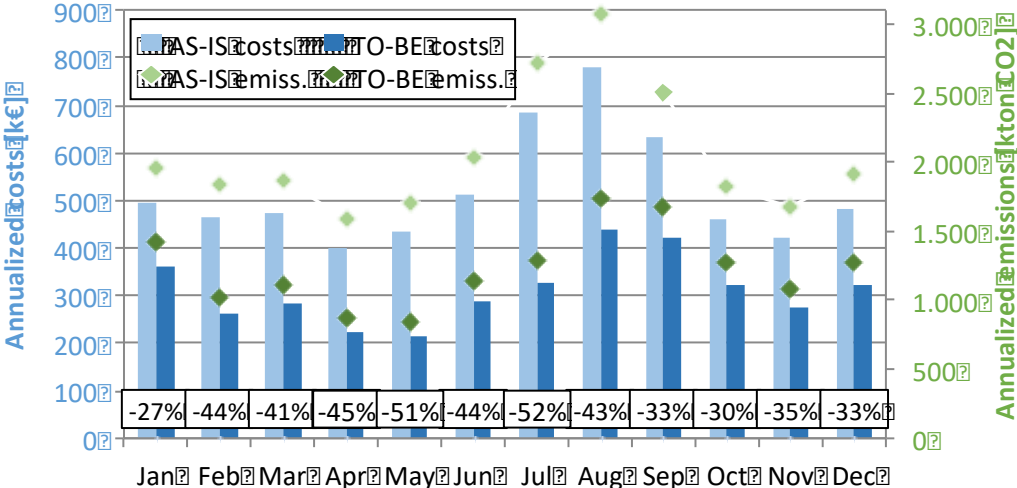


Figure V.67 Monthly economic and emission saving in case study 2.

In order to identify the most convenient size of PVP and STC from an economical point of view, a comparison between cost terms was performed. In detail, considering the results of the twelve optimizations, the operating saving due to the diesel oil supply reduction obtained with variable components sizes is equal to 2,506 k€/year. On the other hand, assuming to install the maximum sizes obtained by the monthly optimizations (16,000 m² of PVP and 3,500 m² of STC), the annualized installation cost would be equal to 453 k€/year (366 k€/year for PV and 87 k€/year for STC, respectively). Thus, assuming the installation of the maximum size of PVP and STC obtained by the twelve simulations equal to the upper bounds of the variables, would cause an investment cost that is about 5.5 times lower than the operating cost saving, providing a very profitable investment. Moreover, since PVP would produce electricity also in January, this energy would cause an additional operating reduction in terms of diesel oil saving, while the higher STC surface would not cause additional savings, since in months between February and October it is already able to cover the whole monthly demand.

V.6 Publications on this topic

- V. Franzitta, D. Curto, D. Milone, and D. Rao, "Assessment of Renewable Sources for the Energy Consumption in Malta in the Mediterranean Sea," *Energies*, vol. 9, no. 12, p. 1034, Dec. 2016.

- V. Franzitta, D. Curto, D. Rao, and A. Viola, "Hydrogen Production from Sea Wave for Alternative Energy Vehicles for Public Transport in Trapani (Italy)," *Energies*, vol. 9, no. 10, p. 850, Oct. 2016.
- V. Franzitta, D. Curto, D. Milone, and A. Viola, "The desalination process driven by wave energy: A challenge for the future," *Energies*, vol. 9, no. 12, pp. 1–16, Dec. 2016.
- V. Franzitta and D. Curto, "Sustainability of the Renewable Energy Extraction Close to the Mediterranean Islands," *Energies*, vol. 10, no. 4, p. 283, Feb. 2017.
- V. Franzitta, D. Rao, D. Curto, and A. Viola, "Greening island: renewable energies mix to satisfy electrical needs of Pantelleria in Mediterranean Sea," in *OCEANS 2016 MTS/IEEE Monterey*, 2016, pp. 1–6.
- A. Viola, D. Curto, V. Franzitta, and M. Trapanese, "Sea water desalination and energy consumption: A case study of wave energy converters (WEC) to desalination applications in sicily," in *OCEANS 2016 MTS/IEEE Monterey*, 2016, pp. 1–5.
- M. Trapanese, F. Raimondi, D. Curto, and A. Viola, "Evaluation of the wave energy density on the Sicilian coast," in *OCEANS 2016 - Shanghai*, 2016, pp. 1–4.
- V. Franzitta, D. Curto, D. Rao, and D. Milone, "Near zero energy island with sea wave energy: The case study of Pantelleria in Mediterranean Sea," in *OCEANS 2016 - Shanghai*, 2016, pp. 1–5.
- V. Franzitta, D. Curto, D. Rao, and A. Viola, "Renewable energy sources to fulfill the global energy needs of a country: The case study of Malta in Mediterranean Sea," in *OCEANS 2016 - Shanghai*, 2016, no. 2012, pp. 1–5.
- A. Viola, V. Franzitta, M. Trapanese, and D. Curto, "Nexus Water & Energy: A Case Study of Wave Energy Converters (WECs) to Desalination Applications in Sicily," *Int. J. Heat Technol.*, vol. 34, no. Special Issue 2, pp. S379–S386, Oct. 2016.
- V. Franzitta, D. Curto, and D. Rao, "Energetic Sustainability Using Renewable Energies in the Mediterranean Sea," *Sustainability*, vol. 8, no. 11, p. 1164, Nov. 2016.
- V. Franzitta, D. Curto, D. Milone, and M. Trapanese, "Energy Saving in Public Transport Using Renewable Energy," *Sustainability*, vol. 9, no. 1, p. 106, Jan. 2017.
- A. Viola and D. Curto, "Numerical simulation of wave energy production through experimental tool," in *2017 IEEE International Conference on Environment and Electrical Engineering and 2017 IEEE Industrial and Commercial Power Systems Europe (EEEIC/I&CPS Europe)*, 2017, no. January, pp. 1–5.
- V. Franzitta, P. Catrini, and D. Curto, "Wave Energy Assessment along Sicilian Coastline, Based on DEIM Point Absorber," *Energies*, vol. 10, no. 3, p. 376, Mar. 2017.

- D. Curto and M. Trapanese, "Experimental tests on hydrogen production from sea waves energy," in *OCEANS – Anchorage*, 2017, 2017, pp. 1-5.
- D. Curto and M. Trapanese, "A Renewable Energy mix to Supply the Balearic Islands: Sea Wave, Wind and Solar," in *2018 IEEE International Conference on Environment and Electrical Engineering and 2018 IEEE Industrial and Commercial Power Systems Europe (EEEIC / I&CPS Europe)*, 2018, pp. 1-6.
- D. Curto, V. Franzitta, A. Viola, M. Cirrincione, A. Mohammadi, and A. Kumar, "A renewable energy mix to supply small islands. A comparative study applied to Balearic Islands and Fiji," *J. Clean. Prod.*, p. 118356, Sep. 2019.
- Crainz et al., "Flexibility Services to Minimize the Electricity Production from Fossil Fuels. A Case Study in a Mediterranean Small Island," *Energies*, vol. 12, no. 18, p. 3492, Sep. 2019.
- M. Trapanese, D. Curto, V. Franzitta, Z. Liu, L. McNabb, and X. Wang, "A Planar Generator for a Wave Energy Converter," *IEEE Trans. Magn.*, vol. 55, no. 12, pp. 1-7, Dec. 2019.
- D. Curto, A. Viola, V. Franzitta, M. Trapanese, and F. Cardona, "A New Solution for Sea Wave Energy Harvesting, the Proposal of an Ironless Linear Generator," *J. Mar. Sci. Eng.*, vol. 8, no. 2, p. 93, Feb. 2020.

VI CONCLUSION

As reported in this thesis, the sea could be a strategic source for water and energy, especially in small islands. The desalination process is nowadays commercially mature, thanks to the development of several techniques, some of them requiring thermal energy and other electricity. In the state of art about desalination (see Chapter II), the commercial techniques have been described, showing their working principles. Other solutions at a prototypical step have been also analyzed.

The statistics, above reported, indicate a quick diffusion of RO in the last years, thanks to the technological development, through which the specific energy consumption to produce freshwater has been drastically reduced. To confirm this, the case studies about small islands enhance the recent installation of new desalination units based on RO, in order to improve the local security of freshwater supply and at the same time the reduction of the energy demand for this industrial process.

About the exploitation of sea wave, despite in the last decades several solutions have been proposed, some of them also tested at full scale size, there are no commercial devices usable to this purpose. According to the state of art reported in Chapter III, there are different ways to extract energy from sea wave. About the first hydrodynamic interaction between the WEC and sea wave, the systems have been classified according to the acronyms OWC, WAB and OD, showing their features, working principles and reporting some examples. About the component adopted to transform sea wave energy into electrical energy, several strategies can be adopted: compression and decompression of chambers full of air to run air turbines; liquid pressurization by piston pumps to run hydraulic motors; water storage in reserves to run low head hydro turbines; the adoption of mechanical motion converters to obtain an usable rotary motion; finally, the utilization of linear generators to use a bidirectional linear motion in order produce directly electrical energy. In any case, a power electronic converter is required to modify the quality of power output, according to the standards required by the electrical loads.

In this context, this thesis proposes an innovative WEC, based on the adoption of linear generators. Focusing on this component, the design step has been reported, showing also the optimization process in order to increase the power output and limit the undesired phenomena, like the end effect of cogging force. As discussed in chapter IV, a relevant value of this disturbing force limits the annual energy producibility of the device, because in this case the WEC runs only if the wave overcomes this force. Thus, the reduction of the cogging force is fundamental to extend the range of sea wave states able to run the WEC.

Simplified mathematical models have been also introduced in order to evaluate the potential annual producibility of the WEC, considering the layout of a point absorber, composed by two buoys, one of which fixed to seabed and the other one able to move up and down to collect the mechanical energy of sea wave.

Different case studies have been reported, in the context of small islands, in order to investigate different aspects. The common condition is the strong dependence on fossil fuels, due to environmental constraints that in the last years have hindered the diffusion of RES supplied technologies, despite they are economical suitable.

The case of Ustica introduces a preliminary economic analysis, considering as target the annual covering of the energy demand from offices and public services. Since this energy consumption is small in comparison with the total energy production in Ustica, the balancing problem was neglected, because it was assumed that this aspect could be managed by the local fossil fuel power plant. As a solution, the adoption of a WEC farm, equipped also with PVP, and the installation of solar plants on public buildings were considered. The environmental and economic benefits have been evaluated in terms of avoided CO₂ emission (221.6 tons per year), discounted cash flow (326594 € after 15 years) and breakeven time (7-8 years).

The case studies of Balearic Islands and Fiji were realized in order to compare different archipelagos, characterized by a similar number of citizens, but different economic and climatic conditions. The idea was to evaluate potential analogies in the energy sectors in these two contexts. Indeed, both regions are affected by a relevant dependence on fossil fuel, but with different boundary conditions. In detail, since Balearic Islands belong to Spain, they are close to mainland and the energy consumption is quite high, this archipelago is equipped with a well-developed electrical grid, connected to the mainland and linking all islands each other. In this way, a significant part of local energy demand is covered by the importation from Spain. However, the diffusion of RES is very limited, thus fossil fuels are the main energy source adopted to satisfy the local energy demand in Balearic Islands. In the case of Fiji, the electrical grid is low developed. Furthermore, each island represents a small standalone system based on the consumption of fossil fuel. The only relevant exception is Viti Levu, the main island where most of population lives. In this context, hydropower is used to cover about half of the total national energy demand. However, the energy demand has been increasing in the last years, thus the installed power capacity should be rise, too. So, both case studies were investigated in order to propose a RES mix based on solar, wind and sea wave, in order to replace some fossil fuel power plants in Balearic islands (where the annual demand is almost stable) and avoid the installation of new fossil fuel plants in Fiji (where the energy demand is increasing). The energy potential of solar, wind and sea wave were investigated, analyzing environmental and economic aspects. About the wind exploitation, two different approaches were introduced in order to use different data banks. In the case of Balearic Islands, the proposed energy mix can avoid the emission of 2.26 million tons of CO₂ per year, requiring an investment between 2220 to 2995 million US dollars. The breakeven time is estimated between 11.96 and 13.31 years. In the case of Fiji, the avoided CO₂ emission is equal to 260,286 tons per year, requiring an investment between 258 to 339 million of US dollar with a breakeven time between 6.19 to 9.12 years.

The case study on Aeolian Islands introduced an economic optimization approach in order to find the best energy mix, by considering the exploitation of solar, wind and sea wave. The idea was to extend the LCOE parameter from a single technology to an entire energy mix and find the condition that minimize this indicator. In detail, LCOE represents the minimal selling price for electrical energy produced by a power plant in order to pay the investment and the operative and maintenance costs. Thus, the definition was modified, in order to include the investments for each technology (solar, wind and sea wave) and the operative and maintenance costs of all plants (including also the local fossil fuel supplied power plant). Thus, fixing the annual share of electricity production from RES, the share of electricity production from solar and wind were varied in a discretized way, evaluating the required installed power capacity and the corresponding LCOE of the energy mix. Some constrains were introduced: each source must produce at least the 10% of the annual energy production, in order to justify the installation of that technology; the total monthly RES production should not exceed a fixed share, in order to consider the balancing problem of the grid and guarantee a certain energy production to the local fossil fuel supplied power plant. These constrains removed some incompatible energy mixes; thus, the best condition was obtained for each one of Aeolian Islands. The proposed energy mix can cover about 50% of the local energy demand, with environmental benefits (20386 tons of CO₂ avoided per year) and economic benefits (9.39 million euros), since the energy price can be reduced, avoiding to pay the additional costs for the corresponding electricity production from fossil fuel.

The same method was applied also in the case of Lampedusa introducing some changes. The fixed maximal monthly share production from RES was firstly adapted, verifying hourly trends of energy producing. In this way, other energy mixes were excluded. The application of LCOE evaluation was applied in order to find the best condition, then the stability analysis was performed. The case study demonstrates the deterioration of the grid stability if specific solutions are not implemented. One of this is the use of diesel engines, running with a limited load, in order to have enough inertia to overcome eventually network disturbances. Some failures in the medium voltage grid were considered. Another solution could be the adoption of more complex power electronic converters, used to connected RES supplied plants to the grid, in order to create an artificial inertia, and help the local power plant in the stability control of the grid.

Finally, the last case study applied to Pantelleria investigates the possibility to use the local desalination plant as modulating load, in order to improve the energy efficiency of the power generation. Since this island is also entrusted to diesel engines and this technology is affected by a significant variation of the energy efficiency at different load conditions, the idea was to adapt the freshwater production in order to shift the corresponding load consumption in some hours of the day and maximize the energy efficiency of the power plant. The main benefit is the reduction of fuel consumption, corresponding to an economic saving and an environmental benefit (avoided CO₂ emission). Secondarily, the modulation of the Domestic Hot Water production during

the day and the installation of RES plant in final users were also performed. In the this case, each domestic client should delegate the management of DHW to the power plant in order to maximize the energy efficiency of the entire system and ensure all client requirements. In the first scenario the annual fuel consumption is reduced by 5383 tons per year, corresponding to an annual economic saving of 1360 k€ and an avoided CO₂ emission of 6300 tons per year. The second scenario requires the installation of 16000 m² of PVP and 3500 m² of STC. The annual economic saving is estimated equal to 2506 k€/y, while the annualized cost for RES installation is 453 k€/y. Thus, this solution is profitable for the owner of the power plant and the clients.

In conclusion, this thesis demonstrated the relevance of desalination and sea wave energy in the context of small islands. The first one is necessary to satisfy the local freshwater demand, avoiding the importation from mainland. The adoption of modern solutions allows the limitation of the energy consumption, required by the process. At the same time a proper management of this plant represents a strategical way to improve the efficiency of the entire electrical grid. In the next future, this approach could be extended in the case of grid with high penetration of RES production. Thanks to the possibility to storage freshwater, the schedule of desalination plants could be managed, according to weather forecast, in order to shift the energy demand when the RES production is greater, helping the traditional fossil fuel plant in the balancing of the electrical grid.

About sea wave, this energy source could be relevant in the next future, especially in small islands. With this purpose a WEC has been proposed, focusing the attention on the designing of the linear generator, usable as PTO. It should be reminded the fact that this kind of technology could solve the problem of RES introduction in small islands, thanks to the fact that this device can be installed in offshore areas, limiting the visual impact (one of the main problem that motivated the environmental restrictions).

This thesis has faced only a part of the design process of WEC, focusing the attention on the optimization of linear generator and evaluating its potential producibility by using data on sea wave climate around Sicily. To complete the sizing of the WEC, other analyses are required, among which:

- The optimization of the shape of the external and internal buoys, considering a detailed evaluation of the hydrodynamic forces, in order to maximize the power extraction from sea wave;
- The designing of the electrical power converter, necessary to transfer the electrical power production to the electrical grid;
- Implementation of control logic, in order to modify the mechanical response of PTO and maximize further the energy extraction in each sea state condition.

Therefore, the research can continue.

VII ALL PUBLICATIONS

- A. Viola, V. Franzitta, M. Trapanese, and D. Curto, "Nexus Water & Energy: A Case Study of Wave Energy Converters (WECs) to Desalination Applications in Sicily," *Int. J. Heat Technol.*, vol. 34, no. Special Issue 2, pp. S379-S386, Oct. 2016.
- V. Franzitta, D. Curto, D. Milone, and D. Rao, "Assessment of Renewable Sources for the Energy Consumption in Malta in the Mediterranean Sea," *Energies*, vol. 9, no. 12, p. 1034, Dec. 2016.
- V. Franzitta, D. Curto, D. Rao, and A. Viola, "Hydrogen Production from Sea Wave for Alternative Energy Vehicles for Public Transport in Trapani (Italy)," *Energies*, vol. 9, no. 10, p. 850, Oct. 2016.
- V. Franzitta, D. Curto, D. Milone, and A. Viola, "The desalination process driven by wave energy: A challenge for the future," *Energies*, vol. 9, no. 12, pp. 1-16, Dec. 2016.
- M. Trapanese, F. Raimondi, D. Curto, and A. Viola, "Evaluation of the wave energy density on the Sicilian coast," in *OCEANS 2016 - Shanghai*, 2016, pp. 1-4.
- V. Franzitta, D. Curto, D. Rao, and D. Milone, "Near zero energy island with sea wave energy: The case study of Pantelleria in Mediterranean Sea," in *OCEANS 2016 - Shanghai*, 2016, pp. 1-5.
- V. Franzitta, D. Curto, D. Rao, and A. Viola, "Renewable energy sources to fulfill the global energy needs of a country: The case study of Malta in Mediterranean Sea," in *OCEANS 2016 - Shanghai*, 2016, no. 2012, pp. 1-5.
- M. Trapanese, F. M. Raimondi, D. Curto, and A. Viola, "A computational magnetohydrodynamic model of a marine propulsion system," in *OCEANS 2016 - Shanghai*, 2016, pp. 1-4.
- V. Franzitta, D. Curto, and D. Rao, "Energetic Sustainability Using Renewable Energies in the Mediterranean Sea," *Sustainability*, vol. 8, no. 11, p. 1164, Nov. 2016.
- V. Franzitta, D. Rao, D. Curto, and A. Viola, "Greening island: renewable energies mix to satisfy electrical needs of Pantelleria in Mediterranean Sea," in *OCEANS 2016 MTS/IEEE Monterey*, 2016, pp. 1-6.
- A. Viola, D. Curto, V. Franzitta, and M. Trapanese, "Sea water desalination and energy consumption: A case study of wave energy converters (WEC) to desalination applications in Sicily," in *OCEANS 2016 MTS/IEEE Monterey*, 2016, pp. 1-5.
- M. Trapanese, F. M. Raimondi, D. Curto, and D. Rao, "A Magnetohydrodynamic Auxiliary Propulsion system for docking assistance of autonomous vehicle," in *OCEANS 2016 MTS/IEEE Monterey*, 2016, pp. 1-4.

- D. Curto, V. Di Dio, D. Rao, M. Trapanese, and A. Viola, "The helicoidal magnetic generator," in *OCEANS 2016 MTS/IEEE Monterey*, 2016, pp. 1-4.
- V. Franzitta, D. Curto, and A. Viola, "Renewable Energy Assessment in Italy and Brazil: An Economic and Political Comparison," in *Proceedings of SWC2017/SHC2017*, 2017, pp. 1-8.
- V. Franzitta and D. Curto, "Sustainability of the Renewable Energy Extraction Close to the Mediterranean Islands," *Energies*, vol. 10, no. 4, p. 283, Feb. 2017.
- V. Franzitta, P. Catrini, and D. Curto, "Wave Energy Assessment along Sicilian Coastline, Based on DEIM Point Absorber," *Energies*, vol. 10, no. 3, p. 376, Mar. 2017.
- A. Viola and D. Curto, "Numerical simulation of wave energy production through experimental tool," in *2017 IEEE International Conference on Environment and Electrical Engineering and 2017 IEEE Industrial and Commercial Power Systems Europe (EEEIC / I&CPS Europe)*, 2017, no. January, pp. 1-5.
- V. Boscaino et al., "Experimental validation of a distribution theory-based analysis of the effect of manufacturing tolerances on permanent magnet synchronous machines," *AIP Adv.*, vol. 7, no. 5, p. 056650, May 2017.
- V. Franzitta, A. Colucci, D. Curto, V. Di Dio, and M. Trapanese, "A linear generator for a waveroller power device," in *OCEANS 2017 - Aberdeen*, 2017, pp. 1-5.
- V. Franzitta, D. Curto, A. Viola, V. Di Dio, V. Boscaino, and M. Trapanese, "Guidelines proposal for a good and durable WEC design," in *OCEANS 2017 - Aberdeen*, 2017, pp. 1-7.
- D. Curto and M. Trapanese, "Experimental tests on hydrogen production from sea waves energy," in *OCEANS - Anchorage*, 2017, 2017, pp. 1-5.
- V. Franzitta, D. Curto, D. Milone, and M. Trapanese, "Energy Saving in Public Transport Using Renewable Energy," *Sustainability*, vol. 9, no. 1, p. 106, Jan. 2017.
- D. Curto, S. Neugebauer, A. Viola, M. Traverso, V. Franzitta, and M. Trapanese, "First Life Cycle Impact Considerations of Two Wave Energy Converters," in *2018 OCEANS - MTS/IEEE Kobe Techno-Oceans (OTO)*, 2018, pp. 1-5.
- F. M. Raimondi, D. Milone, and D. Curto, "An innovative mechanical motion converter for sea wave applications," in *2018 Thirteenth International Conference on Ecological Vehicles and Renewable Energies (EVER)*, 2018, pp. 1-6.
- F. M. Raimondi, D. Curto, V. Franzitta, and D. Milone, "Energy savings for indoor lighting in a shopping mall: A case of study," in *2018 Thirteenth International Conference on Ecological Vehicles and Renewable Energies (EVER)*, 2018, pp. 1-6.
- F. M. Raimondi, D. Curto, and D. Milone, "Environmental sustainability in non-residential buildings by automating and optimization LENI index," in *2018*

Thirteenth International Conference on Ecological Vehicles and Renewable Energies (EVER), 2018, no. 1, pp. 1-6.

- D. Curto and M. Trapanese, "A Renewable Energy mix to Supply the Balearic Islands: Sea Wave, Wind and Solar," in *2018 IEEE International Conference on Environment and Electrical Engineering and 2018 IEEE Industrial and Commercial Power Systems Europe (EEEIC/I&CPS Europe)*, 2018, pp. 1-6.
- D. Curto and D. Milone, "Improvement of Energy Efficiency for Indoor Lighting in a Big Shopping Center," in *2018 IEEE International Conference on Environment and Electrical Engineering and 2018 IEEE Industrial and Commercial Power Systems Europe (EEEIC/I&CPS Europe)*, 2018, pp. 1-6.
- D. Curto, F. Montana, and D. Milone, "Energy Saving Optimizing the Ventilation Control in a Big Shopping Center," in *2018 IEEE International Conference on Environment and Electrical Engineering and 2018 IEEE Industrial and Commercial Power Systems Europe (EEEIC/I&CPS Europe)*, 2018, pp. 1-6.
- M. Trapanese, V. Boscaino, G. Cipriani, D. Curto, V. Di Dio, and V. Franzitta, "A Permanent Magnet Linear Generator for the Enhancement of the Reliability of a Wave Energy Conversion System," *IEEE Trans. Ind. Electron.*, vol. 0046, no. c, pp. 1-1, 2018.
- M. Trapanese, F. M. Raimondi, D. Curto, and A. Viola, "A Magnetohydrodynamic Generator for Marine Energy Harvesting," in *OCEANS 2018 MTS/IEEE Charleston*, 2018, pp. 1-4.
- D. Curto, V. Franzitta, and M. Trapanese, "Designing an innovative system for sea wave utilization," in *OCEANS 2018 MTS/IEEE Charleston*, 2018, pp. 1-6.
- D. Curto, V. Franzitta, S. Longo, F. Montana, and E. Riva Sanseverino, "Investigating energy saving potential in a big shopping center through ventilation control," *Sustain. Cities Soc.*, vol. 49, no. January, p. 101525, Aug. 2019
- Crainz et al., "Flexibility Services to Minimize the Electricity Production from Fossil Fuels. A Case Study in a Mediterranean Small Island," *Energies*, vol. 12, no. 18, p. 3492, Sep. 2019.
- D. Curto, V. Franzitta, A. Viola, M. Cirrincione, A. Mohammadi, and A. Kumar, "A renewable energy mix to supply small islands. A comparative study applied to Balearic Islands and Fiji," *J. Clean. Prod.*, p. 118356, Sep. 2019.
- M. Trapanese, D. Curto, V. Franzitta, Z. Liu, L. McNabb, and X. Wang, "A Planar Generator for a Wave Energy Converter," *IEEE Trans. Magn.*, vol. 55, no. 12, pp. 1-7, Dec. 2019.
- D. Curto, V. Franzitta, and M. Trapanese, "Supplying small islands with solar, wind and sea wave. An economic approach to find the best energy share," in *OCEANS 2019 MTS/IEEE SEATTLE*, 2019, pp. 1-7.
- V. Muteri et al., "Review on Life Cycle Assessment of Solar Photovoltaic Panels," *Energies*, vol. 13, no. 1, p. 252, Jan. 2020.

- D. Curto, A. Viola, V. Franzitta, M. Trapanese, and F. Cardona, "A New Solution for Sea Wave Energy Harvesting, the Proposal of an Ironless Linear Generator," *J. Mar. Sci. Eng.*, vol. 8, no. 2, p. 93, Feb. 2020.
- D. Curto, V. Franzitta, M. Trapanese, and M. Cirrincione, "A Preliminary Energy Assessment to Improve the Energy Sustainability in the Small Islands of the Mediterranean Sea," *J. Sustain. Dev. Energy, Water Environ. Syst.*, pp. 1-19, 2020.

VIII ABBREVIATIONS

SiGLE	DESCRIPTION
AGMD	Air Gap Membrane Distillation
BAT	Best Available Technology
CPP	Conventional Power Plant
CDF	Cumulative Density Function
CDI	Capacitive Deionization
COD	Coefficient of Determination
COP	Coefficient of Performance
CRF	Capital Recovery Factor
CSP	Concentrated Solar Power
DCMD	Direct Contact Membrane Distillation
DES	Desalination plant
DG	Diesel Generator
DHW	Domestic Hot Water
DWEER	Dual Work Exchanger Energy Recovery
ED	Electro-Dialysis
EER	Energy Efficiency Ratio
EFL	Energy Fiji Limited
ERD	Energy Recovering Device
ESS	Electrical Storage
FEM	Finite Element Method
FO	Forward Osmosis
GDP	Gross Domestic Product
GIS	Geographic Information System
GIWH	Grid Integrated Water Heating
GWI	Global Water Intelligence
HDH	Humidification Dehumidification
HEMI	Hydraulic Energy Management Integration
HPP	High-Pressure Pump
HP	Heat Pump
HWSS	Hot Water Storage
HY	Hydration
IXR	Ion Exchange Resin
JONSWAP	Joint North Sea Wave Observation Project
LCOE	Levelized Cost of Electricity
MAE	Mean Absolute Error
MCDI	Membrane Capacitive Deionization
MD	Membrane Distillation
MED	Multi-Effects Distillation
MFS	Multi Flash Stages desalination
MILP	Mixed Integer Linear Programming
MVC	Mechanical Vapor Compression

Sigle	Description
NF	Nanofiltration
NSPL	Non-Synchronous Penetration Level
NUP	National Unique Price
OD	Overtopping Device
OWC	Oscillating Water Column
PDF	Probability Density Function
PM	Permanent Magnets
PTO	Power Take Off
PVP	Photovoltaic Panel
RES	Renewable Energy Source
RMSE	Root Mean Square Error
RO	Reverse Osmosis
RoCoF	Rate of change of frequency
RPX	Rotary Pressure Exchanger
RR	Recovery Ratio
SG	Synchronous Generator
SGMD	Sweeping Gas Membrane Distillation
SIDS	Small Island Developing Country
SRF	Secondary Refrigerant Freezing
STC	Solar Thermal Collector
SWL	Surface Water Level
TBT	Top Brine Temperature
TVC	Thermal Vapor Compression
VC	Vapor Compression
VF	Vacuum Freezing
VMD	Vacuum Membrane Distillation
WAB	Wave Activated Body
WEC	Wave Energy Converter
WMO	World Meteorological Organization
WSS	Freshwater Storage

IX REFERENCES

- [1] A. M. Hamiche, A. B. Stambouli, and S. Flazi, "A review of the water-energy nexus," *Renew. Sustain. Energy Rev.*, vol. 65, pp. 319–331, 2016.
- [2] J. Liu, C. Mei, H. Wang, W. Shao, and C. Xiang, "Powering an island system by renewable energy – A feasibility analysis in the Maldives," *Appl. Energy*, vol. 227, no. August, pp. 18–27, Oct. 2018.
- [3] U.S. Department of Energy, "The Water-Energy Nexus: Challenges and Opportunities," 2014.
- [4] P. H. Gleick, "Water and Energy," *Annu. Rev. Energy Environ.*, vol. 19, no. 1, pp. 267–299, Nov. 1994.
- [5] M. A. Eltawil, Z. Zhengming, and L. Yuan, "A review of renewable energy technologies integrated with desalination systems," *Renew. Sustain. Energy Rev.*, vol. 13, no. 9, pp. 2245–2262, Dec. 2009.
- [6] Department of Economic and Social Affairs Disability, "#Envision2030: 17 goals to transform the world for persons with disabilities." [Online]. Available: <https://www.un.org/development/desa/disabilities/envision2030.html>. [Accessed: 24-Sep-2019].
- [7] United Nations, *Paris Agreement*. 2015.
- [8] United Nations, *Kyoto Protocol to the United Nations Framework – Convention on Climate Change*. United Nations, 1998.
- [9] H. D. Matthews, N. P. Gillett, P. A. Stott, and K. Zickfeld, "The proportionality of global warming to cumulative carbon emissions," *Nature*, vol. 459, no. 7248, pp. 829–832, Jun. 2009.
- [10] A. K. Misra, "Climate change and challenges of water and food security," *Int. J. Sustain. Built Environ.*, vol. 3, no. 1, pp. 153–165, 2014.
- [11] IEA, "Energy and Climate Change," Paris, Nov. 2015.
- [12] J. Rogelj *et al.*, "Zero emission targets as long-term global goals for climate protection," *Environ. Res. Lett.*, vol. 10, no. 10, p. 105007, Oct. 2015.
- [13] M. Meinshausen *et al.*, "Greenhouse-gas emission targets for limiting global warming to 2 °C," *Nature*, vol. 458, no. 7242, pp. 1158–1162, Apr. 2009.
- [14] K. Biel and C. H. Glock, "Systematic literature review of decision support models for energy-efficient production planning," *Comput. Ind. Eng.*, vol. 101, pp. 243–259, 2016.
- [15] Enerdata, "Global Energy Statistical Yearbook 2019." [Online]. Available: <https://yearbook.enerdata.net/>. [Accessed: 26-Dec-2019].
- [16] IEA, *World Energy Outlook 2018*. 2018.
- [17] IRENA, "Renewable Power Generation Costs in 2017," 2018.
- [18] IEA, "World Energy Investment 2019," 2019.

- [19] C. S. Lai and M. D. McCulloch, "Levelized cost of electricity for solar photovoltaic and electrical energy storage," *Appl. Energy*, vol. 190, pp. 191–203, Mar. 2017.
- [20] I. Shiklomanov, "World fresh water resources," in *Water in crisis a guide to the world's fresh water resources*, 1993, pp. 13–24.
- [21] "World Climate Maps." [Online]. Available: <https://www.climate-charts.com/World-Climate-Maps.html>. [Accessed: 23-Sep-2019].
- [22] FAO, WFP, and IFAD, "The State of Food Insecurity in the World - Economic growth is necessary but not sufficient to accelerate reduction of hunger and malnutrition," Rome, 2012.
- [23] IEA, "Water for Energy: Is energy becoming a thirstier resource?," in *World Energy Outlook 2012*, 2012, pp. 1–33.
- [24] L. Guppy and K. Anderson, "Global Water Crisis: The facts," 2017.
- [25] UN-WWAP, *The United Nations World Water Development Report 2015: Water for a Sustainable World*. 2015.
- [26] I. Kougiyas, S. Szabó, A. Nikitas, and N. Theodossiou, "Sustainable energy modelling of non-interconnected Mediterranean islands," *Renew. Energy*, vol. 133, pp. 930–940, Apr. 2019.
- [27] M. Gleick, P. and Heberger, "Water and conflict: events, trends and analysis (2011 - 2012)," in *The World's Water Volume 8*, 2014, pp. 159–171.
- [28] A. Hira and L. G. de Oliveira, "No substitute for oil? How Brazil developed its ethanol industry," *Energy Policy*, vol. 37, no. 6, pp. 2450–2456, 2009.
- [29] R. Moya, C. Tenorio, and G. Oporto, "Short rotation wood crops in Latin American: A review on status and potential uses as biofuel," *Energies*, vol. 12, no. 4, 2019.
- [30] E. Mathioulakis, V. Belessiotis, and E. Delyannis, "Desalination by using alternative energy: Review and state-of-the-art," *Desalination*, vol. 203, no. 1–3, pp. 346–365, Feb. 2007.
- [31] A. Viola, V. Franzitta, M. Trapanese, and D. Curto, "Nexus Water & Energy: A Case Study of Wave Energy Converters (WECs) to Desalination Applications in Sicily," *Int. J. Heat Technol.*, vol. 34, no. Special Issue 2, pp. S379–S386, Oct. 2016.
- [32] D. Airolidi *et al.*, "Scenari di sviluppo delle FER nelle isole minori italiane non interconnesse e analisi di casi studio," 2017.
- [33] Crainz *et al.*, "Flexibility Services to Minimize the Electricity Production from Fossil Fuels. A Case Study in a Mediterranean Small Island," *Energies*, vol. 12, no. 18, p. 3492, Sep. 2019.
- [34] Legambiente, "ISOLE SOSTENIBILI. Osservatorio sulle isole minori. Energia, Economia Circolare, Acqua, Mobilità. Le sfide per le isole minori italiane e le buone pratiche nel mondo.," 2018.
- [35] N. Lior, *Advances in Water Desalination*. Hoboken, NJ, USA: John Wiley & Sons, Inc., 2012.
- [36] G. Wetterau *et al.*, *Desalination of Seawater - M61*, First Edit. Denver: American

Water Works Association, 2011.

- [37] A. Cipollina, G. Micale, and L. Rizzuti, "A critical assessment of desalination operations in Sicily," *Desalination*, vol. 182, no. 1-3, pp. 1-12, Nov. 2005.
- [38] A. M. K. El-Ghonemy, "Performance test of a sea water multi-stage flash distillation plant: Case study," *Alexandria Eng. J.*, vol. 57, no. 4, pp. 2401-2413, 2018.
- [39] K. P. Lee, T. C. Arnot, and D. Mattia, "A review of reverse osmosis membrane materials for desalination-Development to date and future potential," *J. Memb. Sci.*, vol. 370, no. 1-2, pp. 1-22, 2011.
- [40] M. Rognoni, *La Dissalazione dell'acqua di mare. Descrizione, analisi e valutazione delle principali tecnologie*, 1st ed. Palermo: Dario Flaccovio Editore s.r.l., 2010.
- [41] W. V. Weir, *The Weir Group: The History of a Scottish Engineering Legend*. Profile Books, 2008.
- [42] A. M. Al-Mutawa *et al.*, "Desalination in the GCC. The History, the Present & the Future," 2014.
- [43] AMIO WATER TREATMENT LTD., "AMIO Water Technology." [Online]. Available: <http://www.amiowater.com/technology>. [Accessed: 12-Apr-2019].
- [44] E. Jones, M. Qadir, M. T. H. van Vliet, V. Smakhtin, and S. mu Kang, "The state of desalination and brine production: A global outlook," *Sci. Total Environ.*, vol. 657, pp. 1343-1356, 2019.
- [45] A. Alkaisi, R. Mossad, and A. Sharifian-Barforoush, "A Review of the Water Desalination Systems Integrated with Renewable Energy," *Energy Procedia*, vol. 110, no. December 2016, pp. 268-274, Mar. 2017.
- [46] Z. Zimerman, "Development of large capacity high efficiency mechanical vapor compression (MVC) units," *Desalination*, vol. 96, no. 1-3, pp. 51-58, 1994.
- [47] T. Xu, "Ion exchange membranes: State of their development and perspective," *J. Memb. Sci.*, vol. 263, no. 1-2, pp. 1-29, 2005.
- [48] M. Talaeipour, J. Nouri, A. H. Hassani, and A. H. Mahvi, "An investigation of desalination by nanofiltration, reverse osmosis and integrated (hybrid NF/RO) membranes employed in brackish water treatment," *J. Environ. Heal. Sci. Eng.*, vol. 15, no. 1, pp. 1-9, 2017.
- [49] J. S. Sangwai, R. S. Patel, P. Mekala, D. Mech, and M. Busch, "Desalination of seawater using gas hydrate technology - Current status and future direction," in *18th International Conference on Hydraulics, Water Resources, Coastal and Environmental Engineering, HYDRO 2013 International*, 2013, no. July 2015, pp. 434-440.
- [50] M. Al-Shammiri and M. Safar, "Multi-effect distillation plants: state of the art," *Desalination*, vol. 126, no. 1-3, pp. 45-59, Nov. 1999.
- [51] O. K. Buros, "The ABCs of Desalting," 2000.
- [52] M. Shatat and S. B. Riffat, "Water desalination technologies utilizing conventional and renewable energy sources," *Int. J. Low-Carbon Technol.*, vol. 9, no. 1, pp. 1-19,

Mar. 2014.

- [53] S. Sethi and G. Wetterau, "Seawater Desalination Overview," in *Desalination of Seawater - Manual of Water Supply Practices, M61*, 1st Editio., American Water Works Association (AWWA), 2011, p. 13.
- [54] M. Shatat, S. Riffat, and S. Ghabayen, "State of Art Water Desalination Technologies using Conventional and Sustainable Energy Sources," *4th Int. Eng. Conf. -Towards Eng. 21st century*, pp. 1-16, 2012.
- [55] H. Sharon and K. S. Reddy, "A review of solar energy driven desalination technologies," *Renew. Sustain. Energy Rev.*, vol. 41, pp. 1080-1118, 2015.
- [56] I. C. Karagiannis and P. G. Soldatos, "Water desalination cost literature: review and assessment," *Desalination*, vol. 223, no. 1-3, pp. 448-456, 2008.
- [57] R. Tenno and P. Nguyen, "Multistage Flash Evaporator Control in PDE Representation," *IFAC-PapersOnLine*, vol. 49, no. 24, pp. 70-75, 2016.
- [58] A. Al-Karaghoul and L. L. Kazmerski, "Energy consumption and water production cost of conventional and renewable-energy-powered desalination processes," *Renew. Sustain. Energy Rev.*, vol. 24, pp. 343-356, Aug. 2013.
- [59] Research Office Legislative Council Secretariat, "Seawater desalination technologies," 2015.
- [60] F. Helfer, C. Lemckert, and Y. G. Anissimov, "Osmotic power with Pressure Retarded Osmosis: Theory, performance and trends - A review," *J. Memb. Sci.*, vol. 453, pp. 337-358, 2014.
- [61] P. Silvestroni, *Fondamenti di Chimica*. 1996.
- [62] G. Han, S. Zhang, X. Li, and T. S. Chung, "High performance thin film composite pressure retarded osmosis (PRO) membranes for renewable salinity-gradient energy generation," *J. Memb. Sci.*, vol. 440, pp. 108-121, 2013.
- [63] C. Fritzmann, J. Löwenberg, T. Wintgens, and T. Melin, "State-of-the-art of reverse osmosis desalination," *Desalination*, vol. 216, no. 1-3, pp. 1-76, 2007.
- [64] L. Henthorne and B. Boysen, "State-of-the-art of reverse osmosis desalination pretreatment," *Desalination*, vol. 356, pp. 129-139, 2015.
- [65] J. Martin and D. Eisberg, "Brackish Water Desalination - Energy and Cost Considerations," *Int. Desalin. Assoc. World Congr. Desalin. Water Reuse 2007*, vol. 22, no. 1, pp. 99-131, 2007.
- [66] J. Gebel and S. Yüce, *An Engineer's Guide to Desalination*. VGB PowerTech Service GmbH, 2008.
- [67] M. J. Guirguis, "Energy Recovery Devices In Seawater Reverse Osmosis Desalination Plants With Emphasis On Efficiency And Economical Analysis Of Isobaric Versus Centrifugal Devices," University of South Florida, 2011.
- [68] E. Oklejas and J. Hunt, "Integrated pressure and flow control in SWRO with a HEMI turbo booster," *Desalin. Water Treat.*, vol. 31, no. 1-3, pp. 88-94, 2011.
- [69] Advanced Flow, "Energy Recovery Device," 2015. [Online]. Available: <https://www.advancedflow.com/largest-us-desalination-plant-opens-in-san->

diego-county-media-2/. [Accessed: 02-May-2019].

- [70] Forward Aqua, "SWRO Energy Recovery," 2010. [Online]. Available: <https://forwardaqua.wordpress.com/2010/11/22/swro-energy-recovery/>. [Accessed: 03-May-2019].
- [71] S. Mirza, "Reduction of energy consumption in process plants using nanofiltration and reverse osmosis," *Desalination*, vol. 224, no. 1-3, pp. 132-142, 2008.
- [72] J. O. Kessler and C. D. Moody, "Drinking water from sea water by forward osmosis," *Desalination*, vol. 18, no. 3, pp. 297-306, 1976.
- [73] J. R. McCutcheon, R. L. McGinnis, and M. Elimelech, "A novel ammonia-carbon dioxide forward (direct) osmosis desalination process," *Desalination*, vol. 174, no. 1, pp. 1-11, 2005.
- [74] L. Chekli *et al.*, "A comprehensive review of hybrid forward osmosis systems: Performance, applications and future prospects," *J. Memb. Sci.*, vol. 497, pp. 430-449, 2016.
- [75] Y. N. Wang, K. Goh, X. Li, L. Setiawan, and R. Wang, "Membranes and processes for forward osmosis-based desalination: Recent advances and future prospects," *Desalination*, vol. 434, no. October 2017, pp. 81-99, 2018.
- [76] Trevi Systems, "Making Water shouldn't Waste Water," 2016. [Online]. Available: <https://www.trevisystems.com/technology->. [Accessed: 04-May-2019].
- [77] A. W. Mohammad, Y. H. Teow, W. L. Ang, Y. T. Chung, D. L. Oatley-Radcliffe, and N. Hilal, "Nanofiltration membranes review: Recent advances and future prospects," *Desalination*, vol. 356, pp. 226-254, 2015.
- [78] M. Greiter, S. Novalin, M. Wendland, K. Kulbe, and J. Fischer, "Electrodialysis versus ion exchange: comparison of the cumulative energy demand by means of two applications," *J. Memb. Sci.*, vol. 233, no. 1-2, pp. 11-19, Apr. 2004.
- [79] A. Hassanvand, K. Wei, S. Talebi, G. Chen, and S. Kentish, "The Role of Ion Exchange Membranes in Membrane Capacitive Deionisation," *Membranes (Basel)*, vol. 7, no. 3, p. 54, Sep. 2017.
- [80] H. Li and L. Zou, "Ion-exchange membrane capacitive deionization: A new strategy for brackish water desalination," *Desalination*, vol. 275, no. 1-3, pp. 62-66, 2011.
- [81] S. Porada, R. Zhao, A. van der Wal, V. Presser, and P. M. Biesheuvel, "Review on the science and technology of water desalination by capacitive deionization," *Prog. Mater. Sci.*, vol. 58, no. 8, pp. 1388-1442, Oct. 2013.
- [82] A. Alkhudhiri, N. Darwish, and N. Hilal, "Membrane distillation: A comprehensive review," *Desalination*, vol. 287, pp. 2-18, 2012.
- [83] S. Gunko, S. Verbych, M. Bryk, and N. Hilal, "Concentration of apple juice using direct contact membrane distillation," *Desalination*, vol. 190, no. 1-3, pp. 117-124, 2006.
- [84] S. T. Hsu, K. T. Cheng, and J. S. Chiou, "Seawater desalination by direct contact membrane distillation," *Desalination*, vol. 143, no. 3, pp. 279-287, 2002.

- [85] F. A. Banat and J. Simandl, "Membrane distillation for dilute ethanol," *J. Memb. Sci.*, vol. 163, no. 2, pp. 333-348, 1999.
- [86] M. Khayet, C. Cojocaru, and A. Baroudi, "Modeling and optimization of sweeping gas membrane distillation," *Desalination*, vol. 287, pp. 159-166, 2012.
- [87] M. A. E. R. Abu-Zeid, Y. Zhang, H. Dong, L. Zhang, H. L. Chen, and L. Hou, "A comprehensive review of vacuum membrane distillation technique," *Desalination*, vol. 356, pp. 1-14, 2015.
- [88] P. Guyer, "An Introduction to Ion Exchange Techniques for Water Desalination," 2012.
- [89] L. Tavani, "Desalination Process by Ion Exchange," 3,618,589, 1971.
- [90] J. Lindblom, "Solar Thermal Technologies for Seawater Desalination : state of the art," *Renew. Energy Syst.*, no. August, pp. 1-17, 2010.
- [91] D. Lawal, M. Antar, A. Khalifa, S. Zubair, and F. Al-Sulaiman, "Humidification-dehumidification desalination system operated by a heat pump," *Energy Convers. Manag.*, vol. 161, no. January, pp. 128-140, 2018.
- [92] S. Gorjian, T. T. Hashjin, and B. Ghobadian, "Seawater Desalination using Solar Thermal Technologies : state of the art," no. October 2018, pp. 4-7, 2011.
- [93] H. Müller-Holst, M. Engelhardt, and W. Schölkopf, "Small-scale thermal seawater desalination simulation and optimization of system design," *Desalination*, vol. 122, no. 2-3, pp. 255-262, 1999.
- [94] M. Qasim, M. Badrelzaman, N. N. Darwish, N. A. Darwish, and N. Hilal, "Reverse osmosis desalination: A state-of-the-art review," *Desalination*, vol. 459, no. December 2018, pp. 59-104, Jun. 2019.
- [95] Global Water Intelligence, "DesalData." [Online]. Available: <https://www.desaldata.com>. [Accessed: 02-Jun-2019].
- [96] A. Al-Karaghoul and L. L. Kazmerski, "Comparisons of Technical and Economic Performance of the Main Desalination Processes with and without Renewable Energy Coupling."
- [97] J. H. Lindemann, "Wind and solar powered seawater desalination. Applied solutions for the Mediterranean, the Middle East and the Gulf countries," *Desalination*, vol. 168, no. 1-3, pp. 73-80, 2004.
- [98] Q. Ma and H. Lu, "Wind energy technologies integrated with desalination systems: Review and state-of-the-art," *Desalination*, vol. 277, no. 1-3, pp. 274-280, Aug. 2011.
- [99] K. H. Mistry, R. K. McGovern, G. P. Thiel, E. K. Summers, S. M. Zubair, and J. H. Lienhard, "Entropy generation analysis of desalination technologies," *Entropy*, vol. 13, no. 10, pp. 1829-1864, 2011.
- [100] N. Kahraman and Y. A. Cengel, "Exergy analysis of a MSF distillation plant," *Energy Convers. Manag.*, vol. 46, no. 15-16, pp. 2625-2636, Sep. 2005.
- [101] Y. Cerci, "The minimum work requirement for distillation processes," *Exergy, An Int. J.*, vol. 2, no. 1, pp. 15-23, Jan. 2002.

- [102] A. Piacentino, "Application of advanced thermodynamics, thermoeconomics and exergy costing to a Multiple Effect Distillation plant: In-depth analysis of cost formation process," *Desalination*, vol. 371, pp. 88–103, Sep. 2015.
- [103] Y. Cerci, "Exergy analysis of a reverse osmosis desalination plant in California," *Desalination*, vol. 142, no. 3, pp. 257–266, Mar. 2002.
- [104] K. H. Mistry and J. H. Lienhard, "Generalized least energy of separation for desalination and other chemical separation processes," *Entropy*, vol. 15, no. 6, pp. 2046–2080, 2013.
- [105] W. L. Ang, A. W. Mohammad, N. Hilal, and C. P. Leo, "A review on the applicability of integrated/hybrid membrane processes in water treatment and desalination plants," *Desalination*, vol. 363, pp. 2–18, 2015.
- [106] A. Kasaeian, F. Rajaei, and W.-M. Yan, "Osmotic desalination by solar energy: A critical review," *Renew. Energy*, vol. 134, pp. 1473–1490, Apr. 2019.
- [107] L. García-Rodríguez, "Renewable energy applications in desalination: state of the art," *Sol. Energy*, vol. 75, no. 5, pp. 381–393, Nov. 2003.
- [108] A. Ritschel and O. Esan, "Renewable energy desalination for small islands," *IRENA – MARTINIQUE Conf. Isl. energy transitions Pathways Accel. uptake renewables*, no. June, pp. 8–10, 2015.
- [109] V. Franzitta, P. Catrini, and D. Curto, "Wave Energy Assessment along Sicilian Coastline, Based on DEIM Point Absorber," *Energies*, vol. 10, no. 3, p. 376, Mar. 2017.
- [110] J. P. Sierra, C. Martín, C. Mösso, M. Mestres, and R. Jebbad, "Wave energy potential along the Atlantic coast of Morocco," *Renew. Energy*, vol. 96, no. August, pp. 20–32, Oct. 2016.
- [111] V. Vannucchi and L. Cappietti, "Wave Energy Assessment and Performance Estimation of State of the Art Wave Energy Converters in Italian Hotspots," *Sustainability*, vol. 8, no. 12, p. 1300, Dec. 2016.
- [112] M. Monteforte, C. Lo Re, and G. B. B. Ferreri, "Wave energy assessment in Sicily (Italy)," *Renew. Energy*, vol. 78, no. August, pp. 276–287, Jun. 2015.
- [113] Matthew J. Hannon, A. Vantoch-Wood, M. Carcas, S. Bradley, and World Energy Council, "World Energy Resources - Marine Energy," 2016.
- [114] A. Lewis *et al.*, "Ocean Energy," in *Renewable Energy Sources and Climate Change Mitigation. Special Report of the Intergovernmental Panel on Climate Change*, 2011, pp. 497–534.
- [115] Agence Française De Développement and Indian Renewable Energy Development Agency Limited, "Study on Tidal & Waves Energy in India: Survey on the Potential & Proposition of a Roadmap," 2014.
- [116] Tethys, "Roosevelt Island Tidal Energy (RITE) Project Pilot," 2019.
- [117] SeaPower Scrl, "KOBOLD: VERTICAL AXIS MARINE TURBINE." [Online]. Available: <http://www.seapowerscrl.com/ocean-and-river-system/kobold>. [Accessed: 17-Jun-2019].

- [118] D. Deans, "Failed Ramsey Sound tidal energy scheme 'faulty for months,'" *BBC News*, 2016.
- [119] MarineEnergy.biz, "MORE assists Oceanflow's tidal decommissioning," 2017.
- [120] EMEC, "OPEN HYDRO," 2019. [Online]. Available: <http://www.emec.org.uk/about-us/our-tidal-clients/open-hydro/>. [Accessed: 17-Jun-2019].
- [121] World Energy Council, "World Energy Resources: Marine Energy 2016," p. 79, 2016.
- [122] M. Z. Zainol, N. Ismail, and I. Zainol, "A REVIEW ON THE STATUS OF TIDAL ENERGY TECHNOLOGY," *Sci. Int.*, vol. 29(3), no. June, pp. 659-667, 2017.
- [123] S. P. Neill *et al.*, "Tidal range energy resource and optimization - Past perspectives and future challenges," *Renew. Energy*, vol. 127, pp. 763-778, 2018.
- [124] X. Yang, K. A. Haas, and H. M. Fritz, "Evaluating the potential for energy extraction from turbines in the gulf stream system," *Renew. Energy*, vol. 72, pp. 12-21, Dec. 2014.
- [125] J. Guo, Z. Zhang, C. Xia, B. Guo, and Y. Yuan, "Topographic-baroclinic instability and formation of Kuroshio current loop," *Dyn. Atmos. Ocean.*, vol. 81, no. 6, pp. 15-29, 2018.
- [126] M. Krug, D. Schilperoort, F. Collard, M. W. Hansen, and M. Rouault, "Signature of the Agulhas Current in high resolution satellite derived wind fields," *Remote Sens. Environ.*, vol. 217, no. February, pp. 340-351, 2018.
- [127] H. Yuan, J. Zhao, L. Wang, and N. Mei, "Investigation into a multi-stage rotor rotating magnetic field generator powered by ocean current," *Energy Procedia*, vol. 136, pp. 121-126, 2017.
- [128] B. Li *et al.*, "The economics of electricity generation from Gulf Stream currents," *Energy*, vol. 134, pp. 649-658, 2017.
- [129] R. Pelc and R. M. Fujita, "Renewable energy from the ocean," *Mar. Policy*, vol. 26, no. 6, pp. 471-479, 2002.
- [130] H. Aydin, H.-S. Lee, H.-J. Kim, S. K. Shin, and K. Park, "Off-design performance analysis of a closed-cycle ocean thermal energy conversion system with solar thermal preheating and superheating," *Renew. Energy*, vol. 72, pp. 154-163, Dec. 2014.
- [131] Asian Development Bank, *Wave Energy Conversion and Ocean Thermal Energy Conversion Potential in Developing Member Countries*. 2014.
- [132] Okinawa Prefecture, "Okinawa Prefecture Deep Sea Water Power Generation Demonstration Project." [Online]. Available: <http://otecokinawa.com/en/index.html>. [Accessed: 18-Jun-2019].
- [133] A. Tamburini, F. Giacalone, A. Cipollina, F. Grisafi, G. Vella, and G. Micale, "Pressure retarded osmosis: A membrane process for environmental sustainability," *Chem. Eng. Trans.*, vol. 47, no. i, pp. 355-360, 2016.
- [134] R. Cascajo, E. García, E. Quiles, A. Correcher, and F. Morant, "Integration of

marine wave energy converters into seaports: A case study in the port of Valencia," *Energies*, vol. 12, no. 5, 2019.

- [135] A. Laing *et al.*, *Guide to wave analysis and forecasting*, vol. 1998, no. 702. 1998.
- [136] E. B. L. Mackay, "Resource Assessment for Wave Energy," in *Comprehensive Renewable Energy*, vol. 8, Elsevier, 2012, pp. 11–77.
- [137] B. G. Reguero, I. J. Losada, and F. J. Méndez, "A global wave power resource and its seasonal, interannual and long-term variability," *Appl. Energy*, vol. 148, pp. 366–380, Jun. 2015.
- [138] L. H. Holthuijsen, *Waves in Oceanic and Coastal Waters*. New York: Cambridge University Press, 2007.
- [139] A. Cornett, "A global wave energy resource assessment," *Sea Technol.*, no. October, pp. 1–9, 2008.
- [140] F. Arena *et al.*, "Wave climate analysis for the design of wave energy harvesters in the Mediterranean Sea," *Renew. Energy*, vol. 77, pp. 125–141, May 2015.
- [141] H. E. Krogstad and Ø. A. Arntsen, "Linear Wave Theory. Part A. Regular waves," 2000.
- [142] K. Gunn and C. Stock-Williams, "Quantifying the global wave power resource," *Renew. Energy*, vol. 44, pp. 296–304, 2012.
- [143] A. Toffoli and E. M. Bitner-Gregersen, "Types of Ocean Surface Waves, Wave Classification," *Encycl. Marit. Offshore Eng.*, pp. 1–8, 2017.
- [144] C. Iuppa, L. Cavallaro, D. Vicinanza, and E. Foti, "Investigation of suitable sites for wave energy converters around Sicily (Italy)," *Ocean Sci.*, vol. 11, no. 4, pp. 543–557, 2015.
- [145] J. P. Sierra, C. Mösso, and D. González-Marco, "Wave energy resource assessment in Menorca (Spain)," *Renew. Energy*, vol. 71, pp. 51–60, 2014.
- [146] G. Mattiazzo, E. Giorcelli, D. Poggi, G. Sannino, and A. Carillo, "Progettazione di un sistema di produzione di energia da moto ondoso in scala reale," 2013.
- [147] S. Akar and D. A. Akdoğan, "Environmental and Economic Impacts of Wave Energy: Some Public Policy Recommendations for Implementation in Turkey," in *Handbook of Research on Green Economic Development Initiatives and Strategies*, no. January 2016, 2016.
- [148] T. Aderinto and H. Li, "Ocean Wave energy converters: Status and challenges," *Energies*, vol. 11, no. 5, pp. 1–26, 2018.
- [149] G. Mořk, S. Barstow, A. Kabuth, and M. T. Pontes, "Assessing the Global Wave Energy Potential," in *29th International Conference on Ocean, Offshore and Arctic Engineering: Volume 3*, 2010, no. 2008, pp. 447–454.
- [150] L. Liberti, A. Carillo, and G. Sannino, "Wave energy resource assessment in the Mediterranean, the Italian perspective," *Renew. Energy*, vol. 50, pp. 938–949, Feb. 2013.
- [151] A. F. de O. Falcão, "Wave energy utilization: A review of the technologies," *Renew. Sustain. Energy Rev.*, vol. 14, no. 3, pp. 899–918, Apr. 2010.

- [152] B. Drew, A. R. Plummer, and M. N. Sahinkaya, "A review of wave energy converter technology," *Proc. Inst. Mech. Eng. Part A J. Power Energy*, vol. 223, no. 8, pp. 887–902, Dec. 2009.
- [153] R. Bhattacharyya and M. E. McCormick, "Wave Power Activities in Northern Europe," in *Wave Energy Conversion*, 1st ed., Elsevier Science, 2003, pp. 95–123.
- [154] O. Malmo and A. Reitan, "Development of the Kvaerner Multiresonant OWC," in *Hydrodynamics of Ocean Wave-Energy Utilization*, no. October, Berlin, Heidelberg: Springer Berlin Heidelberg, 1986, pp. 57–67.
- [155] M. Ravindran and P. M. Koola, "Energy from sea waves – the Indian wave energy programme," *Curr. Sci.*, vol. 60, no. 12, pp. 676–680, 1991.
- [156] WavePowerLab, "Kvaerner Brug's OWC device," 2014. [Online]. Available: <http://wavepowerlab.weebly.com/what-is-that-wec/kvaerner-brugs-owc-device>. [Accessed: 02-Aug-2019].
- [157] J. Khan and G. S. Bhuyan, "Ocean Energy: Global Technology Development Status," 2009.
- [158] A. F. O. Falcão and J. C. C. Henriques, "Oscillating-water-column wave energy converters and air turbines: A review," *Renew. Energy*, vol. 85, no. January, pp. 1391–1424, 2016.
- [159] Tethys, "Pico Oscillating Water Column." [Online]. Available: <https://tethys.pnnl.gov/annex-iv-sites/pico-oscillating-water-column>. [Accessed: 02-Aug-2019].
- [160] Tethys, "Mutriku Wave Power Plant." [Online]. Available: <https://tethys.pnnl.gov/annex-iv-sites/mutriku-wave-power-plant>. [Accessed: 02-Aug-2019].
- [161] L. Mouffe *et al.*, "Annual report. An Overview of Ocean Energy Activities in 2017," 2017.
- [162] Y. Masuda, T. Yamazaki, Y. Outa, and M. McCormick, "Study of Backward Bent Duct Buoy," in *OCEANS '87*, 1987, pp. 384–389.
- [163] DTI, "Near Shore Floating Oscillating Wave Column: Prototype Development and Evaluation," 2004.
- [164] JAMSTEC, "JAMSTEC Gallery. Mighty Whale." [Online]. Available: http://www.jamstec.go.jp/gallery/j/research/system/images/system_002_1.jpg. [Accessed: 06-Aug-2019].
- [165] B. Wu, T. Chen, J. Jiang, G. Li, Y. Zhang, and Y. Ye, "Economic assessment of wave power boat based on the performance of 'Mighty Whale' and BBDB," *Renew. Sustain. Energy Rev.*, vol. 81, no. March 2016, pp. 946–953, 2018.
- [166] Y. Washio, H. Osawa, and T. Ogata, "The open sea tests of the offshore floating type wave power device 'Mighty Whale' -characteristics of wave energy absorption and power generation," in *MTS/IEEE Oceans 2001. An Ocean Odyssey. Conference Proceedings (IEEE Cat. No.01CH37295)*, 2002, vol. 1, pp. 579–585.
- [167] D. Vicinanza, L. Margheritini, J. P. Kofoed, and M. Buccino, "The SSG Wave Energy Converter: Performance, Status and Recent Developments," *Energies*, vol.

- 5, no. 2, pp. 193–226, Jan. 2012.
- [168] R. Yemm, D. Pizer, C. Retzler, and R. Henderson, “Pelamis: experience from concept to connection,” *Philos. Trans. R. Soc. A Math. Phys. Eng. Sci.*, vol. 370, no. 1959, pp. 365–380, Jan. 2012.
- [169] A. Poullikkas, “Technology Prospects of Wave Power Systems,” *Electron. J. Energy Environ.*, vol. 2, pp. 47–69, 2014.
- [170] A. M. Magro Marques, “Magnetic Circuit Study of a Permanent Magnet Linear Generator for Wave Energy Recovery,” Instituto Tecnico Superior Lisboa, 2018.
- [171] K. Tarrant and C. Meskell, “Investigation on parametrically excited motions of point absorbers in regular waves,” *Ocean Eng.*, vol. 111, pp. 67–81, 2016.
- [172] S. Patel, “Ocean Power Technologies Deploys Commercial PowerBuoy with Energy Storage,” 2016. [Online]. Available: <https://www.powermag.com/ocean-power-technologies-deploys-commercial-powerbuoy-energy-storage/>. [Accessed: 09-Aug-2019].
- [173] J. Blackledge, E. Coyle, D. Kearney, R. McGuirk, and B. Norton, “Estimation of wave energy from wind velocity,” *Eng. Lett.*, vol. 21, no. 4, pp. 158–170, 2013.
- [174] M. Corpuz, “CETO system: Using oceanic wave to generate clean electricity and desalinate water,” *Version Daily*, 2016.
- [175] H. Hastie, “Resurfacing: Collapsed WA wave energy company wants \$5m for a rebirth,” *The Sydney Morning Herald*, 2019.
- [176] J. Falnes, “A review of wave-energy extraction,” *Mar. Struct.*, vol. 20, no. 4, pp. 185–201, 2007.
- [177] “Salter’s Nodding Duck.” [Online]. Available: <https://baonguyen1994.wordpress.com/introduction-to-wave-energy/ocean-wave-technologies/terminators/salters-nodding-duck/>. [Accessed: 09-Aug-2019].
- [178] R. C. Thomson, J. P. Chick, and G. P. Harrison, “An LCA of the Pelamis wave energy converter,” *Int. J. Life Cycle Assess.*, vol. 24, no. 1, pp. 51–63, 2019.
- [179] Wikipedia, “Pelamis Wave Energy Converter,” 2019. [Online]. Available: https://en.wikipedia.org/wiki/Pelamis_Wave_Energy_Converter. [Accessed: 12-Aug-2019].
- [180] P. Evans, “Oyster ocean power system to provide 1 GW by 2020,” *New Atlas*, 2009. [Online]. Available: <https://newatlas.com/oyster-ocean-power-system/11180/>.
- [181] EMEC, “AQUAMARINE POWER,” 2019. [Online]. Available: <http://www.emec.org.uk/about-us/wave-clients/aquamarine-power/>. [Accessed: 12-Aug-2019].
- [182] AW Energy, “WAVEROLLER,” 2018. [Online]. Available: <https://aw-energy.com/waveroller/>. [Accessed: 12-Aug-2019].
- [183] Energy Innovation Cluster, “WAVESTAR.” [Online]. Available: <https://wavepartnership.dk/wavestar-0>. [Accessed: 12-Aug-2019].
- [184] Jordan, “wavestar-002,” 2017. [Online]. Available:

- <https://www.neozone.org/ecologie-planete/wavestar-la-centrale-electrique-qui-utilise-la-houle-pour-produire-de-lenergie/attachment/wavestar-002/>. [Accessed: 12-Aug-2019].
- [185] Eco Wave Power, "Photos," 2019. [Online]. Available: <https://www.ecowavepower.com/gallery/photos/>. [Accessed: 12-Aug-2019].
- [186] P. Zuini and M. Cepellos, "STARTUP USA ONDAS DO MAR PARA GERAR ENERGIA," 2015.
- [187] Ecthelion, "Norwave Wave Power Plant," *sketchfab*, 2017. [Online]. Available: <https://sketchfab.com/3d-models/norwave-wave-power-plant-482851fc4c8041d99d456289c01dc764>.
- [188] P. Bak, J. Peter, Peter Frigaard; Jens Peter Kofoed¹ & Wilfried Knapp², ¹Dept. Civil Engineering; Aalborg University;, and T. U. of Munich, "Wave Dragon: wave power plant using low-head turbines," in *Hidroenergia 04: International Conference and Exhibition on Small Hydropower General*, 2004.
- [189] J. Tedd and J. Peter Kofoed, "Measurements of overtopping flow time series on the Wave Dragon, wave energy converter," *Renew. Energy*, vol. 34, no. 3, pp. 711–717, 2009.
- [190] M. Buccino, D. Banfi, D. Vicinanza, M. Calabrese, G. Del Giudice, and A. Carravetta, "Non breaking wave forces at the front face of Seawave Slotcone Generators," *Energies*, vol. 5, no. 11, pp. 4779–4803, 2012.
- [191] A. Pecher and J. P. Kofoed, *Handbook of Ocean Wave Energy*, vol. 7. Cham: Springer International Publishing, 2017.
- [192] D. Curto, A. Viola, V. Franzitta, M. Trapanese, and F. Cardona, "A New Solution for Sea Wave Energy Harvesting, the Proposal of an Ironless Linear Generator," *J. Mar. Sci. Eng.*, vol. 8, no. 2, p. 93, Feb. 2020.
- [193] I. Boldea and S. A. Nasar, *Linear Electric Actuators and Generators*, 1st ed. Cambridge University Press, 1997.
- [194] W. Li, J. Isberg, J. Engström, R. Waters, and M. Leijon, "Optimization of the power absorption for a linear generator wave energy converter," *Twenty Fifth Int. Offshore Polar Eng. Conf.*, pp. 857–861, 2015.
- [195] J. Faiz and A. Nematsaberi, "Linear electrical generator topologies for direct-drive marine wave energy conversion- an overview," *IET Renew. Power Gener.*, vol. 11, no. 9, pp. 1163–1176, Jul. 2017.
- [196] Supermagnete, "Data sheet article Q-50-15-15-N." pp. 1–3, 2011.
- [197] J. Faiz, M. Ebrahimi-Salary, and G. Shahghplian, "Cogging force alleviation in linear permanent magnet generators," *IEEE AFRICON Conf.*, no. September, 2009.
- [198] M. Vantorre, R. Banasiak, and R. Verhoeven, "Modelling of hydraulic performance and wave energy extraction by a point absorber in heave," *Appl. Ocean Res.*, vol. 26, no. 1–2, pp. 61–72, Feb. 2004.
- [199] P. Balitsky, G. Bacelli, and J. V. Ringwood, "Control-influenced layout optimization of arrays of wave energy converters," *Proc. Int. Conf. Offshore Mech. Arct. Eng. - OMAE*, vol. 9B, no. June, 2014.

- [200] A. Viola, V. Franzitta, D. Curto, V. Di Dio, D. Milone, and G. Rodono, "Environmental Impact Assessment (EIA) of Wave Energy Converter (WEC)," in *OCEANS 2015 - Genova*, 2015, pp. 1–4.
- [201] F. P. Lockett, "Mathematical modelling of wave energy systems," *Renew. Energy*, vol. 9, no. 1–4, pp. 1213–1217, 1996.
- [202] B. R. Munson, *Fundamentals of Fluid Mechanics*, 6th ed. United States of America: Don Fowley, 2009.
- [203] W. Sheng, "Wave energy conversion and hydrodynamics modelling technologies: A review," *Renew. Sustain. Energy Rev.*, vol. 109, no. April, pp. 482–498, 2019.
- [204] P. Wijayatunga, L. George, A. Lopez, and J. A. Aguado, "Integrating Clean Energy in Small Island Power Systems: Maldives Experience," *Energy Procedia*, vol. 103, no. April, pp. 274–279, Dec. 2016.
- [205] M. Gratsea, E. Liakakou, N. Mihalopoulos, A. Adamopoulos, E. Tsilibari, and E. Gerasopoulos, "The combined effect of reduced fossil fuel consumption and increasing biomass combustion on Athens' air quality, as inferred from long term CO measurements," *Sci. Total Environ.*, vol. 592, pp. 115–123, Aug. 2017.
- [206] A. Bridges, F. A. Felder, K. McKelvey, and I. Niyogi, "Uncertainty in energy planning: Estimating the health impacts of air pollution from fossil fuel electricity generation," *Energy Res. Soc. Sci.*, vol. 6, pp. 74–77, Mar. 2015.
- [207] A. R. Keeley, "Renewable Energy in Pacific Small Island Developing States: the role of international aid and the enabling environment from donor's perspectives," *J. Clean. Prod.*, vol. 146, pp. 29–36, 2017.
- [208] R. Ciriminna, M. Pagliaro, F. Meneguzzo, and M. Pecoraino, "Solar energy for Sicily's remote islands: On the route from fossil to renewable energy," *Int. J. Sustain. Built Environ.*, vol. 5, no. 1, pp. 132–140, 2016.
- [209] P. Blechinger, R. Seguin, C. Cader, P. Bertheau, and C. Breyer, "Assessment of the global potential for renewable energy storage systems on small islands," *Energy Procedia*, vol. 46, pp. 294–300, 2014.
- [210] World Health Organization, "Small island developing states: health and WHO: country presence profile," 2017.
- [211] Z. M. A. Bundhoo, K. U. Shah, and D. Surroop, "Climate proofing island energy infrastructure systems: Framing resilience based policy interventions," *Util. Policy*, vol. 55, no. March, pp. 41–51, 2018.
- [212] E. K. Stuart, "Energizing the island community: A review of policy standpoints for energy in small island states and territories," *Sustain. Dev.*, vol. 14, no. 2, pp. 139–147, Apr. 2006.
- [213] M. Beccali *et al.*, "Characterization of a small Mediterranean island end-users' electricity consumption: The case of Lampedusa," *Sustain. Cities Soc.*, vol. 35, no. March, pp. 1–12, 2017.
- [214] M. G. Ippolito, M. L. Di Silvestre, E. Riva Sanseverino, G. Zizzo, and G. Graditi, "Multi-objective optimized management of electrical energy storage systems in an islanded network with renewable energy sources under different design

- scenarios," *Energy*, vol. 64, pp. 648–662, 2014.
- [215] T. L. Jensen, *Renewable Energy on small Islands*, no. April. Copenhagen, 1998.
- [216] IRENA, "Transforming small-island power systems: Technical planning studies for the integration of variable renewables," Abu Dhabi.
- [217] L. Briguglio, "Small Island Developing States and Their Economic Vulnerabilities," *World Dev.*, vol. 23, no. 9, pp. 1615–1632, 1995.
- [218] M. Pelling and J. I. Uitto, "Small island developing states: natural disaster vulnerability and global change," *Glob. Environ. Chang. Part B Environ. Hazards*, vol. 3, no. 2, pp. 49–62, 2001.
- [219] S. Szabó, I. Kougiyas, M. Moner-Girona, and K. Bódis, "Sustainable Energy Portfolios for Small Island States," *Sustainability*, vol. 7, no. 9, pp. 12340–12358, 2015.
- [220] D. Weisser, "On the economics of electricity consumption in small island developing states: A role for renewable energy technologies?," *Energy Policy*, vol. 32, no. 1, pp. 127–140, 2004.
- [221] G. Cannistraro, M. Cannistraro, and G. Trovato, "Islands 'Smart Energy' for eco-sustainable energy a case study 'Favignana Island,'" *Int. J. Heat Technol.*, vol. 35, no. Special Issue1, pp. S87–S95, Sep. 2017.
- [222] F. Petrakopoulou, "On the economics of stand-alone renewable hybrid power plants in remote regions," *Energy Convers. Manag.*, vol. 118, pp. 63–74, Jun. 2016.
- [223] World Energy Council, "World Energy Resources," London, 2016.
- [224] R. G. Shirley and J. Word, "Rights, rivers and renewables: Lessons from hydropower conflict in Borneo on the role of cultural politics in energy planning for Small Island Developing States," *Util. Policy*, vol. 55, no. September, pp. 189–199, 2018.
- [225] Y. Ikeda, "Power Grid with 100% Renewable Energy for Small Island Developing States -- Nexus of Energy, Environment, and Economic Growth," pp. 1–13, 2019.
- [226] G. Lavidas and V. Venugopal, "A 35 year high-resolution wave atlas for nearshore energy production and economics at the Aegean Sea," *Renew. Energy*, vol. 103, pp. 401–417, Apr. 2017.
- [227] S. Bozzi, R. Archetti, and G. Passoni, "Wave electricity production in Italian offshore: A preliminary investigation," *Renew. Energy*, vol. 62, pp. 407–416, 2014.
- [228] E. Rusu and C. Guedes Soares, "Coastal impact induced by a Pelamis wave farm operating in the Portuguese nearshore," *Renew. Energy*, vol. 58, pp. 34–49, Oct. 2013.
- [229] M. Majidi Nezhad, D. Groppi, F. Rosa, G. Piras, F. Cumo, and D. A. Garcia, "Nearshore wave energy converters comparison and Mediterranean small island grid integration," *Sustain. Energy Technol. Assessments*, vol. 30, no. July, pp. 68–76, 2018.
- [230] P. Stenzel, A. Schreiber, J. Marx, C. Wulf, M. Schreieder, and L. Stephan, "Renewable energies for Graciosa Island, Azores-Life Cycle Assessment of

- electricity generation," *Energy Procedia*, vol. 135, pp. 62–74, 2017.
- [231] E. Rusu, "Evaluation of the Wave Energy Conversion Efficiency in Various Coastal Environments," *Energies*, vol. 7, no. 6, pp. 4002–4018, Jun. 2014.
- [232] D. Al Katsaprakakis, B. Thomsen, I. Dakanali, and K. Tzirakis, "Faroe Islands: Towards 100% R.E.S. penetration," *Renew. Energy*, vol. 135, no. 2019, pp. 473–484, May 2019.
- [233] B. Zhao, X. Zhang, P. Li, K. Wang, M. Xue, and C. Wang, "Optimal sizing, operating strategy and operational experience of a stand-alone microgrid on Dongfushan Island," *Appl. Energy*, vol. 113, pp. 1656–1666, 2014.
- [234] S. Selosse, S. Garabedian, O. Ricci, and N. Maïzi, "The renewable energy revolution of reunion island," *Renew. Sustain. Energy Rev.*, vol. 89, no. March, pp. 99–105, 2018.
- [235] K. Sperling, "How does a pioneer community energy project succeed in practice? The case of the Samsø Renewable Energy Island," *Renew. Sustain. Energy Rev.*, vol. 71, no. February 2016, pp. 884–897, May 2017.
- [236] H. C. Gils and S. Simon, "Carbon neutral archipelago – 100% renewable energy supply for the Canary Islands," *Appl. Energy*, vol. 188, pp. 342–355, Feb. 2017.
- [237] E. Zafeiratou and C. Spataru, "Sustainable island power system – Scenario analysis for Crete under the energy trilemma index," *Sustain. Cities Soc.*, vol. 41, no. April, pp. 378–391, 2018.
- [238] Covenant of Mayors Office and Joint Research Centre of the European Commission, "Reporting Guidelines on Sustainable Energy Action Plan and Monitoring," 2014.
- [239] Greenpeace Onlus, "100% rinnovabili: un nuovo futuro per le piccole isole," 2015.
- [240] Ministero dello Sviluppo Economico, *Decreto 14 febbraio 2017. Disposizioni per la progressiva copertura del fabbisogno delle isole minori non interconnesse attraverso energia da fonti rinnovabili*. 2017.
- [241] Wikipedia, "Isole d'Italia per popolazione," 2018. [Online]. Available: https://it.wikipedia.org/wiki/Isole_d%27Italia_per_popolazione. [Accessed: 08-Nov-2019].
- [242] Clean Energy for EU Islands, "26 islands launch clean energy transition with EU Islands Secretariat support." [Online]. Available: <https://euislands.eu/26-islands-launch-transition>. [Accessed: 25-Feb-2019].
- [243] Grundfos, "Addio evaporazione. benvenuta osmosi inversa. Grundfos alle Isole Eolie." [Online]. Available: https://it.grundfos.com/case_stories_pompe/find-case/addio-evaporazione-benvenuta-osmosi-inversa-grundfos-isole-eolie.html. [Accessed: 30-Oct-2019].
- [244] Termomeccanica Ecologica, "Impianto di dissalazione ad osmosi inversa dell'isola di Capraia (LI)." [Online]. Available: http://www.tme.termomeccanica.com/uploaded_files/attachments/200806161213632179/scheda_capraia.pdf. [Accessed: 30-Oct-2019].
- [245] D. Curto, V. Franzitta, M. Trapanese, and M. Cirrincione, "A Preliminary Energy

- Assessment to Improve the Energy Sustainability in the Small Islands of the Mediterranean Sea," *J. Sustain. Dev. Energy, Water Environ. Syst.*, pp. 1-19, 2020.
- [246] Area Marina Protetta, "Isola di Ustica - Zone." [Online]. Available: <http://www.ampustica.it/it/zone.asp?idmenu=4>. [Accessed: 07-May-2019].
- [247] Città Metropolitana di Palermo, "Riserva naturale orientata - Isola di Ustica." [Online]. Available: http://www.provincia.palermo.it/pls/provpa/v3_s2ew_consultazione.mostra_pagina?id_pagina=6236. [Accessed: 07-May-2019].
- [248] V. Puleo, C. M. Fontanazza, V. Notaro, and G. Freni, "Hybrid Energy Generation System for Small Islands Water Supply," in *36th IAHR World Congress*, 2015, pp. 1-6.
- [249] D. Curto and M. Trapanese, "A Renewable Energy mix to Supply the Balearic Islands: Sea Wave, Wind and Solar," in *2018 IEEE International Conference on Environment and Electrical Engineering and 2018 IEEE Industrial and Commercial Power Systems Europe (EEEIC / I&CPS Europe)*, 2018, pp. 1-6.
- [250] V. Franzitta, D. Curto, D. Rao, and A. Viola, "Renewable energy sources to fulfill the global energy needs of a country: The case study of Malta in Mediterranean Sea," in *OCEANS 2016 - Shanghai*, 2016, no. 2012, pp. 1-5.
- [251] V. Franzitta, D. Curto, D. Milone, and D. Rao, "Assessment of Renewable Sources for the Energy Consumption in Malta in the Mediterranean Sea," *Energies*, vol. 9, no. 12, p. 1034, Dec. 2016.
- [252] V. Franzitta, D. Curto, and D. Rao, "Energetic Sustainability Using Renewable Energies in the Mediterranean Sea," *Sustainability*, vol. 8, no. 11, p. 1164, Nov. 2016.
- [253] JRC European Commission, "Photovoltaic Geographical Information System - Interactive Maps," 2017. [Online]. Available: <http://re.jrc.ec.europa.eu/pvgis/apps4/pvest.php?lang=en&map=europe>. [Accessed: 24-Feb-2019].
- [254] Autorità di Regolazione per Energia Reti e Ambiente (ARERA), "Deliberazione 30 Ottobre 2018 n. 544/2018/R/eel," 2018.
- [255] E. C. Bank, "Key ECB interest rates," 2019. [Online]. Available: https://www.ecb.europa.eu/stats/policy_and_exchange_rates/key_ecb_interest_rates/html/index.en.html. [Accessed: 18-Aug-2019].
- [256] Gestore dei Mercati Energetici (GME), "dati di sintesi MPE-MGP - riepilogo," 2019. [Online]. Available: <https://www.mercatoelettrico.org/it/Statistiche/ME/DatiSintesi.aspx>. [Accessed: 18-Aug-2019].
- [257] D. Curto, V. Franzitta, A. Viola, M. Cirrincione, A. Mohammadi, and A. Kumar, "A renewable energy mix to supply small islands. A comparative study applied to Balearic Islands and Fiji," *J. Clean. Prod.*, p. 118356, Sep. 2019.
- [258] AEMET - Agencia Estatal de Meteorologia, "Valores climatológicos normales, Illes Balears," 2016. [Online]. Available:

- <http://www.aemet.es/es/serviciosclimaticos/datosclimatologicos/valoresclimatologicos?k=bal>. [Accessed: 05-Aug-2019].
- [259] Red Eléctrica de España, “Red Eléctrica de España - Statistical Data,” 2019. [Online]. Available: <http://www.ree.es/en/statistical-data-of-spanish-electrical-system/statistical-series/national-statistical-series>. [Accessed: 16-May-2019].
- [260] Australian Bureau of Meteorology and CSIRO, “Climate Variability, Extremes and Change in the Western Tropical Pacific: New Science and Updated Country Reports 2014,” 2014.
- [261] IRENA, “Hydropower,” 2019. [Online]. Available: <http://www.irena.org/hydropower>. [Accessed: 24-Apr-2018].
- [262] R. G. Dean and R. A. Dalrymple, *Water Wave Mechanics for Engineers and Scientists*, vol. 2. WORLD SCIENTIFIC, 1991.
- [263] Y. Fu, X. Liu, and Z. Yuan, “Life-cycle assessment of multi-crystalline photovoltaic (PV) systems in China,” *J. Clean. Prod.*, vol. 86, pp. 180–190, 2015.
- [264] Mitsubishi Electric, “Photovoltaic Modules. MLU series. 255 Wp PV-MLU255HC,” 2017.
- [265] A. Evans, V. Strezov, and T. J. Evans, “Assessment of sustainability indicators for renewable energy technologies,” *Renew. Sustain. Energy Rev.*, vol. 13, no. 5, pp. 1082–1088, Jun. 2009.
- [266] A. Mostafaeipour, M. Rezaei, A. Moftakharzadeh, M. Qolipour, and M. Salimi, “Evaluation of hydrogen production by wind energy for agricultural and industrial sectors,” *Int. J. Hydrogen Energy*, vol. 44, no. 16, pp. 7983–7995, 2019.
- [267] L. Wang, J. Yuan, M. E. Cholette, Y. Fu, Y. Zhou, and A. C. Tan, “Comparative study of discretization method and Monte Carlo method for wind farm layout optimization under Weibull distribution,” *J. Wind Eng. Ind. Aerodyn.*, vol. 180, no. July, pp. 148–155, 2018.
- [268] M. H. Ouahabi, “Analyzing wind speed data and wind power density of Tetouan city in Morocco by adjustment to Weibull and Rayleigh distribution functions,” *Wind Eng.*, no. May, pp. 0–11, 2017.
- [269] meteoblue, “Clima (da modello) Suva,” 2019. [Online]. Available: https://www.meteoblue.com/it/tempo/historyclimate/climatemodelled/suva_figi_2198148. [Accessed: 16-Jul-2019].
- [270] meteoblue, “Clima (da modello) Isole Baleari,” 2019. [Online]. Available: https://www.meteoblue.com/it/tempo/historyclimate/climatemodelled/isole-baleari_spagna_2521384. [Accessed: 16-Jul-2019].
- [271] Senvion, “The MM100. Optimized for low to mid wind locations,” 2018.
- [272] Senvion, “Datasheet 6.3M152,” 2018.
- [273] ADRASE, “Acceso a datos de radiación solar de España,” 2018. [Online]. Available: <http://www.adrase.com/acceso-a-los-mapas/mapa-zona-peninsula.html>. [Accessed: 05-Aug-2019].
- [274] ENEA, “WebGIS - Waves Energy,” 2015. [Online]. Available:

<http://utmea.enea.it/energiadalmare/>. [Accessed: 05-Aug-2019].

- [275] T. Aukitino, M. G. M. Khan, and M. R. Ahmed, "Wind energy resource assessment for Kiribati with a comparison of different methods of determining Weibull parameters," *Energy Convers. Manag.*, vol. 151, no. October, pp. 641–660, 2017.
- [276] A. Abdulkarim, S. M. Abdelkader, and D. John Morrow, "Statistical Analyses of Wind and Solar Energy Resources for the Development of Hybrid Microgrid," 2015, pp. 9–14.
- [277] E. Carpaneto and G. Chicco, "Probability distributions of the aggregated residential load," *2006 9th Int. Conf. Probabilistic Methods Appl. to Power Syst. PMAPS*, 2006.
- [278] E. Carpaneto and G. Chicco, "Probabilistic characterisation of the aggregated residential load patterns," *IET Gener. Transm. Distrib.*, vol. 2, no. 3, p. 373, 2008.
- [279] H. Golpîra, S. Bahramara, S. Abdul Rehman Khan, and Y. Zhang, "Robust bi-level risk-based optimal scheduling of microgrid operation against uncertainty," *RAIRO - Oper. Res.*, Apr. 2019.
- [280] EnergyData.info, "Global Wind Atlas," 2018. [Online]. Available: <https://globalwindatlas.info/>. [Accessed: 05-Aug-2019].
- [281] WACOP, "Fiji Wave Atlas - Wave Power and Energy," 2016. [Online]. Available: <http://wacop.gsd.spc.int/FijiWaveEnergy.html>. [Accessed: 24-Apr-2018].
- [282] M. Boxwell, "Solar electricity handbook - Solar Calculator," 2017. [Online]. Available: <http://solarelectricityhandbook.com/>. [Accessed: 30-Apr-2018].
- [283] S. S. Kutty, M. G. M. Khan, and M. R. Ahmed, "Wind energy resource assessment for Suva, Fiji, with accurate Weibull parameters," *Energy Explor. Exploit.*, vol. 37, no. 3, 2019.
- [284] D. Curto, V. Franzitta, and M. Trapanese, "Supplying small islands with solar, wind and sea wave. An economic approach to find the best energy share," in *OCEANS 2019 MTS/IEEE SEATTLE*, 2019, pp. 1–7.
- [285] A. P. F. Andaloro, R. Salomone, L. Andaloro, N. Briguglio, and S. Sparacia, "Alternative energy scenarios for small islands: A case study from Salina Island (Aeolian Islands, Southern Italy)," *Renew. Energy*, vol. 47, pp. 135–146, Nov. 2012.
- [286] E. González-Roubaud, D. Pérez-Osorio, and C. Prieto, "Review of commercial thermal energy storage in concentrated solar power plants: Steam vs. molten salts," *Renew. Sustain. Energy Rev.*, vol. 80, no. February, pp. 133–148, Dec. 2017.
- [287] K. Branker, M. J. M. Pathak, and J. M. Pearce, "A review of solar photovoltaic levelized cost of electricity," *Renew. Sustain. Energy Rev.*, vol. 15, no. 9, pp. 4470–4482, 2011.
- [288] X. Ouyang and B. Lin, "Levelized cost of electricity (LCOE) of renewable energies and required subsidies in China," *Energy Policy*, vol. 70, pp. 64–73, 2014.
- [289] F. Ueckerdt, L. Hirth, G. Luderer, and O. Edenhofer, "System LCOE: What are the costs of variable renewables?," *Energy*, vol. 63, pp. 61–75, 2013.
- [290] W. Short, D. J. Packey, and T. Holt, "A manual for the economic evaluation of

energy efficiency and renewable energy technologies," 1995.

- [291] C. Parrado, A. Girard, F. Simon, and E. Fuentealba, "2050 LCOE (Levelized Cost of Energy) projection for a hybrid PV (photovoltaic)-CSP (concentrated solar power) plant in the Atacama Desert, Chile," *Energy*, vol. 94, pp. 422–430, 2016.
- [292] I. Pawel, "The cost of storage - How to calculate the levelized cost of stored energy (LCOE) and applications to renewable energy generation," *Energy Procedia*, vol. 46, pp. 68–77, 2014.
- [293] R. A. Abou-Jeyab, Y. P. Gupta, J. R. Gervais, P. A. Branchi, and S. S. Woo, "Constrained multivariable control of a distillation column using a simplified model predictive control algorithm," *J. Process Control*, vol. 11, no. 5, pp. 509–517, 2001.
- [294] D. Vicinanza, L. Cappiotti, V. Ferrante, and P. Contestabile, "Estimation of the wave energy in the Italian offshore," *J. Coast. Res.*, vol. 64, no. 64, pp. 613–617, 2011.
- [295] meteoblue, "Clima Isole Eolie." [Online]. Available: https://www.meteoblue.com/it/tempo/previsioni/modelclimate/isole-eolie_italia_6941096. [Accessed: 24-Feb-2019].
- [296] ENEA, "Waves Energy WebGIS," 2019. [Online]. Available: <http://utmea.enea.it/energiadalmare/>. [Accessed: 24-Feb-2019].
- [297] A. D. Sahin, "Progress and recent trends in wind energy," *Prog. Energy Combust. Sci.*, vol. 30, no. 5, pp. 501–543, 2004.
- [298] H. Chai, W. Guan, X. Wan, X. Li, Q. Zhao, and S. Liu, "A Wave Power Device with Pendulum Based on Ocean Monitoring Buoy," *IOP Conf. Ser. Earth Environ. Sci.*, vol. 108, p. 052013, Jan. 2018.
- [299] N. Guillou and G. Chapalain, "Numerical modelling of nearshore wave energy resource in the Sea of Iroise," *Renew. Energy*, vol. 83, pp. 942–953, Nov. 2015.
- [300] GME, "2018 MGP historical data (in Italian 'Dati Storici MGP. Anno 2018')," 2019. [Online]. Available: <http://www.mercatoelettrico.org/It/download/DatiStorici.aspx>. [Accessed: 20-Feb-2019].
- [301] ARERA, *Deliberation 15 June 2017 n. 428/2017/R/EEL (in Italian "Deliberazione 15 Giugno 2017 n. 428/2017/R/EEL")*. 2017, p. 2.
- [302] V. Franzitta, D. Curto, D. Milone, and A. Viola, "The desalination process driven by wave energy: A challenge for the future," *Energies*, vol. 9, no. 12, pp. 1–16, Dec. 2016.
- [303] S. Favuzza *et al.*, "An Analysis of the Inertial Response of Small Isolated Power Systems in Presence of Generation from Renewable Energy Sources," in *2018 IEEE 4th International Forum on Research and Technology for Society and Industry (RTSI)*, 2018, vol. 2019, pp. 1–6.
- [304] S. Favuzza *et al.*, "System Stability of a Small Island's Network with Different Levels of Wind Power Penetration," in *2018 IEEE 4th International Forum on Research and Technology for Society and Industry (RTSI)*, 2018, vol. 2019, pp. 1–6.

- [305] M. L. Di Silvestre, D. La Cascia, E. Riva Sanseverino, and G. Zizzo, "Improving the energy efficiency of an islanded distribution network using classical and innovative computation methods," *Util. Policy*, vol. 40, pp. 58–66, Jun. 2016.
- [306] V. Lo Brano *et al.*, "Analysis of air conditioning technologies and ICT systems applied to final users in small islands not connected to the NTG to improve the energy efficiency of the island's electrical system (in Italian "Analisi delle tecnologie per la climatizzazione e si," 2016.
- [307] meteoblue, "Climate Lampedusa," 2019. [Online]. Available: https://www.meteoblue.com/en/weather/historyclimate/climatemodelled/lampedusa_italy_2524459. [Accessed: 11-Jun-2019].
- [308] Italian Ministry of Economic Development, "Monthly fuel prices," 2019. [Online]. Available: https://dgsaie.mise.gov.it/prezzi_carburanti_mensili.php?pid=1. [Accessed: 31-Dec-2019].
- [309] ARERA, *Deliberazione 16 Ottobre 2018. 508/2018/R/eel. Determinazione dell'aliquota di integrazione tariffaria, per l'anno 2015, per l'impresa elettrica minore non trasferita ad Enel S.p.A. Selis Lampedusa S.p.A. Italy*, 2018.
- [310] G. M. Caporale and L. A. Gil-Alana, "Long-term interest rates in Europe: A fractional cointegration analysis," *Int. Rev. Econ. Financ.*, vol. 61, no. January, pp. 170–178, 2019.
- [311] "Google maps." [Online]. Available: <https://www.google.it/maps/@42.1830474,10.8934625,1387895m/data=!3m1!1e3?hl=en&authuser=0>. [Accessed: 13-Nov-2019].
- [312] V. Franzitta, D. Rao, D. Curto, and A. Viola, "Greening island: renewable energies mix to satisfy electrical needs of Pantelleria in Mediterranean sea," in *OCEANS 2016 MTS/IEEE Monterey*, 2016, pp. 1–6.
- [313] Presidente della Repubblica Italiana, *DECRETO DEL PRESIDENTE DELLA REPUBBLICA 28 luglio 2016. Istituzione del Parco nazionale «Isola di Pantelleria» e dell'Ente Parco nazionale «Isola di Pantelleria»*. 2016.
- [314] Assessorato dei Beni Culturali ed Ambientali e della Pubblica Istruzione, *Decreto 26 luglio 2000 della Regione Sicilia. Sicilia*, 2000.
- [315] Autorità di Regolazione per l'Energia Reti e Ambiente (ARERA), *Deliberazione 16 Ottobre 2018 n. 511/2018/R/EEL. Determinazione dell'aliquota di integrazione tariffaria, per l'anno 2015, per l'impresa elettrica minore non trasferita ad ENEL SpA, SMEDE Pantelleria SpA*. 2018.
- [316] V. Cosentino *et al.*, "Smart renewable generation for an islanded system. Technical and economic issues of future scenarios," *Energy*, vol. 39, no. 1, pp. 196–204, 2012.
- [317] Autorità di Regolazione per Energia Reti e Ambiente (ARERA), "Indicatori di continuità del servizio relativi alle interruzioni lunghe, brevi e transitorie," 2019. [Online]. Available: https://www.arera.it/it/dati/inter_continuita.htm. [Accessed: 13-Nov-2019].
- [318] Comune di Pantelleria, "Intervento di ricerca e riduzione delle perdite nel sistema di adduzione e distribuzione idrica nell'isola di Pantelleria."

- [319] E. Garofalo *et al.*, "Sviluppo delle Fonti Energetiche Rinnovabili nelle Isole minori non interconnesse," 2015.
- [320] N. Cannata *et al.*, "Multi-Objective Optimization of Urban Microgrid Energy Supply According to Economic and Environmental Criteria," *2019 IEEE Milan PowerTech*, pp. 1-6, 2019.
- [321] G. Attardo, S. Longo, F. Montana, E. Riva Sanseverino, Q. T. T. Tran, and G. Zizzo, "Urban Energy Hubs Economic Optimization and Environmental Comparison in Italy and Vietnam," *IEEE 4th Int. Forum Res. Technol. Soc. Ind. RTSI 2018 - Proc.*, pp. 1-6, 2018.